Vol. 21, No. 5 (Supplent Issue), December, 2022
ISSN (Print): 0972-6268; ISSN (Online) : 2395-3454

Nature Environment & Pollution Technology

A Multidisciplinary, International Journal on Diverse Aspects of Environment

Technoscience Publications
website: www.neptjournal.com

Technoscience Publications
A-504, Bliss Avenue, Balewadi,
Opp. SKP Campus, Pune-411 045
Maharashtra, India

www.neptjournal.com

Nature Environment and Pollution Technology

(An International Quarterly Scientific Research Journal)

EDITORS

Published by : Mrs. T. P. Goel, Technoscience Publications, A-504, Bliss Avenue, Balewadi, Pune-411 045, Maharashtra, India

E-mail : contact@neptjournal.com; operations@neptjournal.com

INSTRUCTIONS TO AUTHORS

Scope of the Journal

The Journal publishes original research/review papers covering almost all aspects of environment like monitoring, control and management of air, water, soil and noise pollution; solid waste management; industrial hygiene and occupational health hazards; biomedical aspects of pollution; conservation and management of resources; environmental laws and legal aspects of pollution; toxicology; radiation and recycling etc. Reports of important events, environmental news, environmental highlights and book reviews are also published in the journal.

Format of Manuscript

- The manuscript (*mss*) should be typed in double space leaving wide margins on both the sides.
- First page of mss should contain only the title of the paper, name(s) of author(s) and name and address of Organization(s) where the work has been carried out along with the affiliation of the authors.

Continued on back inner cover...

Nature Environment and Pollution Technology

Vol. 21, No. 5 (Supplement Issue), December 2022

CONTENTS

The Journal is Currently Abstracted and Indexed in:

- CNKI Scholar (China National Knowledge Infrastructure)
- Scopus CiteScore (2021) 0.70
- Scopus®, SJR (0.169) 2021
- Index Copernicus (2021) = 111.68
- Chemical Abstracts, U.S.A.
- Indian Science Abstracts, New Delhi, India
- Pollution Abstracts, U.S.A.
- Elsevier Bibliographic Databases
- Paryavaran Abstract, New Delhi, India
- Zoological Records
- Electronic Social and Science Citation Index (ESSCI)
- Indian Citation Index (ICI)
- CAB Abstracts, U.K.
- CrossRef (DOI)
- EBSCO: Environment Index™
- Ulrich's (Refereed) database
- Google Scholar
- DOAJ
- Zetoc
- Environment Abstract, U.S.A.
- ProQuest, U.K.
- J-Gate
- WorldCat (OCLC)
- British Library
- Centre for Research Libraries
- Indian Science
- JournalSeek
- Connect Journals (India)
- SHERPA/RoMEO
- Directory of Science
- Research Bible (Japan)
- CSA: Environmental Sciences and Pollution Management
- Elektronische Zeitschriftenbibliothek (EZB)
- Access to Global Online Research in Agriculture (AGORA)
- AGRIS (UN-FAO)
- Present in UGC-CARE List (Group II)

UDL-EDGE (Malaysia) Products like *i*-Journals, *i*-Focus and *i*-Future

www.neptjournal.com

Nature Environment and Pollution Technology

Nature Environment and Pollution Technology
An International Quarterly Scientific Journal

p-ISSN: 0972-6268
(Print copies up to 2016)
e-ISSN: 2395-3454

Vol. 21 | No. 5 (Suppl) | pp. 2015-2023 | 2022

Original Research Paper

https://doi.org/10.46488/NEPT.2022.v21i05.001

Open Access Journal

Support Vector Machine: A Case Study in the Kert Aquifer for Predicting the Water Quality Index in Mediterranean Zone, Drouich Province, Oriental Region, Morocco

Hicham Gueddari*, Mustapha Akodad*, Mourad Baghour*, Abdelmajid Moumen*, Ali Skalli*, Yassine El Yousfi, Hanane Ait Hmeid*, Mohamed Chahban*, Ghizlane Azizi*, Mohamed Chaibi***, Ouassila Riouchi*, Mostapha Maach*, Ahmed Ismail**** and Muhammad Zahid****†**

*Laboratory OLMAN-BPGE, Multidisciplinary Faculty of Nador, Mohamed First University, Oujda, 62700, Nador, Morroco

**Laboratory of Water and Environmental Management Unit, National School of Applied Sciences, Al Hoceima, Abdelmalek Essaadi University, Tangier, 32003, Al Houceima, Morroco

***Team of Renewable Energy and Energy Efficiency, Department of Physics, Faculty of Science, University of Moulay Ismail, Zitoune, Meknes BP 11201, Morocco

****Key Laboratory of Functional Inorganic Material Chemistry, Ministry of Education of the People's Republic of China, Heilongjiang University, Harbin, 150080, China

†Corresponding author: Muhammed Zahid; muhammad93zahid@uop.edu.pk

Nat. Env. & Poll. Tech.
Website: www.neptjournal.com

Received: 03-03-2022
Revised: 04-04-2022
Accepted: 06-04-2022

Key Words:
Groundwater quality
GIS
Water quality index
Support vector machine
Kert aquifer

ABSTRACT

The expansion of urbanization and the amplification of anthropic activities in the Rif region require the establishment of wells. However, the irrational exploitation of water and natural conditions have generated the rise of the water table and the increase in pollution. Thus, the assessment of water quality has emerged as a significant concern. This study's goal is to assess the adequacy of groundwater quality in two aquifers in the vicinity of the Mediterranean Zone - Drouich Province and Oriental Region, Morocco, for drinking water needs by taking 62 water samples of the Kert aquifer for 2019. The Water Quality Index (WQI) classifies water quality: as excellent, good, poor, very poor, etc. That is essential for conveying information about water quality to people and decision-makers in the affected area. The WQI in the Kert aquifer varies from 62.3 to 392.3. The calculation of the water quality index (WQI) of the Kert aquifer view is based that 45.16% of groundwater samples are of poor quality, making them acceptable for drinking. The study's analysis is established with a geographic information system (GIS) setting. The index map provides decision-makers with a complete and interpretable picture for better water resource planning and management. SVM models are shown to account for 87.71% of the varying water quality score. Different statistical and intelligence models may make the index more predictable. These forecasts assist us in better managing the aquifer's water quality.

INTRODUCTION

Public health issues involving the chemical contamination of groundwater must be addressed immediately. The availability of water for human use is a critical global and regional concern (Azizullah et al. 2011, El Yousfi et al. 2022, Schweitzer & Noblet 2018, Vesali Naseh et al. 2018). Water Quality Indices (WQIs) are an easy-to-understand tool that managers and decision-makers can use to evaluate a specific water body's quality and potential applications (Kumari & Sharma 2019, Rawat & Singh 2018). WQI is a mathematical technique for integrating detailed water quality data into a numerical score describing the general view of the water's quality (Gueddari et al. 2022, Mukate et al. 2019, Ponsadailakshmi et al. 2018, Singh et al. 2019) as a whole. In essence, the WQI aims to offer a system for presenting a cumulative score and an expression numerically describing a certain level of water quality (Deshpande et al. 2014, Tziritis et al. 2014). Horton's work led to the development of the first WQI in the US, which has been used in Europe since the 1970s, initially in the UK. Later, the United States National Sanitation Foundation refined this concept (Banda & Kumarasamy 2020, de Andrade Costa et al. 2020,

ORCID details of the authors:

Muhammad Zahid:
https://orcid.org/0000-0002-9618-4814

Kachroud et al. 2019). As a result, the WQI principle has been the subject of extensive effort since then, using concepts that have been slightly modified (Brilli et al. 2013, Eden & Ackermann 2001, Von Zur Gathen & Gerhard 2013).

Prior research in this field has concentrated on groundwater quality (the source of salinity, the aquifer's geochemistry, and investigations of heavy metals). (Elgettafi et al. 2013, Hicham et al. 2021a, 2021b). This publication predicts the Water Quality Index in the unconfined Kert aquifer using a Support Vector Machine.

Water is required for the life of all organisms. As such, it is an irreplaceable resource (Butler 2017, Malekzadeh et al. 2019, Toolabi et al. 2021) We found that the WQI can be predicted using physical values and no sub-index computation of the input for physical and chemical parameters in this study.

MATERIALS AND METHODS

Study Area

North-eastern Morocco is home to the Kert Basin, which covers a space of around 250 square kilometers are shown in Fig. 1. The western Gareb chain forms its eastern boundary. The Kert basin's most important river, the seasonal Temsamane, flows around the massive Temsamane metamorphic mountain, which surrounds the plain to the north and northwest. The river's overall length is 90 km and its catchment area is 2710 sq. km (Zielhofer et al. 2008). According to some studies on the current regular fault system, Kert Basin was formed during the Messinian Paleocene. (Azdimousa 2007). Pump testing and electro-geophysical investigations were used to develop this model. The Kert plain is encircled by an open aquifer that flows through the Miocene Bluish Marls (bedrock aquifer). Numerous hydrogeological formations exist, and their stratification is visible in Fig. 2. Transgressed Miocene marls are overlain by an identical layer of limestone and conglomerate that serves as the aquifer's bedrock. The only other formation in the region, we think, is the Miocene, which contains gypsum. This sequence is completed with villafranchian gravel, silt, and clay. Two Miocene vertical faults created the Kert basin. As a result, the northern and southern bounds of the plain were extended. These faults may connect the aquifer to the Jurassic unit below

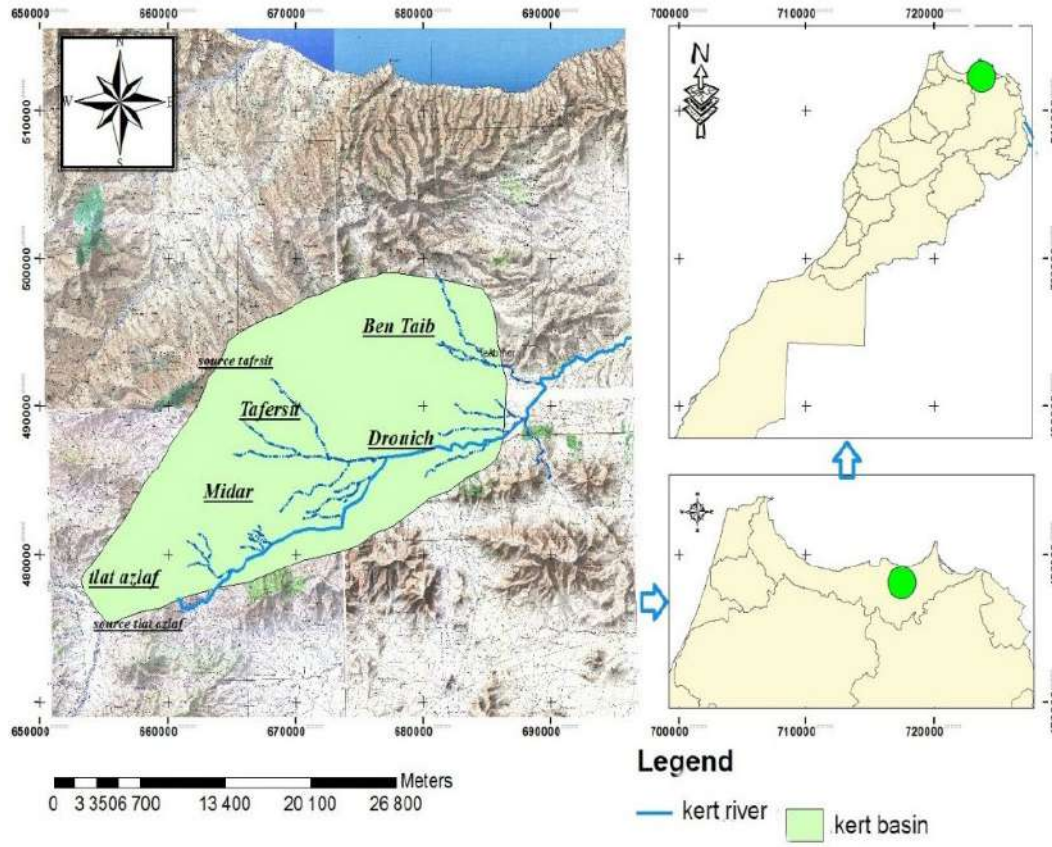

Fig. 1: The Kert basin's placement.

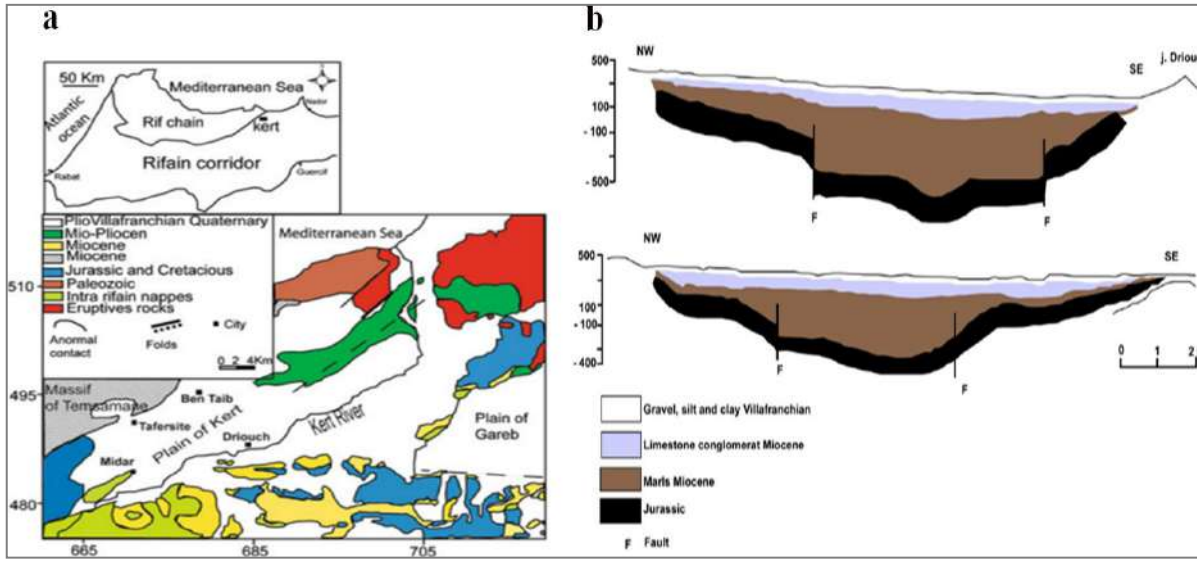

Fig. 2. a - The Kert Plain's base map and b - Hydrogeological section of the kert aquifer system (Carlier 1973).

(Carlier 1973). With an annual rainfall of just 276.9 mm, the area is semi-arid. Temperatures range from 10°C to 25°C annually. The Moulouya Hydraulic Basin Agency pegs the average annual evapotranspiration as 291.6 mm.year^{-1}.

Field Sampling

During the low water season of 2019, sixty wells and two springs are tested from the Kert groundwater. The groundwater samples are subjected to a physicochemical evaluation (Rodier et al. 2009), and a physico-chemical analytical procedure is used. Coolers were used to retain the models at 4^{o}Celsius right away. The ISO 5665 standard is used to collect the samples. The pieces were kept cool (2 to 4°C) in labeled plastic bottles to examine chemical parameters. EC, pH, main elements (Cl^-, Ca^{2+}, Mg^{2+}, K^+, Na^+, SO_4^{2-}, HCO_3^-, NO_3^-, and PO_4^{3-}) were investigated.

Data Processing

Physicochemical data is evaluated using Principal Component Analysis-based multivariate statistical methodologies (PCA). The statistical method is often used in water research to investigate water mineralization and pooling and determine the relationship between WQI and salinity phenomena. The statistical analysis was carried out using the R program. A comparison is made between the measured factors and the quality of drinking water requirements set by the WHO. Thematic maps employing Geographic Information Systems are used to display the results (GIS).

The water quality index (WQI) was developed to quantify the influence of human and natural activities on groundwater chemistry. While assigning weights for the WQI computation, the relative relevance of the physicochemical parameters in determining the overall quality of water for drinking water applications is evaluated. Between one and five, the weight is given. TDS, pH, EC, SO_4, nitrate, and

Table 1: Physicochemical parameters relative weight Parameters (WHO Edition 2011).

Chemical variables	WHO standards (Edition 2011)	Weight (wi)	Relative weight $Wi = wi / \Sigma^{n}_{i=1} wi$
pH (on the scale)	6.5-8.5	4	0.114
EC [mS.cm^{-1}]	250	4	0.114
TDS [mg.L^{-1}]	500	5	0.142
HCO_3^- [mg.L^{-1}]	500	3	0.086
Cl^- [mg.L^{-1}]	600	3	0.086
SO_4^{2-} [mg.L^{-1}]	400	4	0.114
NO_3^- [mg.L^{-1}]	50	5	0.142
Ca^{++} [mg.L^{-1}]	200	2	0.057
Mg^{++} [mg.L^{-1}]	150	1	0.029
Na^+ [mg.L^{-1}]	200	2	0.057
K^+ [mg.L^{-1}]	10	2	0.057

Table 2: WQI-based water quality rating ranges and kinds range water type (Bhargava 1983).

Range	Type of waters
≥50	Excellent water
50-100	Good water
100-200	Poor water
200-300	Very poor water
≤300	Water that is unfit for consumption

HCO_3 have been assigned a maximum weight of 5, 4 for pH, EC, SO_4^{2-}, 3 for HCO_3^-, and two for Ca^{++}, Na^+, and K^+ (Table 1). (Akhtar et al. 2021, Bhimanagouda et al. 2020, Gueddari et al. 2022, Karunanidhi et al. 2021, Selvam et al. 2014)). The comparative weight is calculated using the subsequent equation (eq.1).

$$\mathrm{Wi} = wi / \sum_{i=1}^{ni} wi \quad \ldots(1)$$

Where:

Wi denotes the weight relative to another.

wi denotes the parameter's weight.

The argument count is n.

The level for evaluating the quality of each parameter is determined by dividing each water sample's concentration by the applicable standard (WHO Edition 2011) and multiplying the results by 100 (eq.2).

$$Qi = \left(\frac{ci}{si}\right) \times 100 \quad \ldots(2)$$

Where,

Qi denotes the standard of quality.

ci denotes every chemical parameter's concentration in

The weight of each sample is determined, and the concentration is given in milligrams per liter. si is the recommended limit for every chemical parameter in milligrams per liter by the World Health Organization (WHO Edition 2011). Begin the last phase of WQI calculation by computing the SI for each parameter (Table.2). The water quality index is calculated by adding the SI values for each sample. (Abbasnia et al. 2019, Mukate et al. 2019) (eq.3 and 4).

$$Sli = Wi \times qi \quad \ldots(3)$$

$$WQI = \Sigma Sli \quad \ldots(4)$$

Where

Sli is the i^{th} parameter's sub-index.

qi is the score assigned to the ith parameter depending on its concentration.

The number n denotes the number of parameters.

Physical and Chemical Analysis

Because the parameters vary after sampling, and cannot be identified qualitatively, we took measurements of T (°C) and dissolved oxygen in situ, as well as pH, Cond (S.cm-1), and hydrogen potential (pH) (O2d). For these tests, we utilized a MULTI 350I multi-parameter meter that is easily portable.

Methods for analyzing various other variables were used in a laboratory, as per recommendations from Rodier et al. (2009):

- To identify and quantify (K^+, Na^+), we employed Flame Atomic Absorption Spectrophotometry (Varian Model 475-AA).
- According to the ISO17294-2:2016 standard, the measurements are made using spectrophotometry and colorimetric dose (SO_4^{2-}, NO_3^-, PO_4^{3-}).
- Complexometric measurements are used for calcium and magnesium. To measure the concentration of main anions, we used them as a technique.
- Chloride precipitation and bicarbonate titrimetry with 0.01 N HCl are two methods to determine precipitation. It is common practice to measure chemical levels in $mg.L^{-1}$ units.

Support Vector Machine (SVM)

Identifying the root causes of data is well-suited to the use of SVM-based supervised machine learning models. The statistical learning theory and the notion of structural risk reduction underlie these strategies (Bennett & Demiriz 1999, Evgeniou et al. 2002). The kernel approach in regression transforms non-linear correlations between inputs and outputs into a higher-dimensional regression analysis. (Üstün et al. 2007, Xu et al. 2006). D = x I,y I i = 1: n, where x is the contribution vector, y is the output variable, and n is the number of observations.

The SVR model aims to find the best function f defined (Kavousi-Fard & Kavousi-Fard 2013, Mohammadi & Mehdizadeh 2020) (eq.5):

$$f(x) = w^T \varphi(x) + b \quad \ldots(5)$$

Where *a* is a nonlinear function that translates the data received into high dimensional space, w and b represent the weights and the bias that are determined by minimizing the regularized risk function (eq.6):

$$R = \frac{1}{2} w^T w + C \frac{1}{n} \sum_i^n L_\varepsilon(g(x_i), y_i) \quad \ldots(6)$$

Where L_ε is the ε – I insensitive loss function; $C \frac{1}{n} \sum_i^n L_\varepsilon(g(x_i), y_i)$ is the empirical error and C is a positive Trade-off parameter between the observed error's magnitude and the model's flatness.

When attempting to forecast river water quality using an ungauged catchment in a dual scenario, this study turned to RBF (Model-Based Support Vector Machine Model for Predicting Water Quality) (eq.7).

$$K(x_i, x_j) = \exp\left(-\frac{\| x_i - x_j \|^2}{2\sigma^2}\right) \quad \ldots(7)$$

Where $\|x_i - x_j\|^2$ is the squared Euclidean distance between the two input vectors and, and is the band-

Table 3: Individual water quality index (WQI) categorization.

Wells	WQI	Water quality classification type	Wells	WQI	Water quality classification type
w1	219.4	Very poor water	w34	84.1	Good water
w2	334.98	Water that is unfit for consumption	w35	139.6	Poor water
w3	311.02	Water that is unfit for consumption	w36	190.7	Poor water
w4	264.48	Very poor water	w37	201.5	Very poor water
w5	138.29	Poor water	w38	175.1	Poor water
w6	202.1	Very poor water	w39	206.3	Very poor water
w7	197.5	Poor water	w40	216.2	Very poor water
w8	96	Good water	w41	224.1	Very poor water
w9	138.4	Poor water	w42	322.5	Water that is unfit for consumption
w10	282.8	Very poor water	w43	392.3	Water that is unfit for consumption
w11	179.7	Poor water	w44	301.1	Water that is unfit for consumption
w12	296.5	Very poor water	w45	320.1	Water that is unfit for consumption
w13	234.7	Very poor water	w46	186.7	Poor water
w14	228.6	Very poor water	w47	126.1	Poor water
w15	128.4	Poor water	w48	169.3	Poor water
w16	273.5	Very poor water	w49	74.6	Good water
w17	227.6	Very poor water	w50	138	Poor water
w18	197.7	Poor water	w51	89.6	Good water
w19	223.6	Very poor water	w52	74.9	Good water
w20	260.1	Very poor water	w53	99.5	Good water
w21	318.1	Water that is unfit for consumption	w54	110.2	Poor water
w22	245.2	Very poor water	w55	98.2	Good water
w23	222.6	Very poor water	w56	92	Good water
w24	179.3	Poor water	w57	96	Good water
w25	213.5	Very poor water	w58	152.5	Poor water
w26	116.6	Poor water	w59	158.8	Poor water
w27	109.3	Poor water	w60	185.3	Poor water
w28	139.3	Poor water	S1	95	Good water
w29	183.4	Poor water	S2	69.8	Good water
w30	153.2	Poor water			
w31	128.3	Poor water			
w32	163.2	Poor water			
w33	62.3	Good water			

width parameter of the RBF function (Sun & Fox 2014).

RESULTS AND DISCUSSIONS

Water Quality Index (WQI)

An assessment of water quality and the sustainability of drinking water can only be made using the Water Quality Index (WQI) (Bhimanagouda et al. 2020, Nong et al. 2020, Ponsadailakshmi et al. 2018). The Water Quality Index (WQI) is described as a technique of assessment that delivers the final impact of each water quality indicator (Adimalla 2019, Tripathi & Singal 2019).With an average of 110.16 28.55, 60 wells and two springs are evaluated for the Water Quality Index (WQI). Sixty percent of the water points have a WQI of more than 100, which indicates poor water quality. Because 88.89 percent of these boreholes had Nitrate levels over 50 $mg.L^{-1}$, it seems that high levels of nitrates influence

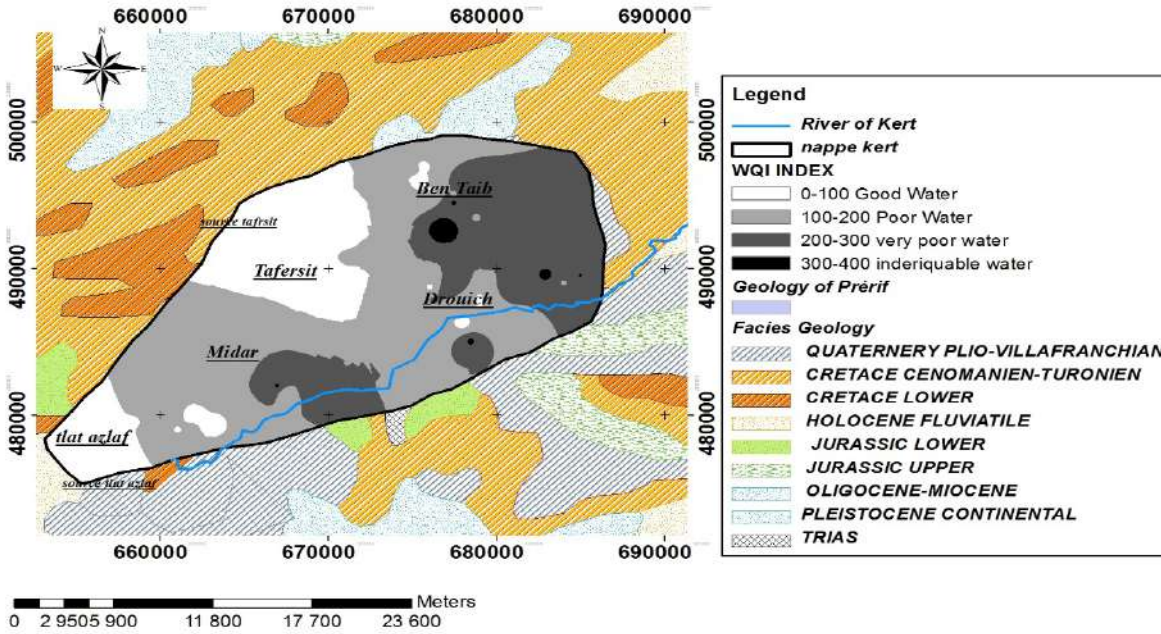

Fig. 3: Water quality classification ranges.

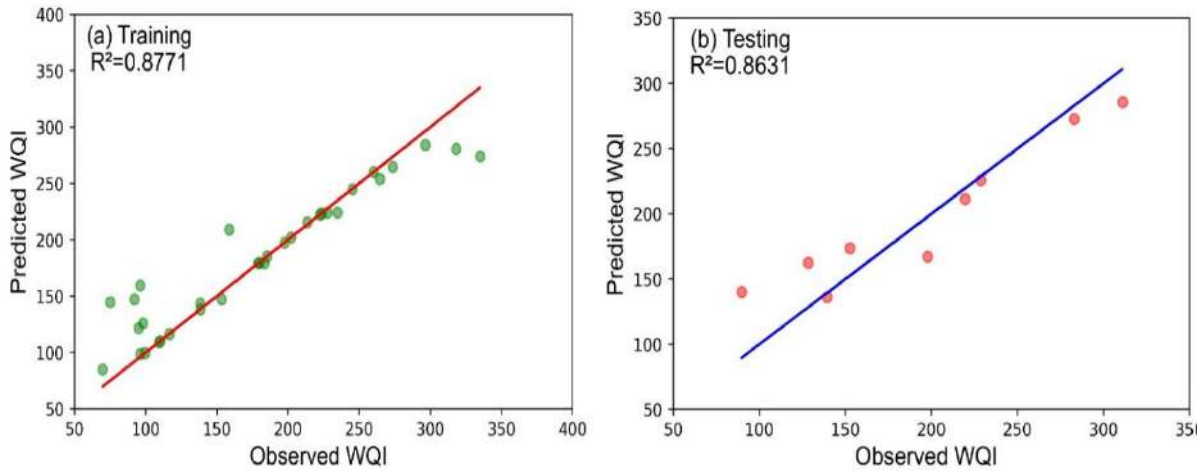

Fig. 4: Plot of prediction versus SVM-Model test data.

the WQI and the deterioration of water quality is shown in (Table.3). Fig. 3 illustrates how an examination of WQI and other metrics demonstrates that natural processes are crucial to the deteriorating water quality of the Kert Aquifer. Gypsum in rock formations may cause this phenomenon since rock salt dissolves readily in water (Gueddari et al. 2022, Liu et al. 2020, Lu et al. 2015, Zaier et al. 2021)). The elevated concentrations of EC, chloride, salt, and calcium demonstrate unequivocally that rock-water interactions are the dominant driver of water quality degradation in the studied region (Kawo & Karuppannan 2018, Mukate et al. 2019, Vaiphei et al. 2020).

All simulations were written with Python 3.8 using the sci-kit-learn library. Table 4 depicts the achieved results in

Table 4: Table predictive performances of the SVM model.

	R^2	RMSE
Training	0.8771	25.6819
Testing	0.8631	25.7497

Table 5: Correlation between variables and factors.

	pH	CE	TDS	Cl^-	Mg^{2+}	Ca^{2+}	K^+	NO_3^-	SO_4^{2-}	HCO_3^-	Na^+	WQI
pH	1.00											
CE	-0.61	1.00										
TDS	-0.55	0.89	1.00									
Cl^-	-0.56	0.95	0.82	1.00								
Mg^{2+}	-0.28	0.58	0.64	0.61	1.00							
Ca^{2+}	-0.37	0.51	0.72	0.37	0.45	1.00						
K^+	-0.19	0.14	0.24	0.05	0.17	0.25	1.00					
NO_3^-	0.11	-0.20	-0.15	-0.19	0.03	-0.14	-0.12	1.00				
SO_4^{2-}	-0.31	0.44	0.78	0.29	0.45	0.82	0.38	-0.12	1.00			
HCO_3^-	0.00	0.23	0.28	0.11	0.03	0.07	-0.14	0.14	0.18	1.00		
Na^+	-0.58	0.89	0.92	0.86	0.40	0.47	0.13	-0.18	0.57	0.31	1.00	
WQI	-0.58	0.86	0.93	0.80	0.57	0.56	0.19	-0.14	0.68	0.31	0.89	1.00

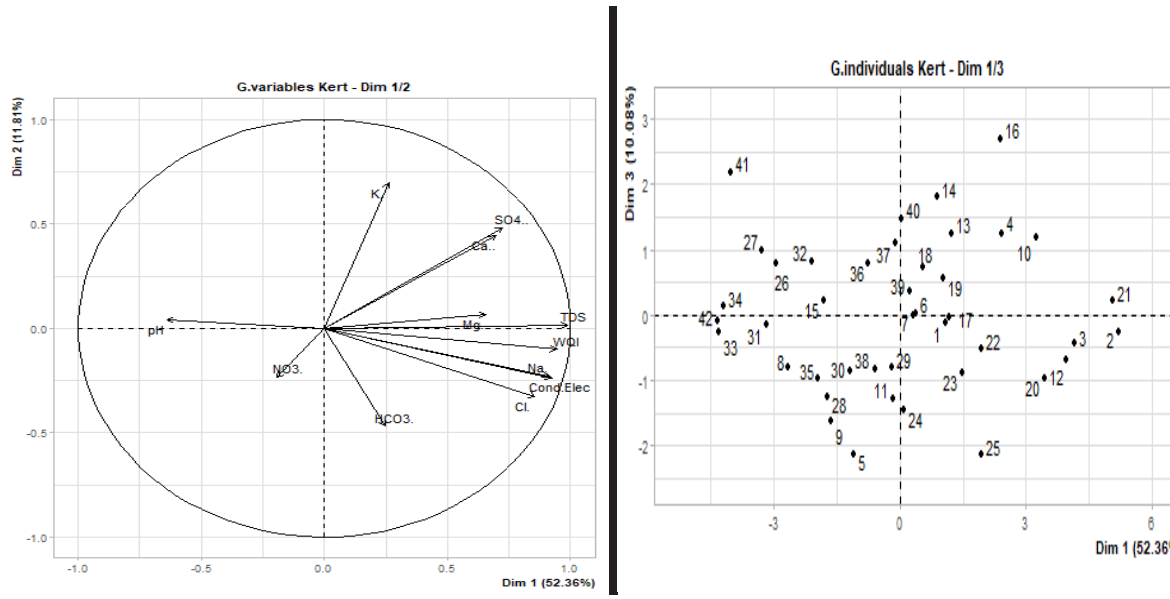

Fig. 5: Main components analysis circle.

both the training and testing stages. As this table indicates, the root means square error rose only by 0.26%, while R^2 decreased slightly by 1.6% during the testing phase. These results showed that the SVM model is stable (Table 4). Fig. 4 illustrates the SVM model's regression plots between the measured and predicted WQI values. As demonstrated by this figure, the SVM model showed a reasonable correlation between observed and estimated values with values of $R^2 = 0.8771$ and $R^2 = 0.8631$ in both the training and testing stages, correspondingly. These results reveal the SVM approach's resilience in predicting WQI.

Statistical Studies

Principal Component Analysis (PCA) is used to analyze the physicochemical data. A table of 15 variables (Ca^{2+}, Mg^{2+}, Na^+, K^+, HCO_3^-, SO_4^{2-}, Cl^-, NO_3^-, PO_4^{2-} Electrical conductivity (Cond), PH, O2d, and T) and 62 persons is used (wells and springs) (Table 5). The correlation matrix (Table 5) for the various parameters investigated revealed a strong link between Na+, SO_4^{2-}, Cl^-, and electrical conductivity. The correlation matrix, a square matrix characterized by a correlation coefficient, may determine the relationship between two variables. All water samples examined were put into a correlation matrix (Table 5).

After examining the correlation matrix, we discovered the following intriguing correlations between the variables:

- TDS (0.93) has the strongest correlation with the WQI, whereas Electric conductivity (0.86), Cl^- (0.8), Na^+ (0.89), SO_4^{2-}(0.68), and Mg^{2+} have modest correlations (0.57). CE and Cl^-(0.95) and CE and Na^+ have strong relationships (0.89). Only a little correlation exists between Calcium and WQI (0.56) and SO_4^{2-}(0.86), showing that the two are intertwined and affect the Kert alluvial aquifer's groundwater quality. The number of essential factors was calculated using the Kaiser criteria (1958). Based on these criteria, aquifer hydrogeochemistry variation can only be explained by components with eigenvalues larger than or equal to one.

A total of 64.83 percent of the variation may be attributed to the four primary kept components as shown in (Table 5). Na^+, Cl^-, WQI, CE and TDS positively influence Principal Component 1, accounting for 52.36 percent of the overall variance. Evaporitic rocks are responsible for this problem, as are residential and agricultural pollutants are shown in Fig. 5. Ca^{2+}, SO_4^{2-}, and K^+ contribute to Principal Component 2, accounting for 11.81 percent of the variation. The salinity of the water is consequently the determining element here. It results from surface salts being dissolved in water and then remineralized. Each of the four variables (components) represents one of the primary processes that explain how to understand how the Kert aquifer acquired and evolved its chemist; it is necessary to look at four variables (components): water-rock interaction, agricultural pollution, and the aquifer itself. As a result of these interactions between water and rock and pollution from home and industrial agriculture, the four variables (or components) reflect the primary processes that explain how the chemist of the Kert aquifer came to be. There are three families of water quality founded on the projection of persons shown in Fig. 5, the first and second of which are situated in the south and eastern regions of the research area, respectively. The third family characterizes Salinity-polluted environments.

CONCLUSIONS

Aquifer lithology and recharge areas, which favor geological dissolution, are connected to groundwater chemistry, associated with the Triassic marl-sulfate formations and the Quaternary evaporate formations. On the other hand, the Kert aquifer's groundwater is of low quality. According to a principal component analysis (PCA) chemical factors, such as sodium, calcium, magnesium, sulfates, and chlorides, have the most significant effect on the quality of Kert's quaternary water table. The Water Quality Index (WQI) reveals that 79% of the drillings had WQI values over 100. As salt levels rise, the Oust of Kert is particularly susceptible since it contains more than the WHO's recommended amount of salinity. Soil treatment is needed in light of this condition and conservative water management measures, such as establishing a strict residential discharge monitoring system.

REFERENCES

Abbasnia, A., Yousefi, N., Mahvi, A. H., Nabizadeh, R., Radfard, M., Yousefi, M. and Alimohammadi, M. 2019. Evaluation of groundwater quality using water quality index and its suitability for assessing water for drinking and irrigation purposes: A case study of Sistan and Baluchistan province (Iran). Human Ecol. Risk Assess. Int. J., 25(4): 988-1005.

Adimalla, N. 2019. Controlling factors and mechanism of groundwater quality variation in the semiarid region of South India: an approach of water quality index (WQI) and health risk assessment (HRA). Environ. Geochem. Health, 5: 1-28.

Akhtar, N., Ishak, M. I. S., Ahmad, M. I., Umar, K., Md Yusuff, M. S., Anees, M.T., Qadir, A. and Ali Almanasir, Y. K. 2021. Modification of the water quality index (WQI) Process for simple calculation using the multi-criteria decision-making (MCDM) method: A Review. Water, 13(7): 905.

Azdimousa, A. 2007. Lithostratigraphy and structure of the Temsamane Unit (Eastern External Rif, Morocco). Rev. Soc. Geol. España, 20(3): 187-200.

Azizullah, A., Khattak, M. N. K., Richter, P. and Häder, D.-P. 2011. Water pollution in Pakistan and its impact on public health; A review. Environ. Int., 37(2): 479-497.

Banda, T.D. and Kumarasamy, M.A. 2020. Review of the existing water quality indices (WQIs). J. Phys. Opt, 2: 1-19.

Bennett, K. and Demiriz, A. 1999. Semi-supervised support vector machines. Adv. Neural Inform. Process. Syst., 11: 368-374.

Bhargava, D.S. 1983. Use of water quality index for river classification and zoning of Ganga River. Environ. Pollut. Ser. B Chem Phys., 6(1): 51-67.

Bhimanagouda, B.P.V., Pinto, S.M., Thejashree, G., Shivakumar, H.V., Vignesh, B. and Nanjappa, K.L. 2020. Multivariate statistics and water quality index (WQI) approach for geochemical assessment of groundwater quality: A case study of Kanavi Halla Sub-Basin, Belagavi, India. Environ. Geochem. Health, 42(9: 2667-2684.

Brilli, R.J., McClead Jr, R.E., Crandall, W.V., Stoverock, L., Berry, J.C., Wheeler, T.A. and Davis, J.T. 2013. A comprehensive patient safety program can significantly reduce preventable harm, associated costs, and hospital mortality. J. Pediat., 163(6): 1638-1645.

Butler, D. 2017. Global challenges. Water, 1(1): 61.

Carlier, P. 1973. The hydrogeological map at 1:50,000 of the Moyen-Kerte plain: Province of Nador, north-eastern Morocco. Ed. Geol. Ser., 16: 1058.

de Andrade Costa, D., de Azevedo, J.P.S., Dos Santos, M.A. and Assumpção, R.S.F.V. 2020. Water quality assessment based on multivariate statistics and water quality index of a strategic river in the Brazilian Atlantic Forest. Sci. Rep., 10(1): 1-13.

Deshpande, A., Yadav, J., and Kharat, V. 2014. Zadeh-Deshpande's approach for the fuzzy description of air and water quality. BVICAM's Int. J. Inform. Technol., 6(1): 484.

Eden, C. and Ackermann, F. 2001. SODA: The principles. Ration. Anal. Prob. World Rev., 9: 21-41.

WHO Edition. 2011. Guidelines for drinking-water quality. WHO Chron., 38(4): 104-108.

Elgettafi, M., Elmandour, A., Himi, M. and Casas, A. 2013. The use of environmental markers to identify groundwater salinization sources in a Neogene basin, Kert aquifer case, NE Morocco. Int. J. Environ. Sci. Technol.,10(4): 719-728.

Evgeniou, T., Poggio, T., Pontil, M. and Verri, A. 2002. Regularization and statistical learning theory for data analysis. Comput Stat. Data Anal., 38(4): 421-432.

Hicham, G, Mustapha, A., Mourad, B., Abdelmajid, M., Ali, S., Yassine, E. Y., Mohamed, C., Ghizlane, A. and Zahid, M. 2021. Assessment of the physico-chemical and bacteriological quality of groundwater in the Kert Plain, northeastern Morocco. Int. J. Energy Water Resour., 7: 1-15.

Hicham, G., Mustapha, A., Mourad, B., Abdelmajid, M., Ali, S., Yassine, E. Y., Hanane, A. H., Mohamed, C., Ghizlane, A. andAbderahmane, R. 2021. Assessment of the metal contamination index in groundwater of the quaternary of the Middle Kert Basin, north□eastern Morocco. Environ. Qual. Manag., 1: 26-34.

Kachroud, M., Trolard, F., Kefi, M., Jebari, S. and Bourrié, G. 2019. Water quality indices: Challenges and application limits in the literature. Water, 11(2): 361.

Kaiser, H.F. 1958. The varimax criterion for analytic rotation in factor analysis. Psychometrika, 23(3): 187-200.

Karunanidhi, D., Aravinthasamy, P., Subramani, T. and Muthusankar, G. 2021. Revealing drinking water quality issues and possible health risks based on the water quality index (WQI) method in the Shanmuganadhi River basin of South India. Environ. Geochem. Health, 43(2): 931-948.

Kavousi-Fard, A. and Kavousi-Fard, F. 2013. A new hybrid correction method for short-term load forecasting based on ARIMA, SVR, and CSA. J. Environ. Exp. Theoret. Artif. Intell., 25(4): 559-574.

Kawo, N.S. and Karuppannan, S. 2018. Groundwater quality assessment using water quality index and GIS technique in Modjo River Basin, Central Ethiopia. J. Afr. Earth Sci., 14: 300-311.

Kumari, R. and Sharma, R.C. 2019. Assessment of water quality index and multivariate analysis of high altitude sacred Lake Prashar, Himachal Pradesh, India. Int. J. Environ. Sci. Technol., 16(10): 6125-6134.

Liu, W., Zhang, X., Fan, J., Zuo, J., Zhang, Z. and Chen, J. 2020. Study on the mechanical properties of man-made salt rock samples with impurities. J. Nat. Gas Sci. Eng., 84: 103683.

Lu, Y., Song, S., Wang, R., Liu, Z., Meng, J., Sweetman, A. J., Jenkins, A., Ferrier, R.C., Li, H. and Luo, W. 2015. Impacts of soil and water pollution on food safety and health risks in China. Environ. Int., 77: 5-15.

Malekzadeh, M., Kardar, S. and Shabanlou, S. 2019. Groundwater for Sustainable Development Simulation of groundwater level using MODFLOW, extreme learning machine, and Wavelet-Extreme Learning Machine models. Groundwater Sustain. Dev., 9: 100279. https://doi.org/10.1016/j.gsd.2019.100279

Mohammadi, B. and Mehdizadeh, S. 2020. Modeling daily reference evapotranspiration via a novel approach based on support vector regression coupled with the whale optimization algorithm. Agric. Water Manag., 237: 106145.

Mukate, S., Wagh, V., Panaskar, D., Jacobs, J.A. and Sawant, A. 2019. Development of a new integrated water quality index (IWQI) model to evaluate the drinking suitability of water. Ecol. Indic., 101: 348-354.

Nong, X., Shao, D., Zhong, H. and Liang, J. 2020. Evaluation of water quality in the South-to-North Water Diversion Project of China using the water quality index (WQI) method. Water Res., 178: 115781.

Ponsadailakshmi, S., Sankari, S.G., Prasanna, S.M. and Madhurambal, G. 2018. Evaluation of water quality suitability for drinking using drinking water quality index in Nagapattinam district, Tamil Nadu in Southern India. Groundwater Sustain. Dev., 6: 43-49.

Rawat, K.S. andSingh, S.K. 2018. Water Quality Indices and GIS-based evaluation of decadal groundwater quality. Geol. Ecol. Landsc., 2(4): 240-255.

Rodier, J., Bernard, K. and Legube, N.M. 2009. Water Analysis. Ninth Edition. Dunod, UNOD (publisher), Paris, Fr. (p. 1600).

Schweitzer, L. and Noblet, J. 2018. Water Contamination and Pollution. Elsevier, The Netherlands. https://doi.org/https://doi.org/10.1016/B978-0-12-809270-5.00011-X

Selvam, S., Manimaran, G., Sivasubramanian, P., Balasubramanian, N. and Seshunarayana, T. 2014. GIS-based evaluation of water quality index of groundwater resources around Tuticorin coastal city, South India. Environ. Earth Sci., 71(6): 2847-2867.

Singh, A.P., Dhadse, K. and Ahalawat, J. 2019. Managing the water quality of a river using an integrated geographically weighted regression technique with a fuzzy decision-making model. Environ. Monit. Assess., 191(6): 1-17.

Sun, Z. and Fox, G. 2014. Traffic flow forecasting is based on the combination of multidimensional scaling and SVM. Int. J. Intell. Transport. Syst. Res., 12(1): 20-25.

Toolabi, A., Bonyadi, Z., Paydar, M., Asghar, A. and Ramavandi, B. 2021. Groundwater for Sustainable Development Spatial distribution, occurrence, and health risk assessment of nitrate, fluoride, and arsenic in Bam groundwater resource, Iran. Groundwater Sustain. Dev., 12: 100543. https://doi.org/10.1016/j.gsd.2020.100543

Tripathi, M. and Singal, S.K. 2019. Use of principal component analysis for parameter selection for development of a novel water quality index: A case study of river Ganga India. Ecol. Indic., 96: 430-436.

Tziritis, E., Panagopoulos, A. and Arampatzis, G. 2014. Development of an operational index of water quality (PoS) as a versatile tool to assist groundwater resources management and strategic planning. J. Hyrdol., 517: 339-350.

Üstün, B., Melssen, W.J. and Buydens, L.M. C. 2007. Visualisation and interpretation of support vector regression models. Anal. Chim. Acta, 595(1-2): 299-309.

Vaiphei, S.P., Kurakalva, R.M. andSahadevan, D.K. 2020. Water quality index and GIS-based technique for assessment of groundwater quality in Wanaparthy watershed, Telangana, India. Environ. Sci. Pollut. Res., 27(36): 45041-45062.

Vesali Naseh, M.R., Noori, R., Berndtsson, R., Adamowski, J. and Sadatipour, E. 2018. Groundwater pollution sources apportionment in the Ghana Plain, Iran. Int. J. Environmental Res. Pub. Health, 15(1): 172.

Von Zur Gathen, J. and Gerhard, J. 2013. Modern Computer Algebra. Cambridge University Press, Cambridge.

Xu, Y., Zomer, S. and Brereton, R. G. 2006. Support vector machines: a recent method for classification in chemometrics. Critic. Rev. Anal. Chem., 36(3-4): 177-188.

Zaier, I., Billiotte, J., Charmoille, A. and Laouafa, F. 2021. The dissolution kinetics of natural gypsum: A case study of Eocene facies in the north-eastern suburbs of Paris. Environ. Earth Sci., 80(1): 1-16.

Zielhofer, C., Faust, D. and Linstädter, J. 2008. Late Pleistocene and Holocene alluvial archives in the Southwestern Mediterranean: Changes in fluvial dynamics and past human response. Quat. Int., 181(1): 39-54.

Nature Environment and Pollution Technology
An International Quarterly Scientific Journal

p-ISSN: 0972-6268
(Print copies up to 2016)
e-ISSN: 2395-3454

Vol. 21 | No. 5 (Suppl) | pp. 2025-2034 | 2022

Original Research Paper

https://doi.org/10.46488/NEPT.2022.v21i05.002

Open Access Journal

Evaluation of Coliform and Faecal Coliform Bacteria in the Lakes of Broknes and Grovnes Peninsula, East Antarctica

L. K. Bhardwaj† and T. Jindal

Amity Institute of Environmental Toxicology, Safety and Management (AIETSM), Sector-125, Amity University, Noida, Uttar Pradesh-201303, India

†Corrsponding author: Laxmi Kant Bhardwaj; bhardwaj.laxmikant@gmail.com

Nat. Env. & Poll. Tech.
Website: www.neptjournal.com

Received: 18-02-2022
Revised: 11-05-2022
Accepted: 22-05-2022

Key Words:
East Antarctica
Larsemann hills
Coliforms
Faecal coliforms
Broknes and Grovnes peninsula
Lake water

ABSTRACT

More than 150 lakes on different peninsulas and islands are situated in the Larsemann Hills. The Larsemann Hills is an ice-free area and are located halfway between the Vestfold Hills and the Amery Ice Shelf on the southeastern coast of Prydz Bay, Princess Elizabeth Land, and East Antarctica. During 34th Indian Scientific Expedition to Antarctica (ISEA) from 2014 to 2015, twenty lake water samples in triplicates were collected from the Broknes & Grovnes peninsula. Coliform and fecal coliform bacteria were analyzed in these samples. Out of twenty, eleven lake water samples were found to be contaminated with coliform bacteria. However, fecal coliform bacteria were absent in all the lake water samples. Coliforms are found in the lakes of Broknes peninsula (P2 Lake & P3 Lake) and Grovnes peninsula (L1C NG, L1D NG, L1E NG, L7 NG, L7A NG, L7B NG, L2 SG, L4 SG & L5 SG). Antarctic lakes water is being polluted due to anthropogenic activities caused by various research activities and tourism. The present study confirms the presence of coliform bacteria in the lakes of East Antarctica which indicates an alarming situation and needs to be investigated further.

INTRODUCTION

Antarctica is the world's most remote and unspoiled continent (Bhardwaj & Pawan 2022). It is the largest pristine wilderness in the world. Lenihan (1992) & Bhardwaj et al. (2021) stated that it is a continent with a pristine environment. Approx. 53 research stations are now located in Antarctica. The population in winter and summer is around 1000 to 4000 people respectively. It is increasing over time due to more researchers taking an interest in research on Antarctica. Antarctic lakes are polluted by sewage waste released from research stations and commercial fishing vessels. Sewage waste which contains food waste and human waste is discharged untreated from research stations to Antarctica and affects its environment. Some local wildlife populations such as seals and sea birds are also releasing their fecal waste in Antarctica. Lenihan et al. (1990) stated that human sewage can be the dominant source of fecal microorganisms in Antarctica and have a significant impact on its environment.

ORCID details of the authors:

L. K. Bhardwaj:
https://orcid.org/0000-0001-7518-4199

Waterhouse (2001) studied the presence of coliforms and fecal coliforms bacteria in Antarctic water and stated that it is due to the activities of the local vertebrates and human populations. These bacteria are nonpathogenic, but their presence indicates the possibility of finding pathogens (Harmon et al. 2014). Mishra et al. (2018) stated that coliforms can be divided into total coliforms and fecal coliforms. Fecal coliform bacteria such as *Escherichia coli* (*E. coli*) are found in feces and their presence in drinking water indicates fecal contamination (Bhardwaj & Sharma 2021). *E. coli* can also be a pathogen itself, so if *E. coli* is found in the water then there is a chance that other pathogens will be present. Fecal coliform is a rod-shaped, gram-negative, non-sporulating, and facultative anaerobic bacterium. It generally originated in the intestine of warm-blooded animals. Coliforms are commonly used microbiological markers of sewage pollution in Antarctica (Hill et al. 1996, Hughes & Blenkharn 2003, Khan & Gupta 2020). Cowan et al. (2011) stated that some strains of coliform bacteria which were found in Antarctica are not indigenous to Antarctica and are transported by anthropogenic activities. Green et al. (1992) studied the different sewage indicators from sewage around Antarctic research stations.

Several researchers studied the different physical factors such as solar radiation, temperature, and ice condition which

affect the survival and distribution of fecal coliform bacteria in Antarctica (Patrick & Bernard 1991, Šolić & Krstulović 1992, Smith et al. 1994). The high level of Ultra-Violet (UV) radiation is also responsible to reduce the viability of sewage microorganisms in Antarctic water and air (Statham & McMeekin 1994, Sinton 1994). The survival rate of fecal bacteria can vary from a few minutes to many days and depends upon the environmental conditions (Statham & McMeekin 1994). Sewage microorganisms can remain viable for prolonged periods in the Antarctic environment while the terrestrial environment is potentially less hospitable due to desiccation stress and wide diurnal temperature ranges (Smith et al. 1994, Upton et al. 1997). Sewage microbes have the potential to infect people and become part of the gut of local wildlife populations in Antarctica (Gardner et al. 1997, Edwards et al. 1998).

In Antarctica, the number of fecal coliform bacteria was found high in early winter due to increased fecal input by migrant wildlife and low doses of solar radiation, while in summer, despite the high population on the research station, the number of fecal coliform bacteria was found low due to the biologically damaging effects from the radiation of solar. According to several scientists after the first human expedition to Antarctica, the disposal of fecal waste has generally been into the sea and either buried in snow or discharged into the Antarctic lakes (McFeters et al. 1993, Parker & Martel 2002, Hughes & Blenkharn 2003, Hughes 2003). Parker & Martel (2002) stated that once the fecal waste is buried in the snow, it remained the same for a long time due to low temperature, it undergoes relatively little degradation and could become a long-term pollution problem in the future in Antarctica. The purpose of this study was to determine the occurrence of coliform and fecal coliform bacteria in the lake water samples of Broknes and Grovnes peninsula of Larsemann Hills, East Antarctica.

MATERIALS AND METHODS

Study Area: Broknes & Grovnes peninsula of Larsemann Hills, East Antarctica was selected as a study area. The location map of the study area is shown in Fig. 1.

Sampling Sites and Collection: The sampling of the lake water samples was carried out in the month of Dec-Feb of 2014-2015. A total of 15 samples were collected randomly from P1 Lake, P2 Lake, P3 Lake, P4 Lake, and Reid Lake from the Broknes peninsula. While 45 samples were collected from L1C NG, L1D NG, L1E NG, L3 NG, L5 NG, L6 NG, L7 NG, L7A NG, L7B NG, Murk Water Lake NG, L1 SG, L2 SG, L3 SG, L4 SG, L5 SG from Grovnes peninsula. Thirty samples from Northern Grovnes and fifteen samples from the Southern Grovnes peninsula were collected respectively. Before taking samples from each site, dark amber color sterile polyethylene (PET) bottles were rinsed twice with the lake water. Three replicates of each sample (1 L) were collected from easily accessible inner areas of each lake. All samples were immediately stored in an ice chest with ice at 4^{o}C and transported to the laboratory after completion of the expedition for fecal coliform and coliform analysis. The sampling sites are shown in Fig. 2, 3 and 4, and Tables 1 and 2.

Requirements (Equipment and Culture Media): Autoclave (Laczene Biosciences Solutions), laminar airflow

Fig. 1: Location map of the study area in Larsemann Hill (downside), Prydz Bay in East Antarctica marked on the continental map of Antarctica (upper side).

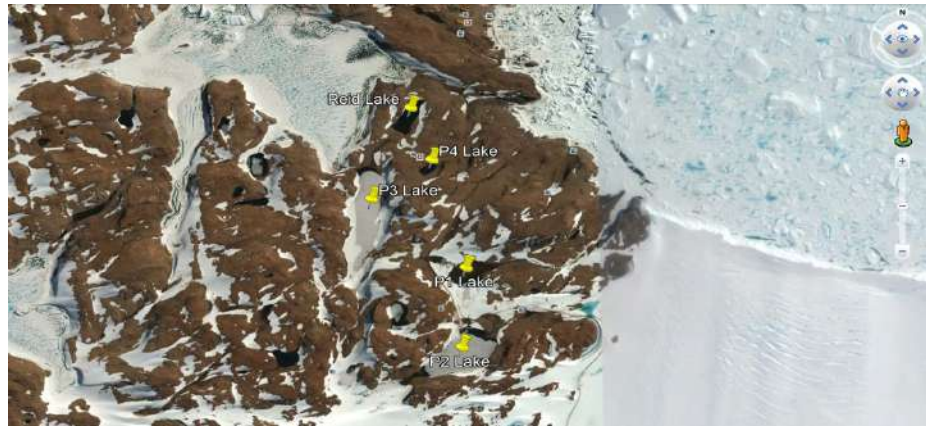

Fig. 2: location of sampling sites mark with pinpoints on Broknes Peninsula, East Antarctica.

Fig. 3: Location of sampling sites mark with pinpoints on Northern Grovnes Peninsula, East Antarctica.

Fig. 4: Location of sampling sites mark with pinpoints on Southern Grovnes Peninsula, East Antarctica.

Table 1: Sample details with geographic coordinates, date of sampling, sample quantity, and name of the lakes at Broknes Peninsula, East Antarctica.

S. No.	Sample ID (Lake Name)	Latitude	Longitude	Replicates	Date of Sampling	Sample Quantity
1	P1 Lake	69°23'49.54" S	76°23'17.43" E	P1-1	17-02-2015	1 L
				P1-2	17-02-2015	
				P1-3	17-02-2015	
2	P2 Lake	69°24'09.005" S	76°23'15.00" E	P2-1	18-02-2015	1 L
				P2-2	18-02-2015	
				P2-3	18-02-2015	
3	P3 Lake	69°23'32.17" S	76°22'17.78" E	P3-1	19-02-2015	1 L
				P3-2	19-02-2015	
				P3-3	19-02-2015	
4	P4 Lake	69°23'22.19" S	76°22'55.82" E	P4-1	20-02-2015	1 L
				P4-2	20-02-2015	
				P4-3	20-02-2015	
5	Reid Lake	69°23'8.83" S	76°22'42.06" E	Reid Lake-1	21-02-2015	1 L
				Reid Lake-2	21-02-2015	
				Reid Lake-3	21-02-2015	

Table 2: Sample details with geographic coordinates, date of sampling, sample quantity, and name of the lakes at Northern and Southern Grovnes Peninsula, East Antarctica.

S. No.	Sample ID (Lake Name)	Latitude	Longitude	Replicates	Date of Sampling	Sample Quantity
1	L1C NG	69°24'25.43" S	76°11'17.66" E	L1C NG-1	25-12-2014	1 L
				L1C NG-2	25-12-2014	
				L1C NG-3	25-12-2014	
2	L1D NG	69°24'22.41" S	76°11'22.26" E	L1D NG-1	25-12-2014	1 L
				L1D NG-2	25-12-2014	
				L1D NG-3	25-12-2014	
3	L1E NG	69°24'23.51" S	76°11'25.20" E	L1E NG-1	26-12-2014	1 L
				L1E NG-2	26-12-2014	
				L1E NG-3	26-12-2014	
4	L3 NG	69°24'27.72" S	76°11'2.70" E	L3 NG-1	26-12-2014	1 L
				L3 NG-2	26-12-2014	
				L3 NG-3	26-12-2014	
5	L5 NG	69°24'32.83" S	76°10'45.75" E	L5 NG-1	27-12-2014	1 L
				L5 NG-2	27-12-2014	
				L5 NG-3	27-12-2014	
6	L6 NG	69°24'37.30" S	76°11'5.13" E	L6 NG-1	27-12-2014	1 L
				L6 NG-2	27-12-2014	
				L6 NG-3	27-12-2014	
7	L7 NG	69°24'34.32" S	76°11'39.41" E	L7 NG-1	28-12-2014	1 L
				L7 NG-2	28-12-2014	
				L7 NG-3	28-12-2014	

S. No.	Sample ID (Lake Name)	Latitude	Longitude	Replicates	Date of Sampling	Sample Quantity
8	L7A NG	69°24'32.78" S	76°11'57.96" E	L7A NG-1	28-12-2014	1 L
				L7A NG-2	28-12-2014	
				L7A NG-3	28-12-2014	
9	L7B NG	69°24'30.05" S	76°11'57.38" E	L7B NG-1	29-12-2014	1 L
				L7B NG-2	29-12-2014	
				L7B NG-3	29-12-2014	
10	Murk Water Lake NG	69°24'53.37" S	76°12'46.16" E	Murk Water Lake NG-1	30-12-2014	1 L
				Murk Water Lake NG-2	30-12-2014	
				Murk Water Lake NG-3	30-12-2014	
11	L1 SG	69°25'13.70" S	76°13'18.33" E	L1 SG-1	02-01-2015	1 L
				L1 SG-2	02-01-2015	
				L1 SG-3	02-01-2015	
12	L2 SG	69°25' 5.10" S	76°12'45.05" E	L2 SG-1	02-01-2015	1 L
				L2 SG-2	02-01-2015	
				L2 SG-3	02-01-2015	
13	L3 SG	69°25'09.07" S	76°12'36.1" E	L3 SG-1	03-01-2015	1 L
				L3 SG-2	03-01-2015	
				L3 SG-3	03-01-2015	
14	L4 SG	69°25'04.46" S	76°12'19.93" E	L4 SG-1	03-01-2015	1 L
				L4 SG-2	03-01-2015	
				L4 SG-3	03-01-2015	
15	L5 SG	69°25'08.65" S	76°11'53.9" E	L5 SG-1	04-01-2015	1 L
				L5 SG-2	04-01-2015	
				L5 SG-3	04-01-2015	

(Laczene Biosciences Solutions), weighing balance (0.01 mg to 220 g, Sartorius), micropipettes, test tubes, Petri discs, inoculation loop, conical flask, Durham's tubes, and spirit lamp were used. MacConkey broth (MCB, M007) Brilliant Green Bile Lactose (BGBL, M121S), Eosin Methylene Blue (EMB, M317) media were procured from HiMedia Laboratories Pvt. Ltd.

Enumeration of Coliform and Faecal Coliform Bacteria: The most probable number (MPN) of coliform and fecal coliform (coliform/100 mL) in lake water samples was determined as per the Indian Standard (IS):1622 (1981). The enumeration was carried out in triplicate and included three phases.

Presumptive Test: Three sets of test tubes were taken for every sample and each set contained five test tubes. 10 mL of double-strength MacConkey broth (MB) was inoculated in each tube of the first set. On the other hand, for the second and third sets of test tubes, 10 mL of single-strength MB was inoculated in each tube. Durham's tube (small tube) was placed inside each tube in an inverted position. Homogenized lake water samples (10 mL, 1 mL & 0.1 mL) were inoculated in the first, second, and third sets of test tubes respectively. All tubes were incubated at 37 ± 1°C for 24-48 h (at 44.5°C for 24 h for fecal coliform). After incubation, the observation was recorded for the gas production (i.e. bubble formation) in Durham's tube. If bubbles were present, then consider that tube positive. If no gas was observed in any test tube, then discontinue the test and record the result as less than 2 organisms/100 mL. This test is shown in Fig. 5.

Confirmative Test: Three sets of test tubes were taken for each positive tube and each set contained five tubes. 10 mL Brilliant Green Bile Lactose (BGBL) broth was inoculated in each test tube. Durham's tube was placed inside each tube in an inverted position. A loopful inoculum from each positive tube was inoculated into three sets of tubes. All tubes were Incubated at 37 ± 1°C for 24-48 h. After incubation, the observation was recorded for gas production in Durham's

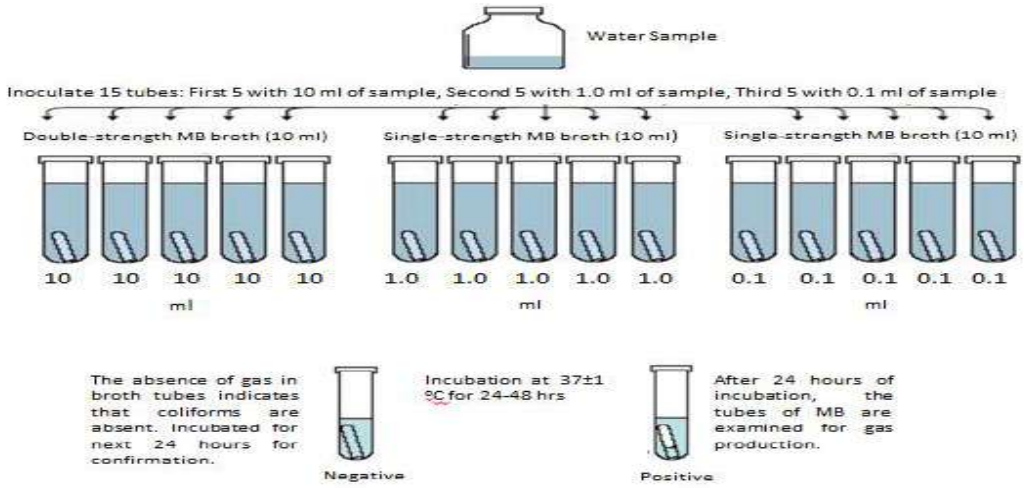

Fig. 5: Presumptive test.

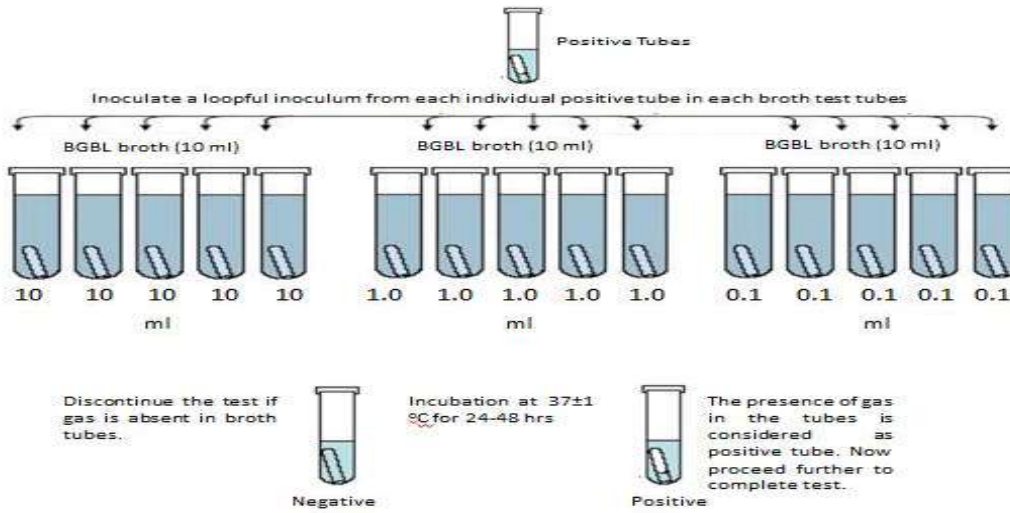

Fig. 6: Confirmative test.

tube. The presence of gas in the tubes was considered a positive tube and record the number of these positive tubes then further proceed to the completed test. In case gas production is not observed in any of the tubes, discontinue the test and record the result as less than 2 organisms/100 mL. This test is shown in Fig. 6.

Completed Test: Eosin Methylene Blue (EMB) media were prepared according to the positive tubes of the confirmative test and then poured into the Petri discs. Three Petri discs were taken for each positive tube. A loopful inoculum from each positive tube was streaked on EMB media plates and these plates were incubated at 37°C for 24 h in an inverted position. The presence of green metallic sheen colonies confirmed the presence of E. Coli. These isolates were further confirmed by Gram's staining for E. Coli as per IS:5887 (1976). This test is shown in Fig. 7.

Quality Assurance/Quality Control (QA/QC): Each sample was analyzed in triplicate. All dilutions and media were prepared in double-distilled water. Based on the number of positive tubes as recorded in a confirmed test calculate the probable number of coliform and fecal coliform/100 mL of lake water sample by using the MPN table. MPN of the organism present per 100 mL of sample is shown in Table 3.

RESULTS

An Occurrence of Coliform and Faecal Coliform Bacteria in the Broknes Peninsula, East Antarctica: No growth was

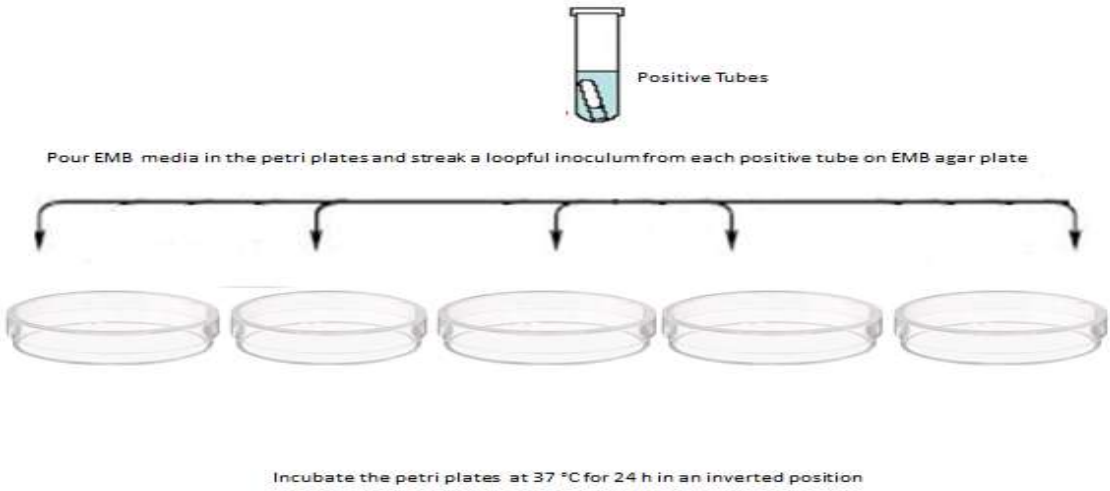

Fig. 7: Completed test.

Table 3: MPN of organism present per 100 mL of sample and confidence limits using 5 tubes of 10 mL, 5 tubes of 1 mL, and 5 tubes of 0.1 mL.

S. No.	Combination of Positive Tubes	MPN Index per 100 mL	95 % Confidence Limits	
			Lower	Upper
1	0-0-0	<2	-	-
2	0-0-1	2	1.0	10
3	0-1-0	2	1.0	10
4	0-2-0	4	1.0	13
5	1-0-0	2	1.0	11
6	1-0-1	4	1.0	15
7	1-1-0	4	1.0	15
8	1-1-1	6	2.0	18
9	1-2-0	6	2.0	18
10	2-0-0	4	1.0	17
11	2-0-1	7	2.0	20
12	2-1-0	7	2.0	21
13	2-1-1	9	3.0	24
14	2-2-0	9	3.0	25
15	2-3-0	12	5.0	29
16	3-0-0	8	3.0	24
17	3-0-1	11	4.0	29
18	3-1-0	11	4.0	29
19	3-1-1	14	6.0	35
20	3-2-0	14	6.0	35
21	3-2-1	17	7.0	40
22	4-0-0	13	5.0	38
23	4-0-1	17	7.0	45
24	4-1-0	17	7.0	46
25	4-1-1	21	9.0	55
26	4-1-2	26	12	63
27	4-2-0	22	9.0	56
28	4-2-1	26	12	65
29	4-3-0	27	12	67
30	4-3-1	33	15	77
31	4-4-0	34	16	80
32	5-0-0	23	9.0	86
33	5-0-1	30	10	110
34	5-0-2	40	20	140
35	5-1-0	30	10	120
36	5-1-1	50	20	150
37	5-1-2	60	30	180
38	5-2-0	50	20	170
39	5-2-1	70	30	210
40	5-2-2	90	40	250
41	5-3-0	80	30	250
42	5-3-1	110	40	300
43	5-3-2	140	60	360
44	5-3-3	170	80	410
45	5-4-0	130	50	390
46	5-4-1	170	70	480
47	5-4-2	220	100	580
48	5-4-3	280	120	690
49	5-4-4	350	160	820
50	5-5-0	240	100	940
51	5-5-1	300	100	1300
52	5-5-2	500	200	2000
53	5-5-3	900	300	2900
54	5-5-4	1600	600	5300
55	5-5-5	□1600	-	-

observed of fecal coliform in all different lake water samples while coliform was present in P2 Lake and P3 Lake. No growth was observed of coliform in P1 Lake, P4 Lake, and Reid Lake. Maximum MPN coliform was found in P2 Lake followed by P3 Lake. An observation of MPN coliform and fecal coliform/100 mL in different lake water samples of Broknes peninsula is shown in Table 4.

An Occurrence of Coliform and Faecal Coliform Bacteria in the Grovnes Peninsula, East Antarctica: No growth was observed of fecal coliform in all different lake water samples while coliform was present in L1C NG, L1D NG, L1E NG, L7 NG, L7A NG, L7B NG, L2 SG, L4 SG, and L5 SG. No growth was observed of coliform in L3 NG, L5 NG, L6 NG, Murk Water Lake NG, L1 SG, and L3 SG. Maximum MPN coliform was found in LIENG followed by L7A NG, L4 SG, L7B NG, L1D NG, L1C NG, L2 SG, and L7 NG. An observation of MPN coliform and fecal coliform/100 mL in different lake water samples of the Grovnes peninsula is given in Tables 5 and 6.

DISCUSSION

In the present study, we assessed the environmental impact of the different sewage markers such as coliform and fecal coliform bacteria. Antarctica is the hub of freshwater lakes (Bhardwaj et al. 2019, Bhardwaj & Jindal 2020). Now, these lakes have been contaminated through anthropogenic activities and wildlife populations, such as seals and penguins. The release of sewage waste in Antarctica can produce microbiological pollution in the lake water. Fecal coliform is a more suitable bacteria for the investigation of the anthropogenic impact on the Antarctic environment. Edwards et al. (1998) & Hughes (2003) studied that some strains of fecal coliforms, such as fecal enterococci and spore-forming bacillus can survive in Antarctica for 30-40 years. Fujioka et al. (1981) and Kapuscinski & Mitchell (1981) have described

Table 4: An occurrence of coliform and faecal coliform bacteria in the lake water samples of Broknes Peninsula, East Antarctica.

S. No.	Sample ID/Lake Name	Altitude [mt]	MPN Coliform/100 mL	MPN Faecal Coliform/100 mL
1	P1 Lake	54	No Growth Observed (<2)	No Growth Observed (<2)
2	P2 Lake	3	40 organisms	No Growth Observed (<2)
3	P3 Lake	24	23 organisms	No Growth Observed (<2)
4	P4 Lake	29	No Growth Observed (<2)	No Growth Observed (<2)
5	Reid Lake	54	No Growth Observed (<2)	No Growth Observed (<2)

Table 5: An occurrence of coliform and faecal coliform bacteria in the lake water samples of Northern Grovnes Peninsula, East Antarctica.

S. No.	Sample ID/Lake Name	Altitude [mt]	MPN Coliform/100 mL	MPN Faecal Coliform/100 mL
1	L1C NG	24	26 organisms	No Growth Observed (<2)
2	L1D NG	22	27 organisms	No Growth Observed (<2)
3	L1E NG	25	60 organisms	No Growth Observed (<2)
4	L3 NG	39	No Growth Observed (<2)	No Growth Observed (<2)
5	L5 NG	30	No Growth Observed (<2)	No Growth Observed (<2)
6	L6 NG	91	No Growth Observed (<2)	No Growth Observed (<2)
7	L7 NG	53	17 organisms	No Growth Observed (<2)
8	L7A NG	51	42 organisms	No Growth Observed (<2)
9	L7B NG	40	32 organisms	No Growth Observed (<2)
10	Murk Water Lake NG	5	No Growth Observed (<2)	No Growth Observed (<2)

Table 6: An Occurrence of coliform and faecal coliform bacteria in the lake water samples of Southern Grovnes Peninsula, East Antarctica.

S. No.	Sample ID	Altitude (mt)	MPN Coliform/100 mL	MPN Faecal Coliform/100 mL
1	L1 SG	8	No Growth Observed (<2)	No Growth Observed (<2)
2	L2 SG	3	21 organisms	No Growth Observed (<2)
3	L3 SG	24	No Growth Observed (<2)	No Growth Observed (<2)
4	L4 SG	28	34 organisms	No Growth Observed (<2)
5	L5 SG	25	11 organisms	No Growth Observed (<2)

the effect of sunlight on E. Coli. Statham & McMeekin (1994) studied the effect of solar radiation on the survival of E. Coli at Davis Research Station, Antarctica, and stated that fecal bacteria were rapidly inactivated when exposed to sunlight in the Antarctic water.

Several scientists have reported the presence of coliform and fecal coliform in the sewage outfall of the Antarctic research stations (Delille 1987, Green et al. 1992, Edwards et al. 1998). Coliforms are less able to survive in Antarctic environmental conditions than spore-forming bacteria. Nedwell et al. (1994) stated that coliform bacteria can survive <50 years while spore-forming bacteria can survive >80 years in Antarctica. The fecal Streptococcus strain was more resistant to the effects of radiation than the gram-negative strains (Statham & McMeekin 1994). Fox Cooper (1998) reported that in some areas of Antarctica, regional warming has caused a decrease in permanent snow cover around nunataks and coastal regions with the result that previously buried toilet pits, depots, and food dumps are now melting out. Green et al. (1992) reported a similar amount of coliform bacteria in the outfall of sewage from the Davis research station, which was reported in the sewage outfall of the McMurdo by Edwards et al. (1998).

In our finding, fecal coliform bacteria were absent in all different lakes of Broknes & Grovnes peninsula, Larsemann Hills, East Antarctica. While coliform bacteria were present in two lakes (P2 Lake and P3 Lake) of Broknes peninsula and nine lakes (L1C NG, L1D NG, L1E NG, L7 NG, L7A NG, L7B NG, L2 SG, L4 SG, and L5 SG) of Grovnes peninsula. The present study confirms that lake water contamination is limited to the immediate vicinity of the sewage outfall and will be useful in the future for the assessment of microbiological pollution in Antarctica.

Hughes & Blenkharn (2003) studied the bacterial reproduction in untreated sewage which was released from the Rothera Research Station, Antarctica. Goldsworthy et al. (2003) reported the presence of feces coliform bacteria in intertidal pools adjacent to sewage effluent from the research stations at Laersemann Hills, East Antarctica. Bruni et al. (1997) reported a high concentration of fecal bacteria (Sediment 94 CFU/100 mL; Water 800 CFU/100 mL) in the sewage outfall from the Italian Research Station, Terra Nova Bay. Hughes and Nobbs (2004) studied the viable fecal coliform bacteria in 30-40 years old human feces which were dumped at Fossil Bluff Field Station, Alexander Island, Antarctic Peninsula. The previous methods of human waste disposal on land are now starting to produce environmental pollution as well as potential health and scientific problems.

CONCLUSIONS AND RECOMMENDATION

Coliform and fecal coliform bacteria are mainly reached Antarctica through anthropogenic activities and are useful indicators of sewage waste. However, other factors may lead to coliform contamination in Antarctica such as the migration of microbes through birds and the transport of food items from the ship to the research station. The presence of coliform bacteria in Antarctic lakes may be due to the human population, which is living at research stations. Our study confirms the presence of coliform bacteria in the lakes of East Antarctica, as reported earlier in other Antarctic regions. Untreated sewage waste released from the research stations is the main cause of the presence of coliform in the Antarctic environment. Due to climate change the rate of snow and ice melting increased and has resulted in previously buried fecal material becoming exposed.

Before release sewage discharge should be fully treated; otherwise, it will leave pathogenic contaminants in the pristine environment of Antarctica. We should give priority to maintaining a relationship between actual human presence and the purification capacity of the plant systems, to reduce as much possible anthropogenic inputs into the Antarctic ecosystem. We need regular monitoring at research stations by which we can control the release of microbiological contaminates. Otherwise, these contaminants can cause several diseases in humans and other animal species. Research on the presence of fecal coliform bacteria in Antarctic Lake water could be helpful to provide a better estimate of the human impact.

ACKNOWLEDGEMENTS

The authors are thankful to the Director of the National Centre for Polar and Ocean Research (NCPOR) & Ministry of Earth Sciences (MoES) for our participation in the 34th Indian Scientific Expedition to Antarctica (ISEA). The authors are also thankful to the expedition leader for his motivation and constant support.

REFERENCES

Bhardwaj, L.K and Jindal, T. 2019. Contamination of Lakes in Broknes peninsula, East Antarctica through the Pesticides and PAHs. Asian-Journal of Chemistry., 31 (7): 1574-1580. https://asianpubs.org/index..php/ajchem/article/view/301.

Bhardwaj, L.K, Sharma, S., Ranjan, A. and Jindal, T. 2019. Persistent organic pollutants in lakes of Broknes peninsula at Larsemann Hills area, East Antarct. Ecotoxicol., 5)28): 589-596. https://doi.org/10.1007/s10646-019-02045-x

Bhardwaj, L.K. and Bharti, P.K. 2022. Noise monitoring and assessmentat Larsemann Hills, East Antarctica. Indian Journal of Environmental Protection., 42(9): 1027-1033. https://co.in/42-9-1027-1033/

Bhardwaj, L.K., Chauhan, A., Ranjan, A. and Jindal, T. 2018. Persistent

organic pollutants in biotic and abiotic components of an Antarctic pristine environment. Earth Syst. Environ., 1)2): 35-54. https://doi.org/10.1007/s41748-017-0032-8

Bhardwaj, L.K., Sharma, S. and Jindal, T. 2021. Occurrence of Polycyclic Aromatic Hydrocarbons (PAHs) in the Lake Water at Grovnes Peninsula Over East Antarctica. Chem. Afr., 4(4): 965-980. https://doi.org/10.1007/s42250-021-00278-0

Bhardwaj, L.K. and Sharma, A. 2021. Estimation of physico-chemical, trace metals, microbiological, and phthalate in PET Bottled Water. Chem. Afr., 4(4): 981-991. https://doi.org/10.1007/s42250-021-00267-3

Bruni, V., Maugeri, T.L. and Monticelli, L. 1997. Fecal pollution indicators in the Terra Nova Bay (Ross Sea, Antarctica). Marine Pollut. Bull., 11)34): 908-912. DOI: https://doi.org/10.1016/S0025-326X(97)00050-7

Cowan, D.A., Chown, S.L., Convey, P., Tuffin, M., Hughes, K., Pointing, S. and Vincent, W.F. 2011. Non-indigenous microorganisms in the Antarctic: Assessing the risks. Trends Microbiol., 19(11): 540-548. DOI: https://doi.org/10.1016/j.tim.2011.07.008

Delille, D. 1987. Spatial distribution of coastal Antarctic seawater bacteria: Relationship with avifauna. Polar Biol., 8(1): 55-60. DOI: https://doi.org/10.1007/BF00297165

Edwards, D.D., McFeters, G.A. and Venkatesan, M.I. 1998. Distribution of Clostridium perfringens and fecal sterols in a benthic coastal marine environment influenced by the sewage outfall from McMurdo Station, Antarctica. Appl. Environ. Microbiol., 7)64): 2596-2600. DOI: https://doi.org/10.1128/AEM.64.7.2596-2600.1998

Fox, A.J. and Cooper, A.P.R. 1998. Climate-change indicators from archival aerial photography of the Antarctic Peninsula. Ann. Glaciol., 27: 636-642. DOI: https://doi.org/10.3189/1998AoG27-1-636-642

Fujioka, R.S., Hashimoto, H.H., Siwak, E.B. and Young, R.H. 1981. Effect of sunlight on survival of indicator bacteria in seawater. Appl. Environ. Microbiol., 41(3): 690-696. DOI: https://doi.org/10.1128/aem.41.3.690-696.1981

Gardner, H., Kerry, K., Riddle, M., Brouwer, S. and Gleeson, L. 1997. Poultry virus infection in Antarctic penguins. Nature, 6630)387): 245-245. DOI: https://doi.org/10.1038/387245a0

Goldsworthy, P.M., Canning, E.A. and Riddle, M.J. 2003. Soil and water contamination in the Larsemann Hills, East Antarctica. Polar Record, 39(4): 319-337. DOI: https://doi.org/10.1017/S003224740300305X

Green, G., Skerratt, J.H., Leeming, R. and Nichols, P.D. 1992. Hydrocarbon and coprostanol levels in seawater, sea-ice algae and sediments near Davis Station in Eastern Antarctica: a regional survey and preliminary results for a field fuel spill experiment. Marine Poll. Bull., 25(9-12): 293-302. DOI: https://doi.org/10.1016/0025-326X(92)90685-Y

Harmon, S.M., West, R.T. and Yates, J.R. 2014. Identifying fecal pollution sources using 3M™ Petrifilm™ count plates and antibiotic resistance analysis in the Horse Creek Watershed in Aiken County, SC (USA). Environ. Monit. Assess., 186(12): 8215-8227. DOI: https://doi.org/10.1007/s10661-014-3999-8

Hill, R.T., Straube, W.L., Palmisano, A.C., Gibson, S.L. and Colwell, R.R. 1996. Distribution of sewage indicated by Clostridium perfringens at a deep-water disposal site after the cessation of sewage disposal. Appl Environ. Microbiol., 62(5): 1741-1746. DOI: https://doi.org/10.1128/aem.62.5.1741-1746.1996

Hughes, K.A. 2003. Influence of seasonal environmental variables on the distribution of presumptive fecal coliforms around an Antarctic research station. Appl. Environ. Microbiol., 69(8): 4884-4891. DOI: https://doi.org/10.1128/AEM.69.8.4884-4891.2003

Hughes, K.A. and Blenkharn, N. 2003. A simple method to reduce the discharge of sewage microorganisms from an Antarctic research station. Marine Pollut. Bull., 46(3): 353-357. DOI: https://doi.org/10.1016/S0025-326X(02)00224-2

Hughes, K.A. and Nobbs, S.J. 2004. Long-term survival of human fecal microorganisms on the Antarctic Peninsula. Antarct. Sci., 3)16): 293-297. DOI: https://doi.org/10.1017/S095410200400210X

Indian Standard:1622. 1981. Methods of Sampling and Microbiological Examination of Water. First Revision February 2003. https: Rlaw.resource.org/pub/in/bis/S02/is.1622.1981.pdf

Indian Standard:5887. 1976. Methods for Detection of Bacteria Responsible for Food Poisoning. First revision 2005. https://law.resource.org/pub/in/bis/S06/is.5887.2.1976.pdf

Kapuscinski, R.B. and Mitchell, R. 1981. Solar radiation induces sublethal injury in Escherichia coli in seawater. Appl. Environ. Microbiol., 41(3): 670-674. DOI: https://doi.org/10.1128/aem.41.3.670-674.1981

Khan, F.M. and Gupta, R. 2020. Escherichia coli (E. coli) as an Indicator of Fecal Contamination in Groundwater: A Review. Int. conf. Sustain. Develop. Water Environ., 61: 225-235. https://doi.org/10.1007/978-3-030-45263-6_21

Lenihan, H.S. 1992. Benthic marine pollution around McMurdo Station, Antarctica: a summary of findings. Marine Pollut. Bull., 25(9-12): 318-323. DOI: https://doi.org/10.1016/0025-326X(92)90689-4

Lenihan, H.S., Oliver, J.S., Oakden, J.M. and Stephenson, M.D. 1990. Intense and localized benthic marine pollution around McMurdo Station, Antarctica. Marine Pollut. Bull., 21(9): 422-430. DOI: https://doi.org/10.1016/0025-326X(90)90761-V

McFeters, G.A., Barry, J.P. and Howington, J.P. 1993. Distribution of enteric bacteria in Antarctic seawater surrounding a sewage outfall. Water Res., 27(4):645-650. DOI: https://doi.org/10.1016/0043-1354(93)90174-G

Mishra, M., Arukha, A.P., Patel, A.K., Behera, N., Mohanta, T.K. and Yadav, D. 2018. Multi-drug resistant coliform: water sanitary standards and health hazards. Front, Pharmacol., 9: 311. DOI: https://doi.org/10.3389/fphar.2018.00311

Nedwell, D.B., Russell, N.J. and Cresswell-Maynard, T. 1994. Long-term survival of microorganisms in frozen material from early Antarctic base camps at McMurdo Sound. Antarct. Sci., 6(1): 67-68. DOI: https://doi.org/10.1017/S095410209400009X

Parker, L.V. and Martel, C.J. 2002. Long-term survival of enteric microorganisms in frozen wastewater. Appl. Environ. Microbiol., 53(11): 3110-3127. DOI: https://hdl.handle.net/11681/5398

Patrick, M. and Bernard, B. 1991. Distribution and survival of motile Aeromonas spp. in brackish water receiving sewage treatment effluent. Appl. Environ. Microbiol., 57(9): 2459-2467. DOI: https://doi.org/10.1128/aem.57.9.2459-2467.1991

Sinton, L.W., Davies-Colley, R.J. and Bell, R.G. 1994. Inactivation of enterococci and fecal coliforms from sewage and meatworks effluents in seawater chambers. Appl. Environ. Microbiol., 60(6): 2040-2048. DOI: https://doi.org/10.1128/aem.60.6.2040-2048.1994

Smith, J.J., Howington, J.P., and Mcfeters, G.A. 1994. Survival, physiological response, and recovery of enteric bacteria exposed to a polar marine environment. Appl. Environ. Microbiol., 8)60) :2984-2977. DOI: https://doi.org/10.1128/aem.2984.1994-60.8.2977

Šolić, M. and Krstulović, N. 1992. Separate and combined effects of solar radiation, temperature, salinity, and pH on the survival of fecal coliforms in seawater. Marine Poll. Bull., 8)24): 411-416. DOI: https://doi.org/10.1016/0025-326X(92)90503-X

Statham, J.A. and McMeekin, T.A. 1994. Survival of fecal bacteria in Antarctic coastal waters. Antarct. Sci., 6(3):333-338. DOI: https://doi.org/10.1017/S0954102094000507

Upton, M., Pennington, T.H., Haston, W. and Forbes, K.J. 1997. Detection of human commensals in the area around an Antarctic research station. Antarct. Sci., 9(2): 156-161. DOI: https://doi.org/10.1017/S0954102097000205

Waterhouse, E.J. (Ed.). 2001. Ross Sea Region 2001: A State Of The Environment Report for the Ross Sea Region of Antarctica. New Zealand Antarctic Institute, NZ.

Nature Environment and Pollution Technology
An International Quarterly Scientific Journal

p-ISSN: 0972-6268
(Print copies up to 2016)
e-ISSN: 2395-3454

Vol. 21 | No. 5 (Suppl) | pp. 2035-2054 | 2022

Original Research Paper

https://doi.org/10.46488/NEPT.2022.v21i05.003

Open Access Journal

Role of Channel Migration and Influencing Hydro-Geomorphic Attributes in Dibru River Basin Using Remote Sensing and GIS

Gulap Sonowal*, Gitika Thakuriah† and Satyendra Hazarika***
*Department of Geography, Darrang College, Gauhati University, Tezpur, Assam
**Department of Geography, Cotton University, Guwahati, Assam
†Corresponding author: Gitika Thakuriah; gthakuriah@yahoo.in

Nat. Env. & Poll. Tech.
Website: www.neptjournal.com

Received: 11-07-2022
Revised: 26-08-2022
Accepted: 07-09-2022

Key Words:
Channel migration
Remote sensing
GIS
Channel avulsion
Dibru river basin

ABSTRACT

The action of the river is dynamic and exhibits morphological changes over time. River channel migration may take place because of sedimentation, geology, soil properties, geomorphic setup, precipitation, land use pattern, natural bank geometry (e.g., channel width, meander length, meander wavelength, amplitude, the radius of curvature, arc angle, and sinuosity), discharges of various frequencies (Brice 1982, MacDonald et al. 1991, Garcia et al. 1994), distribution of riparian vegetation, and vertical and horizontal heterogeneity of floodplain soils (Motta et al. 2012), etc. are some factors for channel migration. The present study is undertaken in the Dibru River Basin, the left-bank tributary of the Brahmaputra River. To identify the Spatio-temporal changes, satellite imagery is used in the GIS environment. The extraction of the river is done from the GIS software (Arc GIS 10.4) by digitizing process and tries to overlay the different time periods of shifting of the river and find out the rate of magnitude and nature of the river course changes. An interval of 10 years is taken to find the rate of magnitude and nature of changes in the river courses from satellite imagery. The time period is taken from 1977-2020 at 10 years intervals. Along with the rate of river course changes, channel avulsion is also shown with the help of satellite imagery. The Dibru Saikhowa National Park falls within the Dibru river basin, where numerous streams are found, within the national park. The Saikhoa river and Ajuka river flow within the national park. The Sursa river is a small channel linked with the Dangori river. With phases of time, the river made a headward erosion and confluence with the Ajuka river and formed a channel. The Saikhoa river flowed till 1987; due to deposition, the river abandoned its original course. In 1988, the Ajuka river and Sursa river merged and flowed northwest direction. The high discharges of the Lohit river diverted towards the Ajuka and Sursa Rivers and took a new channel named the Lower course of Lohit river within the study area. It can be called an avulsion channel because it changed its direction from its original to a new course in 1990. Since 1990, the course of the channel has been tremendously expanding its length and breadth, causing a flood, bank erosion, and deposition nearby human habitats and Dibru Saikhowa National Park. From the multi-temporal satellite imagery, the river courses were studied, and found the year of avulsion took place in the channel. Multi-temporal satellite imagery is used to identify the channel's avulsion. An avulsion is the rapid separation of a river channel to form a new course, which is only possible due to flood, high discharge, soil properties or tectonic activity, etc. that creates instability and causes the channel avulsion..

INTRODUCTION

River morphology is changeable and active in varying environmental landscapes over both spatio-temporal scales. An avulsion is a process by which flow is diverted from the parent channel into a new course in the floodplain. A local avulsion forms a new channel that joins its parent channel downstream (Heller & Paola 1996). Channel diversion mainly occurs within the floodplain region, and bank erosion is held because of lateral shifting of the course. Usually, it is a natural process, but with the ages of time, its terms as semi-natural because of human intervention. Changing channel courses create great havoc on the socio-economic life of the people living in the region. Sometimes, many people lose their homes, agriculture fields, and infrastructure due to channel migration. It is variable; some changes are gradual and some are unnoticeable, while others depend upon the phenomena like extreme floods and droughts. Channel avulsion is a natural process associated with changing channel patterns over space and time. Different channel patterns are identified in the same river course because of the behavior of the river. In foodplains, sinuous

to meandering channel patterns are common in the river course.

The Brahmaputra River has been causing severe bank erosion along different parts of its alluvial banks in Assam. Among the localities afflicted by severe bank erosion in Assam (such as Majuli, Moriahola, Kaziranga, Laharighat, Palasbari, Gomi, Mokalmua, and Bogribari), the Rohmoria area has the highest rate of bank erosion in the south bank of the Brahmaputra (Sarma & Phukan 2006). An attempt has been made for the first time to evaluate the role of a neotectonic fault on rapid bankline migration vis-à-vis bank erosion of the Brahmaputra River around Rohmoria locality of Assam (Sarma & Acharjee 2012).

The Dibru River is a left-bank tributary of the Brahmaputra river. The Dibru river is a northward-flowing river system that drains into the Brahmaputra River in the plains region. The Dibru river origin near the village name called Natun Maithang bujiliban and flows northwards to drain into the Brahmaputra river. The Dangori river is a sub-tributary of the Dibru river and confluence at the Raidang wetland. It is just a tributary of the mainstream river but changes its morphological characteristics by expanding its bank over time. Before, it was just a tiny channel or Nala. Now, Dangori is known as the second Brahmaputra by the local people of the study area. The river creates great havoc on the physical and socio-economic landscapes. The 20 m wide small channel of the Dangori river of 1995 has become about 2,000 m wide channel of the Lohit in 2007 causing severe bank erosion, flooding, and loss of life and property (Sarma et al. 2011).

GIS is the most sophisticated tool used for environmental deterministic research studies. Various multi-temporal satellite imagery is used to identify the temporal change of the Dibru river course and the lower course of the Lohit river. The advantage of using advanced tools for geo-referencing, image processing, visualization, overlay, water bodies extraction, and channel migration position over multiple years to a single extensive system. The high-resolution images give accurate and precise data for a particular region and are essential to evaluating the trend of river shifting. This will be helpful for ordinary people for earlier vulnerability to communities living on the flood plains.

OBJECTIVES OF THE STUDY

1. To identify the high-risk point of channel migration of the Dibru river using satellite imagery.
2. To assess the magnitude of channel change of the Dibru river using geospatial tools.
3. To study the hydro-geomorphic indicator of channel migration.

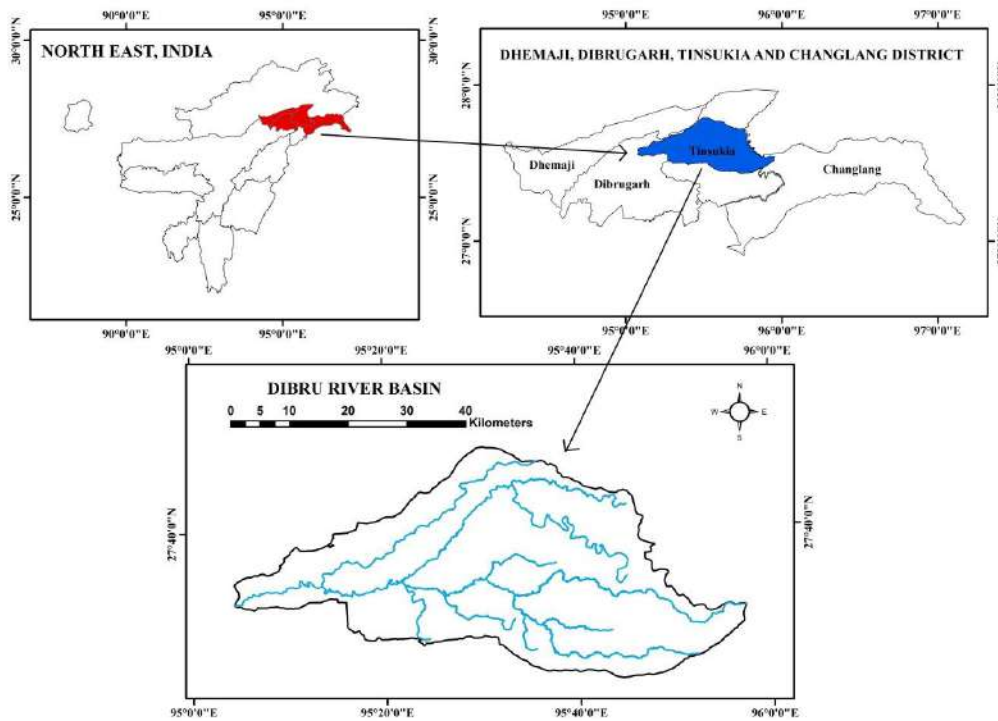

Fig. 1: Location map of the study area.

4. To study the impact on human activities.

STUDY AREA

The Dibru River is a left-bank tributary of the Brahmaputra River. The basin drains into the plain region of Assam experience the great sub-Himalayan terrain and is bounded by the river Brahmaputra and the Lohit in the north, Noa Dihing river in the eastern, and some tributaries of the Burhi Dihing river in the southern and western borders of the basin. Geographically, its latitude and longitudinal extensions are 27º25´30″ N-27º46´30″ N and 95º6´0″ E-95º58´30″ E covering about 1,779 sq. km area of Tinsukia, Dibrugarh, Dhemaji district of Assam and a small part of the Changlang district of Arunachal Pradesh (Fig. 1) with ever-green and semi-deciduous forests and the climatic condition is high humidity and moderate temperature. The slope of the basin varies from a gentle slope to a base-level slope (0^o-5^o).

The Dibru river origins at an altitude of about 155 m above mean sea level and run up to 132.95 km, where the channel gradient is 0.35 $m.km^{-1}$.

A major portion of the study area is a plain region. The population concentration is very high in the southern part of the basin. The Dibru River Basin consists of four revenue circles viz- Chabua, Doom Dooma, Margherita, and Tinsukia revenue (Fig. 20).

DATABASE

The Dibru River basin is delineated from Survey of India topographical Sheets No: 83M/2, 83M/5, 83M/6, 83M/7, 83M/9, 83M/10, 83M/11, 83M/13, 83M/14, and 83M/15 at 1: 50,000 scale. To understand the dynamic nature of the Dibru River Basin, Multi-temporal Landsat satellite data and LISS III data for the years 1977, 1987, 1997, 2007, and 2020 were used. The details of the satellite images for channel migration are given below in Table 1.

To study the Channel Avulsion satellites imagery details are given in Table 2. To understand the flow characteristics of the river, the fluvial and geomorphic databases are collected from the Flood observatory.colorado.edu website. Along with it, we have also used a secondary database, especially the Soil map prepared by the National Bureau of Soil Survey and Land Use Planning Regional Centre, a Geological map from the Geological Survey of India. Rainfall data had collected from various rainfall gauge site stations within and around the basin for a period of 9 years. A primary survey was carried out within the affected villages' areas by lateral migration and their impact on households, tea gardens, and others activities.

Table 1: Details of Satellite imagery of changes in the course of the river:

Sensor	Date of acquisition	Bands used	Resolution
MSS	6 February 1977	MTL	60 m
MSS	22 March 1987	2,3,4	30 m
MSS	16 February 1997	2,3,4	30 m
LISS III	1 February 2007	2,3,4	24 m
OLI and TIRS	22 December 2020	3,4,5	30 m

Table 2: Details of the satellite imagery for channel avulsion.

Sensor	Date of Acquisition	Band	Resolution
MSS	22 March 1987	2,3,4	30 m
MSS	27 October 1988	2,3,4	30 m
MSS	12 January 1989	2,3,4	30 m
MSS	18Nov 1990	2,3,4	30 m
MSS	7Dec 1991	2,3,4	30 m
MSS	7 November 1990	2,3,4	30 m
MSS	28 December 1993	2,3,4	30 m
MSS	28 October 1994	2,3,4	30 m

MATERIALS AND METHODS

For the identification of the spatio-temporal migration of the Dibru River, the satellite image is projected at the same coordinate system units, and that is WGS_1984_UTM_Zone_46N. The whole work and the dynamic nature of the Dibru river over different years are digitized and analyzed with ArcGIS 10.4 software. The channel avulsion is carried out from satellite imagery from 1987 to 1994.

The morphometric parameters like long profile, Sinuosity Index and channel gradient, channel slopes, etc., are computed using the Survey of India toposheet at a 1:50,000 scale and contour interval of 20 m. The affected villages are identified by overlaying the layer of the river course of 2020 over the map of the village. In this way, the numbers of affected villages are identified and for the ground truth, a primary survey was carried out with the help of GPS.

RESULTS AND DISCUSSION

Morphological Changes in the Dangori River (Lower Course of Lohit River)

The Dangori river was just a tiny channel or Nala as per the toposheet (SOI), 1966. But with phases of time, the small channel changes its nature and behavior. The Dangori river has small streams like the Sursa river. Many small streams are found within the Dibru Saikhowa National park. This national park is shaped by the erosion and deposition

works of the Dibang, Dihang, and Lohit rivers, which bring tremendous siltation from hilltops and are deposited at the foothill of Assam. The Dibru Saikhowa National Park, where numerous streams are found, and the Saikhoa river and Ajuka river flow within the study area. The Sursa river is a small channel linked with the Dangori river. With phases of time, the river made a headward erosion and confluence with the Ajuka river and formed a channel. The Saikhowa river flowed till 1987; due to deposition, the river abandoned its original course. In 1988, the Ajuka river and Sursa river merged and flowed in a northwest direction. The high discharges of the Lohit river diverted towards the Ajuka and Sursa Rivers and took a new channel named the Lower course of Lohit river within the study area. It can be called an avulsion river because it changed its direction from its original to a new course in 1990. Avulsion can result from high peak discharges, sediment accretion, uplift or lateral tilting (tectonic), jamming of the channel through the exogenous process, etc. (Miall 1996, Slingerland & Smith 1998, Jones & Schum 1999). Since 1990, the course of the channel has been tremendously expanding its length and breadth, causing flood, erosion, and deposition nearby human habitats and Dibru Saikhowa National Park.

From the Multi-temporal satellite imagery, the river courses were studied, and fond the year of avulsion took place in the channel (Fig. 2). A multi-temporal satellite imagery is

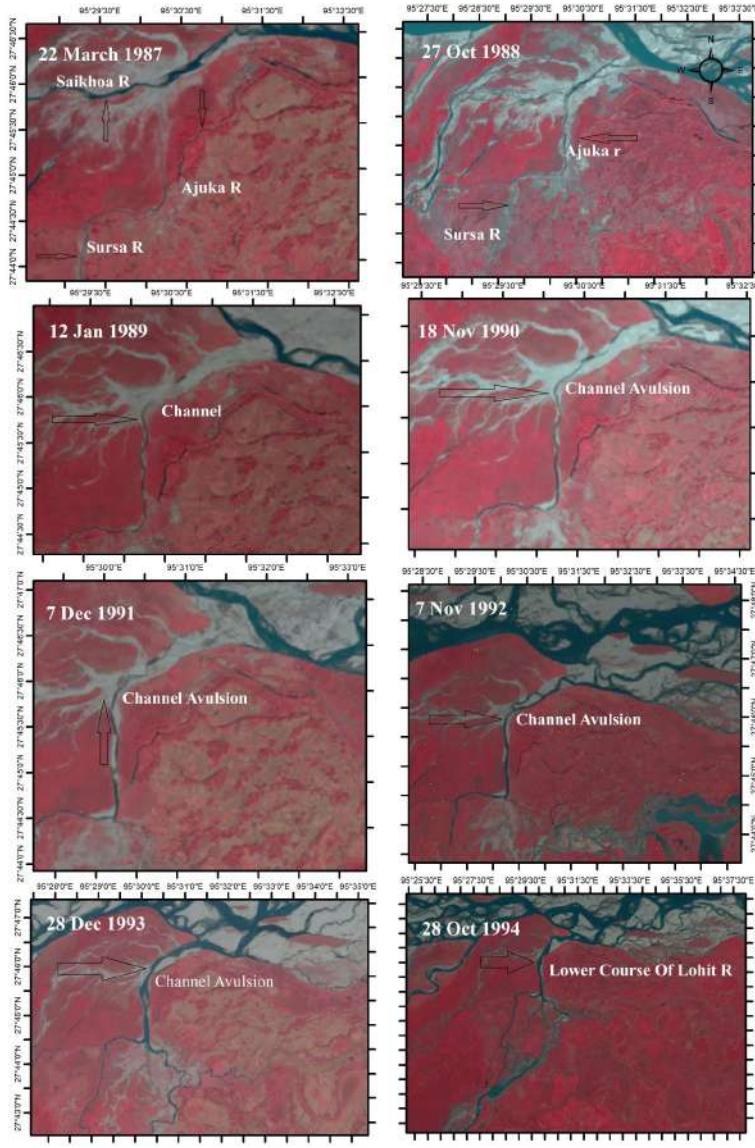

Fig. 2: Morphological changes of Dangori River (Lower Course of Lohit River).

Table 3: Magnitude of changes rate in some selected cross sections:

Cross Section	1977-1987		1987-1997		1997-2007		2007-2020	
	R [km]	L [km]	R [km]	L [km]	R [km]	L [km]	R [km]	L [km]
A-A1	0	0.08	0.82	-	0.54	-	0.07	-
B-B2	0.10	-	-	0.48	-	0.41	0.60	-
C-C3	0.13	-	-	0.37	-	0.48	0.63	-
D-D4	0	0.03	0.22	-	0.02	-	-	0.07
E-E5	0	0.01	-	0.01	-	1.28	0.42	-
F-F5	0	0.04	0.017	-	-	0.83	-	0.83

used to identify the channel's avulsion. An avulsion is the rapid separation of a river channel to form a new course, which is only possible due to flood, high discharge, soil properties or tectonic activity, etc., that creates instability and cause the channel avulsion. A local avulsion forms a new channel that joins its parent channel downstream (Heller & Paola 1996).

Magnitude Changes of Some Selected Cross-Sections Within the Course of the River

Channel Changes (Cross Section AA') during 1977-2020

In 1977, the channel was in a left direction along cross section AA.' In the early age of 1980, the channel shifted towards the left direction with an extent of 0.08 km in the year 1987 again its extent to the right in the year 1997, 2007 and continue till 2020, with a rate of 0.82 km, 0.54 km, and 0.07 km (Table 3). This can occur due to the soil characteristics and high discharge flows (Fig. 3 & 9)

Channel Changes (Cross-Section BB ') during 1977-2020

From 1977-1987 the channel was in the right direction along cross-section BB,' and in the early age of 1990, the channel was shifted towards the left direction with an extent of 0.48 km and 0.41 km in the year 1987-2007 (Table 3). Again from 2007-2020, it shifts towards the right at 0.60 km (Fig. 4 & 10).

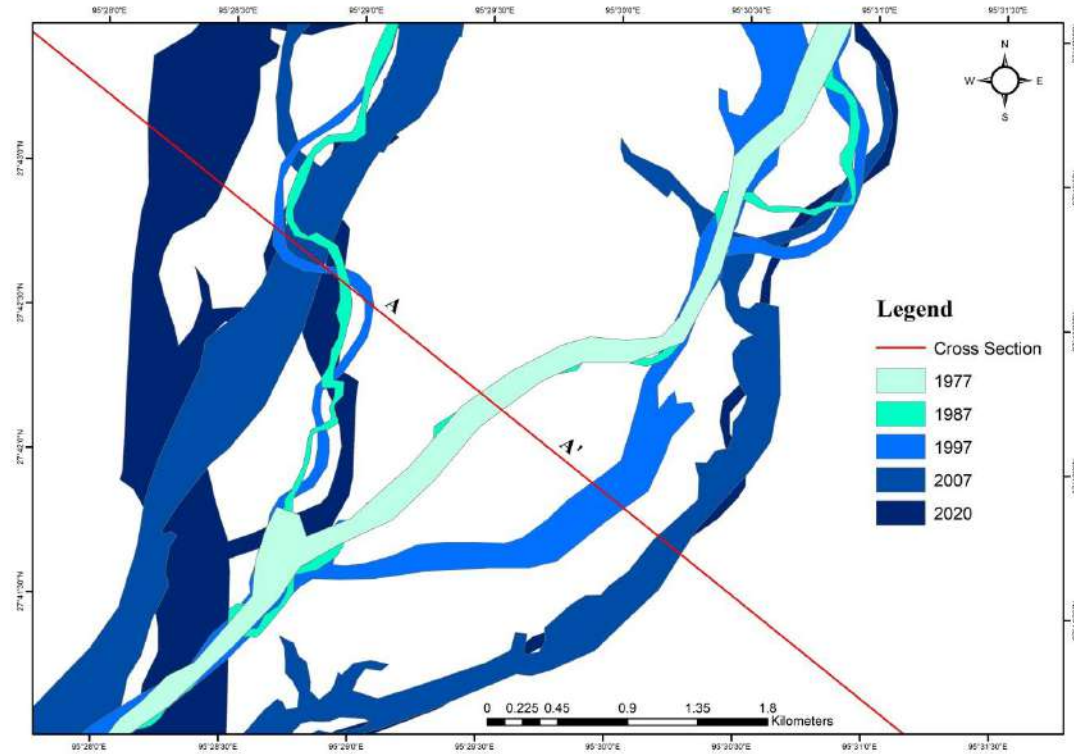

Fig. 3: Cross Section AA'.

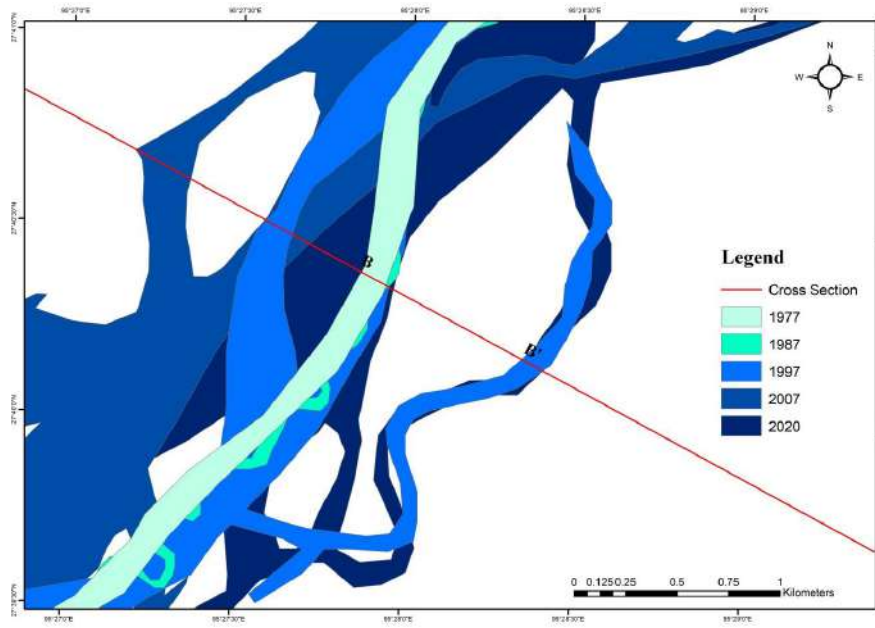

Fig. 4: Cross-section BB'.

Channel Changes (Cross-Section CC', DD' and EE') During 1977-2020

From (Fig. 5 & 10) 1977-1987, CC's cross-section channel was in the right direction and shifted towards the left in 1997 and 2007 at the rate of 0.37 km and 0.48 km, again shifting towards the right in the year 2020 at the rate of 0.63 km (Table 3). From (Fig. 6 & 11, 7 & 11) 1977-1987, cross-section DD' and EE' was in the left direction, cross-section DD' shifted towards the right in the year 1997-2007, and again shifted towards the left direction. And cross-section EE' was a left direction until 1997-2007 and shifted to the right in 2020 (Table 3).

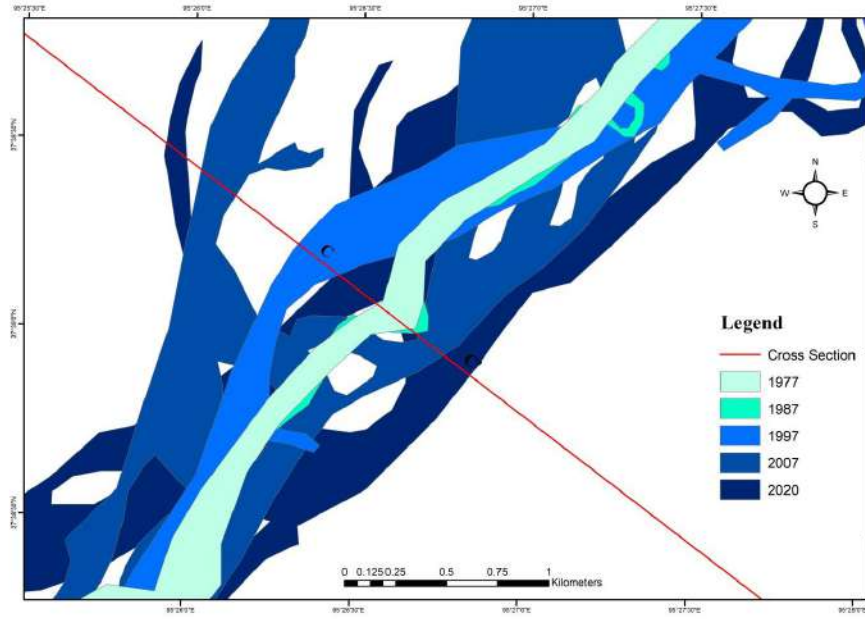

Fig. 5: Cross-section CC'.

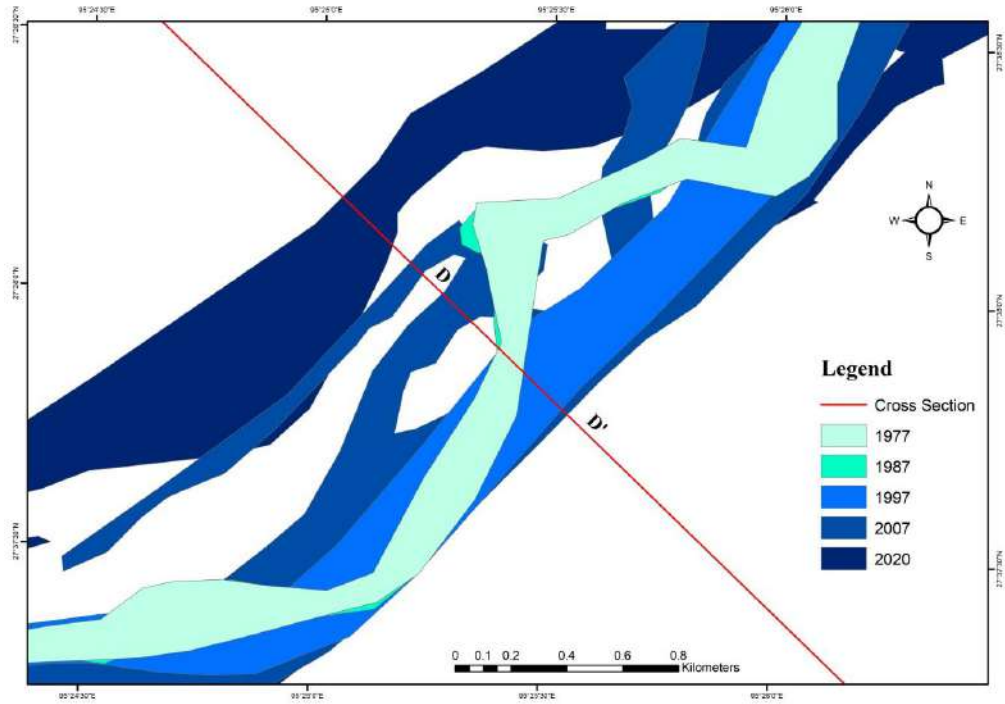

Fig. 6: Cross section DD'.

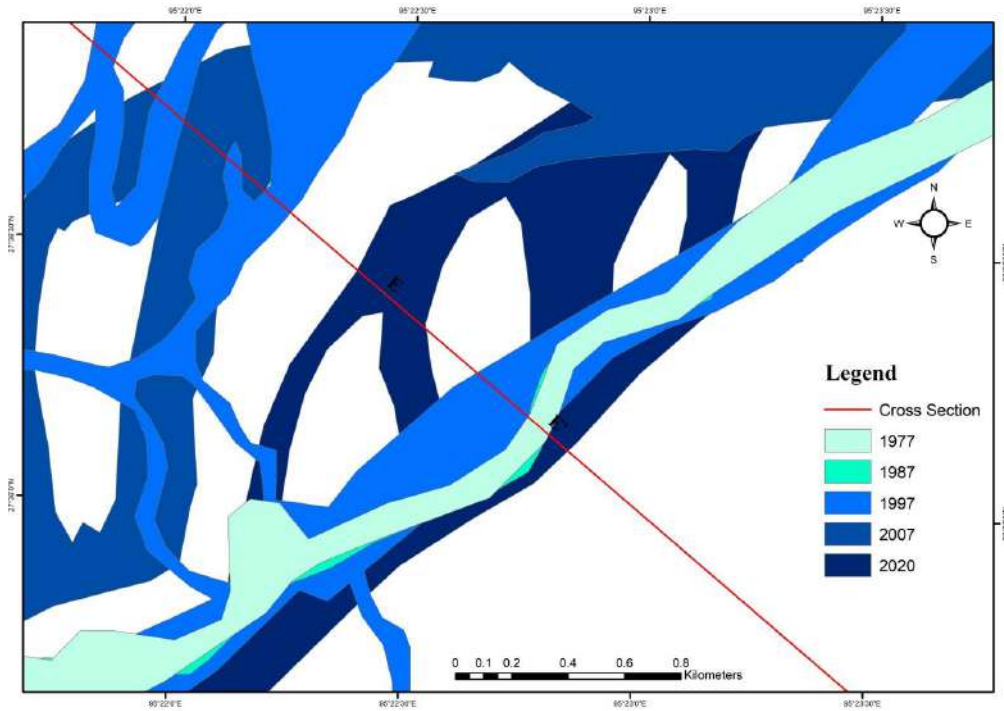

Fig. 7: Cross-section EE'.

Channel Changes (Cross Section FF') During 1977-2020

From 1977-1987, the FF' cross section channel was in the Left direction and shifted towards the right in 1997 at the rate of 0.0.17 km, again shifting towards the left in 2007 and 2020 at the rate of 0.83 km constantly till 2020 (Table 3). In (Fig. 8 & 12), the channel is rapidly progressive in meander formation because of the cliff slope of the channel. The helical flow of the meander bend plays a vital role in sediment transport and deposition (Azpiroz-Zabala et al. 2017).

Hydro-Geomorphic Attributes

Longitudinal River

A long profile is defined as the channel length from source to mouth. It depends on the grade of the slope. Slope declines downwards due to discharge, tectonic activity, geologic structure, sediment transport, flow resistance, width, and depth. From the source to the mouth, the river carries its materials and deposits sediment where it finds the equilibrium point or base level. Displacement along the graded profile would indicate disequilibrium due to tectonic uplift or rock perturbations (Mackin 1948, Leopold & Maddock 1953, Whipple & Tucker 2002, Whittaker et al. 2007). The Dibru river originates at about 155 m above mean sea level and runs up to 132.95 km (Fig. 13). The river is at the mature stage, forming a concave valley. The Dangori river originates at about 145 m above mean sea level and runs to 87.02 km (Fig. 14). The river is at the mature stage, forming a concave valley.

Sinuosity Index (S. I.)

According to Brice (1982) sinuosity index is the ratio of the length of the channel to the length of the meander belt axis. The river has a sinuosity of 1.5, called sinuous or meandering. The Sinuosity Index of the Dibru river and Dangori river were 1.36 and 1.46 in 1966. It shows that the headstream of the Dibru river and Dangori river is sinuous, and in the future, it will be in meandering and braided channels. It is significant in the evolution of landscapes and beneficial for geomorphologists, hydrologists, and Geologists.

Channel Slope

The slope ratio is the ratio between the degree slopes of any given order to the next successive higher order of the basin. It is mathematically expressed as

$$\text{Rs} = \frac{Su}{S_{u+1}}$$

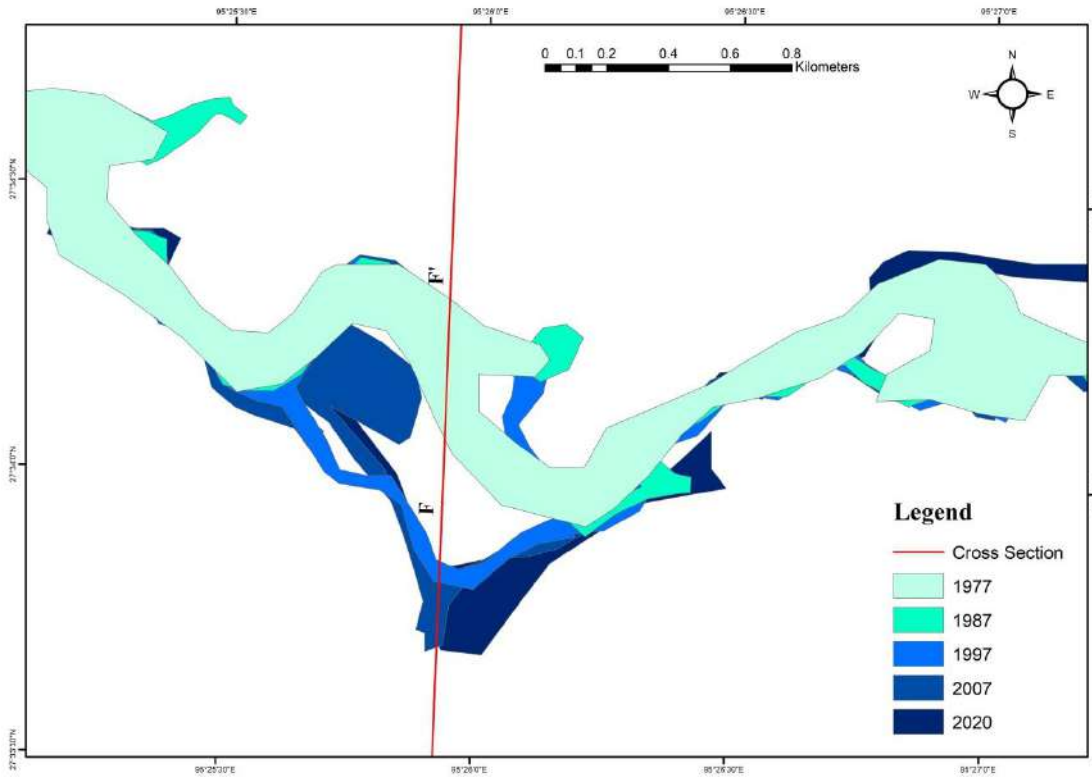

Fig. 8: Cross Section FF'.

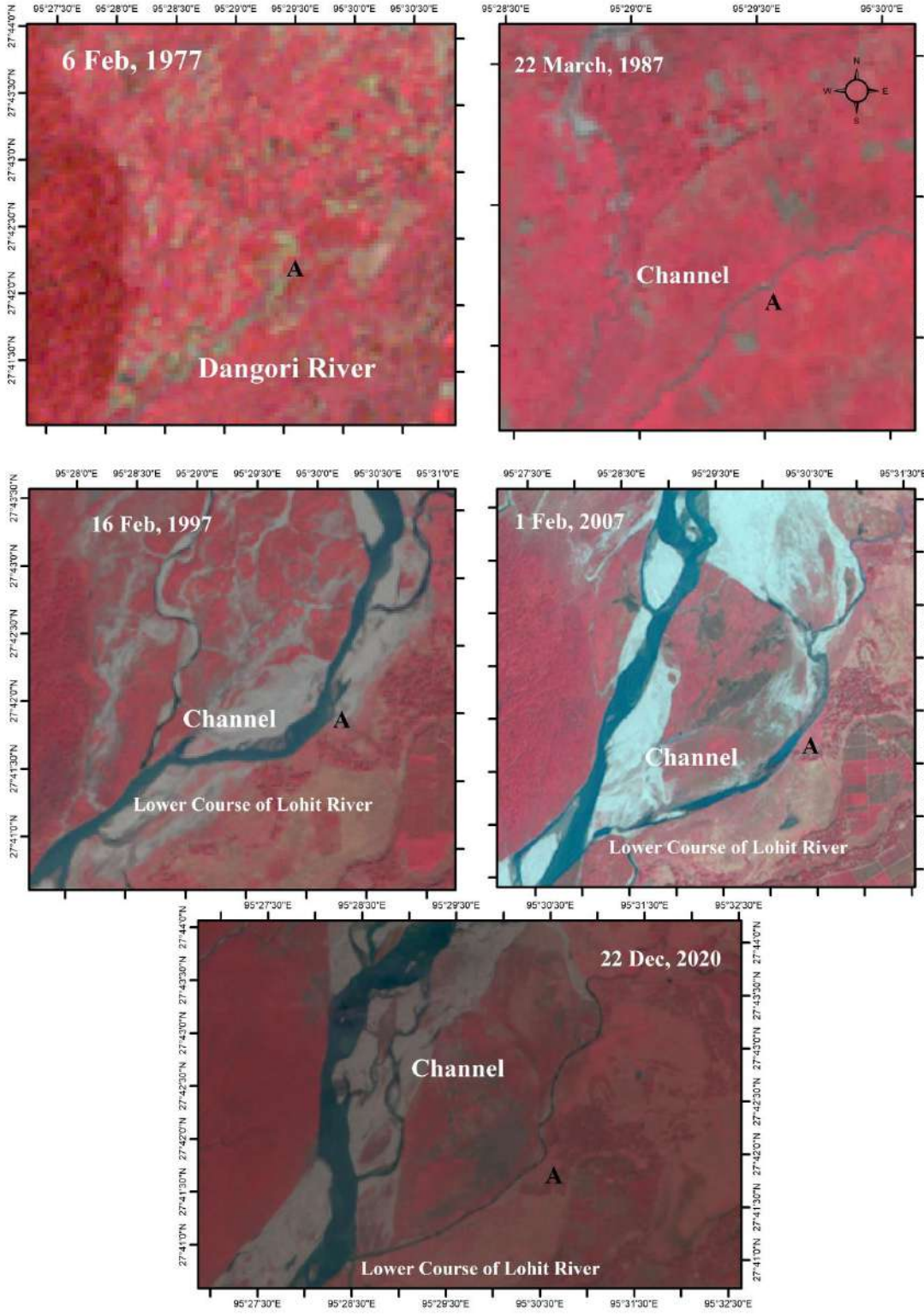

Fig. 9: Satellite imagery of each cross-section.

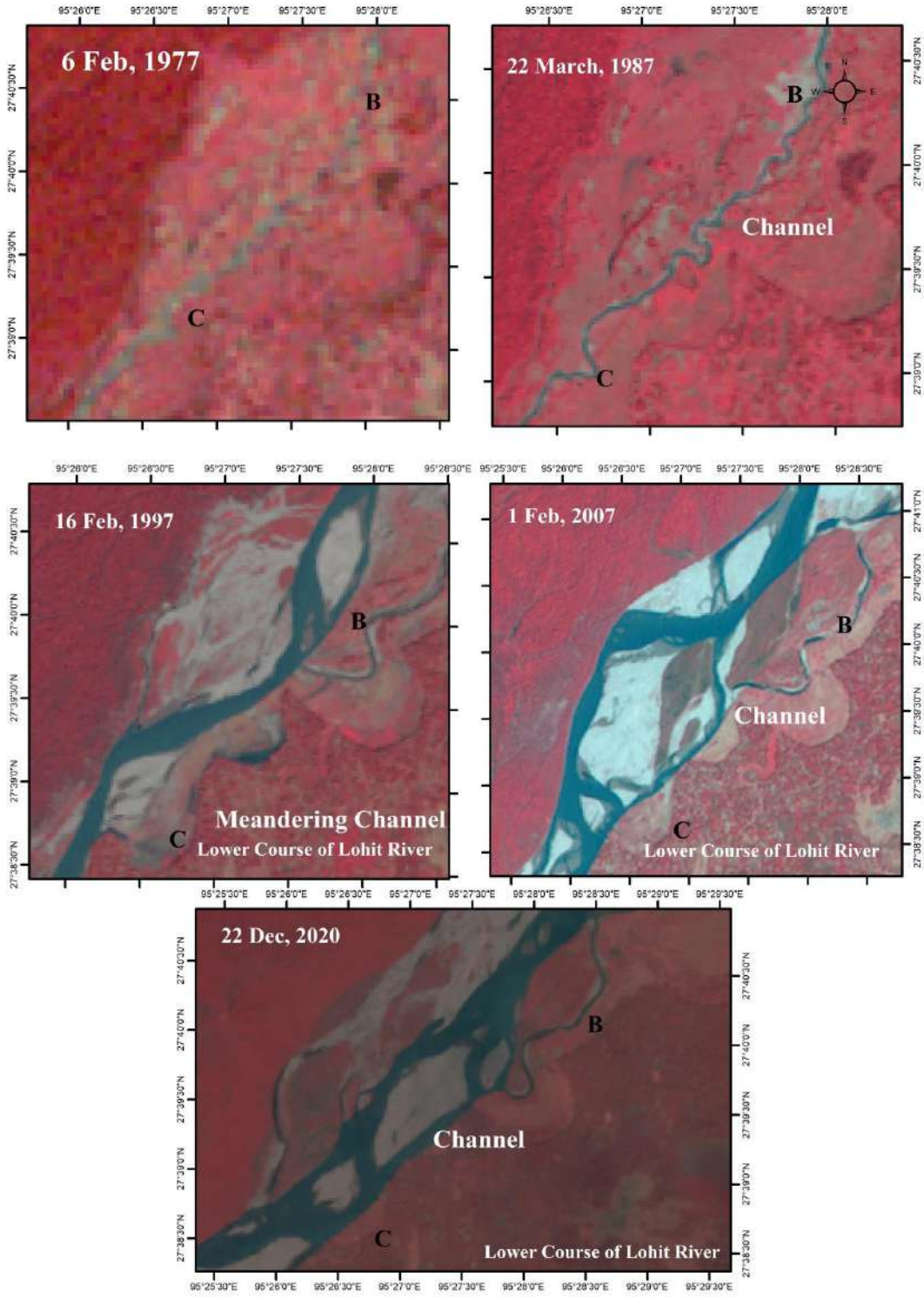

Fig. 10: Satellite imagery of each cross-section.

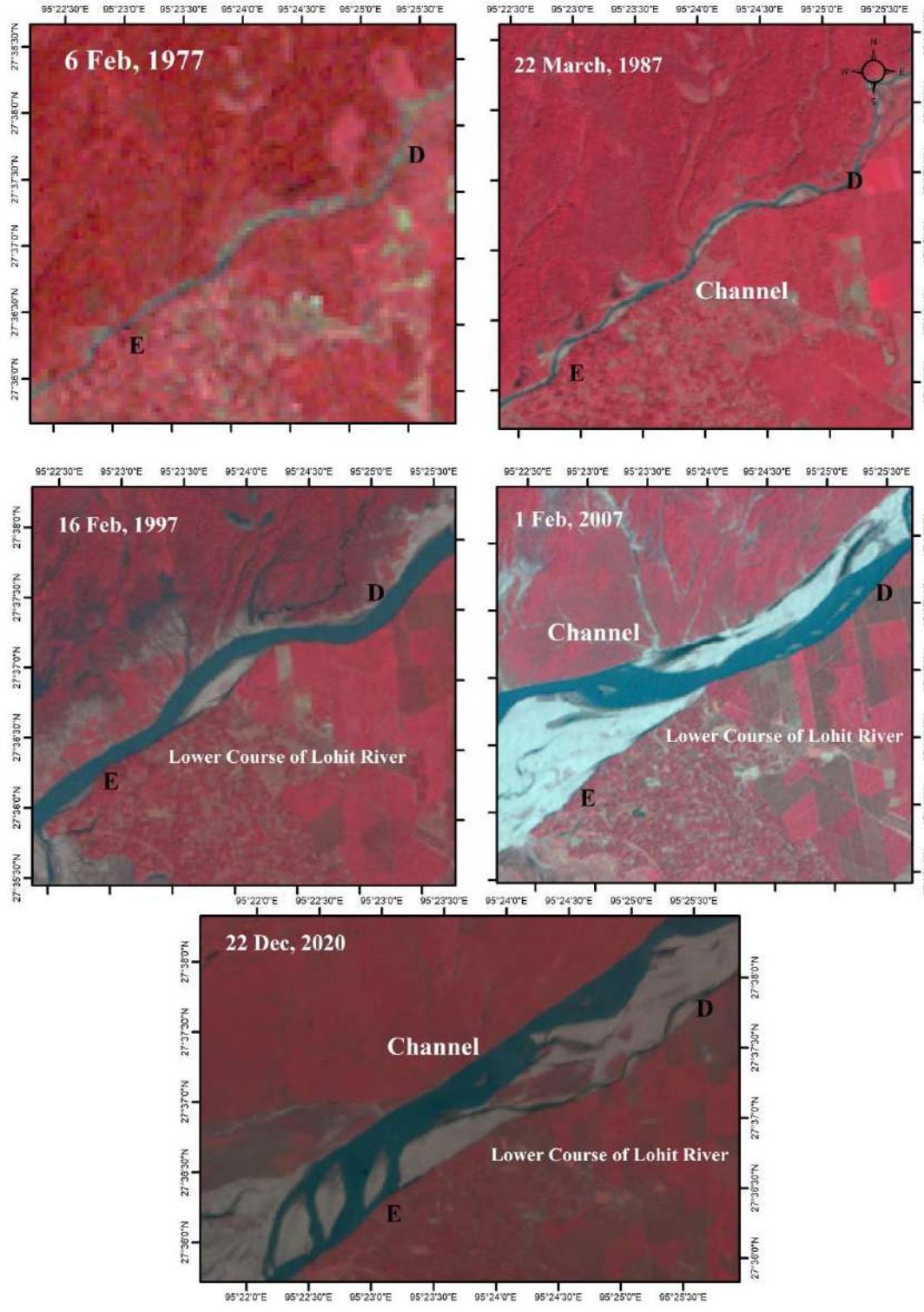

Fig. 11: Satellite imagery of each cross-section.

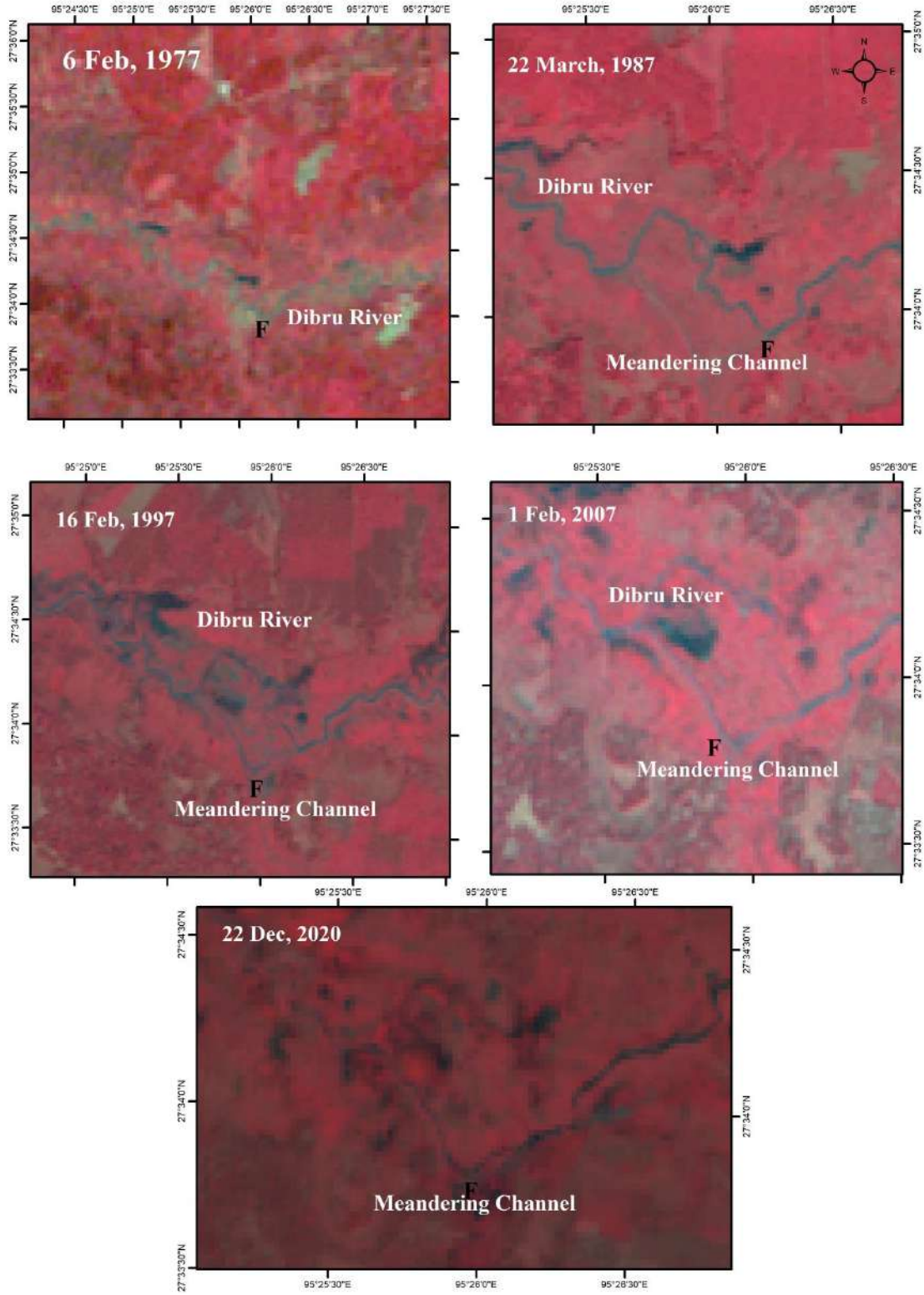

Fig. 12: Satellite imagery of each cross-section.

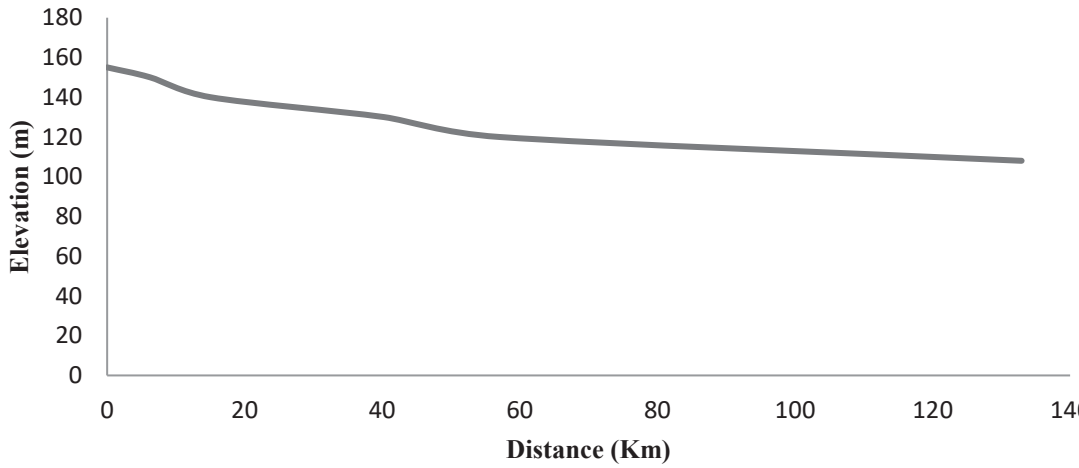

Fig. 13: Longitudinal profile of Dibru river.

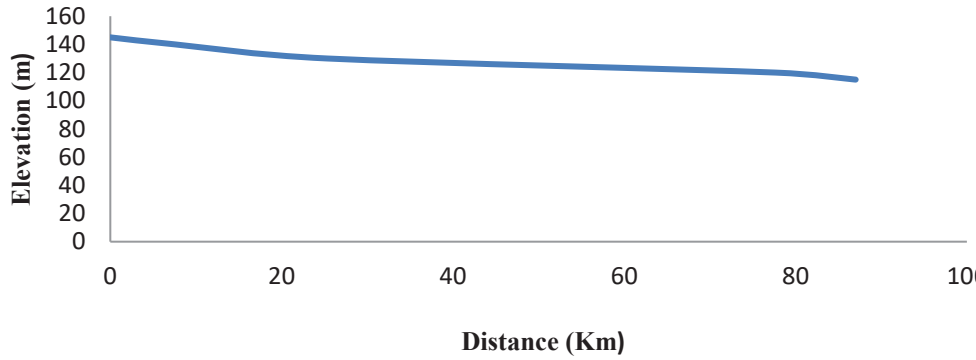

Fig. 14: Longitudinal profile of Dangori river.

Where *Su* is the slope of a given order, S_{u+1} is the slope of the next higher order

The Law of Channel slope is usually measured from the upper stage of the first-order stream to the lower stage of the last-order stream of the single master stream of the river. Usually, the Law of channel slope is finding out the ratio of vertical drop to increase in a horizontal distance of each order. The mean channel slope of each order is then derived and tabulated (Table 4).

Table 4: order wise slope ratio.

Order	Slope in degree	Slope ratio
1	0º4′26.63″	1.279
2	0º3′28.33″	1.052
3	0º3′18.01″	1.066
4	0º3′5.64″	3.750
5	0º0′49.5″	1.302
6	0º0′38″	-

'The Law of channel slope' as propounded by R.E Horton and applied by M. Morisawa and Leopold and Miller (1956), states that mean channel slope decrease with increasing next order in geometric series with constant slope ratio (Fig. 15). The exponential function is fitted to mean channel slope and stream order.

Flow Characteristics

A flow characteristic is essential to know about the discharge within the channel. Discharge leads to erosion and deposition of material within or outside the bank. Variability of water discharge highly impacts bank erosion, especially in the bank-full stage (Dragicevic et al. 2017).

From (Fig. 16), predictions can be made to know the channel's maximum and minimum peak flow. According to this, planning and management can be done within the study area.

Climatic Indication

Dibru River Basin is situated in the humid sub-tropical belt

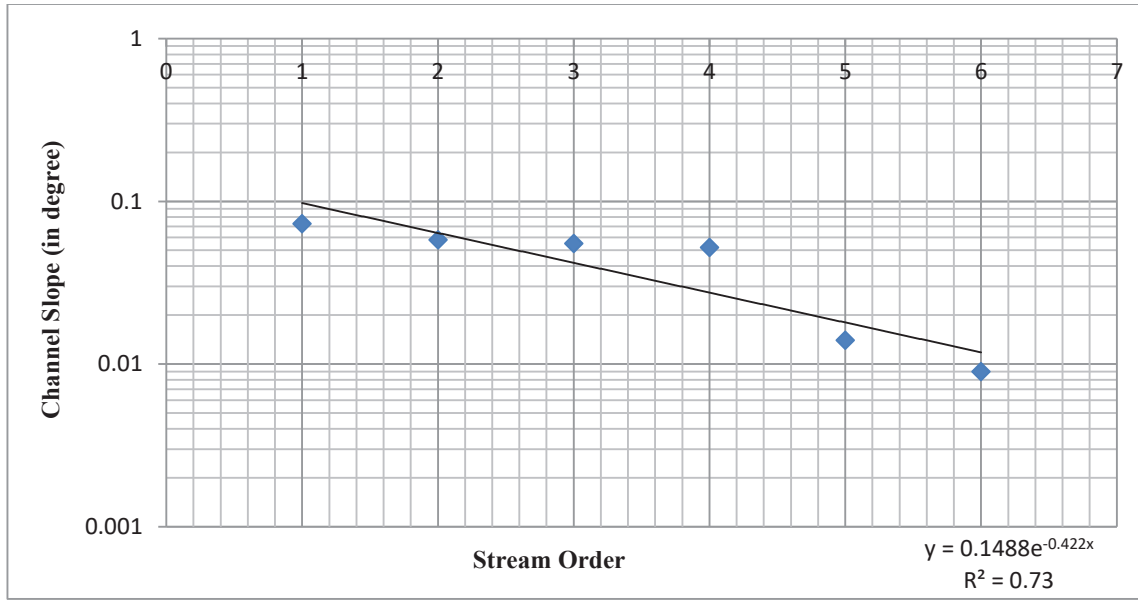

Fig. 15: Channel slope of Dibru River.

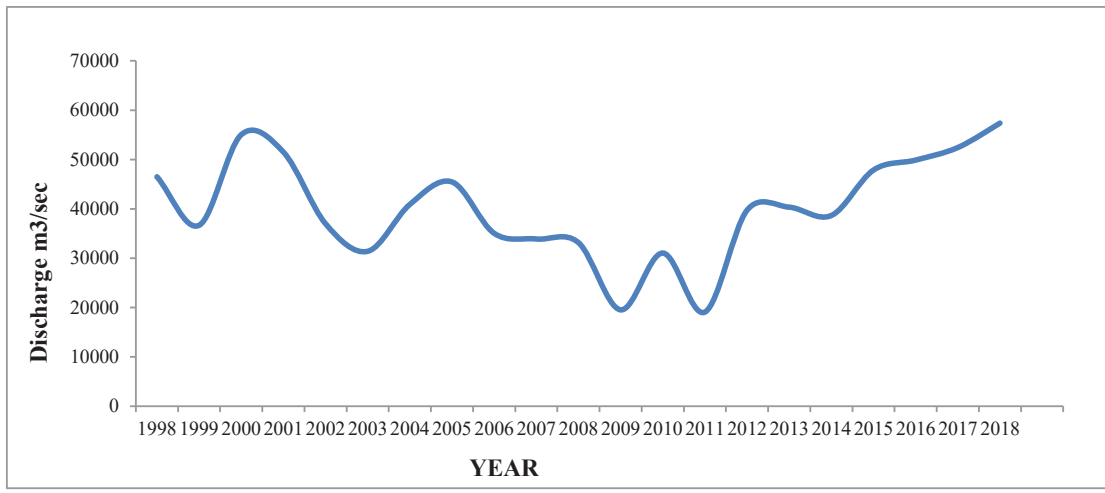

Fig. 16: Annual hydrograph 1998-2019.

within the Brahmaputra River basin. The region experienced a typical subtropical monsoon climate that has some local variations due to its geographic location. In the North and northeast direction of the basin, Arunachal Pradesh and Naga hills develop a sustainable variation in rainfall. The average annual rainfall of the study area is 185.55 cm. The amount of rain received in the Dibru River Basin is not uniform throughout the year. The simplest way of representing the seasonal pattern of variation is the graphical representation of monthly rainfall for different months of the year. The monthly average data for 2011-2019 shows the seasonal variation of rainfall. The monthly averages for the 9 years of record from 2011-2019 are shown in Fig. 17. The ideal graph gives a fairly monthly cycle in a smooth shape. The peak starts from April to September. The maximum amount of rainfall is recorded in July. The rain begins decreasing in October and becomes minimum in December. Maximum precipitation can describe the study area's monthly precipitation patterns during the summer or high sun, insolation at its peak, and a dry season during winter or winter solstice.

The primary peak appearing in April is associated mainly with the pre-monsoon rainstorm caused by the convective activity of ground heating. During the pre-monsoon season, a severe thunderstorm over northeast India generally gives rise

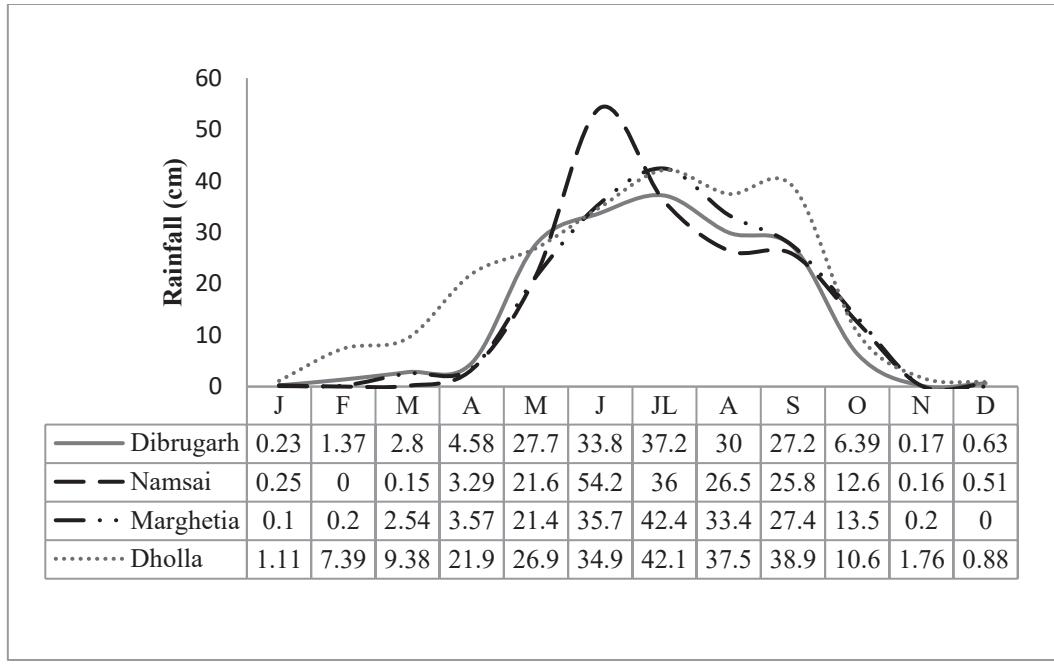

	J	F	M	A	M	J	JL	A	S	O	N	D
Dibrugarh	0.23	1.37	2.8	4.58	27.7	33.8	37.2	30	27.2	6.39	0.17	0.63
Namsai	0.25	0	0.15	3.29	21.6	54.2	36	26.5	25.8	12.6	0.16	0.51
Marghetia	0.1	0.2	2.54	3.57	21.4	35.7	42.4	33.4	27.4	13.5	0.2	0
Dholla	1.11	7.39	9.38	21.9	26.9	34.9	42.1	37.5	38.9	10.6	1.76	0.88

Fig. 17: Rainfall graph of Dibru river basin.

to intense precipitation, leading to the formation of precipitation peaks from April. The maximum rainfall that occurs in July is the effect of the onset of the southwest monsoon.

From August, there is a decline in rainfall due to the effect of a break in monsoon or retreat monsoon taken in September. The deviation of mean monthly rainfall from averages of mean monthly rainfall is observed from October to March. It is found that a highly negative deviation occurs from December to January due to low rain**.**

Geology

The geological map also gives us an idea about geological conditions in particular areas, including rock units and structures. The geological map is prepared by the Geological Survey of India with a scale of 1:50,000 and the map is arranged according to the Age of the formation of the rock layer from the Pleistocene-Holocene to the Meghalayan Age (Fig. 18).

1. Pleistocene-Holocene
2. Holocene
3. Meghalayan

Geologically, the Dibru River Basin was formed during the Pleistocene-Holocene to Meghalaya Age. Pleistocene-Holocene Age covered significant parts of the basin and belonged to older alluvium and consists of rocks oxidized to feebly oxidized sand, silt and clay. Western parts of the basin consist of the Meghalaya Age with newer alluvium and white to greyish sand, silt, pebble, and clay.

The Geological map of the study area is classified into three categories along with their characteristics, and they are mentioned below (Table 5).

Soil

Soil is a naturally complex mixture of inorganic and organic materials. It is a product of a continuing process of evolution in a parent material through physical and chemical weathering processes. It is influenced by the activity and accumulated residues of numerous microscopic and macroscopic plants and animals (Hillel 1998). Soil is one of the pivotal factors in landform development and modification.

Table 5: Geology of Dibru River Basin.

Age	Group_Name	Formation	Lithologic
Pleistocene-Holocene	Older Alluvium	Sorbhog	Oxidized to feebly oxidized sand, silt, and clay
Holocene	Newer Alluvium	Hauli	Established and unoxidized sand, silt, and clay
Meghalayan	Newer Alluvium	Barpeta-I	White to greyish sand, silt, pebble, and clay

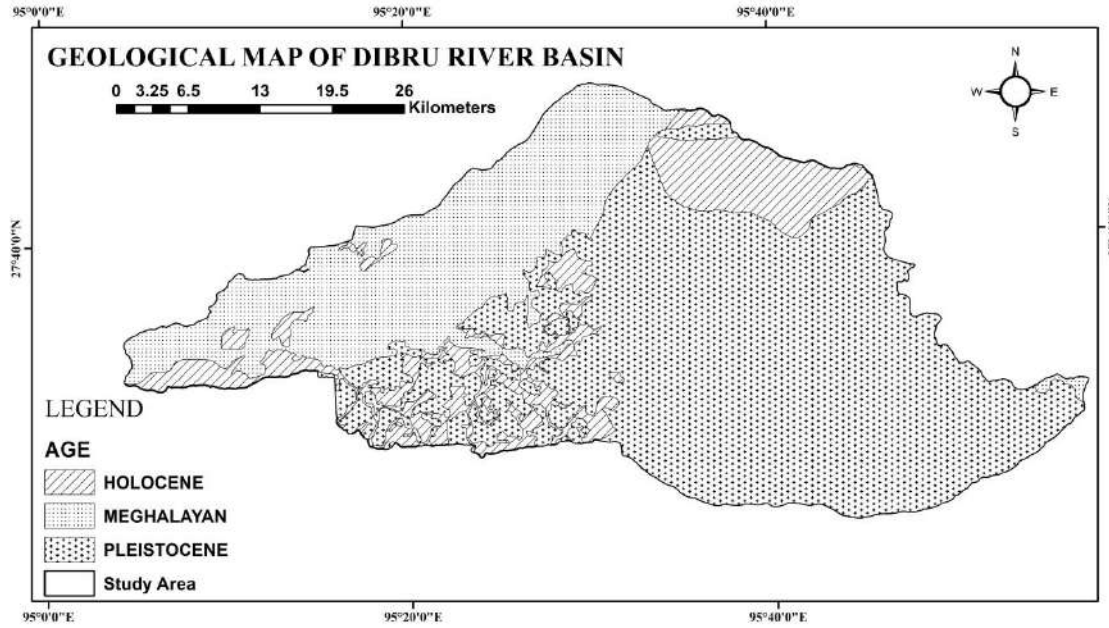

Fig. 18: Geology map.

Thus, it reflects the topographic, geomorphic, hydrologic, and environmental dynamics and impacts the domain of fluvio-geomorphology.

There is a number of factors that have contributed to the processes of soil formation in the Dibru River Basin. Among these factors, the most significant role is played by climate and lithology. Heavy rainfall has contributed to the leaching and lateralization process. Similarly, the diurnal and seasonal temperature variation has contributed to the occurrence of rocks' mechanical disintegration.

The topography and climate have played an essential role in the process of soil formation in the Dibru River Basin. The influence of these two features is more predominant in the rate of surface runoff and erosion. Further, biological features like decayed parts of plants and microorganisms play an essential role in soil formation. The sub-tropical vegetation of the Dibru River Basin the decayed parts and decayed parts of micro-organisms have accelerated the process of soil formation.

The soil of the Dibru River Basin can be classified as Fine-loamy, Coarse-loamy, Fine-Silty, and Sandy. The Soils of the Dibru River Basin have been broadly classified on the published soil map of the Dibru River Basin prepared by the National Bureau of Soil Survey and Land Use Planning (NBSS&LUP) Regional Centre Jorhat, Assam, India (Fig. 19). The soil of the Dibru River Basin can be classified into the following categories based on Soil Taxonomy. The different Soil Taxonomy is mentioned in Table 6.

Earthquake

Earthquakes are one of the most destructive natural hazards in Assam. Assam experienced several devastating events that led to many deaths and severe property damage in Assam. Geo-morphologically, Assam falls within the earthquake-prone zone of the Indian Sub-continent. Much of Assam lies in the Brahmaputra valley, except for a few in southern districts. Northern and Eastern valleys are bounded by Himalayan frontal thrust. Himalayan is a result of a continent-

Table 6: Soil Description of Dibru River Basin.

Soil Taxonomy	Description
Fine-clayey	Very deep, well-drained, clayey soils occur on the undulating plain with slight erosion
Fine-loamy	Very deep, well-drained, fine loamy soil occurring on undulating upland having a loamy surface with slight erosion
Coarse-loamy	Very deep, well-drained, coarse loamy soil occurring on undulating upland having a sandy surface with moderate erosion
Fine silty	Very Deep, poorly drained, fine silty soil occurring on very gently sloping flood plain having a loamy surface with moderate erosion
Sandy	Deep, well-drained, sandy soil occurring on the level to nearly level active flood plain having a loamy surface and severe flooding

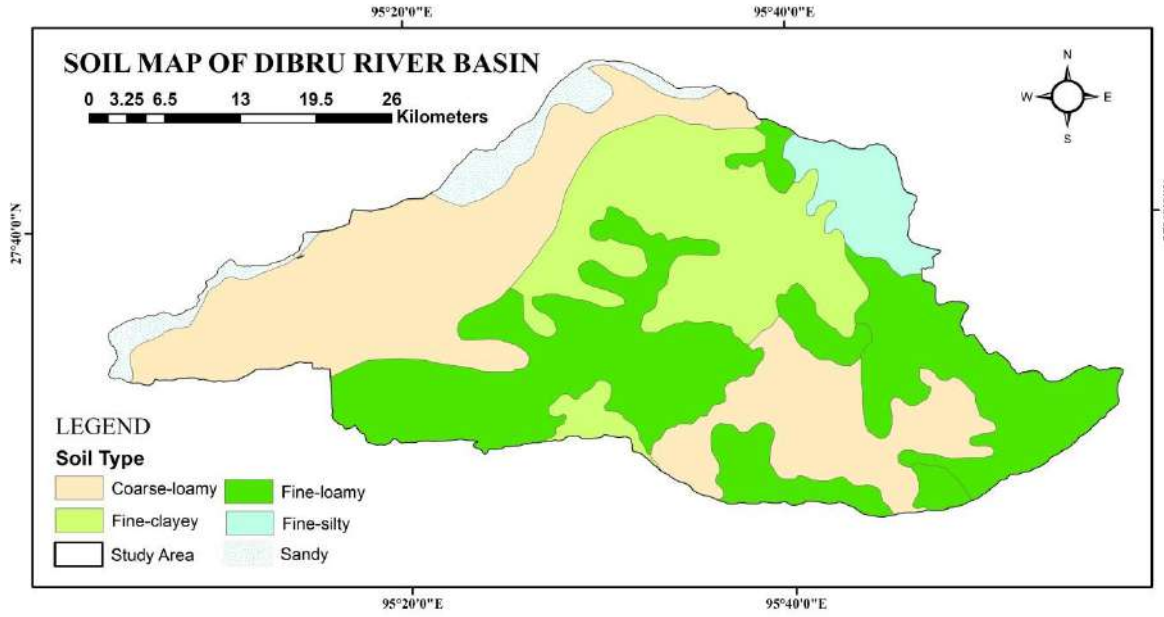

Fig. 19: Soil map.

continent collision with Eurasian plates. In the eastern part, there is Lohit and Naga thrust. In 1897 and 1950, large earthquake events occurred in Assam, and their magnitude was 8.7. According to some documents, these earthquakes were so intense that rivers changed their courses, and ground elevations were immensely affected. Sliced between two tectonic plate collision boundaries, the Himalayan in the north and the Indo-Burman in the east, the northeastern region is the seismically most active region of the world.

Anthropogenic Indication

The role of Anthropogenic in channel migration can be analyzed in terms of changes in the land use pattern. The alteration of the land surface, where the topsoil and vegetation lose their holding capacity of the soil, can lead to changes in the landscapes.

Table 7: Details of Flood-affected villages by lateral migration, Revenue Circle wise.

Parameters	Revenue Circle		
	Doom Dooma	Tinsukia	Chabua
Total village	317	108	19
Total households	48644	22827	1570
Total population	248835	113094	7853
Field surveyed village	04	01	03
Surveyed household	176	15	76
Surveyed population	3312	330	1261
Affected village	32	06	10
Recorded wiped-out villages	23	05	09
Recorded wiped-out household	757	77	426
Recorded the Population shift from wiped-out villages	7664	316	1261
Total village area lost **(hectares)**	4964.51	772.87	1954.85
Total no. of Tea Garden lost	03	02	01
Total no. of Tea Gardens on the urge of the trend of erosion	02	-	-
The total area of the Tea Garden lost (hectares)	522.25	401.83	28.0

Source: Village Map (Census 2011) and Field Survey

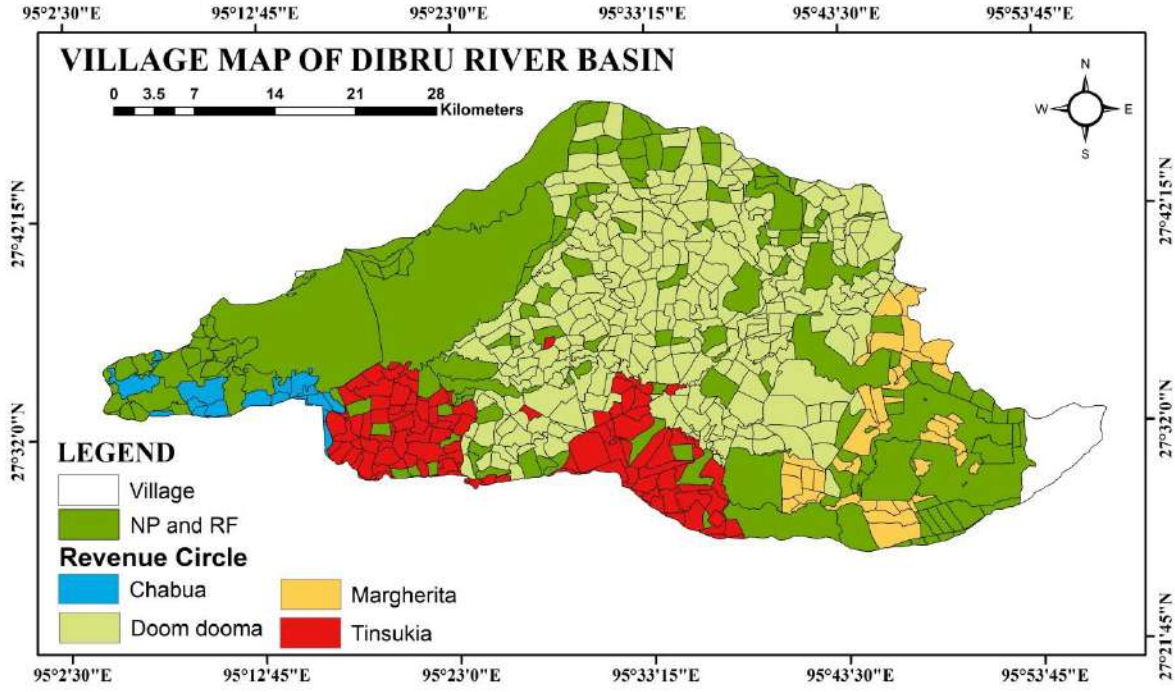

Fig. 20: Village map.

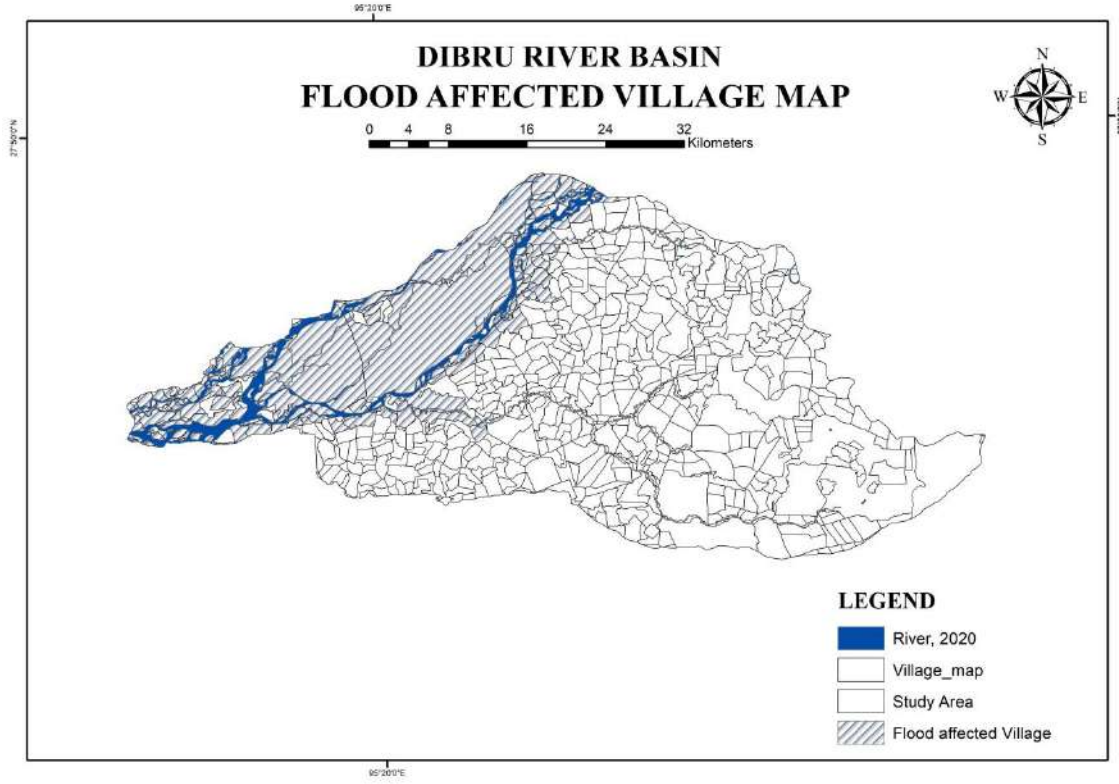

Fig. 21: Flood-affected map.

Consequences of Lateral Migration

Channel migration leads to many changes in the landscapes. They can erode the surface where many villages, tea gardens, households, horticulture, and poultry can lose their life and property. It is a natural process and is usually found in the lower course of each river in the plains region of Assam. Table 7 shows the details of flood-affected villages by the Lower course of the Lohit river, 2020. Since 1966, the river has expanded its wings in recent times and will continue in the future if we don't go for some preventive measures within the study area.

CONCLUSION

The study of the channel migration of the Lower Course of the Lohit river (Dangori) and the Dibru river concludes by using the application of GIS and remote sensing techniques, which helps us to give a glimpse of the channel migration and the nature of the channel. It is difficult to predict the nature of channel migration because of the nature and behavior of the river. Still, we can study the past 54 years of the behavior of the river course and the channel migration from the SOI toposheet and satellite imagery. Using multi-temporal satellite images of the Landsat sensor and LISS sensor of the resolution, we can detect the nature of their shifting and its consequences on the physical and cultural landscapes. Soil properties, Geology structure, tectonic activities, high discharge, precipitation, and the influence of human activities are the leading causes of the channel migration of the Lower Course of the Lohit river (Dangori) and the Dibru river. If we look at the hydro-geomorphic attributes, the profile of the dibru and dangori rivers is in the mature stage, and the river is in a sinuous pattern. This basic help in the shifting and migration of the channel and the channel slope is almost 0° which generally occurs in the plain region. Channel migration is also linked with the climatic indication and soil properties, as the soil of the study area falls in coarse-loamy and fine loamy. The region experiences a great variation of rainfall within and around the basin. The flow characteristic of the river mainly drives the channel migration because of high discharge. If we look at the graph (Fig.16), the discharge rate increased from 2011 to 2018, and the geology structure of the river falls in newer alluvium, as alluvium is linked with floodplain morphology. The most important significance of channel migration is to help to maintain the riparian ecosystem. Riparian ecosystem means the wetlands, ox-bow land, bills, etc. This riparian ecosystem is the home of many species and sustenance the livelihoods of the local people.

The avulsion process is observed within the study area's upper part. Due to this, the Sursa river and Ajuka river merged which led to the flow of the Lohit river within the study area and gave birth to a new channel course as the Lower Course of Lohit river in Dibru River Basin, Tinsukia District.

The rapid expansion of the lower course of the Lohit river led to flood, bank erosion, shifting, and deposition within the study area. In 1966, the channel is expanding its wing and caused much great havoc in physical and cultural landscapes. With the increase in population, the physical landscapes is been converted to cultural landscapes, and alter the changes in land use and land cover of the study area. The region is also fond of the seismic zone. The channel migration erodes many villages, households, and tea gardens near the bank of the river. A total of 37 villages had been wiped out because of channel migration, and 48 are almost affected due to flood and bank erosion problems (Fig. 21). People shifted from their original homeland to new land. Because of channel migration, 5 tea gardens had been wiped out and 2 are on the urge of the trend of erosion. If these problems continue with time, in the coming days many villages, tea gardens, and crop land will be under water. With the help of geospatial tools, we can analyze the rate of shifting and prepare a risk management map to bring awareness to the communities and government to look at these issues and try to mitigate the hazards.

REFERENCES

Azpiroz-Zabala, M., Cartigny, M.J.B., Sumner, E. J., Clare, M.A., Talling, P.J., Parsons, D.R. and Cooper, C. 2017. A general model for the helical structure of geophysical flows in channel bends. Geophys. Res. Lett., 44: 11932–11941. DOI: org/10.1002/2017GL075721

Brice, J.C. 1982. Stream channel stability assessment. Report FHW A/ RD-82/021, US Department of Transportation Federal Highway Administration, Washington, DC, p. 42.

Dragicevic, S., Pripuzic, M., Novkovic, I., Kostadinov, S., Langovic, M., Milojkovic, B. and Cvorovic, Z. 2017. Spatial and temporal variability of bank erosion during the period 1930-2016: Case Study- Kolubara River Basin (Serbia). Water, 9(10): 748. Doi:10.3390/w9100748.

Garcia, M.H., Bittner, L. and Nino, Y. 1994. Mathematical modeling of meandering streams in Illinois: a tool for stream 64 FD. Shields, Jr, A. Simon and L.J. Steffen management and engineering, Unpublished report, University of Illinois, Urbana, IL, USA, p. 49.

Heller, P.L. and Paola, C. 1996. Downstream changes in alluvial architecture: an exploration of controls on channel-stacking patterns. J. Sed. Res., 66(2): 297-306.

Hillel, D. 1998. Environmental Soil Physics: General Physical Characteristics of Soils. Academic Press, London, p. 3.

Horton, R.E. 1945. Erosional development of streams and their drainage basins: Hydrophysical approach to quantitative morphology. Geol. Soc. Am. Bull., 56: 275-370.

https.//censusindia.gov.in

Jones, L.S. and Schumm, S.A. 1999. Causes of avulsion: An overview. Spec. Publ. Int. Assoc. Sedimental., 28: 171-178.

Leopold, L.B. and Maddock, T. 1953. The hydraulic geometry of stream channels and some physiographic implications. Geol. Surv. Prof. Paper, 16: 252.

MacDonald, T.E., Parker, G. and Leuthe, D.P. 1991. Inventory and Analysis of Stream Meander Problems in Minnesota, St Anthony Falls Laboratory, University of Minnesota, Minneapolis, MN, USA, p. 37.

Mackin, H.J. 1948. Concept of the Graded River. Geol. Soc. Am., 55: 463-512.

Miall, A.D., 1996. The Geology of Fluvial Deposits. Springer-Verlag, Berlin.

Motta, D., Abad. J.D., Langendo, E.J. and Gracia, M.H. 2012. A simplified 2D model for meander migration with physically-based bank evolution. Geomorphology, 10: 163-164.

Sarma, J.N. and Acharjee, S. 2012. Bank erosion of the Brahmaputra River and Neo-tectonic activity around Rohmoria, Assam, India. Comun. Geol., 99(1): 33-38.

Sarma, J.N. and Phukan, M.K. 2006. Bank erosion and banking migration of the river Brahmaputra in Assam, India, during the twentieth century. Journal. Geol. Soc. of India, 68. 1023-1036.

Sarma, J.N., Acharjee, S. and Gogoi, C. 2011. Application of DEM, Remote sensing, and geomorphic studies in identifying a recent (or perhaps Neogene) upwarp in the Dibru River Basin, Assam, India. J. Indian Soc. Remote Sens., 15: 115. DOI 10.1007/s12524-011-0115-1.

Slingerland, R. and Smith, D. 1998. Necessary conditions for a meandering-river avulsion. Geology, 26(5): 435-438.

Whipple, K. & Tucker, G. 2002. Implications of sediment flux dependent river incision models for landscape evolution, J. Geophys. Res., 107: 44. https://doi.org/10.1029/200JB000044.

Whittaker, A.C., Cowie, P.A., Attal, M., Tucker, G.E. and Roberts, G.P. 2007. Bedrock channel adjustment to tectonic forcing: Implications for predicting river incision rates. Geol. Soc. Am., 35(2): 103-106.

Nature Environment and Pollution Technology
An International Quarterly Scientific Journal

p-ISSN: 0972-6268
(Print copies up to 2016)
e-ISSN: 2395-3454

Vol. 21 | No. 5 (Suppl) | pp. 2055-2071 | 2022

Original Research Paper

https://doi.org/10.46488/NEPT.2022.v21i05.004

Open Access Journal

An Overview of the Role of Smallholders in Oil Palm Production Systems in Changing Climate

Ahmed Abubakar and Mohd Yusoff Ishak†
Faculty of Forestry and Environment, Universiti Putra Malaysia, 43400 Serdang, Selangor, Malaysia
†Corresponding author: Mohd Yusof Ishak; m_yusoff@upm.edu.my

Nat. Env. & Poll. Tech.
Website: www.neptjournal.com

Received: 23-04-2022
Revised: 16-05-2022
Accepted: 01-07-2022

Key Words:
Smallholder
Oil palm
Food security
Climate change

ABSTRACT

Oil palm production contributes tremendously to the economies of tropical countries, a location where cultivation takes place. The cultivation of oil palm is usually dominated by smallholders and produces about 40% of global palm oil demand. Therefore, in this study, we aim to investigate the role of smallholder oil palm growers in ensuring palm oil production in a changing climate. This study was based on a conventional literature review. Relevant articles were retrieved using search terms such as "climate change" or "oil palm" or "climate change and oil palm" OR "oil palm smallholders" OR "oil palm growers". The documents were selected by (i) examining the title of the document, (ii) the abstract (iii) and the content of the document sequentially. Only documents that meet the inclusion criteria were selected for the review. The results of this study demonstrated that global climatic changes have a greater negative effect on oil palm production in the tropics. Rising temperatures result in water stress to the palms, as does variability in rainfall, which reduces productivity, declining floral abortion, increase in pests and diseases infestation, and yield loss. Oil palm smallholder growers contribute immensely to global food security. Smallholders are estimated to manage approximately 40% of the global oil palm planted area, producing 40% of the global palm oil demand. In Africa, smallholders produced more than 60% of palm oil demand, 33% in Papua New Guinea, and 40% in Malaysia. In Latin America, where 87% of oil palm growers are smallholders, they produce over 60% of the demand for palm oil. Oil palm production creates jobs and poverty alleviation, provides the most efficient oil, provides vitamins for body-building, and provides nutritious and healthy food. This study recommends long-term and short-term policies on climate change and oil palm, improved regional academic leadership, with a focus on collaboration with scientists in consumer countries, improved institutional research, and collaboration in research between producer and major consumer countries.

INTRODUCTION

One of the fastest-growing crops in Southeast Asia is oil palm (Food and Agriculture Organization 2009, Sheil et al. 2009, Paterson et al. 2018, Paterson 2019, Ahmed et al. 2021). In addition to being used in food all over the world, palm oil and palm kernel can be found in cosmetics, detergents, plastics, chemicals, and pharmaceuticals (Paterson et al. 2013, 2018). Furthermore, biodiesel from palm oil helps Malaysia meet its fuel needs (Paterson et al. 2009, 2013). By 2015, oil palm had surpassed all other edible oils as the most widely consumed globally (Boyce 2017).

About 72% of palm oil production is consumed by the processed foods industry, while the personal care and cleaning products industry consumes 18%, and the biofuels industry consumes 10% (Voora et al. 2019). Asia consumes almost 70% of all palm oil production in the world; China, India, and Indonesia consume 40% of all palm oil produced as food-grade. When the demand for palm oil is broken down by region, Asia is by far the biggest and fastest-growing consumer (Tullis 2019, Jadhav 2019). The European Union and the United States of America account for 14% of global palm oil consumption (Voora et al. 2019). Global vegetable oil and fat production primarily use oil palm as a source, which makes the plant a highly utilized one (Paterson et al. 2013). Globally, 3 billion people use palm oil as their primary energy and vitamin source (d'Enghien 2016). Among the top ten producers of oil palm are Indonesia, Malaysia, Thailand, Nigeria, Colombia, the Ivory Coast, Brazil, Costa Rica, and the Democratic Republic of Congo (Corley & Tinker 2003, Maluin et al. 2020). Oil palm production, for example, is a significant industry in Guatemala, accounting for approximately 1% of the country's GDP and 4.01% of export volume in 2018 (Guillaume & Soledad 2010). The top ten countries for palm oil exports include China, India, the Netherlands, Pakistan, the Philippines,

Turkey, the United States, Kenya, South Korea, and Italy (MPOC 2021).

In the late 19th century Africa began exporting palm oil and kernel and experienced rapid growth, although Malaysia and Indonesia were the first to establish commercial plantations. In the 1920s, plantations were established in the DRC Congo, as well as in some parts of West Africa. The plant is currently grown at latitudes of 19°N (Dominican Republic) and 15°S (Brazil) (Carr 2011). In 2017, Indonesia (USD 18.7 billion), Malaysia (USD 9.8 billion), and the Netherlands (reexport) (USD 1.2 billion) were the top three exporters of crude palm oil and its fractions (refined and unrefined). India (USD 6.5 billion), China (USD 3.5 billion), and Pakistan (USD 2.2 billion) were the biggest buyers (Brack et al. 2016, Workman 2019, Voora et al. 2019). According to the 2016 export figures, palm oil (crude) and palm kernel (refined) were valued at USD 28.2 and USD 3.7 billion, respectively. In 2016, the sector's (retail) market value was at least USD 65 billion, and it contributed significantly to the global economy: global GDP and tax revenues were boosted by USD 39 billion and USD 4.3 billion, respectively (Voora et al. 2019). According to Voora et al. (2019) "In 2013/2014, the sector provided 2.9 million downstream jobs, with people employed in industries that use palm oil derivatives to make food ingredients, pastries, margarine, animal feed, and personal care products".

Oil palm cultivation, both large and small-scale, has made a huge change to regions in the tropics, the lives of people, and the profit margins of palm oil companies. Oil palm has a high production rate and is easy to establish, which in addition to its low cost of operation makes it highly profitable; the crop is also highly efficient economically, and does not use much land, pesticides, and fertilizer (Dislich et al. 2017, Paterson et al. 2018). Palm oil is produced mainly by Malaysia and Indonesia, which together produce 85–90% of overall global palm oil production (Voora et al. 2019). Almost 2/3 (60%) of the global production of palm oil comes from plantations owned by corporations or states, while the rest comes from 3 million smallholder growers (Voora et al. 2019). Recognizing the importance of palm oil in global food security, food sources such as oil palm must be managed carefully in the face of changing climate (Paterson et al. 2013). A significant negative effect will be imposed by changing climate on the cultivation of oil palm, particularly by 2100 (Paterson et al. 2015, 2017). Plantations will expand in the event of climatic changes and variability, as new areas become available - assuming biodiversity issues are overcome - and oil palm growers will need to adjust their methods to the changing climate (Rival 2017, Paterson et al. 2018).

The capability of oil palm growers to produce nutritious palm oil and allied products in sufficient quantities to meet local needs while meeting growing global demand is critical to the development of global food security (Nesadurai 2013, Khatun et al. 2020). Millions of households in developing countries face the globally critical threat of food security, which is an issue that must be solved by ramping up the processes of food production while overcoming the issues of advancing climate change and damage to the environment (FAO 2010). Palm oil is widely acknowledged to be the most efficient plant-derived oil, with the potential to feed the progressively increasing universal population (Meijaard et al. 2018, Weckx et al. 2019, Maluin et al. 2020). Due to such benefits to rural Malaysians and Indonesians, palm oil has now become a remarkable factor in lessening poverty, etc. (Santika et al. 2019), inevitably raising the standard of living of these households and allowing them to have access to improved healthcare and education (Qaim et al. 2020). In addition to meeting the universal demand for non-renewable resources and meeting food security challenges, palm oil is an optimal key solution for food crises and insecurity (Nesadurai 2013, MPOC 2019).

This study employed a conventional literature review to provide a current overview of the effect of changing climate on oil palm production and the role of oil palm smallholders in palm oil production. Several search engines were used to find articles relevant to this study, including Web of Science, Scopus, Elsevier, ProQuest, ResearchGate, and Google Scholar. Documents were found using suitable and appropriate search terms, such as "climate change" OR "oil palm" "climate change and oil palm" OR "oil palm smallholders" OR "oil palm growers" and so on. At this stage, the title and abstracts of the searched documents were thoroughly reviewed to categorize them into various themes and associations. Duplicate documents were removed, and the relevant documents were saved for future reference. Documents and articles that were not published in English, as well as articles that predated the year 2000, were excluded. The objective of this study is to investigate the role of smallholder oil palm growers in oil palm production in a changing climate. Oil palm's international importance as a vegetable oil source is a comparatively new phenomenon, boosted mainly by the initiative of Malaysian businesses and government over the past 3 to 4 decades, which established the crop and developed the industry through constant research support (Carr 2011). The findings of this study have the potential to benefit policymakers/stakeholders and the palm oil industry by providing mechanisms to adapt to the effect of climatic changes as well as enhancing the capacity of smallholders to improve oil palm production for global food security.

MATERIALS AND METHODS

Phase 1: Searching and Identification of Documents

Documents and articles pertinent to this review were obtained from reliable database systems such as Google Scholar, Scopus, ProQuest, Elsevier, and Web of Science. Documents and related articles were obtained from search engines via relevant search terms such as "climate change" OR "oil palm" or "climate change and oil palm" OR "oil palm smallholders" OR "oil palm growers" etc. Initial search 1,500 documents were returned from the search engines.

Phase 2: Screening and Selection of Relevant Documents

In this stage, the title, abstracts, and content of the searched documents were comprehensively reviewed and evaluated for categorization into various themes, topics, and associations. Duplicate documents were sorted out and the relevant original documents were retained for further review. Documents that were not written in English were excluded, as well as articles that pre-dates the year 2000 (Table 1).

Phase 3: Inclusion and Exclusion Criteria (Table 1)

Phase 4: Reviewing of Included Articles

Documents included in this review were selected from articles that specifically indicated in their titles or abstracts commitments to oil palm smallholder and food security directly or indirectly. Also included were full-text reviews and assessments of documents that reported the role of oil palm in feeding the world and the economies of oil palm smallholders. Papers that reported difficulties faced by smallholders in changing climate and the effect of changing temperature and rainfall on oil palm were also included.

Oil Palm

A native of West Africa, the oil palm (Elaeis guineensis), is normally found between Angola and The Gambia (Dislich et al. 2017, Nambiappan et al. 2018). The oil palm range in West African forests, where semi-wild palm trees have long grown around farmsteads and supported village economies (Carr 2011). The species is widely utilized in palm oil production (Corley & Tinker, 2003, Dislich et al. 2017, Nambiappan et al. 2018). Palm plantations have been established widely in many tropical countries where the climate is favorable. Oil palm is widely regarded as a highly efficient and profitable oil crop globally, which is easy to set up and establish, requires minimal capital, and has high-yielding productivity (Wahid et al. 2005). Oil palm is now farmed in the lowlands of tropical-humid countries (about 18.1 million hectares spread over 43 nations); production, 7.1 million hectares in Indonesia, and 4.6 million hectares in Malaysia, together make up approximately 85% of global palm oil production output (Dislich et al. 2017). Oil palm can be grown on various soil types, even on soils not favored by most other crops, within a pH range of 4-8 if sufficiently moist (Corley & Tinker 2003, Paterson et al. 2013).

Water is essential for oil palm growth, flowering, and fruit development. The range, distribution, and parameters relating to rainfall must be taken into consideration when selecting suitable plantation areas. A suitable amount of rainfall for oil palm trees is between 2,000 and 3,000 millimeters per year, or more than 200 rainy days annually (Carr 2011, Unjan et al. 2017). At temperatures below 15°C, growth may cease. Maximum and minimum temperatures range from 30-32°C and 21-24°C, respectively. (Paterson 2013, Ahmed et al. 2021, Abubakar et al. 2021). Oil palms are sensitive to high temperatures, with photochemical efficiency declining to above 35°C (Paterson et al. 2013). Palms require a relative

Table 1: Criteria for including and excluding retrieved articles.

Inclusion	Exclusion
Documents published in English	Documents not published in English
Google Scholar, Scopus, ProQuest, Elsevier, and Web of Science	Articles, textbooks on purchase or request
Documents indexed in Web of Science, Scopus, Elsevier, ProQuest, ResearchGate, and Google Scholar from 2000 to 2021	Pre-2000 documents that are not available through Web of Science, Scopus, Elsevier, ProQuest, Research Gate, or Google Scholar
Reviews, conferences, and articles	Magazine articles, patents, films, television broadcasts, generic documents, and statutes
Phase 2: title, abstract and full-text review	
Oil palm	Another crop rather than oil palm
Oil palm smallholders	Non-smallholders
Climate change and adaptation	Mitigation, the vulnerability only
Smallholders and food security	Large scale growers
Role of palm oil	Other vegetable oils

humidity between 75 and 80% and solar radiation should be not less than 16 or 17MJ m^{-1} d^{-1} (Unjan et al. 2017, Oettli et al. 2018); it also does not grow in areas subjected to continuous flooding (Carr 2011, Paterson et al. 2013). Palm oil production costs are minimal compared to other plants as it requires a comparatively low input of fertilizer (Dislich et al. 2017). The production capacity of oil palm trees reaches its maximum at age 9-18 years (USDA FAS 2012, Dislich et al. 2017). The palm tree normally reaches a height of approximately 10 m and is productive for 25-30 years before needing to be replanted (Corley & Tinker 2003, Abubakar et al. 2021).

Climate Change Impact on Oil Palm Production

In most parts of the world, weather and climate are the most important factors influencing oil palm productivity (Zhai & Zhuang 2009). Agricultural regions have seen a rapid evolution of climate change in the past few decades with a broad increase in atmospheric carbon dioxide (CO_2) throughout the world (Lobell & Gourdji 2012). The essential confidence that climatic changes and CO_2 will persist in the long term tends to raise several concerns on the security of food supply and agricultural production, a key question is how climatic variations would then affect global crop production (Lobell & Gourdji 2012). The Intergovernmental Panel on Climate Change has outlined the Low Emission Scenario (B1) and the High Emission Scenario (A1FI) as a means of determining global temperatures which predict to rise by 1.8°C to 4.0°C, which will negatively impact oil palm and other crop production (IPCC 2007a). Several factors contribute to the effect of climate change on oil palm, including changes in pests and diseases, site conditions, and climatic conditions (Fleiss et al. 2017, Paterson 2021). When growing conditions are unfavorable for oil palm, for example, temperatures that are higher or water deficiencies, the trees may be more susceptible to pests and diseases, resulting in lower yield. The pollination of oil palm may also be negatively declined as a result of changing climate, which results in lower yield (Fleiss et al. 2017). In most cases, climatic factors such as temperature and rainfall, as well as abiotic factors such as diseases, pests, and pollinators, will have a negative effect on the cultivation of palms (Rival 2017, Paterson 2020). Rising temperatures, deviations in rainfall records, droughts, floods, and persistent extreme weather are all evidence of climate change (Tang 2019). The quality, quantity, and price of palm oil produced per palm depend on the weather conditions and variabilities (Shanmuganathan & Narayanan 2012).

As a result of climate change and its indirect effects, palm production in Malaysia has decreased (Zainal et al. 2012). Malaysian CPO production fell by 3.3% in 2009 (MPOB 2010). In Western Malaysia, the average FFB fell by 7.5%, 4.7% in Sabah, and 2.6% in Sarawak (See Fig. 1 for global oil palm FFB production in 2018) (MPOB 2010). A higher number of abortions, elongated inflorescences, reduced productivity, rotten fruit bunches, water stress, and colonization of lance leaves (fronds) are other impacts of climate change on oil palm production (Ahmed et al. 2021). These significantly decreased productivity in oil palm globally. Climate change reduces male and female flowering, dehydrates tissue and cells, and reduces nutrient uptake (Abubakar et al. 2021). Other impacts include; general metabolism disruption and negative effects on photosynthesis; rising temperatures cause pests and diseases pandemics by changing the fertility and life-cycle of the pests, as well as influencing the pollination process and changing the mode of operation of pollinating insects such as *Elaeidobius kamerunicus* (Ahmed et al. 2021).

The Effect of Changing Temperatures on Oil Palm Production

The impact of changing temperatures on oil palm production is wide-ranging. When temperatures rise by 1-4°C, there will be a 10-40% decrease in palm oil production (Sarkar et al. 2020). Changes in temperature that results in drought conditions would cause approximately 208,000 ha of the present cultivated areas to become marginal and unsuitable for oil palm production in Malaysia (Zainal et al. 2012). A rise of 2°C in temperature could lower oil palm yields by 30% (MNRE 2010, Paterson et al. 2018, Abubakar et al. 2020). A warmer environment results in the quicker evaporation of soil water, causing water stress on the palms and a more intense effect of dry periods (Oettli et al. 2018). These result in loss of FFB yield, disruption in photosynthesis and respiration, and general metabolism of the palms (Fleiss et al. 2017). Although warming alone is unlikely to have severe impacts, projections indicate that oil palm cultivation in Southeast Asia will become challenging in 2100 as global temperatures are projected to rise (Corley & Tinker 2015, Paterson et al. 2015). For example, Zainal et al. (2012) reported that for every 1°C rise in temperature, oil palm revenue is expected to decline by RM 44.52 (USD 10.63), RM 45.60 (USD 10.89), and RM 37.70 (USD 9.01) for Peninsular Malaysia, Sabah, and Sarawak. The future projection indicates that on average, oil palm losses will be (RM/hectare) RM 341.29 (USD 81.52) by the year 2029, RM 127.43 (USD 30.44) by the year 2059, and RM 51.80 (USD 12.37) by the year 2099 for Peninsular Malaysia, Sabah and Sarawak respectively (Zainal et al. 2012).

The Effect of Changing Rainfall on Oil Palm Production

Rainfall has a marginal effect of reducing net revenue per hectare by RM 4.59 (USD 1.10) and RM 1.60 (USD 0.38) for Sabah and Sarawak, respectively (Zainal et al. 2012). A water deficit of 100 mm in an oil palm plantation during the phase of sex determination reduces yield by 6% (Ambar Suharyanti et al. 2020). In contrast, the decline in productivity during the floral abortion phase is more signed up to 7% and has a greater effect on bunch quantity as opposed to bunch weight (Ambar Suharyanti et al. 2020). A study by Carr (2011) indicates that increasing the water deficit by 100 mm in a single year can result in an 8-10% reduction in production the following year, and a 3-4% reduction the following year. Similarly, Corley & Tinker (2015) gave a more detailed explanation concerning water deficit; in the flowering phase of the plant, a 100 mm water deficit can adversely affect the following three components: 1) floral initiation (1-3% yield loss per 100 mm water deficit); 2) sex determination (3-4% yield loss per 100 mm loss); 3) floral abortion (8-10% yield loss per 100 mm loss).

A study conducted on the influence of water and nutrient management on oil palm yield trends on a large-scale plantation in Ghana indicates that as the water deficit increases, oil palm production decreases in tandem, the results of the research can be summarised as follows: A yearly water deficit of 150 mm yields 22-25 tonnes/ha FFB, a yearly water deficit of 250 mm yields 16-18 tonnes/ha FFB, and a yearly water deficit of 400 mm yields 6-7 tonnes/ha FFB (Rhebergen et al. 2019). Similarly, Carr (2011) reported that each 100 mm rise in soil water deficit results in a loss of approximately 10% in productivity. Moisture shortages in oil palm plantations can be the reason for lower nutrient uptake in oil palm trees (Teh 2016, Shafiq 2017), which impacts flower development and causes a rise in abortion, lowered productivity, and extended inflorescences that last about 8-9 months (Shafiq 2017, Woittiez et al. 2017). Two months consecutively or longer of reduced rainfall will result in a depressed oil extraction rate about 11 months later (Muhamad Rizal & Tsan 2008). Higher rainfall, which caused flooding, reduced crude palm oil (CPO) production and quality, with the events being attributed to influencing the ripening process of the FFB and reflecting on the yield in later months (Shanmuganathan et al. 2014).

Climate Change Adaptation for Oil Palm Sustainability

Adaptation to climate change involves "adjustment in natural or human systems in response to actual or anticipated climatic stimuli or their effects, which mitigates harm or capitalizes on beneficial opportunities" (IPCC TAR 2001). Oil palm growers specialized in adapting to climate change. Recent techniques for adaptation were employed to address the effect of climatic changes and variability in plantations. These adaptation options include; the use of improved variety, soil, and water conservation practices, mulching, silt pit, agroecological practices, such as sustainable use of recommended fertilizer, integrated pest management, frond management, land clearing without slash burning, intercropping, patronizing extension services, access to government subsidies and incentives, livelihood diversification, loan and or credit, buying of crop insurance, etc (Nabara & Norsida 2018, Abubakar et al. 2021)

Oil Palm and Global Food Security

Food security is a general concern globally, with the FAO reporting that over 815 million people are chronically malnourished (FAO 2020). Essentially palm oil had an important role to play in feeding and nourishing the world, both directly and indirectly, and will go on to play a vital part in addressing this issue head- on (Nesadurai 2013, Vel et al. 2016, Sibhatu 2019, Ayompe et al. 2021). At the 1996 World Food Summit, food security was defined as "existing when all people, at all times, have physical and economic access to sufficient, safe, and nutritious food that meets their dietary needs and food preferences for an active and healthy life" (FAO 2008). Food security "is determined by availability (having an adequate supply of suitable food), access (having enough income or other resources to access food), and utilization/consumption (having adequate dietary intake and the ability to absorb and use nutrients in the body)" (Molotoks et al. 2021). The role of palm oil in food security has not been fully explained as a topic in literature (Hervas 2021). The development of oil palm has some success in alleviating poverty, improving food security, and contributing to employment and economic development, especially in Malaysia and Indonesia (Hervas 2021, Ajonina & Okanyene 2021). Ajonina & Okanyene (2021) reported that oil palm production has increased food security in Cameroon.

Global Oil Palm Production

Many countries grow a small amount of oil palm, but only two dominate the global market: Indonesia and Malaysia (Abubakar et al. 2021). In terms of oil palm planted area, Indonesia has (7.1 million ha) (Dislich et al. 2017), Malaysia (has 5.9 million ha), Thailand (has 2.3 million ha), Colombia (524 thousand ha), Guatemala (has 190,000 ha), Ecuador (290,000 ha), and Cameroon (250,000 ha) in 2019 (Ordway et al. 2017, MPOC 2021, Statista 2021a). The expansion of oil palm plantations occupies 24% (4.5 Mha) hectares globally (Ordway et al. 2017). There were 16 million hectares of oil

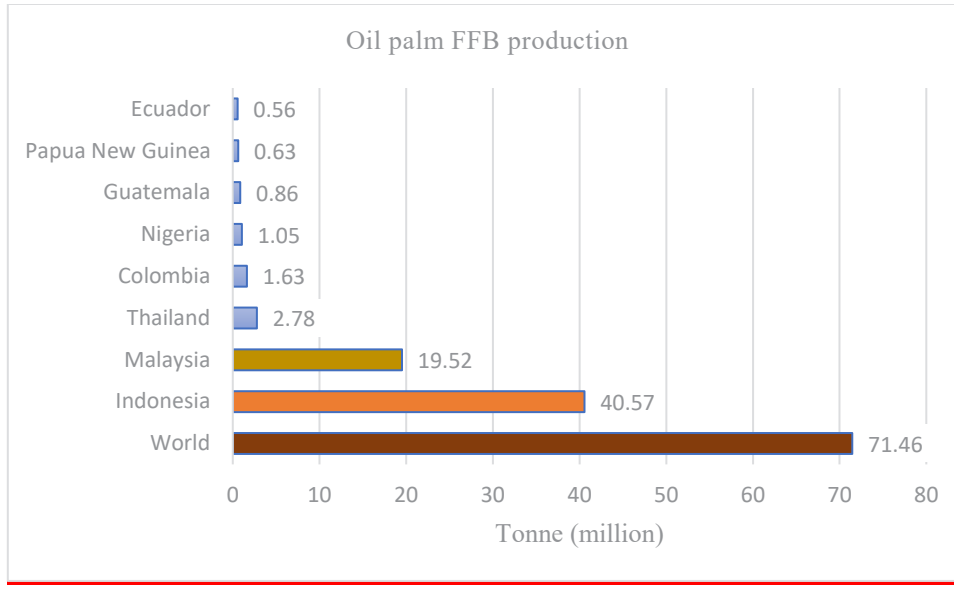

Fig. 1: Oil palm FFB production in 2018.
Source: Oil World (2021)

palm planted globally between 1990 and 2010, accounting for approximately 10% of the global land under permanent crops (Pirker et al. 2016). The planting areas in Malaysia and Indonesia increased by 150% and 40%, respectively, as a result of this dynamic development (Pirker et al. 2016, Killeen et al. 2013).

In the past half-century, the production of palm oil has increased dramatically (Abubakar et al. 2021). Total global output in 1970 was only 2 million tonnes, and this has more than tripled: global output in 2018 was 72 million tonnes (See Fig. 2 for global palm oil production) (Hannah & Max 2021). Indonesia produced 57% of this (41 million tonnes),

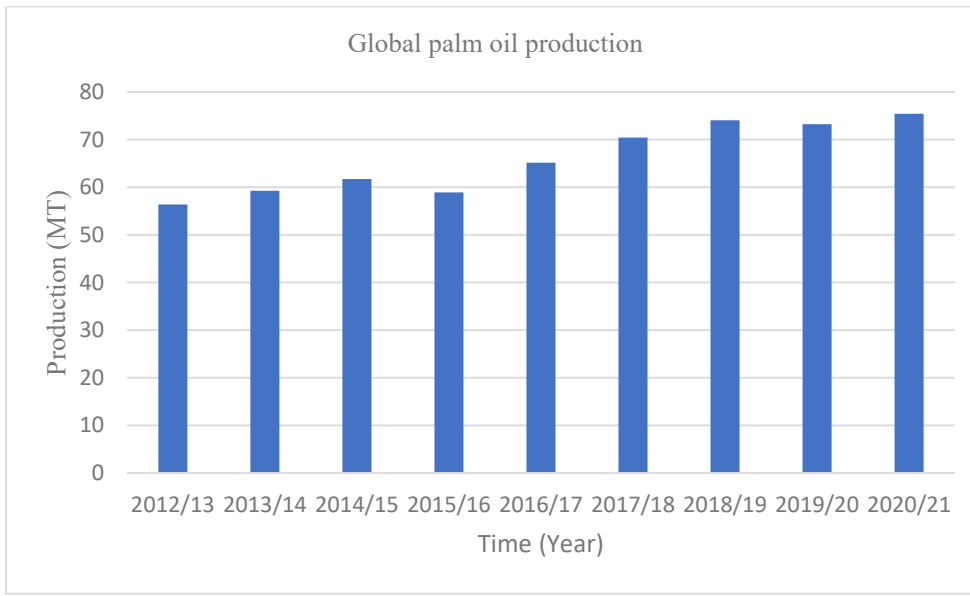

Fig. 2: Global trend of palm oil production (Statista 2021).

Table 2: Palm oil production by country in 2020.

Country	Productions (tonnes/million)
Indonesia	48.3
Malaysia	19.7
Thailand	3.1
Colombia	1.6
Nigeria	1.28
Philippines	0.90
Guatemala	0.88
Sierra Leone	0.75
Benin Republic	0.75
Honduras	0.60
Papua New Guinea	0.56
Angola	0.55
Côte d'Ivoire	0.51
Cameroon	0.46
Ghana	0.36
Cost Rica	0.27
Mexico	0.23
Peru	0.20

Statista (2021) and United States Department of Agriculture (2021).

with Malaysia producing 27% (20 million tonnes). Table 2 presents palm oil production by country in 2020.

Global Palm Oil Consumption

Global consumption of palm oil had surpassed 73 million metric tonnes by 2019/2020, with that figure expected to rise to roughly 75.45 million metric tonnes in the subsequent year (Statista 2021a). In Germany, the food sector consumption of palm oil and palm kernel oil was 246,500 tonnes and 30,100 tonnes respectively in 2017 (Meo Carbon Solutions 2018). In 2017, the feed sector consumed approximately 148,250 tonnes of palm oil in Germany, while pharmaceuticals and other chemical industries consumed approximately 120,000 tonnes of palm oil and 15,000 tonnes of palm kernel oil (Meo Carbon Solutions 2018). Oil palm domestic consumption by country in 2021 showed that Indonesia consumed about (15,225MT), India (8,550MT), China (7,170MT), EU-27 (6,765MT), Pakistan (3,495MT), Malaysia (3,450MT), Thailand (2,677MT), Nigeria (1,740MT), Bangladesh (1,630MT), and USA (1,470MT) (USDA 2021a, 2021b). Palm oil consumption in Colombia was estimated to be more than one million metric tonnes in 2019, while consumption in Brazil was estimated to be (750,000 MT). In contrast, the consumption of palm oil in Venezuela was estimated to be only (58,000 MT) that year (Statista 2021a). In 2019, about 500,000 MT of palm oil was consumed domestically in Cameroon (Statista 2021a). In the year 2019, Latin America accounts for 1.1 million MT of palm oil consumption (Statista 2021a). Global palm oil consumption is shown in Fig. 3.

The Role of Palm Oil in Feeding the World

Alleviating Poverty

Following years of decline, the trend of global hunger has increased since 2014 (FAO et al. 2018). Overall, the global percentage share of people who are malnourished rose to 10.6 % in 2015, and then declined to 11 % in 2016 (United Nations 2018, Molotoks et al. 2021). In 2017, the global undernourished population was estimated to be 821 million, or roughly one in every nine people (FAO et al. 2018). This increase in food insecurity represents a momentous risk of being unable to meet the Sustainable Development Goal (SDG) target of which by 2030, hunger

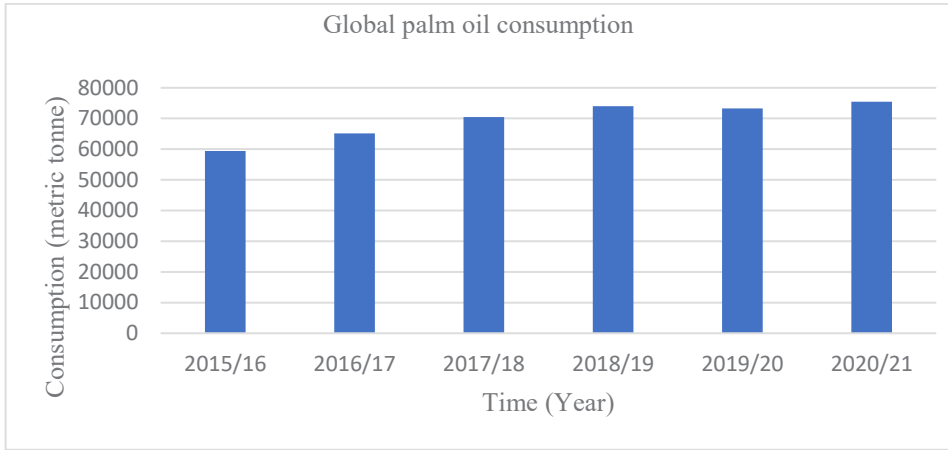

Fig. 3: Global palm oil consumption (Statista 2021).

will be eradicated (FAO et al. 2018, Molotoks et al. 2021).

Oil palm cultivation is increasingly being promoted by Indonesia and Malaysia as a means of alleviating poverty and promoting development in jungle areas (Majid Cooke 2012, Potter 2012, Santika et al. 2019). Other developing countries taking similar steps are Brazil, Peru, Colombia, Nigeria, Gabon, Ghana, and Rwanda (Villela et al. 2014, Byerlee et al. 2009, 2017, Meijaard et al. 2018). The Malaysian plantation sector employs a large number of people, guaranteeing many rural residents a monthly income and employment, and over 2 million people rely on the palm industry for a living, aside from providing economic benefits to the country and job opportunities (Ahmad et al. 2020). More than 600,000 Malaysians are engaged effectively in the oil palm industries, which includes both skilled and unskilled labor. According to Basiron (2007), "the quality of life of people has improved as a result of their involvement in cultivation or downstream activities". The oil palm industry employs 1.7–2 million people in Indonesia (Wakker 2006, Zen et al. 2006). Agricultural smallholders in Indonesia have an average annual household income of IDR 30,417,441 (USD 2,132), with oil palm farming making up 85.8%, non-oil palm farming at 8%, and farming at 6.2% (Ramadhana et al. 2021). More than 63% of the household income of smallholders comes from oil palm-based activities in Indonesia (Susila 2004). In Malaysia, oil palm accounts for 66.7% of smallholders' income (Dayang Norwana et al. 2011). The proportion of oil palm-related assets in total household assets is also very high, estimated to be around 63-72% in Indonesia (Susila 2004). Oil palm growers in Nigeria earn between N35,000 and N40,000 per month, employing up to 4 million people and providing income to many growers and their families (High Carbon Stock 2015). In Peru, smallholder farmers earn about USD 3,336 annually from oil palm plots, which can go up to 14,500/USD/ha/year when prices are at their highest (Bennett et al. 2019).

There are two types of planters identified in the palm oil sector. The organized companies are in contrast to the smallholders and the independent growers. A variety of businesses are available in the oil palm production and processing channel, counting on producers, milling units, relationships among industries and producers, and intermediary actors (Feintrenie 2013). In comparison to scheme and managed smallholder households, independent small-scale farmers have incomes that are lower monthly from oil palm cultivation (IDR 2.17 million) (USD 189.18) (Lee et al. 2014). The income and consumption of households are adversely affected by these factors (Santika et al. 2019). Palm plantation expansion in some areas has resulted in higher incomes, especially among smallholder and wealthier growers (Shahputra & Zen 2018, Santika et al. 2019). Nevertheless, the economic benefits of oil palm differ significantly between locations that have varying biophysical characteristics and communities with dissimilar starting socioeconomic situations (Shahputra & Zen 2018, Santika et al. 2019). Similarly, Santika et al. (2019) in their study of Kalimantan oil palm farmers, recorded an overall rise in the base indicators of physical and financial well-being between 2000 and 2014. Usually, rural areas where oil palms are grown tend to have lower average rural poverty, such as in North Sumatra, Riau, Central Kalimantan, and Southern Nigeria (Shahputra & Zen 2018). For example, in five years, Riau experienced a decline in rural poverty from 21% to 10% (2009-2013). It is clear that, in terms of gross development disparities, the cultivation of oil palm has lowered the disparity between Java and the outer islands of Indonesia significantly (Shahputra & Zen 2018). Ramadhana et al. (2021) observed several factors like "household income, level of education, family size, family members earning an income, number of children attending school, and amount of credit taken by the household that has a strong and positive effect on the expenditure of oil palm smallholders".

In terms of wide-ranging benefits, according to the industry, the oil palm sector employs nearly 6 million individuals, most of whom are elevated out of economic hardship (Goenadi 2008). The cultivation of oil palm provides a consistent cash inflow from consistent yields and ever-present demand, which has given money to thousands of smallholders to invest in plantations and environmental improvements and to provide an education for their families (Jezeer et al. 2019). Oil palm has also aided in the reduction of disparities between urban and rural populations. It has improved access to healthcare and education for rural populations, ensuring a higher quality of life and standard of living for themselves and their children.

The Most Efficient Vegetable Oil

Approximately 9.1 billion people will live on the planet by 2050, an increase of 34% from the current figure (FAO 2009). Feeding ever-growing and possibly urban populations, food production must increase by 70% (FAO 2009, 2017). The estimated annual quantity of oils and fats to meet this demand will be 150 million additional tonnes of oils and fats (d'Enghien 2016). It is a significant challenge to produce 150 million tonnes of oil (d'Enghien 2016) from the point of edible oil resources and the perspective of which plants can compete with oil palm. Oil palm is the only vegetable oil plant that meets all standards on all environmental measures when compared to sunflower, rapeseed, soybean, and others

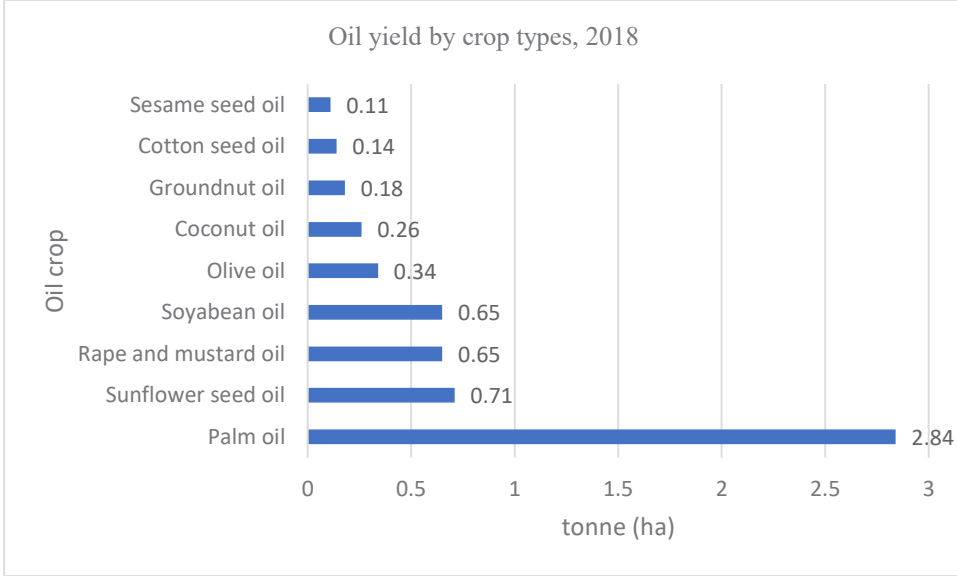

Fig. 4: Oil yield by crop types, 2018.
Source: Oil World 2020.
Note: Global oil yields are measured as the average amount of vegetable oil produced per hectare of land. This is different from the total yield of the crop since only a fraction is available as vegetable oil.

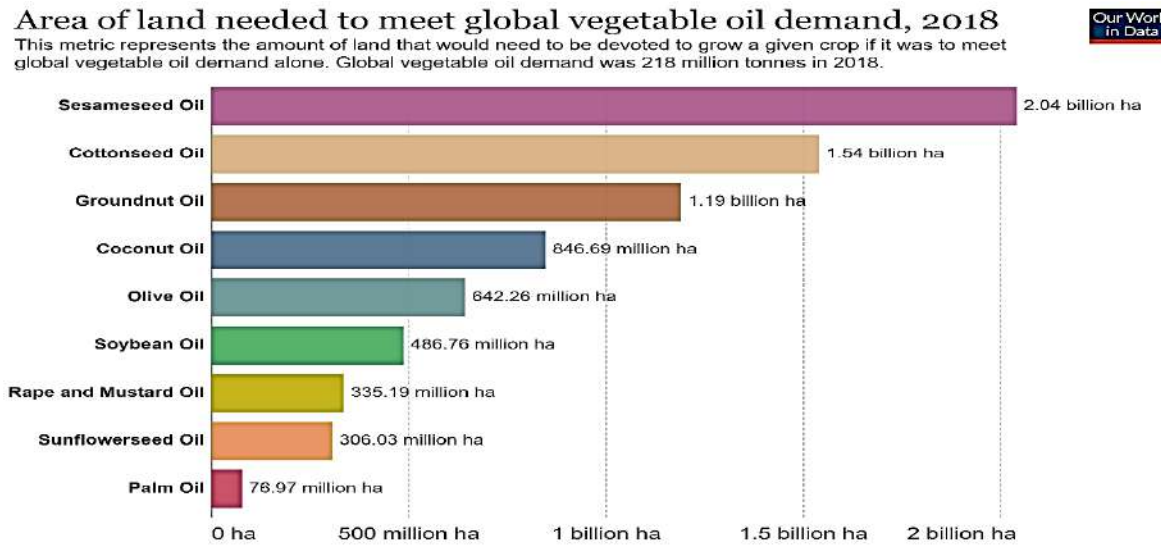

Fig. 5: The amount of land required to meet global vegetable oil demand.
Source: Calculated by Our World in Data based on data from the UN Food and Agriculture Organization (FAO)
OurWorldInData.org/palm-oil CC BY

(Basiron & Chan 2004, Tang & Al Qahtani 2020). Fig. 4 presents oil yield by crop types, 2018.

For example, soybean will necessitate 400 million ha of farmland, 187 million ha of rapeseed, and 250 ha of sunflower (d'Enghien 2016). Palm oil, on the other hand, will require only 38 million ha of farmland (d'Enghien 2016). It is ultimately the most versatile and efficient vegetable oil crop on earth, which produce more oil per hectare as compared to other plants that produce vegetable oil (Murphy 2014). When compared to many oil-bearing plants, oil palm produced 4-10 times the amount of oil per unit area (Roundtable on Sustainable Palm Oil 2017). The push to replace oil palm

would then necessitate the use of more land, as well as the use of more fertilizer and pesticides (d'Enghien 2016). The issue of food security, in contrast, is critical for the developing world and future generations (Pawlak & Kołodziejczak 2020). Palm oil is an existing lifeblood of the developing world with about 3 billion people worldwide currently using palm oil for its high energy and vitamin content, including India, Sub-Saharan Africa, and South-East Asia (d'Enghien 2016). As the struggle for available land grows, the potential for oil palm to produce a higher quantity of food from a lower acreage will be even more critical (Varsha et al. 2016, d'Enghien 2016, Khatiwada et al. 2021). Fig. 5 presents the amount of land required to meet global vegetable oil demand.

Vitamin Supplementation

The World Health Organization (WHO) estimates that approximately 190 million children of preschool age in developing nations, particularly in Africa and Southeast Asia, lack vitamin A in their diets (WHO 2011, Loganathan et al. 2017). These result in liver disorder, impaired immunity, stunted growth, and hematopoiesis, and cause rashes and other distinctive ocular effects (e.g., xerophthalmia, night blindness) (Sommer 2008, Akhtar et al. 2013, Stevens et al. 2015). There is widespread use of palm oil in the food and nutrition industries due to its versatility and balanced fatty acid content (~50% saturated, ~50% unsaturated) (Daud et al. 2012). Furthermore, pro-vitamin A and vitamin E are also found abundantly in crude palm oil (Daud et al. 2012). There are a high number of carotenoids (500-700 ppm) and vitamin E (600-1000 ppm) in crude palm oil (Daud et al. 2012). CPO has the potential effectiveness in overcoming deficiencies of vitamin A in children and pregnant women, improving vitamin A deficiency that results in ocular problems, as protection against ischemic heart disease, promoting normal reproductive potential in males and females, aid in diabetes management, ameliorate harmful effects of chemotherapy, and aiding in the management of hypobaric conditions (Loganathan et al. 2017). Palm oil contains a variety of trace components that benefit humans, which include tocotrienols, tocopherols, and carotenoids. Tocotrienols and tocopherols are vitamin E family members that possess well-publicized health benefits, including having antioxidant, anti-inflammatory, anticancer, neuroprotective, and skin protection actions. They also benefit cognition, bone health, and longevity, as well as reducing plasma cholesterol levels (Cestaro et al. 2017). Several studies conducted in Europe, South Africa, India, Burkina Faso, Tanzania, and Nigeria found that intake of palm oil improved Vitamin A status in children, adults, and pregnant and lactating women (van Stuijvenberg et al. 2020, Lietz et al. 2001, 2006, Olmedilla et al. 2002, Ajose et al. 2004, Zeba et al. 2006, Daud et al. 2012). The use of CPO in edible cooking could solve the problem of vitamin deficiency, particularly vitamin A deficiency, in countries where deficiency is a public health issue (Daud et al. 2012).

Producing Nutritious and Healthier Food

Palm oil has a distinct composition that prevents it from containing trans fats. Trans fat is unhealthy, and many health authorities, including the WHO, now advise against it because it has been clinically proven to increase the risk of cardiovascular disease (Ismail et al. 2018). Aside from being a source of fatty acids, and various vital fat-soluble micronutrients, it also has a high calorific content, which provides us with the energy we need to perform our daily activities (MPOC 2021). According to Singh (2014), "Palm oil supplies fatty acids as well as important fat-soluble micronutrients like carotenoids (including pro-vitamin A), vitamins D, E and K". In relation to other vegetable oils, unrefined palm oil is a naturally rich source of carotenoids – 15 times higher than carrots and 30 times higher than tomatoes (MPOC 2021). The cells in the human body need fatty acids as raw materials to build their membranes, including in our bones, nervous system, and brain. The human body also needs these micronutrients to maintain its cells and their daily functions (MPOC 2021). Palm oil has a high calorific content. Palm oil contains 9 Kcal of energy per gram, twice the amount of protein (4 Kcal) or carbohydrates (4 Kcal) in 1 gram (MPOC 2021). All food groups must be included as sources of energy, not least fats, and oils. Expert estimates of the average adult energy requirements are 1,800 to 2,000 Kcal daily, with fats and oils accounting for up to 30% of that total (MPOC 2021).

Palm oil is found in nearly everything, making up almost half of all packaged products found on supermarket shelves, which include pizza, doughnuts, and chocolate (Hannah & Max 2021). Palm oil is also used as an animal feed component in various parts of the world (Ghani 2020). As an edible oil, palm oil is highly versatile and possesses varied properties and functions, which have made it an extremely important and widely used oil. It has a semi-solid form at room temperature, which keeps spreads or spreadable; it resists oxidation, giving products a longer shelf life; it has high stability at elevated temperatures, which gives fried foods their crispy and crunchy texture; and it does not change the taste or smell of food products most common use of palm oil in Asia and Africa is for cooking (Ghani 2020). Because of its high melting point, the oil is in a semi-solid form at room temperature. By substituting other vegetable fats for palm oil, the hydrogenation process is avoided, which results in unhealthy trans fats in products. Palm oil acts as a natural preservative in processed foods. This makes oil palm more

useful in the food industry. The global demand for palm oil in 2019 was projected to be 74.6 million tonnes and is anticipated to grow at a volume-based CAGR of 2.3% from 2020 to 2027. The market growth is expected to be driven by higher demand from end-use industries, which is combined with an increase in consumer awareness of the nutritional benefits of palm oil.

Oil Palm Smallholders

Plantations of oil palms are usually large-scale (3000-20000 ha) (Sheil et al. 2009) or smallholder which is defined as 50 hectares, most of which are about 2 hectares and run by local family concerns (Vermeulen & Goad 2006, Dislich et al. 2017). Smallholder oil palm growers are considered the major block in palm oil production. There is some consistency in the definitions of "smallholder" in relation to palm oil production and other commodities. A smallholder, for example, grows a maximum of 2 ha, whereas small-scale growers cultivate plantations sized up to 40 to 50 ha. Nonetheless, these definitions depend on continents or regions. In Colombia, 40 ha would make a farmer a small grower, whereas, in Sierra Leone, a farmer with 40 ha would be considered a large-scale producer (Jezeer et al. 2019). Furthermore, regardless of their land size, smallholders can be differentiated by various factors, for example, their level of organization, whether they have company contracts or otherwise, assets deployed by them, geography, capacities, family or hired labor, and so on. In the discussion of policy and market instruments' impacts on smallholder growers, it is critical to take this diversity into account (Jezeer et al. 2019).

For example, around 400,000 ha are occupied by oil palm plantations in Colombia, 280,000 ha in Ecuador, 103,000 ha in Honduras, 150,000 ha in Brazil, and 2000 ha in Guatemala (Robinson 2013), 117,625 ha in Nigeria (RMRDC 2004). As of 2019, there were estimated to be 6.04 million hectares of oil palm estates in Indonesia. In Malaysia, independent smallholders cultivate 986,331 million ha of land (Rahman 2020). Smallholder plantations account for approximately 40% of oil palm growing land in Indonesia and 13% in Malaysia (MPOC 2021, Azhar et al. 2014; Central Bureau of Statistics Indonesia 2014). Approximately three million smallholders are estimated to be involved in the production of palm oil globally (Rival & Levang 2014), and this number is rising. In Malaysia, there are about 650,000 smallholder growers. In Ecuador, there are about 7,000 smallholder oil palm growers, 7,300 in Honduras, and 1,435 in Brazil (Robinson 2013, Ahmad et al. 2020).

Smallholders can work independently or as part of a team. These smallholders are characterized by being self-financing, involved in managing their plantations, and may have direct dealings with their favorite local operators of palm oil mills; they may even process their palm oil at their own mills or manual presses owned by the local community (Zoological Society London 2015). As a result of the support they receive, smallholders have access to big plantations, receive inputs and training, and receive assistance in establishing their plantations (Sheil et al. 2009). In exchange for the support received, these smallholders agree to sell their harvests at a predetermined price to large-scale companies to be processed at nearby mills, whereas the company deduced any fraction of the loan from the revenue (Dislich et al. 2017).

The Economics of Oil Palm Smallholders

For smallholders looking for a good return from low inputs, oil palm is a rewarding industry (Belcher et al. 2004). According to the 1997 Indonesian Palm Oil Statistics, oil palm smallholders' average annual net income was seven times that of subsistence farmers' (Hartemink 2005). Preparation and planting of land cost NGN 69, 452.70 (USD 169.39) per hectare per year, and land preparation and planting costs NGN 57, 600.00 (USD 140.49) per hectare per year, in Nigeria. Seedlings per hectare were NGN 42, 900.00 (USD 104.63). Cutlass from the 1st to 4th year was NGN 76,800.00 (USD 187.32), and from the 5th year onward was NGN 43,200.00 (USD 105.37) per hectare per year. Pruning (death fronds, epiphytes, etc) up to the 10th year was NGN 4,800.00 (USD 11.71) per hectare per year, and pruning after the 10th year was NGN 3,600.00 (USD 8.78) per hectare per year. The fertilizer application was NGN 4, 800.00 (USD 11.71) per ha per annum (Ukwuteno et al. 2018). Ukwuteno et al. (2018) report that "oil palm plantation maintenance/ running cost with cost of materials required for five years and above was found to be NGN 303, 152.70 (USD 739.310) annually, for oil palm plantation in Nigeria". The costs of production vary with the geography and economic strength of a particular country. The cost of oil palm production in other countries may be higher or lower compared to Nigeria. The average yield in Nigeria is 13.56 ($t\ ha^{-1}\ yr^{-1}$), in Malaysia is 15-18 ($t\ ha^{-1}\ yr^{-1}$), in Indonesia is 14.82 ($t\ ha^{-1}\ yr^{-1}$), in Peru, it is 14 ($t\ ha^{-1}\ yr^{-1}$), and 14.6-22.5 ($t\ ha^{-1}\ yr^{-1}$) in Kalimantan (Lee et al. 2014, De Vos et al. 2021). In Peru, an oil palm plantation requires an average investment usually assessed at around USD 3,000–3,500 for each hectare (Bennett et al. 2019). The disparity in yield between countries depends on geography, whereas, higher yields were largely attributed to planting material and harvesting frequency. Strong group organization is another factor that might contribute to pre-certification conditions (De Vos et al. 2021).

Loans, credit, and subsidies are available to smallholder growers. For example, in Brazil, a smallholder is entitled to USD 125,000 for plantation establishment at an interest rate of 5.75% (Brandão & Schoneveld 2015). Smallholders

in Malaysia have access to loans of RM 26,600 (equal to about USD 62,001) with a 15-year maturity and a 6.25% interest rate (lower than the market rate) (Bronkhorst et al. 2017). In Peru, USD 2,117,700 has been set aside to assist 160 families in establishing an oil palm plantation (Bennett et al. 2019). Smallholder growers were provided with 700 plants (equivalent to 5 ha) at no charge and needed to get loans from banks to cover the remaining financial cost of establishing their plantations (fertilizer, pesticide, transportation) (Bennett et al. 2019).

The Role of Smallholder Farmers in Food Security

A substantial number of empirical studies contend that smallholders remain critical to nutrition and food security globally (Bennett et al. 2019, Paloma et al. 2020). Smallholder plantations are increasingly being seen as having a positive impact on food security, and nutrition, as well as promoting overall development around the world. Smallholder oil palm production, particularly when it is integrated fully into a diversified rural economy and agrifood value chain, has the potential to contribute even more to inclusive growth and job creation (Paloma et al. 2020).

The contribution of smallholders to food security is significantly different across regions (Jezeer et al. 2019). The cultivation of oil palm in Southeast Asia was initially in the form of a monoculture plantation crop driven by government and private companies and reliant on outside labor (Jezeer et al. 2019). Smallholders came into the picture much later as part of mill-related resettlement schemes such as nucleus estate plasma schemes in Indonesia and through the Federal Land Development Authority (FELDA) in Malaysia (Jezeer et al. 2019). Oil palm has always been a smallholder crop in Africa, where it is a native tree, self-planted, self-processed, and is not usually planted in monoculture form. In Latin America, only a small number of corporations and smallholder farmers were involved in biofuels, which were primarily sold in the domestic market (Jezeer et al. 2019). The Nucleus Estate Company in Papua New Guinea uses oil palm fruit from smallholders to operate its mills. Smallholders produce approximately 33% of PNG's palm oil, the majority of which is produced in West New Britain Province (WNBP) (Koczberski et al. 2012). Malaysian crude palm oil production totalled approximately 19.86 million metric tonnes in 2019, of which a total of 40% of the product is produced by small-scale producers, either independently or organized (2020). Around 40% of the global oil palm plantations are under smallholder management and produce almost a third (30%) of the global palm oil output (Saadun et al. 2018). Palm oil and allied products contributed 3.3% to the agricultural GDP in Colombia, 15% in Ecuador, 16% in Honduras, 3.7% in Malaysia, and 1% in Guatemala (Robinson 2013, Department of Statistics 2020, Hervas 2021).

Approximately 25% of Indonesia's oil palm plantations are managed by private smallholders or farmers who operate on a small scale and are not affiliated with companies or mills. This makes up a substantial portion of an industry with an oil output of 31 million tons annually (Thontowi et al. 2018). In both Brazil and Mexico, oil palm smallholder plantations began in the 1940s and 1950s by converting livestock into plantations (Lesage & Feintrenie 2018). Mexico witnessed a tremendous increase in palm oil production from 79, 000 metric tonnes in 2010 to about 140 thousand metric tonnes in 2019 (Statista 2021c). Brazil produced 346 thousand metric tonnes of palm oil in 2016, with production anticipated to exceed half a million metric tonnes in 2018 (Statista 2021b). Smallholder growers contributed immensely to the rise in palm oil production, for example in Honduras smallholder growers produced 620 thousand metric tons in 2016 (Statista 2021a). Similarly, In Ghana, Nigeria, Panama, Nicaragua, Peru, Ecuador (over 87% of all growers are smallholders and contributed 40% of the planted area), and the Dominican Republic more than 60% of FFB and palm oil are produced by smallholder growers (Robinson 2013, Lesage & Feintrenie 2018, Khatun et al. 2020). In Honduras, 7,300 growers with 1-10 ha, control 68% of the planted area and produce more than 60% of the palm oil (Robinson 2013). Up to 2012, the areas under cultivation by smallholder producers in Cameroon made up about 70% of the land area planted with oil palm, an increase of 570% from 1970s figures (Hoyle & Levang 2012, Ordway et al. 2017), and produced 110,000 tonnes of CPO (Nkongho et al. 2014). These account for almost 80% of the demand for edible oil in Cameroon, with smallholders accounting for 30% (Frank et al. 2011, Ordway et al. 2017). Most African oil palm companies promote smallholders to produce more, rather than engage in new plantation development due to the high costs (Nkongho et al. 2015).

Smallholders are expected to increase their production capacity to twice what it is now in the coming decade and are expected to control about 60% of the total oil palm plantation area in Indonesia by 2030 (i et al. 2018). Globally, more than 3 million smallholders rely on palm oil for a living. The smallholders produce around 40% of the world's palm oil, and even though their farms are much smaller than industrial plantations, they contribute immensely to the sustainability of the oil palm industry as well as food security (RSPO 2021, 2012).

Smallholders typically intercrop oil palms with other plant species or fruit trees (Kremen et al. 2012, Fu et al. 2010; Azhar et al. 2017). Depending on the age of the oil

palm, the other crops include both annual and perennial plants. Lam et al. (2009) and Azhar et al. (2017) reports that among the annual plants are "pineapple (Ananascomosus), sugarcane (Saccharum officinarum), sweet potato (Ipomoea batatas), capsicum (Capsicum annuum), lemon grass (*Cymbopogon citratus*), banana (*Musa* spp.), pumpkin (*Cucurbita moschata*), and corn (*Zea mays*). Perennial plant examples are papaya (*Carica papaya*), coconut (*Cocos nucifera*), coffee (*Coffea canephora*), kaffir lime (*Citrus hystrix*), and cassava (*Manihot esculenta*). Examples of fruit trees include mango (*Mangifera indica*), breadfruit (*Artocarpus integer*), Cocoa (*Theobroma cacao*), jackfruit (*Artocarpus hetero-phyllus*), key lime (*Citrus aurantifolia*), sukun (*Artocarpus altilis*), and guava (*Psidium guajava*) which are cultivated by independent smallholders in their planted fields". In addition to intercropping, the integration of grazing livestock (e.g. cattle, goats, and sheep) with oil palm planting is practiced by oil palm smallholders to increase protein sources for consumption locally. Tscharntke et al. (2012) put forward that "agriculture practiced under smallholder farmer-dominated landscapes rather than large-scale farming, is the backbone of global food security in developing countries". The availability of secondary crops may serve as an alternative for smallholders to cope with economic uncertainties resulting from crop failures or price drops in the palm oil market (Simien & Penot 2011).

Challenges Faced by Smallholders

Pre-harvest oil palm growers are constrained by numerous socioeconomic, environmental, and political challenges. The major challenges faced by smallholder growers include; land unavailability and lack of ownership, limited credit and loan facilities, availability of better planting materials, training and skills deficiencies, processing facility obstacles, costly agricultural input, lack of technological expertise, pests and diseases, lack of adoption of innovation and technology, lack of knowledge to keep up with advanced agricultural practices, climate change (rising temperatures, rainfall variability, the impact of El-Nino and La-Nina), lack of labor and manpower, social sustainability (problem-solving and thinking outside box) and soil fertility challenges have all had a negative impact on smallholder production globally, Jelsma et al. 2017, Aznie et al. 2018, Junaidi et al. 2020, et al. 2021, Ahmed et al. 2021, Abubakar et al. 2021).

Post-harvest, other challenges include reliance on dealers for selling products, which is vulnerable to highly volatile market prices. Smallholders also faced uncertain market conditions as a result of rising production costs and weak exports, high duties imposed by importing countries, as well as stiff competition from the major players in the industry (Ahmad et al. 2020). Sustainable certification is constrained by the high cost of the certification, lack of standard knowledge and practice, and lack of incentives for certification (Abazue et al. 2019), and the EU supports a resolution to sanction palm oil imports for the biofuel sector, and impose the adoption of a single sustainable certification for palm oil entering the European market. As a result, this scenario is expected to have a significant impact on the income of over 650,000 palm oil smallholders (Brandi et al. 2015, Ahmad et al. 2020, Zakaria et al. 2020).

CONCLUSION

The results suggest that due to climate change, temperature, and rainfall variability, there could be a significant loss of oil palm yield. The contribution of oil palm smallholder growers to the global palm oil demand is immense. Globally, smallholders dominate palm oil production and oil palm cultivation, except for Malaysia and Indonesia. Despite the impacts of climate change, from 1970 to 2020, all palm oil-producing countries recorded a tremendous increase in CPO output per hectare. The global consumption of palm oil had increased dramatically and is projected to reach 75.45 million metric tonnes in 2021. This is attributed to its health benefits and nutrition. Dealing with climate change entails empowering and enhancing the capacity of smallholders. This study suggests the following: improvements in academic integration at the national and regional levels, with a focus on collaboration with researchers in consumer countries, increasing institutional research capacity, enhancing access to finance, embracing best development practices, sustainable market policies that favor smallholders, access to inputs at subsidized prices, integration of smallholders in decision making, adhering to national policies, and it is critical to developing climate-resilient varieties with high-tolerance planting materials and new crop varieties in response to changing climate conditions.

ACKNOWLEDGMENT

I would like to acknowledge the Tertiary Education Trust Fund (TETFUND) for funding this review study. Grant number TETF/UNIV/JIGAWA STATE/TSAS/2019.

REFERENCES

Abazue, C.M., Choy, E.A. and Lydon, N. 2019. Oil palm smallholders and certification: exploring the knowledge level of independent oil palm smallholders to certification. J. Biosci. Agric. Res., 19(1): 1589-1596.

Abubakar, A., Ishak, M.Y. and Makmom, A.A. 2021. Impacts of and adaptation to climate change on the oil palm in Malaysia : A systematic review. Environ. Sci. Pollut. Res., 28(33): 1-23.

Ahmad, A., Osman, H., Raflis, A., Omar, C., Rahman, M.R. and Ishak, S. 2020. Contributions and challenges of palm oil to smallholders in Malaysia. Int. J. Sci. Res., 9(6): 269-273.

Ahmed, A., Mohd, Y.B.I. and Abdullah, A.M. 2021. Oil palm in the face of climate change: A review of recommendations. IOP Conf. Ser. Environ. Earth Sci., 646(1): 1-10

Ajonina, U. P., and Okanyene, B. B. 2021. Impact of oil palm (Elaeis guineensis) cultivation on soil physico-chemical properties and food security of rural households within Mundemba sub-division, Cameroon. J. Agric. Ecol., 22(3): 32-46.

Ajose, O.A., Adelekan, D.A. and Ajewole, E.O. 2004. Vitamin status of pregnant Nigerian Women: Relationship to dietary habits and morbidity. Nutr. Health, 17(4): 325-333.

Akhtar, S., Ahmed, A., Randhawa, M. A., Atukorala, S., Arlappa, N., Ismail, T., and Ali, Z. 2013. Prevalence of vitamin A deficiency in South Asia: causes, outcomes, and possible remedies. J. Health Popul. Nutr., 31(4): 413-423.

Ambar Suharyanti, N., Mizuno, K. and Sodri, A. 2020. The effect of water deficit on inflorescence period at palm oil productivity on peatland. E3S Web Conf., 211: 2-11.

Azhar, B., Puan, C.L., Zakaria, M., Hassan, N. and Arif, M. 2014. Effects of monoculture and polyculture practices in oil palm smallholdings on tropical farmland birds. Basic. Appl. Ecol., 15: 336-346.

Azhar, B., Saadun, N., Prideaux, M. and Lindenmayer, D.B. 2017. The global palm oil sector must change to save biodiversity and improve food security in the tropics. J. Environ. Manage., 203: 457-466.

Aznie, R., Lyndon, N., Azlan, M., Besar, J. A. and Rohizaq, M. 2018. Independent Oil Palm Smallholders' challenges in Malaysia's independent oil palm. Int. J. Acad. Res. Bus. Soc. Sci., 8(13): 68-75.

Basiron, Y. 2007. Palm oil production through sustainable plantations. Eur. J. Lipid. Sci. Technol., 109: 289-295.

Basiron, Y. and Chan, K.W. 2004. Palm oil and its sustainability. J. Oil Palm Res., 16(1): 1-10.

Begum, H., Siwar, C., Er, A.C. and Alam, A.S.A.F. 2016. Environmentally friendly practices of oil palm cultivators. Int. J. Adv. Appl., 3(2): 15-19.

Belcher, B., Imang, N. and Achdiawan, R. 2004. Rattan, rubber, or oil palm: cultural and financial considerations for farmers in Kalimantan. Econ. Bot 58: S77-S87.

Bennett, A., Ravikumar, A., McDermott, C. and Malhi, Y. 2019. Smallholder oil palm production in the Peruvian Amazon: Rethinking the promise of associations and partnerships for economically sustainable livelihoods. Front. for. Glob. Change, 2(4): 1-16.

Boyce, J. 2017. The Palm Oil Debate: What You Need to Know. Nature's Path. https://www.naturespath.com/ en-us/blog/the-palm-oil-debate-what-you-need-to-know/. Accessed 25 June 2021

Brack, D., Glover, A. and Wellesley, L. 2016. Agricultural Commodity Supply Chains Trade, Consumption, and Deforestation. https://www.chathamhouse.org/sites/default/files/publications/research/2016-01-28-agricultural-commodities-brack-glover-wellesley.pdf. Accessed 13 May 2021

Brandão, F. and Schoneveld, G. 2015. The state of oil palm development in the Brazilian Amazon: Trends, value chain dynamics, and business models, vol. 198. CIFOR.

Brandi, C., Cabani, T., Hosang, C., Schirmbeck, S., Westermann, L. and Wiese, H. 2015. Sustainability standards for palm oil: Challenges for smallholder certification under the RSPO. J. Environ. Dev., 24(3): 292-314.

Bronkhorst, E., Cavallo, E., van Dorth tot Medler, M.M., Klinghammer, S., Smit, H.H., Gijsenbergh, A. and van der Laan, C. 2017. Current Practices and Innovations in Smallholder Palm Oil Finance in Indonesia and Malaysia: Long-term Financing Solutions To Promote Sustainable Supply Chains. Occasional Paper 177. Bogor, Indonesia: CIFOR.

Byerlee, D., de Janvry, A. and Sadoulet, E. 2009. Agriculture for development: Toward a new paradigm. Annu. Rev. Resour. Econ., 1: 15-31.

Byerlee, D., Falcon, W.P. and Naylor, R.L. 2017. The Tropical Oil Crop Revolution: Food, Feed, Fuel, and Forest. Oxford University, Press, Oxford, UK.

Carr, M.K.V. 2011. The water relations and irrigation requirements of oil palm (Elaeis guineensis): A review. Exp. Agric., 47(4): 629-652.

Central Bureau of Statistics Indonesia. 2014. Indonesian Oil Palm Statistics 2013. https://www.neliti.com/pt/publications/49002/indonesian-oil-palm-statistics-2013. Accessed 08 March 2020.

Cestaro, B., Porta, M., Della, K. and Cazzola, R. 2017. Palm oil: Health risks and benefits. Agro. Food Indus. Hi-Tech., 28(6): 57-59.

Corley, R.H.V. and Tinker, P.B. (ed) 2003. The Oil Palm. Wiley Blackwell, London, p. 680.

Corley, R.H.V. and Tinker, P.B. (ed) 2015. The Oil Palm. World Agricultural Series, Wiley Blackwell, London, p. 680.

d'Enghien, P.B. 2016. Palm Oil-Essential for Food Security. http://theoilpalm.org/palm-oil-essential-for-food-security/. Accessed 10 April 2021.

Daud, Z.A.M., Kaur, D. and Khosla, P. 2012. Health and nutritional properties of palm oil and its components. palm oil: Production, processing, characterization, and uses. 9: 545-560.

De Vos, R.E., Suwarno, A., Slingerland, M., Van Der Meer, P.J. and Lucey, J.M. 2021. Independent oil palm smallholder management practices and yields: Can RSPO certification make a difference? Environ. Res. Lett., 16(6): 1-10

Department of Statistics. 2020. Selected Agricultural Indicators, Malaysia, 2020. https://www.dosm.gov.my/v1/index.php?r=column/ctheme-ByCat&cat=72&bul_id=RXVKUVJ5TitHM0cwYWxlOHcxU3d-Kdz09&menu_id=Z0VTZGU1UHBUT1VJMFlpaXRRR0xpdz09. Accessed 28 May 2021

Dislich, C., Keyel, A.C., Salecker, J., Kisel, Y., Meyer, K.M., Auliya, M., Barnes, A.D., Corre, M.D., Darras, K., Faust, H., Hess, B., Klasen, S., Knohl, A., Kreft, H., Meijide, A., Nurdiansyah, F., Otten, F., Pe, G., Steinebach, S. and Wiegand, K. 2017. A review of the ecosystem functions in oil palm plantations, using forests as a reference system. Biol. Rev., 49: 1539-1569.

FAO et al. 2018. The State of Food Security and Nutrition in the World 2018. Building climate resilience for food security and nutrition, Rome, FAO.

Fleiss, S., Hill, J.K., Mcclean, C., Lucey, J.M. and Reynolds, G. 2017. Potential Impacts of Climate Change on Oil Palm Cultivation: A Science-for-Policy. Available at: http://www.sensorproject.net/wp-content/uploads/2018/01/Climate-change-report-FINAL.pdf. Accessed 27 December 2020.

Food and Agriculture Organization (FAO). 2009. How to Feed the World in 2050. Rome: FAO. https://www.fao.org/fileadmin/templates/wsfs/docs/expert_paper/How_to_Feed_the_World_in_2050.pdf. Accessed 28 June 2021.

Food and Agriculture Organization (FAO). 2017. The Future Of Food and Agriculture Trends and Challenges.. https://www.fao.org/3/i6583e/i6583e.pdf. Accesed 07 September 2021.

Food and Agriculture Organization (FAO). 2019. FAO Statistics. Available online at: http://www.fao.org/faostat/en. Accessed 28 September 2021.

Food and Agriculture Organization (FAO). 2020. The World Is at Critical Juncture: The State of Food Security and Nutrition in the World 2021 http://www.fao.org/state-of-food-security-nutrition. Accessed 15 August 2021

Frank, N.E.G., Albert, M.M.F., Lavendure, D.E.F. and Paul, K. 2011. Assessment of the quality of crude palm oil from smallholders in Cameroon. J. Stored Prod. Postharvest Res., 2: 52-56.

Fu, Y., Chen, J., Guo, H., Hu, H., Chen, A. and Cui, J. 2010. Agrobiodiversity loss and livelihood vulnerability as a consequence of converting from subsistence farming systems to commercial plantation-dominated systems in Xishuangbanna, Yunnan, China: A household level analysis. Land Degrad. Dev., 21(3): 274-284.

Ghani, M. 2020. 8 things to Know about Palm oil. https://www.wwf.org.uk/updates/8-things-know-about-palm-oil. Accessed 19 December 2021.

Goenadi, D.H. 2008. Perspective on Indonesian palm oil production. Paper to 41st IPC Seminar Food, Fuel, and Forests: A Seminar on Climate

Change, Agriculture, and Trade. Bogor, Indonesia, 12 May 2008. International Food and Agricultural Trade Policy Council. http://www.agritrade.org/ events/documents/Goenadi2008.pdf. Accessed 30 June 2021.

Guillaume, G. and Soledad, Z. 2010. BACI: International Trade Database at the Product Level. The 1994-2007 Version. Working Papers 2010-23, CEPII Research Center, France.

Hannah, R. and Max, R. 2021. Forests and Deforestation. Published online at OurWorldInData.org. https://ourworldindata.org/forests-and-deforestation. Accessed 13 May 2021.

Hartemink, A. E. 2005. Plantation agriculture in the tropics: environmental issues. Outlook Agric. 34: 11-21.

Hervas, A. 2021. Mapping oil palm-related land use change in Guatemala, 2003-2019: Implications for food security. Land Use Policy, 109: 1-14

High Carbon Stock. 2015. Nigeria: A Smallholder Case Study. https://www.simedarbyplantation.com/sites/default/files/sustainability/high-carbon-stock/consulting-reports/socio-economic/hcs-consulting-report-13-nigeria-a-smallholder-case-study.pdf. Accessed 14 May 2021.

Hoyle, D. and Levang, P. 2012. Oil Palm Development in Cameroon. WWF, Yaoundé, Cameroon.

IPCC 2007a: Climate Change 2007. The physical science basis. contribution of working group i to the fourth assessment report of the intergovernmental panel on climate change. Cambridge University Press, Cambridge, United Kingdom and New York, NY, USA, 996 pp.

IPCC TAR. 2001. Climate Change 2001. Impacts, Adaptation, and Vulnerability. IPCC Third Assessment Report, Cambridge University Press, Cambridge, MA.

Ismail, S.R., Maarof, S.K., Ali, S.S. and Ali, A. 2018. A systematic review of palm oil consumption and the risk of cardiovascular disease. PLoS ONE, 13(2): 1-16.

Jadhav, R. 2019. India's Palm Oil Imports Could Hit Record on Rising Demand: Analyst. Reuters. https://in.reuters. com/article/india-palmoil-imports-idINKBN1WA17P. Accessed 15 April 2021.

Jelsma, I., Schoneveld, G.C., Zoomers, A. and van Westen, A.C.M. 2017. Unpacking Indonesia's independent oil palm smallholders: An actor-disaggregated approach to identifying environmental and social performance challenges. Land Use Policy, 69(8): 281-297.

Jezeer, R. E., Verweij, P. A., Boot, R. G. A., Junginger, M., and Santos, M. J. 2019. Influence of livelihood assets, experienced shocks and perceived risks on smallholder coffee farming practices in Peru. J. Environ. Manage., 242: 496-506.

Junaidi, A.B., Mohd F.M.J., Ahmad Rizal, M.Y., Al-Amril Othman, R.F. 2020. Socio-economic development of palm oil smallholders in Malaysia. Int. J. Adv. Appl., 7(7): 109-118.

Khatiwada, D., Palmén, C. and Silveira, S. 2021. Evaluating the palm oil demand in Indonesia: Production trends, yields, and emerging issues. Biofuels, 12(2): 135-147.

Khatun, K., Maguire-Rajpaul, V.A., Asante, E.A. and McDermott, C.L. 2020. From agroforestry to agroindustry: Smallholder access to benefits from oil palm in Ghana and the implications for sustainability certification. Front. Sustain. Food Syst., 4(4): 1-13.

Killeen, T. J., Harris, N. L., Brown, K., Netzer, M. and Gunarso, P. 2013. Projections of Oil Palm Expansion in Indonesia, Malaysia and Papua New Guinea From 2010 To 2050. Rspo.Org, September 2013, 89-112.

Koczberski, G., Curry, G.N. and Bue, V. 2012. Oil palm, food security, and adaptation among smallholder households in Papua New Guinea. Asia Pac. Viewp., 53(3): 288-299.

Kremen, C., Iles, A. and Bacon, C. 2012. Diversified farming systems: An agroecological, systems-based alternative to modern industrial agriculture. Ecol. Soc., 17(4): 1-19.

Lam, M. K., Tan, K. T., Lee, K. T. and Mohamed, A. R. 2009. Malaysian palm oil: Surviving the food versus fuel dispute for a sustainable future. Renewable Sustainable Energy Rev., 13(6-7): 1456-1464.

Lee, J.S.H., Ghazoul, J., Obidzinski, K. and Koh, L.P. 2014. Oil palm smallholder yields and incomes are constrained by harvesting practices and type of smallholder management in Indonesia. Agron. Sustain. Dev., 34(2): 501-513.

Lesage, C. and Feintrenie, L. 2018. Are Sustainable Pathways Possible for Oil Palm Development in Latin America? 2018 World Bank Conference On Land And Poverty. The World Bank, Washington DC.

Lietz, G., Henry, C.J.K., Mulokozi, G., Mugyabuso, J.K.L., Ballart, A., Ndossi, G.D., Lorri, W. and Tomkins, A. 2001. Comparison of the effects of supplemental red palm oil and sunflower oil on maternal vitamin A status. Am. J. Clin. Nutr., 74(4): 501-509.

Lietz, G., Mulokozi, G., Henry, J.C.K. and Tomkins, A.M. 2006. Xanthophyll and hydrocarbon carotenoid patterns differ in the plasma and breast milk of women supplemented with red palm oil during pregnancy and lactation. Nutr. J., 136(7): 1821-1827.

Lobell, D.B. and Gourdji, S.M. 2012. The influence of climate change on global crop productivity. Plant Physiol., 160(4): 1686-1697.

Loganathan, R., Subramaniam, K.M., Radhakrishnan, A.K., Choo, Y.M. and Teng, K.T. 2017. Health-promoting effects of red palm oil: Evidence from animal and human studies. Nutr. Rev., 75(2): 98-113.

Majid Cooke, F. 2012. In the name of poverty alleviation: Experiments with oil palm smallholders and customary land in Sabah, Malaysia. Asia Pac. Viewp., 53(3): 240-253.

Maluin, F.N., Hussein, M.Z. and Idris, A.S. 2020. An overview of the oil palm industry: Challenges and some emerging opportunities for nanotechnology development. Agron., 10(3): 1-20

Meijaard, E., Garcia-Ulloa, J., Sheil, D., Carlson, K. and Wich, S.A. 2018. Oil Palm and Biodiversity – A Situation Analysis. IUCN Oil Palm Task Force, Gland, Switzerland.

Meo Carbon Solutions. 2018. The Palm Oil Market in Germany in 2017, 2018. Online available at https://www.forumpalmoel.org/imglib/Palmoelstudie%202017_Meo_FONAP_ho.pdf. Accessed 24 August 2021.

MNRE. 2010. Malaysia's second National Communication (NC2) submitted to the United Nations framework convention on climate change (UNFCCC), Ministry of Natural Resources and Environment (MNRE), Federal Government of Malaysia, Putrajaya.

Molotoks, A., Smith, P. and Dawson, T. P. 2021. Impacts of land use, population, and climate change on global food security. Food Energy Secur., 10(1): 1-20.

MPOB. 2010. Overview of the Malaysian Palm Oil Industry. Available at: Report.http://bepi.mpob.gov.my/images/document/overview202010_final.pdf. Accessed 11 December 2020.

MPOC. 2019. Palm Oil Holds Promise for Current and Future Food Security. http://palmoiltoday.net/palm-oil-holds-promise-for-current-and-future-food-security/. Accessed 23 September 2021.

MPOC. 2021. Monthly Palm Oil Trade Statistics: January – July 2021. http://mpoc.org.my/monthly-palm-oil-trade-statistics-2021/. Accessed 23 September 2021

Muhamad Rizal, A.R. and Tsan, F.Y. 2008. Low Rainfall for Two or More Months in Succession Will Depress OER about 11 Months Later. Available at: http://www.iipm.com.my/ipicex2014/docs/posters/Muhamad%20Rizal%20and%20Tsan.pdf. Accessed 13 July 2021.

Murphy, D.J. 2014. The future of oil palm as a major global crop: Opportunities and challenges. J. Oil Palm Res., 26(3): 1-24.

Nabara, I.S. and Norsida, M. 2018. The role of extension in activity-based adaptation strategies towards climate impact among oil palm smallholders in Malaysia : A systematic review. J. Agric. Vet. Sci., 11: 37-44.

Nambiappan, B., Ismail, A., Hashim, N., Ismail, N., Shahari, D. N., Idris, N. A. N., Omar, N., Salleh, K. M., Hassan, N. A. M. and Kushairi, A. 2018. Malaysia: 100 years of resilient palm oil economic performance. J. Oil Palm Res., 30(1): 13-25.

Nesadurai, H. E. S. 2013. Food security, the palm oil-land conflict nexus, and sustainability: A governance role for a private multi-stakeholder regime like the RSPO? Pacific Review, 26(5): 505-529.

Nkongho, R.N., Feintrenie, L. and Levang, P. 2014. The Non-Industrial Palm Oil Sector in Cameroon. Working Paper 139. CIFOR, Bogor, Indonesia.

Nkongho, R.N., Ndjogui, T.E. and Levang, P. 2015. History of a partnership between agro-industries and oil palm smallholders in Cameroon. OCL Oilseeds Fats, 22(3): 1-15

Oettli, P., Behera, S.K. and Yamagata, T. 2018. Climate-based predictability of oil palm tree yield in Malaysia. Sci. Rep., 8(1): 1-13.

Oil world 2020. Oil yield by crop types 2018. https://ourworldindata.org/grapher/oil-yield-by-crop Accessed 21 March 2021.

Olmedilla, B., Granado, F., Southon, S., Wright, A.J.A., Blanco, I., Gil-Martinez, E., Den Berg, H., Van, Thurnham, D., Corridan, B., Chopra, M. and Hininger, I. 2002. A European multicentre, placebo-controlled supplementation study with -tocopherol, carotene-rich palm oil, lutein or lycopene: Analysis of serum responses. Clin. Sci., 102(4): 447-456.

Ordway, E.M., Naylor, R.L., Nkongho, R.N. and Lambin, E.F. 2017. Oil palm expansion in Cameroon: Insights into sustainability opportunities and challenges in Africa. Glob. Environ. Change., 47(8): 190-200.

Paloma, S.G., Riesgo, L. and Louhich, K. (ed) 2020. The Role of Smallholder Farms in Food and Nutrition Security. Gewerbestrasse, Cham, Switzerland., p. 253.

Paterson, R., Russell M. and Lima, N. 2018. Climate change affecting oil palm agronomy, and oil palm cultivation increasing climate change, require amelioration. Ecol. Evol., 8(1): 452-461.

Paterson, R., Russell M., Kumar, L., Taylor, S. and Lima, N. 2015. Future climate effects on suitability for growth of oil palms in Malaysia and Indonesia. Sci. Rep., 5: 1-11.

Paterson, R.R.M, Sariah, M. and Lima, N. 2013. How will climate change affect oil palm fungal diseases ? Crop Prot., 46: 113-120.

Paterson, R.R.M. 2019. Ganoderma boninense disease was deduced from simulation modeling with large data sets of future Malaysian oil palm climate. Phytoparasitica, 47(4): 1-11

Paterson, R.R.M. 2020. Oil palm survival under climate change in Malaysia with future basal stem rot assessments. For. Pathol., 50(6): 1-8.

Paterson, R.R.M. 2021. Modeling longitudinal trends to oil palm refuges and oil palm mortalities in South America under future climate. J. Agric. Crop Manag., 2(1): 1-7.

Paterson, R.R.M., Kumar, L., Shabani, F. and Lima, N. 2017. World climate suitability projections to 2050 and 2100 for growing oil palm. J. Agric. Sci., 155(5): 659-702.

Paterson, R.R.M., Moen, S. and Lima, N. 2009. The feasibility of producing oil palm with altered lignin content to control Ganoderma disease. J. Phytopathol., 157(11-12): 649-656.

Pawlak, K. and Kołodziejczak, M. 2020. The role of agriculture in ensuring food security in developing countries: Considerations in the context of the problem of sustainable food production. Sustainability, 12(13): 1-20

Pirker, J., Mosnier, A., Kraxner, F., Havlík, P. and Obersteiner, M. 2016. What are the limits to oil palm expansion? Global Environmental Change, 40: 73-81.

Potter, L. 2012. New transmigration "paradigm" in Indonesia: Examples from Kalimantan. Asia Pac. Viewp., 53(3): 272-287.

Qaim, M., Sibhatu, K. T., Siregar, H., and Grass, I. 2020. Environmental, economic, and social consequences of the oil palm boom. Annu. Rev. Resour. Eco., 12: 321-344.

Rahman, S. 2020. Malaysian Independent Oil Palm Smallholders and their Struggle to Survive 2020. ISEAS Perspective, pp. 1-16.

Ramadhana, A., Ahmed, F. and Thongrak, S. 2021. The impact of oil palm farming on household income and expenditure in Indonesia. J. Asian Fin. Econ. Bus., 8(4): 539-547.

Rhebergen, T., Fairhurst, T., Giller, K.E. and Zingore, S. 2019. The influence of water and nutrient management on oil palm yield trends on a large-scale plantation in Ghana. Agric. Water Manag., 221(5): 377-387.

Rival, A. 2017. Breeding the oil palm (Elaeis guineensis Jacq.) for climate change. Crops and Lip., 24(1): 1-7.

Rival, A. and Levang, P. 2014. Palms of controversies: Oil palm and Development Challenges. CIFOR, Bogor, Indonesia.

RMRDC. 2004. Report On Survey Of Selected Agricultural Materials. Raw Materials Research and Development Council, Malaysia.

Robinson, D. 2013. Smallholder Oil Palm Growers in Latin America. The Proforest Initiative. www.proforestinitiative.org. Accessed 28 February 2021.

Roundtable on Sustainable Palm Oil 2017. Would it not be better to replace palm oil? https://askrspo.force.com/s/article/Would-it-not-be-better-to-replace-palm-oil#:~:text=This%20is%20because%20palm%20oil,be%20converted%20into%20agricultural%20land (Accessed 21 March 2021).

RSPO 2021. RSPO smallholders. https://rspo.org/smallholders. Accessed 23 March 2021.

RSPO. 2012. Why Palm Oil Matters In Your Everyday Life. https://www.rspo.org/file/RSPO_DesignFactSheet.pdf. Accessed 12 March 2021.

Saadun, N., Lim, E.A.L., Esa, S.M., Ngu, F., Awang, F., Gimin, A., Johari, I.H., Firdaus, M.A., Wagimin, N.I. and Azhar, B. 2018. Socio-ecological perspectives of engaging smallholders in environmental-friendly palm oil certification schemes. Land Use Policy, 72(1): 333-340.

Santika, T., Wilson, K.A., Budiharta, S., Law, E.A., Poh, T.M., Ancrenaz, M., Struebig, M.J. and Meijaard, E. 2019. Does oil palm agriculture help alleviate poverty? A multidimensional counterfactual assessment of oil palm development in Indonesia. World Dev., 120(4): 105-117.

Sarkar, M.S.K., Begum, R.A. and Pereira, J.J. 2020. Impacts of climate change on oil palm production in Malaysia. Environ. Sci. Pollut. Res., 27(9): 9760-9770.

Shafiq, K.M. 2017. The Effect of Rainfall Distribution on Production of Oil Palm in Different Locations. Dissertation, University of Tecknologi, Malaysia.

Shahputra, M.A. and Zen, Z. 2018. Positive and negative impacts of oil palm expansion in Indonesia and the prospect to achieve sustainable palm oil. IOP Conf. Seri. Environ. Earth Sci., 122(1): 1-7.

Shanmuganathan, S. and Narayanan, A. 2012. Modeling the climate change effects on Malaysia's oil palm yield. 2012 IEEE Symposium on E-Learning, E-Management, and E-Services, IS3e 2012, 21-24 October 2012, KL, Malaysia, IEEE, Piscataway, US, pp. 71-76.

Shanmuganathan, S., Narayanan, A., Mohamed, M., Ibrahim, R. and Khalid, H. 2014. A hybrid approach to modeling the climate change effects on Malaysia's oil palm yield at the regional scale. Adv. Intell. Syst., 287: 335-346.

Sheil, D.A. Casson, Meijaard, E., van Noordwijk, M., Gaskell, J., Sunderland-Groves, J., Wertz, J.K. and Kanninen, M. 2009. The Impacts and Opportunities of Oil Palm in Southeast Asia: What Do We Know and What Do We Need to Know? Occasional Paper No. 51., CIFOR, Bogor, Indonesia.

Simien, A. and Penot, E. 2011. Current evolution of smallholder rubber-based farming systems in southern Thailand. J. Sustain. For., 30(3): 247-260.

Singh, R.P. 2014. Cost-effectiveness of palm oil in comparison to other oils and fats in the country with special emphasis on lower income group. Indian J. Community Health, 26(5): 37-44.

Sommer, A. 2008. Vitamin A deficiency and clinical disease: An historical overview. J. Nutr., 138(10): 1835-1839.

Statista. 2021a. Palm Oil Consumption Worldwide from 2015/2016 to 2020/2021. https://www.statista.com/statistics/274127/world-palm-oil-usage-distribution/. Accessed 23 April 2021

Statista. 2021b. Production of Palm Oil in Brazil in 2016 and 2018. https://www.statista.com/statistics/876428/palm-oil-production-volume-brazil/. Accessed 23 March 2021.

Statista. 2021c. Production of Palm Oil in Mexico from 2010 to 2019. https://www.statista.com/statistics/955211/mexico-palm-oil-production-volume/. Accessed 16 October 2021.

Statista. 2021d. Production Volume of Palm Oil in Indonesia from 2012 to 2020. https://www.statista.com/statistics/706786/production-of-palm-oil-in-indonesia/. Accessed 22 May 2021.

Stevens, G. A., Bennett, J. E., Hennocq, Q., Lu, Y., De-Regil, L. M., Rogers, L., Danaei, G., Li, G., White, R. A., Flaxman, S. R., Oehrle, S. P., Finucane, M. M., Guerrero, R., Bhutta, Z. A., Then-Paulino, A., Fawzi, W., Black, R. E. and Ezzati, M. 2015. Trends and mortality effects of vitamin A deficiency in children in 138 low-income and middle-income countries between 1991 and 2013: A pooled analysis of population-based surveys. Lancet Glob. Health, 3(9): e528-e536.

Susila, W. R. 2004. Contribution of oil palm industry to economic growth and poverty alleviation in Indonesia. J. Litbang, 23(1): 107-114.

Tang, K.H.D. 2019. Climate change in Malaysia: Trends, contributors, impacts, mitigation, and adaptations. Sci. Total Environ., 650: 1858-1871.

Tang, K.H.D. and Al Qahtani, H.M.S. 2020. Sustainability of oil palm plantations in Malaysia. Environ. Dev. Sustain., 22(6): 4999-5023.

Teh, C.B.S. 2016. Availability, use, and removal of oil palm biomass in Indonesia. Rep. Int. Council Clean Transport., 2: 1-39.

Thontowi, A., Suhada, B.B. and Saleh, S. 2018. Smallholder Farmers Are Key to Making the Palm Oil Industry Sustainable. https://www.wri.org/insights/smallholder-farmers-are-key-making-palm-oil-industry-sustainable. Accessed 22 November 2021.

Tscharntke, T., Clough, Y., Wanger, T.C., Jackson, L., Motzke, I., Perfecto, I., Vandermeer, J. and Whitbread, A. 2012. Global food security, biodiversity conservation, and the future of agricultural intensification. Biol. Conserv., 151(1): 53-59.

Tullis, P. 2019. How the World Got Hooked on Palm Oil. The Guardian. https://www.theguardian.com/news/2019/feb/19/palm-oil-ingredient-biscuits-shampoo-environmental. Accessed 19 October 2021.

Ukwuteno, S.O., Eboh, E.C. and Ocheja, J.O. 2018. Determination of costs and returns of oil palm production in Kogi State, Nigeria. Int. J. For. Res., 5(1): 27-33.

United Nations 2018. The Sustainable Development Goals Report. United Nations, New York.

Unjan, R., Nissapa, A. and Chiarawipa, R. 2017. Climatic considerations support the choice between natural rubber and oil palm in Nakhon Si Thammarat, southern Thailand. Kasetsart J. Soc. Sci., 38(3): 273-281.

USDA FAS. 2012. Malaysia: Stagnating Palm Oil Yields Impede Growth. United States Department of Agriculture Foreign Agricultural Service. https://ipad.fas.usda.gov/highlights/2012/12/Malaysia/. Accessed 15 November 2021.

USDA. 2021a. Palm Oil Domestic Consumption By Country in 1000MT. https://www.indexmundi.com/agriculture/?commodity=palm-oil&graph=domestic-consumption. Accessed 23 January 2021.

USDA. 2021b. Palm Oil Production By Country in 1000MT. https://www.indexmundi.com/agriculture/?commodity=palm-oil. Accessed 06 March 2021

van Stuijvenberg, M.E., Faber, M., Dhansay, M.A., Lombard, C.J., Vorster, N. and Benadé, A.J. 2000. Red palm oil as a source of beta-carotene in a school biscuit used to address vitamin A deficiency in primary school children. Int. J. Food Sci. Nutr., 51(1): 43-50.

Varsha, V., Stuart, L., Pimm, C.N. and Jenkins, S.J.S. 2016. The impacts of oil palm on recent deforestation and biodiversity loss. Nature, 391(6670): 835-836.

Vermeulen, S. and Goad, N. 2006. Toward Better Practice in Smallholder Palm Oil Production. International Institute for Environment and Development, London.

Villela, A.A., Jaccoud, D.B., Rosa, L.P. and Freitas, M.V. 2014. Status and prospects of oil palm in the Brazilian Amazon. Biomass Bioenergy, 67: 270-278.

Voora, V., Cristina, L., Steffany, B. and Sofia, B. 2019. Global Market Report: Palm Oil. https://www.iisd.org/system/files/publications/ssi-global-market-report-palm-oil.pdf. Accessed 16 June 2021.

Wahid, M.B., Abdullah, S.N.K. and Henson, I.E. 2005. Oil Palm: Achievements and potential. Oil Palm Bull., 50: 1-13.

Wakker, E. 2006. The Kalimantan Border Oil Palm Mega-project. Friends of the Earth Netherlands and the Swedish Society for Nature Conservation (SSNC), Amsterdam.

Weckx, S., Inzé, D. and Maene, L. 2019. Tissue culture of oil palm: Finding the balance between mass propagation and somaclonal variation. Front. Plant Sci, 10: 1-17.

WHO. 2011. Guideline: Vitamin A Supplementation in Infants and Children 6-59 Months of Age. World Health Organization, Geneva, Switzerland.

Woittiez, L.S., van Wijk, M.T., Slingerland, M., van Noordwijk, M. and Giller, K.E. 2017. Yield gaps in oil palm: A quantitative review of contributing factors. Eur. J. Agron., 83: 57-77.

Workman, D. 2019. Palm Oil Imports By Country: World's Top Exports. http://www.worldstopexports.com/palmoil-imports-by-country/. Accessed 04 June 2021.

Zainal, Z., Shamsudin, M.N., Mohamed, Z.A. and Adam, S.U. 2012. The economic impact of climate change on Malaysian palm oil production. Trends Tech. Sci. Res., 7:872-880.

Zakaria, Z., Rahim, A.R A. and Aman, Z. 2020. Issues and challenges of oil palm cooperatives towards greater sustainability: A proposal of conceptual framework. Int. J. Acad. Res. Bus. Soc. Sci., 10(1): 46-69.

Zeba, A.N., Prével, Y.M., Somé, I.T. and Delisle, H.F. 2006. The positive impact of red palm oil in school meals on vitamin A status: Study in Burkina Faso. Nutr. J., 5: 1-10.

Zen, Z., Barlow, C. and Gondowarsito, R. 2006. Oil palm in Indonesian socio-economic improvement: A review of options. J. Oil Palm Res., 6: 18-29.

Zhai, F. and Zhuang, J. 2009. Agricultural Impact of Climate Change: A General Equilibrium Analysis with Special Reference to Southeast Asia. ADBI Working Paper 131, Asian Development Bank, Tokyo.

Zoological Society London. 2015. Sustainable Palm Oil Platform. Available at: http://www.sustainablepalmoil.org/growers-millers/ growers/ smallholders/. Accessed 26 June 2021.

Nature Environment and Pollution Technology
An International Quarterly Scientific Journal

p-ISSN: 0972-6268
(Print copies up to 2016)
e-ISSN: 2395-3454

Vol. 21 | No. 5 (Suppl) | pp. 2073-2087 | 2022

Original Research Paper

https://doi.org/10.46488/NEPT.2022.v21i05.005

Open Access Journal

Seasonal Characterization and Possible Solutions for Municipal Solid Waste Management in the City of Patna, Bihar, India

F. A. Siddiqui*, R. Singh* and Prashant*†

*Department of Environmental Science, Central University of South Bihar, Gaya-824236, India

†Corresponding author: Prashant; drprashant@cub.ac.in

Nat. Env. & Poll. Tech.
Website: www.neptjournal.com

Received: 18-04-2022
Revised: 31-05-2022
Accepted: 22-06-2022

Key Words:
Municipal solid waste
Characterization
Moisture content
Calorific value

ABSTRACT

The present study aims to characterize the municipal solid waste (MSW) generated in the municipality of Patna, the second-largest city in Eastern India. MSW is heterogeneous and the composition varies with seasons and within the different parts of the city. MSW samples were characterized for the three different seasons Winter (November), Summer (May), and Monsoon (August) to select feasible waste treatment methods. The physical characterization indicates that the major fractions of the MSW were biodegradable (48.83%) and inert (18.26%), which shows variations in different seasons of about ~5%. On a seasonal basis, the chemical characterization of MSW revealed that the moisture content varies between 43.21% to 51.78%, and volatile matter between 20.18% to 29.45%. ash content between 20.20% to 26.23% and fixed carbon between 4.11% to 5.91%. The C/N was found to be between 15.81 to 28.84 and the calorific value lies between 1212 to 2627 kcal.kg^{-1} during different seasons. The characterization of MSW highlights the virtue of waste segregation at the source and developing an efficient MSW system, including the potential for recycling, composting, anaerobic digestion, and production of refuse-derived fuels (RDFs). The outcomes of the present study will be helpful for Patna Municipal Corporation (PMC) in the planning for implementing suitable waste treatment technologies for integrated solid waste management systems (ISWM).

INTRODUCTION

Globally, the population is increasing, resulting in the consumption of more and more resources. The industrial revolution promised that human resourcefulness could solve many problems. As the take-make-waste model of industrialization and resource consumption pattern disregarded environmental concerns, hence heaps of waste were added to the environment. Waste is an unnecessary evil and a byproduct of consumption and the outcome of most processes (Chen et al. 2020). The poorly managed waste is causing diseases, harming animals, choking sewers, polluting rivers and oceans, emitting Green House Gases (GHGs), local air pollution, and loss of revenues on tourism fronts (Kaza et al. 2018). It is said that a city, which is unable to manage its waste wisely is rarely able to manage its other services like health, education, or transportation (Hoornweg & Bhada-Tata 2012). In the fast-growing world, the poor handling and mismanagement of MSW in an unscientific manner has become an environmental threat and serious concern for local and central agencies in most developing nations (Parihar et al. 2017).

The waste management issues evolve as the countries and their cities in due course of time, educe from low-income to middle- and high-income economies (Kaza et al. 2018). Indian cities are experiencing continuous growth in population and urban expansion (Census 2011, Dinda et al. 2021). In the past decade, India has witnessed a growth of 31.8% in urban sprawl (Singhal et al. 2021). The total MSW generated by India is about 150847.1 tons per day (TPD). Out of the total waste generated, 96.8 % of waste is collected, and only 47% of the collected waste is treated (CPCB 2019-20). According to the latest report of the Central Pollution Control Board (CPCB), the rate of waste collection has increased but the amount of waste being treated is still on the lower side. The primary reason behind such a low rate of treatment is the unavailability of segregated waste and the lack of data on the physical composition and chemical characteristics of MSW at the city level, which eventually helps in setting up treatment facilities. Thus, the open dumping and burning of the MSW is the most preferable practice in India (Singhal & Goel 2021). Unscientific and improper municipal solid waste management (MSWM) coupled with inefficient and outdated practices, and techniques pose a serious threat to environmental and human health. So, there is an urgent need for proper quantification, upscaling segregation, and processing and treatment of waste following the concept of the circular economy.

Indian cities require a systematic way forward to channel the waste management system to cope with the ever-increasing volume of waste. The take-make-use-waste model does not support the treatment, processing, and recycling of the MSW; rather an ISWM approach shall be adopted as a sustainable waste management option. The ISWM is a comprehensive program encompassing waste prevention, recycling, processing, and safe disposal. It strives to make a balance between environmental effectiveness (waste prevention and reduction methods), social acceptability (behavioral aspects and citizen's awareness), and economic affordability (cost-effective processing and disposal methods) (Marshall & Farahbakhsh 2013). Furthermore, the Indian legislation named Solid Waste Management Rules 2016 (SWMR 2016) is in line with the concept of ISWM. Acknowledging the problem of waste shall be the very first step of the waste management program. The choice of treatment/ processing and disposal option depends on the quantity and characteristics of the MSW. Additionally, the information about characteristics of waste stream based upon seasonal variations aids in making an ISWM robust. In developing nations, it has been reported that the major fraction of MSW is organic waste (Srivastava et al. 2014). On average, Indian cities produce 41% of organic waste (Sharholy et al. 2008, Kumar et al. 2017). Studies on characterization based upon location, viz. household level, community bins, and dumpsite/landfill in developing countries, including India have been conducted (Azam et al. 2020, Rawat & Davey 2018, Sujauddin et al. 2008, Kumar & Goel 2009, Mboowa et al. 2017), but very few studies are available on the seasonal characterization of MSW. Some studies show that seasonal variation affects the MSW composition and characteristics (Sliusar et al. 2020, Singhal et al. 2021, Cheela et al. 2021, Ibikunle et al. 2020, Abylkhani et al. 2019, Sethi et al. 2013, Dasgupta et al. 2013, Gómez et al. 2009). There is a dearth of studies on seasonal variation of MSW characteristics at the city level. A study on the seasonal variation of MSW composition and characteristics may help in scheduling the capacities of the treatment and processing facility (Composting/ vermicomposting, ethanol production, biomethanation, and waste to energy i.e. WtE plants).

The present study was conducted in the capital city, Patna, one of the four upcoming smart cities in Bihar. There is a paucity of data on the seasonal characterization of MSW at Patna. This paper presents a detailed characterization of MSW on a seasonal basis to assess suitable waste processing techniques. The outcome of the present study will assist the policymakers of MSWM in making a way forward toward ISWM with a holistic approach.

MATERIALS AND METHODS

Study Area and its Sanitation Setup

Patna, the capital of Bihar is one of the oldest and second-largest cities in eastern India with a population of 1,683,200 (Census 2011). The city is situated between 25.5941° North and 85.1376° East geographical coordinates on the southern bank of the river Ganges. Being an entirely landlocked area, it enjoys a humid subtropical climate with quite hot summers (temperature 37-45 degrees Celsius) from

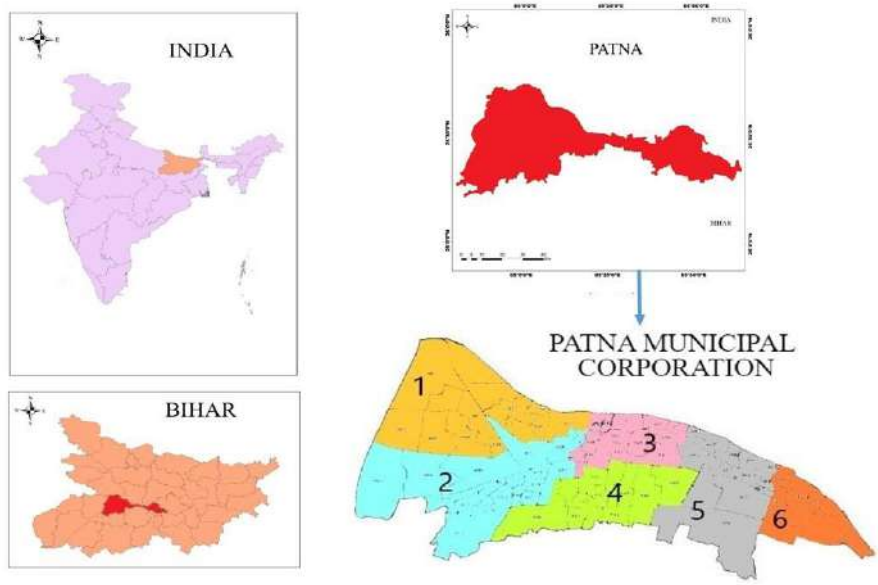

Fig. 1: Study area map with six divisions of PMC. Source: Created with software "ArcGIS 10.4.1 for Desktop".

March to June. The city receives an average rainfall of 1143 mm, from June to September and mild to chilly winters from November to February when the temperature falls up to 5 degrees Celsius.

Patna was also listed in the third round of the "100 Smart Cities Mission", an initiative of the Government of India (GoI) dated 23 June 2017 (MoUD 2017). Under *Swachha sarvekshann* (Cleanliness Survey), an annual survey of cleanliness, hygiene, and sanitation in cities and towns across India, Patna bagged 47th rank, the last among all the participating cities in 2020, and 44th out of 48 cities in 2021 (Faryal 2020, Tripathi 2021).

Solid waste management (SWM) in the city is under the Patna Municipal Corporation (PMC), one of the oldest civic bodies, established on 15th August 1952, in accordance with The PMC Act, 1951. The total area under PMC is around 109 km^2, divided into 6 divisions and 75 municipal wards (Fig. 1). Out of the total area of PMC, 47.55% comprises residential premises, which contributes to 49.56 km2. An effective SWM system is a labor-intensive service and relies upon adequate staffing (Gupta & Gupta 2015). The SWM hierarchy of PMC in the context of its supervisory and field officials is outlined in Fig. 2. As per the estimate, the city generates around 1105 TPD of MSW (BUIDCO 2020).

PMC initiated a door-to-door collection of MSW in 2018, and now this facility is being provided in all the wards of Patna. The primary collection (door-to-door) is done by PMC workers in open and closed tippers, electric tricycles, and hand carts. After primary collection, the waste is either transferred directly to the dumpsite or the transfer stations. Presently there is no treatment and processing facility for the collected waste. PMC is focusing solely on the collection and disposal of MSW in open dumpsites. The existing dumpsite (Bairiya) is an unlined dumping area of about 78 acres located on the northern side of NH 83. The present MSWM is depicted in Fig. 3. The civic body has started sensitizing the people about source segregation and cleanliness by engaging the citizens under the campaign named "one dream Patna clean" and "*Roko-Toko* (Stop and Nag)" to bring behavioral change and create a positive attitude among citizens towards SWM (Megha 2022). SWMR 2016 has made it mandatory to segregate the waste at the source of generation.

Sample Collection, Segregation and Preparation

The sampling of MSW generated in the city from all six divisions was done in accordance with ASTM D5231-92 (2016). As per this method, vehicles reaching the dumpsite from identified divisions were chosen randomly during each day of the one-week sampling period.

Fig. 2: Schematic representation of hierarchy of officials in PMC.

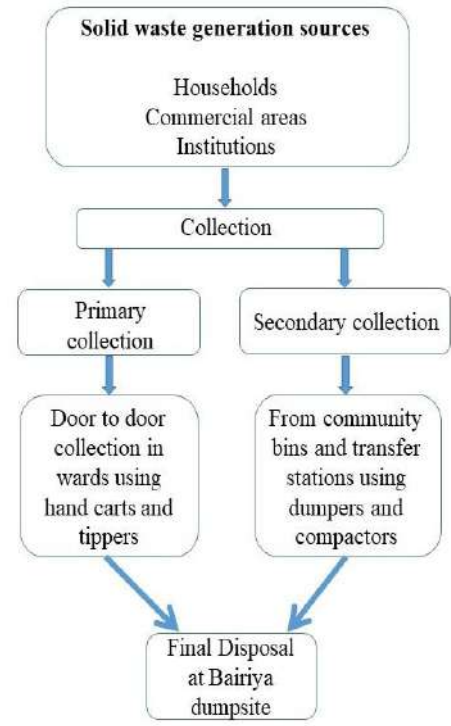

Fig. 3: Schematic representation of solid waste management in Patna.

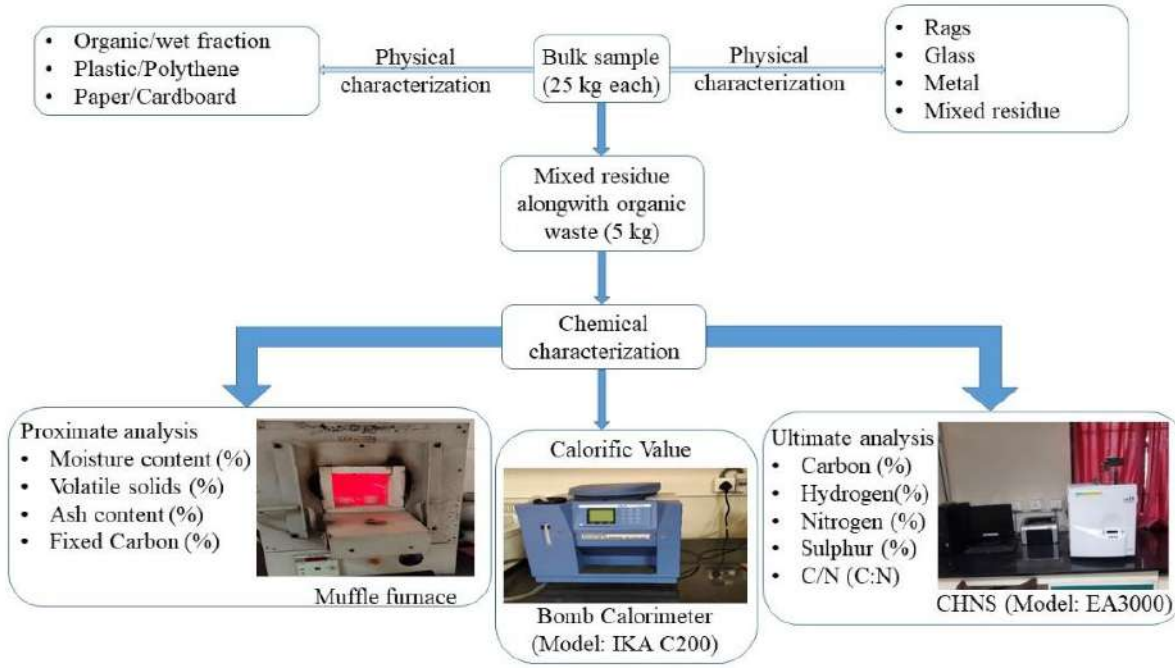

Fig. 4: Schematic diagram showing sample fractions and parameters analyzed and instruments used (Muffle furnace, Bomb calorimeter, and CHNS analyzer).

To acquire knowledge about the seasonal characteristics of MSW, the sampling was carried out for the three different seasons (Winter, Summer, and Monsoon) November, May, and August. The tippers/trucks reaching the dumpsite from the identified division were emptied by directing them to place their waste on a plastic sheet to prevent the co-mingling of underneath soil/waste. Around 100 kg of sample was collected from the waste placed on a plastic sheet for each identified division. The 100 kg of waste was collected from each division for a period of one-week sampling during each of the three seasons.

The Coning and Quartering method was implemented to obtain a representative waste sample. In this method, 100 kg of waste sample was mixed thoroughly to obtain a homogenous sample and later divided into four quarters. Further, two opposite quarters were removed and the remaining were mixed again. In this way, a representative sample of about 25 kg was obtained for each division for one week for the mentioned seasons. 5 kg of samples extracted from each representative sample were further analyzed for physical and chemical characteristics of MSW. A schematic representation of sample collection, segregation, and analysis has been presented in Fig. 4.

Physical Sorting and Composition of MSW Samples

The waste samples were hand-sorted manually with the help of waste handlers and staff present at the dump site. The samples were analyzed on a wet-weight basis. Various components like paper, polythene, plastic bottles, and other materials, milk pouches, tetra packs, concrete, stone, ash, glass, metals, soft drink cans, cartons, soiled textiles, etc. were segregated manually under the categories like organic/wet waste, plastics/polythene, paper/cardboard, soiled clothes/ textiles, glass, metal and inert or construction and demolition waste and street sweepings. The physical characterization of the MSW sample was determined seasonally for all six divisions. Different components obtained after segregation were weighed separately to obtain the percentage composition in the total waste sample.

Chemical Characterization of Collected Waste Samples

Chemical characterization of collected waste samples was done to examine their potential for different waste treatment methods including composting, incineration, and refused derived fuel (RDF). Chemical characterization includes two broad analysis procedures i.e. proximate and ultimate analysis. The proximate analysis is a specific measurement used to estimate the capability of MSW as fuel (Pichtel 2020) and in evaluating the combustion properties of waste. A limitation of the proximate analysis is that it does not indicate possible pollutants emitted during combustion. It was done to obtain the percent of moisture content, volatile solids, ash content, and fixed carbon by following the procedure described by Ibikunle et al. (2021) and Pichtel (2020).

Moisture content (MC)- The organic waste sample of 5 gm was taken into crucibles and dried in the oven at 105°C for 1 h based on ASTM D1348-94. The crucible with the sample was then cooled in a desiccator and weighed. The difference found in weight is moisture content denoted in percentage.

Volatile solids (VS)- The sample used for MC determination was then covered and heated in the muffle furnace at 950°C for 7 minutes, based on ASTM D3175-11. The sample was then cooled down and weighed. The loss in weight is taken as the percentage of volatile matter.

Ash content (AC)- It was determined by heating the remaining part of the sample in the crucible after VS estimation without lid/cover at 750°C for 30 minutes. The sample was then placed into a desiccator and cooled. The loss in weight is ash content.

Fixed Carbon (FC)- This, in the waste sample, was determined by subtracting the sum of MC (%), VS (%), and AC from 100 i.e. 100-(MC+VS+AC). The calorific value was estimated using the Bomb calorimeter (Model IKA C200). Samples were dried, ground, sieved, and made into pellets (1 gm) for energy estimation in terms of Kcal/kg.

The ultimate analysis is useful during mass balance calculations for chemical or thermal processes. The organic fraction of MSW is characterized through ultimate analysis for the determination of chemical composition. The ultimate analysis also includes the nutrient ratios, such as C/N for biological conversion processes such as composting. It involves percentage determination of total elemental analysis of Carbon, Hydrogen, Nitrogen, and Sulphur in dried samples. This was done using a CHNS analyzer (Model EA 3000) according to ASTM D3176-09. The organic sample was firstly air dried, ground to powder and again dried in a hot air oven at 105°C for 24-48 hours to remove all the moisture content.

MSWM IN PATNA: AT A GLANCE

Primary Collection and Street Sweeping

The sanitary workers (*Safai mitra*) associated with waste collection collect the waste in the morning, starting from 6 am in all six divisions (75 wards), and dump it at the nearest secondary collection/transfer station. The door-to-door collection and street sweeping are conducted in closed and open tippers respectively. In narrow and congested streets, hand carts and electric tricycles are used for waste collection. Each waste-carrying vehicle except hand carts and electric tricycles is equipped with a GPS device with a defined route for waste collection. Secondary collection points or transfer stations are open spaces provided by PMC located nearby residential areas without paved surfaces. Informal waste recycling activities are very common near secondary collection points/transfer stations. Rather than the transfer of waste from smaller to larger vehicles, no other facilities such as mechanical or manual sorting, recyclable material drop-off for citizens, and screening of MSW fractions are available at transfer stations. In some areas, these points are located near a dense population which creates a nuisance for residents. Primary collection is impeded when the vehicles used in waste collection or transportation break down.

Secondary Collection and Transportation

The secondary collection within the city is carried out using compactor trucks and open trucks (*Tata 407*), which carry the waste from secondary storage points to the Bairiya dumpsite (open dumpsite) for final disposal. The loading of waste into these vehicles is done by a skid loader, also known as a *bobcat,* or manually with the help of sanitary workers. Each division is provided with vehicle stands from where vehicles are operated and parked after waste collection. There are two vehicle workshops within the PMC boundary for the servicing and maintenance of vehicles in divisions 2 and 4 only.

Final Disposal of MSW

The fate of collected MSW ends up in an open dumping area, Bairiya dumpsite, surrounded by agricultural land. The site has been used for the last 25-30 years by the PMC. Approximately 1105 tons of MSW are dumped every day by the PMC (BUIDCO 2020). There are huge heaps of waste that can be seen from far away. The MSW dumped in the dumpsite is made to be spread by the poclain machine and leftover without proper soil coverage which causes a foul smell and unhygienic conditions. During the summer season, the case of fire breakouts occurs, releasing toxic fumes and creating a suffocating situation for onsite waste handlers and the nearby population. A weighbridge has been installed at the dump site for the quantification of waste being carried by the vehicles. There is no leachate collection system or groundwater monitoring well. Thus the leachate so generated may ooze into the soil and potentially contaminate the groundwater.

There are several infrastructures developed in very close proximity to the dump site. A school within 100 m, several godowns, and informal recycling centers with residences have been established (Fig. 5). SWMR 2016 states that groundwater monitoring well within 50 m and a buffer zone of no development activity around the dumpsite shall be maintained. As the dumpsite is surrounded by agricultural land, the associated farmers have issues with leachate runoff to their agricultural land.

Fig. 5: a) Poclain machines at the dumpsite, b) waste dumping, c) A school near the dumpsite; (Images captured during field/sampling work by researchers at different time-periods during 2021-2022 using camera model- Nikon D 3300).

RESULTS AND DISCUSSION

Physical Composition of MSW

The physical characterization of MSW is the first step and plays a crucial role in selecting waste management techniques. The results of the physical characterization of MSW of six divisions of PMC are presented in Table 1 and Fig. 6. It was observed that the organic waste (49%) remained the most prominent fraction during three different seasons in all the divisions, followed by inert (18.3%), plastic (11.3%), and paper (10.3%) (Table 1).

Rags and other waste constituted approximately 7.47% and 2.9% respectively. The presence of glass (.75%) in a low fraction in the MSW stream may be because of selling glass to the recyclers by generators and waste handlers/rag pickers in exchange for instant cash. Other studies carried out in eastern India (Kharagpur and Dhanbad), north-central India (Allahabad), and Silicon Valley of India (Bengaluru) reported 0.5%, 0.7%, and .65% of glass in MSW respectively (Sharholy et al. 2007, Kumar & Goel 2009, Mboowa et al. 2017, Ramachandra et al. 2018).

The metal fraction in MSW was 0.22% (Table 1). This negligible value indicates the practice of storing the metal at the household level and selling it to ragman (*kabaddi wala*). The manual scavenging of metal pieces by rag-pickers from secondary collection points or the roadside is also a reason for the lower percentage of metals in the MSW stream coming to the dumpsite (personal observations during sampling).

Seasonal Characterization of MSW

The variations in the composition of MSW in different seasons can be referred to the geographic location, climatic conditions, food consumption behaviors, cultural, and economic status, and religious events (CPCB 2012, Denafas et al. 2014, Ghosh 2017). As per Table 1 and Fig. 6, the difference in the seasonal variations was found in MSW components such as compostable, plastic/polythene, paper/cardboard, rags, and inert materials. Food residue or compostable fractions were higher in summer being, around 51.3% as compared to winter (46%) and monsoon (49.1%) seasons. The possible cause behind more food/compostable waste generation in summer could be the availability and

Table 1: Tabular representation of the physical composition of MSW for various divisions of Patna city on seasonal basis.

MSW Fractions		Div. 1	Div. 2	Div. 3	Div. 4	Div. 5	Div. 6	Average
Compostable/ organic	Winter	44.4	44.2	44.23	46	57	40.18	46.00
	Summer	51	51.5	48	52.3	59.5	46	51.38
	Monsoon	48.2	50.5	46.88	48.77	55.6	44.6	49.09
	Average	47.87	48.73	46.37	49.02	57.37	43.59	48.83
Plastic/Polythene	Winter	12.15	9.5	13.88	9.5	6.88	8.32	10.04
	Summer	16	14.8	17.7	14.6	10	7.15	13.38
	Monsoon	13	11.3	14	11.65	8.2	5.26	10.57
	Average	13.72	11.87	15.19	11.92	8.36	6.91	11.33
Paper/Cardboard	Winter	9	13.2	9.5	14.4	10	13.2	11.55
	Summer	8.3	8.6	7.8	7.28	6.2	9.66	7.97
	Monsoon	7.36	11	12	11.86	13.4	12.55	11.36
	Average	8.22	10.93	9.77	11.18	9.87	11.80	10.30
Rags	Winter	11.5	9.2	12.32	8.48	5.6	6.16	8.88
	Summer	7.6	3.6	8.5	7.2	5	5.25	6.19
	Monsoon	9.5	6.48	8	6.3	6.37	7.39	7.34
	Average	9.53	6.43	9.61	7.33	5.66	6.27	7.47
Glass	Winter	1.26	0	0.6	0.4	1.3	0	0.59
	Summer	0	1.5	0	1.3	1	2.3	1.02
	Monsoon	0	0	2.2	0	1	0.6	0.63
	Average	0.42	0.50	0.93	0.57	1.10	0.97	0.75
Metal	Winter	0.8	0.2	0.1	0	0.8	0	0.32
	Summer	0	0.2	0.1	0	0	1.6	0.32
	Monsoon	0	0.13	0	0	0	0.1	0.04
	Average	0.27	0.18	0.07	0.00	0.27	0.57	0.22
Inert	Winter	19.55	22.2	18.37	20.02	15.8	29.6	20.92
	Summer	13.33	16.4	14.4	16	13.3	26	16.57
	Monsoon	14.84	17.45	15.23	18.67	11	26.5	17.28
	Average	15.91	18.68	16.00	18.23	13.37	27.37	18.26
Others*	Winter	1.34	1.5	1	1.2	2.62	2.54	1.70
	Summer	4	3.4	3.5	1.32	5	2.04	3.21
	Monsoon	7.1	3.14	1.69	2.75	4.43	3	3.69
	Average	4.15	2.68	2.06	1.76	4.02	2.53	2.87

All the values are in percentage; *Includes waste like dry leaves, thermocol and coconut shells.

consumption of various fruits and peeled vegetables and their wastage due to rotting caused by high temperatures. A seasonal characterization study conducted in Guwahati city revealed that the MSW contained approximately 49% (Singhal et al. 2021) of compostable or food waste in the summer season, which is similar to the results found in the present study. Plastic or polythene wastes were found to be high during summer (13.38%) as compared to winter and monsoon seasons (10% and 10.57% respectively), which is likely due to the consumption of different types of drinks contained in plastic-made bottles (Sethi et al. 2013). Plastic ice cream cups were also found in high amounts. A study conducted by Cheela et al. (2021) in Vishakhapatnam has shown similar findings (9.39-9.86%), with no significant changes in plastic waste fractions in winter and pre and post-monsoon seasons. The paper/cardboard and soiled cloth/ textile wastes were higher in the winter season being 11.5 and 8.8% respectively. During the winter season, several

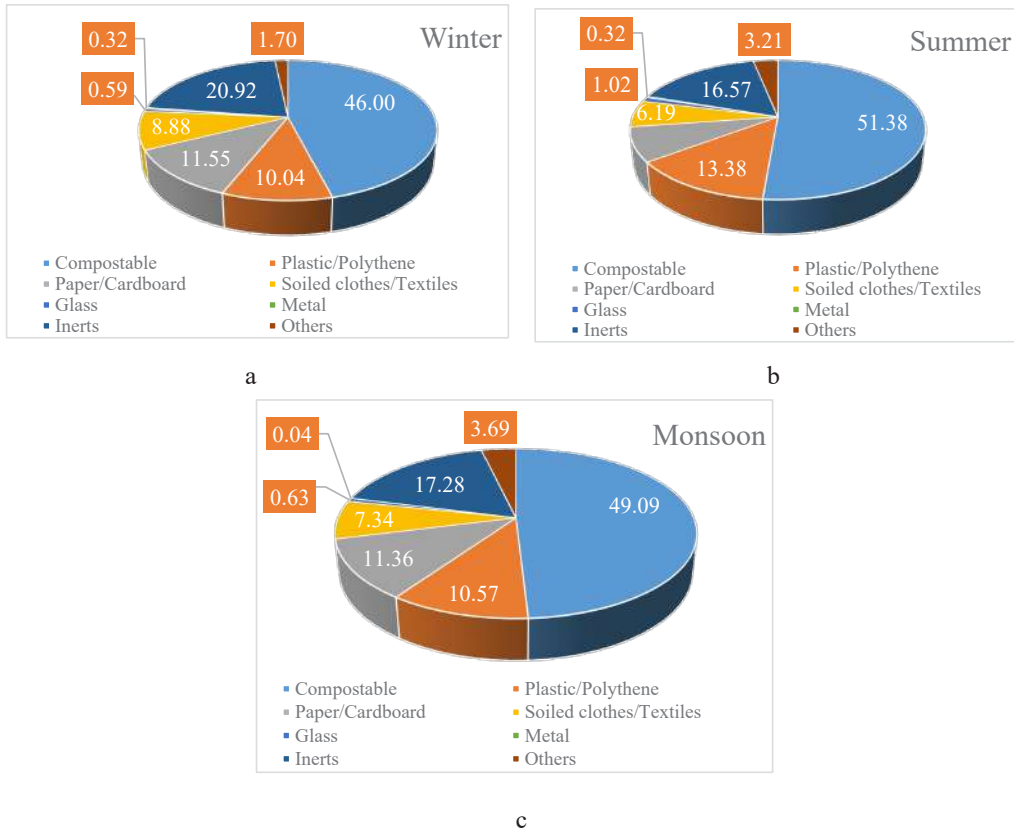

Fig. 6: Pie diagrams representing average variation in seasonal composition of MSW.

festivals are celebrated in this region of India such as *Diwali* followed by a festival named "*Chhath*" an ancient and most holy festival historically native to the Indian subcontinent, more specifically, the Indian state of Bihar. In the lead-up to these festivals, celebrants prepare for a month-long by cleaning, renovating, and decorating their homes and workplaces (Kumar 2008) which could be a strong reason for the generation of paper and rags during the winter season. Inert waste is the second most abundantly present component in the MSW stream. The inert waste contains sand, stones, concrete, ash, grits, and construction and demolition waste. The highest amount of inert waste was witnessed in the winter season (21%). The possible reason for this is the practice of burning wood, coal, etc. to get protection against cold. Local public administration also provides this facility along the roadside and at various nooks of the city for people which adds up during street sweeping to the inert material in the MSW stream. The other reasons for highly inert materials are unpaved roads, street sweeping, construction activities under smart area development projects, and dredging and cleaning of a storm drain (Miezah et al. 2015, Khan et al. 2016, Kumar et al. 2017). Several other waste components such as dry leaves, thermocol, and coconut shells were mostly found in higher quantities in the summer and monsoon seasons (3.21% and 3.69%).

Spatial Variation in MSW Composition

The mean values of different waste components based on the divisions in the study area are presented in table 3. Compostable waste fraction (CWF) is the major component of the MSW in each division. CWF fraction of 57.3% was significantly present in division 5, as this division has several vegetable markets and is attributed to the low-income group. The low-income group generates more CWF (Rana et al. 2018) as solid fuels such as coal, wood, briquette, and dung cakes are used for cooking purposes (Khan et al. 2016). The highest amount of plastic and rags wastes were found to be 15.3% and 9.61% respectively from division 3, which is dominated by commercial establishments, institutions, and offices. The major activities contributing to plastic waste generation are the use of plastics as packaging materials, bottling drinks, and carrying bags (Miezah et al. 2015). On the other hand, some area of division 3 is situated along the bank of the river Ganges which has several cremations ground that adds up to the rag fractions. The lowest CWF and highest inert fraction were found in division 6. It may be

Table 2: Division-wise population of PMC.

Div. 1	Div. 2	Div. 3	Div. 4	Div. 5	Div. 6
367053	313821	254090	282332	293356	173570

Source: PMC 2011; https://www.censusindia.co.in/towns/patna-population-patna-bihar-801373

Fig. 7: Transportation of sand in open tractor trolleys. (Image captured during field/sampling work by researchers at different time-periods during 2021-2022 using camera model- Nikon D 3300).

because of the considerably higher population in this division rear cattle and utilize the generated CWF as cattle feed. Hence linked to a comparatively lesser generation of CWF with the least population among all the divisions (Table 2). Inert waste was found in the highest quantity in divisions 2 and 6 due to infrastructure development (construction work) and sand mining along the banks of the river Ganges. The transportation of sand in open tractor trolleys causes spill-off on the roads as shown in Fig. 7 (taken during the field survey).

Chemical Characterization of MSW

The chemical characterization provides an insight into the percentage of elements present in the MSW, which further aids in deciding the appropriate treatment technology that needs to be incorporated (Rana et al. 2018). The results of the proximate and ultimate analysis are presented in Table 4 and Table 5 respectively.

The MC of MSW ranged between 43% to 52% across the seasons. The data on MC helps develop suitable methods for the treatment of MSW (Cheela et al. 2021). The earlier study for Indian cities with a population between 1-2 million reported the MC between 25% - 65% (Kumar et al. 2009). In a study conducted in the Tricity region of Northern India (Chandigarh, Mohali, and Panchkula) the MC was reported

Table 3: Characterization of MSW on a divisional basis.

MSW Fractions	Div. 1	Div. 2	Div. 3	Div. 4	Div. 5	Div. 6
Compostable	47.87	48.23	46.20	49.02	57.37	43.59
Plastic/ Polythene	13.72	12.20	15.31	12.25	8.77	6.91
Paper/ Cardboard	8.22	10.93	9.79	11.91	9.87	11.80
Soiled clothes/ Textiles	9.53	6.43	9.61	6.03	4.99	6.27
Glass	0.42	0.54	1.13	0.13	1.10	0.97
Metal	0.27	0.18	0.07	0.00	0.27	0.57
Inert	15.91	18.82	16.07	18.56	13.03	27.37
Others	4.05	2.67	1.82	2.08	4.61	2.53

All the values are in percentage (%).

to be between 40% - 50% (Rana et al. 2018). The MC thus found in the Tricity region is quite similar to the present study. The high MC was observed in the Monsoon season, while the lowest was in the summer season. The high MC was due to rainfall. During the field visits, it was observed that most of the waste-carrying vehicles are not designed to meet the requirements of the existing situation and are incapable of achieving the design value. Additionally, due to uncovered transport of the MSW in the vehicle during rains, disposing of the MSW on wetland margins and urban sewer drains leads to high MC (43%-51%). The volatile solids (VS) were observed between 20%-29%. Based on the results of MC and VS, composting and biomethanation can be suggested as the MSW treatment option. Ash content was between 20% - 26%. The possible reason for the high ash content (26%) in the winter season could be the presence of inert material in this season. The ash content in the mixed waste sample from a dumpsite in Chennai was found to be 21% (Peter et al. 2019).

While looking into the elemental composition, Carbon (C) ranges between (16%-20%), Hydrogen (H) (1.6%-5%), Oxygen (O) (13%-17%), and Nitrogen (N) and Sulphur (S) together comprised of 1%. The Highest C content was found in division 5. It may be due to the presence of large vegetable markets and a holy place of Sikhs, *Gurudwara Patna Saheb*, where a large dining hall (*Langar Seva*) utilizing tons of vegetables and other natural foods is run throughout the year which leads to the generation of vegetable and food wastes. An optimum range of C/N ratio was observed in divisions 1 and 4, due to the segregation of waste at the secondary dumping/collection point for composting by PMC.

Thus, there exists a possibility of a decentralized approach to implementing composting and vermicomposting facilities in these divisions. However, the average C/N ratio

Table 4: Tabular description of proximate analysis of MSW.

		Div. 1	Div. 2	Div. 3	Div. 4	Div. 5	Div. 6	Average
Moisture	Winter	49	51.3	47	50.55	51.5	39.26	48.10
	Summer	47.5	45.6	43.3	48.25	42.6	32	43.21
	Monsoon	55.6	53	53.6	53.6	53.4	41.5	51.78
	Average	50.70	49.97	47.97	50.80	49.17	37.59	47.70
Volatile matter	Winter	17.7	20	22	20.6	20.15	20.64	20.18
	Summer	25.3	28	31	30.2	34.6	27.6	29.45
	Monsoon	16.3	28.6	24.8	22.45	22	29.8	23.99
	Average	19.77	25.53	25.93	24.42	25.58	26.01	24.54
Ash content	Winter	27.3	26	26.2	24.6	21.3	32	26.23
	Summer	20.65	20.4	20	17.3	17.5	33.6	21.58
	Monsoon	25.29	15.2	17.2	20.18	20.8	22.5	20.20
	Average	24.41	20.53	21.13	20.69	19.87	29.37	22.67
Fixed carbon	Winter	6	2.7	5.7	4.12	7.1	8.4	5.67
	Summer	6.5	6	5.6	4.95	5.6	6.8	5.91
	Monsoon	2.81	3.2	4.5	3.78	3.8	6.55	4.11
	Average	5.10	3.97	5.27	4.28	5.50	7.25	5.23

All the values are in percentage (%).

of the mixed MSW was low (23%) to be used directly for composting. It may increase and the optimum range of 30:1 can be achieved after segregation. The calorific value (CV) of the MSW from all the divisions during the studied seasons was in the range of 823-3839 kcal.kg^{-1} (Table 6). On average the estimated CV was 1700 Kcal/Kg. The CV, only during the summer season was in the range prescribed under SWMR 2016 (>1500Kcal/kg) for incineration or RDF generation. The CV was below the prescribed limit during the monsoon and winter seasons which may render the incineration and

Table 5: Tabular description of the ultimate analysis of MSW.

Elements	Div. 1	Div. 2	Div. 3	Div. 4	Div. 5	Div. 6	Average
Carbon	16.15	15.5	18.34	13.65	21.43	19.8	17.48
Hydrogen	3.9	4.55	3.74	4.68	2	1.6	3.41
Nitrogen	0.56	0.93	1.16	0.47	1.07	0.72	0.82
Sulfur	0.013	0.031	ND	ND	0.65	0.045	0.18
Oxygen	13.6	14.26	13.2	14	17.43	13.01	14.25
C/N	28.839	16.66	15.81	29.04	20.02	27.5	22.98

All the values are in percentage (%) except the C/N ratio.

Table 6: Seasonal variations in calorific value of MSW (in kcal/kg).

Divisions	Winter	Summer	Monsoon
Div. 1	1435	2540	1345
Div. 2	1223	2704	1035
Div. 3	1142	2887	1166
Div. 4	1546	3839	1673
Div. 5	1302	2458	1232
Div. 6	912	1336	823
Average	1260	2627.33	1212.33

WtE generation process. A WtE plant of 400 MW of green power is under the planning stage at the dumpsite (CPCB 2019-20). In this context, the government alongwith the civic body may have to adopt the latest and the most advanced technology for the thermal treatment of MSW which may require additional fuel (Wilson et al. 2012) and provisions for adequate fund allotment in the budget for waste management (CPHEEO 2016).

Existing MSW Processing Techniques in Patna

Composting

After the implementation of SWMR 2016 and the Swachha Bharat Mission, the PMC initiated the installation of composting plants in various areas within the boundary of the PMC. In the first phase of installation 15 such plants have been installed with an input load of 2000 kg and 500 kg capacity per day of biodegradable waste. The civic body has set a target to install 22 more composting plants in the city (Faryal 2021). Till now, no to very less potential buyers have been identified and the compost so produced is being stored. Composting in open windrows is preferred because of the ambient temperature of the city. In comparison with available MSW treatment technologies, from installation, and maintenance to operation, composting requires the lowest capital investment.

Waste Recycling

The PMC itself directly is not indulged in the recycling facility. The recycling activity is generally carried out by small or large-scale recyclers. Recyclable junk such as plastics, paper, cardboard, metals, and glasses are either sold directly by households or by waste handlers. Most of the recycling businesses flourish in the near vicinity of the waste dumping areas, as the waste pickers found abundant recyclable material there which they use to pick, sort, and sell for their livelihood.

In most developing nations, waste is perceived as a valuable resource for the informal sector. The scavenging activities by the informal sector where there is no established municipal structure in operation provide employment, reduce littering, increase the lifespan of the landfill, pollution is abated and ultimately, the flow of waste is reduced (Damghani et al. 2008, Monirozzaman et al. 2011, Ezeah et al. 2013). In India, there are around 2 million waste-pickers (Swaminathan 2018, Chaturvedi 2010) though some figures say that almost 40 percent of waste-pickers are less than 18 years of age (Swaminathan 2018). In the informal sector, activities are usually carried out by persons or family groups. Fig. 8 represents and describes the role of various sectors from bottom to top i.e. from waste picking (segregation) to processing and its use as raw material in manufacturing industries.

Suggestions and Possible Solutions for Enhanced SWM in Patna

The science of waste management is dependent upon the physical composition and chemical characteristics of the MSW. Presently, the established waste management system in Patna city follows a linear fashion which neither includes proper source segregation nor the pre-treatment of MSW (Fig. 9). There seems to be an urgent need to redesign the current MSWM system which should include appropriate waste treatment technology in compliance with

(Source: Modified Wilson et al. 2006)

Fig. 8: Hierarchy of informal sector recycling

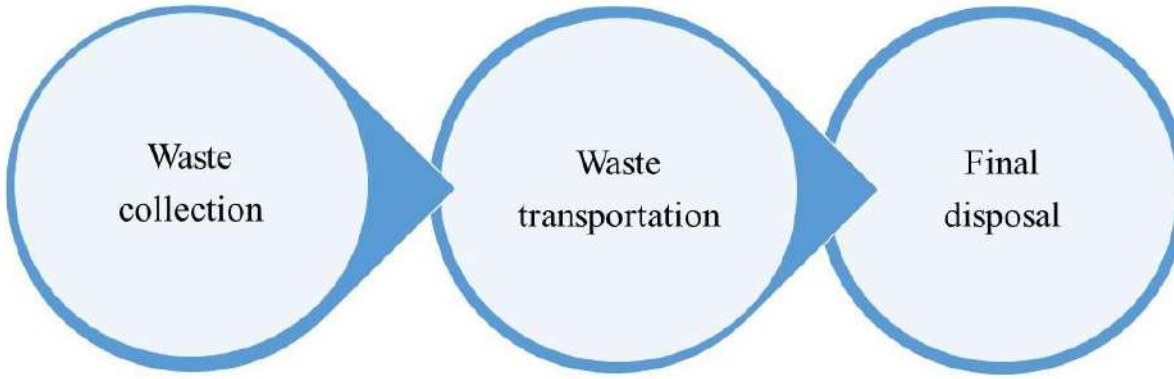

Fig. 9: Linear fashion of present waste management at Patna.

SWMR 2016. Based on the findings of the study following recommendations have been put forward.

Source Segregation and Collection of MSW

The segregation of waste at the source or household level is the first and crucial step for the successful implementation of available waste treatment technologies. The findings indicate that a large fraction of the MSW is organic and inert. Thus ensuring the segregation of MSW at the source of generation, scheduling of collection of recyclables at the household level and segregation facility at transfer stations to prevent the co-mingling during secondary collection and transportation is a dire need.

- The principal step in source segregation is educating, sensitizing, and creating awareness in the population at a massive level.
- Secondly, providing and implementing basic amenities such as two or three-bin systems for separate collection of waste is recommended.
- Additionally, Urban local bodies (ULBs) need to facilitate the infrastructure development and train the field staff for separate collection of waste to prevent the comingling of organic waste with inert fractions.
- The sources of inerts in the MSW stream are street sweepings, construction activities, sand, and grits from unpaved roads. A separate waste collection system must be implemented to ensure separate collection.
- The inert fraction so collected may be used for daily covers at landfills or dumpsites.
- The capacity of containers needs to be designed by the civic body based on the population density and waste generation rate.

Recycling and Recovery

Although recycling ranks third in the waste management hierarchy, it can be given priority as the recyclable fractions (22%) in MSW streams are present in noticeable amounts. However, recycling or recovery activities can be achieved at a higher potential only when the practice of source segregation is implemented strictly. The plastic recovery rate in India is estimated to be around 40% which is far better and much higher than in developed nations having only a recycling rate of 10-15% (Srivastava et al. 2005, Srivastava & Jain 2007, Sethi et al. 2013, Srivastava et al. 2014, Rana et al. 2018)

- SWMR 2016 suggests that the degradable (organic fraction) and non-biodegradable (recyclables/dry waste) shall be stored separately at the household level in separate bins and collected separately by ULBs. Thus, proper segregation of MSW can increase the potential for scientific treatment and disposal.
- Informal waste segregation by waste pickers was observed in several parts of the city and at the dump site. The PMC should focus on formalizing informal waste sectors by registering them under a state policy of SWM strategy with stakeholders including the representative of informal waste handlers.
- The segregation of recyclable materials and organic fractions of MSW by formalizing the waste recycling chain can provide a source of revenue generation that may be used for infrastructure development as well as a better-quality end product in the form of compost.

Anaerobic Digestion or Biomethanation

Anaerobic digestion (AD) is a process through which bacteria break down organic matter such as animal manure, wastewater bio-solids, and food wastes in the absence of oxygen that produces biogas and liquid slurry (Demirbas 2016). The composition of biodegradable waste (46%-51%) and MC (43%-51%) of MSW of the city along with humid weather, provide suitable conditions for AD. The C/N ratio

(23) and VS (25%) are somewhat low, and incompatible to favour the AD process. However, with proper waste segregation at the household level, the MSW can be used for AD. There is a difference in the composition of MSW within the different divisions of the city. Thus implementing a decentralized system for waste treatment by AD may reduce the transportation cost of the waste for final disposal to the dumpsite and hence burden on the landfill. The biogas thus produced may take the route to electricity generation or can be converted into biofuel.

Composting

Alternative to AD, several studies have recommended that composting (aerobic digestion) can play an important role in managing the biodegradable waste fraction of MSW (Giusti 2009, Rawat et al. 2013, Pathania et al. 2014, Mengistu et al. 2017). Except for a few fractions, almost all the compostable waste is dumped directly into the dumpsite in an unscientific manner.

- In this regard, composting could be seen as a suitable 'baseline' waste treatment method to be applicable in Patna city.
- The results of physical and chemical characterization of the MSW in the study area revealed that almost half the fraction of the total MSW generated is organic with high moisture content in the range of 43%-51% which makes composting an attractive and preferable waste treatment option.
- The average C/N ratio estimated in the study area was found to be 23 which is lower than the optimum C/N ratio for composting (30:1). Still, with proper waste segregation, the optimum range can be achieved.
- The leachate production in the dumpsite is mainly due to biodegradable waste. In this context, a decentralized composting mechanism can reduce the burden on dumpsites and thus, leachate production.

Refuse Derived Fuel

As mentioned in part II section 3 (ii) of the SWMR 2016, RDF is the combustible fraction of MSW that is converted into pellets by drying, shredding, dehydrating, and compacting. At present throughout the world, approximately 84% of the electricity is generated by burning fossil fuels, which is a non-renewable natural resource (Kumar & Samadder 2017). In this regard, RDFs seem to be an alternative and sustainable option to be co-processed with coal in large coal-based industries such as cement kilns and thermal power plants. However, there are several limitations to the co-processing and use of RDFs in industries because of irregular supply, lack of established practice, and retrofitting of the existing mechanism to make the present machinery use RDF as fuel. As per Central Public Health and Environmental Engineering Organisation (CPHEEO 2016), these shortcomings can be overcome by producing crude RDFs and transporting them to industries from multiple locations. Furthermore, based on specific requirements the crude RDFs can be refined by the industries themselves. There is a total of 129 RDF/ palletization plants operational in India. Madhya Pradesh has 83, the maximum number of RDFs plants installed and operational till now (CPCB 2019-20).

The average CV of the MSW in the study area is also appropriate for the generation of good-quality RDFs. The PMC has started sorting legacy waste by installing trommel machines with sieving sizes of 8mm, 20-30 mm, and 40 mm at the dumpsite with a plan to segregate the fresh MSW shortly. The legacy waste thus segregated produces compost, fine earth, and crude RDFs. The crude RDFs is sold and transferred to the cement industry situated in the Aurangabad district of Bihar. The compost so produced is being purchased by the local farmers for their agricultural purposes.

CONCLUSION

The study is based on the seasonal characterization of MSW, which provides baseline data to outline the effective waste management strategy and best available MSW processing technologies for the city of Patna. In addition, the lacking and issues alongwith possible solutions in the functional elements of waste management have been discussed. The compositional analysis of MSW of the city of Patna shows the approximate average composition of biodegradable matter, plastic/polythene, paper/cardboard, rags, glass, metals, inert, and others to be 49%, 11.33%, 10.3%, 7.5%, 0.75%, 0.22%, 18.26%, and 3% respectively. The results of physical characterization revealed that the major fractions of the MSW stream were biodegradable (49%) and inert waste (18%). A difference of ~5% in the biodegradable, ~3% in the plastic/polythene, and ~3.6% in the paper/cardboard fractions of the MSW was observed during the winter and summer seasons. Inert fraction must be considered, as its presence in a high amount generally hinders the treatment process. The inert fraction which includes sand, street sweepings, and C&D waste, must be prevented from mixing up with the MSW and collected separately. Chemical characterization including MC, VM, AC, C, H, N, and S has also shown variations during three different seasons. The MC was highest in monsoon (~52%) while lowest in the summer season. The VM was found to be high during summers (~29%) while AC was high in the winter season (~26%). While looking into the energy content (CV) of the MSW, the average CV was determined as 1700 kcal.Kg^{-1} which was noticeably highest

in summer (2627 kcal.kg^{-1}) and lowest in monsoon season (1212 kcal.kg^{-1}).

The characterization of MSW in the study area unveils the fact that the ULB has several options for treatment technology. Composting alongwith vermicomposting facilities is simple, low budget, and easy to maintain technology is an urgent need to treat compostable waste. The city of Patna has content of recyclables such as plastics and papers which have a high potential for producing RDFs or to be used again by installing a formal chain supply of recycling facilities. Still, the practice of source segregation is the key step for strengthening the broader concept of waste to wealth. Currently, in the city of Patna, the MSW is present in mixed form, which makes the treatment quite difficult and costly. So, the city has to gear up to improve the SWM practices and increase the ranking in the Cleanliness survey (*Swachha Survekshann)* for holistic development including the concept of ISWM.

ACKNOWLEDGEMENTS

The authors are thankful to the University Grants Commission (UGC) for providing funding support as a Research Fellowship (NET-JRF/SRF) to the first author, Faiz Ahmad Siddiqui for completing this work as a part of his Ph.D. research. Furthermore, the authors are grateful to the municipal commissioner, Shri Keshav Ranjan Prasad for granting permission to collect samples at the landfill site. The cooperation and help extended by the onsite workers at the dumpsite are also acknowledged.

REFERENCES

Abylkhani, B., Aiymbetov, B., Yagofarova, A., Tokmurzin, D., Venetis, C., Poulopoulos, S., Sarbassov, Y. and Inglezakis, V.J. 2019. Seasonal characterization of municipal solid waste from Astana city, Kazakhstan: Composition and thermal properties of the combustible fraction. Waste Manag. Res., 37(12): 1271-1281.

ASTM Method D1348-94. 2008. Standard Method for Moisture in Cellulose. West Conshohocken: ASTM International.

ASTM Method D3175-11 2013. America Society for Testing and Materials, for Volatile Matters. West Conshohocken: ASTM International, 504-509.

ASTM. 2016. Standard Test Method for Determination of the Composition of Unprocessed Municipal Solid Waste. D5231–92. West Conshohocken, PA, USA: American Society for Testing and Materials.

Azam, M., Jahromy, S.S., Raza, W., Raza, N., Lee, S.S., Kim, K.H. and Winter, F. 2020. Status, characterization, and potential utilization of municipal solid waste as a renewable energy source: Lahore case study in Pakistan. Environ, Int., 134: 105291.

BUIDCO 2020. Tender notice for Patna and Gaya municipal corporations, Bihar Urban Infrastructure Development Corporation Limited, 1: 1-82. http://www.buidco.in/Application/TenderDoc/556_07-Nov-2020_Bid%20Document%20Patna%20n%20Gaya%20Part%201.pdf

Census 2011. Census of India 2011. Government of India. Provisional Population Totals. https://censusindia.gov.in/2011-prov results/paper2/data_files/india2/1.%20data%20highlight.pdf

Census 2011. Census of India 2011. Government of India. Provisional Population Totals. https://web.archive.org/web/20120507135928/http:/www.censusindia.gov.in/2011-prov-results/paper2/data_files/India2/+_2_PR_Cities_1Lakh_and_Above.pdf

Central Pollution Control Board (CPCB) 2020. Annual Report 2019-20 on Implementation of Solid Waste Management Rules, 2016. CPCB, New Delhi, pp 1-143.

Chaturvedi, B. 2010. Mainstreaming waste pickers and the informal recycling sector in municipal solid waste. Handling and Management Rules 2000. A discussion paper, WEIGO, Women in Informal Employment: Globalizing and Organizing, UK.

Cheela, V.R.S., Goel, S., John, M. and Dubey, B. 2021. Characterization of municipal solid waste based on seasonal variations, source, and socio-economic aspects. Waste Disp. Sustain. Energy, 3(4): 275-288.

Chen, D.M.C., Bodirsky, B.L., Krueger, T., Mishra, A. and Popp, A. 2020. The world's growing municipal solid waste: Trends and impacts. Environ. Res. Lett., 15(7): 074021.

CPCB 2012. Consolidated Annual Review Report on implementation of municipal solid wastes (management and handling) Rules, 2000, Central Pollution Control Board, New Delhi.

CPHEEO 2016. Municipal Solid Waste Management Manual (MSWMM) (Part I and II), 2016. Central Public Health and Environmental Engineering Organization (CPHEEO). Swachh Bharat Mission. 1(1).

Damghani, A.M., Savarypour, G., Zand, E. and Deihimfard, R. 2008. Municipal solid waste management in Tehran: Current practices, opportunities, and challenges. Waste Manag., 28(5): 929-934.

Das, S. and Bhattacharyya, B.K. 2013. Municipal solid waste characteristics and management in Kolkata, India. In The 19th International Conference on Industrial Engineering and Engineering Management (pp. 1409-1399). Springer, Berlin, Heidelberg.

Dasgupta, B., Yadav, V.L. and Mondal, M.K. 2013. Seasonal characterization and present status of municipal solid waste (MSW) management in Varanasi, India. Adv. Environ. Res., 2(1): 51-60.

Demirbas, A., Taylan, O. and Kaya, D. 2016. Biogas production from municipal sewage sludge (MSS). Energy Sources, Part A: Recovery, Utilization, and Environmental Effects, 38: 3027-3033.

Denafas, G., Ruzgas, T., Martuzevičus, D., Shmarin, S., Hoffmann, M., Mykhaylenko, V., Ogorodnik, S., Romanov, M., Neguliaeva, E., Chusov, A. and Turkadze, T. 2014. Seasonal variation of municipal solid waste generation and composition in four East European cities. Resour. Conserv. Recycl., 89: 22-30.

Dinda, S., Chatterjee, N.D. and Ghosh, S. 2021. An integrated simulation approach to the assessment of urban growth pattern and loss in urban green space in Kolkata, India: A GIS-based analysis. Ecol. Indic., 121: 107178.

Ezeah, C., Fazakerley, J.A. and Roberts, C.L. 2013. Emerging trends in informal sector recycling in developing and transition countries. Waste Manag., 33(11): 2509-2519.

Faryal, Rumi 2020. Patna last among 47 cities in Swachh Survekshann, The Times of India (ToI), August 21, 2020. Available at: https://timesofindia.indiatimes.com/city/patna/patna-last-among-47-cities-in-swachh-survekshan/articleshow/77660860.cms.

Faryal Rumi 2021. Patna to get 22 more waste composting plants: Civic body, The Times of India (ToI), March 12, 2021. Available at: https://timesofindia.indiatimes.com/city/patna/civic-body-patna-to-get-22-more-waste-composting-plants/articleshow/81454115.cms

Ghosh, S.K. 2017. Centre for regional development, Country Chapter. United Nations, NY.

Giusti, L. 2009. A review of waste management practices and their impact on human health. Waste Manag., 29: 2227-2239.

Gómez, G., Meneses, M., Ballinas, L. and Castells, F. 2009. Seasonal characterization of municipal solid waste (MSW) in the city of Chihuahua, Mexico. Waste Manag., 29(7): 2018-2024.

Gupta, N. and Gupta, R. 2015. Solid waste management and sustainable

cities in India: the case of Chandigarh. Environ. Urban., 27(2): 573-588.

Hoornweg, D. and Bhada-Tata, P. 2012. What a waste: a global review of solid waste management. World Bank Publications, Washington DC.

Ibikunle, R.A., Titiladunayo, I.F., Dahunsi, S.O., Akeju, E.A. and Osueke, C.O. 2021. Characterization and projection of dry season municipal solid waste for energy production in Ilorin metropolis, Nigeria. Waste Manag. Res., 39(8): 1048-1057.

Ibikunle, R.A., Titiladunayo, I.F., Lukman, A.F., Dahunsi, S.O. and Akeju, E.A. 2020. Municipal solid waste sampling, quantification and seasonal characterization for power evaluation: Energy potential and statistical modeling. Fuel, 277: 118-122.

Kaza, S., Yao, L., Bhada-Tata, P. and Van Woerden, F. 2018. What a waste 2.0: a global snapshot of solid waste management to 2050. World Bank Publications, Washington DC.

Khan, D., Kumar, A. and Samadder, S.R. 2016. Impact of socioeconomic status on municipal solid waste generation rate. Waste Manag., 49: 15-25.

Kolekar, K.A., Hazra, T. and Chakrabarty, S.N. 2016. A review on prediction of municipal solid waste generation models. Procedia Environ. Sci., 35: pp. 238-244.

Kumar, A. and Samadder, S.R. 2017. A review of technological options of waste to energy for effective management of municipal solid waste. Waste Manag., 69: 407-422.

Kumar, K.N. and Goel, S. 2009. Characterization of municipal solid waste (MSW) and a proposed management plan for Kharagpur, West Bengal, India. Resour., Conserv. Recycl., 53(3): 166-174.

Kumar, P. 2008. Meri Khoj Ek Bharat Ki. ISBN -1240-4357-1-978 9. Archived from the original on 10 January 2022

Kumar, S., Bhattacharyya, J.K., Vaidya, A.N., Chakrabarti, T., Devotta, S. and Akolkar, A.B. 2009. Assessment of the status of municipal solid waste management in metro cities, state capitals, class I cities, and class II towns in India: An insight. Waste Manag., 29(2): pp.883-895.

Kumar, S., Smith, S.R., Fowler, G., Velis, C., Kumar, S.J., Arya, S., Rena, Kumar, R. and Cheeseman, C. 2017. Challenges and opportunities associated with waste management in India. Royal Soc. Open Sci., 4(3): 160764.

Marshall, R.E. and Farahbakhsh, K. 2013. Systems approach integrated solid waste management in developing countries. Waste Manag., 33(4): 988-1003.

Mboowa, D., Qureshi, S., Bhattacharjee, C., Tonny, K. and Dutta, S. 2017. Qualitative determination of energy potential and methane generation from municipal solid waste (MSW) in Dhanbad (India). Energy, 123: 386-391.

Megha 2022. Swachh survey: PMC to boost public participation in cleanliness efforts, Hindustan Times (HT), February 14, 2022. https://www.hindustantimes.com/cities/patna-news/swachh-survey-pmc-to-boost-public-participation-in-cleanliness-efforts-101644808448169.html

Mengistu, T., Gebrekidan, H., Kibret, K., Woldetsadik, K., Shimelis, B. and Yadav, H. 2018. Comparative effectiveness of different composting methods on the stabilization, maturation, and sanitization of municipal organic solid wastes and dried fecal sludge mixtures. Environ. Syst. Res., 6(1): 1-16.

Miezah, K., Obiri-Danso, K., Kádár, Z., Fei-Baffoe, B. and Mensah, M.Y. 2015. Municipal solid waste characterization and quantification as a measure towards effective waste management in Ghana. Waste Manag., 46: 15-27.

Moniruzzaman, S.M., Bari, Q.H. and Fukuhara, T. 2011. Recycling practices of solid waste in Khulna city, Bangladesh. J. Solid Waste Technol. Manag., 37(1): 1-15.

Parihar, R.S., Ahmed, S., Baredar, P. and Sharma, A. 2017. Characterization and management of municipal solid waste in Bhopal, Madhya Pradesh, India. Waste Resour. Manag., 170: 95-106. Thomas Telford Ltd.

Pathania, R., Bhardwaj, S.K. and Verma, S. 2014. Analysis of urban solid waste generation in Solan town and its bio-recycling through composting. Agric. Sustain. Develop., 2(2): 149-152.

Peter, A.E., Nagendra, S.M.S. and Nambi, M.I. 2019. Environmental burden by an open dumpsite in urban India. Waste Manag., 85: 151-163.

Pichtel, J. 2014. Waste management practices: municipal, hazardous, and industrial. CRC Press, Boca Raton.

PMC 2011. Patna Population, Religion, Caste, Working Data Patna, Bihar - Census 2011. https://www.censusindia.co.in/towns/patna-population-patna-bihar-801373

Ramachandra, T.V., Bharath, H.A., Kulkarni, G. and Han, S.S. 2018. Municipal solid waste: Generation, composition and GHG emissions in Bangalore, India. Renew. Sustain. Energy Rev., 82: 1122-1136.

Rana, R., Ganguly, R. and Gupta, A.K. 2018. Physico-chemical characterization of municipal solid waste from Tricity region of Northern India: A case study. J. Mater. Cycl. Waste Manag., 20: 678-689.

Rawat, M., Ramanathan, A.L. and Kuriakose, T. 2013. Characterization of municipal solid waste compost (MSWC) from selected Indian cities-a case study for its sustainable utilization. Scientific Research, 4: 163-171.

Rawat, S. and Daverey, A. 2018. Characterization of household solid waste and current status of municipal waste management in Rishikesh, Uttrakhand. Environ. Eng. Res., 23(3): 323-329.

Sethi, S., Kothiyal, N.C., Nema, A.K. and Kaushik, M.K. 2013. Characterization of municipal solid waste in Jalandhar city, Punjab, India. J. Hazard. Toxic Radioact. Waste, 17(2): 97-106.

Sharholy, M., Ahmad, K., Mahmood, G. and Trivedi, R.C. 2008. Municipal solid waste management in Indian cities–A review. Waste Manag., 28(2): 459-467.

Sharholy, M., Ahmad, K., Vaishya, R.C. and Gupta, R.D. 2007. Municipal solid waste characteristics and management in Allahabad, India. Waste Manag., 27(4): 490-496.

Singhal, A. and Goel, S. 2021. Spatio-Temporal Analysis of Open Waste Dumping Sites Using Google Earth: A Case Study of Kharagpur City, India. Springer, Cham, pp. 137-151.

Singhal, A., Gupta, A.K., Dubey, B. and Ghangrekar, M.M. 2021. Seasonal characterization of municipal solid waste for selecting feasible waste treatment technology for Guwahati city, India. J. Air Waste Manag. Assoc., 72(2): 147-160.

Sliusar, N., Polygalov, S., Ilinykh, G.I., Korotaev, V., Vaisman, Y. and Stanisavljevic, N. 2020. Seasonal changes in the composition and thermal properties of municipal solid waste: A Case study of the city of Perm, Russia. Environ. Res. Eng. Manag., 76(2): 54-64.

Srivastava, A. and Jain, V.K. 2007. A study to characterize the suspended particulate matter in an indoor environment in Delhi, India. Build. Environ., 42(5): 2046-2052.

Srivastava, P.K., Kulshreshtha, K., Mohanty, C.S., Pushpangadan, P. and Singh, A. 2005. Stakeholder-based SWOT analysis for successful municipal solid waste management in Lucknow, India. Waste Manag., 25(5): 531-537.

Srivastava, R., Krishna, V. and Sonkar, I. 2014. Characterization and management of municipal solid waste: a case study of Varanasi city, India. Int. J. Curr. Res. Acad. Rev., 2(8): 10-16.

Sujauddin, M., Huda, S.M.S. and Hoque, A.R. 2008. Household solid waste characteristics and management in Chittagong, Bangladesh. Waste Manag., 28(9): 1688-1695.

Swaminathan, M. 2018. How can India's waste problem see a systemic change? Econ. Polit. Week., 53: 16.

Tripathi, P. 2021. Bihar is last among 13 states in Swachh Survekshann; Patna at 44th position out of 48 cities, The Times of India (ToI), November 20, 2021. Available at: https://timesofindia.indiatimes.com/city/patna/bihar-last-among-13-states-in-swachh-survekshan-patna-at-44th-position-out-of-48-cities/articleshow/87821036.cms

Wilson, D.C., Rodic, L., Scheinberg, A., Velis, C.A. and Alabaster, G. 2012. Comparative analysis of solid waste management in 20 cities. Waste Manag. Res., 30: 237-254.

Nature Environment and Pollution Technology
An International Quarterly Scientific Journal

p-ISSN: 0972-6268
(Print copies up to 2016)
e-ISSN: 2395-3454

Vol. 21 | No. 5 (Suppl) | pp. 2089-2102 | 2022

Review Research Paper

https://doi.org/10.46488/NEPT.2022.v21i05.006

Open Access Journal

Responses of Grass Species to Elevated CO_2 – A Review of Three Decades of Research and Future Direction

N. C. Sashna, Aparna Sreekumar and C. C. Harilal†
Environmental Science Division, Department of Botany, University of Calicut, Thenhipalam 673635, Malappuram, Kerala, India
†Corresponding author: C. C. Harilal; ccharilal22@gmail.com

Nat. Env. & Poll. Tech.
Website: www.neptjournal.com

Received: 25-05-2022
Revised: 28-06-2022
Accepted: 30-06-2022

Key Words:
Elevated CO_2
Photosynthesis
Stomatal conductance
Water use efficiency
Biomass
Grass species

ABSTRACT

Rising atmospheric carbon dioxide accelerates growth and modifies physiological responses in plants. Over the last 40 years, the global scientific community had taken up initiatives to make out the role of plants in capturing and storing atmospheric carbon dioxide. This review consolidates the research of the past three decades on the responses of grass species to elevated levels of CO_2. An enhancement in intercellular CO_2 concentration, water use efficiency, photosynthesis, total non-structural carbohydrates, and total biomass was noticed in grass species under controlled growth systems supplied with varying levels of CO_2. Each of these responses reflects the potency of grasses to survive and store ample carbon in CO_2-enriched environments. Reduction in stomatal conductance, transpiration rate, and total nitrogen concentration was in effect positive responses, in connection with the acclimatization of plants at CO_2-enriched environments. This review ascertains that in experimental microclimatic environments with varying CO_2 regimes or varying treatment duration, grasses show positive growth responses. Thus it illustrates the efficient atmospheric carbon sequestration of grasses irrespective of their photosynthetic pathway (whether C_3/C_4).

INTRODUCTION

Over the last 50 years, an amplified global temperature scenario was caused by increased greenhouse gas emissions (Khan 2017), primarily from carbon dioxide (CO_2). Considering the present levels of atmospheric carbon dioxide and its hazardous effects on climate and ecosystems, there is a pressing need to develop technologies for their capture and storage. A recent report of the Intergovernmental Panel on Climate Change (IPCC 2018) set forth the urgent need for keeping global warming levels below 1.5°C to circumvent the upcoming issues in the area of climate change.

Various strategies are framed worldwide for lowering the levels of atmospheric CO_2, such as geological and oceanic confiscation, energy use reduction, low or no carbon fuel development, carbon sequestration through engineering approaches and other forestry/agro-forestry practices (Dhyani et al. 2020). Carbon sequestration is the process of taking out carbon from various sources and depositing it in long or short-lived reservoirs (Nogia et al. 2016). Of various methods, carbon sequestration in terrestrial biomass is a meaningful and cost-effective approach for reducing the ill effects of climate change.

Over the past 40 years, dedicated efforts have been taken up by the international scientific community for the study of direct responses of terrestrial ecosystems to CO_2 enrichment. Since the end of 1980, a sizable number of original research, synthesis, and review papers have been published in the area of elevated CO_2 effects on plants, interacting organisms' and ecosystems (Leuzinger & Hattenschwiler 2013). Experiments on the responses of grasses to elevated CO_2 found momentum at the beginning of the 1990s. Among terrestrial plants, grasses (Poaceae) are one of the most ecologically adapted angiosperm groups and are distributed in all possible habitats (Tzvelev 1989). Poaceae is the fifth most species-rich angiosperm family with approximately 11000 species (Clayton et al. 2015). The world's savannas and grasslands are dominated by C_3 and C_4 grasses. These ecosystems extend to more than 20% of the Earth's terrestrial surface and contribute to 30% of global net primary productivity (Mishra & Young 2020). Savannas and grasslands have a much influential role in carbon and nutrient cycles. Grasslands, constituted by a multitude of species have an immense potential for carbon storage (O'Mara 2012). The underground biomass of grasslands also serves as a sink for carbon storage (Frank et al. 2004). Many of these grasses

are with an extensive root system, which helps them in the transfer and storage of carbon into the soil annually, by shedding widespread roots (Anderson et al. 2008, Fissore et al. 2009, Odiwe et al. 2016). Further, it influences the global land-atmosphere energy balance (Mishra & Young 2020). Unlike grasslands, owing to the growth or life cycle patterns, many grass species are less studied as sinks of carbon storage. Annual grasses are short-lived, and thus need to be managed each year and with perennial grasses, there are defoliation-related management issues. Further, perennial grasses require quite different ecological conditions; hence climatic limitations may hinder the cultivation of these plants (Scordia & Cosentino 2019). Thus researches on elevated CO_2 responses of individual grass species become limited. Even then, individual performances of selected grass species under controlled conditions, with elevated CO_2 were reported. A broad synthesis of elevated CO_2 responses in grass species has not been attempted yet. Strengthening the knowledge base on the responses of grasses to elevated CO_2 will improve our ability for the selection of ideal species and conditions for effective CO_2 mitigation efforts.

The present review consolidated the physiological and growth responses of grass species (C_3 and C_4) maintained under different growth systems to elevated levels of CO_2. The specific objective of this synthesis was to provide estimates of the significance and reasons for CO_2 enrichment effects on photosynthetic rate (Pn), intercellular CO_2 concentration (Ci), stomatal conductance (g_s), transpiration rate (E), water use efficiency (WUE), total nonstructural carbohydrate (TNC), biomass responses and nitrogen concentration (N) in grasses. Since these responses are the basic direct plant responses towards a changed environment as enrichment in CO_2, this consolidation will urge a selection of the best grasses for carbon mitigation efforts.

CARBON DIOXIDE ELEVATION AND ASSOCIATED CLIMATIC FACTORS

Studies on the effect of varying concentrations of CO_2 on the growth/development/physiology and biochemistry of 24 grass species were considered in this synthesis. The authors set well-established micro-environmental systems to maintain a near-natural condition for the growth of grasses at CO_2 enrichment (Table 1). Growth responses of grasses at elevated CO_2 are linked with other climatic factors too. Cold temperatures and nutrient-poor soil down-regulate growth stimulation, however, at low light and water-stressed conditions growth enhancement was evident (Poorter & P´erez-Soba 2002). Besides, at increased levels of ozone concentration, plants show a much stronger response, since CO_2 elevation ameliorates ozone toxicity in plants due to reduced stomatal conductance (Turcsanyi et al. 2000). Some of the scrutinized CO_2 elevation experiments maintained grasses under different conditions such as water stress, varying nutrient supply, drought stress, temperature stress including warming temperatures and low/high light. These interaction effects will play an important role in formulating adaptive strategies in the future. Temperature is an important determinant of plant responses at elevated CO_2, since an

Table 1: Experimental models & designs used for CO_2 enrichment experiment on grasses.

Sl. No.	Experimental model	Volume/other dimensions	Design	Microclimatic environment	Author
1.	Controlled environmental chamber	-	Aluminum panel Foamed polyurethane insulation	350ppm aCO_2 675ppm eCO_2 14h photoperiod Temperature : light/dark- 29/20°C RH: light/dark -70/100	Riechers and Strain (1988)
2.	Closed top chamber	3.165m^3	Cylindrical	337 ± 32 ppm aCO_2 658 ± 81 ppm eCO_2	Kirkham et al. (1992)
3.	Growth cabinet	-	-	340 ± 15 ppm aCO_2 680 ± 15 ppm eCO_2	Ryle et al. (1992)
4.	Large OTC	63.578m^3	Cylindrical UV-resistant polyethylene film and aluminum frame	350 ppm aCO_2 700 ppm eCO_2 Intermittent nutrient supply	Knapp et al. (1993)
5.	OTC	1.286m^3	Cylindrical PVC sheet	340 ppm aCO_2 680 ppm eCO_2	Baxter et al. (1994 a, 1994b)
6.	OTC	0.331m^3	Cylindrical	Ambient Ambient +350 ppm eCO_2 Sandstone soil, no nutrient or water supply	Jackson et al. (1995)

Table cont....

Sl. No.	Experimental model	Volume/other dimensions	Design	Microclimatic environment	Author
7.	FACE	18m diameter	FACE ring	340 ppm aCO_2 600 ppm eCO_2 2 nutrient regimes-low & high	Jongen et al. (1995)
8.	OTC	63.578m^3	Cylindrical 1.5mm thick UV-resistant polyethylene Aluminum frame with frustrum*	350 ppm aCO_2 700 ppm eCO_2	Bremer et al. (1996)
9.	Expt.1: glass dome Expt.2: growth chamber Expt.3: a glass house	-	Naturally lit glass dome Growth chamber lit by metal halide & incandescent bulbs Naturally lit glass house	700 ppm eCO_2 Expt 1: RH exceeding 90% Temperature : 30°C/25°C for 15/9 h day/night Low light (9.2 mol m^{-2} d^{-1} irradiance)/high light (24.9 mol m^{-2} d^{-1} irradiance)treatment Expt 2: PPFD 750 Expt 3: RH 60 % Irradiance midday peak 1350 µmol m^{-2} S^{-1}	Ghannoum et al. (1997)
10.	OTC	1.3m between parallel sides 1.95m^2 soil area	Hexagonal 3mm polycarbonate sheet	365-380ppm aCO_2 716-720ppm eCO_2 (1995) 751-756ppm eCO_2 (1996) A cooling system to decrease the temperature	Oijen et al. (1999)
11.	OTC	1.13m^3	Cylindrical UV-stabilized plastic sheet Lightweight steel frame	360 ppm aCO_2 700 ppm eCO_2 Half of the chambers- moderate nutrient supply Half of the chambers-low nutrient supply	Davey et al. (1999)
12.	OTC	61.70m^3	Hexagonal Galvanized steel frame Clear Lexan panels with Lexan frustum	360 ± 20 aCO_2 720 ± 20 eCO_2 The outlet fan equilibrated the pressure inside & outside the chambers	Morgan et al. (2001)
13.	Growth chamber	-	-	350ppm aCO_2 700ppm eCO_2 Day/night temperature - 24°C/16°C RH- 70% PPFD- 600-1200µmol$m^{-2}S^{-1}$	Goverde et al. (2002)
14.	OTC	6.18m^3	Cylindrical	370ppm aCO_2 720ppm eCO_2 PPFD- 1500 µmol$m^{-2}s^{-1}$	De Souza et al. (2008)
15.	OTC	-	-	370-380ppm aCO_2 600 ± 50 ppm eCO_2	Bhatt et al. (2010)
16.	Environmental growth chamber	-	-	400 ± 10 ppm aCO_2 800 ± 10 ppm eCO_2 Average Day/Night temperature-21°C/18°C PAR-650µmol$m^{-2}s^{-1}$ RH-60% 14h photoperiod Fertilized with Hoagland's solution	Burgess and Huang (2014)
17.	CO_2 growth chambers	2m^3	Closed topped PVC frame Polyester sheeting	400ppm aCO_2 800ppm eCO_2 Draught/non-draught treatment	Nackley et al. (2014)

Table cont....

Sl. No.	Experimental model	Volume/other dimensions	Design	Microclimatic environment	Author
18.	Environmental growth chamber	-	-	400 ± 20ppm aCO_2 800 ± 20ppm eCO_2 5 temperature treatments (15/12,20/17,25/22,30/27,35/32-day/night) RH-70 % PAR-660 µmol $m^{-2}s^{-1}$ 12h photoperiod	Song et al. (2014)
19.	Glass dome	700m^3	Semi-open design with adjustable window	385ppm aCO_2 700 ppm eCO_2 PAR-1200 µmol $m^{-2}s^{-1}$	Klem et al. (2017)
20.	OTC inside a glass house	1.53m^3	-	345.43 ± 38.59ppm aCO_2 & room temperature 345.55 ±38.47 aCO_2 & room temperature + 3°C 714.63 ± 89.40 eCO_2 & room temperature 724.56 ± 88.85 eCO_2 & room temperature + 3°C	Faria et al. (2018)
21.	Growth chamber	152.102m^3		400 ppm aCO_2 950 ppm eCO_2 Temperature day/night 25/22°C RH 70% - 80%	Tom Dery et al. (2018)
22.	OTC	3.378m^3	Hexahedron	390 ppm aCO_2 550 ppm eCO_2 5 precipitation patterns	Wang et al. (2019)

Note: OTC = Open top chamber; FACE = Free air CO_2 enrichment; *= portion between two parallel planes create artificial microclimate; aCO_2 = ambient CO_2; eCO_2 = elevated CO_2; RH = Relative humidity; PPFD = Photosynthetic photon flux density; PAR = photosynthetically active radiation

increase in CO_2 causes warming. Due to a consequence of elevated CO_2, maximum biomass enrichment happens in tall grass prairie in dry years with high temperatures and abundant solar radiation (Knapp et al. 1993). In *Poa pratensis* elevated CO_2 alleviated the adverse effect of severely high temperatures (Song et al. 2014). The authors attributed this alleviation effect to the accumulation of soluble sugars and total non-structural carbohydrates. A study on the combined effect of CO_2 elevation and higher temperature on Brazilian Cerrado biome grasses shows that the species are tolerant to high temperatures and could even benefit from temperature rise. Nackley et al. (2014) reported drought tolerance of *Arundo donax* at elevated CO_2. Here elevated CO_2-induced decline in transpiration rate is ascribed to increased water use efficiency and thereby drought tolerance. Soil nutrient profiles and elevated CO_2 responses are also attempted by previous authors. Open-top chamber study on UK grassland species reveals stimulation of photosynthesis under low nutrient supply (Davey et al. 1999). This is the most important stimulation in carbon acquisition.

During the period of evaluation, a gradual increase in experimental CO_2 supply from 600 to 950 ppm has been noticed. This was in concurrence with the increase in CO_2 levels in the ambient atmosphere from a global perspective. The duration of CO_2 treatment studies under experimental conditions was from 40 days to 3 years. The most measured response factors were net photosynthetic rate (Pn) and biomass. Authors also evaluated the effect of elevated CO_2 on intercellular CO_2 concentration (Ci), stomatal conductance (gs), transpiration rate (E), water use efficiency (WUE), total nonstructural carbohydrates (TNC) and total nitrogen concentration (N) on various grass species.

ELEVATED CARBON DIOXIDE AND PHOTOSYNTHETIC RESPONSES IN C_3/C_4 PATHWAYS

Photosynthetic responses of plants are considered as an important measure of carbon capture efficiency in CO_2 sequestration studies. Augmentation in CO_2 levels leads to increased photosynthetic rate (Ziska et al. 1999, Aranda et al. 2020). This review also signifies a positive response in the photosynthetic rate of 86.36% of grasses (Table 2). However, species like *Andropogon gerardii* (Kirkham et al. 1992) and *Pascopyrum smithii* (Davey et al. 1999) lack a significant response in photosynthetic rate under elevated levels of CO_2. *Arundo donax* exhibits a negative

Table 2: Changes in the photosynthetic rate at elevated CO_2.

Sl. No.	Plant species	Duration of CO_2 treatment	Pn	Reference
1.	*Andropogon gerardii* (C_4)	40 days	+ 8.75% (NS)	Kirkham et al. (1992)
2.	*Poa pratensis* (C_3)	40 days	+ 141%	Kirkham et al. (1992)
3.	*Lolium perenne* (C_3)	49 days	+ 50%	Ryle et al. (1992)
4.	*Andropogon gerardii* (C_4)	2 growing seasons one with water stress	+	Knapp et al. (1993)
5.	*Agrostis capillaris* (C_3)	79 days	+	Baxter et al. (1994 a, 1994b)
6.	*Avena barbata* (C_3)	One growing season	+ 20%	Jackson et al. (1995)
7.	*Panicum laxum* (C_3)	1.5 months with low light/high light	+18%in low light NS	Ghannoum et al. (1997)
8.	*Panicum antidotale* (C_4)	1.5 months with low light/high light	+10% in high light (NS)	Ghannoum et al. (1997)
9.	*Triticum aestivum* (C_4)	2 growing seasons	+ 30%	Oijen et al . (1999)
10.	*Agrostis capillaries* (C_3)	2 years with nutrient supply(low & moderate)	+38% at low +12% at moderate	Davey et al. (1999)
11.	*Pascopyrum smithii* (C_3)	2 years with nutrient supply(low & moderate)	NS	Davey et al. (1999)
12.	*Bouteloua gracilis* (C_4)	7 months	+	Morgan et al. (2001)
13.	*Pascopyrum smithii* (C_3)	7 months	+	Morgan et al. (2001)
14.	*Saccharum officinarum* (C_4)	50 weeks	+ 30%	De Souza et al. (2008)
15.	*Panicum maximum* (C_4)	2 growing seasons	+ 53%	Bhatt et al. (2010)
16.	*Agrostis stolonifera* (C_3)	84 days	+ 21%	Burgess and Huang (2014)
17.	*Arundo donax* (C_3)	78days(28days drought stress)	- NS	Nickley et al. (2014)
18.	*Poa pratensis* (C_3)	2 weeks (temperature treatment)	+	Song et al. (2014)
19.	*Calomagrostis arundinacea* (C_3)	3years	+	Klem et al. (2017)
20.	*Urochloa brizantha* (C_4)	75 days with temperature treatment	+	Faria et al. (2018)
21.	*Megathyrsus maximus* (C_4)	75 days with temperature treatment	+	Faria et al. (2018)
22.	*Stipa baicalensis* (C_3)	3 months	+93.4%-158%	Wang et al. (2019)

Note: Pn = photosynthetic rate; + = increase; - = decrease; NS = not significant

photosynthetic response (Nickley et al. 2014). Feedback inhibition is associated with an excess of unutilized N and carbon resources, consequent to the lack of carbohydrate sinks attributed to the down-regulation of photosynthesis during CO_2 enrichment in *Arundo donax* in its specific experimental conditions (Paul & Foyer 2001). A comparative evaluation of the CO_2 elevation experiment conducted in *Poa pratensis* and *Andropogon gerardii* (Kirkham et al.1992) reveals a rise in the photosynthetic rate in *Poa pratensis* (C_3) owing to the domination of carboxylation activity of Rubisco enzyme under high CO_2 environment. Yet there is no significant change in the assimilation rate of A. gerardii (C4). In C3 at CO_2 limited environment, Rubisco catalyzes the oxygenation of Ribulose-1, 5-bisphosphate (RubP), a reaction that is competitively inhibited by CO_2 (Drake et al., 1997). Kranz anatomy eliminates this phenomenon in C4.Thus CO2 elevation is not much beneficial to C4. CO_2 enrichment treatment eliminates energy-losing photorespiration under a doubled CO_2 environment in C_3 plants and growth is stimulated to a range of 40-45%, whereas in C_4 plants, growth only to a range of 10-20% (Ghannoum et al. 2000). Thus CO_2 elevation is more advantageous to C_3

plants than C_4 (Waggoner 1984). This advantage is apparent in the photosynthetic rate of 84.62% of C_3 grasses scrutinized.

Contrary to the C_3 advantage, the positive photosynthetic response is also shown by 88.88% of C_4 grasses reviewed in the present study. Arid environments with temperature ascending and limited nutrients favor C_4 plants and eventually exhibit positive responses at CO_2 elevation (Ghannoum et al. 2000, Sage & Kubein 2003). Even though CO_2 concentrating mechanism makes C_4 plants insensitive to elevated CO_2, superior photosynthetic nitrogen use efficiency (Sage & Kubein 2003) is more advantageous to them at elevated CO_2 than C_3 plants. Rubisco accounts for about 30% of leaf nitrogen content in C_3 plants, while only 4 - 21% in C_4 species (Sage et al. 1987, Evans & Von Caemmerer 2000). Carbohydrate dilution of nitrogen content (Wong 1990, Kuehny et al. 1991, Gifford et al. 2000) at elevated CO_2 decreases nitrogen use efficiency of C_3 plants, thus C_3 leaves need to invest more nitrogen on Rubisco. Such nitrogen requirements down-regulate C_3 plants at elevated CO_2 environments (Lara & Andreo 2011).In the case, of C_3 plants like *Panicum laxum* and *Arundo donax*, reduction in assimilation are attributed to decreased Rubisco activity (Ghannoum et al. 1997). Photosynthetic acclimatization and down-regulation reported for long-term exposure of plants to elevated CO_2 are attributed to this decline in Rubisco activity (Fredeen et al. 1995, Sicher & Bunce 1997). Enhanced cellular carbohydrate levels may down-regulate genes transcribing Rubisco and other photosynthetic proteins (Stitt 1991, Krapp et al. 1991). Another observation states that an increased requisite of ATP (required for RuBP regeneration) for increased carbon fixation before CO_2 elevation results in a decline in the Rubisco activation state. Such reduction was also observed in previous studies (Sage et al. 1988, Cen & Sage 2005). Besides augmented levels of CO_2, nutrient conditions and other factors of a microenvironmental condition such as temperature, light intensity, and treatment duration also influence the response of grasses. Nevertheless, most of the grasses (86.36%) assessed here respond almost identically in various microclimatic conditions.

ELEVATED CARBON DIOXIDE - INTERCELLULAR CO_2 CONCENTRATIONS AND STOMATAL CONDUCTANCE

Stomatal responses occur due to the intensity of intercellular CO_2 concentration (Ci), preceded by mesophyll CO_2 demands (Mott 1988). With the rise in atmospheric CO_2, intercellular CO_2 concentration raises (Kirkham et al. 1992). C_3 plants have a higher Ci than C_4 plants. C_4 plants maintain a lower Ci due to its CO_2 concentrating mechanism with a special arrangement of bundle sheath cells and mesophyll cells (kranz anatomy). Few studies on C_3 and C_4 grasses measured Ci and an increase is evident in both cases, while stomatal conductance decreased in these grasses, with the exception of *Panicum maximum, Urochloa brizantha,* and

Table 3: Changes in intercellular CO_2 concentration and stomatal conductance at elevated CO_2.

Sl. No.	Plant species	Duration of CO_2 treatment	Ci	g_s	Reference
1.	*Andropogon gerardii* (C_4)	40 days	+180%		Kirkham et al. (1992)
2.	*Poa pratensis*(C_3)	40 days	+67.79%		Kirkham et al. (1992)
3.	*Andropogon gerardii* (C_4)	2 growing seasons one with water stress		-52%	Knapp et al. (1993)
4.	*Andropogon gerardii* (C_4)	6 months		-54.4%	Bremer et al. (1996)
5.	*Sorghastrum nutans* (C_4)	6 months		-39.6%	Bremer et al. (1996)
6.	*Panicum laxum* (C_3)	1.5 months with low light/high light		-50%	Ghannoum et al. (1997)
7.	*Panicum antidotale* (C_4)	1.5 months with low light/high light		- 50%	Ghannoum et al. (1997)
8.	*Saccharum officinarum* (C_4)	50 weeks		-37%	De Souza et al. (2008)
9.	*Panicum maximum* (C_4)	2 growing seasons	+	+	Bhatt et al. (2010)
10.	*Agrostis stolonifera* (C_3)	84 days		-40%	Burgess and Huang (2014)
11.	*Arundo donax* (C_3)	78days(28days drought stress)	+	-	Nickley et al (2014)
12.	*Calomagrostis arundinacea* (C_3)	3years		-	Klem et al. (2017)
13.	*Urochloa brizantha* (C_4)	75 days with temperature treatment		+	Faria et al. (2018)
14.	*Megathyrsus maximus* (C_4)	75 days with temperature treatment		+	Faria et al. (2018)
15.	*Cenchrus pedicellatus* (C_4)	68days(wet&dry treatment)		-40%	Tom Dery et al. (2018)
16.	*Stipa baicalensis* (C_3)	3 months	+72.3 - 129.6		Wang et al. (2019)

Note: Ci = intercellular CO_2 concentration; g_s = stomatal conductance; + = increase; - = decrease

Megathyrsus maximus (Table 3). The grasses undergone experimentation so far showed a decreased range of stomatal conductance, between 35-55%. Previous reviews on plant CO_2 responses support this view (Curtis & Wang 1998, Wand et al. 1999, Ainsworth et al. 2002, Ainsworth & Rogers 2007, Aranda et al. 2020). The positive response of *Panicum maximum* is attributed to the lack of stomatal functioning effect at higher CO_2 concentrations (600 ± 50) (Bhatt et al. 2010). Elevated temperature treatment in combination with elevated CO_2 explains positive stomatal conductance rates of *Urochloa brizantha* and *Megathyrsus maximus* (Faria et al. 2018). A feedback mechanism works to decrease stomatal conductance under elevated CO_2 in most plants. It has been implicit that guard cells sense the concentration of CO_2 in the intercellular spaces, and as the mesophyll requirement for CO_2 increases, Ci decreases, causing stomatal opening and increasing Ci (Mott 1988). Depolarization of the guard cell membrane is the main requirement for stomatal closure (Assmann 1999). At elevated CO_2, depolarization happens to a larger extent, which leads to the reduced stomatal aperture (Ainsworth & Rogers 2007). Reduced stomatal conductance shown by plants at long-term elevated CO_2 exposure is ascribed to the changes in stomatal aperture or stomatal index or stomatal density (Pritchard & Rogers 2007). A putative 3-keto acyl-coenzyme A synthase encoded by HIC (high carbon dioxide) gene is a negative regulator of stomatal development (Gray et al. 2000) and is also reported to be related to stomatal closure.

ELEVATED CARBON DIOXIDE - TRANSPIRATION RATE AND WATER USE EFFICIENCY

The transpiration rate was noted to decline for individual grasses scrutinized (Table 4). Yet *Panicum maximum* responds positively to elevated levels of CO_2 and is attributed to increased chamber temperature (Bhatt et al. 2010). Declining transpiration is a stress protection method that limits water loss and minimizes damage linked with desiccation. Plants and ecosystems under drought condition experience greater WUE (Water Use Efficiency) (Field et al. 1997; Arp et al. 1998). Increased WUE is also said to be a result of morphological adjustments rather than stomatal (Norby & O'Neill 1991) under elevated CO_2. Studies indicate that crop plants grown at higher CO_2 environments have larger and highly branched root systems, which increases the capacity for resource acquirement but at lesser efficiency (Pritchard & Rogers 2000). Day et al. (1996) observed higher root production towards nutrient-available surfaces and water-available depths in a sandy nutrient-poor Oak-palmetto system. Upon review of the literature on root growth under elevated CO_2, Wullschleger et al. (2002) found that elevated CO_2 increases root growth and it leads to enhanced water uptake and improved water balance, thus helping to evade water deficits. Yet when soil moisture is sufficient to meet transpirational loss of water, the CO_2 effect on root volume is seemingly extraneous, thus this mechanism could be

Table: 4: Changes in transpiration rate and water use efficiency at elevated CO_2.

Sl. No.	Plant species	Duration of CO_2 treatment	E	WUE	Reference
1.	*Andropogon gerardii* (C_4)	40 days	- 54%	+ 41.6%	Kirkham et al. (1992)
2.	*Poa pratensis* (C_3)	40 days	-7%	+158%	Kirkham et al. (1992)
3.	*Lolium perenne* (C_3)	49 days			Ryle et al. (1992)
4.	*Andropogon gerardii* (C_4)	6 months	-18%		Bremer et al. (1996)
5.	*Sorghastrum nutans* (C_4)	6 months	-22%		Bremer et al. (1996)
6.	*Saccharum officinarum* (C_4)	50 weeks		+62%	De Souza et al. (2008)
7.	*Panicum maximum* (C_4)	2 growing seasons	+	+	Bhatt et al. (2010)
8.	*Agrostis stolonifera* (C_3)	84 days	-40%	+30%	Burgess and Huang (2014)
9.	*Arundo donax* (C_3)	78days(28days drought stress)	-100%	+	Nickley et al. (2014)
10.	*Calomagrostis arundinacea* (C_3)	3years	-	+	Klem et al. (2017)
11.	*Urochloa brizantha* (C_4)	75 days with temperature treatment		+	Faria et al. (2018)
12.	*Megathyrsus maximus* (C_4)	75 days with temperature treatment		+	Faria et al. (2018)
13.	*Stipa baicalensis* (C_3)	3 months		+87.2%	Wang et al. (2019)

Note: E = transpiration rate; WUE = water use efficiency; + = increase; - = decrease

detected only under specific conditions (Wullschleger et al. 2002). Since the rise in atmospheric CO_2 usually upholds WUE, there will be a tendency for plants to tolerate draught in the future (Beerling et al. 1996).

ELEVATED CARBON DIOXIDE AND TOTAL NON-STRUCTURAL CARBOHYDRATES

The principal non-structural carbohydrates present in leaves are total soluble sugars and starch. Evaluation of literature on individual grasses explains a significant increase in non-structural carbohydrates (Table 5) in CO_2rich environments. Growth and development of grasses thrive with an accumulation of non-structural carbohydrates; which are also related to environmental stress tolerance (Moraes et al. 2013). Elevated CO_2 exposure creates a considerable increase in soluble sugar and starch content (Teng et al. 2006). Previous investigations revealed that augmented levels of soluble sugars and starch contents in leaves are due to increased assimilation rates (Delucia et al. 1985, Long & Drake 1992, Moore et al. 1997, Teng et al. 2006). Elevated CO_2-based increases in sugar levels may also be due to an indirect effect of declined nitrogen concentrations leading to lowered respiration rates (Oijen et al. 1999). Storage of non-structural carbohydrates such as starch and fructans is common among some grasses (Morvan-Bertrand et al. 2001, Xue et al. 2009). Temperate climate grasses usually store carbohydrates as fructans (Halford et al. 2011). Fructans are formed from imported sucrose and the site of synthesis is the vacuolar lumen (Pollock et al. 2003). A limited number of grasses use starch as a carbohydrate storage pool and is synthesized in plastids or amyloplasts (Slewinski 2012). The storage of carbohydrate polymers increases the sequestration capability of grasses. Drought stress tolerance of non-structural carbohydrates is hypothesized by previous authors (Moraes et al. 2013). Low hydraulic conductance of grass stems due to the accumulation of soluble sugars facilitates easy conductance of water from the soil to plant parts (Fu et al. 2011). Along with carbon sequestration capability, this adaptation for draught tolerance will also be advantageous for grasses in facing future environmental challenges.

ELEVATED CARBON DIOXIDE AND BIOMASS RESPONSES

Growth and biomass responses of plants to elevated levels of CO_2 are widely studied. Literature reveals that the biomass has increased to varying levels at elevated CO_2 environments (Table 6). Even though C_4 grasses have no additional benefit at elevated CO_2 owing to internal CO_2 concentrating mechanisms, increased photosynthetic rates or increased biomass are reported in C_4 grasses. These increases are resulting in faster development of inflorescence, changes in partitioning, delayed leaf senescence, or enhanced water potential at CO_2 elevation (Carter & Petersen 1983, Potvin & Strain 1985, Knapp et al. 1993). Other studies state that the increase in growth and biomass at CO_2 ascent is attributed to an enhancement in leaf area (Poorter & Remkes, 1990). Roumet & Roy (1996) also stated a positive correlation of plant growth to specific leaf area (leaf surface area per unit of leaf weight) and leaf area ratio (leaf area per unit

Table 5: Changes in total non-structural carbohydrates at elevated CO_2.

Sl. No.	Plant species	Duration of CO_2 treatment	TNC	Reference
1.	*Agrostis capillaris* (C_3)	79 days	+	Baxter et al. (1994 a, 1994b)
2.	*Festuca vivipara* (C_3)	189 days	+	Baxter et al. (1994 a, 1994b)
3.	*Lolium perenne*-Root (C_3)	One growing season	+46.9%	Jongen et al. (1995)
4.	*Panicum laxum* (C_3)	1.5 months with low light/high light	NS	Ghannoum et al. (1997)
5.	*Panicum antidotale* (C_4)	1.5 months with low light/high light	NS	Ghannoum et al. (1997)
6.	*Triticum aestivum* (C_4)	2 growing seasons	+	Oijen et al. (1999)
7.	*Agrostis stolonifera* (C_3)	65 days	+	Goverde et al. (2002)
8.	*Anthoxanthum odoratum* (C_3)	65 days	+	Goverde et al. (2002)
9.	*Festuca rubra* (C_3)	65 days	+	Goverde et al. (2002)
10.	*Poa pratensis* (C_3)	65 days	+	Goverde et al. (2002)
11.	*Poa pratensis* (C_3)	2 weeks (temperature treatment)	+38% at 25 - 35°C	Song et al. (2014)
12.	*Urochloa brizantha* (C_4)	75 days with temperature treatment	+	Faria et al. (2018)
13.	*Megathyrsus maximus* (C_4)	75 days with temperature treatment	+	Faria et al. (2018)

Note: TNC = total non-structural carbohydrates; + = increase; NS = not significant

of total plant dry weight) in 11 closely related types of grass.

Changes in moisture relationships have a key role in grassland productivity (Owensby et al. 1993). Previous investigations revealed that elevated CO_2 significantly stimulated plant growth even at water-limited conditions (Gifford & Morison 1985, King & Greer 1986, Samarakoon & Gifford 1995, Owensby et al. 1996). According to Pritchard et al. (1999), stimulation of cell wall-related genes at elevated CO_2 uphold enhanced cell production and cell elongation. This view is a possible explanation for biomass increase at elevated CO_2. Temperature is yet another factor, which defines growth at elevated CO_2. Growth and storage of carbohydrates are limiting at low temperatures, however, an increase in temperature creates a positive response towards growth at elevated CO_2. This view is supported by Oliveira et al. (2013), where the accumulation of biomass and enhanced grain yield in wheat is noticed under elevated CO_2, combined with high-temperature treatment. The same authors imply that the combination of high temperature and elevated CO_2 will lessen the awful effects of terminal drought. Fisher et al. (1994) estimated the carbon sequestration potential of deep-rooted grasses in South American savannas and reported a sequestration of 100-507 Mt carbon per year. Through this study, the authors 'demonstrated the importance of grass biomass as a major sink of atmospheric carbon.

Table 6: Changes in plant biomass at elevated CO_2.

Sl. No.	Plant species	Duration of CO_2 treatment	Biomass	Reference
1.	*Bouteloua gracilis* (C_4)	7 weeks	+35%	Riechers and Strain (1988)
2.	*Lolium perenne* (C_3)	49 days	+	Ryle et al. (1992)
3.	*Andropogon gerardii* (C_4)	2 growing seasons one with water stress	+41%	Knapp et al. (1993)
4.	*Agrostis capillaries* (C_3)	79 days	+	Baxter et al. (1994 a, 1994b)
5.	*Poa alpinia* (C_3)	105 days	+	Baxter et al. (1994 a, 1994b)
6.	*Festuca vivipara* (C_3)	189 days	-48%	Baxter et al. (1994 a, 1994b)
7.	*Lolium perenne*-Root (C_3)	One growing season	+48%	Jongen et al. (1995)
8.	*Panicum laxum* (C_3)	1.5 months with low light/high light	+1.41 fold in low light +1.71 fold in the highlight	Ghannoum et al. (1997)
9.	*Panicum antidotale* (C_4)	1.5 months with low light/high light	+1.28 fold in the highlight	Ghannoum et al. (1997)
10.	*Triticum aestivum* (C_4)	2 growing seasons	+	Oijen et al . (1999)
11.	*Agrostis capillaries* (C_3)	2 years with nutrient supply(low & moderate)	-23% at low -16% at moderate	Davey et al. (1999)
12.	*Lolium perenne* (C_3)	2 years with nutrient supply(low & moderate)	-29% at low -17% at moderate	Davey et al. (1999)
13.	*Bouteloua gracilis* (C_4)	7 months	+	Morgan et al. (2001)
14.	*Pascopyrum smithii* (C_3)	7 months	+	Morgan et al. (2001)
15.	*Agrostis stolonifera* (C_3)	65 days	NS	Goverde et al. (2002)
16.	*Anthoxanthum odoratum* (C_3)	65 days	+	Goverde et al. (2002)
17.	*Festuca rubra* (C_3)	65 days	+	Goverde et al. (2002)
18.	*Poa pratensis* (C_3)	65 days	NS	Goverde et al. (2002)
19.	*Saccharum officinarum* (C_4)	50 weeks	+40%	De Souza et al. (2008)
20.	*Panicum maximum* (C_4)	2 growing seasons	+	Bhatt et al. (2010)
21.	*Agrostis stolonifera* (C_3)	84 days	+35%	Burgess and Huang (2014)
22.	*Poa pratensis* (C_3)	2 weeks (temperature treatment)	+	Song et al. (2014)
23.	*Urochloa brizantha* (C_4)	75 days with temperature treatment	+54.5%	Faria et al. (2018)
24.	*Megathyrsus maximus* (C_4)	75 days with temperature treatment	+56.7%	Faria et al. (2018)
25.	*Stipa baicalensis* (C_3)	3 months	+	Wang et al. (2019)

Note: + = increase; - = decrease; NS = not significant

ELEVATED CARBON DIOXIDE AND NITROGEN CONCENTRATION IN PLANT PARTS

CO_2 elevation brings about a negative response on N concentration among most of the grasses considered (Table 7). A reduction in total leaf nitrogen content has been reported in previous studies (Davey et al. 1999). Cotrufo et al. (1998) reviewed experiments regarding elevated CO_2 effects on nitrogen concentration of plants including grasses and found a statistically significant decline in N concentration in plants grown under elevated CO_2 than control. Due to increased assimilation at elevated CO_2, up to 30% of leaf nitrogen is transported to Rubisco (Evans 1989). At elevated CO_2, a major portion of leaf nitrogen is reallocated to other photosynthetic and non-photosynthetic processes (Sage 1994). A contradictory opinion by Coleman et al. (1993) is that the CO_2-induced reduction in N concentration is not due to physiological changes, but is size dependent and results from enhanced plant growth. The actual mechanism responsible for the reduction of N under elevated CO_2 is not yet established; however, there are substantial hypotheses explaining this phenomenon (Taub & Wang 2008). The same authors opined increased carbohydrate levels and decreased N uptake as key mechanisms affecting plant N concentration at elevated CO_2. Observations by McDonald et al. (2002) also testify to these hypotheses. The same study states that the plants with high WUE possess morphological, allocational, and physiological root traits, thus there is a low transpiration-mediated N supply, compared with the rate of carbon accumulation. There are further reports on the inhibition of N uptake and transport under CO_2 elevation due to reduced transpiration rates (Correia et al. 2005, Jauregui et al. 2016). A recent report (Padhan et al. 2020) illustrates the genetic mechanisms behind N reduction under elevated CO_2. Their CO_2 elevation experiment on bread wheat had shown the down-regulation of ammonia assimilating genes and up-regulation of reactive oxygen species at CO_2 enrichment.

FUTURE STEPS

The carbon mitigation potential of terrestrial plants has been proven effective and profitable. Grasses possess more special adaptations and characteristics than other plant groups. Their fast growth even under unfavorable environmental conditions such as limited water and nutrient supply, higher temperature, higher CO_2 environments, etc. attribute to more consideration in CO_2 mitigation programs. Approximately 11000 species of grasses are reported worldwide (Clayton et al. 2015), but the carbon sequestration potential of a major share of them is still unexplored. Extensive experimentations on the CO_2 mitigation potential of remaining grass species over the world's savannas and grasslands is an upcoming need to improve our ability for selecting ideal species for CO_2 mitigation efforts. Effective utilization of grasses for

Table 7: Changes in nitrogen concentration at elevated CO_2.

Sl. No.	Plant species	Duration of CO_2 treatment	N	Reference
1.	*Lolium perenne*(C_3)	49 days	-	Ryle et al. (1992)
2.	*Agrostis capillaris* (C_3)	79 days	NS	Baxter et al. (1994 a, 1994b)
3.	*Poa alpinia* (C_3)	105 days	NS	Baxter et al. (1994 a, 1994b)
4.	*Festuca vivipara* (C_3)	189 days	-	Baxter et al. (1994 a, 1994b)
5.	*Avena barbata* (C_3)	One growing season	-25%	Jackson et al.1995
6.	*Lolium perenne*–Root (C_3)	One growing season	-	Jongen et al. (1995)
7.	*Panicum laxum* (C_3)	1.5 months with low light/high light	NS	Ghannoum et al. (1997)
8.	*Panicum antidotale* (C_4)	1.5 months with low light/high light	NS	Ghannoum et al. (1997)
9.	*Triticum aestivum* (C_4)	2 growing seasons	-	Oijen et al . (1999)
10.	*Bouteloua gracilis* (C_4)	7 months	-	Morgan et al. (2001)
11.	*Pascopyrum smithii* (C_3)	7 months	-	Morgan et al. (2001)
12.	*Agrostis stolonifera* (C_3)	65 days	-	Goverde et al. (2002)
13.	*Anthoxanthum odoratum* (C_3)	65 days	-	Goverde et al. (2002)
14.	*Festuca rubra* (C_3)	65 days	-	Goverde et al. (2002)
15.	*Poa pratensis* (C_3)	65 days	-	Goverde et al. (2002)
16.	*Stipa baicalensis* (C_3)	3 months	-9.7%	Wang et al. (2019)

Note: - = decrease; NS = not significant

agro-forestry practices is yet another option for effective and profitable mitigation of atmospheric carbon dioxide and soil stabilization.

CONCLUSION

This review aimed to consolidate experimental findings on the physiological and growth responses of grass species at elevated CO_2 and to establish the significance and reasons for their responses. Positive responses of photosynthetic rate and total biomass at elevated CO_2 signify the potency of grass species to cope with CO_2-enriched environments. Gas exchange parameters such as Ci and g_s showed contradictory responses. Augmented levels of Ci could be considered an admirable response as it can further enhance the photosynthetic rate. As well, the stomatal conductance declined at elevated levels of CO_2 due to the feedback mechanism. This decline is also connected with parameters of water relations such as transpiration and WUE. The transpiration rate decreased and WUE increased at CO_2 elevation. Thus in effect, the decline in stomatal conductance is a positive response, as the grasses can survive in environments with enriched CO_2 and associated drought. TNC and plant biomass are yet other factors, which reflect carbon capture and storage. Increased TNC affects plant N concentration at elevated CO_2. A C_3-C_4 controversy exists in each of these plant responses discussed. C_3 plants benefit more at elevated CO_2 since it eliminates photorespiration. However, at longer periods of carbon dioxide ascend, C_4 grasses could nurture well due to their high water use and nitrogen use efficiency. After all, each grass species stores plentiful carbon in soil annually through the shedding of its fine-spread roots. This review ascertains that, despite the treatment condition, treatment duration, or photosynthetic pathway (C_3/C_4), the grasses subjected to experimentation could respond identically to elevated CO_2. In CO_2-enriched environments, grasses have the potential to mitigate atmospheric carbon dioxide and store photosynthates in their biomass and this ensures their effective utilization for carbon mitigation strategies.

ACKNOWLEDGEMENT

The work is supported through funding by the Council of Scientific and Industrial Research (CSIR, Ministry of Science & Technology, Govt. of India). HRDG (CSIR) Sanction letter no. /file no.09/043 (0196)/2018 EMR-1).

REFERENCES

Ainsworth, E.A. and Rogers, A. 2007. The response of photosynthesis and stomatal conductance to rising [CO_2]: Mechanisms and environmental interactions. Plant Cell Environ., 30(3): 258-270.

Ainsworth, E.A., Davey, P.A., Bernacchi, C.J., Dermody, O.C., Heaton, E.A., Moore, D.J. and Curtis, P.S. 2002. A meta-analysis of elevated [CO_2] effects on soybean (*Glycine max*) physiology, growth, and yield. Glob. Change Biol., 8(8): 695-709.

Anderson, J.L., Beduhn, R.A., Current, D., Espeleta, J.F., Fissore, C., Gangeness, B. and Reich, P.B. 2008. The Potential for Terrestrial Carbon Sequestration in Minnesota: A Report to the Department of Natural Resources from the Minnesota Terrestrial Carbon Sequestration Initiative. http://files.dnr.state.mn.us/aboutdnr/reports/carbon.pdf

Aranda, I., Cadahía, E. and de Simón, B.F. 2020. Leaf eco-physiological and metabolic response in *Quercus pyrenaica* Willd. seedlings to moderate drought under an enriched CO_2 atmosphere. J. Plant Physiol., 244: 153083.

Arp, W.J., Van Mierlo, J.E.M., Berendse, F. and Snijders, W. 1998. Interactions between elevated CO_2 concentration, nitrogen, and water: effects on growth and water use of six perennial plant species. Plant Cell Environ., 21(1): 1-11.

Assmann, S.M. 1999. The cellular basis of guard cell sensing of rising CO_2. Plant Cell Environ., 22(6): 629-637.

Baxter, R., Ashenden, T.W., Sparks, T.H. and Farrar, J.F. 1994a. Effects of elevated carbon dioxide on three montane grass species: I. Growth and dry matter partitioning. J. Exp. Bot., 45(3): 305-315.

Baxter, R., Gantley, M., Ashenden, T.W. and Farrar, J.F. 1994b. Effects of elevated carbon dioxide on three grass species from montane pasture II. Nutrient uptake, allocation, and efficiency of use. J. Exper. Bot., 45(9): 1267-1278.

Beerling, D.J., Heath, J., Woodward, F.I. and Mansfield, T.A. 1996. Drought - CO_2 interactions in trees observations and mechanisms. New Phytol., 134(2): 235-242.

Bhatt, R.K., Baig, M.J., Tiwari, H.S. and Roy, S. 2010. Growth, yield, and photosynthesis of *Panicum maximum* and *Stylosanthes hamata* under elevated CO_2. J. Environ. Biol., 31: 549-552.

Bremer, D.J., Ham, J.M. and Owensby, C.E. 1996. Effect of elevated atmospheric carbon dioxide and open-top chambers on transpiration in a tallgrass prairie. J. Environ. Qual., 25(4): 691-701.

Burgess, P. and Huang, B. 2014. Growth and physiological responses of creeping bentgrass (*Agrostis stolonifera*) to elevated carbon dioxide concentrations. Horticul. Res., 1(1): 1-8.

Carter, D.R. and Peterson, K.M. 1983. Effects of a CO_2-enriched atmosphere on the growth and competitive interaction of a C_3 and a C_4 grass. Oecologia, 58(2): 188-193.

Cen, Y.P. and Sage, R.F. 2005. The regulation of Rubisco activity in response to variation in temperature and atmospheric CO_2 partial pressure in sweet potato. Plant Physiol., 139: 979-990.

Clayton, W.D., Vorontsova, M.S., Harman, K.T. and Williamson, H. 2016. Grassroots e-floras in the Poaceae: Growing grass base and grass world. PhytoKeys, (48): 73-84.

Coleman, J.S., Mc Connaughay, K.D.M. and Bazzaz, F.A. 1993. Elevated CO_2 and plant nitrogen use: is reduced tissue nitrogen concentration size-dependent? Oecologia, 93(2): 195-200.

Correia, C.M., Pereira, J.M.M., Coutinho, J.F., Björn, L.O. and Torres-Pereira, J.M. 2005. Ultraviolet-B radiation and nitrogen affect the photosynthesis of maize: A Mediterranean field study. Europ. J. Agron., 22(3): 337-347.

Cotrufo, M.F.,` Ineson, P. and Scott, A. 1998. Elevated CO_2 reduces the nitrogen concentration of plant tissues. Glob. Change Biol., 4(1): 43-54.

Curtis, P.S. and Wang, X. 1998. A meta-analysis of elevated CO_2 effects on woody plant mass, form, and physiology. Oecologia, 113(3): 299-313.

Davey, P.A., Parsons, A.J., Atkinson, L., Wadge, K. and Long, S.P. 1999. Does photosynthetic acclimation to elevated CO_2 increase photosynthetic nitrogen-use efficiency? A study of three native UK grassland species in open-top chambers. Funct. Ecol., 13: 21-28.

Day, F.P., Weber, E.P., Hinkle, C.R. and Drake, B.G. 1996. Effects of elevated atmospheric CO_2 on fine root length and distribution in an oak-palmetto scrub ecosystem in central Florida. Glob. Change Biol., 2(2): 143-148.

Faria, A.P., Marabesi, M.A., Gaspar, M. and França, M.G.C. 2018. The increase of current atmospheric CO_2 and temperature can benefit leaf gas exchanges, carbohydrate content and growth in C_4 grass invaders of the Cerrado biome. Plant Physiol. Biochem., 127: 608-616.

Oliveira, E.D., Bramley, H., Siddique, K.H., Henty, S., Berger, J. and Palta, J.A. 2013. Can elevated CO_2 combined with high temperature ameliorate the effect of terminal drought in wheat? Funct. Plant Biol., 40(2): 160-171.

De Souza, A.P., Gaspar, M., Da Silva, E.A., Ulian, E.C., Waclawovsky, A.J., Nishiyama, M.Y. and Buckeridge, M.S. 2008. Elevated CO_2 increases photosynthesis, biomass, and productivity, and modifies gene expression in sugarcane. Plant Cell Environ., 31(8): 1116-1127.

Delucia, E.H., Sasek, T.W. and Strain, B.R. 1985. Photosynthetic inhibition after long-term exposure to elevated levels of atmospheric carbon dioxide. Photosynth. Res., 7(2): 175-184.

Dhyani, S.K., Ram, A., Newaj, R., Handa, A.K. and Dev, I. 2020. Agroforestry for Carbon Sequestration in Tropical India. In Ghosh, P.K., Mahanta, S.K., Mandal, D. and Mandal, B. (eds), Carbon Management in Tropical and Sub-Tropical Terrestrial Systems. Springer, Singapore, pp. 313-331.

Drake, B.G., Gonzàlez-Meler, M.A. and Long, S.P. 1997. More efficient plants: a consequence of rising atmospheric CO_2? Annual Rev. Plant Biol., 48(1): 609-639.

Evans, J.R. 1989. Photosynthesis and nitrogen relationships in leaves of C_3 plants. Oecologia, 78(1): 9-19.

Evans, J.R. and von Caemmerer, S. 2000. Would C_4 rice produce more biomass than C_3 rice?. Studies in Plant Science, 7: 53-71.

Field, C., Lund, C., Chiariello, N. and Mortimer, B. 1997. CO_2 effects on the water budget of grassland microcosm communities. Glob. Change Biol., 3(3): 197-206.

Fisher, M.J., Rao, I.M., Ayarza, M.A., Lascano, C.E., Sanz, J.I., Thomas, R.J. and Vera, R.R. 1994. Carbon storage by introducing deep-rooted grasses in the South American savannas. Nature, 371(6494): 236-238.

Fissore, C., Espeleta, J., Nater, E.A., Hobbie, S.E. and Reich, P.B. 2010. Limited potential for terrestrial carbon sequestration to offset fossil-fuel emissions in the upper Midwestern US. Front. in Ecol. Environ., 8(8): 409-413.

Frank, A.B., Berdahl, J.D., Hanson, J.D., Liebig, M.A. and Johnson, H.A. 2004. Biomass and carbon partitioning in switchgrass. Crop Sci., 44(4): 1391-1396.

Fredeen, A.L., Koch, G.W. and Field, C.B. 1995. Effects of atmospheric CO_2 enrichment on ecosystem CO_2 exchange in a nutrient and water-limited grassland. J. Biogeogr., 12: 215-219.

Fu, Q., Cheng, L., Guo, Y. and Turgeon, R. 2011. Phloem loading strategies and water relations in trees and herbaceous plants. Plant Physiol., 157(3): 1518-1527.

Ghannoum, O., Caemmerer, S.V., Ziska, L.H. and Conroy, J.P. 2000. The growth response of C_4 plants to rising atmospheric CO_2 partial pressure: A reassessment. Plant Cell Environ., 23(9): 931-942.

Ghannoum, O., von Caemmerer, S., Barlow, E.W. and Conroy, J.P. 1997. The effect of CO_2 enrichment and irradiance on the growth, morphology and gas exchange of a C_3 (*Panicum laxum*) and a C_4 (*Panicum antidotale*) grass. Funct. Plant Biol., 24(2): 227-237.

Gifford, R.M. and Morison, J.I. 1985. Photosynthesis, water use, and growth of a C_4 grass stand at high CO_2 concentration. Photosynth. Res., 7(1): 77-90.

Gifford, R.M., Barrett, D.J. and Lutze, J.L. 2000. The effects of elevated [CO_2] on the C: N and C: P mass ratios of plant tissues. Plant Soil, 224(1): 1-14.

Goverde, M., Arnone III, J.A. and Erhardt, A. 2002. Species-specific reactions to elevated CO_2 and nutrient availability in four grass species. Basic Appl. Ecol., 3(3): 221-227.

Gray, J.E., Holroyd, G.H., Van Der Lee, F.M., Bahrami, A.R., Sijmons, P.C., Woodward, F.I. and Hetherington, A.M. 2000. The HIC signaling pathway links CO_2 perception to stomatal development. Nature, 408(6813): 713-716.

Halford, N.G., Curtis, T.Y., Muttucumaru, N., Postles, J. and Mottram, D.S. 2011. Sugars in crop plants. Annals of Appl. Biol., 158(1): 1-25.

He, H., Kirkham, M.B., Lawlor, D.J. andKanemasu, E.T. 1992. Photosynthesis and water relations of big bluestem (C_4) and Kentucky bluegrass (C_3) under high concentration carbon dioxide. Trans. Kansas Acad. Sci., 19(03): 139-152.

IPCC. 2018: Summary for Policymakers. In Masson-Delmotte, P., Zhai, H.O., Pörtner, D., Roberts, J., Skea, P.R., Shukla, A., Pirani, W., Moufouma-Okia, C., Péan, R., Pidcock, S., Connors, J.B.R., Matthews, Y. Chen, X., Zhou, M.I., Gomis, E., Lonnoy, T., Maycock, M. and Tignor, T.W. (eds.), Global Warming of 1.5°C: An IPCC Special Report On The Impacts Of Global Warming Of 1.5°C Above Pre-Industrial Levels And Related Global Greenhouse Gas Emission Pathways, in the Context Of Strengthening the Global Response to the Threat of Climate Change, Sustainable Development, and Efforts to Eradicate Poverty. World Meteorological Organization, Geneva, Switzerland, pp. 1-32.

Jackson, R.B., Luo, Y., Cardon, Z.G., Sala, O.E., Field, C.B. and Mooney, H.A. 1995. Photosynthesis, growth, and density for the dominant species in a CO_2-enriched grassland. J. Biogeogr., 54: 221-225.

Jauregui, I., Aparicio-Tejo, P.M., Avila, C., Cañas, R., Sakalauskiene, S. and Aranjuelo, I. 2016. Root–shoot interactions explain the reduction of leaf mineral content in Arabidopsis plants grown under elevated [CO2] conditions. Physiol. Plant., 158(1): 65-79.

Jongen, M., Jones, M.B., Hebeisen, T., Blum, H. and Hendrey, G. 1995. The effects of elevated CO_2 concentrations on the root growth of *Lolium perenne* and *Trifolium repens* grown in a FACE* system. Glob. Change Biol., 1(5): 361-371.

Khan, M.Z.A. 2017. Causes and consequences of greenhouse effect & its catastrophic problems for earth. Int. J. Sustain. Manag. Information Technologies, 3(4): 34.

King, K.M. and Greer, D.H. 1986. Effects of carbon dioxide enrichment and soil water on maize. Agron. J., 78(3): 515-521.

Klem, K., Holub, P. and Urban, O. 2017. Elevated CO_2 concentration affects the vertical distribution of photosynthetic activity in *Calamagrostis arundinacea* (L.) Roth. Beskydy, 10(1-2): 67-74.

Knapp, A.K., Hamerlynck, E.P. and Owensby, C.E. 1993. Photosynthetic and water relations responses to elevated CO_2 in the C_4 grass *Andropogon gerardii*. Int. J. Plant Sci., 154(4): 459-466.

Krapp, A., Quick, W.P. and Stitt, M. 1991. Ribulose-1, 5-bisphosphate carboxylase-oxygenase, other Calvin-cycle enzymes, and chlorophyll decrease when glucose is supplied to mature spinach leaves via the transpiration stream. Planta, 186(1): 58-69.

Kuehny, J.S., Peet, M.M., Nelson, P.V. and Willits, D.H. 1991. Nutrient dilution by starch in CO_2-enriched Chrysanthemum. J. Exper. Bot., 42(6): 711-716.

Lara, M.V. and Andreo, C.S. 2011. C_4 plants adapt to high levels of CO_2 and drought environments. Abiotic Stress Plants-Mech Adapt., 20: 415-428.

Leuzinger, S. and Hättenschwiler, S. 2013. Beyond global change: Lessons from 25 years of CO_2 research. Oecologia, 171(3): 639-651.

Long, S.P. and Drake, B.G. 1992. Photosynthetic CO_2 assimilation and rising atmospheric CO_2 concentrations. Topics Photosynth., 12: 69-103.

McDonald, E.P., Erickson, J.E. and Kruger, E.L. 2002. Research note: Can decreased transpiration limit plant nitrogen acquisition in elevated CO_2? Funct. Plant Biol., 29(9): 1115-1120.

Mishra, N.B. and Young, K.R. 2020. Savannas and grasslands. Terr. Ecosyst. Biodivers., 20: 235.

Moore, B.D., Palmquist, D.E. and Seemann, J.R. 1997. Influence of plant

growth at high CO_2 concentrations on leaf content of ribulose-1, 5-bisphosphate carboxylase/oxygenase, and intracellular distribution of soluble carbohydrates in tobacco, snapdragon, and parsley. Plant Physiol., 115(1): 241-248.

Moraes, M.G., Chatterton, N.J., Harrison, P.A., Filgueiras, T.S. and Figueiredo-Ribeiro, R.C.L. 2013. Diversity of non-structural carbohydrates in grasses (Poaceae) from Brazil. Grass Forage Sci., 68(1): 165-177.

Morgan, J.A., Lecain, D.R., Mosier, A.R. and Milchunas, D.G. 2001. Elevated CO_2 enhances water relations and productivity and affects gas exchange in C_3 and C_4 grasses of the Colorado short grass steppe. Glob. Change Biol., 7(4): 451-466.

Morvan-Bertrand, A., Boucaud, J., Le Saos, J. and Prud'homme, M.P. 2001. Roles of the fructans from leaf sheaths and the elongating leaf bases in the regrowth following defoliation of *Lolium perenne* L. Planta, 213(1): 109-120.

Mott, K.A. 1988. Do stomata respond to CO_2 concentrations other than intercellular? Plant Physiol., 86(1): 200-203.

Nackley, L.L., Vogt, K.A. and Kim, S.H. 2014. *Arundo donax* water use and photosynthetic responses to drought and elevated CO_2. Agric. Water Manag., 136: 13-22.

Nogia, P., Sidhu, G.K., Mehrotra, R. and Mehrotra, S. 2016. Capturing atmospheric carbon: biological and non-biological methods. International J. Low-Carbon Technol., 11(2): 266-274.

Norby, R.J. and O'neill, EG. 1991. Leaf area compensation and nutrient interactions in CO_2-enriched seedlings of yellow-poplar (*Liriodendron tulipifera* L.). New Phytolog., 117(4): 515-528.

Odiwe, A.I., Olanrewaju, G.O. and Raimi, I.O. 2016. Carbon sequestration in selected grass species in tropical lowland rainforest at Obafemi Awolowo University, Ile-Ife, Nigeria January 26, 2017. J. Tropical Biol. Conserv., 11: 13.

O'Mara, F.P. 2012. The role of grasslands in food security and climate change. Annals Bot., 110(6): 1263-1270.

Owensby, C.E., Coyne, P.I., Ham, J.M., Auen, L.M. and Knapp, A.K. 1993. Biomass production in a tallgrass prairie ecosystem exposed to ambient and elevated CO_2. Ecol. Appl., 3(4): 644-653.

Owensby, C.E., Ham, J.M., Knapp, A., Rice, C.W., Coyne, P.I. and Auen, L.M. 1996. Ecosystem-level responses of tall grass prairie to elevated CO_2. In Koch, G. and Roy, J. (eds), Carbon Dioxide and Terrestrial Ecosystems. Elseiver, Netherlands, pp. 147-162

Padhan, B.K., Sathee, L., Meena, H.S., Adavi, S.B., Jha, S.K. and Chinnusamy, V. 2020. CO_2 Elevation accelerates phenology and alters carbon/nitrogen metabolism vis-à-vis ROS abundance in bread wheat. Front. Plant Sci., 11, 1061.

Paul, M.J. and Foyer, C.H. 2001. Sink regulation of photosynthesis. J. Exp. Bot., 52(360): 1383-1400.

Pollock, C., Farrar, J., Tomos, D., Gallagher, J., Lu, C. and Koroleva, O. 2003. Balancing supply and demand: the spatial regulation of carbon metabolism in grass and cereal leaves. J. Exp. Bot., 54(382): 489-494.

Poorter, H. and Perez-Soba, M. 2002. Plant growth at elevated CO_2. Encycl. Glob. Environ. Change, 2: 489-496.

Poorter, H. and Remkes, C. 1990. Leaf area ratio and net assimilation rate of 24 wild species differing in relative growth rate. Oecologia, 83(4): 553-559.

Potvin, C. and Strain, B.R. 1985. Effects of CO_2 enrichment and temperature on growth in two C_4 weeds, Echinochloa crus-galli and Eleusine indica. Canadian Journal of Botany, 63(9), 1495-1499.

Pritchard, S.G. and Rogers, H.H. 2000. Spatial and temporal deployment of crop roots in CO_2-enriched environments. New Phytol., 147(1): 55-71.

Pritchard, S.G., Rogers, H.H., Prior, S.A. and Peterson, C.M. 1999. Elevated CO_2 and plant structure: a review. Glob. Change Biol., 5(7): 807-837.

Riechers, G.H. and Strain, B.R. 1988. Growth of blue grama (*Bouteloua gracilis*) in response to atmospheric CO_2 enrichment. Canad. J. Bot., 66(8): 1570-1573.

Roumet, C. and Roy, J. 1996. Prediction of the growth response to elevated CO_2: A search for physiological criteria in closely related grass species. New Phytol., 134(4), 615-621.

Ryle, G.J.A., Powell, C.E. and Tewson, V. 1992. Effect of elevated CO_2 on the photosynthesis, respiration, and growth of perennial ryegrass. J. Exp. Bot., 43(6): 811-818.

Sage, R.F. 1994. Acclimation of photosynthesis to increasing atmospheric CO_2: the gas exchange perspective. Photosynth. Res., 39(3): 351-368.

Sage, R.F. and Kubien, D.S. 2003. Quo Vadis C_4? An ecophysiological perspective on global change and the future of C_4 plants. Photosynth. Res., 77(2-3): 209-225.

Sage, R.F., Pearcy, R.W. andSeemann, J.R. 1987. The nitrogen use efficiency of C_3 and C_4 plants: III. Leaf nitrogen effects on the activity of carboxylation enzymes in *Chenopodium album* (L.) and *Amaranthus retroflexus* (L.). Plant Physiol., 85(2): 355-359.

Sage, R.F., Sharkey, T.D. and Seemann, J.R. 1988. The in-vivo response of the ribulose-1, 5-bisphosphate carboxylase activation state and the pool sizes of photosynthetic metabolites to elevated CO_2in *Phaseolus vulgaris* L. Planta, 174(3): 407-416.

Samarakoon, A.B. and Gifford, R.M. 1995. Soil water content under plants at high CO_2 concentration and interactions with the direct CO_2 effects: a species comparison. J. Biogeogr., 193-202.

Scordia, D. and Cosentino, S.L. 2019. Perennial energy grasses: Resilient crops in changing European agriculture. Agriculture, 9(8): 169.

Sicher, R.C. and Bunce, J.A. 1997. Relationship of photosynthetic acclimation to changes of Rubisco activity in field-grown winter wheat and barley during growth in elevated carbon dioxide. Photosynth. Res., 52(1): 27-38.

Slewinski, T.L. 2012. Non-structural carbohydrate partitioning in grass stems: a target to increase yield stability, stress tolerance, and biofuel production. J. Exp. Bot., 63(13): 4647-4670.

Song, Y., Yu, J. and Huang, B. 2014. Elevated CO_2-mitigation of high-temperature stress associated with maintenance of positive carbon balance and carbohydrate accumulation in Kentucky bluegrass. PLoS One, 9(3): 545.

Stitt, M. 1991. Rising CO_2 levels and their potential significance for carbon flow in photosynthetic cells. Plant Cell Environ., 14(8): 741-762.

Taub, D.R. and Wang, X. 2008. Why are nitrogen concentrations in plant tissues lower under elevated CO_2? A critical examination of the hypotheses. J. Integr. Plant Biol., 50(11): 1365-1374.

Teng, N., Wang, J., Chen, T., Wu, X., Wang, Y. and Lin, J. 2006. Elevated CO_2 induces physiological, biochemical, and structural changes in leaves of *Arabidopsis thaliana*. New Phytol., 172(1): 92-103.

Tom Dery, D., Eller, F., Jensen, K. and Reisdorff, C. 2018. Effects of elevated carbon dioxide and climate change on biomass and nutritive value of Kyasuwa (*Cenchrus pedicellatus*Trin.). J. Appl. Bot. Food Qual., 91: 88-95.

Turcsányi, E., Cardoso-Vilhena, J., Daymond, J., Gillespie, C., Balaguer, L., Ollerenshaw, J. and Barnes, J. 2000. Impacts of tropospheric ozone: past, present and likely future. In Trace Gas Emissions and Plants (pp. 272-249). Springer, Dordrecht.

Tzvelev, N. 1989. The system of grasses (Poaceae) and their evolution. Bot. Rev., 55(3): 141-203.

Oijen, V.M., Schapendonk, A.H.C.M., Jansen, M.J.H., Pot, C.S. and Maciorowski, R. 1999. Do open-top chambers overestimate the effects of rising CO_2 on plants? An analysis using spring wheat. Glob. Change Biol., 5(4): 411-421.

Waggoner, P.E. 1984. Views: Agriculture and Carbon Dioxide: If the levels of carbon dioxide in the atmosphere increase as expected, will agricultural productivity decline? Am. Sci., 72(2): 179-184.

Wand, S.J., Midgley, G.F., Jones, M.H. and Curtis, P.S. 1999. Responses of wild C_4 and C_3 grass (Poaceae) species to elevated atmospheric CO_2 concentration: a meta-analytic test of current theories and perceptions. Glob. Change Biol., 5(6): 723-741.

Wang, H., Zhou, G., Jiang, Y., Shi, Y. and Xu, Z. 2019. Effects of elevated CO_2 on *Stipa baicalensis* photosynthesis depend on precipitation and growth phase. Ecol. Res., 34(6): 790-801.

Wong, S.C. 1990. The elevated atmospheric partial pressure of CO_2 and plant growth. Photosynth. Res., 23(2): 171-180.

Wullschleger, S.D., Tschaplinski, T.J. and Norby, R.J. 2002. Plant water relations at elevated CO_2–implications for water-limited environments. Plant Cell Environ., 25(2): 319-331.

Xue, G.P., McIntyre, C.L., Rattey, A.R., van Herwaarden, A.F. and Shorter, R. 2009. Use of dry matter content as a rapid and low-cost estimate for ranking genotypic differences in water-soluble carbohydrate concentrations in the stem and leaf sheath of *Triticum aestivum*. Crop Pasture Sci., 60(1): 51-59.

Ziska, L.H., Sicher, R.C. and Bunce, J.A. 1999. The impact of elevated carbon dioxide on the growth and gas exchange of three C_4 species differing in CO_2 leak rates. Physiol. Plant., 105(1): 74-80.

Nature Environment and Pollution Technology
An International Quarterly Scientific Journal

p-ISSN: 0972-6268
(Print copies up to 2016)
e-ISSN: 2395-3454

Vol. 21 | No. 5 (Suppl) | pp. 2103-2115 | 2022

Original Research Paper

https://doi.org/10.46488/NEPT.2022.v21i05.007

Open Access Journal

Mountainous City Landscape Water Supply System Potential Carbon Footprint: Case of the Philippines' Catbalogan Sky City Mega Project

Ronald L. Orale*(**)† and Doris Montecastro*
*School of Engineering and Architecture, Ateneo de Davao University, Davao City, Philippines
**Samar State University, Catbalogan City, Philippines
†Corresponding author: Ronald Orale; ronald.orale@ssu.edu.ph

Nat. Env. & Poll. Tech.
Website: www.neptjournal.com

Received: 17-06-2022
Revised: 30-07-2022
Accepted: 03-08-2022

Key Words:
Water supply system
Carbon footprint
Land use impact
Low impact development
Rainwater harvesting
Antiao watershed

ABSTRACT

Catbalogan Sky City Mega Project (CSCMP) is a climate-change (CC) adaptation strategy proposed after Typhoon Haiyan devastated the Philippines in November 2013. It is currently being built on top of a hill about 120m from sea level to avoid the impact of storm surges, sea-level rise, and flooding. With the city's continued expansion, water demand further worsens the supply gap. This study focused on determining the carbon footprint of the proposed water supply scarcity solution. This solution includes the construction of a reservoir to receive runoff water from the watershed where the CSCMP is located. Results of the study show that the reservoir can supply the water requirement for the entire city. However, the carbon footprint of the recommended solution is between 123% and 557% due to water treatment of heavily contaminated runoff water and the power consumption in distributing water to higher elevations. There is a need for the city to design a harvesting system that will reduce the need for more intense water treatment (i.e., reducing exposure of runoff water to contaminants) and the use of renewable energy in powering pumps and other treatment activities.

INTRODUCTION

The global population has continuously grown by more than 80 million per year, and the rate expects to grow by 2 billion annually by 2050 (Population Matters 2018). The growth rate in urban areas continues to grow despite having low fertility attributed to migration. By 2050, the urban population share is expected to increase to 68% from 54% in 2018 (Bolay & Kern 2019, United Nations 2018). Some countries in Latin and North America, including the Caribbean, have their population share reaching about 80% in urban centers than in the countryside (Bolay & Kern 2019). Overall, Asian countries share about 54% of the global urban population, while Europe and Africa have 13% each (United Nations 2018).

Many urban areas are scarce with available land. Cities need to expand to accommodate people attracted to the urban centers. Cities either expand horizontally (new growth areas) or vertically through high-rise buildings (Al-Kodmany 2018, Wennersten 2018, Tosics 2015). Either way, both approaches have climate-change-related challenges. Going vertical makes cities denser and requires more energy, while the horizontal expansion will require changing land use and scarcity of land for some. Urban expansion (vertical or horizontal) will always increase population density. Densely populated urban areas are very vulnerable to the impacts of CC, especially those coming from low- and middle-income countries (Dodman 2009) like the Philippines.

Water resources are vital for any community's survival (Green Facts 2008); cities need this resource to be competitive; water is life (National Geographic nd). History explains that communities are established where water abounds, like coastal zones, nearby rivers, or the river mouth. Today, most of these communities' water resources are severely affected due to the intensifying CC phenomenon (Misra 2014, Talat 2021). Because of CC, some areas have more water during extreme hydrological events that lead to floods, while others experience water scarcity (Pingale et al. 2014, Steeneveld et al. 2018). Some cities in the world look for strategic approaches to address water scarcity. One good example is Singapore, which has four sources: runoff waters captured in catch basins, imported water from Malaysia, recycled water, and desalinated water (PUB nd.a, Hsien et al. 2019). Other water-scarce areas make use of rainwater as a viable resource. Rainwater harvesting is not new but remains one of the most influential alternative water supply options (Liu et al. 2020). In Singapore, runoff water is drained into canals, and those that exist in streams and rivers are treated before it is used for various purposes

(PUB nd.a, Hsien et al. 2019). The choice of water production process depends on many factors, the primary consideration is financial resources. While countries like Singapore can supply water to their population despite being water-scarce, other economically challenged countries face difficulty. In 2018, the water production cost in Singapore is pegged at $1.78 (PUB nd.c), while in the Philippines, it is US$0.21 per cubic meter for the first 40 cubic meters (MWSS 2017). The vast gap can be attributed to the cost of water production and the economic status of the countries.

The Philippines improving economy facilitated the growth of communities in major cities and those in the countryside. As it grows, the need for new areas for development is paramount. Equipped with information about disasters like Typhoon Haiyan, cities like the Catbalogan in the Eastern Visayas region embarked on an ambitious project dubbed the Catbalogan Sky City Mega Project (TAP nd., Orale & Novilla 2016, Hurtado 2019) or CSCMP. The project received positive reviews in the Philippines and abroad (Catbalogan LGU 2019, Meniano 2018, CDIA Asia 2016), but some questions remain, such as water supply requirements for the city to thrive.

This study aimed to present the likely water supply scenario if no suitable land use plan exists and a scientifically backed-runoff water collection system is incorporated. Information about the old city and the CSCMP, such as current and future water demand and the wastewater production profile, was determined to answer this. The water supply production and distribution cost were calculated based on the information gathered. Also, the potential contribution to CC was estimated.

MATERIALS AND METHODS

The paper focused on the characterization of the water supply for the Catbalogan Sky City project, specifically the runoff harvesting, treatment, distribution, and production cost, as well as the carbon footprint. The plans were based on secondary data; the current master plan for the Sky City and the drainage system collecting the runoff water and gray water are based on prevailing designs used by the LGU of Catbalogan and the indicative plans for the city. There is no active Comprehensive Land Use Plan (CLUP) in the City of Catbalogan.

Study Site Profile

The study site profile, specifically it is land utilization in the study site, was derived from secondary sources, mainly from unpublished Local Government of Catbalogan City reports. This information was validated through a physical survey using a drone to capture the current condition of the study sites, specifically land cover. Without an updated Comprehensive Land Use Plan (CLUP), the proposed Sky City Mega Project plans were based on the concept proposals submitted by the LGU of Catbalogan to various funding institutions. Population demographics are estimated based on the 2020 census population from the Philippine Statistics Authority. The researcher also referred to drone shots of the watershed and visited areas in the study sites for validation, especially along the groundcover parameters for the HEC-HMS-based modeling. The drone shots and other plans were georeferenced for QGIS analysis. Handheld GPS was used to locate specific areas seen in the drone images.

Water and Waste Water Production, Treatment and Distribution Profile

The current production, treatment, and distribution profile were extracted from the reports available at the Catbalogan Water District (CWD). From these reports, the proportion of production (PP) from each of the sources (PS_i) per month for n sources (e.g., Spring/groundwater; Caramayon, Masacpasac, Tomalistis, Executive, Lagundi; surface water Kulador and Sky City lagoon; and other minor sources) was calculated using equation (a);

$$PP = \frac{PS_i}{\sum PS_n} \quad \ldots(1)$$

The distribution according to the type of use (i.e., domestic use or DU, and non-domestic use or NDU) was also calculated based on the reports of CWD. Equations used for the PDU (proportion for DU) and PNDU (proportion of NDU) are (b) and (c) respectively;

$$PDU = \frac{DU}{(DU+NDU)}\ 100\% \quad \ldots(2)$$

$$PNDU = \frac{NDU}{(DU+NDU)}\ 100\% \quad \ldots(3)$$

The water system flow network was generally described based on inspections made to at least 20 households, 15 commercial establishments, and five institutional sectors. Documentary reviews and informal interviews with other sectors involved in the system and supplemented with technical reports by Gomba et al. (2007a, 2007b). The system's water supply network draws from water sources to collection and treatment facilities, then to domestic (households or DU) and non-domestic clients (i.e., industrial, commercial, institutional/government, others or NDU) utilization, then followed by wastewater production and disposal. The volume of wastewater is a function of water use. Information about wastewater production and disposal is unavailable in many parts of the Philippines (Claudio 2015, ADB 2013), including Catbalogan City. The UN Water estimates that around 80% of used water becomes

wastewater. Most of the wastewater in Catbalogan City finds its way to waterbodies (Orale & Fabillar 2011); others seep into the grounds. Canals and waterways in Catbalogan are either concreted (with poor water tightness attributed to construction defects or poor maintenance/cracked) or unlined (like Antiao River and Antiao Creek). Seepage into the soil strata is governed by permeability, texture, bulk density, porosity, and others (Rai et al. 2017). The loss in water due to seepage and evaporation was estimated using a modified ponding method described by Rai et al. (2017). The modification includes creating a 1m x 1m x 1m pond filled with water until the soil is saturated to mimic an active drainage canal condition. After it is saturated, the pond is filled with canal water, and the drop in height is the loss estimate. The seepage and evaporation loss in the three sites was 16, 27, and 45, or an average of 29.33 or approximately 30%.

The future water supply network was based on the assumption that no specialized intervention exists. Here, the manner of production, treatment, and distribution of water and wastewater, including disposal, was analyzed similarly. The collection of runoff water as an additional water source was incorporated into the system.

Water Supply and Demand

Water demand and available water supply are based on a projected scenario of the future. This future is based on the plans such as the currently being updated Catbalogan Comprehensive Land Use Plan (CLUP) and the Sky City concept proposals, which were available during the study. Formulation and the implementation of planned developments like CLUP face many challenges (Lech & Leppert 2018, Salazar-Quitaleg & Orale 2016, Huang & Cantada 2019) that lead to the non-realization of the plan. For this paper, the realization rate of the planned future was set to only between 5% to 25% considering the low compliance of the city to zoning regulations and the variability of a future scenario affecting the implementation of the planned future. Available Water Supply (AWS) is from the CWD sources (CWS) and the extractable water at the planned lagoon (EWL). The subscript "t" stands for the time/year, specifically 2022 and 2040;

$$AWS_t = CWS_t + EWL_t \quad \ldots(4)$$

The CWS is from at least three primary water sources and other groundwater wells (CWD 2018) and is assumed will not decrease or increase over time. The quantities were extracted from the monthly official reports of CWD (CWD 2015, CWD 2021, CWD 2022). The EWL, on the other hand, is the water collected from various drains to the lagoon. The quantity of EWL is estimated using the Hydrologic Engineering Center - Hydrologic Modeling System (HEC-HMS) of the US Army of Engineers (USACE nd.). Equation (e) is for the water demand for 2022 and 2040.

$$WD_t = DD_t + CD_t + ID_t + GID_t + OD_t \quad \ldots(5)$$

The WD was estimated from five groups of users; residential/domestic (DD), commercial (CD), industrial (ID), government offices/institutional (GID), and others (OD). These are estimated based on current and future scenarios. For example, the DD estimate considered the entire population and not only those who are serviced with CWD. Current water demand from the rest of the consumers was based on the 2020 monthly records of the CWD (CWD 2021).

Future water demand was based on the projected development scenario by 2040. The allocation of new residential, commercial and industrial zones will result in a higher population primarily through migration. The water demand by 2040 (WD_{2040}) under the 5% future development scenario is calculated as;

$$WD_{2040} = (LA_{2040})(5\%)(CR_{2022}) \quad \ldots(6)$$

where LA is the land allocation for specific land use (e.g. residential/domestic, commercial, industrial, government/institutional, and others), and the term CR_{2022} is the base consumption rate for 2022 for the specific land use. For example, CR_{2022} for residential land use is calculated as;

$$CR_{2022(residential)} = \frac{LA_{2022(residential)}}{WD_{2022(residential)}} \quad \ldots(7)$$

equation (f) and (g) is similar for other land uses. The consumption rate (CR_{2022}) for occupied residential, commercial, industrial, and institutional lands is estimated to be 2.45, 2.31, 0.14, and 1.0 cubic meters of water per square meter.

Wastewater Production Profile

Catbalogan wastewater production is unknown. Globally, it is estimated that around 80% of consumed water is transformed into wastewater, and the remaining 20% is a function of evaporation and unaccounted water (UN Water 2021a, UN Water 2021b, UNESCO nd.). In the Philippines, only 10% of all wastewater is treated, and only 5% of the total population is connected to a sewer network (Claudio 2015), Catbalogan City has almost none. Institutional/governmental, commercial, and Industrial wastewater production will be calculated similarly to domestic wastewater. The calculation of wastewater (WW) produced is 80% of water demand (WD). Formula (h) was used for all wastewater production per type of land use.

$$WW_{2040} = (WD_{2040})(80\% \quad \ldots(8)$$

Runoff Water Estimation and Stormwater Collection System

Rainfall-runoff discharge estimation was through the HEC-HMS version 4.5 developed by the US Corps of Engineers – Institute for Water Resources Hydrologic Engineering Center. As shown in Table 1, the simulation data that were kept constant are the land allocation area and soil type, while the average monthly rainfall data was based on the 2021 reports from the Philippine Astronomical Geophysical and Astronomical Administration (PAGASA) for Catbalogan City. The impervious layer, lag time, and SCS-CN values were estimated based on the possible land utilization.

The stormwater collection system was assumed to be similar to what Catbalogan City currently uses. Runoff water enters the canal bringing in sediments, solid waste, and contaminants. The runoff waters, including those drained from roofs of buildings/houses, roads, lawns, and other pavements, including those from vegetated grounds, are most often heavily contaminated with chemical and biological matters. Without a detailed plan of the Sky City, it is assumed in this paper that roadsides have a drainage system leading to the impounding dam.

Carbon Footprint of Water Supply Production and Distribution

Carbon Footprint is estimated using CO_2-e or the Carbon Dioxide Equivalent; several metric tons of CO_2 emissions with the same global warming potential as one metric ton of another greenhouse gas (EPA 2022). The entire operation of the CSCMP will generate a Carbon Footprint designated as Carbon Dioxide equivalent or CO_2-e; one of which is the production, treatment, and distribution of water supply. In this paper, only the carbon footprint due to pumping water from the source to treatment plants and clients, as well as chemicals (i.e., chlorimide) was considered. Based on CWD reports for 2021, about 0.632 kWh of energy was used to pump out water from the source to the treatment facility and distribution. About 78% of the energy used was used for production and 22% for distribution. The exact value will be used to pump out water from the lagoon to households. Therefore, the carbon footprint in water production (CFWP) and distribution (CFWD), considering the type of energy used (CFET) in Catbalogan City, is based on current practice is;

$$CFWP = WD[(0.632)(78\%)](\%EM_{nr})(CFET) \quad \ldots(9)$$

$$CFWP = WD[(0.632)(78\%)](\%EM_{nr})(CFET) \quad \ldots(10)$$

The $\%EM_{(nr)}$ is the percent of the energy used that is non-renewable. Energy production from renewable sources like geothermal energy has a very low carbon footprint (Pehl et al. 2017, EIA nd.), thus was not considered. The value used for this study is 43% extracted from the 2020 and 2021 energy mix used by the local power supplier, the Samar II Electric Cooperative (SAMELCO II 2020, SAMELCO II 2021). The CFET for energy from coal-powered electrical plants is about 0.79 kg of CO_2e per kWh of energy produced (Richie 2020, Scherer & Pfister 2016). The distribution cost for the case of the CSCMP is 0.632 kWh of energy per cubic meter.

The current treatment process includes sedimentation, rapid and slow sand filtration, and finally, chlorination

Table 1: Parameters used in the HEC-HMS simulation.

Land Allocation	HEC Parameters	Year (Development Scenario)		
		2022	2040 (5%)	2040 (25%)
Sky City Area: 0.909 km2	SCS-CN	77	85	92
	Impervious Layer [%]	5	50	80
	Lag Time [min]	30	20	15
Outside Area: 1.55 km2	SCS-CN	77	80	90
	Impervious Layer [%]	5	10	25
	Lag Time [min]	30	25	18
Green Area: 0.616 km2	SCS-CN	77	77	77
	Impervious Layer [%]	1	1	1
	Lag Time [min]	45	45	45
Lagoon Area: 0.309 km2	SCS-CN	77	77	77
	Impervious Layer [%]	1	5	5
	Lag Time [min]	5	5	5

(CWD nd.). For this study, the current carbon footprint is based solely on the chlorination process, while by 2040, it is assumed that it will become more advanced. The carbon footprint to produce potable water from groundwater/spring water, and surface water from the river in 2022 is 0.02 and 0.08 kg CO_2e per cubic meter, respectively. By 2040, the carbon footprint for groundwater/spring water, surface water (i.e Antiao River or other imported water from rivers of other nearby towns), and runoff water are estimated at 0.05, 0.10 (Biswas & Yek 2016), 0.39 kg of CO_2e (Hsien et al. 2019) per cubic meter of water respectively.

The SCMP will harvest runoff water and store it in a lagoon as a reservoir. There is no available runoff water harvesting design making it potentially heavily contaminated. The current runoff collection system for the City of Catbalogan also receives wastewater from all sources, the reason for it being treated as gray water.

RESULTS AND DISCUSSION

All cities are called upon to respond to the challenges posed by global warming. However, the responses of every city vary; most often than not, these actions lack evaluation of whether it is a solution or contributing to the problem they aimed to address. The foregoing will present the CC adaptation of a small city in the Philippines and examine the carbon footprint of the approach. The study delimits its scope to water supply, one of the challenges the new project will face.

Catbalogan Sky City Profile

Catbalogan is a coastal component city and the capital of the province of Samar Philippines (PhilAtlas nd.a) The 106,440 population as of the 2020 census is distributed to its 57 barangays or villages (PhilAtlas nd.b), most of which is concentrated in the city center, which is only about 2% of the total land area (Orale 2006). With a 2.47% growth rate, the city will reach 173,396 thousand by 2040. The actual population density in the city center will likely reach around 10,000 people per square kilometer (Orale 2006), one of the highest in the Eastern Visayas Region. These numbers do not include the transient workers coming to the city for work and other purposes but returning to nearby municipalities/

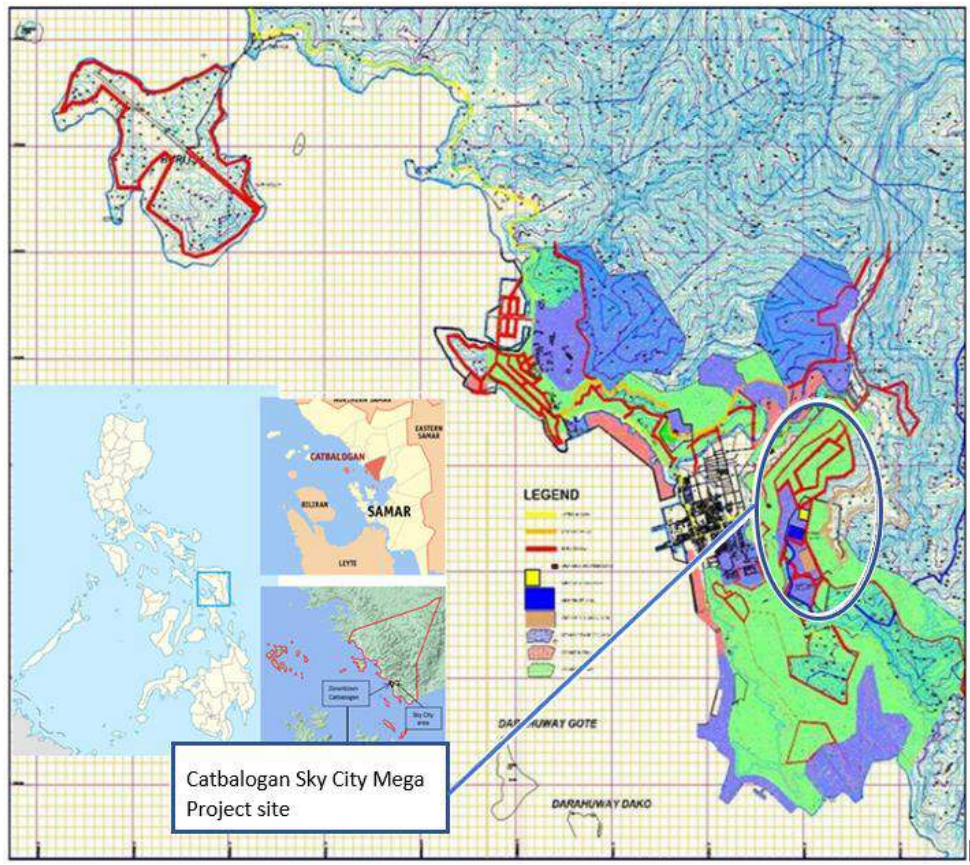

Fig. 1: Comprehensive development map of the entire Catbalogan; inset is the Sky City Mega Project.

cities at night. The City of Catbalogan has an economic activity among others that is among the highest based on the Competitiveness Index report since 2016 (DTI nd.), further attracting investors to the city. There is, however, minimal land area for the growing demand for expansion as the city has only about 15% flat to gently sloping land surface. Fig. 1 shows the Comprehensive Development Plan (CDP) of the City of Catbalogan and the site of the proposed CSCMP. This CDP is expected to be part of the currently formulated Comprehensive Land Use Plan (CLUP) of the City of Catbalogan.

The 2013 impact of the tropical super typhoon Haiyan resulted in the birth of the CSCMP (Hurtado 2019); a new township located 120m above sea level (Skyscraper City 2015) found northeast of the old Catbalogan City downtown area. The project aims to be an example of localizing the Sustainable Development Goals (SDGs), the Sendai Framework, and the New Urban Agenda to create a resilient, safe, and sustainable city (Hurtado 2019). The project area covers about 440 hectares, and the first phase of initiatives is on its way (CDIA Asia 2016). The new city will utilize 50% open space and 50% buildable space for hotels, resorts, health and wellness center, education and training hubs, and multi-purpose complexes (Skyscraper City 2015). The plan was praised in many venues here and abroad; in 2015, the project was among the few proposals promoted by Urban-Low Emission Development Strategies cities out of 150 submissions (Meniano 2018). The estimated and proposed Catbalogan land use distribution is mentioned in Table 2.

Water & Wastewater Production and Distribution Profile

The main source of water for Catbalogan use is springs supplemented with groundwater pumping. The main sources are heavily influenced by precipitation. This water supply, distribution, and consumption as well as water loss are shown in Figs. 3 and 4.

As of 2022, the water supply system network: As of March 2022, Catbalogan City, through its Catbalogan Water District (CWD), supplies water from at least six sources, as shown in Fig. 2. About 10% is from surface water (river), and the rest is from groundwater. Around 86% are extracted at the mouth of springs, and around 4% are pumped from deep wells. The said waters are post-processed differently; the surface water

Table 2: Estimated current (2022) and proposed (2040) Catbalogan land use distribution.

Land use with buildings*	Land Area [m^2]			
	2022		2040	
	Old City	Sky City	Old City	Sky City
Residential	144,804	0	6,452,091	185,833
Commercial	10,478	0	466,854	378,896
Industrial	44,204	0	1,969,635	218,319
Others	39,709	0	1,769,333	89,507
Reservoir	0	0	0	387,875
Remaining lands without buildings	1,730,001,203	0	165,054,663	0

*Values were estimated from Google Map Image and Drone Shots (2022) and Fig. 1 (2040).

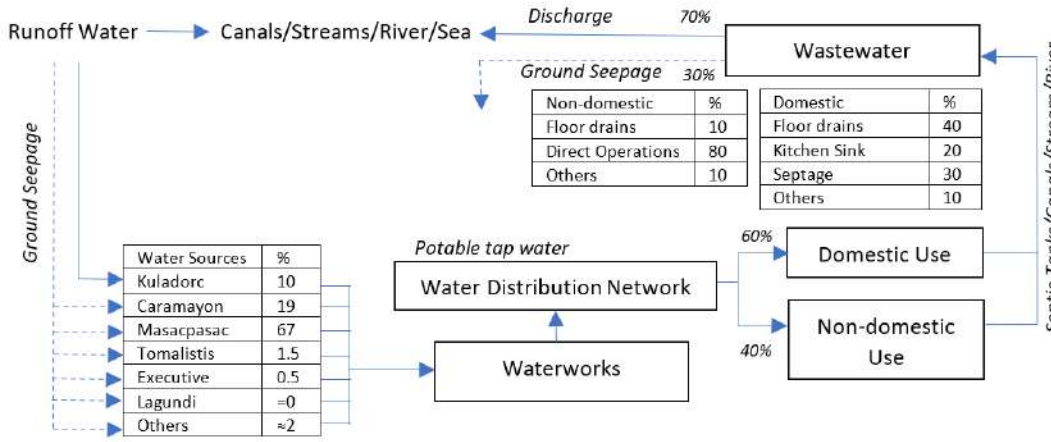

Fig. 2: Current Catbalogan city water and wastewater production and distribution.

undergoes several steps to remove sediments and passes through a rapid and slow sand filtration system (CWD nd.), while other sources are not subjected to it. All sources, however, are treated with chlorine compound to eliminate any pathogenic bacteria present. After water treatment, it is distributed to at least 26 of the 57 barangays of the City of Catbalogan. As of the study period, there are about 8,144 households serviced by the CWD, 153 government offices/ units, and 924 commercial/industrial service connections (CWD 2021). Approximately there will be around 39,740 individuals, or 37.3% of the Catbalogan populace, served by CWD. The remaining population secures their water from public and private artesian wells, open wells, and boxed spring water like those houses near the CSCMP site.

More than three-quarters of the water produced by the CWD is used for domestic purposes, and the rest is for commercial/industrial and institutional uses. Waste water produced, therefore, is mostly coming from households. The volume of waste is about 80% of the water consumed. At household levels, about 40% exit from floor drains, 20% from kitchens, 30 % disposed of in septic tanks, and about 10% from other domestic activities like watering plants, cleaning lawns, swimming pool, and other minor uses. Except for wastewater deposited in septic tanks, other wastewater is disposed of directly in drainage systems, canals, streams, rivers, or the sea. Even wastewater from septic tank leaching chambers finds its way to the drainage canals. Some of this wastewater seeps into the ground, risking contamination of groundwater aquifers. The manner of wastewater disposal deteriorated waters of the only river in Catbalogan (Antiao River) to a level comparable to sewage water (Amascual et al. 2020). Antiao River is the receiver of the majority of drainage waters in the City of Catbalogan.

Plausible scenario of water supply system network by 2040: If the LGU of Catbalogan observes the same manner of runoff management, the water collected in the catchment basin (lagoon as shown in Fig. 3-Right) will be very contaminated, and cleaning it will be very expensive for the people of Catbalogan. Shown in Fig. 4 is the likely water supply network cycle from the source of water, treatment, distribution, utilization, disposal of wastewater, and back to the source. There is also a possibility that if the watershed

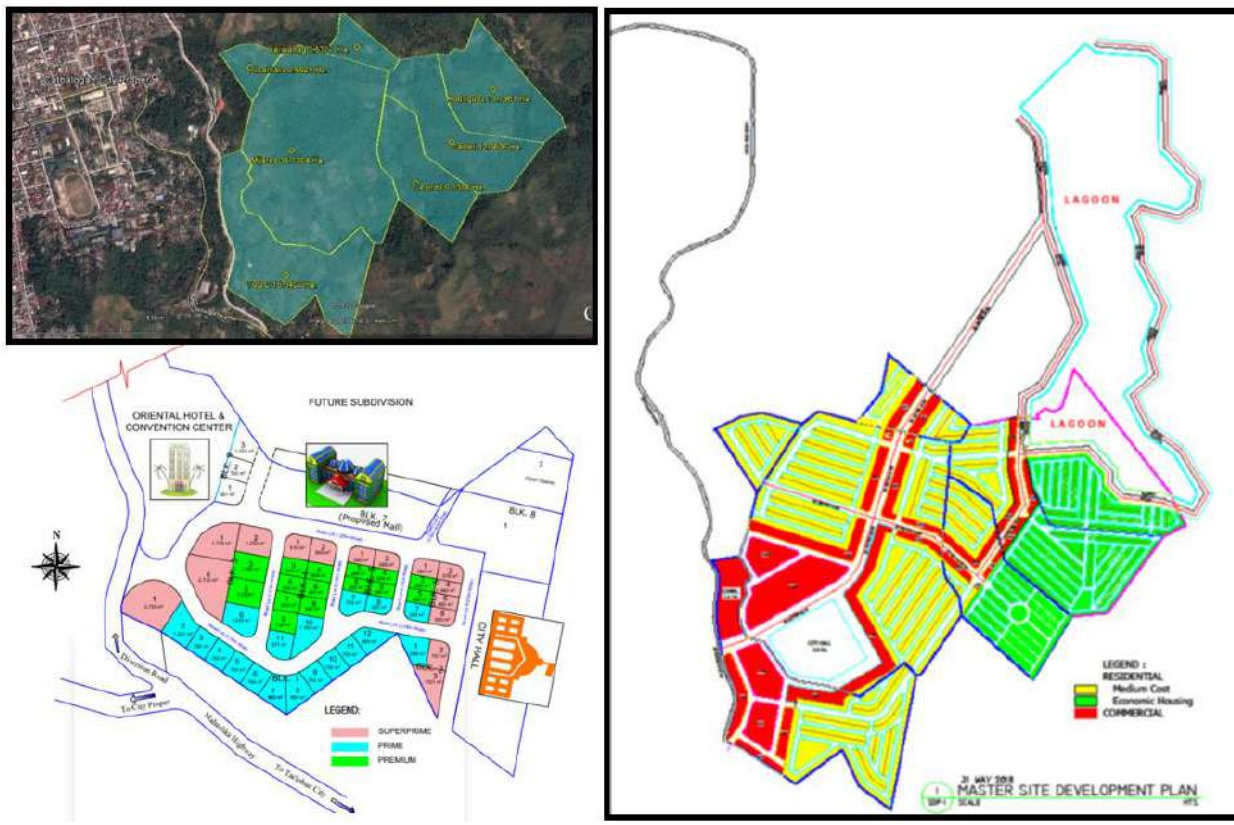

Fig. 3: The Sky City mega project; (Right) Master site development plan, (Upper-Left) Site for Phase 1, (Lower-Left) Lot allocation for Phase 1.

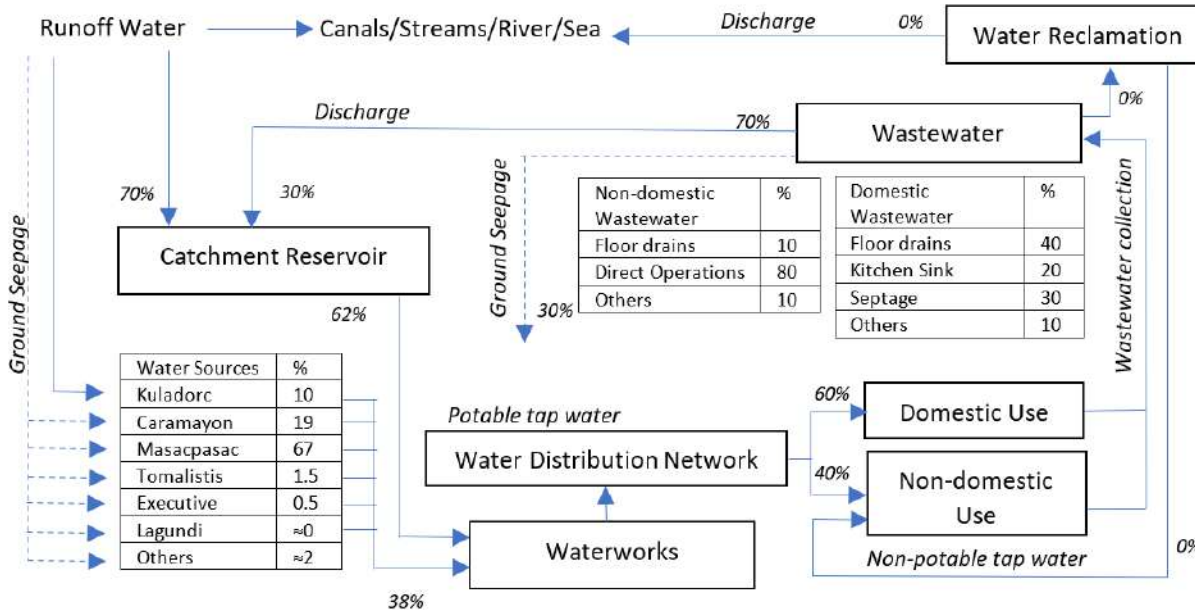

Fig. 4: Projected Catbalogan city water and wastewater production and distribution.

is not improved, the 38% share of the water supply may be further reduced. Satellite images and ocular inspection of the watershed reveal continuing degradation of ground cover due to various illegal ground cover-changing activities, including increasing agricultural activity in the area. The area's transformation into the CSCMP alone will change the land use from vegetated lands to urban centers.

With improved commercial and institutional activities, the water demand will be more than the capacity of the current water supply source. Commercial buildings require a substantial volume of water depending on the size. The Catbalogan Sky City Mega Project will house hotels, resorts, a health and wellness center, education and training hubs, and a multi-purpose complex, to name a few (Skyscraper City 2015). These facilities will require water in their operation. For example, every square meter of an educational facility may need around 1.62 cubic meters of water per day ($m^3.d^{-1}$). Every type of facility will have different demands; a healthcare facility will need 5.17 $m^3.d^{-1}$, lodging/hotels about 4.64 $m^3.d^{-1}$, a mall will need 1.40 $m^3.d^{-1}$, and public assembly centers will require 2.86 $m^3.d^{-1}$ (2017).

Plans often are not realized as it is expected due to many factors. Complicated processes govern the development phase, and events like COVID-19 or a disastrous typhoon like Yolanda change government priorities, often halting planned developments. In some cities abroad, they found that land use conformity to master plans is less than 50% and significantly varies depending on the location within the city (Huang & Cantada 2019). Conformance to planned land use is more challenging in the Philippines due to conflicting policies, influential land owners, overlapping mandates between government authorities, and political interference (Lech & Leppert 2018). In Samar, even the formulation of CLUPs alone is a severe challenge, many do not have, and others have inactive plans (Salazar-Quitalig & Orale, 2016). This situation is true in the case of Catbalogan City; based on its old (inactive) land use plan, a small portion of the plans became a reality. Considering a more complicated case for the Philippines and the observations made to CLUP implementation in Catbalogan, a conservative 5%, and 25% realization was considered for rainfall-runoff simulation purposes.

A 5% development scenario will result in a water demand of about 71,572 cubic meters per month for the CSCMP alone and another 552,030 cubic meters for the old city, or a total of about 623,602 cubic meters per month. The published production capacity of the CWD is pegged at 387,474 cubic meters per month (CWD 2021). Incorporating losses from extraction, treatment, to distribution will make the current capacity of CWD not even enough for the current demand of about 398,167 cubic meters per month. In higher development scenarios (e.g 25%), the gap between available water resources and the demand will increase by 980,001 or about 253%. The development planners must therefore look for additional water sources to supply the water demand of the near future like what Singapore did (WWF 2012, Hsien et al. 2019, PUB nd.b), securing water elsewhere while developing systems to make self-sufficient in the very near future (IWA nd.).

Table 3: Catbalogan city water requirements.

Land use with buildings	Monthly Water Demand (m^3)					
	2022		2040 (05%)		2040 (25%)	
	Old City*	Sky City	Old City	Sky City	Old City	Sky City
Residential**	355,996	0	459,848	22,843	563,699	114,216
Commercial	24,167	0	53,839	43,696	269,196	218,478
Industrial	6,041	0	13,460	1,492	67,302	7,460
Institutional	10,462	0	23,308	1,179	116,540	5,896
Others	1,500	0	1,575	2,362	1,875	2,812
Sub Total	398,167	0	552,030	71,572	1,015,613	348,862
Total	398,167		623,603		1,367,475	

*based on CWD records
**estimated demand for the entire population

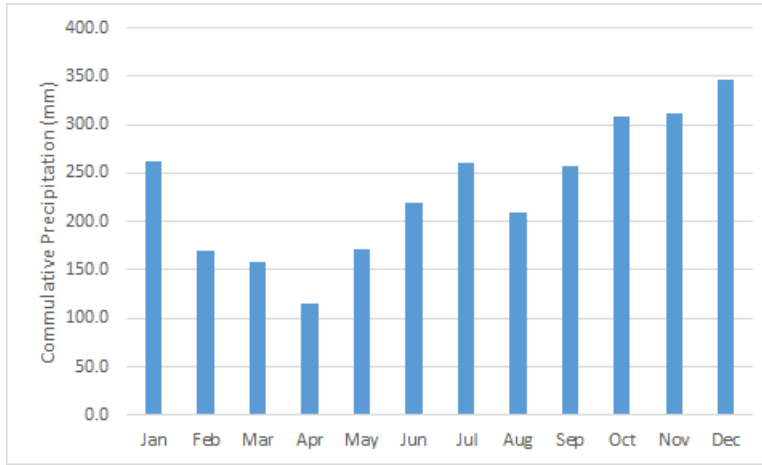

Fig. 5: Average monthly precipitation per month (1948-2021; PAGASA).

Runoff Water Production

Catbalogan City has an average precipitation rate of 180 mm per month. The highest recorded monthly precipitation is about 1,140 mm, and the largest single-day rain was more than 350 mm (Orale 2015). With the degraded ground cover in the area, most of this rainwater will run off the surface and exit into the Antiao River. It was predicted that the construction and development of the CSCMP would result in a larger volume of runoff water which may swell the river and flood the old city (Orale & Novilla 2016). Collecting the runoff water from the CSCMP and storing it in a reservoir will reduce this risk.

The Local Government of Catbalogan allocated around 387,875 square meters as the catchment basin for the lagoon. In the absence of engineering plans for the said reservoir, it is assumed that the lagoon will have an average depth of one meter resulting in a capacity of 387,875 cubic meters of water on any given day if enough precipitation is available. Fig. 5 shows 73-year average monthly precipitation characteristics in Catbalogan from the database of the Philippine Atmospheric, Geophysical, and Astronomical Services Administration (PAGASA) Catbalogan City Office. The rain will be the primary source of water for the water reservoir.

Fig. 5 shows that April and December receive the least and the most rain, respectively. Low-rain months include February, March, and May. On the other hand, October and November are considered high-rain months. There are also occasions when one month rain is poured in few hours which often chokes waterways resulting into floods.

Fig. 6 shows the amount of runoff water the lagoon receives during December and April, the driest and wettest months in Catbalogan. These values were derived from the HEC-HMS modeling using the parameters given in Table 1. For the April and December 2021 rain, the total volume of water harvested during low-rain months like April is about

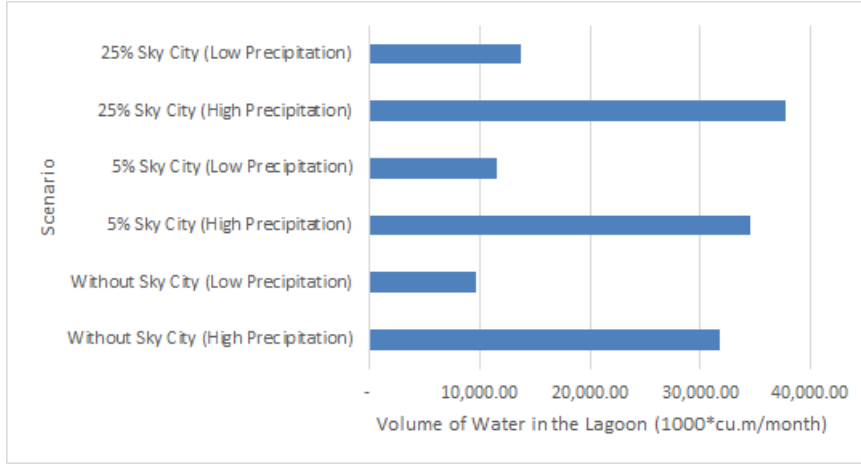

Fig. 6: Volume of harvested runoff water at the lagoon.

9,715,000 cubic meters in current condition, and it will reach 13,698,300 by 2040 in a 25% development scenario. The volume of runoff water collected is higher by 175% to 228% during peak rain months like December. This means that the lagoon can supply water demand not only for the CSCMP but for the entire City of Catbalogan. There will be a surplus of about 12,330,825 cubic meters per month, even in low-rain months.

Therefore, the lagoon's designed capacity must be greater than the city's water demand for any future scenario. As given in Table 3, in a 25% development scenario by 2040, the city needs about 1.4 million cubic meters of water per month or about 46,000 cubic meters per day. The lagoon can provide much-needed water every day. While abundant water is available for Catbalogan City, treating it is another challenge.

Runoff Collection Treatment and Distribution System

The CSCMP has no plans for how the runoff water will be collected, treated, and distributed. It is assumed in this paper that construction methods for roads, drainage systems, building designs and execution, and wastewater management will be similar to what exists in the old city. There will be canals that will receive runoff water from roads, lawns, paved and unpaved grounds, stormwater from buildings, and even wastewater from the kitchen, toilet drains, and excess water from septic tanks of buildings. According to the Environmental Protection Agency of the USA (EPA 2003), urban runoff is exposed to a variety of pollutants such as sediments, wastes from motor vehicles like oil, excess fuels, grease, and other chemical compounds, most of which are toxic. Agricultural activities also contribute to wastewater from pesticides and excess nutrients from fertilizers. Runoff waters may contain viruses and bacteria from the effluents of toilets. It may also contain heavy metals from various sources. These canals will drain the wastewater to the catchment basin or the lagoon. The water in the reservoir will be treated separately from other CWD water sources. Since the water collected is heavily contaminated, the treatment required will also be more complex, like the reclamation of blackwater. The treatment of similar wastewater in Singapore requires filtration, reverse osmosis, and disinfection (PUB nd.e, Thompson & Powell 2003) instead of the usual surface water treatment which includes coagulation, sedimentation, filtration, disinfection, biological activated carbon, and mineralization (PUB nd. d). Currently, the CWD only uses coagulation, filtration, and disinfection to treat surface water from Kulador and only disinfection for groundwater and spring water sources.

A strategic approach to minimizing the contamination of rainwater to other runoff water (i.e from lawns, roads, etc) must be explored. Rainwater harvesting at the building level will reduce exposure of this excess water to contamination. This harvesting will reduce the energy required to pump water from the treatment facility to the users. Less contaminated water means a reduced need for chemicals to make the water potable or safe for domestic and other uses.

Catbalogan Sky City Water Supply Carbon Footprint

Current water supply production and distribution. The CWD uses power extensively to pump water from various sources and to its clients. Most of the carbon footprint comes from water production and distribution. Depending on the water supply condition, the CWD spends up to 334,267 kWh per month, especially during dry seasons. SAMELCO II, the energy distributor, has varied sources; most are from the nearby geothermal power, and the rest are from fossil-

based power plants. Considering the energy mixes of the power distributor, the CO_2e equivalent for the collection and distribution is shown in Table 4. The CO_2e equivalent for water treatment is also shown in Table 4.

The carbon footprint for the current water supply production, treatment, and distribution reaches 2,222 $kgCO_2.e.day^{-1}$, 627 $kgCO_2.e.day$ $e.day^{-1}$, and 627 $kgCO_2.e.day^{-1}$, respectively, or a total of about 3,194 kg CO_2-e/day. The collection of water from the source is a heavy contributor to the carbon footprint profile sharing about 69% compared to 11% for treatment and 20 for distribution. This is because water extraction from CWD sources relies heavily on pumps. Using renewable resources in powering pumps that extract water can significantly reduce the carbon footprint.

The current treatment process used by CWD only covers simple steps; sedimentation, slow and fast sand, and chlorination. The carbon footprint estimates come primarily from the chemicals and minimal energy used in making the water potable. CWD uses a chloramine (e.g. monochloramine) compound totaling about 326 kg per month. With CWD water extracted mainly from groundwater sources, the treatment is minimal. The carbon footprint for groundwater and surface water sources is estimated at only 0.02 and 0.08 kg of CO_2-e per cubic meter of water produced (Biswas & Yek 2016). As shown in Fig. 3, the water supply comes from 10% surface (Kulador) and 90% different groundwater/spring sources. This means that water treatment for 398,162 cubic meters per month water is about 10,352 kilograms of CO_2-e per month.

Runoff water-based water supply production and distribution carbon footprint. The CSCMP proposes a runoff water harvesting feature. This feature is both a flood mitigation measure for the old city and, at the same time, provide the much-needed water not only for the CSCMP but for the old city as well. As shown in Table 3, the current theoretical available volume of water supply according to CWD estimates cannot accommodate even the current water demand. No engineering details are yet available on how runoff water will be collected and drained to the lagoon. Runoff water in the City of Catbalogan mixes with wastewater dumped into existing drainage systems. This will make the runoff water collected contaminated and

Table 4: Carbon footprint of water supply production and distribution.

Processes	CO_2-e [$kg.month^{-1}$]				
	2022	2040**			
	Old City*	Old City (5%)	Sky City (5%)	Old City (25%)	Sky City (25%)
Treatment	10,352	72,554	27,054	248,923	131,870
Collection	66,676	74,449	0.00	96,486	0.00
Distribution	18,806	26,578	15,366	48,616	74,897
Total	95,835	173,582	42,420	394,025	206,767

*estimate if 100% of the population is served
**conservative estimates assuming 5% or 25% of planned development is attained

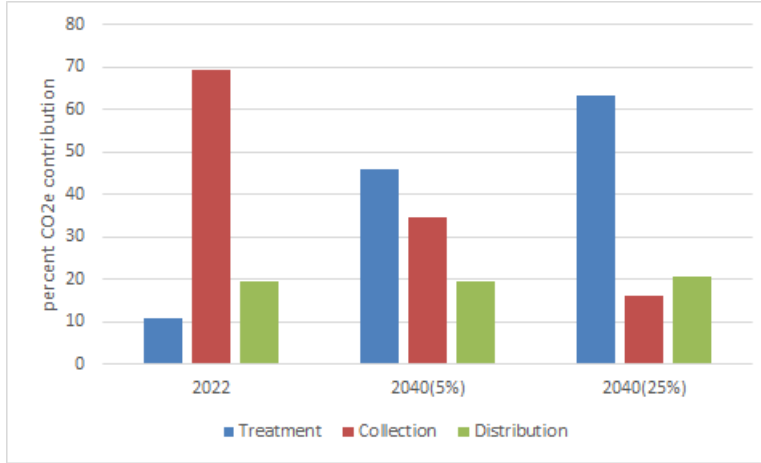

Fig. 7. Per cent CO_2e contribution in the production, treatment, and distribution of water supply.

require specialized water treatment far beyond the current processes.

The carbon footprint increases by about 125% and 526% for a 5% and 25% development scenario by 2040 compared to the 2022 condition. As shown in Fig. 7, the treatment required will increase by about 862% and 3,578% for the 5% and 25% development scenarios by 2040. The decrease in the carbon footprint contribution from the water collection processes cannot compensate for the increase from water treatment processes. The carbon footprint of the proposed water system for the CSCMP is 123% and 557% for the same scenario in 2040, respectively.

Overall, the CSCMP will result in a significantly higher carbon footprint because of increased water demand for Catbalogan City. The lagoon at the CSCMP will provide much-needed water for the new and the old city. The effort to reduce the contamination of runoff water and use renewable energy to extract, treat and distribute water must be continuously explored. The introduction of better rainwater harvesting technology may be explored to minimize at least the treatment requirements. Rainwater harvesting at a lot owner's building or lawn level may be considered for investigation.

CONCLUSIONS AND RECOMMENDATIONS

Catbalogan City lacks both water and area for expansion. In light of the global impact of CC, it proposed to inhabit higher elevated land away from the threats of lowland flooding for unusually heavy rains and sea level rise in the future. The CSCMP was packaged as a CC adaptation; however, if not properly designed, it can contribute more to CC than help address it. While the local government unit of Catbalogan implements the Sky City, the old city is also poised to receive additional development activities, further widening the gap between the available water and the water demand. It is estimated that in a 5% development success scenario, about 623,603 cubic meters of water per month is needed, or about 60% deficient. The lagoon at the CSCMP can supply the needed water for the city even at a 25% development scenario by 2040. If the rainwater harvesting is not properly engineered, the treatment alone is estimated to produce more than 8 to 36 folds of CO_2-e. Therefore, the local government unit of Catbalogan must legislate and implement green-engineering building standards to ensure any development like the CSCMP will be low-impact. A well-engineered runoff water collection and distribution system can be formulated and implemented to minimize carbon footprint and make CSCMP a successful climate adaptation strategy for mountainous city landscapes.

REFERENCES

ADB. 2013. Philippines: Water Supply and Sanitation Sector Assessment Strategy, and Road Map. Asian Development Bank, Mandaluyong City, Philippines

Al-Kodmany, K. 2018. The Vertical City: A Sustainable Development Model. WIT Press, England.

Amascual, R., Panganoron, H., Gamba, A., Irene, E. and Amparado, M.L. 2020. Water Quality Assessment of Antiao River in Samar, Philippines. Samar State University, Catbalogan City, Samar.

Biswas, W. and Yek, P. 2016. Improving the carbon footprint of water treatment with renewable energy: A Western Australian case study. Renew. Wind, Water Solar, 3(14): 45.

Bolay, J. and Kern, A. 2019. Intermediate cities. Blackwell, London.

Catbalogan LGU. 2019. Catbalogan Sky City Mega Project Gets the Nod from Tourism. (Catbalogan LGU) Retrieved March 5, 2022, from http://www.catbalogan.gov.ph/catbalogan-sky-city-mega-project-gets-the-nod-from-tourism-investors/

Catbalogan LGU. nd. Local Heritage. Retrieved September 12, 2020, from The Official Website of the City Government of Catbalogan: http://www.catbalogan.gov.ph/for-visitors/local-heritage/

CDIA Asia. 2016. From CIIPP, Catbalogan's Sky City Project Gets Funding from the Private Sector. Retrieved March 4, 2022, from https://cdia.asia/2016/09/13/from-ciipp-catbalogans-sky-city-project-gets-funding-from-the-private-sector/

Claudio, L. 2015. Wastewater Management in the Philippines. Retrieved March 3, 2022, from https://www.wipo.int/edocs/mdocs/mdocs/en/wipo_ip_mnl_15/wipo_ip_mnl_15_t4.pdf

CWD. 2015. 2015 Monthly Data Sheet. Retrieved 2022 1, 2015, from https://catbaloganwd.gov.ph/files/MDS%202015.pdf

CWD. 2018. About Us. Retrieved March 1, 2022, from https://www.catbaloganwd.gov.ph/about%20us.html

CWD. 2020. Water Production Graph Per Source. Retrieved October 15, 2020, from Catbalogan Water District: https://www.catbaloganwd.gov.ph/

CWD. 2021. Catbalogan Water District. Retrieved March 1, 2022, from https://catbaloganwd.gov.ph/files/MDS%20Jan-Dec%202020.pdf

CWD. 2022. Transparency Seal - Catbalogan Water District. Retrieved 1 2022, 2022, from https://catbaloganwd.gov.ph/transparency%20seal.html

CWD. nd. Kulador Treatment Plant. Retrieved March 3, 2022, from http://catbaloganwd.gov.ph/Kulador.html

Dodman, D. 2009. Urban Density and Climate Change. United Nations Population Fund (UNFPA), NY.

DTI. nd. Rankings of Cities and Municipalities. Retrieved October 5, 2020, from Cities & Municipalities Competitiveness Index: https://cmci.dti.gov.ph/pages/rankings/

EIA. 2017. 2012 Commercial Buildings Energy Consumption Survey: Water Consumption in Large Buildings Summary. Retrieved October 8, 2020, from Commercial Buildings Energy Consumption Survey (CBECS): https://www.eia.gov/consumption/commercial/reports/2012/water/

EIA. nd. Geothermal Explained - Geothermal Energy and the Environment. Retrieved March 2, 2022, from https://www.eia.gov/energyexplained/geothermal/geothermal-energy-and-the-environment.php

EPA. 2003. Protecting Water Quality from Urban Runoff. Retrieved February 14, 2022, from https://www3.epa.gov/npdes/pubs/nps_urban-facts_final.pdf

EPA. 2022. Convert emissions or energy data into concrete terms you can understand - such as the annual CO_2 emissions of cars, households, and power plants. Retrieved July 10, 2022, from https://www.epa.gov/energy/greenhouse-gas-equivalencies-calculator

Gomba, F.E., Orale, R.L. and Uy, R.S. 2007a. Stochastic Process Applied to Catbalogan Supply Resource Planning. 10th National Convention on Statistics (NCS), Catbalogan City.

Gomba, F., Orale, R. and Uy, R. 2007b. Assessment of Masacpasac Water Supply: A Technical Study. Catbalogan Water District, Catbalogan City.

Green Facts. 2008. Water Resources. Retrieved March 2, 2022, from https://www.greenfacts.org/en/water-resources/index.htm

Hsien, C., Low, J.S., Fuchen, S.C. and Han, T.W. 2019. Life cycle assessment of water supply in Singapore: A water-scarce urban city with multiple water sources. Resour. Conserv. Recycl., 6: 151.

Huang, C. and Cantada, I. 2019. Challenges to Implementing Urban Master Plans - What Are We Missing? Retrieved July 24, 2022, from World Bank Blogs: https://blogs.worldbank.org/sustainablecities/challenges-implementing-urban-master-plans-what-are-we-missing

Hurtado, A. 2019. Catbalogan Sky City Mega Project Gets the Nod from Tourism Investors. Retrieved October 7, 2020, from The Official Website of the City Government of Catbalogan: http://www.catbalogan.gov.ph/catbalogan-sky-city-mega-project-gets-the-nod-from-tourism-investors/

IWA. nd. City Water Stories: Singapore. Retrieved February 28, 2022, from https://iwa-network.org/wp-content/uploads/2016/12/IWA_City_Stories_Singapore.pdf

Lech, M. and Leppert, G. 2018. Current Issues of the Philippine Land Use Planning and Management System. German Institute for Development Evaluation, Bonn, Germany.

Liu, Y., Wang, M., Webber, M., Zhou, C. and Zhang, W. 2020. Alternative water supply solutions: China's South-to-North-water-diversion in Jinan. J. Environ. Manag., 16: 276.

Meniano, S. 2018. Catbalogan's Mega Project Attracts Big Companies. Retrieved October 10, 2020, from Philippine News Agency: https://www.pna.gov.ph/articles/1040995

Misra, A.K. 2014. Climate change and challenges of water and food security. Int. J. Sustain. Built Environ., 3(1): 153-165.

MWSS. 2017. MWSS Approves New Rates Effective January 1, 2018. Retrieved February 3, 2022, from https://www.manilawater.com/customer/agos/2017-12-15/mwss-approves-new-rates-effective-january-1--2018#:~:text=Once%20the%20new%20rates%20take,increase%20from%20P305%20to%20P306.

National Geographic. nd. Freshwater Crises. Retrieved March 1, 2022, from https://www.nationalgeographic.com/environment/article/freshwater-crisis

Orale, R. 2006a. Land Use Zoning for industrial use based on geohazard assessment. Eng. Pebble, 12:135-165.

Orale, R. 2006b. Landslide Suceptibility Assessment in Catbalogan, Samar: Proposed Hazard Control Program. International Civil Engineering Congress 2006 (ICEEC 2006) and the 7th National Civil Engineering Education Congress 2006 (7th NCEEC). Angeles City, Pampanga Philippines.

Orale, R. 2015. Flood risk assessment in post-Antiao river control project in Catbalogan City, Philippines. Country. Dev. Res. J., 3(2): 39-52.

Orale, R. and Fabillar, L.A. 2011. Coastal waste transport in Catbalogan City, Philippines, and nearby towns. Iran. J. Energy Environ., 1(2): 56.

Orale, R. and Novilla, R. 2016. Flood risk at various stages of Catbalogan Sky City project development. Country. Dev. Res. J., 4(1): 82-94.

Pehl, M., Arvesesn, A., Humpenoder, F., Popp, A., Hertwich, E. and Luderer, G. 2017. Understanding future emissions from low-carbon power systems by integration of life cycle assessment and integrated energy modeling. Nat. Energy, 2: 939-945.

PhilAtlas. nd.a. Catbalogan, Province of Samar. Retrieved February 5, 2022. from https://www.philatlas.com/visayas/r08/samar/catbalogan.html#sectionEconomy

PhilAtlas. nd.b. Catbalogan, Province of Samar. Retrieved September 18, 2020. from Philippine Atlas: https://www.philatlas.com/visayas/r08/samar/catbalogan.html

Pingale, S.M., Jat, M.K. and Khare, D. 2014. Integrated urban water management modeling under climate change scenarios. Resour. Conserv. Recycl., 83: 176-189.

Population Matters. 2018. Climate Change. Retrieved October 10, 2020, from Population Matters: https://populationmatters.org/the-facts/climate-change

PUB. nd.a. Four National Tap. Retrieved March 31, 2021, from https://www.pub.gov.sg/watersupply/fournationaltaps

PUB. nd.b. Singapore Water Story. Retrieved March 3, 2022, from https://www.pub.gov.sg/watersupply/singaporewaterstory

PUB. nd.c. Water Price. Retrieved January 31, 2022, from https://www.pub.gov.sg/watersupply/waterprice

PUB. nd.d. Water Treatment. Retrieved March 1, 2022, from https://www.pub.gov.sg/watersupply/watertreatment

PUBb. nd.e. Domestic & Non Domestic. Retrieved March 1, 2022, from https://www.pub.gov.sg/usedwater/treatment/usedwatertreatmentprocess

Rai, R.K. Singh, V.P. and Upadhyay, A. 2017. Planning and Evaluation of Irrigation Projects. Methods and Implementation. Elseiver, Netherlands

Richie, H. 2020. What are the Safest and Cleanest Sources of Energy? Retrieved February 20, 2022, from https://ourworldindata.org/safest-sources-of-energy

Salazar-Quitalig, R. and Orale, R.L. 2016. Comprehensive land use planning capacity of local government units in Samar Philippines. Country. Dev. Res. J., 4(1): 36-52

SAMELCO II. 2020. Generation Mix Rate. Retrieved March 1, 2022, from https://samelcodos.com/generation-mix-rate/

SAMELCO II. 2021. Generation Mix Rate 2021. Retrieved March 1, 2022, from https://samelcodos.com/generaiion-mix-rate-2021/

Scherer, L. and Pfister, S. 2016. Hydropower's biogenic carbon footprint. PLoS One, 11(9): 548.

Skyscraper City. 2015. Catbalogan Sky City. Retrieved September 12, 2020, from Skyscraper City: https://www.skyscrapercity.com/threads/catbalogan-catbalogan-sky-city-mix.1813878/

Steeneveld, G., Klompmaker, J.O., Groen, R.J. and Holtslag, A.A. 2018. An urban climate assessment and management tool for combined heat and air quality judgments at neighborhood scales. Resour. Conserv. Recycl., 132, 204-217.

Talat, N. 2021. Urban water-supply management: indirect issues of climate change leading to water scarcity scenarios in developing and underdeveloped nations. In Thokshorn, B., Qiu, P. and Iyer, P.K. (eds), Water Conservation in the Era of Global Climate Change. Elsevier, The Netherlands, pp. 47-71.

TAP. nd. Catbalogan Sky City Mega Project. Retrieved March 3, 2022, from https://tap-potential.org/projects/catbalogan-sky-city-mega-project/

Thompson, M. and Powell, D. 2003. Case Study-Kranji High-Grade Water Reclamation Plant, Singapore. Proceedings of IMSTEC 3.

Tosics, I. 2015. Growing Cities: How to Expand in a Sustainable and Integrated Way? Retrieved October 1, 2020, from URBACT: https://urbact.eu/growing-cities-how-expand-sustainable-and-integrated-way

UN Water. 2021a. Water Quality and Wastewater. Retrieved March 1, 2022, from https://www.unwater.org/water-facts/quality-and-wastewater/

UN Water. 2021b. Summary Progress Update 2021: SDG 6 - Water and Sanitation for All. UN Water, Geneva, Switzerland.

UNESCO. nd. The United Nations World Water Development Report. Retrieved March 1, 2022, from http://www.unesco.org/new/en/natural-sciences/environment/water/wwap/wwdr/

United Nations. 2018. 68% of the World Population is Projected to Live in Urban Areas By 2050, says UN. Retrieved October 1, 2020, from United Nations - Department of Economics and Social Affairs: https://www.un.org/development/desa/en/news/population/2018-revision-of-world-urbanization-prospects.html

USACE. nd. HEC-HMS - Hydrologic Engineering Center - US Army Corps of Engineers Retrieved January 11, 2022, from https://www.hec.usace.army.mil/software/hec-hms/

Wennersten, R. 2018. Chapter 6. Development of New Sustainable Urban Areas: Horizontal or Vertical Planning Systems for Resource Efficient Cities. In Y. Ergen, An Overview of Urban and Regional Planning (pp. 103-120). IntechOpen.

WWF. 2012. Singapore Water Management. Retrieved March 20, 2022, from https://wwf.panda.org/wwf_news/?204587/Singapore-water-management

Nature Environment and Pollution Technology
An International Quarterly Scientific Journal

p-ISSN: 0972-6268
(Print copies up to 2016)
e-ISSN: 2395-3454

Vol. 21 | No. 5 (Suppl) | pp. 2117-2127 | 2022

Original Research Paper

https://doi.org/10.46488/NEPT.2022.v21i05.008

Open Access Journal

Assessment of Corrosion Potential Based on Water Quality Index in the Distribution Network of Urban Patna, Bihar, India

Saurabh Kumar, Reena Singh† and N. S. Maurya
Department of Civil Engineering, National Institute of Technology, Patna 800005, Bihar, India
†Corresponding author: Reena Singh; reena@nitp.ac.in

Nat. Env. & Poll. Tech.
Website: www.neptjournal.com

Received: 02-06-2022
Revised: 12-07-2022
Accepted: 13-07-2022

Key Words:
Water quality index
Corrosiveness index
Water supply
Distribution network

ABSTRACT

Corrosion in the distribution network pipe can lead to pipe failure and water quality problems. This study assesses the corrosion or scaling potential based on the Water Quality Index (WQI) of drinking water in the distribution networks of Patna, Bihar, India. The water samples were collected from 18 points of the distribution network. In situ parameters like temperature, pH, electrical conductivity, and TDS were measured. Other parameters such as Alkalinity, Total hardness, Calcium, Magnesium, Chloride, Residual chlorine, Sulfate, Nitrate, and Dissolved oxygen were examined in the laboratory. Corrosiveness indicators, such as the Langelier saturation index (LSI), Ryznar stability index (RSI), Puckorius scaling index (PSI), Larson-Skold index (Ls), and Aggressive index (AI) are being used for water sample corrosion prediction. Experimental Corrosion rate (CR) is analyzed to show the actual prediction of corrosion. WQI was calculated to observe the effect of water quality on Corrosiveness indices and CR. A general conclusion was reached that LSI concludes 66.67% corrosive, 22.22% scaling, and 11.11% neutral, RSI concludes 88.88% corrosive, 5.56% scaling, and 5.56% neutral, PSI indicates 38.88% corrosive, 5.56% scaling, and 55.56% neutral, Ls indicates 94.44% scaling, and 5.56% corrosive, AI indicates 77.78% corrosive, and only 22.22% scaling. The average Experimental Corrosion rate is found at 1.91 mils per year. In this study, a weak correlation ($r = 0.35$) between Corrosion rate and WQI has been observed. A weak correlation is also observed between corrosion rate and corrosiveness indices ($r < 0.5$). It is concluded that the Corrosiveness Indices fail to represent the actual behavior of water.

INTRODUCTION

Corrosion in the pipeline of the distribution network can impact water quality, infrastructure performance, structural integrity, and scaling. Many water quality problems are caused by internal corrosion of distribution network piping and home plumbing, including health concerns, discoloration, and smell (AWWA 2011). A corroded cast iron pipe may produce rusted water or reddish water due to ferric iron (FeIII) (Khiari 2002). Corrosion of cast iron may also produce musty tastes and odors (Kirmeyer & Passarelli 2000). Pipe and valve failures are often caused by corrosion of distribution network piping. A change in the quality of the distribution water can cause red water, an increase in lead or copper concentration in tap water, or other issues (Mirzabeygi et al. 2016). The Water Quality Index of any particular field or particular source may be ascertained by applying water quality parameters which are chemical, physical, and biological parameters (Singh & Kumar 2022). The value of these parameters is risky for human health if the quantity of the parameter exceeds the permissible limits (Kumar & Singh 2021).

Many indices have been developed, but none have been able to quantify and predict the corrosive or scaling effects of water. They can only provide a rough indication (Rossum & Merrill 1983). These are the two common methods of calculating the stability of water: the Langelier saturation index (LSI) and the Ryznar stability index (RSI). In terms of the calcium carbonates scale, LSI and RSI are designed as predictive tools. Scales such as those containing calcium phosphate, calcium sulfate, silica, and magnesium silicate cannot be estimated using these techniques (Alsaqqar et al. 2014). Other tools are used as the Puckorius scaling index (PSI), Aggressive index (AI), and Larson-Skold index (Ls).

These indices are derived using numerical equations. In the case of drinking water, numerical equations have not yet been developed to accurately calculate corrosion. In distribution systems, there are so many factors that contribute to corrosion that these indices are limited (Slavíčková et al. 2013). Many factors affect a given Corrosion environment, including dissolved oxygen, pH, temperature, alkalinity, hardness, suspended solids, organic matter, ammonia, specific anions (phosphoric acid, nitrite, sulfate, and

chloride), and biological slimes (EPA 1984). The indices used as LSI, RSI, PSI, Ls, and AI are however dependent upon the seven factors such as pH, temperature, total dissolved solids, calcium hardness, alkalinity, chloride, and sulfate (Kumar et al. 2022). It is, therefore, necessary to monitor corrosion with a direct method such as the corrosion weight loss method.

The objective of this study is to assess the corrosion and scaling potential of the Patna water supply distribution network based on the water quality index (WQI). Along with, demonstrating how changes in water quality can impact corrosion potential. The focus of this study is also on analyzing corrosion potential and comparing it to experimental analysis of corrosion rate.

MATERIALS AND METHODS

Study Area

The study area is Patna urban distribution network, located at N and E. Fig. 1 shows the study area and the sampling points of the water supply distribution network. A total of 18 sampling points were selected. The location of sampling points was S1- Sumitra Nagar, S2- Gurudwara, S3- Old City Court, S4- Gandhi Maidan, S5-Near Sadaqat Ashram, S6- Digha, S7- Danapur, S8- Near Paras Hospital, S9- Rajbanshi Nagar, S10- Patna Station, S11- Rajendra Nagar, S12- Kadamkuna, S13- Chitkohra. S14- Phulwari Sharif, S15- AIIMS Patna, S16- Mithapur Farm Area, S17- Kumhrar, S18- Begampur.

Sample Collection

The sampling procedure was followed using the methods described in the Standard method (APHA 1989). The water samples were collected from 18 different points of the distribution network from October to November 2021. Polyethylene bottles with a capacity of 2 liters were used to collect the samples. The bottles were sealed tightly so that no leakage would occur and stored at 4°C in a dark, dry place within 3 h of collection.

Determination of Physicochemical Parameters

All experiment was followed using the method described in the standard method (APHA 1989). A pH probe tester pen was used to measure the pH on a site. (Eutech instrument cyberxan CON11) was used to measure temperature, conductivity, and TDS at a site. A titration method was used to examine total hardness, calcium hardness, magnesium hardness, and alkalinity. The concentration of chloride was determined by the argentometric method. Nitrate and Sulfate were analyzed using UV Spectrophotometers (220 & 275 nm for Nitrate and 420 nm for Sulfate). Winklers method (iodometric method) was used to measure Dissolved Oxygen using an oxidation-reduction titration method. A method of iodometric titration was used to measure residual chlorine.

Determination of Corrosion Potential

The corrosion potential of water samples was determined using the indicators LSI, RSI, PSI, Ls, and AI. These indices are calculated using seven physicochemical parameters

Table 1: Mathematical Equations and classification of Corrosiveness indices.

Index	Equation	Index value	Water condition
Langelier Saturation Index (LSI)	LSI = pH - pHs pHs = (9.3 +A + B) - (C + D) A = (Log (TDS)-1)/10 B = -13.2(Log (°C + 273)) + 34.55 C = Log (Ca^{++} + $CaCO_3$) D = Log (Alkalinity as $CaCO_3$)	LSI < 0 LSI = 0 LSI > 0	Corrosion occurs Neutral Scaling occurs
Ryznar Stability Index (RSI)	RSI= 2pHs -pH	RSI < 5.5 5.5 < RSI < 6.2 6.2 □ RSI □ 6.8 6.8 < RSI < 8.5 RSI □ 8.5	High scale forming Low scale-forming Neutral Low corrosive High corrosive
Puckorius Scaling Index (PSI)	PSI = 2pHs - pHeq pHeq = 1.465log (Alkalinity) + 4.54	PSI > 7 PSI < 6	Corrosion occurs Scaling occurs
Larson-Skold Index (Ls)	Ls = $(C_{Cl^-} + C_{SO_4^-})/(C_{HCO_3^-} + C_{CO_3^-})$ C = Concentration in $mg.L^{-1}$	Ls > 1.2 0.8 □ Ls □ 1.2 Ls < 0.8	Greater corrosion rate High corrosion occurs Scaling occurs
Aggressive Index (AI)	AI = pH + log ((Ca^{++}) (Alkalinity))	AI < 10 10 □ AI □ 12 AI > 12	Corrosion occurs Moderately corrosive Scaling occurs

pH = Actual, pHs = Saturated pH, pHeq = Equivalent pH

including pH, Temperature, TDS, Alkalinity, Calcium hardness, Chloride, and Sulfate. Corrosiveness indices are presented in Table 1 (Acharya et al. 2018, Alimoradi et al. 2018, García-Ávila et al. 2018).

Determination of Corrosion Rate

The method described in ASTM G1 was used for the determination of the corrosion rate (ASTM G1-90 1999). Galvanized iron (GI) specimens were used as test coupons. The size of the test coupon was 25 mm 17.9 mm 1.5 mm. The test coupon had been precleaned using the corrosion cleaning reagent. It was a mixture of Hydrochloric acid (500 mL) and Hexamethylene tetramine (3.5 g) and made to 1000 mL in distilled water. Further, the test coupon was washed followed by distilled water, acetone, and distilled water. The initial weight of the dried test coupon was measured with an accuracy of 0.0001 g. Then the test coupon was immersed in the 300 mL test sample of water for 30 days. After the completion of the period test coupons were taken from the test water sample. Cleaning procedures were repeated as initial then final weighing was taken. Eq. (1) of corrosion rate in mils per year (MPY) is given as follows (EPA 1984):

$$\textbf{Corrosion rate (MPY)} = \frac{\mathbf{K\,W}}{\mathbf{DAT}} \quad ...(1)$$

Where

W = Weight loss (mg)

D = Density of specimen ($g.cm^{-3}$)

A = Surface Area ($inch^2$)

T = Time period (hours)

K = Constant (534)

Determination of Water Quality Index (WQI) (Brown et al. 1970)

The method described by (Brown et al. 1970) was used for the determination of the water quality index. A total of 10 parameters were used for the calculation of WQI including pH, TDS, Alkalinity, TH, Calcium, Magnesium, Sulfate, Chloride, Nitrate, and DO. Determination of WQI was a three steps process.

In the first step Water Quality Rating (Qi) was determined using Eq. (2) given below:

$$\mathbf{Qi} = \frac{[\mathbf{Xa} - \mathbf{Xi}]}{[\mathbf{Xs} - \mathbf{Xi}]} \times \mathbf{100} \quad ...(2)$$

Where,

Qi = Water quality rating of the parameter

Xa = Calculated value of the water quality parameter

Xi = Ideal value of a parameter

Xs = Standard permissible value for the water quality parameter

In the second step, Relative Unit Weight was determined using Eq. (3).

$$\mathbf{Wi} = \frac{\boldsymbol{K}}{\boldsymbol{Xs}} \quad ...(3)$$

Where,

Wi = Unit weight for the parameter

Xs = Standard permissible value of the parameters

K = Proportionality constant

The proportionality constant (K) was determined using Eq. (4).

$$\boldsymbol{K} = \frac{\mathbf{1}}{\boldsymbol{\Sigma Xs}} \quad ...(4)$$

Where,

Xs = Standard permissible value of the parameters.

In the third step, Water Quality Index was determined using Eq. (5).

$$\mathbf{WQI} = \frac{\sum \mathbf{WiQi}}{\sum \mathbf{Wi}} \quad ...(5)$$

Where,

Wi = Unit weight for the parameter

Qi = Water quality rating of the parameter

Statistical and Graphical Analysis

Microsoft Excel office 2019 is used for statistical analysis. QGIS 3.14 is used to create a map of the study area and sample locations. Statistical correlation of corrosion rate with indices is calculated using the IBM SPSS Statistics version 28.

RESULTS AND DISCUSSION

The Technique Used for the Selection of the Study Area

As there is no map available of the distribution network (Patna), the main roads of Patna were assumed to be the layout of the distribution network. The samples were collected at a distance of 4 to 6 km beside the main road (Fig. 1). The Physicochemical analysis is shown in Table 2.

Physicochemical Parameters Analysis

Physicochemical results were compared to drinking water standards as provided by the (BIS 2012) mentioned in Table 3. Water temperature was found in the range of

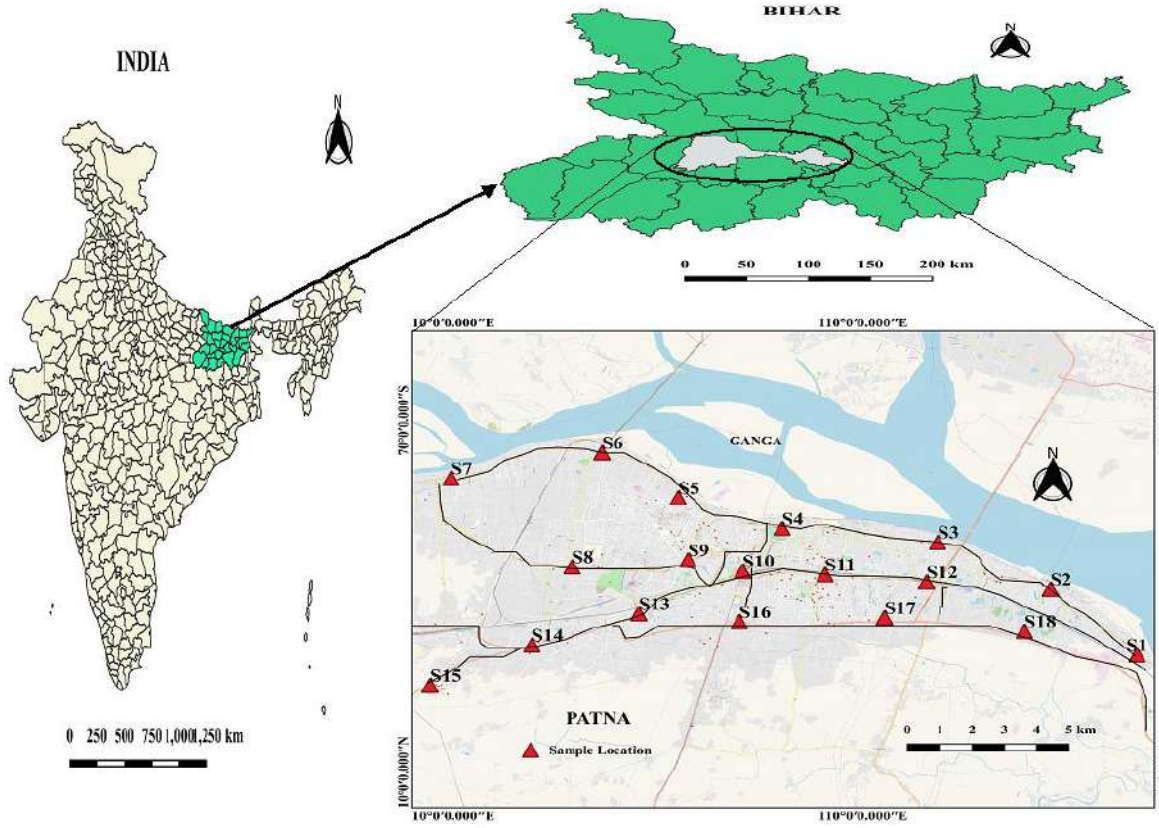

Fig. 1: Study area and sampling points.

Table 2: Physicochemical analysis of the samples.

Sample No.	TDS mg.L^{-1}	Temp. °C	Cond. µS/cm	pH	Alkalinity mg.L^{-1}	TH mg.L^{-1}	Ca^{2+} mg.L^{-1}	Mg^{2+} mg.L^{-1}	Cl^{-} mg.L^{-1}	SO_4^{2-} mg.L^{-1}	NO_3^{-} mg.L^{-1}	DO mg.L^{-1}
S1	733	23.3	1033	7.48	176	256	152	104	36	37	0	4
S2	765	23.4	1078	7.48	184	280	192	88	44	76.30	0	3.4
S3	2180	23.6	3080	7.15	492	664	560	104	140	385	13	3.4
S4	578	22.8	815	7.19	324	296	180	116	44	96.45	0.3	4.8
S5	619	25.4	874	7.38	328	80	40	40	40	10.70	0	4
S6	663	25.6	948	7.59	376	56	30	26	24	7.80	0.8	4
S7	1240	25.2	1736	7.32	568	80	50	30	120	84.80	11	4
S8	646	25.3	909	7.67	328	48	40	8	40	8.40	0.2	3
S9	708	25.2	995	7.38	304	64	40	24	152	12.24	0.5	2.8
S10	565	24.6	796	6.95	200	240	144	96	20	12.50	0	5.2
S11	415	24.4	586	7.45	300	300	200	100	60	41.50	1.8	5.2
S12	540	24.3	767	7.30	280	300	240	60	130	57.50	0.2	4.6
S13	727	24.2	1032	6.81	240	336	216	120	44	33	0	3
S14	696	24.2	982	6.98	200	256	160	96	40	19.50	0.7	5.4
S15	495	24.6	697	7.02	160	248	160	88	20	16.50	0	5.4
S16	643	22.5	910	7.05	320	328	176	152	28	34.57	0.1	5.2
S17	611	23.3	890	6.98	340	336	196	140	60	117.61	0.7	4.2
S18	592	23.6	830	7.47	360	260	196	64	74	17.24	0.5	4

TDS = Total dissolved solid, Temp.=Temperature, Cond.=Conductivity, TH = Tota hardness, DO = Dissolved oxygen

22.5 to 25.6°C. The range is not defined by WHO or BIS, however, the temperature of the water has an impact on the chemical and biological quality. As temperatures increase, corrosion reactions also increase. Therefore, hot water is more corrosive than cold water (EPA 1984). Each of the water samples showed a pH between 6.5 and 8.5 (BIS 2012). Corrosion rates increase with a lower pH value. pH values above 7.0 enhance scaling and protect the pipe (EPA 1984). Only S3 (Old City Court) and S7 (Danapur) exceeded the permissible limit (WHO 2006) for electrical conductivity. The limit of Electrical Conductivity (EC) is not defined by the (BIS 2012). The total dissolved solids in 16 water samples exceeded the permissible limit set by BIS (500 $mg.L^{-1}$ as $CaCO_3$). Water samples S11-Rajendra Nagar (415 $mg.L^{-1}$) and S15-AIIMS Patna (495 $mg.L^{-1}$) had TDS within the range. Electrical conductivity increases as TDS increases. The electrochemical circuit is completed by water when the EC increases. As a result, it generates a corrosive current (EPA 1984). Alkalinity concentrations in 15 water samples exceeded the (BIS 2012) permissible limit (200 mg/L as $CaCO_3$). The highest alkalinity is 492 $mg.L^{-1}$ as $CaCO_3$ in water sample number S3 (Old city court). Alkalinity produces $CaCO_3$ coatings on pipe surfaces. Hardness levels in 13 water samples exceeded the permissible limit (200 $mg.L^{-1}$ $CaCO_3$) specified by (BIS 2012). Hardness levels in samples S5, S6, S7, S8, and S9 fell within acceptable ranges. Sample number S3 (Old city court) had the highest hardness value of 664 $mg.L^{-1}$. The hardness of water is classified into soft water (<75 $mg.L^{-1}$ as $CaCO_3$), slightly hard water (75-150 $mg.L^{-1}$ as $CaCO_3$), moderately hard water (150-300 $mg.L^{-1}$ as $CaCO_3$), and very hard water (>300 $mg.L^{-1}$) (Tyagi & Sarma 2020). Hard water is generally less corrosive than soft water (EPA 1984). Hardness is classified into carbonate hardness (Due to $CO_3^{--}$and HCO_3^-) and non-carbonate hardness (Due to Cl^-, NO_3^-, SO_4^{2-} etc.). Carbonate hardness was found in all water samples. Non-carbonate hardness was found in 9 water samples. Carbonate hardness is called temporary hardness. Non-carbonate hardness is called permanent hardness. Softening is done to remove the hardness from water both temporary and permanent hardness. The Lime soda process and Zeolite process have used the removal of the permanent hardness (Tchobanoglous et al. 2003). The range of carbonate hardness was found 48-492 $mg.L^{-1}$ and non-carbonate hardness was 0-172 $mg.L^{-1}$. It was found that 16.67% of water samples have fallen under soft water and 11.11% of water samples lie in slightly hard water and 50% of water samples lie in moderately hard water and 22.22% of water samples fell in very hard water. Calcium hardness was found to be higher than 75 $mg.L^{-1}$ in 13 of the water samples (BIS 2012), while calcium hardness was within safe limits in water samples S5, S6, S7, S8, and S9. Calcium hardness was highest at 560 $mg.L^{-1}$ in water sample number S3 (Old city court). Calcium helps to reduce corrosion by forming a protective $CaCO_3$ layer (EPA 1984). In 14 water samples, magnesium hardness was greater than (30 $mg.L^{-1}$ as $CaCO_3$) permissible limit defined by (BIS 2012). Mg hardness in water samples S6, S7, S8, and S9 was within the range. The chloride concentration in all water samples was found within the permissible limit (200 $mg.L^{-1}$) prescribed by (BIS 2012). Similarly, the sulfate concentration in all 17 samples was within the limit described by (BIS 2012). Sample number S3 (Old city court) contained the largest amount of sulfate. Chloride is three times more affinity than sulfate (EPA 1984). Nitrate levels were found within a permissible range (45 $mg.L^{-1}$) prescribed by the (BIS 2012). Nitrate is an indicator of organic matter. The presence of organic matter, directly and indirectly, affects the corrosion rate. It may increase or decrease the corrosion rate (EPA 1984). Water sample numbers S10, S11, S14, S15, and S16 contain more than 5 $mg.L^{-1}$ of dissolved oxygen, and the other samples contain less than 5 $mg.L^{-1}$. A higher level of Dissolved Oxygen in the pipeline increases its corrosion rate. However, a lower level indicates microbial activity (EPA 1984). No residual chlorine was found in any samples, indicating a lack of disinfection.

Corrosion Potential of Water Samples

Langelier Saturation Index (LSI)

LSI and RSI are the main predictors of the corrosiveness of water (Pisigan & Singley 1985). LSI incorporates a useful indicator for corrosive water in its indices. LSI can be defined as the difference between the actual pH of the water and the calculated pH as follows: LSI = pH actual - pH calculated (Langelier 1936). LSI of water samples is given in Fig 2. (a) and corrosive behavior is mentioned in Table 4. This index measures the formation and scale-out of calcium carbonate from water. It is based on pH. LSI < 0 indicates the corrosive potential of water and LSI > 0 indicates the scaling potential of water. LSI of sample number S2 (Gurudwara) was almost zero (0.02). LSI of sample number S4 (Gandhi Maidan) was also nearly zero (-0.05). These water samples exhibit neither scaling nor corrosive tendency of water. LSI of sample number S3 (Old City Court) was found a maximum value of 0.54. It exhibits the scaling tendency of water due to the high value of TDS, Alkalinity, and Ca hardness. LSI of sample number S10 (Patna Station) was found a minimum value of -0.56. It exhibits a corrosive tendency of water due to slightly acidic (pH = 6.95) in nature. The mean value of LSI was -0.17 which represents the corrosive tendency of water. LSI represents 66.67% of water samples Corrosive, 22.22% Scaling, and 11.11% Neutral.

Table 3: Descriptive statistics of water quality parameters with limits specified by (BIS 2012).

Variable	Minimum	Maximum	Mean	Standard Deviation	BIS
Temperature (°C)	22.50	25.60	24.19	0.93	-
pH	6.81	7.67	7.26	0.25	6.5-8.5
Conductivity (μS/cm)	586.00	3080.00	1053.22	558.09	-
TDS (mg/L)	415.00	2180.00	745.33	396.07	500
Alkalinity (mg/L as a $CaCO_3$)	160.00	568.00	304.44	106.91	200
TH (mg/L as a $CaCO_3$)	48.00	664.00	246.00	147.75	200
Ca Hardness (mg/L as a $CaCO_3$)	30.00	560.00	165.11	120.65	75
Mg Hardness (mg/L as a $CaCO_3$)	8.00	152.00	80.89	41.90	30
Chloride (mg/L)	20.00	152.00	62.00	43.08	250
Sulfate (mg/L)	7.80	385.00	59.37	87.82	200
Nitrate (mg/L)	0.00	13.00	1.65	3.81	45
DO (mg/L)	2.80	5.40	4.20	0.87	>5

Ryznar Stability Index (RSI)

RSI is defined as the difference between the calculated pH and actual pH of water, as follows: 2 × calculated pH - actual pH (Ryznar 1944). RSI of water samples is given in Fig 2. (b) and corrosive behavior is mentioned in Table 4. This index measures the formation and scale-out of calcium carbonate from water. It is based on pH. RSI is a modification of the LSI which has higher accuracy than LSI. RSI exhibits neutral in the range of 6.2 to 6.8. The RSI of sample number S18 (Begampur) was nearly 6.8 (6.82). It exhibits neither scaling nor the corrosive tendency of water. RSI of sample number S3 (Old City Court) was a minimum value of 6.07. It was found in the range of 5.5 to 6.2 which represents low-scale forming. All water samples except S3 and S18 had RSI values between 6.8 and 8.5, indicating that they have low corrosive potential. The mean value of RSI was found at 7.59 representing the low corrosive tendency of water. The result of RSI indicates that 88.88% of water samples are low corrosive, 5.56% low scaling, and 5.56% neutral. In comparison to LSI, RSI indicates more corrosive, less scaling, and less neutral.

Puckorius Scaling Index (PSI)

The Puckorius Scaling Index indicates a greater accumulation of sediments created in equilibrium due to the buffer capacity (Taghipour et al. 2012). The mathematical equation of PSI is derived to replace the actual pH in the equation of LSI and RSI with the equilibrium pH. PSI of the water samples is shown in Fig 2. (c) and corrosive behavior is mentioned in Table 4. PSI < 6 represents the scaling tendency of water and PSI > 7 represents the corrosive tendency of water. PSI of sample number S3 (Old City Court) was a minimum value of 4.73. It exhibits the scaling tendency of water. PSI of sample numbers S2 and S14 were nearly 7 (7.06 & 7.05) representing neither scaling nor corrosive. Otherwise, the PSI of sample numbers S4, S7, S11, S12, S13, S16, S17 & S18 lie in the range of 6 to 7 representing the neutral behavior of water. PSI of water samples S1, S5, S6, S8, S9, S10 & S15 were found greater than 7. These are representing the corrosive behavior of water. The mean value of PSI was 6.71 which indicates neither scaling nor corrosive tendency of water. PSI indicates that 38.88% of water samples are Corrosive, 5.56% Scaling, and 55.56% Neutral.

Larson-Skold Index (Ls)

RSI is a corrosion rate indicator tool for steel and cast iron pipes that are modified by Larson-Skold (Larson & Skold 1958). The mathematical equation of Ls is derived by the use of parameters such as the concentration of chloride, sulfate, carbonate, and bicarbonate alkalinity. Ls < 0.8 represents the scaling tendency of water, 0.8 < Ls < 1.2 represents the corrosion tendency of water, and Ls > 1.2 represents a greater corrosion rate. Ls of water samples are shown in Fig 2. (d) and corrosive behavior is mentioned in Table 4. A low value of chloride and sulfate was detected in all water samples except S3, which indicates the scaling tendency of water. A corrosion tendency was found for sample number S3 (Old City Court). This is due to the high levels of chloride and sulfate in the sample. The mean value of Ls was found 0.38 which represents the scaling tendency of water. Ls value indicates 5.56% of water samples are highly corrosive and 94.44% was scaling tendency.

Aggressive Index (AI)

An aggressive index is used to detect corrosion in asbestos-cement pipes (Taghipour et al. 2012). It is a useful indicator for the selection of materials or treatment for corrosion control. The equation of AI is derived by the use of

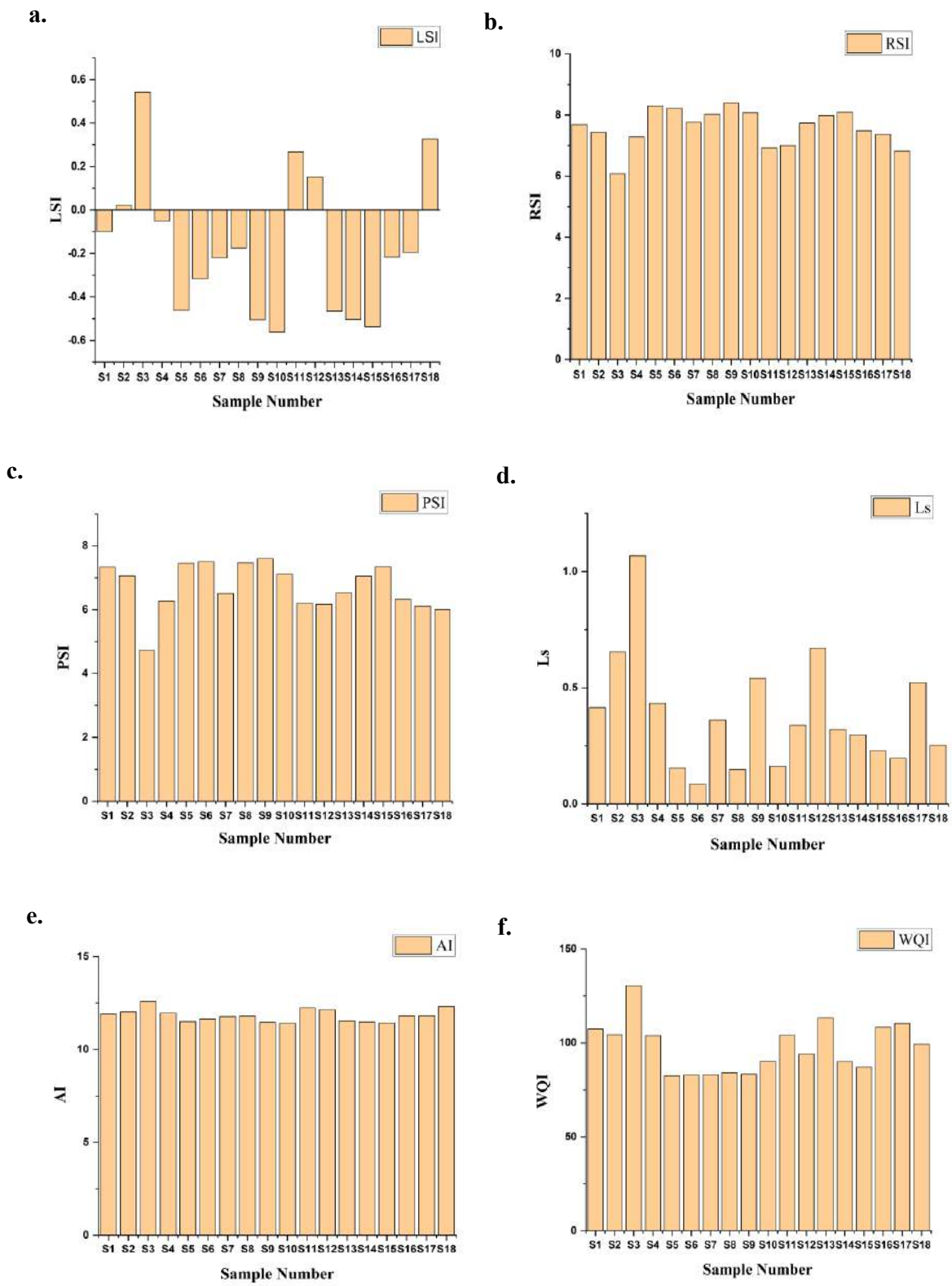

Fig 2: Represents Corrosiveness indices and WQI (a) LSI, (b) RSI, (c) PSI, (d) Ls, (e) AI, (f) WQI.

Table 4: Corrosive behavior and quality status of water samples.

S. No.	LSI	RSI	PSI	Ls	AI	WQI
S1	Corrosive	Low corrosive	Corrosive	Scaling	Moderately Corrosive	NUD
S2	Neutral	Low corrosive	Neutral	Scaling	Moderately Corrosive	NUD
S3	Scaling	Low Scaling	Scaling	High Corrosive	Scaling	NUD
S4	Neutral	Low corrosive	Neutral	Scaling	Moderately Corrosive	NUD
S5	Corrosive	Low corrosive	Corrosive	Scaling	Moderately Corrosive	WWQ
S6	Corrosive	Low corrosive	Corrosive	Scaling	Moderately Corrosive	WWQ
S7	Corrosive	Low corrosive	Neutral	Scaling	Moderately Corrosive	WWQ
S8	Corrosive	Low corrosive	Corrosive	Scaling	Moderately Corrosive	WWQ
S9	Corrosive	Low corrosive	Corrosive	Scaling	Moderately Corrosive	WWQ
S10	Corrosive	Low corrosive	Corrosive	Scaling	Moderately Corrosive	WWQ
S11	Scaling	Low corrosive	Neutral	Scaling	Scaling	NUD
S12	Scaling	Low corrosive	Neutral	Scaling	Scaling	WWQ
S13	Corrosive	Low corrosive	Neutral	Scaling	Moderately Corrosive	NUD
S14	Corrosive	Low corrosive	Neutral	Scaling	Moderately Corrosive	WWQ
S15	Corrosive	Low corrosive	Corrosive	Scaling	Moderately Corrosive	WWQ
S16	Corrosive	Low corrosive	Neutral	Scaling	Moderately Corrosive	NUD
S17	Corrosive	Low corrosive	Neutral	Scaling	Moderately Corrosive	NUD
S18	Scaling	Neutral	Neutral	Scaling	Scaling	WWQ

WWQ-worst water quality, NUD-Not used for drinking

parameters such as calcium hardness, pH, and total alkalinity. AI <10 represents the corrosion tendency of water, 10 < AI <12 represents the moderately corrosive behavior of water, and AI > 12 represents the scaling tendency of water. AI of water samples is given in Fig 2. (e) and corrosive behavior is mentioned in Table 4. Sample numbers S3, S11, S12 & S18 were found AI greater than 12, which indicates that the water is scaling. AI of the remaining samples ranged from 10 to 12, which indicates a moderately corrosive tendency of the water. The mean value of AI was 11.82 which represents the moderately corrosive tendency of water. AI indicates 77.78% of water samples are moderately corrosive and 22.22% are scaling.

Corrosion Rate Analysis (CR)

Coupon Weight Loss Method was used for corrosion rate analysis. The corrosion rate (30 days) of Galvanised iron specimen is shown in Fig 3. Corrosion rate (CR) has been confirmed that the corrosion has occurred in all samples. The corrosion rate of water samples was lie in the range of 1.31-2.29 MPY. Corrosion rates were highest in water sample 10 (Patna station) and lowest in S14 (Phulwari Sharif). Corrosion-weight loss method only informs about uniform corrosion.

Table 4 illustrates that all the indices have a different tendency for the same water sample. One index is showing the same water sample to be corrosive, while another index shows scaling or neutral. One index is showing highly corrosive levels for the same water sample, while another index shows low corrosive levels. It is challenging to depict the actual behavior of water samples using these indices. When all the indices give the same result, it is easy to make a decision. The same problem has also been observed in Acharya et al. 2018, Alimoradi et al. 2018, Kalyani et al. 2017, Mirzabeygi et al. 2016, Taghavi et al. 2019, Tyagi & Sarma 2020. The corrosion rate is therefore calculated experimentally to provide strong evidence. It has found less deviation (1.91 MPY).

Water Quality Index Analysis (WQI)

If Qi = 0 indicates the absence of pollutants. If 0 < Qi < 100 indicates the pollutants are in the prescribed range. If Qi >100 indicates the pollutants are above the prescribed range. Water quality rating is divided into five grades i.e., 'A' for best water quality, 'B' for good water quality, 'C' for bad water quality, 'D' for worst water quality, and 'E' for not use for drinking. WQI rating is mentioned in Table 5 (Brown et al. 1970). WQI of the water sample is given in Fig 2. (f) and the quality status of water samples is mentioned in Table 4. The water Quality rating (Qi) of 8 water samples was found

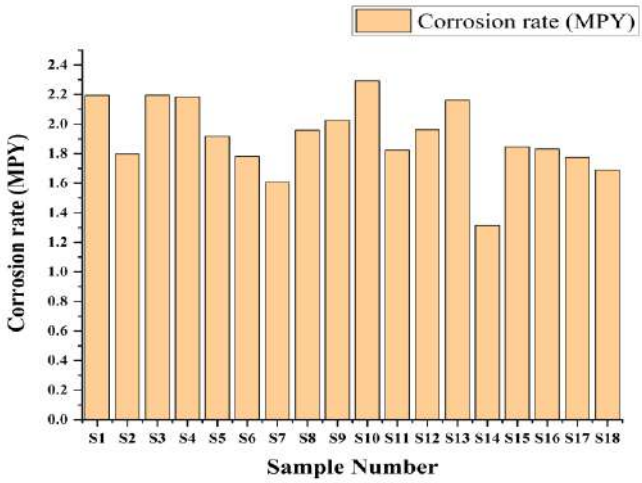

Fig. 3: Represents Corrosion rate of water samples in mils per year.

greater than 100. These indicate the pollutants are above the value of the standards. WQI was found in the range of 82-130. WQI of 8 water samples was found above 100. It means water is not used for drinking purposes graded as 'E'. WQI of the remaining ten water samples lies in the range of 76-100. This indicates the worst water quality is graded as 'D'. The mean value of WQI was found at 97.66 which represents the worst water quality. Overall, the analysis of WQI no sample lies in the range of best water quality zone and good water quality zone. The values of WQI are higher in this study due to excess magnesium and less amount of dissolved oxygen out of ten physicochemical parameters.

Effect of Water Quality on Corrosion Indices and Corrosion Rate

The Pearson Correlation method is used for the indication of correlation presented in Table 6. Pearson correlation mainly explained the relationship between two or more variables. It states weak or strong relationships and directions between two or more variables. Pearson coefficient 'r' indicates a linear relationship between two or more variables (Positive shows the proportional relationship and Negative shows an inverse relationship). If the coefficient of correlation r < 0.5 states weakly relates and r 0.5 states strongly relates (Tyagi & Sarma 2020). A weak correlation exists between the experimental Corrosion rate and WQI (Table 6). But Corrosiveness indices are strongly correlated with WQI. WQI is strongly and positively correlated with LSI (r = 0.594), & AI (0.63) and strongly and negatively correlated with RSI (-0.776), & PSI (-0.767) at a significant level of $p < 0.01$. It concludes a low quality of water indicates the possibility of scale. High-quality water indicates a corrosive tendency of water. Ls are strongly and positively correlated with WQI (0.63) at a significant level of $p < 0.01$. It concludes if water quality is excellent, then scaling tendency occurs otherwise corrosive tendency. Water quality follows corrosive or scaling behavior with LSI, RSI, PSI, and AI but is contradictory with Ls. WQI indicates all water samples lie in grade 'D' (Worst water quality) or 'E' (Not used for drinking). Therefore, LSI, RSI, PSI, and AI should indicate the scaling tendency of water, and Ls should indicate the corrosive tendency of water. Practically it is not found in Table 4.

There is a weak correlation exists between corrosion rate and corrosiveness indices ($r < 0.5$) (Table 6). Several studies such as (Kalyani et al. 2017, Pisigan & Singley 1987) also report that the corrosion rate weakly correlates with the corrosiveness index. LSI is strongly and inversely correlated with RSI (-0.924) and PSI (-0.757) both significant at $p < 0.01$. LSI exhibits true relation with RSI and PSI. It concludes as LSI increases whenever RSI or PSI decreases the scaling behavior of water increases. As LSI decreases whenever RSI or PSI increases the corrosive behavior of water increases. LSI is strongly and positively correlated with Ls (0.6) at a significant level of $p < 0.01$. It indicates contradictory results. If LSI increases scaling behavior of water increases whenever Ls increases corrosive behavior of water increases. LSI is strongly and positively correlated with AI (0.998) at a significant level of $p < 0.01$. LSI exhibits true relation with AI. If LSI or AI increases scaling behavior of water increases. If LSI or AI decreases corrosive behavior of water increases. (Kalyani et al. 2017) have told that AI can be used in the place of LSI due to a higher correlation of about 1. Similarly, it has been found that RSI is strongly and positively correlated with PSI (0.927) and negatively correlated with Ls (-0.676), and AI (-0.935) at a significant level of $p < 0.01$. RSI exhibits true relation with PSI and AI and contradictory relation with Ls. PSI is strongly and negatively correlated with Ls (-0.634), and AI (-0.777) both significant at $p < 0.01$. PSI exhibits true relation with AI and contradictory relation with Ls. Ls are strongly and positively correlated with AI (0.625) at a significant level of $p < 0.01$. Ls exhibits contradictory relations with AI. Based on the correlation, LSI, RSI, PSI, and AI should have the same tendency of water but be contradictory to Ls. Practically it is not found in Table 4.

Strategy to Reduce Corrosion Potential in the Water Distribution Network

In this study, pH was found to be nearly acidic and basic. The pH of water plays an important role in its corrosion or scaling behavior. Water quality can be improved using pH adjustment (near neutral pH = 7) using soda ash and sodium

Table 5: WQI rating.

WQI range	water quality rating	Grade
0-25	Best water quality	A
26-50	Good water quality	B
51-75	Bad water quality	C
76-100	Worst water quality	D
Above 100	Not used for drinking	E

bicarbonate. Also, alkalinity and hardness were found to be greater in water that was deposited on the pipe surface. To remove the hardness and alkalinity, a softener or zeolite basin can be used. The most common oxidants such as dissolved oxygen, chlorine, and sulfate can rapidly react with iron pipe and feed the pipe (Zhang et al. 2022). In Patna, the distribution system is mostly cast iron. Therefore, the DO must be controlled and chloride and sulfate are removed from it. A literature review suggests that selecting appropriate materials and designing a distribution system can reduce corrosion. $CaCO_3$, inorganic phosphate, sodium silicate, and other chemical inhibitors may be used. These chemicals form a protective film on the surface of a pipe and provide a barrier between the water and the pipe. Corrosion-resistant coatings and paints such as epoxy paint, polyethylene, and coal tar should be used (EPA 1984).

CONCLUSIONS

A general conclusion was reached that LSI concludes 66.67% water sample corrosive, 22.22% scaling, and 11.11% neutral. RSI concludes 88.88% water sample is corrosive, 5.56% scaling, and 5.56% neutral. PSI indicates 38.88% water sample corrosive, 5.56% scaling, and 55.56% neutral. Ls indicates 94.44% water sample scaling, and 5.56% corrosive. AI indicates 77.78% water sample corrosive, and only 22.22% scaling. It has been found all indices give different tendencies of water. Therefore, it is difficult to conclude whether the tendency of the water sample is corrosive or scaling. That's a reason, experimentally corrosion rate has been found in all water samples. It is observed that the Experimental Corrosion rate is independent of Corrosiveness indices. The average corrosion rate has been found 1.91 MPY. It has been observed that the corrosiveness indices are not able to show the actual behavior of water. In this study, Corrosiveness indices are found not a suitable tool for corrosion monitoring. Dissolved oxygen (DO) influences the corrosion rate but no corrosiveness indices included the DO. The minimum DO is found which may indicate less corrosion rate, may indicate microbial activity. It was also observed that Water quality failed to define the Corrosion rate and tendency of Corrosiveness indices.

ACKNOWLEDGEMENTS

We would like to thank the National Institute of Technology Patna for its financial support.

REFERENCES

Acharya, S., Sharma, S.K. and Khandegar, V. 2018. Assessment and hydro-geochemical characterization for evaluation of corrosion and scaling potential of groundwater in South West Delhi, India. Data in Brief, 18:928-938.

Alimoradi, J., Naghipour. D., Kamani. H., Asgari. G., Naimi-Joubani, M. and Ashrafi, S.D. 2018. Data on corrosive water in the sources and distribution network of drinking water in the north of Iran. Data in Brief, 17: 105-118.

Alsaqqar, A.S., Khudair, B.H. and Ali, S.K. 2014. Evaluating water stability indices from water treatment plants in Baghdad City. J. Water Resour. Protect., 6: 1344-1351.

APHA. 1989. Standard Methods for Examination of Water And Wastewater, Part 3, Determination of Metals. 17th, American Public Health Association, Washington DC, p. 164.

ASTM G1-90. 1999. Standard Practice for Preparing, Cleaning and Evaluating Corrosion Test Specimens. https://www.astm.org/g0001-90r99e01.html

AWWA. 2011. Internal Corrosion Control in Water Distribution Systems AWWA MANUAL M58 First Edition.

Table 6: Correlation of Corrosion rate (CR) with indices.

	CR	LSI	RSI	PSI	Ls	AI	WQI
CR	1						
LSI	0.075	1					
RSI	-0.118	**-0.924[c]**	1				
PSI	-0.096	**-0.757[c]**	**0.927[c]**	1			
Ls	0.238	**0.6[c]**	**-0.676[c]**	**-0.634[c]**	1		
AI	0.084	**0.998[c]**	**-0.935[c]**	**-0.777[c]**	**0.625[c]**	1	
WQI	0.35	**0.594[c]**	**-0.776[c]**	**-0.767[c]**	**0.63[c]**	**0.63[c]**	1

[c]Correlation is significant at 0.01 level (2-tailed). Bold: r > 0.5 indicates a strong correlation.

BIS. 2012. Indian Standard Drinking Water Specification (Second Revision). https://www.indiawaterportal.org/articles/indian-standard-drinking-water-bis-specifications-10500-1991

Brown, R .M., McClelland. N.I., Deininger, R.A. and Tozer, .G. 1970. A-water-quality-index-do-we-dare? Data Instrument. Water Qual. Manag., 61: 339-343.

EPA. 1984. Corrosion Manual for Internal Corrosion of Water Distribution Systems. https://www.osti.gov/biblio/6808456

García-Ávila, F., Ramos-Fernández, L., Pauta, D. and Quezada D. 2018. Evaluation of water quality and stability in the drinking water distribution network in Azogues city, Ecuador. Data in Brief, 18: 111-123.

Kalyani, D.S., Rajesh, V., Reddi, E.U.B., Kumar, K.C. and Rao, S.S. 2017. Correlation between corrosion indices and corrosiveness of groundwater: A study with reference to selected areas of Krishna District, Andhra Pradesh, India. Environ. Earth Sci., 76: 544.

Khiari, D. 2002. Distribution Generated Taste-And-Odor Phenomena. AWWA Research Foundation and American Water Works Association. Denver

Kirmeyer, G. and Passarelli, S.M. 2000. Guidance manual for Maintaining Distribution System Water Quality. AWWA Research Foundation and American Water Works Association, Denver & Alexandria.

Kumar, S. and Singh, R. 2021. Qualitative assessment and corrosiveness of the Ganga water: A comparative assessment. Mater. Today Proceed., 45: 5695-5701.

Kumar, S., Singh, R. and Maurya, N.S. 2022. Water quality analysis and corrosion potential in the distribution network Patna, Bihar. J. Environ. Eng. Sci., 16: 1-6.

Langelier, W.F. 1936. The analytical control of anti-corrosion water treatment. J. Am. Water Works Assoc., 28: 1500-1521.

Larson, T.E. and Skold, R.V. 1958. Laboratory studies relating mineral quality of water to corrosion of steel and cast iron. Corrosion, 14: 43-46.

Mirzabeygi, M., Naji, M., Yousefi, N., Shams, M., Biglari, H. and Mahvi, A.H. 2016. Evaluation of corrosion and scaling tendency indices in the water distribution system: A case study of Torbat Heydariye, Iran. New Pub. Balaban, 57: 25918-25926.

Pisigan, R.A. and Singley, J. 1987. Influence of buffer capacity, chlorine residual, and flow rate on corrosion of mild steel and copper. AWWA, 79: 62.

Pisigan, R.A. and Singley, J.E. 1985. Effects of water quality parameters on the corrosion of galvanized steel. J. Am. Water Works Assoc., 77: 76-82.

Rossum, J.R. and Merrill, D.T. 1983. An evaluation of the calcium carbonate saturation indexes. J. Am. Water Works Assoc., 75: 95-100.

Ryznar, J.W. 1944. A new index for determining the amount of calcium carbonate scale formed by water. J. Am. Water Works Assoc., 36: 472-483.

Singh, R. and Kumar, S. 2022. Assessment and Suitability Analysis of Water Quality of River Ganga in Patna, Bihar. Springer, Cham, pp. 251-258.

Slavíčková, K., Grünwald, A. and Šťastný, B. 2013. Monitoring of the corrosion of pipes used for the drinking water treatment and supply. Civil Eng. Architect., 1: 61-65.

Taghavi, M., Mohammadi, M.H., Radfard, M., Fakhri, Y. and Javan, S. 2019. Assessment of scaling and corrosion potential of drinking water resources of Iranshahr. MethodsX, 6: 278-283.

Taghipour, H., Shakerkhatibi, M., Pourakbar, M. and Belvasi, M. 2012. Corrosion and scaling potential in drinking water distribution system of Tabriz, Northwestern Iran. Health Promo. Perspect., 2: 103.

Tchobanoglous, G., Burton, F.L. and Stensel, H.D. 2003. Wastewater Engineering: Treatment and Reuse. Fourth Edition. McGraw-Hill, NY.

Tyagi, S. and Sarma, K. 2020. Qualitative assessment, geochemical characterization, and corrosion-scaling potential of groundwater resources in Ghaziabad district of Uttar Pradesh, India. Groundwater Sustain. Develop., 10:100370.

WHO 2006. WHO Guidelines for Drinking-Water Quality. Fourth Edition. WHO, Washington DC.

Zhang, H., Liu, D., Zhao, L., Wang, J., Xie, S., Liu, S., Lin, P., Zhang, X. and Chen, C. 2022. Review on corrosion and corrosion scale formation upon unlined cast iron pipes in drinking water distribution systems. J. Environ. Sci., 117:173-189.

Nature Environment and Pollution Technology
An International Quarterly Scientific Journal

p-ISSN: 0972-6268
(Print copies up to 2016)
e-ISSN: 2395-3454

Vol. 21 | No. 5 (Suppl) | pp. 2129-2139 | 2022

Original Research Paper

https://doi.org/10.46488/NEPT.2022.v21i05.009

Open Access Journal

Scenedesmus obliquus and *Chlorella vulgaris* – A Prospective Algal Fuel Source

V. Hariram*†, J. Godwin John, E. Sangeethkumar**, B. Gajalakshmi***, V. Ramanathan**, M. Vinothkumar*, R. Selvakumar** and M. Balachandar***

*Department of Mechanical Engineering, Hindustan Institute of Technology and Science, Padur, Chennai-603103, Tamil Nadu, India

**Department of Automobile Engineering, Hindustan Institute of Technology and Science, Padur, Chennai-603103, Tamil Nadu, India

***Department of Chemistry, Hindustan Institute of Technology and Science, Padur, Chennai-603103, Tamil Nadu, India

†Corresponding author: V. Hariram; connect2hariram@gmail.com

Nat. Env. & Poll. Tech.
Website: www.neptjournal.com

Received: 08-04-2022
Revised: 02-05-2022
Accepted: 16-05-2022

Key Words:
Biofuel
Chlorella vulgaris
Greenhouse gas
Scenedesmus obliquus

ABSTRACT

In recent years, the prospective use of algae as an alternate fuel source for petroleum-based fuels has increased drastically. It has been researched extensively and proven that it can be used as a sustainable feedstock for producing green energy considering environmental safety. This article focused on the economically viable algal feedstock for the production of lipid content for its use as a feedstock for biodiesel production. For this purpose, the algal species *Scenedesmus obliquus* and *Chlorella vulgaris* were selected, and it was grown under lab and open ambient conditions with two Blue green Medium (BG-11) and Bold Basal medium (BBM). Upon the yield, it was noticed that the BG-11 medium gave optimum lipid yield for both species. Hence, it was determined that through this medium higher lipid yield can be expected, and based on the GC-MS result it was notified that it can be a viable source of alternate fuel.

INTRODUCTION

Fuel price increase in India demands the presence of an alternate fuel that can neutralize the burden of a common person in terms of economy. Not just the economy but also global warming which increases the greenhouse gas (GHG) emissions in the atmosphere. This is of greater concern considering the environmental conditions (Hariram et al. 2017a, 2017b).

Moreover, in India, industrialization increases due to economic growth, and the population also increases day by day, both influences the annual emission of carbon dioxide which acts as a major emission source in global warming. For decades, researchers have been working on biodiesel that can be produced from algae which actively supports its use in terms of performance and emission characteristics through better combustion (Godwin et al. 2017).

Species of blue-green and green algae were isolated and the selected strain chlorella vulgaris under certain optimized conditions was cultured to produce the biomass. Biomass was then converted to oils and its calorific value was determined to possess closer fuel values. This shows that this energy source can be utilized as an alternate form while it also mitigates greenhouse gases (Ghayal et al. 2013). Algae-based biofuel showed great potential in replacing petroleum-based fuels. One of the greater influences was that its carbon-neutral character helps in environment-cleaning applications. The focus was made to have a bio-refinery feedstock which was found to be economically possible (Trivedi et al. 2015). Microalgal refinery design can be made with certain optimal production conditions. *Scenedesmus obliquus* was taken as the base model organism and the research detailed that a good refinery can be made with optimal development like nutrient conditions so that the biomass can be improved. From 100 grams of *Scenedesmus obliquus* biomass, the following products were yielded namely, 0.06 gram of βcarotene, 38 grams of biodiesel, 2 grams of omega-3 fatty acids, 3 grams of glycerol and 17 grams of ethanol (Reeza et al. 2015). The research study was done to develop the *Scenedesmus obliquus* in various conditions for lipid and biomass production. The study was to implement the application also for wastewater treatment. The mixotrophic condition was found suitable for this application. It was noted that the palmitoleic acid-rich *Scenedesmus obliquus* strain developed in mixotrophic

conditions can be utilized for wastewater treatment along with good algal biomass production and better algal oil yield (Yanan et al. 2021). The research was carried out to develop Levulinic acid from microalgae wherein methyl-sulphonic acid mediated conversion method was utilized. The study proved that the microalgae Scenedesmus obliquus was a promising feedstock (Gwi-Taek & Sung-Koo 2021). Researchers did a study on the development of strategies involving Mixotrophic cultivation to improve biomass production in freshwater microalga *Scenedesmus obliquus* by using sodium acetate in an appropriate concentration. Both autotrophic and mixotrophic lab scale study was done in which mixotrophic condition favored the situation. Also, the sodium acetate used should have an appropriate concentration to enhance the photosynthetic reaction and for better biomass production (Jie et al. 2021). From the microalgae *S. obliquus*, the production of bioethanol and biodiesel was studied. During this study, the growth was incorporated with the waste glycerol taken from biodiesel production as a nutrient supplement. It was also noticed that increased bioethanol occurred after sequential fermentation after lipid extraction (Shannan et al. 2019). An energy study was carried out by authors wherein the centrifugation and flocculation methods were undergone to compare the yield. Lipid recovery was found to be 17.4% for centrifugation and 20.7% for flocculation, but the bio-oil yield was a little lesser. The energy output in biodiesel production from centrifugation and flocculation was 0.87 and 0.68 GJ per ton. From the comparison, it was concluded that flocculation would be the optimized method for biodiesel production (Shuang et al. 2019). A study on harvesting and drying methods was done for the microalgae *Scenedesmus obliquus*. The method for harvesting was flocculation and centrifugation, while freeze drying, freezing, drying, and hot-oven dehydrating were incorporated for testing. It was determined that for polyunsaturated acid yield freeze drying and biodiesel production from biomass freezing would be more appropriate. Moreover, it was found that centrifugation was the best method (Carlos et al. 2020). Among various Scenedesmus species, it was also determined that S. Obliquus yielded with highest biomass productivity. It was also noted that the Cetane number and viscous value of *S.obliquus* FAME met the international standard (Mostafa et al. 2018).

From these studies, it was noted that *Chlorella vulgaris* and *Scenedesmus obliquus* showed promising results. Henceforth, an analysis was undergone to study both these microalgae for potential fuel sources.

Scope of Both the Species

Chlorella vulgaris acts as an encouraging bioenergy source. It is viewed as a good substitute comparing the current biodiesel crops like corn, rapeseed, or soybean, as it supplements increased productivity and is not competing with edible food crops. It can yield enormous quantities of bio-lipids up to 15 times greater than the feedstocks benchmarked for biodiesel production. The literature revealed that *Chlorella vulgaris* also contains a notable quantity of starch which could be a value-added feedstock for bio-ethanol production. However, biofuel yielded from microalgae has a competitive gap with conventional fossil fuel due to its controversial sustainability and higher production cost.

Bio-Oil Extraction

Although Scenedesmus algal family can produce numerous varieties of bioenergy such as biodiesel, bioethanol, bio-hydrogen, and drop-in fuels, all-encompassing investigations have been carried out towards the production of biodiesel. Similar to the algal bioenergy ecosystem, operational challenges in the cohesive biodiesel production from the Scenedesmus family are encountered with implementation commercially. A few of the key encounters include gas and fluid transfer, recycling, nutrient supply, cultural integrity, PAR (Photosynthetically Active Radiation) delivery, water-land availability, environmental control, and genetic and metabolic engineering harvesting (Godwin et al. 2018).

Bio-Diesel Production

Literature confirms that the Scenedesmus microalga family is capable of producing a notable quantity of lipids and a higher concentration of biomass when compared with other blue-green and green algae with a limited supply of micro and macronutrients. This was also showcased by many researchers in the production of biodiesel. The Scenedesmus microalga family has proved to yield increased lipid and biomass concentration at optimized environmental conditions in heterotrophic surroundings than in autotrophic circumstances. Variable and optimized supply of micro-macro nutrients in nitrogen-carbon-di-oxide deficient conditions enhanced the production of biomass and lipids significantly. Recent studies reported that Scenedesmus retain maximum lipid and biomass at its complete growth cycle at around 62% in dry cell weight. Assimilation of carbon-di-oxide was also found to be better in Scenedesmus algae in comparison with other blue-green algae. The growth environment with nitrogen deficit conditions promoted the concentration of lipids significantly. Despite notable lipid content, its separation using chemical methods with alcohols and its recovery is a challenging factor as its increases the production cost greatly.

Bioethanol

Chlorella vulgaris and *Scenedesmus obliquus* were found to possess a higher concentration of carbohydrates (more than

47% by dry weight) making them competitive feedstock in the production of bio-ethanol. An investigation reported that *Scenedesmus obliquus* at nitrate deficient condition produced higher biomass and lipid with a notable increase in carbohydrates. Hydrolysis of carbohydrates with sulphuric acid underwent a fermentation reaction for four hours yielding 8.45 grams of bio-ethanol in the ratio of 0.214-gram ethanol per gram of biomass.

Wastewater Management

Scenedesmus obliquus and *Chlorella vulgaris* were also found to be very effective in removing the phosphorus and ammonia content from the waste waters of the agro-industrial sector. *Scenedesmus obliquus* reacted with the wastewater effectively for the removal of ammonia in a cylindrical bio-reactor whereas phosphorous removal was found to be similar with bot both species. In the presence of Algal Turf Scrubber (ATS), *Scenedesmus obliquus* and *Chlorella vulgaris* were very active and operative in the removal of phosphorus and ammonia from the polluted waters. Literature reported that the metallic phosphorous removal cost was brought down to 24$ from 77$ when the system is employed with *Scenedesmus obliquus*. On the other hand, the substrates used of *Scenedesmus obliquus* growth could also be used as an organic fertilizer, cattle feed, and paper industry as a value-added feedstock.

The above-mentioned are all the scope and needs which can be fulfilled by using these two algal species. In this article, the lipid extraction from these two species will be studied for the effective usage of these lipids as fuel sources.

MATERIALS AND METHODS

Chlorella Vulgaris

Chlorella vulgaris, under the classification of genus *Chlorella*, is a green eukaryotic microalga. The species name was derived from the Greek-Latin language, Chloros (□□□□ó□) referring to its size which is a microscopic – single-celled organism in nature. Martinus Willam Beijerinck discovered *Chlorella vulgaris* in 1890 possessing a prominent nucleus. In the early 1990s, German researchers identified a spike protein in *Chlorella vulgaris* which make it suitable for edible purpose also. Due to its enhanced medicinal value, protein-rich content, and enriched dietary supplements, Japan consumes it largely across the globe. *Chlorella vulgaris* is a eukaryotic, unicellular green alga existed on the earth for more than 2.4 billion years. Its natural higher protein level and higher mineral content transformed it into a major multivitamin supplement and hydration enhancer. Nowadays, due to its significant concentration in lipids under certain growth environments, it played a vital role in biodiesel production. It was estimated that *C. vulgaris* possess lipid at about 42.5% which was 22% greater than sugarcane, corn, or soybean making it a viable and promising feedstock for biodiesel production. Fig. 1 shows the microscopic view of *Chlorella vulgaris*.

Scenedesmus Obliquus

Scenedesmus obliquus is a flat plate, unicellular green algae belonging to the genus of Chlorophyceae. It a

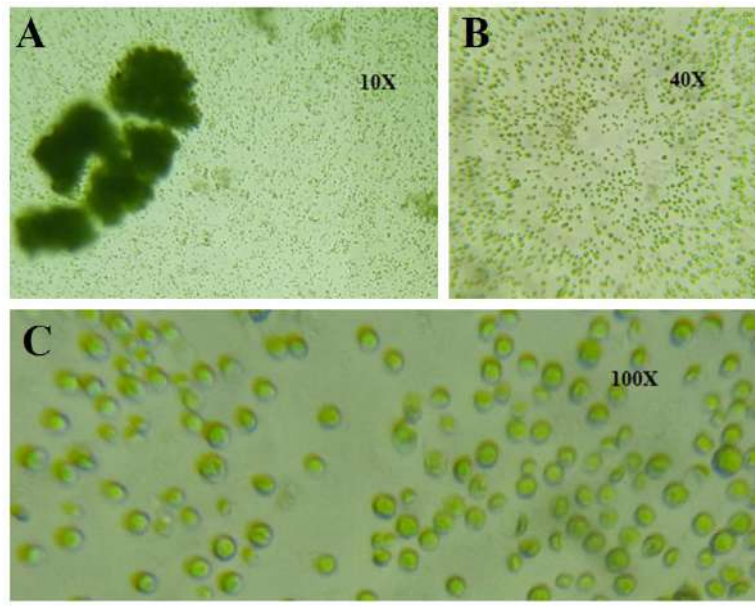

Fig. 1: Microscopic view of *Chlorella vulgaris* in various lenses at 10X (A), 40X (B), and 100X (C).

microscopically small, colonial in nature, and non-motile. The microscopic view distinguishes the chloroplast and a pyrenoid which is mono-parietal visible. Its view under a scanning electron microscope at 10X magnification released the cell wall membrane is not flat but with reticulations and bumps. Vast studies were reported on *Scenedesmus obliquus* with emphasis on potential nutrient value. Recent literature showcased it to be a promising aquatic organism with produces variable proportions of carbohydrates and lipids enhancing its value addition. The latest technologies transform and promote the usefulness of *Scenedesmus obliquus* more towards bioenergy-producing fuel feedstocks and supporting green energy. Numerous investigations were carried out in NREL (National Renewable Energy Laboratory, India) to understand its oil production capacity and it was evidenced that it could yield 19 to 21 times more bio-oil than oil-producing crops.

This investigational study focuses on the oil production capability of *Scenedesmus obliquus* on a laboratory scale with optimized environmental conditions. The advantages of using *Scenedesmus obliquus* are easy accessibility, eco-friendly nature, and renewability. The algal reproduction was through the conventional photosynthesis process providing luminescence and a pre-determined quantity of micro-macro nutrients along with carbon-di-oxide. Upon achieving exponential growth upto 10^4 to 10^6 cells.cm^{-1}, the harvesting of biomass was carried out. Centrifugation and soxhlet extraction process expelled the lipids from *Scenedesmus obliquus.* The microscopic view of *Scenedesmus Obliquus* is shown in Fig. 2.

Morphology of *Chlorella Vulgaris* and *Scenedesmus obliquus*

Table 1 signifies the algal class and division of *Scenedesmus obliquus* and *Chlorella vulgaris*. *Chlorella vulgaris*, is a spherical and small unicellular green algae sizing between 5 and 10 µm. is small, spherical algae that have a size of 5-10µm. The microscopic structure of *Chlorella vulgaris* showed mixtures of 16 chromosomes between 0.97 Mb and 3.8 Mb which may be due to the isolated geographical locations of the strains. *Scenedesmus obliquus* was microscopically seen with spikes and cell patterns. A few cells were also seen with pointed ends which lack spikes. Few cells were also arranged in colonies with the oblong-ovate arrangement and even the absence of spikes. The abundance of unicellular *Scenedesmus obliquus* was identified in rows with the presence of spikes

Table 1: Micro algae division information.

Parameters	*Chlorella vulgaris*	*Scenedesmus obliquus*
Hierarchy	Taxonomic (Beijerinck 1890) & (IT IS – Taxonomic Serial No: 5815)	Taxonomic: (Turpin) (Kützing 1833)
Kingdom	Plantae	Plantae
Sub-kingdom	Viridiplantae	Viridiplantae
Division	Cholorphyta	Cholorphyta
Subdivision	Cholorphytina	Cholorphytina
Class	Trebouxiophyceae	Chlorophyceae
Genus	Chlorella	Scenedesmus
Family	Oocystaceae	Scenedesmaceae
Order	Chlorellales	Sphaeropleales

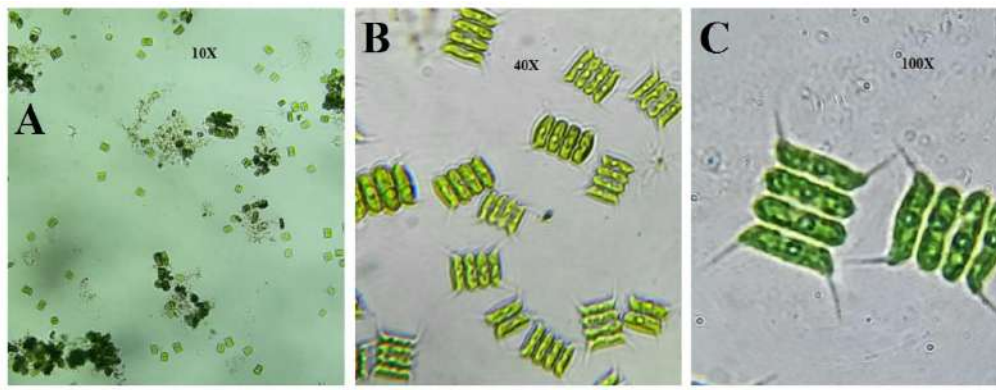

Fig. 2: Microscopic view of *Scenedesmus obliquus* at 10X (A), 40X (B), and 100X (C).

between 3 and 33 with attachments in the outer periphery of the cell wall membrane. The morphologies of *Scenedesmus obliquus* showcased unicellular and multicellular cells influenced by surrounding abiotic and biotic factors which will affect its growth significantly.

Cell Wall

Chlorella vulgaris is composed of carbohydrates inhibiting cellulose up to 82% in its cell wall membrane. As a result, it was very rigid and integrated with the other surrounding membranes thus serving as a protecting layer. *Scenedesmus obliquus* was seen as unicellular and multicellular as well and found in colonies with 2 to 8 cells covered with the parental cell wall membrane. The concentration of unicellular organisms was found to be higher in the amalgamated medium but proper illumination and elevated surrounding temperature pronounced unicellular growth significantly in a non-colonial manner.

Reproduction

Chlorella vulgaris assimilates natural sunlight through the chloroplast along with a minimal quantity of micro and macro nutrient for its reproduction. Further, it in-digests carbon-di-oxide to perform the process of photosynthesis in fresh clean water in an aseptic condition. As the strains of *Chlorella vulgaris* start multiplying on the water surface, it blocks the natural sunlight from the top surface thereby deteriorating the growth of *Chlorella vulgaris* and eventually dying underneath. This could be avoided by supplying proper aeration and artificial luminance for their growth.

Light Conditions

Since *Chlorella vulgaris* and *Scenedesmus obliquus* are autotrophic, the photosynthetic process gains importance greatly as it promotes algal growth. In the open pond culture system, the biomass production cost was brought down significantly due to the availability of natural sunlight. On the other hand, open pond cultivation deteriorates the algal growth in a few instances of lack of proper care, the mother algae become a parasite to the other living organism which could affect the growth of *Chlorella vulgaris* and *Scenedesmus obliquus* largely.

Natural sunlight compresses numerous components based on its wavelength, visibility, x-ray, gamma ray, and others. The photosynthesis process uses only natural sunlight between the wavelength of 370 nm and 740 nm for promoting algal growth. Filtering the light rays from the amalgamation was difficult and also leads to a negative impact on the algal biomass concentration. The climatic condition in the area of the open pond system selected for the algal growth also plays a vital role in its growth.

Growth Medium

The two main media used in the biomass cultivation of, *Chlorella vulgaris* are Bold's Basal medium BG11. These two media are often used which successfully supports growth without denaturing the cells and there nurture the cells by supplying them with essential nutrients and other compounds. The vital role of the medium is to support the growth of the cells but here the medium not only supports the growth of the cells but also nurtures them and helps to keep the constituents and compounds present together without any distortion. Each medium will have a composition different from one another which marks the uniqueness of each medium. Thus, the medium used here is unique as they contribute to the growth of the microalgae as well as supports it by maintaining the micro algal cells throughout their growth without causing damage to the cells and their components.

RESULTS AND DISCUSSION

In this section, the methods for optimization of the algal growth towards lipid production are detailed for both the species *Chlorella vulgaris* and *Scenedesmus obliquus*.

Microalgal Cultivation

To optimize the process, both the microalgae species were inoculated to two different mediums (BBM & BG-11) after collecting 3ml of each species sample, later which was cultured in a plant tissue culture lab and made up to 250 mL of each species in a sterile conical flask and maintained in a different environment for the optimization process. The Bold Basal Medium (BBM) and Blue-Green medium (BG-11) were used to cultivate microalgae of two different species in different environments to analyze the growth of algae and production of lipids, and toidentify the best medium for the fast growth of algae and high lipid production.

Ambient Condition Control

Three different types of environmental temperatures (16°C, 25°C, and 32°C) were selected and cultured for both the microalgae species to identify a suitable environmental temperature to get a high specific growth rate and biomass productivity of algae.

At 16°C, the sample was placed in a plant tissue culture lab under a fixed artificial light provided by a fluorescent tube and the effects of light on the growth of the algae were calculated by the total cell count. At 25°C, the sample was

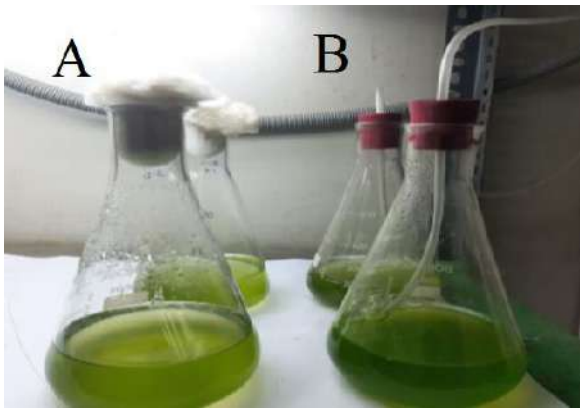

Fig. 3: Non-aerated (A) and aerated culture (B).

placed in a window side of the lab receiving partial sunlight and at room temperature with manual agitates for every one-hour interval gap to enhance the growth and mixing of the medium and culture.

At 32°C, the sample was placed in a window side of the lab receiving partial sunlight and at room temperature with manual agitates for every one-hour interval gap to enhance the growth and mixing of the medium and culture. In the culture lab, the sample was also tested with aeration, and without aeration, aeration was supplied through an aerating pump. The flow rate of the pump was 3L.min^{-1}, which mixes the medium and sample for 24 h and enhances the growth as shown in Fig. 3. The growth results were then compared with the non-aerated. For non-aeration, the supply was added to the culture medium, it was cultured in a plant tissue culture lab and agitated manually for a 1h interval gap to avoid the sedimentation of the culture and to enhance the mixing of the culture with the medium. The aeration can be seen as shown in Fig. 3.

Chlorella Vulgaris and *Scenedesmus obliquus* Morphology

The morphological studies of the two microalgae species *Chlorella vulgaris* and *Scenedesmus obliquus* were performed to observe and study the growth of the cells from the young stage to the mature stage. Hence, microscopic studies were done on the 7th day after inoculation of the sample into the medium and it was carried out for one month with seven days of interval gap. The sample for the morphological studies is collected from different environments maintained for the optimization process. The growth rate is detailed in the form of a graphical representation shown below in Figs. 4, 5, 6, 7, 8 and 9.

The growth determination of samples 1 (BBM) & 2 (BG-11) of microalgae *Chlorella vulgaris* and samples 1 (BBM) & 2 (BG-11) of microalgae *Scenedesmus obliquus* were performed by taking the growth density readings with the help of colorimeter at three respective nanometers (620 nm, 680 nm & 700 nm) at the different time intervals (9 am, 12 pm & 3 pm). The maximum growth of the two microalgae species was observed at the absorbance of 620nm. The total cell count of the microalgae was studied to identify the growth rate of algae in the interval gap of seven days for four weeks where the hemocytometer was used for the total cell count. The result of the phytochemical screening is shown below in Table 2.

The preliminary phytochemical screening of the microalgae of *Chlorella vulgaris* and *Scenedesmus obliquus* showed the methanolic extracts containing alkaloids, amino acids and proteins, carbohydrates, fixed oils and fats, and phenols and tannins. The phytochemical screening demonstrated the presence of different types of phytocompounds which could be responsible for the various pharmacological &

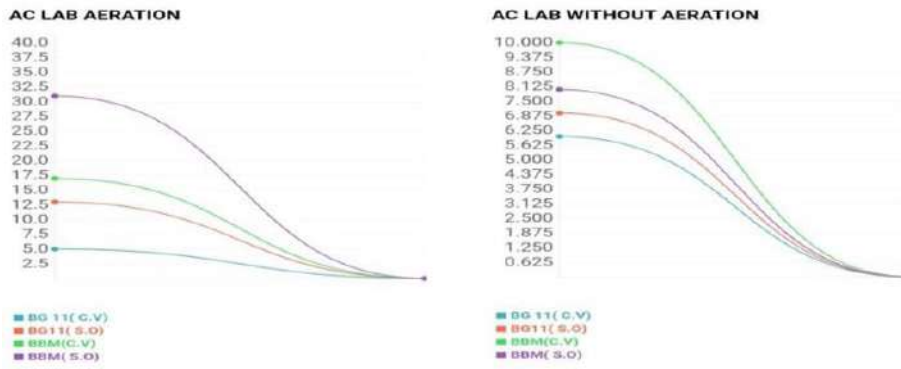

Fig. 4: Growth rate study with and without aeration at 620 nm.

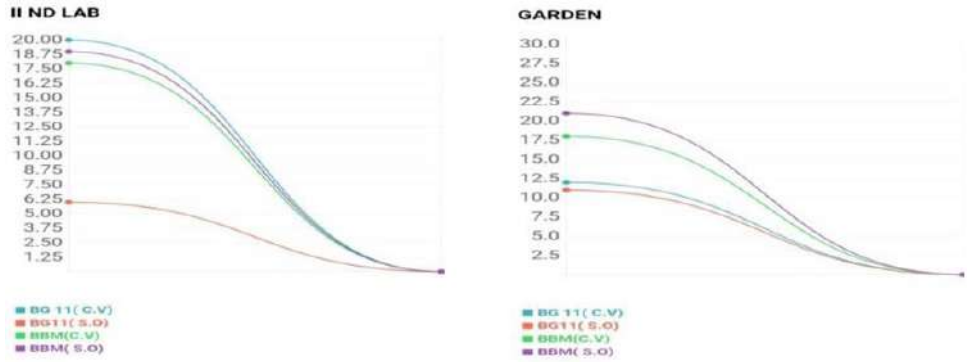

Fig. 5: Growth rate study in lab and garden at 620 nm.

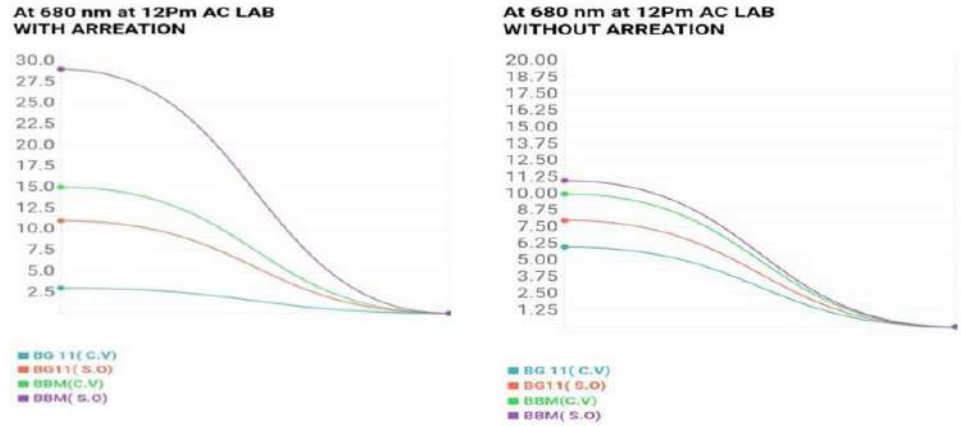

Fig. 6: Growth rate study with and without aeration at 680 nm.

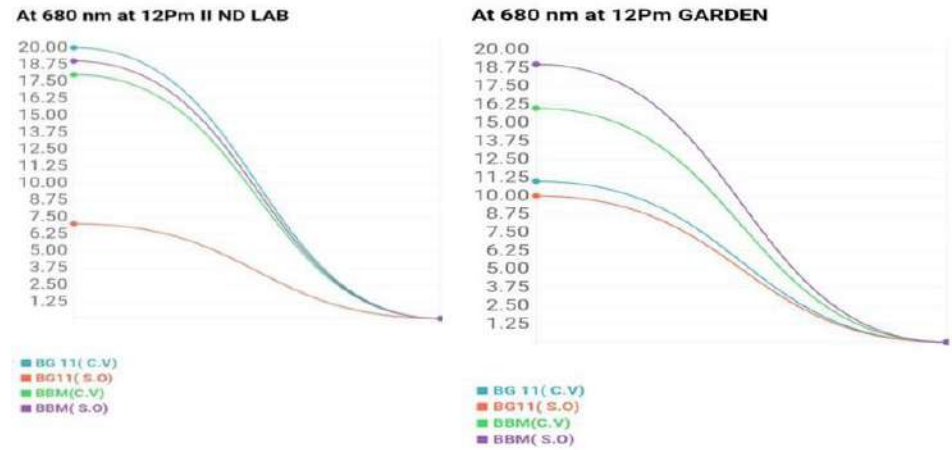

Fig. 7: Growth rate study in lab and garden at 680 nm.

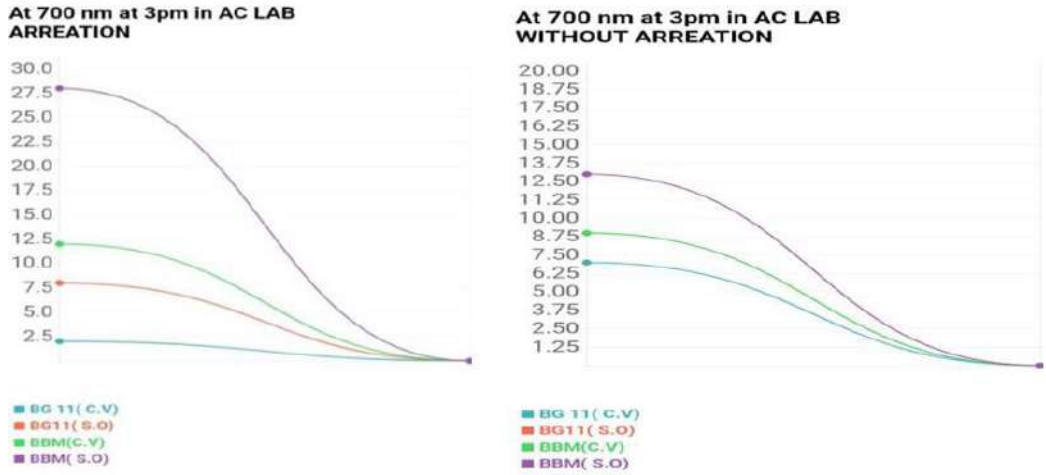

Fig. 8: Growth rate study with and without aeration at 700 nm.

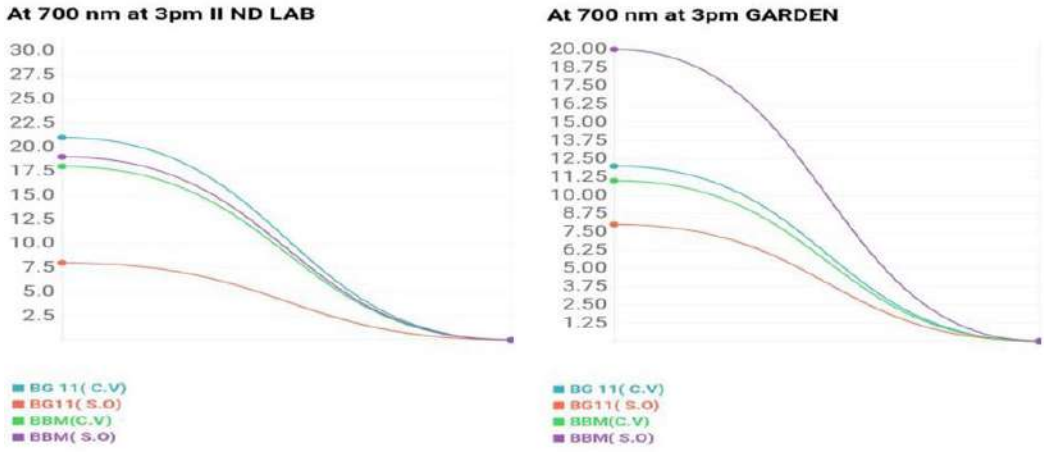

Fig. 9: Growth rate study in lab and garden at 700 nm.

Table 2: Phytochemical screening.

Phytochemical Test	Reagents used (Test performed)	Result for (*C.vulgaris*) (BBM)/(BG)		Result for (*S.obliquus*) (BBM)/(BG)	
Alkaloid test	Mayer's test	+	+	+	+
Amino acids & proteins	Ninhydrin test	-	+	+	+
Carbohydrates	Benedict's test	+	+	+	+
Fixed oils & fats	Saponification test	+	+	+	+
Phenolic compounds &tannins	Ferric chloride testLead acetate test	+	+	+	+
		+	+	+	+

Table 3: Lipid Content in *Chlorella Vulgaris* and *Scenedesmus Obliquus.*

Algae	*Chlorella vulgaris*		*Scenedesmus obliquus*	
Medium	BG11	BBM	BG11	BBM
Lipid Content [%]	17.630 ± 0.002	11.560 ± 0.002	26.320 ± 0.003	19.760 ± 0.003

Table 4: Major chemical composition determined from GCMS of *Chlorella vulgaris* and *Scenedesmus obliquus.*

S.No.	*Chlorella vulgaris*	*Scenedesmus obliquus*
1	Heptaldehyde	3-hexadecyloxycarbonyl-5-(2-hydroxyl)-4-methylimidazolium
2	Octadecenoic acid, methyl ester	dodecanoic acid 3-hydroxy3.32%,
3	Hexadecanoic acid	9-octadecenoic acid (Z)41.59%,
4	3-Decyn-2-Ol	9,12,15-octadecadienoic acid2.42%,
5	(E)- 3,7,11,15-tetramethylhexadec-2-ene	2-hexadecenal 5.11%,
6	Heptadecane-1,2,3,4,5-pentol	quercetin 7,30,40-trimethoxy 13.48%,
7	Docosane, 4-methyl	octasiloxane

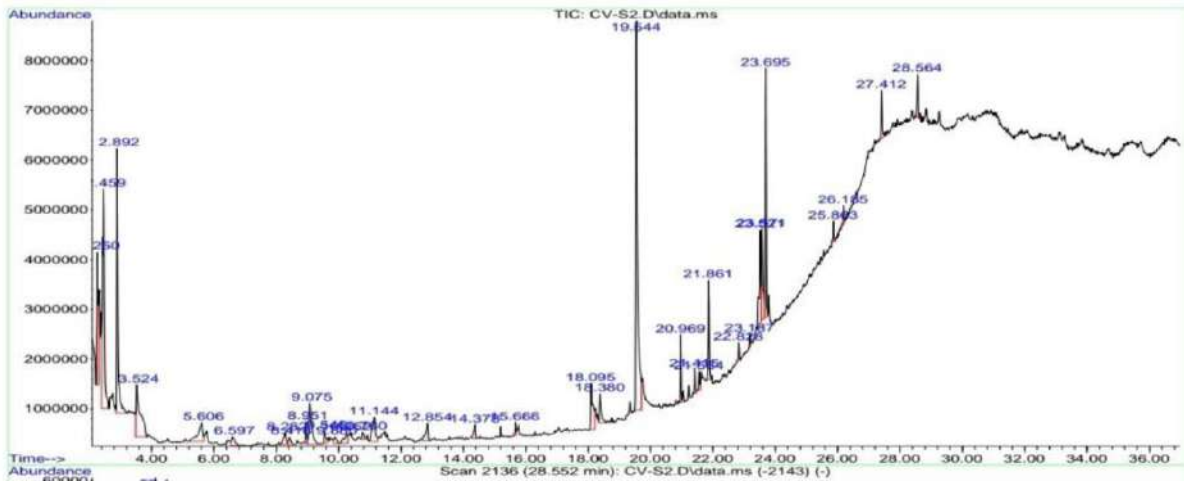

Fig. 10: GCMS of *Chlorella vulgaris* in BBM.

medicinal properties. Among these compounds, fixed oils and fats are important. Secondary metabolites are responsible principles for the biofuel properties of the microalgae.

Lipid Extraction

To extract the lipid content, Folch's extraction procedure was used which is one of the most popular methods for isolating lipidsfrom biological samples. In this method, 200 mL of the sample was taken and mixed with 1.5 mL of methanol, then vortexed with 3 ml of chloroform and then incubated for 1 h at room temperature. After which, 1.25 mL of water content was added and left for 10 min. Later, the centrifugation was performed for 10 min at 10 rpm which extracted the lipid at the lower phase which was collected for testing. From the extracted lipid, it was noted that BG11 medium supported better yield in both species which can be noted in Table 3.

GC-MS

The GC-MS analysis of the microalgae *C.vulgaris* and *S.obliquus* revealed the presence of various compounds. The major chemical compounds present in *Chlorella vulgaris* and Scenedesmus *obliquus* were confirmed based on the peak area and retention time which is shown in Table 4. The identification of compounds on the mass spectrum of GC-MS was done using the database NIST - National Institute of Standard and Technology, which details that it can be used as a biofuel. The graph obtained with its peak was shown below in Figs.10, 11, 12, and 13. Similar GC-MS testing was also done by Supriya et al. (2012).

Fig. 11: GCMS of *Chlorella vulgaris* in BG11 medium.

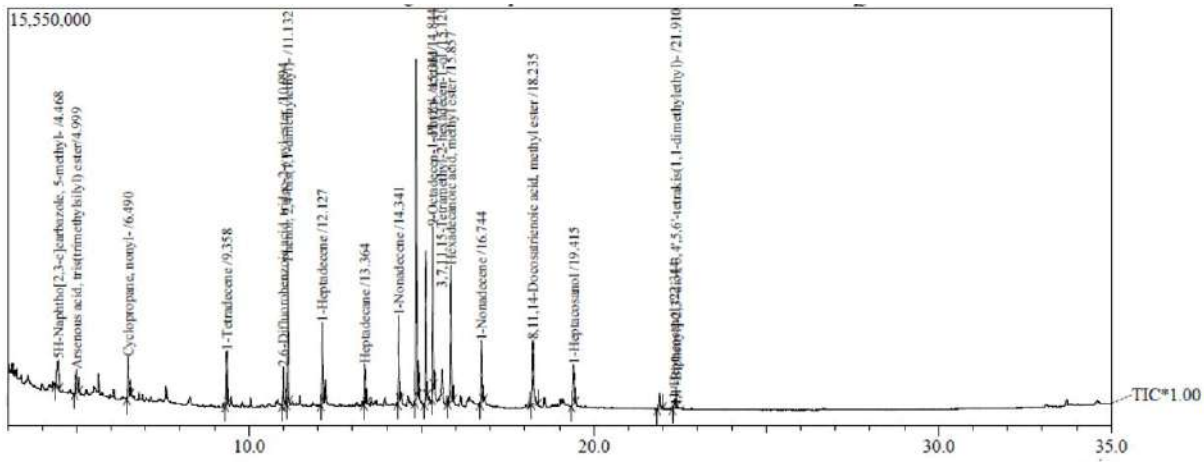

Fig. 12: GCMS of Scenedesmus Obliquus in BBM.

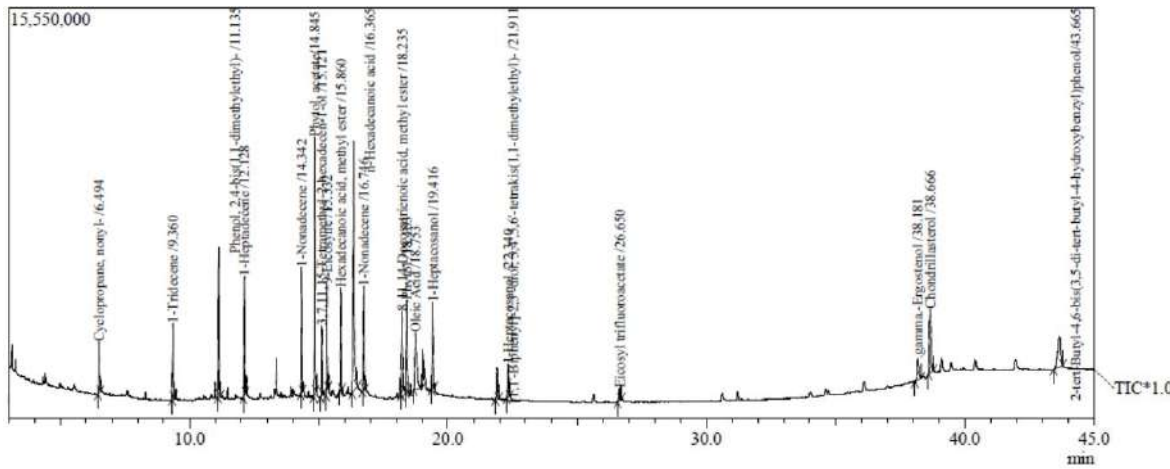

Fig. 13: GCMS of *Scenedesmus obliquus* in BG11 medium.

CONCLUSION

This study mainly focused on the optimization and comparative analysis of the *Chlorella vulgaris* and *Scenedesmus obliquus* microalgae growth and high lipid productions. The growth determination of the microalgae revealed the time period of the algae growth which was observed at 620nm. The phytochemical analysis was performed for the microalgae species to check the phytoconstituents. It was revealed that the concentration was more in theBG-11 medium from both samples. The GC-MS analysis of the microalgae *C.vulgaris* and *S.obliquus* revealed the presence of various compounds. The presence of major compounds in *C.vulgaris* and *S.obliquus* was confirmed based on the peak area and retention time, which concludes that these extracts can be utilized as a biofuel. From the analysis, it can also be concluded that the *Chlorella vulgaris* and *Scenedesmus obliquus* growth is more in the BG-11 medium than in the BBM medium.

REFERENCES

Carlos, Y.B.O., Thayna, L.V., Rafael, G.L., Herculano, C.R.S.M., Aline, T.S., Nelson, R.A.F. and Roberto, B.D. 2020. A comparison of harvesting and drying methodologies on fatty acids composition of the green microalga. Biomass Bioenerg., 132: 105437.

Ghayal, M.S and Pandya, M.T. 2013. Microalgae biomass: A renewable source of energy. Energy Proced., 32: 242-250.

Godwin, J., Hariram, V and Seralathan, S. 2018. Emission reduction using improved fuel properties of algal oil biodiesel and its blends. Energy Sour. Part A Recov. Utiliz. Environ. Effects, 40(1): 45-53.

Godwin, J., Hariram, V., Seralathan, S. and Jaganathan, R. 2017. Effect of oxygenate on emission and performance parameters of a CI engine fuelled with blends of diesel-algal biodiesel. Int. J. Renew. Energy Res., 7(4): 2041-2047.

Gwi-Taek, J. and Sung-Koo, K. 2021. Methanesulfonic acid-mediated conversion of microalgae Scenedesmus obliquus biomass into levulinic acid. J. Ind. Eng. Chem., 63:111-121. DOI. org/10.1016/j.jiec.2021.08.013.

Hariram, V. Godwin John, J. and Seralathan, S. 2017b. Spectrometric analysis of algal biodiesel as a fuel derived through base-catalyzed transesterification. Int. J. Amb. Energy, 40(2): 195-202.

Hariram, V., John J. Godwin, Seralathan Sivamani. 2017a. Data set for extraction and transesterification of bio-oil from Stoechospermum marginatum, brown marine algae. Elsevier, 14: 623-628.

Jie, C., Wenxin, F. and Linggang, Z. 2021. Development of a mixotrophic cultivation strategy for simultaneous improvement of biomass and photosynthetic efficiency in freshwater microalga *Scenedesmus obliquus* by adding appropriate concentration of sodium acetate. Biochem. Eng. J., 176: 108177.

Mostafa, E., Abd El-Fatah, A., Hamed, E., Mohamed, B. and Soha, M. 2018. Screening of different species of Scenedesmus isolated from Egyptian freshwater habitats for biodiesel production. Renew. Energy, 129: 114-120.

Reeza, P. and Nirupama, M. 2015. Utilization of Scenedesmus obliquus biomass as feedstock for biodiesel and other industrially important co-products: An integrated paradigm for microalgal biorefinery. Algal Res., 12: 328-336.

Shannan, X., Mahdy, E., Gehan, A.I., Chunhou, L., Shuang, L. and Wang, A. 2019. Evaluation of bioethanol and biodiesel production from Scenedesmus obliquus grown in biodiesel waste glycerol: A sequential integrated route for enhanced energy recovery. Energy Conv. Manag., 197: 111907.

Shuang, W., Mukhambet, Y., Abd El-Fatah, A., Sherif, E. and Qian, W. 2019. Microalgae harvest influences the energy recovery: A case study on chemical flocculation of *Scenedesmus obliquus* for biodiesel and crude bio-oil production. Bioresour. Technol., 286: 121371.

Supriya, G. and Ramachandra, T.V. 2012. Optimal extraction of lipids from microalgae, and microcystins. Nature Environ. Pollut. Technol., 11(2): 213-218.

Trivedi, J., Aila, M., Bangwal, D.P., Kaul, S. and Garg, M.O. 2015. Algae based biorefinery—how to make sense? Renewable and Sustainable Energy Reviews, 47: 295-307.

Yanan, S., Xiaodan, W., Hongli, C., Chunli, J., Jinai, X., Xiaoyun, J., Ruiyan, M. and Runzhi, L. 2021. Enhancing growth and oil accumulation of a palmitoleic acid–rich *Scenedesmus obliquus* in mixotrophic cultivation with acetate and its potential for ammonium-containing wastewater purification and biodiesel production. J. Environ. Manag., 297: 113273.

Nature Environment and Pollution Technology
An International Quarterly Scientific Journal

p-ISSN: 0972-6268
(Print copies up to 2016)
e-ISSN: 2395-3454

Vol. 21 | No. 5 (Suppl) | pp. 2141-2163 | 2022

Original Research Paper

https://doi.org/10.46488/NEPT.2022.v21i05.010

Open Access Journal

Assessing the Suitability of Oil Palm (*Elaeis guineensis*) Production in Peninsular Malaysia based on Soil, Climate and Land Use

A. Abubakar, M. Y. Ishak**†, A. B Aisyah**, Md. K. Uddin*** and M. H. Ahmad******

**Faculty of Forestry and Environment, Universiti Putra Malaysia, 43400 Serdang, Selangor, Malaysia
***Faculty of Agriculture, University Putra Malaysia, 43400 Serdang, Selangor, Malaysia
****Department of Geography, Ahmadu Bello University, Zaria, Nigeria
†Corresponding author: Mohd Yusoff Ishak; m_yusoff@upm.edu.my

Nat. Env. & Poll. Tech.
Website: www.neptjournal.com

Received: 22-09-2022
Revised: 18-10-2022
Accepted: 19-10-2022

Key Words:
Land use
Climate
Oil palm production
Water deficit

ABSTRACT

In recent years, palm oil production has grown rapidly as a result of rising demand. Oil palm plantations have been established on thousands of acres to meet this demand. The objective of this study is to assess the suitability of oil palm production as driven by soil, climate, and land use. The land suitability assessment (LSA) method was adopted in this study. We use geospatial techniques of overlay mapping as a suitable land suitability assessment method, in which the evaluation criteria are recorded as superimposed layers. A land suitability map is produced by integrating these layers into a single layer. The method is also applied to delineate available areas for growing oil palm in Peninsular Malaysia. The findings revealed that suitable soil areas for oil palm production are extensively found in the selected regions of Peninsular Malaysia, in states like Selangor and some parts of Kedah, Kelantan, and Terengganu with clay loam and sandy loam soil properties, while in the southern region like Melaka, moderate suitability for oil palm production was found due to the domination of clay soil in the area. Highly suitable areas were estimated (mean annual water deficit <150 mm) to be 3688254.00 ha (29.54%) of the total land area; suitable areas (mean annual water deficit <250 mm) were 6540669.00 ha (52.38%); moderately suitable areas were (mean annual water deficit <400 mm) 2227500.00 ha (17.84%), and unsuitable areas (mean annual water deficit >400mm) for oil palm production as a result of poor water availability was 31104.00ha (0.25%). The Land Use Land Cover Map of Peninsular Malaysia revealed the suitable areas to cover an average of 10885001.46 ha (82.45%), water bodies 1239505.58 ha (9.39%), built-up areas (unsuitable areas) 1051544.34 ha (7.96%), and bare surface areas are also not suitable areas for oil palm production at 26509.73 ha (0.20%). This study recommends that oil palm plantations be expanded into areas with highly suitable soils and climates.

INTRODUCTION

West and southwest Africa is home to the oil palm (Elaeis guineensis), mainly in the region between Angola and the Gambia 10°N and 10°S and extending to a 200-300 km coastal belt from approximately 15°N to 15°S (Paterson et al. 2013). In the case of this species, guineensis refers to the name of the area where it was found, not the country now known as Guinea (Verheye 2010, Paterson et al. 2013, Nambiappan et al. 2018, Abubakar et al. 2021, Abubakar et al. 2022a, 2022b). The Bogor Botanical Garden in Indonesia is believed to have been the first to plant oil palm in Southeast Asia in 1848 (Nambiappan et al. 2018). In Malaysia, the first commercial plantation was established in 1917 at Tennamaran Estate in Kuala Selangor (Basiron 2007, Dunn et al. 2011, Nambiappan et al. 2018). The main product of the crop is vegetable oil, and it is grown mainly for industrial purposes (Verheye 2010). Oil palm requires a suitable climate for optimum production (Abubakar et al. 2021). Temperatures between 27 and 28°C are optimal daily, with maximums of 30-32°C on a monthly basis and minimums of 21-24°C (Verheye 2010, Zainal et al. 2012, Paterson et al. 2013, Abubakar et al. 2021). In the coldest month, the minimum temperature should be > 18°C (Abubakar et al. 2022a, 2022b). Seedling growth ceases at temperatures < 15°C, and when temperature drop below 18°C growth is stopped (Verheye 2010, Zainal et al. 2012, Paterson et al. 2013). There should be at least 85% relative humidity in the air (Verheye 2010, Oettli et al. 2018). In addition, solar radiation should be at least 16 or 17 MJ m^{-1} d^{-1} (Oettli et al. 2018). A typical requirement for oil palms is 150mm of rain per month, with an annual rainfall of 2000-2500mm, and a dry period of no more than 2-3 months (Verheye 2010, Paterson et al. 2015). Oil palm can be grown on a

wide variety of soils (Verheye 2010, Paterson et al. 2013, Rhebergen et al. 2016, Pirker et al. 2016; Abubakar et al. 2021). A well-drained, deep soil is essential for palm trees (Paterson et al. 2013, Abubakar et al. 2022a, 2022b). Low-elevation tropical lowlands are the primary growing areas for the crop where the original vegetation cover of these areas was dense rainforests (Verheye 2010). Physical soil properties are more important in oil palm plantations than soil fertility (Verheye 2010). Soil physical properties, such as soil moisture, are more important than nutrient supply, which can be corrected by fertilizer application (Verheye 2010). The best place for planting the crop is on the flat or gently undulating ground (Verheye 2010, Paterson et al. 2013, Abubakar et al. 2022a, 2022b). Oil palm is a very lucrative crop and a high-yielding oil plant (Corley & Tinker 2008, Castiblanco et al. 2013). It is economically the most efficient of all oil crops because of its ease of establishment, low costs, and high output (Dislich et al. 2017). Palm oil and other products derived from oil palm are found in a variety of products such as lipstick, pizza dough, instant noodles, shampoo, ice cream, detergent, margarine, chocolate, cookies, biodiesel, soap, packaged bread. The product is also found in frying fats, biscuits, snack foods, bakery products, cosmetics, candles, pharmaceuticals, and supermarket goods, etc. (Nagaraj 2009, Teoh 2010, Sutton & Kpentey 2012, Castiblanco et al. 2013, Paterson & Lima 2018). Oil palm is highly produced by the following countries: Indonesia, Malaysia, Nigeria, the Democratic Republic of Congo, the Ivory Coast, Brazil, Colombia, Costa Rica, and Ecuador (Corley & Tinker 2003, Paterson et al. 2013, Abubakar et al. 2022a, 2022b, Abubakar et al. 2022a, 2022b). Indonesia and Malaysia, palm oil accounts for over 85% of global demand (Varkkey et al. 2018, Rahman 2020, Ayompe et al. 2021). Among the major palm oil export destinations are India, China, the European Union (EU), the United States (USA), Pakistan, Bangladesh, Nigeria, and the Philippines etc. (Kushairi et al. 2018, 2019, Maluin et al. 2020, Abubakar et al. 2022a, 2022b).

Over the past few decades, oil palm production has witnessed a sharp rise, particularly in terms of the area that has been produced and the amount of oil produced (McCarthy & Cramb 2009, Sayer et al. 2012). National export revenues have increased significantly due to the expansion of the oil palm industry, particularly during the Asian financial crisis of the late 1990s, and today it dominates the landscape in Malaysia (Khiabani & Takeuchi 2020). Oil palm production has increased in recent years due to a rise in global demand for fats and oils (Abazue et al. 2015). In Malaysia, rapid oil palm plantation expansion began in 1980 when the expansion reached 1.0 million ha and subsequently reached 2.9 million ha in 1991, 3.1 million ha in 1998, 3.8 million ha in 2004, 4.9 million ha in 2010, and 5.9 million ha in 2019 (Malaysian Palm Oil Board 2020). Recent years have seen stiff competition for plantation land in Peninsular Malaysia, where acres of land have been taken over by oil palm plantations (Koh & Wilcove 2008, McCarthy & Cramb 2009, Koh et al. 2011, Shevade & Loboda 2019, Charters et al. 2019).

The distribution of oil palm is restricted by climate on a large scale; nevertheless, local factors such as terrain and soil texture may also have an impact (Paterson et al. 2015, Rhebergen et al. 2016, Abubakar et al. 2022a, 2022b, Paterson 2021a, 2021b). Monitoring land use changes and observing the transition from forests to plantations and evaluating the effects of these changes in Malaysia could benefit from the use of remote sensing (Vadivelu et al. 2014). The first step in oil palm plantation is a land-suitability evaluation (He et al. 2011, Vasu et al. 2018). Several methods and theories have been employed since the early twentieth century to evaluate soils. A number of these include; Land capability classifications (LCC) (Klingebiel & Montgomery 1966), the Storie index (SI) (Storie 1978), the FAO land suitability assessment (FAO 1976), the parametric method (Sys et al. 1991), Land Suitability Evaluation, and GIS-based multi-criteria analysis, to name a few examples (Elsheikh et al. 2013, Nguyen et al. 2015). Biophysical suitability evaluation methods are used to examine the physical state of the environment for a certain crop (Pirker 2015, 2016, Rhebergen et al. 2016, Vasu et al. 2018, Khiabani & Takeuchi 2020, Jaroenkietkajorn & Gheewala 2021, Abubakar et al. 2022a, 2022b).

Because of the rapid growth of oil palm trees' vegetation cover and their spectral similarity to other land covers such as natural forests and rubber plantations, mapping the distribution of oil palms using optical satellite remote sensing, particularly the image-based approach, is a difficult task (Gutiérrez-Vélez & DeFries 2013, Li et al. 2015, Torbick et al. 2016). In this study, geographic information systems (GIS) are used to evaluate land suitability for oil palm production and assess the land available for oil palm cultivation in Peninsular Malaysia using soil, climate, and land use data. Using data from the literature, we explain the agro-ecological conditions and develop environmental criteria that determine whether or not a region is an ideal place to grow oil palms. Identifying suitable land for oil palm cultivation as well as determining its yield is imperative for policymakers and entrepreneurs. In addition, this study will assist investors and the government in exploring suitable areas left for oil palm expansion in Peninsular Malaysia.

MATERIALS AND METHODS

The Study Area

Located between longitude 99° and 105° east, the study area

stretches between latitudes 1° and 7° north (Fig. 1). Malaysia is bordered on the North by Thailand; on the East by the South China Sea; on the South by the Strait of Johore; and on the West by the Strait of Malacca and the Andaman Sea, with a total boundary length of 2,068 km (Zulkifli et al. 2020). The Highlands, floodplains, and coastal zones dominated the region with a total land area of 132,000 km^2 (Abubakar et al. 2022a, 2022b). Peninsular Malaysia experiences a tropical climate all year round that is warm and humid (Sarkar et al. 2020). There is a temperature range of 25° to 32°C in the region (Abubakar et al. 2022a, 2022b). There are two monsoon seasons in the region: the southwest monsoon from May to September and the northeast monsoon from November to March, which is associated with high rainfall (Wong et al. 2009). Annual rainfall varies between 2000 and 4000 mm in the region (Muhammad et al. 2020, Abubakar et al. 2022a, 2022b).

Land Suitability Assessment

In Malaysia, as in many other countries around the world, land suitability maps are used to plan land use and identify areas that can grow crops at the lowest possible cost to the economy and the environment through land suitability assessments (LSAs) (Bandyopadhyay et al. 2009, Olaniyi et al. 2015, Mugiyo et al. 2021). Assessing the suitability of a piece of land for agriculture or determining whether it is suitable for its intended use is called land suitability assessment (Olaniyi et al. 2015). In general, land suitability assessments are conducted on locations based on their biophysical and ecological characteristics to assess their potential for agriculture (Olaniyi et al. 2015, Doula et al. 2017). To determine land and crop production suitability indexes, land features and site-specific comparisons with crop requirements are considered (Rhebergen et al. 2016).

In this study, geospatial overlay mapping is used to assess land suitability, where the criteria for evaluating the suitability of a site are recorded as layers overlaid one over the other (Malczewski 2004). A land suitability map is then produced from these layers by integrating them into a single data layer. The method we used allowed us to define

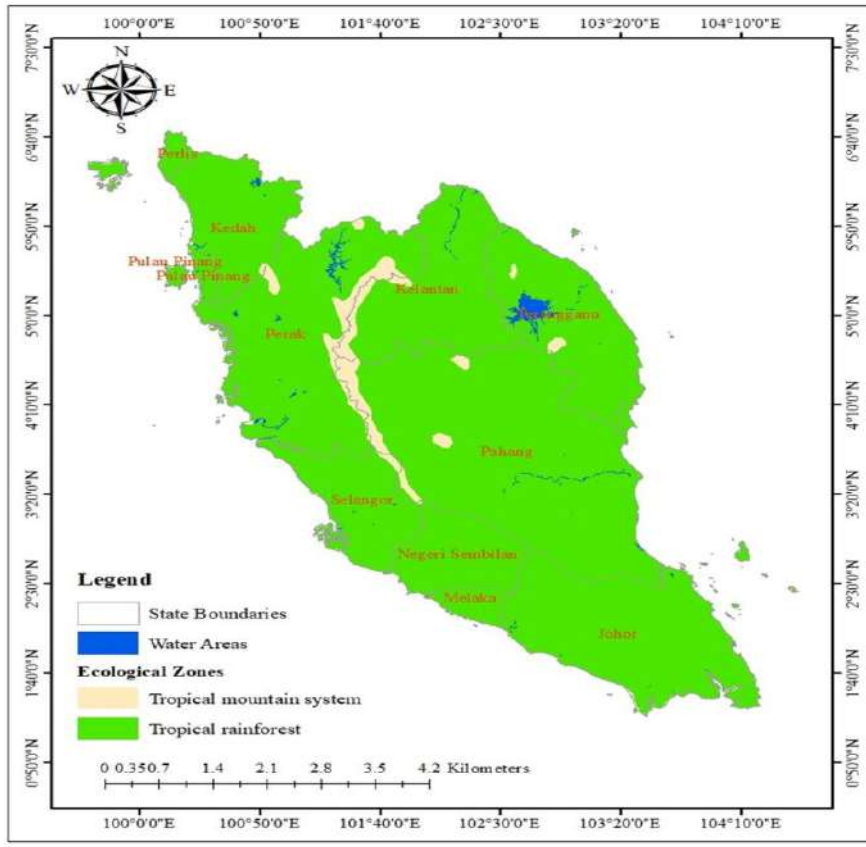

Fig. 1: Study area map.
Source: A Malaysian administrative map is adopted and modified, in 2022.

Table 1: Biophysical parameters indicating suitability for oil palm production.

Criterion	Suitability Class 4 (Highly suitable)	Suitability Class 3 (Suitable)	Suitability Class 2 (Moderate)	Suitability Class 1 (Unsuitable)
Mean annual rainfall (mm)	1700-2875	1450-1700	1000-1450	<1000
Annual mean temperature (°C)	>22	22-20	20-18	<18
Slope (°)	0-8	8-16	16-50	>50
Elevation (m)	0-1500	>1500	>1500	>1500
Mean annual water deficit	<150	<250	<400	>400
Soil texture	Clay loam	Sandy loam	Clay	Sandy
Solar radiation MJ M^{-2} day^{-1}	>16	16 - 21	< 21	> 21

both the suitable and the available locations in Peninsular Malaysia for oil palm cultivation. Based on mean annual water deficits, we identified climatically suitable oil palm production areas (Rhebergen et al. 2016). Oil palm yields are significantly affected by water scarcity (Corley & Tinker 2003, Rhebergen et al. 2016).

Rhebergen et al. (2016) argued that determining and grouping areas with similar climatic conditions for the production of oil palm can be accomplished by using mean annual water deficits. The authors further stated that generally, oil palm production is not feasible in areas with water deficits greater than 400 mm per year. In oil palm plants, it is assumed that the critical water deficit is 200 mm a year, after which growth and yield begin to suffer (Corley & Tinker, 2003). This assumption led us to define four categories of water deficit based on Olivin's suitability assessment methods (1968). An oil palm production feasibility study in Ghana by Rhebergen et al. (2016) utilized a similar approach. A water deficit approach, developed by Olivin (1968), and van der Vossen (1969) was used in this study to determine soil, climate, and land use suitability for oil palm production in Peninsular Malaysia.

i. Highly suitable zones with a mean annual water deficit of <150 mm;
ii. Moderate: zones with mean an annual water deficit of <250 mm;
iii. Suitable: zones with mean an annual water deficit of <400 mm; and
iv. Unsuitable: zones with mean an annual water deficit of >400 mm

Nonetheless, we categorized biophysical constraints into suitable and unsuitable areas based on climatic conditions (Table 1). After water deficit, rainfall, solar radiation, temperature, slope, and elevation are the most significant factors that influence oil palm yields (Paramananthan 2003). Rhebergen et al. (2016) argued that the amount of solar radiation suitable for oil palm production cannot be determined precisely because it is difficult to isolate its effect from other factors affecting production. When there is at least >16 MJ^{-2} day^{-1} of solar radiation per day, oil palm grows best (Oettli et al. 2018). In addition to reducing stomatal aperture and leaf temperature, excessive solar radiation can slow the rate of carbon dioxide absorption (Paramananthan 2011). Photodamage can also occur to the palms when they are exposed to high levels of solar radiation (Kasahara et al. 2002). Costly management interventions can only modify elevation out of these constraints.

In addition, this study examines protected areas and land uses, including national parks, forest reserves, world heritage sites, wetlands, and wildlife. A protected area is defined as geographical space, recognized, dedicated, and managed, through legal or other effective means, to achieve the long-term conservation of nature with associated ecosystem services and cultural values (Najihah et al. 2018). Population counts (people), settlement points, and light levels at night distinguish urban settlements from rural ones. Table 2 presents the data type and sources for this study.

Data Collection (Table 2)

Data Processing

Sentinel 2A Image Preprocessing

During the Level-2A processing, top-of-atmosphere (TOA) Level-1C, orthoimages are classified and atmospheric corrections are applied. Level-2A's main output is an orthoimage Bottom-Of-Atmosphere (BOA) corrected reflectance product. Level-2A output image products were resampled and generated with an equal spatial resolution for all bands (10 m, 20 m, or 60 m). There are three separate folders in the standard distributed product containing all resolution envelopes:

- 10m: containing spectral bands 2, 3, 4, 8, a True Color Image (TCI), and an Aerosol Optical Thickness (AOT) and Water Vapour (WV) maps resampled from 20 m.

Table 2: Data type and sources.

Data	Variable	Unit/Format	Resolution	Period/year	Source
Land Cover	Ecological Zones	- /Shapefile	-	-	https://data.review.fao.org/map/catalog/srv/eng/catalog.search#/metadata/74bab234-3a1e-442d-93cf-0b34859e9a60 Accessed 07/06/2022
Urban extent	Urban places	- /Shapefile	-		https://sedac.ciesin.columbia.edu/data/set/grump-v1-urban-extents/data-download
Rainfall	Average monthly rainfall	mm $month^{-1}$/Raster	30 arc-seconds (~ 1km)		https://www.worldclim.org/ Accessed 20/06/2022
Temperature	Minimum, maximum, and mean temperature (monthly) The temperature of the coldest month	^{o}C/Raster	30 arc-seconds (~ 1km)		https://www.worldclim.org/ Accessed 15/06/2022
Solar radiation	Average monthly solar radiation	$kJm^{-2}day^{-1}$	30 arc-seconds (~ 1km)		https://www.worldclim.org/ Accessed 15/06/2022
Digital Elevation Model (DEM) of Shuttle Radar Topography Mission (SRTM)	Elevation	Meters (above sea level)	3 arc-seconds (~ 100m)	2008	https://srtm.csi.cgiar.org/srtmdata/ Accessed on 20/06/2022
Soil Properties	Soil type	Unit/Shapefile	-	2012	https://www.fao.org/soils-portal/soil-survey/soil-maps-and-databases/harmonized-world-soil-database-v12/en/ Accessed 18/06/2022
	Soil texture	%/Raster	30 arc-seconds (~ 1km)		
Sentinel 2A	Satellite Imagery	-/Raster	10m		https://scihub.copernicus.eu/dhus/#/homeAccessed 12/02/2022
Protected area	Protected areas	- /Shapefile	-	-	https://www.protectedplanet.net/country/MY Accessed 18/06/2022
Population	Inhabitants' population	-/Raster	30 arc-seconds (~ 1km)		https://sedac.ciesin.columbia.edu/data/collection/gpw-v4 Accessed 13/07/2022
MODIS Terra NDVI data (MOD 13)	NDVI	Raster	1km		Land Processes Distributed Active Archive Center (LP DAAC), NASA. Accessed 18/02/2021

- 20m: containing spectral bands 2-7, the bands 8A, 11, and 12, a True Color Image (TCI), a Scene Classification map (SCL), and an AOT and WV map. The band B8 is omitted as B8A provides more precise spectral information.
- 60m: containing all components of the 20 m product resampled to 60 m and additionally the bands 1 and 9. The cirrus band 10 is omitted, as it does not contain surface information.

A tool known as Sen2Core in SNAP software was used in the preprocessing (Pałas & Zawadzki 2020). Combined with a scene classification module, Sen2Cor uses state-of-the-art atmospheric correction techniques tailored to the Sentinel-2 environment (Muller-Wilm et al. 2013, Skakun et al. 2022). However, the scene classification algorithm allows the detection of clouds, snow, and cloud shadows and the generation of a classification map, which consists of three different classes for clouds (including cirrus), together with six different classifications for shadows, cloud shadows, vegetation, not vegetated, water and snow (Hughes & Hayes 2014, Zekoll et al. 2021).

The preprocessed images were imported to ArcGIS for layer stacking. Band 4, band 3, and band 2 were used respectively to obtain the natural color combination 432.

The image was then mosaic using the mosaic operator to the new raster tool.16-bit unsigned was used for the pixel type, the mosaic operator was set to maximum and a mosaic color map was set to match. The image was then clipped using the respective shape file of the states.

Image Classification

The unclassified images were subjected to clustering of similar spectral signatures for different LULC classes in ArcGIS. Four temporary classes were generated (water bodies, built-up areas, bare surfaces, and vegetation). Field sampling was done with the help of high-resolution (Google Earth Imagery) using the printed (unsupervised) map. The information generated using high-resolution images includes areas that have mixed clusters like water bodies and vegetation, built-up areas, cropland, etc. During the data collection, different feature identifiers (IDs) were generated for all the land uses, and the data was collected from on-screen digitization and photographs of the identified land uses.

As part of supervised classification, it is essential to identify the types of information that are relevant to the image (e.g., land cover types). Based on the reflectances for each information class, the software system develops a statistical characterization (see Table 3). The signature analysis stage involves deriving a characterization of the reflectance on each band, such as the mean or the range, or it may involve analyzing the variances and covariances of all bands systematically. As soon as a statistical characterization is obtained for each information class, a classification decision is made based on which signature the image most closely resembles based on the reflectance of each pixel. Table 3 presents the description of land cover categories used

A supervised maximum likelihood classification (MLC) method in ArcGIS was used, creating training samples from the acquired data generated from the Google Earth imagery to create the classes required for the LULC map.

Accuracy Assessment

The process of classification requires the assessment of accuracy. In the investigation area, the objective is to determine if pixels were grouped into the appropriate feature classes. However, one basic accuracy measure is the overall accuracy, which is calculated by dividing the correctly classified pixels (sum of the values in the main diagonal) by the total number of pixels checked.

Table 3: Detailed descriptions for each land cover category.

LULC Type	Description
Water Body	Lakes, ponds, rivers, wetlands, and reservoirs
Built-Up Area	Transportation, business, and residential services
Vegetation	All types of plants, including parks, playgrounds, trees, grasslands, forests, and shrublands
Bare Surface	Landfills, open spaces, and bare soils

Overall accuracy (%) = (correctly classified pixels/total number of pixels) …(1)

1. In addition to the overall accuracy, each class can also be classified with an equal degree of accuracy. Further, we need to determine how the accuracy is distributed across the categories because the overall accuracy doesn't indicate how it is distributed. The overall accuracy method, however, considers these categories as having equivalent or similar accuracy even though the categories could have dramatically different accuracy values. To determine the accuracy of individual categories, there are two methods available (Bharatkar & Patel 2013).
2. Therefore, Users' accuracy is calculated by dividing the number of correctly classified pixels by the total number of pixels classified in a LULC class – The percentage of correctly classified classes is of concern to users (Bharatkar & Patel 2013).

$$\text{User's accuracy (\%)} = \frac{\text{Correctly classified pixels}}{\text{Classified total pixels}} \quad \ldots(2)$$

For a particular LULC class, The producer's accuracy is the ratio between correctly classified pixels and reference pixels (Bharatkar & Patel 2013, Rwanga & Ndambuki 2017).

$$\text{Producer's accuracy (\%)} = \frac{\text{Correctly classified pixels}}{\text{Reference total pixels}} \quad \ldots(3)$$

Therefore, the Producer's accuracy (%) = (Correctly classified pixels/Reference total pixels) (Bharatkar & Patel 2013).

A summary of each classification's accuracy is shown below;

- Commission error = 1 - user's accuracy
- Omission error = 1 - producer's accuracy
- The kappa coefficient (K) can be computed as follows,

$$K = \frac{P_0 - P_c}{1 - P_c} \quad \ldots(4)$$

Where P_0 = Proportion of units that agree = overall accuracy

P_c = Proportion of units for expected chance agreement

Therefore, The general range for Kappa values is if K

< 0.4, a poor kappa value; while, if 0.4 < K< 0.75, is a good kappa value and if K > 0.75, it is an excellent kappa value (Bharatkar & Patel 2013).

The accuracy assessment was carried out using ArcGIS pro 2.4 in which a stratified sampling method was used.

Data Analysis

The data used in this study was preprocessed and corrected in the ArcGIS environment. Raster grid data is a subset to the extent of Peninsular Malaysia's boundaries using the administrative map of the country. Inverse distance weighted (IDW) interpolation was used to generate maps of rainfall and temperature. To accomplish this, ArcGIS Spatial Analyst was used. The climatic data were organized in Microsoft Excel, saved as a comma-separated value (CSV), and imported as points into ArcGIS, where they were interpolated to generate climatic element maps. A map of the study area was used to delineate the Digital Elevation Model (DEM) of the area from Shuttle Radar Topographic Mapper (SRTM) data in the ArcGIS environment. To georeference the maps, WGS 1984 coordinates were used. After that, the DEM was used to generate the slope map for the area.

One of the most efficient and inexpensive methods for estimating evapotranspiration (ET) is remote sensing, which offers regional and global coverage efficiently and economically (Anderson et al. 2012, Weiss et al. 2020), especially when combined with meteorological data (Salmon et al. 2015). The direct measurement of actual evapotranspiration (AET) is very rare globally (Bates et al. 2008). Based on meteorological data describing climate variations and land use data describing vegetation changes, an alternative solution would be to predict ET variations by using mathematical models (Yang et al. 2008). Whatever the method applied, the spatial scale of the computed value depends on the method used to estimate the ET (Liou & Kar 2014). Climate station-based techniques are rare and produce point estimates, but with the use of the coordinate point of each station, it can be applied in the geographical information system (GIS) to assess the spatial and temporal variation of ET (Hengl et al. 2012). Satellite remote sensing methods are capable of estimating the biophysical properties of land from one pixel up to the regional scale with a certain degree of accuracy (Liou & Kar 2014).

Crop Coefficient ET Estimation Methods

As defined by Jensen et al. (1990), crop coefficients are derived from experimental correlations between actual ETs measured from a specific crop and ETs from a reference crop. To calculate reference ET, one must calculate weather data for a defined reference crop, such as alfalfa or grass, and then use the crop coefficient (Kc) to calculate the ET for a specific crop (Allen et al. 2005, Anapalli et al. 2020).

An important method for managing irrigation water is to estimate AET using the crop coefficient (Kc) (Kamble et al. 2013). ETc estimates derived from the Kc method can differ significantly from actual crop ETc estimates (Allen et al. 2005)

According to Allen et al. (2005) and El-Shirbeny et al. (2014), the crop coefficient (Kc) is a dimensionless number (usually between 0.1 and 1.2) used to calculate the actual evapotranspiration (AET). Using satellite data, Kamble et al. (2013) estimate Kc by evaluating NDVI and the relationship between NDVI and Kc.

$$K_C = \frac{1.2}{NDVI_{dv}}(NDVI - NDVI_{mn}) \quad \ldots(5)$$

Therefore, where; 1.2 is the maximum Kc, $NDVI_{dv}$ is a difference between the minimum and maximum NDVI value for vegetation and $NDVI_{mn}$ is the minimum NDVI value for vegetation (El-Shirbeny et al. 2014).

To calculate monthly potential evapotranspiration, we converted solar radiation into water equivalents for each month based on latitude and year (Hargreaves & Samani 1982). To better reflect potential evapotranspiration (ETP), we included more climatic variables. Using the Hargreaves equation, we estimated ETP (Rhebergen et al. 2016):

$$ETP = 0.0023 \times Ra \times (T - t)^{0.5} 0(t_m + 17.8) \quad \ldots(6)$$

Where:

ETP = Evapotranspiration in mm/day

Ra = Expressed as water equivalent, extraterrestrial solar radiation (mm/day)

T-t = Monthly maximum and minimum temperature difference (°C)

tm = Means air temperature (°C)

Water requirements for crop modeling have been estimated using this method (Kra & Ofosu-Anim 2010). As opposed to Penman-Monteith, this method requires less data (Allen et al. 1998), and similar results are produced by both methods (Hargreaves & Allen 2003). A monthly difference was calculated between the mean maximum and minimum temperatures in the study area using WorldClim climatic variables to generate the ETP layer (Läderach et al. 2013).

A mean annual water balance was calculated from ETP (Surre 1968). All monthly negative water balances were added up to calculate the annual water deficit. A total of 28 meteorological stations provided data on rainfall. There

are some stations on commercial palm plantations, while others are on smallholder plantations. Within the oil palm belt, production sites have various rainfall (mm month^{-1}) distributions. Based on our suitability assessment and Surre's method (1968), we calculated the average annual water deficits for each site. We identified potential oil palm production areas on potentially available land by combining land use data. The maps we used for land suitability excluded protected areas and urban settlements.

The normality test is conducted to determine if climatic data is normally distributed. Empirical probability distributions can be used to analyze normally distributed data. The commonly used test of normality is the Anderson-Darling (A-D) statistic, defined as:

$$A_n^2 = \int_{-\infty}^{\infty} |F_n(x) - F(x)|^2 \Psi(x) f(x) d(x) \quad \ldots(7)$$

Where:

$$\Psi(x) = {}^{n}/_{F(x)\{1 - F(x)\}}$$

n = Data points totaled for the study;

F(x) = distribution function of the fitted distribution;

$f(x)$ =density function of the fitted distribution;

$$F_n = \frac{i}{n}$$

i = The cumulative rank of the data point.

A-D statistics are generally considered to be more useful than K-S statistics because they can account for tail distributions as well as main distributions. This normality test is based on the following hypotheses (Anderson- Darling normality test):

H_0: Data is from the population with a normal distribution;

H_1: Data is not from a population with a normal distribution;

Data distributed normally can be assessed by the Anderson-Darling p-value. Therefore, if the distribution fits the data, the A-D statistic will be small and the associated p-value will be greater than the chosen alpha-level (0.05 and 0.10). AddinSoft Xlstat software was used to analyze the data using the Anderson-Darling Normality test.

SPSS 22 version and Microsoft Excel software were used to compute Mann-Kendall and Sen's slope trend analysis.

We calculated Actual Evapotranspiration, or AET, by combining Kc (from satellite images) with ET (from meteorological station observations). To conduct the analysis, ArcGIS was used.

$$AET = K_C \times ET \quad \ldots(8)$$

Where;

AET = Actual evapotranspiration [mm d^{-1}],

Kc = Crop coefficient [dimensionless],

ET = Reference evapotranspiration [mm d^{-1}].

The difference between AET and PET was used as an agricultural water deficit

Water deficit was generated herein to reflect the agricultural water deficit (AW_D) using the following formula

$$AW_d = PET - AET \quad \ldots(9)$$

Where; AW_D: is the Evapotranspiration deficit defined as the difference between potential water demand (PET) and the actual water supplied (AET) for vegetation. Agriculture experiences more water stress when PET is larger. Agricultural water stress is commonly measured using PET as the measure of crop water stress (Yin et al. 2022).

RESULTS AND DISCUSSION

Land Use Areas Suitable for Palm Production

Fig. 2 presents the Land Use Land Cover Map of Peninsular Malaysia showing suitable areas for oil palm production to cover an average of 10885001.46ha (82.45%), water bodies (1239505.58ha (9.39%), built-up areas (unsuitable areas) 1051544.34ha (7.96%), and bare surface areas that are also areas not suitable for oil palm production (26509.73ha (0.20%). Consequently, many vegetation areas, some of which are sensitive to environmental issues, have been cleared as a result of oil palm spread. Land conversion for oil palm cultivation impacts land use in varying ways, focusing on current land conversion and future land demand projections. In the future, this will be beneficial to the industry. A range of land use options was explored to minimize the pressure on land to be opened up for development and minimize monoculture dependence (Basiran & Ja'afar 2022).

Oil palm plantations are continuously being expanded in

Table 4: Statistics of Land Use Land Cover areas suitable for oil palm production.

Land use Land cover	Area (ha)	Percentage (%)
Vegetation (Suitable)	10885001.46	82.45
Water bodies	1239505.58	9.39
Built-up area (Unsuitable)	1051544.34	7.96
Bare surface	26509.73	0.20
Total	13202561.11	100.00

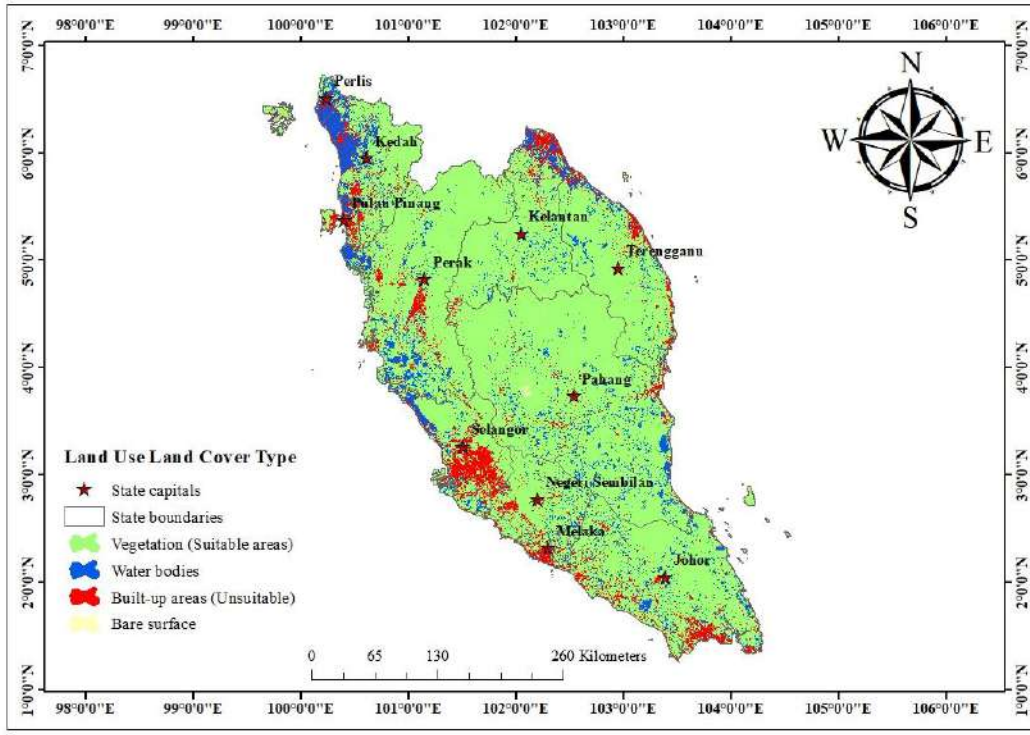

Fig. 2: Land Use Land Cover Map showing Suitable areas for Oil Palm production in Malaysia Peninsular.

Malaysia and Indonesia, and as a result, are accountable for over 85% of global palm oil demand (Tang & Al Qahtani 2020). The growth in the planted area in Peninsular Malaysia from 1975 to 2020 is shown in Fig. 3. Oil palm was planted on

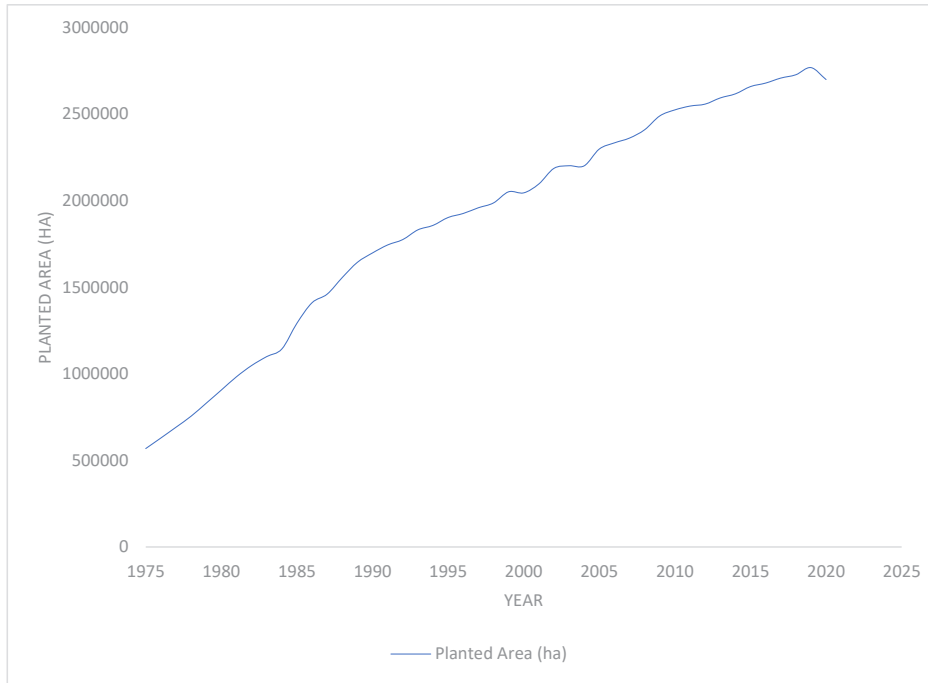

Fig. 3: Oil Palm area planted in Peninsular Malaysia (1975-2020).

2,769,003 hectares in Peninsular Malaysia in 2019 (see Fig. 3) and this was projected to be 4,560,479 hectares, 3,489,022 hectares, and 5,930,442 hectares for the years 2040, 2080, and 2100, respectively (Abubakar et al. 2022). It is unclear whether Malaysia will be able to achieve this target given its ongoing economic and political uncertainties.

The Tennarmaram Estate was the first to commercially plant oil palm in 1917 (Abubakar et al. 2022). A crop diversification program carried out by the government in the 1960s eventually led to the planting of oil palms on a large scale (Teoh 2000). Growth in planted areas of oil palm revealed that in 1975, 1976, and 1977, planted areas of oil palm covered about 568561 ha, 629558 ha, and 691706 ha, respectively. While the areas increased in 2018, 2019, and 2020 to 2,727,608 ha, 2,769,003 ha, and 2,700,004 ha, respectively (see Fig. 3) (Malaysian Palm Oil Board 2020). Oil palm plantations expanded rapidly in 2019 but slowed in 2020 as global economic growth slowed. In 2020, oil palms occupied 5.865 million hectares, down 0.6% from 5.900 million hectares in 2019 (Malaysian Palm Oil Council 2022). This might be on account of an increasing shortage of manpower and the economic impact of COVID-19. The Sabah and Sarawak parts of Malaysia offer greater land availability for the expansion of oil palm plantations. Sabah and Sarawak started developing their oil palm industries in the 1970s as Peninsular Malaysia expanded its oil palm planting in the late 1950s and early 1960s (Khiabani & Takeuchi 2020). In Fig. 3, we see how planted areas have increased over the last several decades.

In a rapidly growing economy such as this, protected areas are crucial to oil palm production (Kanniah et al. 2015). As one of the world's most biodiverse countries, Malaysia is home to some of the oldest rainforests in the world (see Fig. 4). With a GDP of USD 296.2 billion at present, the economic growth rate of Malaysia is 36th in the world (Tulayasathien & Tejapaibul 2017). With almost half of Malaysia's forest cover disappearing since the 1940s, Malaysia's rapid economic growth is negatively impacting the environment. The charismatic Malayan Tiger has also declined rapidly in this region (*Panthera tigris* Jacksoni) (Ten et al. 2021). The wild population has decreased by 10% since 1950 to only 300 individuals (Holzner et al. 2021).

There are 13.2% of protected areas in Peninsular Malaysia. The federal government or the state government

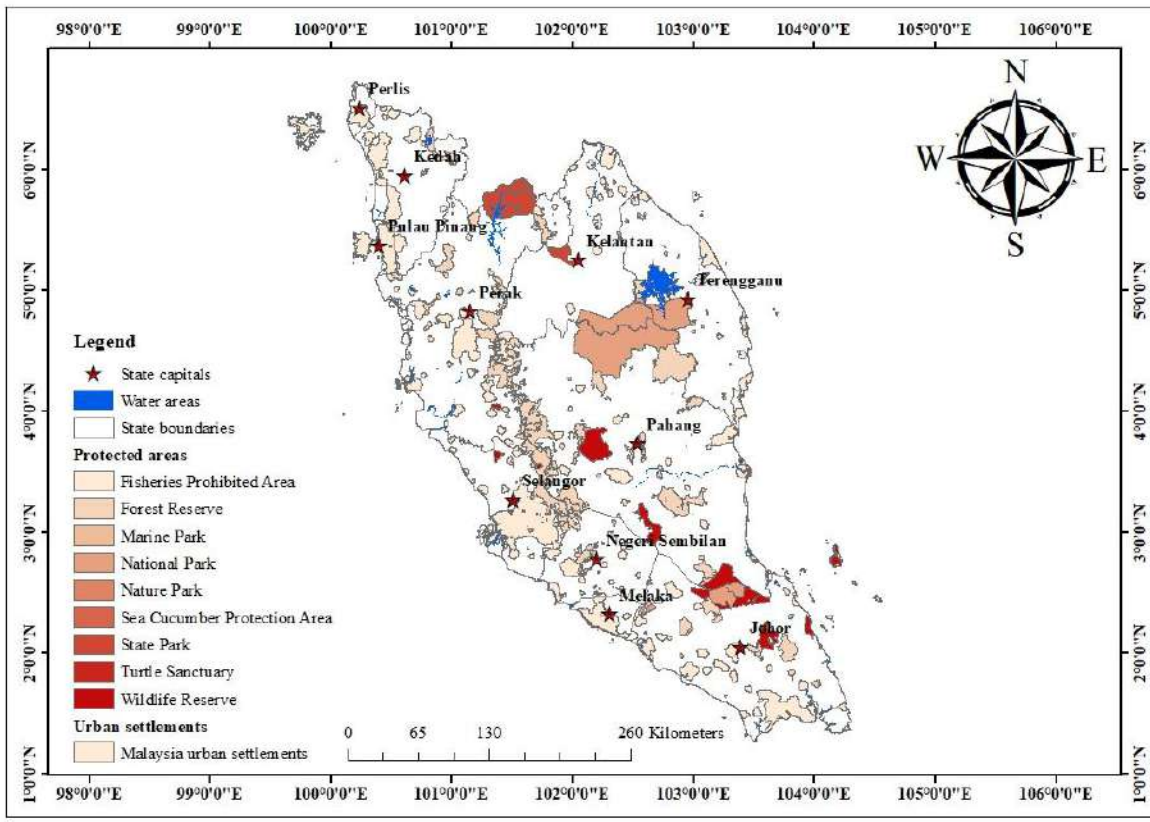

Fig. 4: Potential area for oil palm expansion excluding settlement and protected areas.

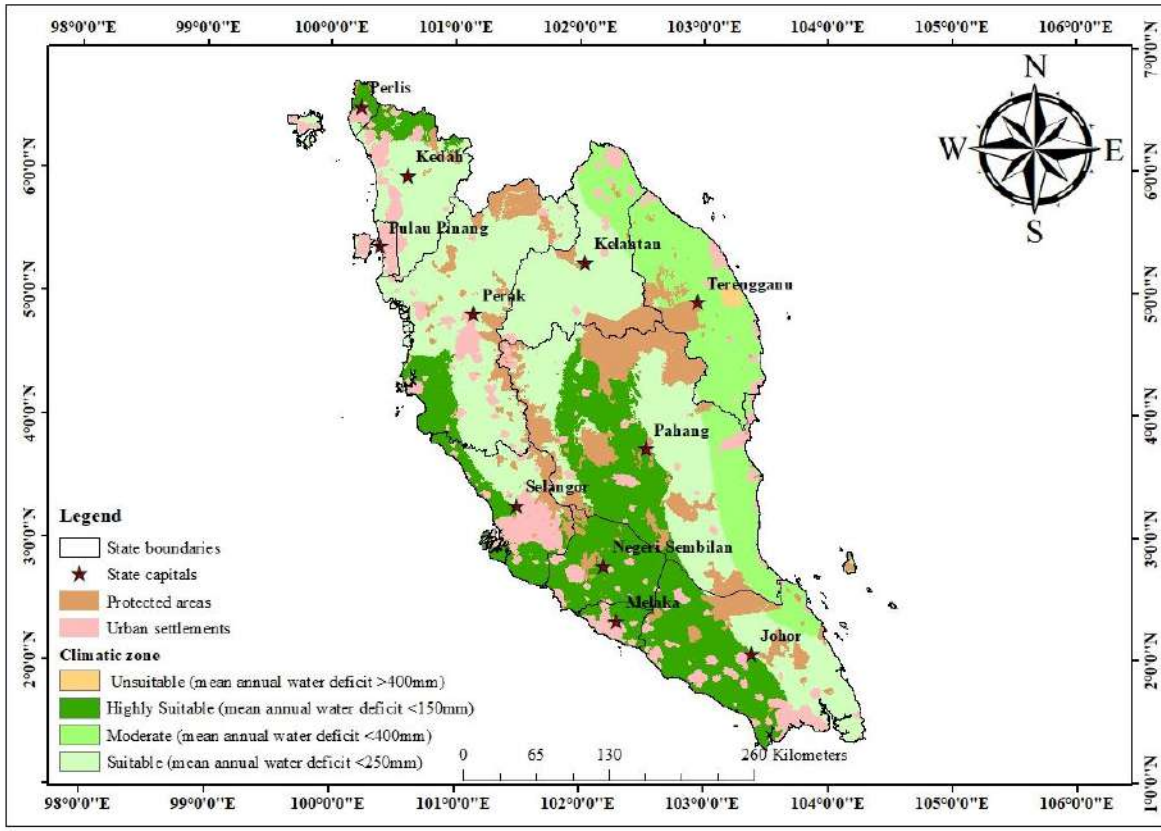

Fig. 5: Climatic zone (water deficit) suitable for oil palm production in Malaysia Peninsular.

manages protected areas (Najihah et al. 2018). At present, there is no system of national protected areas. Land and forest are deemed state matters by Malaysia's constitution, so establishing protected areas is a challenge (Schwabe et al. 2015). In addition to natural resources, states view them as revenue streams to fuel development (Hezri & Nordin Hasan 2006). Fisheries-prohibited areas, forest reserves, marine, and national parks, sea cucumber protection areas, turtle parks, turtle sanctuaries, and wild reserves are the major protected areas in Peninsular Malaysia and could be among the most suitable land left for oil palm production.

Many lowland forests (Fig. 4) have been cleared to expand oil palm production. Concerns have been raised about how future oil palm developments will affect environmental quality, especially for the remaining forest land (Basiron & Weng 2004, Ferdous Alam et al. 2015, Tang & Al Qahtani 2020).

Climatic Zones Suitable for Palm Production

Highly suitable areas were estimated (mean annual water deficit <150mm) for oil palm in Peninsular Malaysia to be 3688254.00 ha (29.54%) of the total land area (Fig. 5).

These areas were found mostly around the north-central and northwestern parts of the Peninsular. Suitable areas (mean annual water deficit <250mm) was 6540669.00 ha (52.38%), moderately suitable areas were (mean annual water deficit <400mm) 2227500.00 ha (17.84%) while unsuitable areas (mean annual water deficit >400mm) for oil palm production as a result of poor water availability was 31104.00 ha (0.25%) (Table 4). However, moderate and unsuitable areas for oil palm production in Peninsular Malaysia were decreased compared to Murphy et al. (2021) and Paterson (2020) projections as a result of increasing cultivation, which poses a negative environmental impact, threatening sustainability. The results of this study demonstrate that Malaysia's oil palm production may be threatened by climate change. On a broad scale, climate change will affect the distribution of oil palm production.

Furthermore, Malaysia has a humid and tropical climate (Abubakar et al. 2021). Mountains and complex interactions between land and sea greatly influence the climate (Abubakar et al. 2022a, 2022b). However, recent years have seen a

Table 5: Statistics of Climate suitability (water deficit) for oil palm production.

Climatic Zone (Water deficit)	Area [ha]	Percentage [%]
Highly Suitable (mean annual water deficit <150 mm)	3688254.00	29.54
Suitable (mean annual water deficit <250 mm)	6540669.00	52.38
Moderate (mean annual water deficit <400 mm)	2227500.00	17.84
Unsuitable (mean annual water deficit >400 mm)	31104.00	0.25
Total	12487527.00	100.00

rise in mild climate-related disasters. The socio-economic status of the country was significantly impacted by floods and droughts (Abubakar et al. 2021). Landslides caused by excessive rainfall and strong winds caused minimal damage to hills and coastal areas. (Abubakar et al. 2021). As a function of the area covered by biodiversity, Malaysia is the second-richest country in Southeast Asia, after Indonesia, with 0.2% of the world's landmass. According to the 2001 Global Diversity Outlook, Malaysia is one of twelve countries with mega-diversity (Abdul Rahman 2018).

Soil Properties Suitable for Palm Production

On the west coast of the Peninsular, suitable soil is primarily found for oil palm cultivation in a state like Selangor and some parts of Kedah with clay loam and sandy loam soil properties, while in the southern region like Johor, moderate suitability of oil palm production was noticed due to the domination of clay-soil in the area. However, sandy soil is only found in a very small area and is not suitable for the production of oil palm (Fig. 6). Kome et al. (2020) argued that climate in the coastal plains of southwest Cameroon did not pose a serious constraint on oil palm production, but oil palm production, however, is limited by soil physical characteristics (primarily clayey texture and poor drainage) and soil fertility.

The impact of climate on soil structure is complex (Várallyay 2010). It is raindrops, surface runoff, and filtrating water that have the greatest direct impact on aggregate destruction. In particular, climate change is contributing to more intense, frequent, and heavy rainstorms, especially during heavy rains and thunderstorms (Ashton-Butt et al. 2018). Changes in vegetation patterns and land use practices cause indirect influences. It is possible to boost fertility by

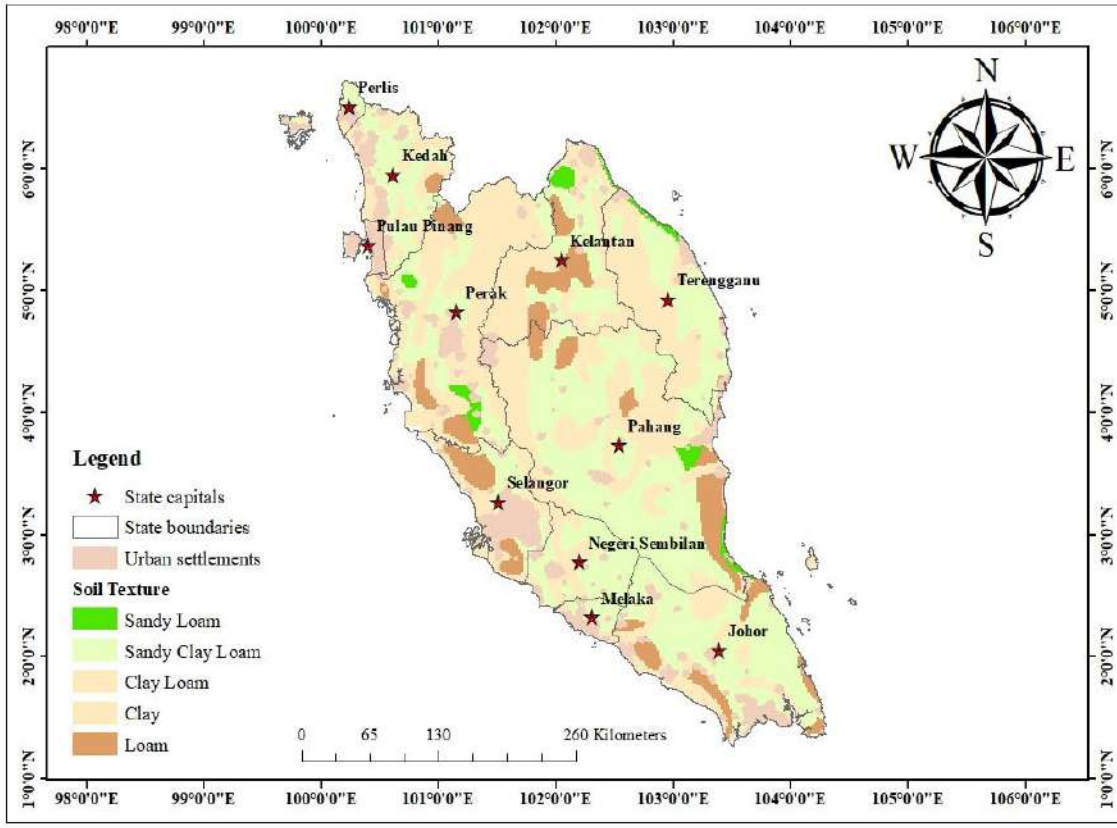

Fig. 6: Soil texture of Peninsular Malaysia showing areas suitable for oil pal production.

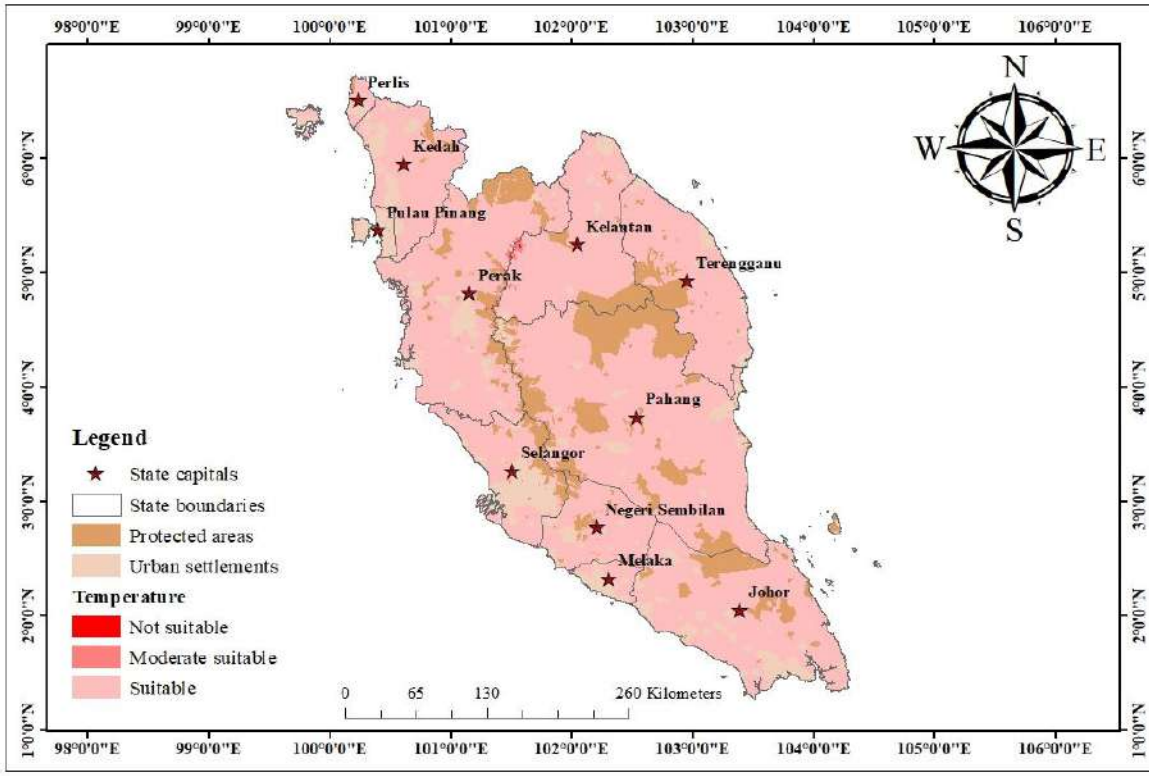

Fig. 7: Climatic zone (Temperature) suitable for oil palm production in Malaysia Peninsular.

using mineral fertilizers and crop residues (Fu et al. 2021). As most soils in the oil palm belt drain well, drainage criteria were not considered in the assessment. Fertile soils are found in the valleys (Annan-Afful et al. 2005); high rainfall periods often cause flooding and water-logging, so they often require costly drainage to avoid flooding (Rhebergen et al. 2014).

Fig. 7 and Table 6 reveal the climatic suitability areas (ha) for oil palm production in Peninsular Malaysia under the influence of temperature (degrees Celsius). Unsuitable areas cover about 6318.00ha (0.05%), moderately suitable areas 95337.00ha (0.76%), while the suitable areas cover a large area of about 12385872.00ha (99.19%).

Table 6: Statistics of Climate suitability (Temperature) for oil palm production

Climatic Zone (Temperature in degree Celsius)	Area (ha)	Percentage (%)
Temperatures <18	6318.00	0.05
Temperatures 18 – 20	95337.00	0.76
Temperatures >18	12385872.00	99.19
Total	12487527.00	100.00

The uplifted edges are found at elevations <1500 asl which cover 12396321.00 (99.45%) and has mean monthly minimum temperatures above >18^{o}C, which signifies suitability for oil palm production in the area (Fig. 7, 8 and Table 5, 6), while the unsuitable areas are at elevation >1500 covers an average area of 68283.00 (0.55%) (Table 7). Slope suitable areas (Fig. 9 and Table 9) reveal the areas with suitable slopes, estimated within the limits for oil palm at 12192606.00ha (99.83%). Almost all slopes >50, 12192606.00ha (99.83%) in the study area were removed from climatically suitable areas for oil palm cultivation. In suitable climate zones, the oil palm belt has undulating terrain with slopes between 0 and 30 degrees. Rendana et al. (2022) disclosed that a gently sloping flank or a low gradient slope margin would be a suitable place to plant oil palm. Urban settlements and protected areas were excluded

Table 7: Statistics of Elevation suitability for oil palm production

Elevation (degrees)	Area (ha)	Percentage (%)
Elevation 0 - 1500m	12396321.00	99.45
Elevation > 1500m	68283.00	0.55
Total	12464604.00	100.00

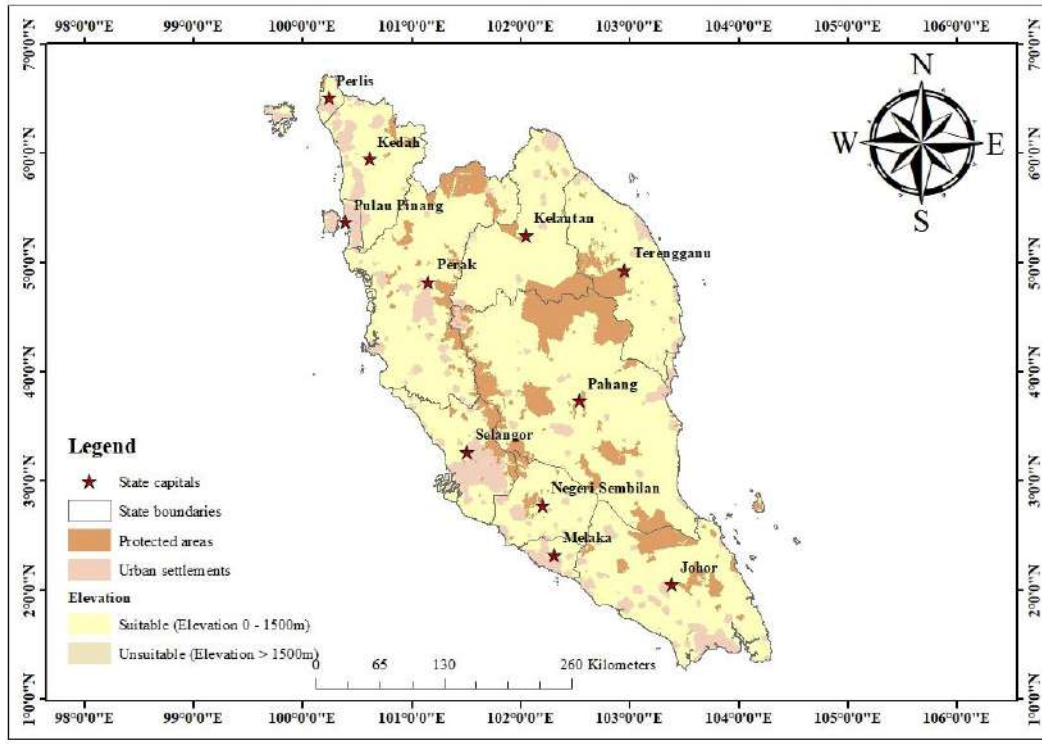

Fig. 8: Elevation areas climatically suitable for oil palm production in Peninsular Malaysia.

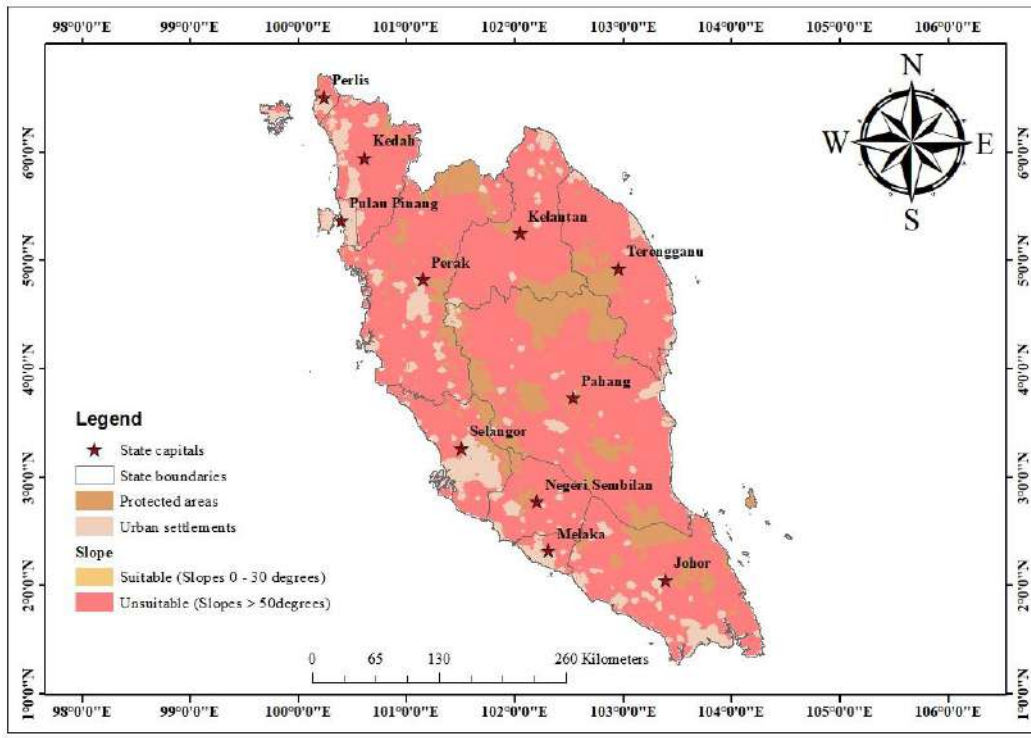

Fig. 9: Slope map showing areas that are climatically suitable for oil palm production in Peninsular Malaysia.

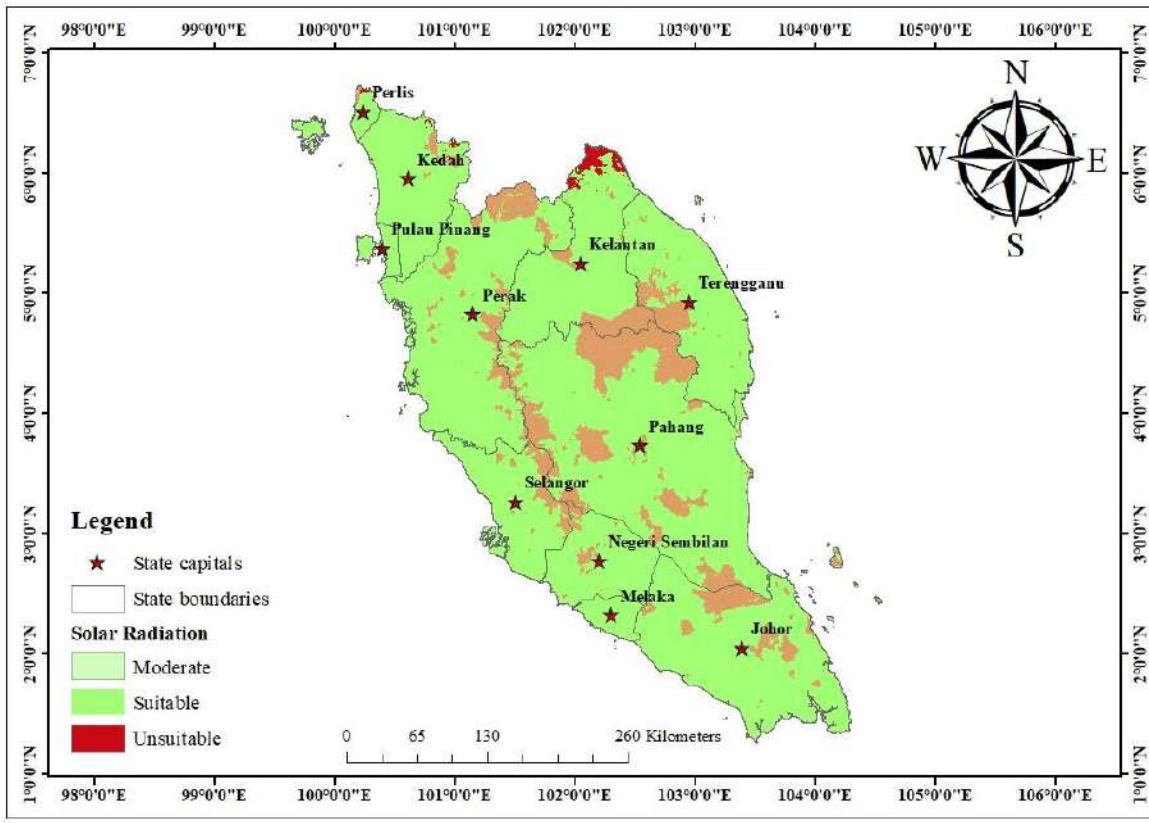

Fig. 10: Solar radiation zones climatically suitable for oil palm production.

from this calculation. Oil palm cultivation has declined due to a shrinking amount of suitable land (Fig. 9). Montgomery et al. (2016) argued that the reduction in agricultural land value has been caused by urbanization and industrialization

Fig. 10 depicts the climate suitability (Solar radiation MJ M^{-2} day^{-1}) area. Within the limits for oil palm production, suitable estimated solar radiation is 12399561.00ha (99.30%), moderate suitable 81.00ha (0.00%), and unsuitable 87885.00ha (0.70%) (Table 8). Fig. 11 presents the annual variation in the monthly average of daily solar radiation, while Fig. 12 presents the mean annual variation of solar radiation at the oil palm plantations region in Peninsular Malaysia.

Table 8: Statistics of climate suitability (Solar radiation) for oil palm production.

Climatic Zone (Solar radiation in MJ M^{-2} day^{-1})	Area (ha)	Percentage (%)
Moderate Suitable (Solar Radiation)	81.00	0.00
Suitable (Solar Radiation)	12399561.00	99.30
Unsuitable (Solar Radiation)	87885.00	0.70
Total	12487527.00	100.00

Climate, Land and Soil Suitability Analysis

To guide governments and policymakers in making decisions, a basic methodology was used to evaluate how much reasonable and accessible land is available in Peninsular Malaysia for oil palm cultivation. The results give a bedrock to the conversation of the ongoing debate on the development of oil palm in the nation and underline the significance of assessing the climatic elements that decide the ongoing and future production of oil palm in the country. Findings from the study reveal that a larger area was found to be suitable for oil palm production in Peninsular Malaysia than that identified by Abubakar et al. (2022). The observed differences may be explained by different methods for determining suitability, although climate variability is

Table 9: Statistics of slope suitability for oil palm production.

Slope	Area [ha]	Percentage [%]
Slopes 0 – 30	20331.00	0.17
Slopes > 50	12192606.00	99.83
Total	12212937.00	100.00

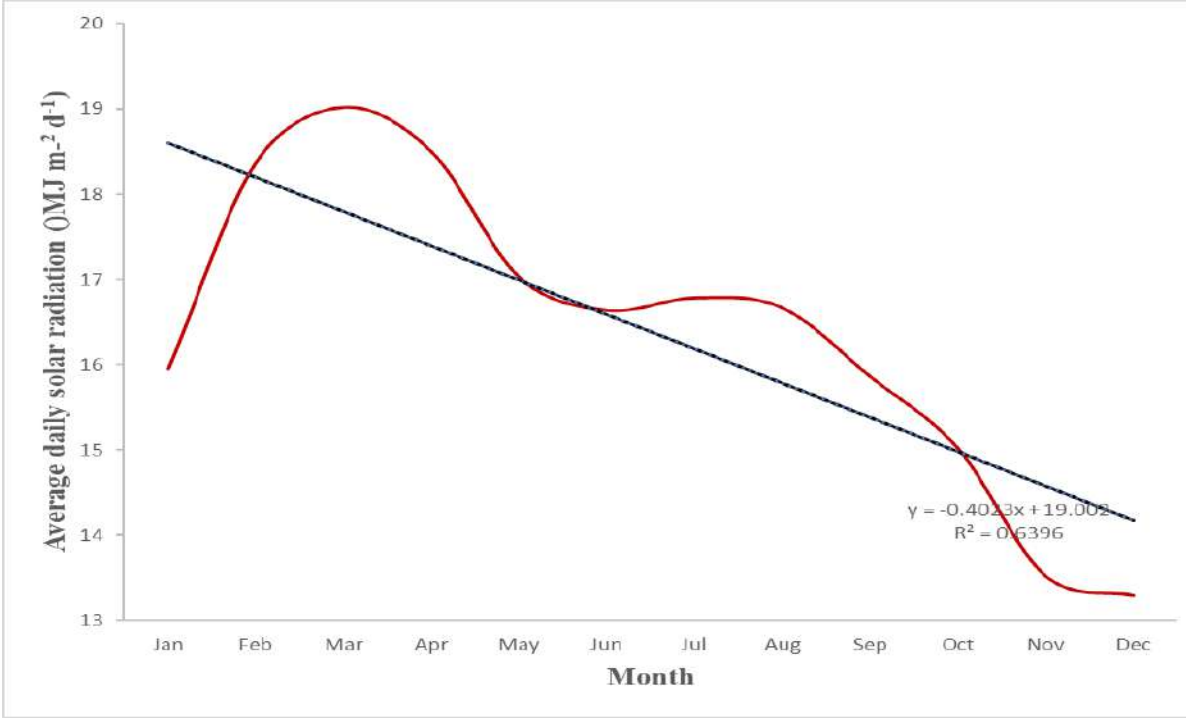

Fig. 11: Annual variation in the monthly average of daily solar radiation at oil palm plantations region in Peninsular Malaysia.

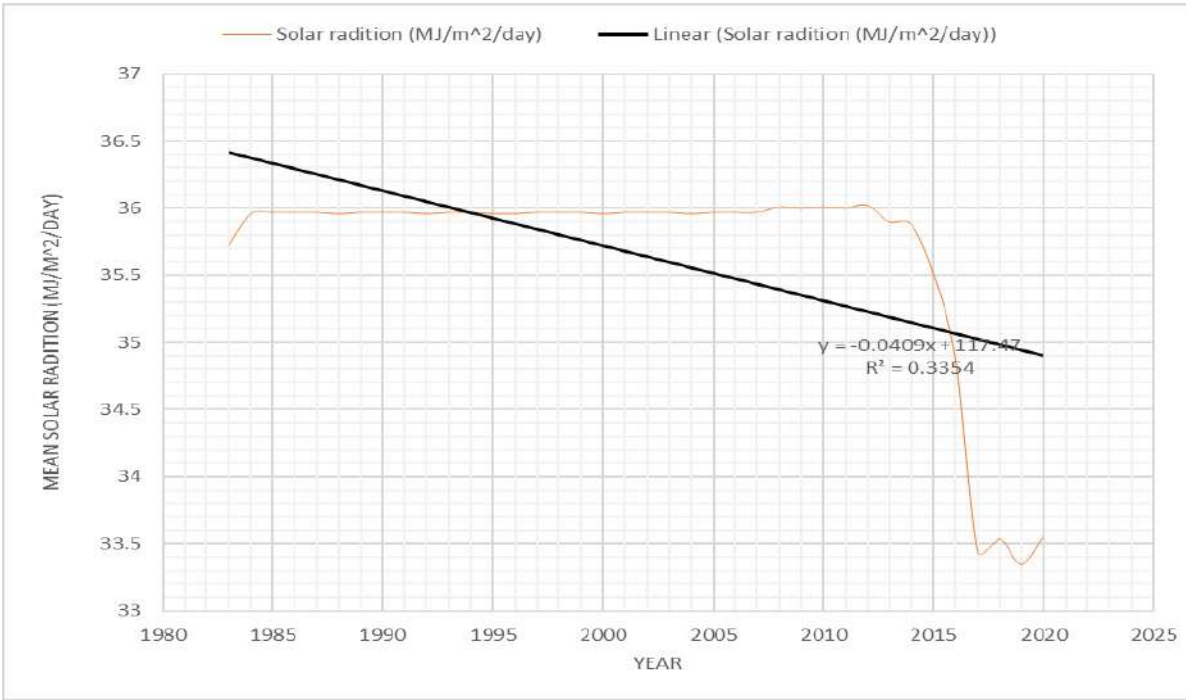

Fig. 12: Mean Annual variation of solar radiation at oil palm plantations region in Peninsular Malaysia from 1983 to 2020.

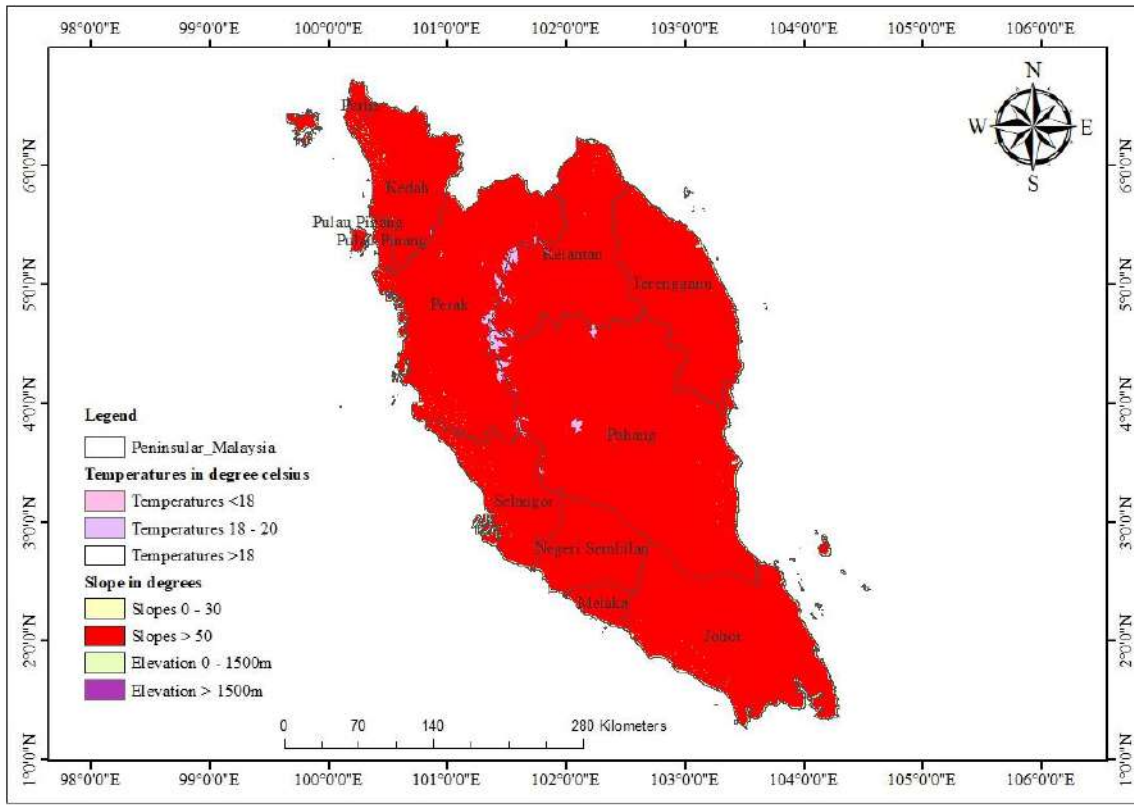

Fig. 13: Combine temperature, slope, and elevation map showing areas climatically suitable for oil palm production in Peninsular Malaysia.

another factor. Fig. 13 shows the combined temperature, slope, and elevation map showing areas climatically suitable for oil palm production in Peninsular Malaysia.

The data on climate, soil, and land use for this study were more detailed than those that were used by Rhebergen et al. (2016). Oil palm production can be made more sustainable with improved knowledge of environmental parameters. Remote sensing and GIS methodologies can explain observed changes in evapotranspiration and water deficit (Mustafa et al. 2011). A land suitability assessment would greatly aid in enhancing and validating the suitability analysis by simulating and analyzing oil palm production under varying climate conditions. The oil palm belt climate has changed dramatically from the early 1980s to the present (Abubakar et al. 2022a, 2022b). The country experienced an increase in temperature from 1980 to 2020 while rainfall remained stable (Abubakar et al. 2021). The WorldClim climate data for 1960–2000 is also used to assess temporal variations in climate. The eco-physiological constraints imposed by the climate determine the distribution ranges of species. Oil palm may not colonize unsuitable sites due to factors like soil properties and biotic interactions (Pareek 2017).

Due to the varying spatial scales at which each factor acts, the interrelationships among these factors can be complex (Murphy et al. 2021). The presence of oil palm plantations in climatically suitable areas can change over time due to other factors becoming more important at the local level (Paterson et al. 2015, Abdul Rahman 2018). It is more important to consider topography and soil texture on a finer scale, as well as nutrient content. Plantations of oil palm are expected to experience significant impacts due to climate change (Paterson et al. 2015, Sarkar et al. 2020).

Over the last four decades, most areas of Malaysia have seen an increase in surface temperature of 2.7-4.0^{o}C (Jegasothy et al. 2021). Since the 1970s, precipitation in Peninsular Malaysia has also increased (Loo et al. 2015). With increased trends in daily maximum rainfall along Peninsular Malaysia's west coast since the mid-1970s, northeast and southwest monsoon rainfall have increased dramatically (Cramb 2020, Kuttippurath et al. 2021). A longer dry spell was also observed during this period. From 1969-2009, Malaysia's average surface temperature rose from 0.6 to 1.20^{o}C and is predicted to rise from 1.5 to 2°C by 2050 (Paterson et al. 2015). A greater degree of fluctuation

may be experienced in rainfall and river flows (Paterson et al. 2015). Daily minimum precipitation in Peninsular Malaysia is expected to fall by 32 to 61%, while maximum precipitation is expected to rise by 51% in Pahang, Kelantan, and Terengganu (Alam et al. 2011). There will be an increase of 10% in rainfall in Kelantan, Pahang, Terengganu, and the northwestern coast, and a decrease of 5% in Johor and Selangor, causing risks and uncertainty for oil palm farmers (Othman et al. 2016).

Agriculture's Role in Malaysia's Economic Development

A significant role has been played by agriculture in Peninsular Malaysia's recent economic transformations (Murad et al. 2008, Austin & Baharuddin 2012). In the years between 1997 and 2010, Malaysia was hit by numerous regional and global economic crises, which were alleviated by agriculture (Olaniyi et al. 2013). Therefore, in Malaysia, the growth in agricultural productivity will mainly be achieved through intensification, among other initiatives, as indicated by the previous and future economic plans (Ming & Chandramohan 2002, Abdullah et al. 2009, Nordin et al. 2014, Varkkey et al. 2018). In accordance with the Malaysian National Economic Development Plans, the National Physical Plan (NPP) was formulated through the Malaysian Town and Country Planning Act 1976 (Kassim 2012). Land suitability maps that are not updated regularly would make this task difficult for agencies. This study found coastal Selangor to be one of the highly climatic suitable areas for the production of oil palm (Fig. 5). The suitability of this area might expose the area to potential environmental degradation from agricultural intensification.

How Climate Change Affects Oil Palm Production in Peninsular Malaysia?

Despite falling from 6.0% of GDP in the 1970s to 3.1% in 2021 (World Bank 2022). Malaysia's development relies heavily on the agriculture sector (Wong 2007, Islam & Siwar 2012, Matahir & Tuyon 2013). There are a variety of subsectors within the sector, such as rubber, livestock, forestry, logging, fisheries, aquaculture, pepper, cocoa, pineapples, coconuts, tobacco, tea, etc. The oil palm industry dominated Malaysian agriculture in 2014, which accounted for 36.6% of the total agricultural production (Sarkar et al. 2020). After Indonesia, Malaysia has the second-highest palm oil production and exports (Abubakar et al. 2022a, 2022b). With 39% of global production and 44% of exports, Malaysia dominates palm oil production and exports (Alam et al. 2015). As a result, Malaysia's economy benefits greatly from oil palm cultivation and production.

Floods, droughts, heat stress, and heavy precipitation are all effects of climate change on crop production. Malaysian oil palm production has decreased due to the direct and indirect impacts of climate change (Paterson & Lima 2018). According to Zainal et al. (2012), Net revenue from oil palm production is significantly affected by climate change. Tropical countries are suffering from adverse effects of climate change on oil palm production (Paterson et al. 2015, 2017).

In addition, Paterson & Lima (2018) predicted that if temperatures exceeded 2°C and rainfall decreased by 10%, oil palm production would decrease by 30% in Malaysia. Oil palm production will be unsuitable beyond 2050 due to the unsuitable climate (Paterson, 2019a, Paterson 2020). Paterson (2019a) predicts a significant decline in oil palm production. The climate change effect on oil palms is expected to worsen between 2070 and 2100 (Paterson 2019b). Oil palm production may not be sustainable based on this projection. Due to climate intensity and severity, climate change can have considerable impacts on oil palm production. Oil palm plantations can become susceptible to diseases and pests if the land is dry or degraded, or if temperatures rise (Akinci et al. 2013).

The Contribution of Oil Palms to National Development

In terms of net contribution to gross national income (GNI), the palm oil industry is ranked fourth in the country with RM53 billion (Mahat 2012). Over the next decade, oil palm will dominate the nation's economy, contributing RM178 billion to the nation's GDP in 2020 (Mahat 2012). Since rubber and tin are being replaced by diversifying the economy, the government has been able to sustain the success of this industry. The oil palm sector was successfully developed as a result of this decision. The Malaysian government decided to promote oil palm plantations as a new agricultural commodity in 1955, in accordance with a World Bank mission recommendation (Teoh 2002). The narrow economic base was widened and diversified to grow the economy more efficiently. To expand palm oil exports, industrial estates are being established and palm oil estates are being expanded. Diversification initiatives were taken to develop manufacturing and expand the export of palm oil (Teoh 2002, Rasiah & Shahrin 2006). By creating wealth for the nation, the palm oil industry changed the economic landscape for the better, as well as alleviating poverty among the poor (Majid Cooke 2012). The Second Malaya Plan (1961-1955) clearly emphasized rural development and poverty alleviation as government priorities (Fredericks 2012). The poverty rate among agricultural farmers was 68.3% in the 1970s. A new program to alleviate poverty

in rural areas was launched in the 1960s through the planting of oil palms. As a result of the government's rural development programs and newly opened lands, three rural development agencies were established to encourage the establishment of large plantation areas, including The Federal Land Development Authority (FELDA), the Federal Land Consolidation and Rehabilitation Authority (FELCRA), and the Rubber Industry Smallholders Development Authority (RISDA) (Teoh 2002, Yap et al. 2021).

Oil Palm Production Opportunities in Peninsular Malaysia

The competitiveness and advantages of palm oil have made it one of the leading sources of vegetable oils (Mekhilef et al. 2011). According to several studies, oil palm has done well in the global market for oils and fats for several reasons (Ming & Chandramohan 2002, Basiron & Balu 2004, Burri 2012, Von Giebler 2013, Goh et al. 2016, Mat Yasin et al. 2017, Kushairi et al. 2018). Palm oil is less expensive than other vegetable oils (Carter et al. 2007, Zimmer 2010). There was an increase of 7.9% in palm oil consumption over the past 40 years, compared to a growth of 5.6% in soy oil over that same period (Abazue et al. 2015). In comparison to other crops, palm oil has the highest productivity per acre (Murphy et al. 2021). The sustainability of palm oil cannot be matched by other vegetable oils, since it has a long lifespan of 25 years and it consumes significantly less energy during production. In comparison to other oil-producing crops, it requires less land and produces more oil per hectare (Sumathi et al. 2008, Lam et al. 2009, Levang et al. 2016). Among the facts that cannot be contested are the high productivity of oil palm, it's commercial profitability at large scales, and the growing demand for palm oil (Sheil et al. 2009). Oil palm profitability makes it an attractive investment for development and wealth creation in Malaysia, by offering a route out of poverty. There are also potential markets for palm oil and allied products as it is used in food products, detergents, cosmetics and, to a small extent, biofuel. Over half of all packaged products consumed by Americans contain palm oil, despite it being a minor component of the American diet. It is possible to improve incomes and quality of life through the development of oil palms if they are well-planned and managed (Meijaard & Sheil 2013). Throughout Peninsular Malaysia, oil palm cultivation is suitable due to the climate and soil conditions (Paterson & Lima 2018, Abubakar et al. 2022a, 2022b). Peninsular Malaysia continues to expand its oil palm production area (Shevade & Loboda 2019). Over 20% of the land is covered by oil palm plantations, and new plantations are being established throughout the region (Shevade & Loboda 2019). Historically, Peninsular Malaysia has been a resource-based economy dominated by plantations, including oil palm plantations that have replaced natural forests (Shevade & Loboda 2019). Finally, the market for palm oil is global and demanding, whereas the climate and soils in Peninsular Malaysia are highly suitable for oil palm cultivation.

CONCLUSION

In this study, we assess the suitability of oil palm production as driven by soil, climate, and land use in Peninsular Malaysia. To determine suitable and available land for oil palm production, remote sensing and GIS overlay were found to be useful methods. To handle digital spatial data, this method was found to be more flexible and accurate. The GIS in this study proves a powerful combination to apply for climate, soil, and land-use suitability analysis. The study shows that good soils and climatic conditions in Malaysia remain one of the most important factors in oil palm cultivation. Recent decades have seen Malaysia's oil palm plantations expand due to suitable soil and climate. In terms of delineating oil palm production sites, combining LSA with GIS enhances policymakers' and planners' decision-making capabilities. The northeastern part of central Peninsular Malaysia is home to the most suitable soils for oil palm production, particularly those in Selangor and Kedah, and Kelantan Terengganu, with clay loams and sandy loams, whereas in the southern regions, such as Melaka, clay soil dominates the area, which makes it moderately suitable for oil palm production. For further research, additional aspects including irrigation schemes, market infrastructure, and socioeconomics should be considered. Further suitability analysis will be possible due to soil databases and land information systems that include information on soil types, soil fertility, terrain, current land use condition, climate, slope, vegetation cover, soil erosion, and land unit maps. For further research, however, irrigation facilities, market infrastructure, and socioeconomic factors should be considered.

ACKNOWLEDGMENT

The author would like to acknowledge the funding provided by TETFUND.

REFERENCES

Abazue, C.M., Er, A.C., Ferdous Alam, A.S.A. and Begum, H. 2015. Oil Palm Smallholders and Its Sustainability Practices in Malaysia. Mediterr. J. Soc. Sci., 6: 482-488.

Abdul Rahman, H. 2018. Climate change scenarios in Malaysia: Engaging the public. Int. J. Malay-Nusantara Stud., 1: 55-77

Abdullah, A.Z., Salamatinia, B., Mootabadi, H. and Bhatia, S. 2009. Current status and policies on the biodiesel industry in Malaysia as the world's leading producer of palm oil. Energy Policy, 37:5440-5448.

Abubakar, A., Ishak, M.Y. and Makmom, A.A. 2021. Impacts of and adaptation to climate change on the oil palm in Malaysia : A systematic review. Environ. Sci. Pollut. Res., 28: 1-23.

Abubakar, A., Ishak, M.Y. and Makmom, A.A. 2022a. Nexus between climate change and oil palm production in Malaysia : a review. Environ. Monit. Assess., 194: 1-22.

Abubakar, A., Ishak, M.Y., Bakar, A.A., Uddin, M.K., Ahmad, M.H., Seman, I.A., Ching, L.M., Ahmad, A. and Hashim, Z. 2022b. Geospatial simulation and mapping of climate suitability for oil palm (Elaeis guineensis) production in Peninsular Malaysia using GIS / remote sensing techniques and analytic hierarchy process. Model Earth Syst. Environ., 8: 1-23.

Akinci, H., Özalp, A.Y. and Turgut, B. 2013. Agricultural land use suitability analysis using GIS and AHP techniques. Comput. Electron. Agric., 97: 71-82.

Alam, A.F., Er, A.C. and Begum, H., 2015. Malaysian oil palm industry: Prospect and problem. J. Food Agric. Environ., 13: 143-148.

Allen, R.G., Clemmens, A.J., Burt, C.M., Solomon, K. and O'Halloran, T. 2005. Prediction Accuracy for Project-wide Evapotranspiration Using Crop Coefficients and Reference Evapotranspiration. J. Irrig. Drain. Eng., 131: 24-36.

Anapalli, S.S., Fisher, D.K., Pinnamaneni, S.R. and Reddy, K.N. 2020. Quantifying evapotranspiration and crop coefficients for cotton (Gossypium hirsutum L.) using an eddy covariance approach. Agric. Water Manag., 233: 1-12

Anderson, M.C., Allen, R.G., Morse, A. and Kustas, W.P. 2012. Use of Landsat thermal imagery in monitoring evapotranspiration and managing water resources. Remote Sens. Environ., 122: 50-65.

Annan-Afful, E., Masunaga, T. and Wakatsuki, T. 2005. Soil properties along the toposequence of an inland valley watershed under different land use in the Ashanti Region of Ghana. J. Plant Nutr., 28: 141-150.

Ashton-Butt, A., Aryawan, A.A. K., Hood, A.S.C., Naim, M., Purnomo, D., Wahyuningsih, R., Willcock, S., Poppy, G.M. and Snaddon, J.L. 2018. Understory vegetation in oil palm plantations benefits soil biodiversity and decomposition rates. Front. For. Glob. Change, 1: 1-13.

Austin, O.C. and Baharuddin, A.H. 2012. Risk in Malaysian agriculture: The need for a strategic approach and a policy refocus. Kajian Malay. J. Malay. Stud., 30: 21-50.

Ayompe, L.M., Schaafsma, M. and Egoh, B.N. 2021. Towards sustainable palm oil production: The positive and negative impacts on ecosystem services and human wellbeing. J. Clean. Prod., 278: 1-10.

Bandyopadhyay, S., Jaiswal, R.K., Hegde, V.S. and Jayaraman, V. 2009. Assessment of land suitability potentials for agriculture using a remote sensing and GIS-based approach. Int. J. Remote Sens., 30: 879-895.

Basiran, I. and Ja'afar, A. 2022. To study the effect of oil palm empty fruit bunch (OPEFB) fibre ratio on the mechanical properties of EFB. Cem. Board Panel., 3: 297-305.

Basiron, Y. and Balu, N. 2004. Palm oil : The driving force of world oils and fats economy. Oil Palm Ind. Econ. J. 4: 1-10.

Basiron, Y. and Weng, C.K. 2004. The oil palm and its sustainability. J. Oil Palm Res., 16: 1-10.

Bentivoglio, D., Finco, A. and Bucci, G. 2018. Factors affecting the Indonesian palm oil market in food and fuel industry: Evidence from a time series analysis. Int. J. Energy Econ. Policy, 8: 49-57.

Bharatkar, P.S. and Patel, R. 2013. Approach to accuracy assessment tor RS image classification techniques. Int. J. Sci. Eng. Res., 4: 79-86.

Burri, B.J. 2012. Evaluating global barriers to the use of red palm oil as an intervention food to prevent vitamin a deficiency. Compr. Rev. Food Sci. Food Saf., 11: 221-232.

Carter, C., Finley, W., Fry, J., Jackson, D. and Willis, L. 2007. Palm oil markets and future supply. Eur. J. Lipid Sci. Technol., 109: 307-314.

Castiblanco, C., Etter, A. and Aide, T.M. 2013. Oil palm plantations in Colombia: A model of future expansion. Environ. Sci. Policy, 27: 172-183.

Charters, L.J., Aplin, P., Marston, C.G., Padfield, R., Rengasamy, N., Bin Dahlan, M.P. and Evers, S. 2019. Peat swamp forest conservation withstands pervasive land conversion to oil palm plantations in North Selangor, Malaysia. Int. J. Remote Sens., 40: 7409-7438.

Corley, R.H.V. and Tinker, P.B. 2003. The Palm Oil. Fourth Edition. Blackwell Publishing, Oxford, UK

Cramb, R. 2020. White gold: The commercialization of rice farming in the lower Mekong Basin. Springer Nature, Singapore, p. 456.

Dislich, C., Keyel, A. C., Salecker, J., Kisel, Y., Meyer, K. M., Auliya, M., Barnes, A. D., Corre, M. D., Darras, K., Faust, H., Hess, B., Klasen, S., Knohl, A., Kreft, H., Meijide, A., Nurdiansyah, F., Otten, F., Pe, G., Steinebach, S. and Wiegand, K. 2017. A review of the ecosystem functions in oil palm plantations, using forests as a reference system. Biol. Rev. 49: 1539-1569.

Doula, M.K., Moreno-Ortego, J.L., Tinivella, F., Inglezakis, V.J., Sarris, A. and Komnitsas, K. 2017. Olive mill waste: Recent advances for the sustainable development of olive oil industry. Olive Mill Waste, 1: 29-56.

Elsheikh, R., Shariff, A.R.B.M., Amiri, F., Ahmad, N.B., Balasundram, S.K. and Soom, M.A.M. 2013. Agriculture Land Suitability Evaluator (ALSE): A decision and planning support tool for tropical and subtropical crops. Comput. Electron. Agric., 93: 98-110.

El-Shirbeny, M.A., Ali, A.M., Badr, M.A. and Bauomy, E.M. 2014. Assessment of wheat crop coefficient using remote sensing techniques. World J. Agric. Res., 1: 12-16.

Fu, B., Chen, L., Huang, H., Qu, P. and Wei, Z. 2021. Impacts of crop residues on soil health: A review. Environ. Pollut. Bioavailab., 33: 164-173.

Fadzillah, N.A., bin Che Man, Y., Rohman, A., Rosman, A.S., Ismail, A. and Mustafa, S. 2015. Detection of butter adulteration with lard by employing 1H-NMR spectroscopy and multivariate data analysis. J. Oleo. Sci., 10: 1-7.

FAO. 1976. A Framework for Land Valuation FAO Soils Bulletin No. 32. FAO, Rome, Italy, pp. 72.

Ferdous Alam, A.S.A., Er, A.C. and Begum, H. 2015. Malaysian oil palm industry: Prospect and problem. J. Food Agric. Environ., 13: 143-148.

Fredericks, L.J. 2012. Exploring the spatial dimensions of rural development models in Malaysia 1957-2007. Institut. Econ., 4: 47-62.

Goh, K.J., Wong, C.K. and Ng, P.H.C. 2016. Oil Palm. Encycl. Appl. Plant Sci., 3: 382-390.

Gutiérrez-Vélez, V.H. and DeFries, R. 2013. Annual multi-resolution detection of land cover conversion to oil palm in the Peruvian Amazon. Remote Sens ., 129: 154-167.

Gutiérrez-Vélez, V.H. and DeFries, R. 2013. Annual multi-resolution detection of land cover conversion to oil palm in the Peruvian Amazon. Remote Sens. Environ., 129: 154-167.

Hargreaves, G.H. and Allen, R.G. 2003. History and evaluation of Hargreaves evapotranspiration equation. J. Irrig. Drain. Eng., 129: 53-63.

Hargreaves, G.H. and Samani, Z.A. 1982. Estimating potential evapotranspiration. J. Irrig. Drain. Eng., 108: 225-230.

He, Y., Yao, Y., Chen, Y. and Luca, O. 2011. Regional land suitability assessment for tree crops using remote sensing and GIS. Proc. Int. Conf. Comput. Distrib. Control Intell. Environ. Monit., 11: 354-363.

Hengl, T., Heuvelink, G.B.M., Tadić, M.P. and Pebesma, E.J. 2012. Spatio-temporal prediction of daily temperatures using time-series of MODIS LST images. Theor. Appl. Climatol., 107: 265-277.

Hezri, A.A. and Nordin Hasan, M. 2006, February. Towards sustainable development? The evolution of environmental policy in Malaysia. In DiSano, J. (ed), Natural Resources Forum, Volume 30, Blackwell Publishing Ltd, Oxford, UK, pp. 37-50.

Holzner, A., Rayan, D.M., Moore, J., Tan, C.K.W., Clart, L., Kulik, L., Kühl, H., Ruppert, N. and Widdig, A. 2021. Occupancy of wild southern pig-tailed macaques in intact and degraded forests in Peninsular Malaysia. Peer J., 9: 12462.

Hughes, M.J. and Hayes, D.J. 2014. Automated detection of cloud and

cloud shadow in single-date Landsat imagery using neural networks and spatial post-processing. Remote Sens., 6: 4907-4926.

Islam, R. and Siwar, C. 2012. The analysis of urban agriculture development in Malaysia. Adv Environ Biol 6: 1068-1078.

Jaroenkietkajorn, U. and Gheewala, S.H. 2021. Land suitability assessment for oil palm plantations in Thailand. Sustain. Prod. Consum., 28: 1104-1113.

Jegasothy, R., Sengupta, P., Dutta, S. and Jeganathan, R. 2021. Climate change and declining fertility rate in Malaysia: The possible connexions. J. Basic Clin. Physiol. Pharmacol., 32: 911-924.

Jensen, M.E., Burman, R.D. and Allen, R.G. 1990. Evaporation and irrigation water requirements. ASCE Manuals and Reports on Eng. Practices No. 70. Am. Soc. Civil Eng., New York, NY, pp. 978-990.

Kamble, B., Kilic, A., Hubbard, K. 2013. Estimating crop coefficients using remote sensing-based vegetation index. Remote Sens., 5: 1588-1602.

Kanniah, K. D., Sheikhi, A., Cracknell, A. P., Goh, H. C., Tan, K. P., Ho, C. S. and Rasli, F. N. 2015. Satellite images for monitoring mangrove cover changes in a fast-growing economic region in southern Peninsular Malaysia. Remote Sens 7: 14360-14385.

Kasahara, M., Kagawa, T., Oikawa, K., Suetsugu, N., Miyao, M. and Wada, M. 2002. Chloroplast avoidance movement reduces photodamage in plants. Nature, 420: 829-832.

Kassim, A. 2014. Recent trends in transnational population inflows into Malaysia: Policy, issues, and challenges. Malays. J. Econ. Stud., 51: 9-28.

Khiabani, P.H. and Takeuchi, W. 2020. Assessment of oil palm yield and biophysical suitability in Indonesia and Malaysia. Int. J. Remote Sens., 41: 8520-8546.

Klingebiel, A.A. and Montgomery, P.H. 1966. Land Capability Classification. Agricultural Hand Book No. 210, USDA, Washington.

Koh, L.P., Miettinen, J., Liew, S.C. and Ghazoul, J. 2011. Remotely sensed evidence of tropical peatland conversion to oil palm. Proc. Natl. Acad. Sci. USA, 108: 5127-5132.

Koh, L.P. and Wilcove, D.S. 2008. Is oil palm agriculture destroying tropical biodiversity ? Conserv. Lett., 1: 60-64.

Kome, G.K., Tabi, F.O., Enang, R.K. and Silatsa, F.B.T. 2020. Land suitability evaluation for oil palm (Elaeis guineensis Jacq.) in coastal plains of southwest Cameroon. Open J. Soil Sci., 10: 257-273.

Kra, E.Y. and Ofosu-Anim, J. 2010. Modeling maize planting date to minimize irrigation water requirements. Aust. J. Agric, Eng., 1: 66-73.

Kushairi, A., Loh, S. K., Azman, I., Hishamuddin, E., Ong-Abdullah, M., Izuddin, Z. B. M. N., Razmah, G., Sundram, S. and Parveez, G. K. A. 2018. Oil palm economic performance in Malaysia and r&d progress in 2017. J Oil Palm Res., 30: n163-195.

Kushairi, A., Ong-Abdullah, M., Nambiappan, B., Hishamuddin, E., Bidin, M. N. I. Z., Ghazali, R., Subramaniam, V., Sundram, S. and Parveez, G. K. A. 2019. Oil palm economic performance in Malaysia and R&D progress in 2018. J. Oil Palm Res., 31: 165-194.

Kuttippurath, J., Murasingh, S., Stott, P.A., Sarojini, B.B., Jha, M.K., Kumar, P., Nair, P.J., Varikoden, H., Raj, S., Francis, P.A. and Pandey, P.C. 2021. Observed rainfall changes in the past century (1901–2019) over the wettest place on Earth. Environ. Res. Lett., 16: 1-14.

Läderach, P, Martinez-Valle, A., Schroth, G. and Castro, N. 2013. Predicting the future climatic suitability for cocoa farming of the world's leading producer countries, Ghana and Côte d'Ivoire. Clim. Change, 119: 841-854.

Lam, M.K., Tan, K.T., Lee, K.T. and Mohamed, A.R. 2009. Malaysian palm oil: Surviving the food versus fuel dispute for a sustainable future. Renew. Sustain. Energy Rev., 13: 1456-1464.

Levang, P., Riva, W.F. and Orth, M.G. 2016. Oil palm plantations and conflict in Indonesia: Evidence from West Kalimantan. In Cramb, R. and McCarthy, J.F. (eds), The Oil Palm Complex: Smallholders, Agribusiness And The State in Indonesia and Malaysia, JSTOR, pp. 283-300.

Li, L., Dong, J., Tenku, S.N. and Xiao, X. 2015. Mapping oil palm plantations in Cameroon using PALSAR 50-m orthorectified mosaic images. Remote Sens., 7: 1206-1224.

Liou, Y.A. and Kar, S.K. 2014. Evapotranspiration estimation with remote sensing and various surface energy balance algorithms-a review. Energies, 7: 2821-2849.

Loo, Y.Y., Billa, L. and Singh, A. 2015. Effect of climate change on seasonal monsoon in Asia and its impact on the variability of monsoon rainfall in Southeast Asia. Geosci Front., 6: 817-823.

Mahat, S.A. 2012. The palm oil industry from the perspective of sustainable development: A case study of Malaysian palm oil industry. Ritsumeikan Asia Pac. Univ. Japan, 12: 1-126.

Majid Cooke, F. 2012. In the name of poverty alleviation: Experiments with oil palm smallholders and customary land in Sabah, Malaysia. Asia Pac. Viewp., 53: 240-253.

Malaysian Palm Oil Board 2020. Malaysian Oil Palm Statistics 2019. 39th (eds). Malaysian Palm Oil Board. Ministry of Plantation Industries and Commodities, Selangor, Malaysia.

Malaysian Palm Oil Council (MPOC). 2022. Malaysian Palm Oil Sector Performance In 2020 and Market Opportunities. https://mpoc.org.my/malaysian-palm-oil-sector-performance-in-2020-and-market-opportunities/

Malczewski, J. 2004. GIS-based land-use suitability analysis: a critical overview. Prog Plann., 62: 3-65.

Maluin, F.N., Hussein, M.Z. and Idris, A.S. 2020. An overview of the oil palm industry: Challenges and some emerging opportunities for nanotechnology development. Agronomy, 10: 1-20.

Mat Yasin, M.H., Mamat, R., Najafi, G., Ali, O.M., Yusop, A.F. and Ali, M.H. 2017. Potentials of palm oil as new feedstock oil for a global alternative fuel: A review. Renew. Sustain. Energy Rev., 79: 1034-1049.

Matahir, H. and Tuyon, J. 2013. The dynamic synergies between agriculture output and economic growth in Malaysia. Int. J. Finance Econ., 5: 56-71.

McCarthy, J.F. and Cramb, R.A. 2009. Policy narratives, landholder engagement, and oil palm expansion on the Malaysian and Indonesian frontiers. Geogr. J., 175: 112-123.

Meijaard, E. and Sheil, D. 2013. Oil-Palm Plantations in the Context of Biodiversity Conservation. Elsevier Ltd, The Netherlands.

Mekhilef, S., Siga, S. and Saidur, R. 2011. A review on palm oil biodiesel as a source of renewable fuel. Renew Sustain. Energy Rev., 15: 1937-1949.

Ming, K.K. and Chandramohan, D. 2002. Malaysian palm oil industry at crossroads and its future direction. Oil Palm Ind. Econ. J., 2: 2-7.

Montgomery, B., Dragićević, S., Dujmović, J. and Schmidt, M. 2016. A GIS-based Logic Scoring of Preference method for evaluation of land capability and suitability for agriculture. Comput. Electron. Agric., 124: 340-353.

Mugiyo, H., Chimonyo, V.G.P., Sibanda, M., Kunz, R., Masemola, C.R., Modi, A.T. and Mabhaudhi, T. 2021. Evaluation of land suitability methods with reference to neglected and underutilized crop species: A scoping review. Land, 10: 1-24.

Muhammad, N.S., Abdullah, J. and Julien, P.Y. 2020. Characteristics of rainfall in peninsular Malaysia. J. Phys. Conf. Ser., 1529: 1-12.

Muller-Wilm, U., Louis, J., Richter, R., Gascon, F. and Niezette, M. 2013, September. Sentinel-2 level 2A Prototype Processor: Architecture, Algorithms and First Results. In Proceedings of the ESA Living Planet Symposium, Edinburgh, UK, pp. 9-13.

Murphy, D.J., Goggin, K. and Paterson, R.R.M. 2021. Oil palm in the 2020s and beyond: challenges and solutions. CABI Agric. Biosci., 2: 1-22.

Mustafa, A.A., Singh, M., Sahoo, R.N., Ahmed, N., Khanna, M. and Sarangi, A. 2011. Land suitability analysis for different crops: A multi-criteria decision-making approach using remote sensing and GIS. Water Technol., 3: 61-84.

Nagaraj, G. 2009. Oilseeds: Properties, Processing, Products, and Procedures. New India Publishing, New Delhi.

Najihah, A., Nor, M., Isnorm, R. A., Abas, M. A., Hanisah, N., Malek, A., Hassin, N. H. and Aziz, H. A. 2018. Landscape Ecological Assessment of Potential Ecotourism in Malaysia. Int. J. Civ. Eng. Technol., 9: 969-979.

Nambiappan, B., Ismail, A., Hashim, N., Ismail, N., Shahari, D.N., Idris, N.A.N., Omar, N., Salleh, K.M., Hassan, N.A.M. and Kushairi, A. 2018. Malaysia: 100 years of resilient palm oil economic performance. J. of Oil Palm Res., 30(1): 13-25.

Nguyen, T.T., Verdoodt, A., Van Y, T., Delbecque, N., Tran, T.C. and Van Ranst, E. 2015. Design of a GIS and multi-criteria-based land evaluation procedure for sustainable land-use planning at the regional level. Agric. Ecosyst. Environ., 200: 1-11.

Nordin, S.M., Noor, S.M. and Bin Md Saad, M.S. 2014. Innovation diffusion of new technologies in the Malaysian paddy fertilizer industry. Proced. Soc., 109: 768-778.

Oettli, P., Behera, S.K. and Yamagata, T. 2018. Climate based predictability of oil palm tree yield in Malaysia. Sci. Rep., 8: 1-13.

Olaniyi, A.O., Ajiboye, A.J., Abdullah, A.M., Ramli, M.F. and Sood, A.M. 2015. Agricultural Land Use Suitability Assessment in Malaysia. Bulg. J. Agric. Sci., 21: 560-572.

Olivin, J. 1968. Study for the location of an industrial oil palm block II. Judging criteria. Oilseeds, 23: 499-504.

Othman, M.A., Zakaria, N.A., Ghani, A.A., Chang, C.K. and Chan, N.W. 2016. Analysis of trends of extreme rainfall events using Mann Kendall test: a case study in Pahang and Kelantan river basins. J. Teknol., 78: 9-4.

Pałas, K.W. and Zawadzki, J. 2020. Sentinel-2 imagery processing for tree logging observations on the billowier forest world heritage site. Forests, 11: 1-16.

Paramananthan, S. 2003. Oil palm. In Fairhurst, T.H. and Härdter, R. (eds), Management for Large and Sustainable Yields, Potash & Phosphate Institute of Canada (PPIC) and International Potash Institute (IPI), Singapore, pp. 27-57.

Paramananthan, S. 2011. Soil Requirements and Land Evaluation for Oil Palms for High Yields. In: Goh, K.J., Chiu, S.B., Paramananthan, S. (Eds.), Agronomic Principles & Practices of Oil Palm Cultivation. Agricultural Crop Trust (ACT), Malaysia, p. 771

Pareek, N. 2017. Climate change impact on soils : Adaptation and mitigation. MOJ Eco. Environ. Sci., 2: 136-139.

Paterson, R.R.M. 2019a. *Ganoderma boninense* disease of oil palm to significantly reduce production after 2050 in Sumatra if projected climate change occurs. Microorganisms, 7: 4-6.

Paterson, R.R.M. 2019b. *Ganoderma boninense* disease was deduced from simulation modeling with large data sets of future Malaysian oil palm climate. Phytoparasitica, 3: 1-11.

Paterson, R.R.M. 2020. Oil palm survival under climate change in Malaysia with future basal stem rot assessments. For. Pathol., 50: 1-8.

Paterson, R.R.M. 2021a. Optimized and systematic suitable climate modeling confirms future longitudinal trends for growing oil palm in Africa. J. Environ. Manage., 300: 113785.

Paterson, R.R.M. 2021b. Longitudinal trends of future climate change and oil palm growth: empirical evidence for tropical Africa. Environ. Sci. Pollut. Res., 28: 21193-21203.

Paterson, R.R.M., Kumar, L., Shabani, F. and Lima, N. 2017. World climate suitability projections to 2050 and 2100 for growing oil palm. J. Agric. Sci., 155: 659-702.

Paterson, R.R.M., Kumar, L., Taylor, S. and Lima, N. 2015. Future climate effects on suitability for growth of oil palms in Malaysia and Indonesia. Sci. Rep., 5: 1-11.

Paterson, R.R.M. and Lima, N. 2018. Climate change affecting oil palm agronomy, and oil palm cultivation increasing climate change, require amelioration. Ecol. Evol., 8: 452-461.

Paterson, R.R.M., Sariah, M. and Lima, N. 2013. How will climate change affect oil palm fungal diseases? Crop Prot., 46: 113-120.

Pirker, J. 2015. Mapping Oil Palm Suitability Protocol. Technical Annex 1. Oil Palm Suitability Map for South West Cameroon. IEL International, p. 23.

Pirker, J., Mosnier, A., Kraxner, F., Havlík, P. and Obersteiner, M. 2016. What are the limits to oil palm expansion? Glob. Environ. Chang., 40: 73-81.

Rahman, S. 2020. Malaysian Independent Oil Palm Smallholders and their Struggle to Survive 2020. ISEAS Perspect, KL, pp. 1-16.

Rasiah, R. and Shahrin, A. 2006. Development of palm oil and related products in Malaysia and Indonesia. University of Malaya, KL, pp.1-54.

Rendana, M., Rahim, S. A., Idris, W. M. R., Rahman, Z. A. and Lihan, T. 2022. Agricultural Land Evaluation Using GIS-Based Matching Method in Highland Areas for Oil Palm Cultivation. J. Sustain. Agric., 37: 100-110.

Rhebergen, T., Fairhurst, T., Zingore, S., Fisher, M., Oberthür, T. and Whitbread, A. 2016. Climate, soil, and land-use based land suitability evaluation for oil palm production in Ghana. Eur. J. Agron., 81: 1-14.

Rwanga, S.S. and Ndambuki, J.M. 2017. Accuracy Assessment of Land Use/Land Cover Classification Using Remote Sensing and GIS. Int. J. Geosci., 08: 611-622.

Salmon, J.M., Friedl, M.A., Frolking, S., Wisser, D. and Douglas, E.M. 2015. Global rain-fed, irrigated, and paddy croplands: A new high-resolution map derived from remote sensing, crop inventories, and climate data. Int. J. Appl. Earth Obs. Geoinf., 38: 321-334.

Sarkar, M.S.K., Begum, R.A. and Pereira, J.J. 2020. Impacts of climate change on oil palm production in Malaysia. Environ. Sci. Pollut. Res., 27: 9760-9770.

Sayer, J., Ghazoul, J., Nelson, P., Klintuni, and Boedhihartono, A. 2012. Oil palm expansion transforms tropical landscapes and livelihoods. Glob. Food Sec., 1: 114-119.

Schwabe, K.A., Carson, R.T., DeShazo, J.R., Potts, M.D., Reese, A.N. and Vincent, J.R., 2015. Creation of Malaysia's Royal Belum State Park: a case study of conservation in a developing country. J. Environ. Dev., 24: 54-81.

Sheil, D., Casson, A., Meijaard, E., van Nordwijk, M., Gaskell, J., Sunderland-Groves, J., Wertz, K. and Kanninen, M. 2009. The Impacts and Opportunities of Oil Palm in Southeast Asia: What Do We Know and What Do We Need to Know? Occasional Paper No. 51. CIFOR, Bogor, Indonesia.

Shevade, V.S. and Loboda, T. V. 2019. Oil palm plantations in Peninsular Malaysia: Determinants and constraints on expansion. PLoS One, 14: 1-22.

Siwar, C., Alam, M., Murad, M.W. and Al-Amin, A.Q. 2009. A review of the linkages between climate change, agricultural sustainability, and poverty in Malaysia. Int. Rev. Bus. Res., 5: 309-321.

Skakun, S., Wevers, J., Brockmann, C., Doxani, G., Aleksandrov, M., Batič, M., Frantz, D., Gascon, F., Gómez-Chova, L., Hagolle, O., López-Puigdollers, D., Louis, J., Lubej, M., Mateo-García, G., Osman, J., Peressutti, D., Pflug, B., Puc, J., Richter, R. and Žust, L. 2022. Cloud Mask Intercomparison eXercise (CMIX): An evaluation of cloud masking algorithms for Landsat 8 and Sentinel-2. Remote Sens. Environ., 274: 1-22.

Storie, R. 1978. Storie Index Soil Rating. University of California, Special Publication 3203, Oakland, CA.

Sumathi, S., Chai, S.P. and Mohamed, A.R. 2008. Utilization of oil palm as a source of renewable energy in Malaysia. Renew. Sustain. Energy Rev., 12: 2404-2421.

Surre, C. 1968. Les besions en eau du palmier à huile. Calcul du bilan de I'eau et ses applications pratiques. Oléagineux, 23: 165-167.

Sutton, J. and Kpentey, B., 2012. An enterprise map of Ghana (Vol. 2). International Growth Centre in Association with the London Publishing Partnership, London.

Sys, C., Van Ranst, E. and Debaveye, J. 1991. Land Evaluation. Part 1:

Principles in Land Evaluation and Crop Production Calculation. General Administration for Development Cooperation, Agric. Publ. No. 7, Brussels.

Tang, K.H.D. and Al Qahtani, H.M.S. 2020. Sustainability of oil palm plantations in Malaysia. Environ Dev. Sustain., 22: 4999-5023.

Ten, D.C.Y., Jani, R., Hashim, N.H., Saaban, S., Abu Hashim, A.K. and Abdullah, M.T., 2021. Panthera tigris jacksoni population crash and impending extinction due to environmental perturbation and human-wildlife conflict. Animals, 11: 1-14.

Teoh, C.H. 2002. The Palm Oil Industry in Malaysia: From Seed to Frying Pan. https://www.rspo.org/files/resource_centre/OP_Chain_Part%20A_new.pdf

Teoh, C.H. 2000. Land use and the oil palm industry in Malaysia. WWF For. Inf. Syst. Database, 9: 129.

Teoh, C.H. 2010. Key Sustainability Issues in the Palm Oil Sector. Discussion Paper, WBG Multi-Stakeholders Collaboration. World Bank Gr., 11: 1-52.

Torbick, N., Ledoux, L., Salas, W. and Zhao, M. 2016. Regional mapping of plantation extent using multisensor imagery. Remote Sens., 8: 1-21.

Tulayasathien, S. and Tejapaibul, A. 2017. Investment Promotion and Liberalization in Selected ASEAN Countries. In Thirawat, N. (ed), Internationalization and Managing Networks in the Asia Pacific. Chandos Publishing, Cambridge, UK, pp. 29-51.

Vadivelu, S., Ahmad, A. and Choo, Y.H. 2014. Remote sensing techniques for oil palm age classification using Landsat-5 Tm satellite. SciInt., 26: 1547-1551.

van der Vossen, H.A.M. 1969. Areas were climatically suitable for optimal oil palm production in the forest zone of Ghana. Ghana J. Agric. Sci., 2: 113-118.

Várallyay, G. 2010. The impact of climate change on soils and their water management. Agron. Res., 8: 385-396.

Varkkey, H., Tyson, A. and Choiruzzad, S.A.B. 2018. Palm oil intensification and expansion in Indonesia and Malaysia: Environmental and socio-political factors influencing policy. For. Policy Econ., 92: 148-159.

Vasu, D., Srivastava, R., Patil, N. G., Tiwary, P., Chandran, P. and Kumar Singh, S. 2018. A comparative assessment of land suitability evaluation methods for agricultural land use planning at the village level. Land Use Policy, 79: 146-163.

Verheye, W. 2010. Growth and production of oil palm. In: Land Use, Land Cover and Soil Sciences. UNESCO-EOLSS Publishers.

Von Geibler, J. 2013. Market-based governance for sustainability in value chains: Conditions for successful standard setting in the palm oil sector. J. Clean. Prod., 56: 39-53.

Weiss, M., Jacob, F. and Duveiller, G. 2020. Remote sensing for agricultural applications: A meta-review. Remote Sens. Environ., 236: 1-19.

Wong, C., Uhlenbrook, S. and Zhou, Y. 2009. Variability of rainfall in Peninsular Malaysia. Hydrol. Earth Syst. Sci. Discuss., 6: 5471-5503.

Wong, L.C. 2007. Development of Malaysia's agricultural sector: Agriculture as an engine of growth. In ISEAS Conf. Malays. Econ. Develop. Chall., 25: 1-22.

World Bank. 2022. GDP growth (Annual %) – Malaysia. https://data.worldbank.org/indicator/NY.GDP.MKTP.KD.ZG?locations=MY

Yang, H., Yang, D., Lei, Z. and Sun, F. 2008. New analytical derivation of the mean annual water-energy balance equation. Water Resour. Res., 44: 1-9.

Yap, P., Rosdin, R., Abdul-Rahman, A. A. A., Omar, A. T., Mohamed, M. N. and Rahami, M. S. 2021. Malaysian Sustainable Palm Oil (MSPO) certification progress for independent smallholders in Malaysia. IOP Conf. Ser. Earth Environ. Sci., 736: 1-5.

Yin, D., Li, Q., Li, X. and Zhu, R. 2022. Annual water deficit in response to climate variabilities across the globe. Environ. Res. Lett., 17: 1-10.

Zainal, Z., Shamsudin, M.N., Mohamed, Z.A. and Adam, S.U. 2012. The economic impact of climate change on Malaysian palm oil production. Trends Appl. Sci. Res., 7: 872-880.

Zekoll, V., Main-Knorn, M., Louis, J., Frantz, D., Richter, R. and Pflug, B. 2021. Comparison of masking algorithms for sentinel-2 imagery. Remote Sens., 13: 1-21.

Zimmer, Y. 2010. Competitiveness of rapeseed, soybeans, and palm oil. J. Oilseed Brassica, 1: 84-90.

Zulkifli, N., Ibrahim, R.I.R., Rahman, A.A.A. and Yasid, A.F.M. 2020. Maritime Cooperation in the Straits of Malacca (2016-2020): challenges and recommendations for a new framework. Asian J. Res. Educ. Soc. Sci., 2: 10-32.

Nature Environment and Pollution Technology
An International Quarterly Scientific Journal

p-ISSN: 0972-6268
(Print copies up to 2016)
e-ISSN: 2395-3454

Vol. 21 | No. 5 (Suppl) | pp. 2165-2175 | 2022

Review Research Paper | https://doi.org/10.46488/NEPT.2022.v21i05.011 | Open Access Journal

Multi Techniques for Agricultural Image Disease Classification and Detection: A Review

M. Amudha* and K. Brindha†**
*School of Information Technology and Engineering, Vellore Institute of Technology, Vellore 632014, India
**School of Information Technology and Engineering, Vellore Institute of Technology, Vellore 632014, India
†Corresponding author: K. Brindha; brindha.k@vit.ac.in

Nat. Env. & Poll. Tech.
Website: www.neptjournal.com

Received: 11-06-2022
Revised: 10-07-2022
Accepted: 13-07-2022

Key Words:
Machine learning
Deep learning
Blight
Plant disease
Deep convolutional

ABSTRACT

The agriculture sector has a significant impact on the market in every country. Identifying crop disease with conventional methods is a hard operation and it needs more time, effort, and experts with continuous farm monitoring. Blight and other crop diseases have severe consequences on crop yields and cause enormous economic losses worldwide. Plant health monitoring and disease detection are critical components of sustainable agriculture. Machine learning and deep learning techniques are used to identify plant diseases and associated with severity detection in plant leaves. The adoption of these techniques still faces several important challenges. In recent years, improvements in technology and researchers' interest in this area have made it possible to obtain an optimal solution. In addition to providing a detailed explanation of the proposed technique, which is deep learning architecture that uses the deep convolutional extreme learning machine (DC-ELM) for faster training, this study focuses on how machine learning and deep learning techniques detect plant diseases and infections that affect different crops. The proposed model is capable of providing good computational performance and allowing the learning process to be completed with less processing time. Finally, several challenges and problems with the existing system, as well as future research objectives, are enumerated and discussed.

INTRODUCTION

Agriculture is an aspect of everybody›s lives, either directly or indirectly. Natural disasters such as disease and pests impair plant growth and may even cause it to die during the entire growing cycle (Conrad et al. 2020). Plant disease is a disorder caused by a change in a plant's morphology, metabolism, or activity. Plant diseases are caused by infectious organisms (fungi, bacteria, or viruses) that are specified in Fig. 1, which are known as biotic diseases (Vishnoi et al. 2021). The most prevalent plant diseases are blight, spot, rust, and canker. Plant disease outbreaks harm agricultural production. Food insecurity will worsen if plant diseases are not detected in time (Chen et al. 2020a). Plant diseases represent a huge hazard to small-scale farmers since they can destroy their whole food supply (Li et al. 2021). Farmers used to follow expert recommendations by inspecting specimens of infected plants with their own eyes, or an expert could visit the field and provide appropriate solutions. To treat plant diseases, farmers were taking prophylactic steps. Finding reliable specialists is challenging, the practice of ongoing expert supervision is costly and time-consuming, and it is ineffective in large fields (Hang et al. 2019). It is important to identify agricultural products and diseases accurately and promptly. So, we need a certain automatic, fast, accurate, and less expensive system to detect plant diseases.

This review article focuses on artificial intelligence approaches for plant disease identification and recognition, comparing them based on the datasets used, prototypes used, and performance metrics compared with other techniques (Liu et al. 2020). This study also looks at how classic machine learning algorithms have evolved since deep learning (Khan et al. 2021). Image processing techniques are also applied to identify and classify plant diseases in a quick, automatic, and accurate manner. Thermal, hyperspectral (Gu et al. 2019, Lin et al. 2020), multispectral, and fluorescent image processing approaches can help detect plant illnesses early. The systematic phases of image processing are image acquisition, image preprocessing, image segmentation, feature extraction, feature selection, and classification. The issue with this technique is its limited accuracy, which necessitates several major operations to achieve higher levels of accuracy. Large amounts of pre-existing data are difficult to implement due to the limited number of manually generated feature parameters. These

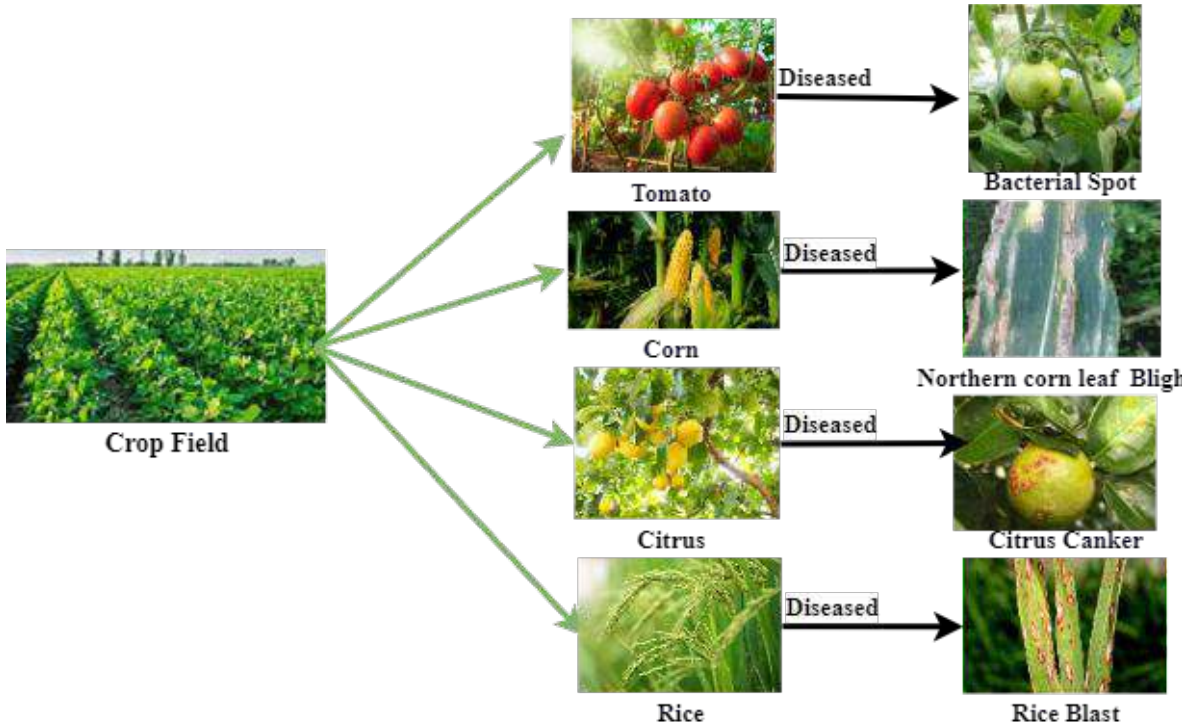

Fig. 1: Sample healthy and diseased crop images.

issues can be solved using artificial intelligence techniques (Yuan et al. 2021).

Traditional machine learning algorithms were initially used to detect plant diseases using plant images, resulting in limited accuracy and dataset range. Due to advancements in artificial intelligence and computer vision technology, deep learning has recently become popular in image identification (Turkoglu et al. 2022). Convolutional Neural Network (CNN) is the most commonly used neural network model in deep learning. CNN has great auto-learning, flexibility, and generalization capabilities (Xiong et al. 2021). CNN is based on biological nervous and visual systems. It is an unsupervised deep-learning classification model which provides more detection and classification accuracy. Deep learning improves accuracy while also broadening the scope of identifying and classifying plant diseases (Sladojevic et al. 2016). There are numerous CNN models obtainable, such as AlexNet, VGG, GoogLeNet, ResNet, and others. Different methods are available based on depth, configuration, nonlinearity, and several units. The dropout rate and learning rate are two variables that can be adjusted in complicated processes for solving Identification and pattern recognition problems.

Section 2. Provides related work Section 3. Proposed DC-ELM model. Section 4. Comparative analysis based on existing technologies. Section 5. The research findings and future work are concluded.

RELATED WORK

There are several methods for examining plant diseases and pests in agriculture. Conventional machine-learning approaches have been widely adopted in agriculture. According to the study, there are different deep learning models with transfer learning that can detect plant diseases more accurately, and transfer learning has been widely applied to speed up training and enhance the performance of deep learning models. Transfer learning is an optimization that allows rapid progress, and is also associated with the issue of multitasking.

Traditional Crop Diseases Detection and Classification Techniques

Image processing techniques are extremely crucial in the automatic detection and early identification of plant diseases to rise plant production and quality. Image processing approaches such as noise removal, image segmentation, feature extraction, classification, and so on (Al-Windi et al. 2021). Techniques for segmentation include with K-Means clustering, fuzzy C-Means clustering, and color segmentation algorithms, among others. The technique of extracting features from different instances of the same class is known as feature extraction (Ali et al .2019). The wheat leaf disease infected severities with powdery mildew were recognized

based on the machine learning algorithm and hyperspectral imaging dataset. The finest model was selected by comparing the accuracy of various dimensionality reduction algorithms, which are principal component analysis (PCA), random forest (RF), and successive projection algorithms, and three different identification models were created by support vector machine (SVM) (Jiang et al. 2020), random forest, and probabilistic neural network. The final result showed that the SVM model with PCA dimensionality reduction ensured the finest result, with a classification accuracy of 93.33% (Zhao et al. 2020).

In this section, the performance of several classification algorithms, such as Random Forest (RF), Support vector machine (SVM), Decision tree(DT), K-nearest neighbors(KNN), and Naive Bayes(NB) on a tomato disease dataset is evaluated, and it is discovered that RF classification techniques beat other algorithms. When compared to other algorithms for classifying plant diseases, the RF algorithm achieves 89% accuracy (Neelakantan 2021). Machine learning-based system for leaf disease classification and detection model utilizes SVM, NB, and convolution neural network (CNN), and Histogram equalization remains used for pre-processing, and the PCA technique is used to extract image features (Pallathadka et al. 2021). The deep features of thirteen CNN models (11 most often used + 2 tiny architectures) were extracted from a specific layer, and the characteristics were then given to an SVM classifier to identify rice leaf disease. The efficiency of the classification models for recognizing rice leaf diseases is evaluated using transfer learning with SVM techniques. Finally, a comparison was made between deep feature plus SVM, transfer learning, bag of features, and classic image classification methods. The comparison of plant disease detection and classification techniques is précised in Table 1.

Table 1: Comparison of various techniques in plant disease detection.

Reference	Plant Name	Technique Used	Metrics	Research Gap
(Rahman et al. 2020)	Rice	Stacked CNN	This architecture reduces the model size by 98% compared to the VGG16 or other similar models.	To use memory-efficient CNN models to get high accuracy.
(Sethy et.al. 2020)	Rice	Deep feature plus SVM	This technique has improved the performance of classification models for identifying rice leaf diseases.	To add more varieties of rice disease data by using a suitable CNN model.
(Wang et al. 2021	Rice	CNN with Bayesian optimization	The model has better test accuracy.	Using different optimization algorithms and hyperparameter tuning will improve the performance.
(Archana & Sahayadhas 2018)	Rice	K-mean clustering	Automatic rice disease identification was achieved.	Some pigments in the leaves are not extracted properly which leads to less accurate results.
(Ramesh & Vydeki 2020)	Rice	Deep neural network, Jaya optimization algorithm(DNN-JOA)	This proposed system archives better Classification and test accuracy.	Improved methods can enhance the best performance.
(Li et al. 2020)	Rice	Custom backbone DCNN network	This approach is capable of detecting diseases using Video images	Real-time crop diseases and pest video detection system is needed
(Shrivastava & Pradhan 2021)	Rice	Support vector machine (SVM) classifier,	SVM achieves the highest classification accuracy compared to the other 7 classifiers.	Results are reported for a small dataset. Training speed was slow.
(Jiang et al. 2021)	Rice	CNN(Improved VGG16)	The proposed model can recognize multiple crop diseases at the same time. The fine-tuning method gives more accuracy than the reuse model method.	Fine-tuning with more parameters will give more accuracy.
(Abbas et al. 2021)	Tomato	Conditional Generative Adversarial Network(C-GAN) DenseNet 121	The proposed system improves network generalizability and C-GAN prevents Overfitting.	The disease identification system is not developed.
(Fuentes et al. 2017)	Tomato	Deep meta-architecture and feature extractor.	The proposed system deals with different illumination conditions, different sizes of images, and different backgrounds of images. This system not only Recognizes the disease but also identifies the location.	This model applies to a single crop.

Table cont....

Reference	Plant Name	Technique Used	Metrics	Research Gap
(Trivedi et al. 2021	Tomato	Deep Convolutional Neural Network (DCNN)	It achieves 98.6%classification accuracy.	Results are reported for biotic diseases in the crop leaf.
(Thangaraj et al. 2021)	Tomato	DCNN model, Adaptive moment estimation (Adam), stochastic gradient descent (SGD)	This proposed model achieves better recognition accuracy on a small dataset.	Results are reported for a single crop.
(Yang et al. 2020)	Tomato	LFC-Net(Location, Feedback and Classification networks)	This model achieves high performance with an accuracy of up to 99.7%	Results are reported for a Limited number of diseases only.
(Gadekallu et al. 2021)	Tomato	PCA, Whale optimization algorithm, DNN	This proposed model achieves better training and testing accuracy. Loss percentage and time is taken for training have reduced.	Results are reported for a single crop.
(Liu & Wang 2020)	Tomato	MobileNetv2-YOLOv3	Limited memory consumption, and higher recognition accuracy.	The results are represented for a single disease.
(Chakraborty et al. 2021)	Tomato	VGG 16	This model achieves high-performance accuracy.	The results are represented for a single disease.
(Yu et al. 2022)	Maize	Multi-stage Grey wolf optimizer (MGWO)	The proposed system can obtain a more accurate solution.	Higher Time complexity
(Singh et al. 2022)	Maize	AlexNet	It gives efficient results in the case of smaller datasets.	It requires more epoch size for attaining high accuracy.
(Subramanian et al. 2022)	Maize	VGG16, , Bayesian optimization	This system efficiently works with the dataset which is not extremely large. Requires low computational power and less training time to retrain some of the top layers	Fewer hyperparameters have been taken for optimization.
(Waheed et al. 2020)	Maize	Optimized DenseNet model	This model achieves better accuracy in identifying three types of diseases	Results are reported for three types of diseases only.
(Khalili et al. 2020)	Soybean	Gradient Tree Boosting (GBT)	The proposed model was the best-performing classifier, giving better accuracy in terms of sensitivity is 96.25% and specificity is 97.33%.	Limited classification accuracy was achieved.
(Yan et al. 2020)	Bean	U-Net-based ResNet model, Robotic perception framework	The proposed system detects the bean leaves accurately from uncontrolled environmental conditions.	For large datasets, efficiency and reliability didn't prove.
(Annrose et al. 2022)	Soybean	Hybrid deep learning model with an optimization algorithm	The proposed method gives better training and testing accuracy.	Data overfitting issues.
(Nihar et al. 2021)	Bean and tomato	Modified convolutional neural network architecture (ModCNN)	Time-effective and cost-effective approaches.	Limited accuracy was achieved. Takes too many epochs to get better accuracy.
(Zeng et al. 2020)	Citrus	Deep Convolutional Generative Adversarial Networks Inception_v3 model	A deep learning model with Augmentation will give better disease severity detection accuracy. Which is 20% more than the model trained on the original dataset.	Real environment image datasets are needed to test in real-time scenarios. Traditional augmented methods are not applied.
(Sharif et al. 2018)	Citrus	Optimized weighted segmentation method, Multi-Class Support Vector Machine (M-SVM)	This system achieves better segmentation accuracy, best features are selected for disease classification.	Results are reported for a small dataset. Overfitting
(Elaraby et al. 2022)	Citrus	AlexNet Stochastic Gradient Descent with momentum	The AlexNet classifier is more accurate than the VGG19 classifier.	This model applies to standard-sized image datasets. It requires more epochs
(Syed-Ab-Rahman et al. 2022)	Citrus	Feature extractor and region proposal network	The region-based classification gives more accurate results.	It is applied to small datasets. Overfitting.
(Zou et al. 2020)	Tea	Decision Tree & Random Forest	Feature selection with random forest made the classification result more accurate.	Lack of datasets.

Table cont....

Reference	Plant Name	Technique Used	Metrics	Research Gap
(Patil & Burkpalli 2021)	Cotton	Multilayer Perceptron, Support Vector	Artificial neural networks (MLP) give 96.69% accuracy, better accuracy compared to other classifiers. Classifier performance was better while using color feature extraction.	It takes a long time to train a large dataset. Texture features are not taken for classification.
(Azadbakht et al. 2019)	Wheat	v-Support Vector Regression	The severity of wheat leaf rust diseases varied under high, medium, and low LAI levels.	It is not possible to extract all wavelengths at each level of the LAI.
(Yebasse et al. 2021)	Coffee	Deep neural network	Achieves better classification accuracy compared to other naive approaches.	Localization is not done on the diseases. Only black box testing does not effectively detect the defective region.
(Singh et al. 2019)	Mango	AlexNet architecture, Multilayer convolutional neural network	This model automatically extracts the image without segmentation.	Training times are high.
(Khan et al. 2022)	Cucumber	Entropy-ELM technique with deep learning	Fine-tuned pre-trained model with augmentation improves accuracy. Feature selection techniques reduce the Computational time.	The augmentation process increases the time. Few features are ignored during the feature selection process.
(Jiang et al. 2019)	Apple	Deep CNNs, GoogLeNet Inception	High accuracy and faster detection speed.	Uniform background images were taken.
(Singh 2019)	Sunflower	Segmentation –particle swarm optimization	The proposed system achieves good segmentation accuracy.	The main limitation of the image segmentation technique is the need for a faster search speed to lower search time.

Originating from Artificial Neural Networks (ANNs) (Ferentinos 2018) are the most prominent algorithms in machine learning. Machine learning algorithms are the best choice for identifying homogeneous plant images captured in a lab environment. Machine learning problems have recently been addressed with deep learning and convolutional neural networks. (Li et al. 2018). Northern maize leaf blight is a deadly disease that affects maize health. The field's varied background and varying light intensities make illness detection more challenging. To identify maize leaf blight, a multi-scale feature fusion instance recognition approach based on a CNN is presented. The NLB dataset is used here. The suggested technique consists of three primary steps: data set preparation, network fine-tuning, and the detection module (Sun et al. 2020). This research investigates the use of discrete lesions and spots for plant disease detection instead of considering the entire leaf (Barbedo 2019). In this study, the CNN technique requires a large and wide variety of datasets, which is an important limitation in deep learning (Barbedo 2018).

MULTI CROP'S DISEASE DETECTION USING DEEP CONVOLUTIONAL EXTREME LEARNING MACHINE

The proposed method for detecting plant diseases based on images employs deep transfer learning with deep convolutional neural networks. Extreme learning machine architecture will be able to maximize the benefits of deep learning

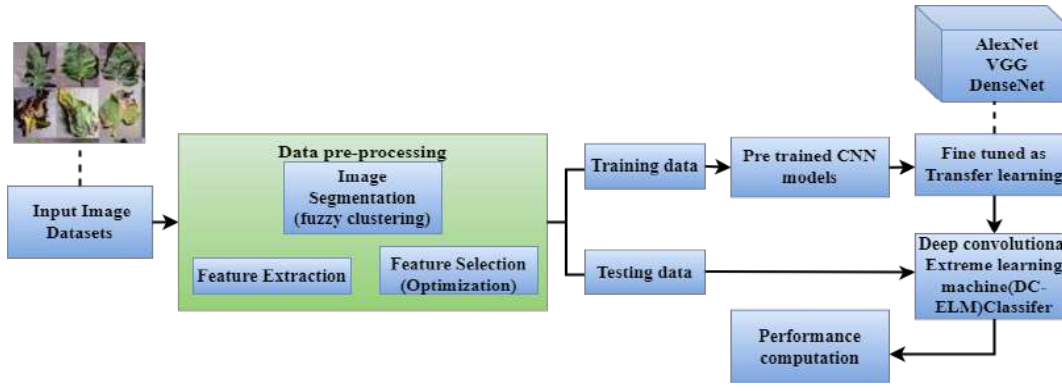

Fig. 2: Block diagram of the proposed DC-ELM System Model.

when used to detect plant diseases using leaf images. Previous research has shown that CNN can effectively recognize plant leaf disease and also suffer from some challenges that as lengthy training time, Iterative methods based on gradient methods can take longer to adjust weights and have a higher computational cost. As a result, it is necessary to investigate alternative approaches; it appears that DC-ELM outperforms other conventional learning algorithms.

The general architecture of the proposed DC-ELM system is illustrated in Fig. 2, which involves input image datasets, pre-processing, the deep learning architecture module, the transfer learning module, the deep convolutional Extreme learning machine, and the performance metrics.

Image Dataset

Deep learning architectures were examined and trained on the input plant leaf image dataset to categorize and recognize diseases in the plant image dataset. The dataset is first divided into two sections. The training data, followed by the test data, with a ratio of 80% and 20%, respectively. The datasets contain images of healthy and diseased leaves (Albattah et al. 2022). An enormous volume of training data is required to effectively train a deep-learning classification model. As a result, augmentation operations have been performed on the training dataset to increase the size of the image dataset used in training and avoid overfitting, which can occur when limited training data is used during training.

Data Pre-Processing

The images are collected in real-time conditions and contain noise. Preprocessing is the process of removing noise, which improves the quality of images (Cristin et al. 2020). Therefore, images are preprocessed before extracting features for the disease detection system to increase its computational accuracy. The time taken to process an image is also reduced when resizing and cropping an image. The simplest way to prevent over-fitting is to train the model on a significant amount of data. Augmentation is the process of creating additional training data from existing data. Throughout the training, the images were exposed to augment such as brightness, and contrast in color augmentation techniques, and image flipping left-right, flipping up-down, scaling, and rotating are position augmentation techniques were randomly used to make the model more effective (Gajjar et al. 2021), To augment the data, several techniques such as Generative adversarial networks (GANs) (Nerkar & Talbar 2021), neural style transfer, and adversarial training are used. Segmentation is used to divide an image into interesting regions (Sai Reddy & Neeraja 2022).

Features are relevant and discriminating attributes/information associated with objects that differentiate one object from others. Features are useful for identifying objects and classifying them. Feature extraction is key to building the classification/recognition model and determining the relevant attribute characteristics of each class (Kurmi et al. 2022). Generally, features such as shape, color, size, corners, edges, and so on are taken into account for object recognition. Feature selection techniques are employed to find the most applicable features from the characteristic vector. Analysis (PCA) score, entropy, and covariance of extracted points are measured for extracted features are measured

Pre-Trained Deep Learning Models

Artificial neural networks are mathematical models which reflect common principles of brain function through their neurons and synapses. CNNs (Zekiwos & Bruck 2021) are a subset of traditional artificial neural networks that are mainly concentrated on applications with repeated patterns in various areas of the modeling of an image-based recognition system. Pre-trained models, which were trained previously on different datasets, perform tasks like classification, and feature extraction. The core CNN architectures are AlexNet, DenseNet, and the VGG16 metrics phase. The pre-trained model architecture requires less training and effort to build.

AlexNet Model

AlexNet (Wang 2022) is a 60-million-parameter eight-layer deep network with five convolutional layers and three completely connected layers. It is a conventional convolutional neural network model that employs dropout to avoid overfitting by randomly disregarding some neurons and employs a rectified linear unit (RELU) as an activation function. The model uses two GPUs at the same time to accelerate neural network training. As a result, when compared to other models, AlexNet (Dhaka et al. 2021) excels at image categorization and object recognition.

DenseNet Model

DenseNet (Vallabhajosyula et al. 2021) is used in CNN networks to optimize the connecting patterns between layers. To overcome the drawback of maximum data flow, each layer in this network is directly connected to the other layers. DenseNet has fewer feature maps than regular CNN. DenseNet solves gradient-related issues. The DenseNet model's layers have direct access to the results from the input images as well as a gradient loss function. The DenseNet uses a typical feed-forward network, with each layer's output being linked to the previous layer via a composite operation. These operations include layer pooling, batch normalization, and an activation function. The DenseNet concept can be

broken down into small dense blocks. The transition layers in the dense blocks are responsible for down-sampling while batch normalization is applied.

VGG16 Model

The VGG16 (Abed et al. 2021) model is a deep convolution model with 13 convolutional layers, five pooling layers, and three fully connected layers. Six block structures are present in all VGG configurations. The feature extraction layer is made up of these six blocks, with the remaining three completely connected layers serving as the classification layer.

Transfer Learning

Transfer learning is the process of re-applying a formerly trained deep learning model to a new problem. We describe a unique approach for fusing data at multiple levels of abstraction to improve transfer learning efficiency (Cruz et al. 2017). Transfer learning (Johnson et al. 2021) is a common deep learning strategy that involves transferring pre-trained model weights to a new classification problem, as shown in Fig. 3. As a concern, training is more efficient than it improves the performance of the model also improves computational efficiency. TL is particularly important in deep convolutional neural networks (Chen et al. 2020b). Transfer learning involves the concept of fine-tuning. Fine-tuning improves accuracy on lesser datasets and is quicker than starting from scratch. To improve accuracy, hyperparameters are fine-tuned using a transfer learning approach.

Deep Convolutional Extreme Learning Machine (DC-ELM)

An Extreme Learning Machine (ELM) (Aqel et al. 2021, Zhang et al. 2017) is a classification technique for Single Hidden Layer Feed Forward Neural Networks (SLFNs) or Multiple Hidden Layer Feed-Forward Neural Networks (MLFNs). It improves the speed of convergence training and eliminates the need for multiple iterations to change the hidden layer weights (Imran & Raman 2020). ELM is a one-of-a-kind training method because it does not use gradient calculations to update network weights (Alagumariappan et al. 2020). The ELMs are believed to have the ability to learn thousands of times faster than networks trained using the backpropagation technique (Bhatia et al. 2020). The DC-ELM (Santos et al. 2019) is a deep convolutional extreme learning machine that integrates the speed of ELM training with the capability of CNN. In the final hidden layer, DC-ELM employs stochastic pooling to drastically reduce feature dimensionality. This saves both training time and computational resources (Pang & Yang 2016). The DC-ELM combines the convolutional neural network's feature abstraction performance with the extreme learning machine for fast training (Rodrigues et al. 2021). The example architecture of DC-ELM is shown in Fig. 4.

The Optimizer Used in DL and TL

Image processing requires bio-inspired optimization strategies. By reducing noise and blurring, it improves image

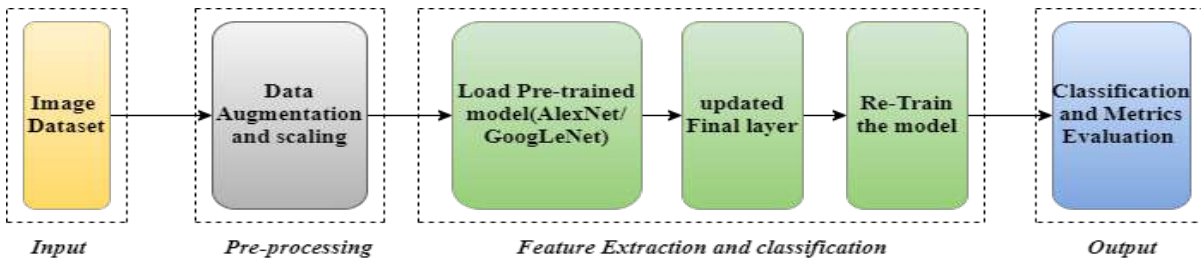

Fig. 3: Classification based on transfer learning.

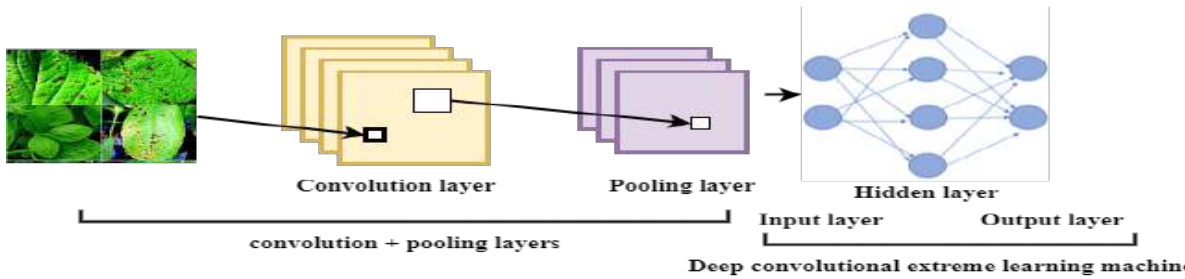

Fig. 4: Example of a CNN-based DC-ELM architecture.

enhancement, restoration, segmentation, edge detection, and pattern recognition. So far, various optimization strategies for various image-processing applications have been proposed (Jino Ramson et al. 2019). The accuracy of the deep learning model is greatly influenced by optimization algorithms. To train a neural network architecture, create a loss function that measures the difference between model predictions and the label that wish to predict. Various optimizers can be used to adjust your weights and learning rate. On the other hand, choosing the best optimizer is dependent on the application. DL optimization approaches include (SGD) Stochastic Gradient Descent (Saleem et al. 2020, Gong et al. 2020) and (Adam) Adaptive Moment Estimation (Alzubaidi et al. 2021).

An optimization method is used in the plant disease detection system for feature selection and feature extraction. This optimization technique aids in the selection of the best features, which improves the performance of the classifier.

Performance Computation

The confusion matrix elements are used to calculate the performance measures, used to evaluate the models' performance (Hariri & Avsar 2022). A relative study using the accuracy, sensitivity, and specificity metrics demonstrate the method's efficacy. Accuracy, Sensitivity, Specificity, Precision, Recall, and F1 Score are some of the performance metrics that are evaluated (Djimeli-Tsajio et al. 2022).

The accuracy rate at which a plant disease is detected, and is calculated as the ratio of correctly identified positive and negative samples to total samples, as shown below. The sample count is evenly distributed across the different classes of diseases.

$$\text{Accuracy} = \frac{\text{number of samples correctly identified}}{\text{total number of sample}} \times 100\%$$

The loss function should be calculated using training loss with accuracy, training result, and validation loss with accuracy, validation loss. This F1 score assists us in determining both recall and precision of the total number of classes specified in the diseases.

$$\text{F1 Score} = 2 * \frac{\text{Precision} - \text{Recall}}{\text{Precision} + \text{Recall}}$$

The proposed DC-ELM models perform the metrics in terms of classification accuracy, loss function, and F1-Score.

COMPARATIVE ANALYSIS BASED ON THE EXISTING TECHNIQUE

To evaluate the performance, a comparison was made with existing approaches presented in the survey. The survey found TL with optimization outperforms the vast majority of associated tasks. While analyzing the performance of TL-based approaches to other state-of-art techniques, specific, accurate, and appropriate comparisons were made between

Table 2: Comparison of deep learning model used in plant disease classification with accuracy.

Type of plant	Type of diseases	Method used	Classification Accuracy	References
Rice	Bacterial Leaf Blight, Rice Blast, Sheath Blight, Healthy Leave	Support vector machine (SVM) classifier	94.65	(Shrivastava & Pradhan 2021)
Wheat	wheat leaf rust	v-Support Vector Regression	95	(Azadbakht et al. 2019)
Tea	Anthracnose, Brown leaf spot, tea white star	Decision Tree & Random Forest	80	(Zou et al. 2020)
Rice Wheat	Bacterial blight, brown spot, leaf blast Leaf rust, powdery mildew	CNN (improved VGG16)	97.22 98.75	(Jiang et al. 2021)
Tomato	Early blight, bacterial leaf spot, curl virus, fruit canker, and powdery Mildew.	DCNN	99.55	(Thangaraj et al. 2021)
Corn	corn common rust, gray leaf spot, northern corn leaf blight	CNN (DenseNet)	98.06	(Waheed et al. 2020)
Bean Tomato	Mosaic Virus Tomato curl leaf	ModCNN	97.69	(Nihar et al. 2021)
Citrus	Anthracnose, Black spot, Citrus Canker	Multi-Class Support Vector Machine (M-SVM)	97	(Sharif et al. 2018)
Cotton	bacterial blight	Multilayer Perceptron, Support Vector (ANN)	96.69	(Patil & Burkpalli 2021)
Coffee	Coffee leaf rust	Deep neural network (DNN)	98	(Yebasse et al. 2021)

the Deep learning and ML-based strategies used to solve the specific problem addressed in each study. Deep learning is currently struggling to model numerous complicated data modalities at the same time. Another important area of modern deep learning research is multi-tasking with extreme learning machines.

The accuracy of the classification of machine learning and deep learning methods is compared in Table 2. The classification accuracy of different CNN models and machine learning models for plant disease identification was discovered. The comparison result shows that deep learning models outperform machine learning models in terms of accuracy.

CONCLUSION

Deep learning with DC-ELM concepts is used in the proposed model to accurately identify plant diseases that can automatically identify signs of plant disease and is performed with high accuracy. In comparison to traditional image processing methods, which handle plant disease and pest recognition tasks in multiple steps. We conducted a survey on the detection and classification of diseases in various agricultural products using image processing, machine learning, and deep learning techniques. We identified 60 relevant studies by evaluating the specific region and issue they concentrate on, practical aspects of the models used, datasets used, data preprocessing and data augmentation techniques used, and overall performance according to the achievement criteria listed by each paper. Then, in terms of performance, we compared transfer learning to other existing approaches. As per the comparison transfer learning with optimization and DC-ELM beats other common imaging approaches. In the future, we intend to extend the broad concepts and best-practices ensemble learning technique, as detailed to additional sectors of agriculture where this modern method has not yet been fully implemented, to improve the performance of the model the research is extended based on multi-task learning with extreme learning machine.

REFERENCES

Abbas, A., Jain, S., Gour, M. and Vankudothu, S. 2021. Tomato plant disease detection using transfer learning with C-GAN synthetic images. Comput. Electron. Agric., 187: 106279.

Abed, S.H., Al-Waisy, A.S., Mohammed, H.J. and Al-Fahdawi, S. 2021. A modern deep learning framework in robot vision for automated bean leaves disease detection. Int. J. Intell. Robot. Appl., 5(2): 235-251.

Alagumariappan, P., Dewan, N.J., Muthukrishnan, G.N., Raju, B.K.B., Bilal, R.A.A. and Sankaran, V. 2020. Intelligent plant disease identification system using Machine Learning. Eng. Proceed., 2(1): 49.

Albattah, W., Nawaz, M., Javed, A., Masood, M. and Albahli, S. 2022. A novel deep learning method for detection and classification of plant diseases. Compl. Intell. Syst., 8(1): 507-524.

Al-Windi, B.K.M.A., Abbas, A.H. and Mahmood, M.S. 2021. Wheat stem rust leaf disease detection using image processing. Mater. Proceed., 61: 151-163.

Ali, M.M., Bachik, N.A., Muhadi, N.A., Yusof, T.N.T. and Gomes, C. 2019. Non-destructive techniques of detecting plant diseases: A review. Physiol. Mol. Plant Pathol., 108: 101426.

Alzubaidi, L., Zhang, J., Humaidi, A.J., Al-Dujaili, A., Duan, Y., Al-Shamma, O. and Farhan, L. 2021. Review of deep learning: concepts, CNN architectures, challenges, applications, future directions. Journal of Big Data, 8(1): 1-74.

Annrose, J., Rufus, N., Rex, C.R. and Immanuel, D.G. 2022. A cloud-based platform for soybean plant disease classification using Archimedes optimization-based hybrid deep learning model. Wirel. Personal Commun., 122(4): 2995-3017.

Aqel, D., Al-Zubi, S., Mughaid, A. and Jararweh, Y. 2021. Extreme learning machine for plant diseases classification: A sustainable approach for smart agriculture. Clust. Comput., 1-14.

Archana, K.S. and Sahayadhas, A. 2018. Automatic rice leaf disease segmentation using image processing techniques. Int. J. Eng. Technol., 7(3.27): 182-185.

Azadbakht, M., Ashourloo, D., Aghighi, H., Radiom, S. and Alimohammadi, A. 2019. Wheat leaf rust detection at canopy scale under different LAI levels using machine learning techniques. Comput. Electron. Agric., 156: 119-128.

Barbedo, J.G.A. 2019. Plant disease identification from individual lesions and spots using deep learning. Biosyst. Eng., 180: 96-107.

Barbedo, J.G.A. 2018. Impact of dataset size and variety on the effectiveness of deep learning and transfer learning for plant disease classification. Comput. Electron. Agric., 153: 46-53.

Bhatia, A., Chug, A. and Prakash Singh, A. 2020. Application of extreme learning machine in plant disease prediction for highly imbalanced dataset. J. Stat. Manag. Syst., 23(6): 1059-1068.

Chakraborty, S., Kodamana, H. and Chakraborty, S. 2021. Deep learning aided automatic and reliable detection of tomato begomovirus infections in plants. J. Plant Biochem. Biotechnol., 21: 1-8.

Chen, J., Zhang, D. and Nanehkaran, Y. A. 2020a. Identifying plant diseases using deep transfer learning and enhanced lightweight network. Multimedia Tool Appl., 79(41): 31497-31515.

Chen, J., Chen, J., Zhang, D., Sun, Y. and Nanehkaran, Y. A. 2020b. Using deep transfer learning for image-based plant disease identification. Comput. Electron. Agric., 173: 105393.

Conrad, A.O., Li, W., Lee, D.Y., Wang, G.L., Rodriguez-Saona, L. and Bonello, P. 2020. Machine learning-based presymptomatic detection of rice sheath blight using spectral profiles. Plant Phenom., 2: 10.

Cristin, R., Kumar, B.S., Priya, C. and Karthick, K. 2020. Deep neural network-based Rider-Cuckoo Search Algorithm for plant disease detection. Artif. Intell. Rev., 53(7): 4993-5018.

Cruz, A.C., Luvisi, A., De Bellis, L. and Ampatzidis, Y. 2017. Vision-based plant disease detection system using transfer and deep learning. ASABE, 20: 171

Dhaka, V.S., Meena, S.V., Rani, G., Sinwar, D., Ijaz, M.F. and Woźniak, M. 2021. A survey of deep convolutional neural networks applied for prediction of plant leaf diseases. Sensors, 21(14): 4749.

Djimeli-Tsajio, A. B., Thierry, N., Jean-Pierre, L. T., Kapche, T. F. and Nagabhushan, P. 2022. Improved detection and identification approach in tomato leaf disease using transformation and a combination of transfer learning features. Journal of Plant Diseases and Protection, 1-10.

Santos, M.M., da Silva Filho, A.G. and dos Santos, W.P. 2019. Deep convolutional extreme learning machines: Filters combination and error model validation. Neurocomputing, 329: 359-369.

Elaraby, A., Hamdy, W. and Alanazi, S. 2022. Classification of citrus diseases using optimization deep learning approach. Comp. Intell. Neurosci., 2022.

Ferentinos, K.P. 2018. Deep learning models for plant disease detection and diagnosis. Comput. Electron. Agric., 145: 311-318.

Fuentes, A., Yoon, S., Kim, S.C. and Park, D.S. 2017. A robust deep-learning-based detector for real-time tomato plant diseases and pests recognition. Sensors, 17(9): 202.

Gadekallu, T.R., Rajput, D.S., Reddy, M., Lakshmanna, K., Bhattacharya, S., Singh, S. and Alazab, M. 2021. A novel PCA–whale optimization-based deep neural network model for classification of tomato plant diseases using GPU. J. Real-Time Image Process., 18(4): 1383-1396.

Gajjar, R., Gajjar, N., Thakor, V. J., Patel, N. P. and Ruparelia, S. 2021. Real-time detection and identification of plant leaf diseases using convolutional neural networks on an embedded platform. Vis Comput., 11: 1-16.

Gong, D., Zhang, Z., Shi, Q., van den Hengel, A., Shen, C. and Zhang, Y. 2020. Learning deep gradient descent optimization for image deconvolution. IEEE Trans. Neural Netw. Learn. Syst., 31(12): 5468-5482.

Gu, Q., Sheng, L., Zhang, T., Lu, Y., Zhang, Z., Zheng, K. and Zhou, H. 2019. Early detection of tomato spotted wilt virus infection in tobacco using the hyperspectral imaging technique and machine learning algorithms. Comput. Electron. Agric., 167: 105066.

Hang, J., Zhang, D., Chen, P., Zhang, J. and Wang, B. 2019. Classification of plant leaf diseases based on improved convolutional neural network. Sensors, 19(19): 4161.

Hariri, M. and Avşar, E. 2022. Tipburn disorder detection in strawberry leaves using convolutional neural networks and particle swarm optimization. Multimedia Tool Appl., 81(8): 11795-11822.

Imran, J. and Raman, B. 2020. Deep motion templates and extreme learning machine for sign language recognition. Vis Comput., 36(6): 1233-1246.

Jiang, P., Chen, Y., Liu, B., He, D. and Liang, C. 2019. Real-time detection of apple leaf diseases using deep learning approach based on improved convolutional neural networks. IEEE Access, 7: 59069-59080.

Jiang, F., Lu, Y., Chen, Y., Cai, D. and Li, G. 2020. Image recognition of four rice leaf diseases based on deep learning and support vector machine. Comput. Electron. Agric., 179: 105824.

Jiang, Z., Dong, Z., Jiang, W. and Yang, Y. 2021. Recognition of rice leaf diseases and wheat leaf diseases based on multi-task deep transfer learning. Comput. Electron. Agric., 186: 106184.

Jino Ramson, S. R., Lova Raju, K., Vishnu, S. and Anagnostopoulos, T. 2019. Nature-inspired optimization techniques for image processing—A short review. Nature Inspired Optimization Techniques for Image Processing Applications, 113-145.

Johnson, J., Sharma, G., Srinivasan, S., Masakapalli, S. K., Sharma, S., Sharma, J. and Dua, V. K. 2021. Enhanced field-based detection of potato blight in complex backgrounds using deep learning. Plant Pheno., 2: 21.

Khalili, E., Kouchaki, S., Ramazi, S. and Ghanati, F. 2020. Machine learning techniques for soybean charcoal rot disease prediction. Front. Plant Sci., 11: 2009.

Khan, M.A., Alqahtani, A., Khan, A., Alsubai, S., Binbusayyis, A., Ch, M. and Cha, J. 2022. Cucumber leaf disease recognition using multi-level deep entropy-ELM Feature Selection. Appl. Sci., 12(2): 593.

Khan, R.U., Khan, K., Albattah, W. and Qamar, A.M. 2021. Image-based detection of plant diseases: From classical machine learning to the deep learning journey. Wirel. Commun. Mob. Comput., 2021.

Kurmi, Y., Saxena, P., Kirar, B.S., Gangwar, S., Chaurasia, V. and Goel, A. 2022. Deep CNN model for crops diseases detection using leaf images. Multidim. Syst Signal Process., 16: 1-20.

Li, J., Wang, N., Wang, Z. H., Li, H., Chang, C.C. and Wang, H. 2018. New secret sharing scheme based on faster R-CNNs image retrieval. IEEE Access, 6: 49348-49357.

Li, L., Zhang, S. and Wang, B. 2021. Apple leaf disease identification with a small and imbalanced dataset based on lightweight convolutional networks. Sensors, 22(1): 173.

Li, D., Wang, R., Xie, C., Liu, L., Zhang, J., Li, R. and Liu, W. 2020. A recognition method for rice plant diseases and pests video detection based on deep convolutional neural network. Sensors, 20(3): 578.

Lin, F., Guo, S., Tan, C., Zhou, X. and Zhang, D. 2020. Identification of rice sheath blight through spectral responses using hyperspectral images. Sensors, 20(21): 6243.

Liu, B., Tan, C., Li, S., He, J. and Wang, H. 2020. A data augmentation method based on generative adversarial networks for grape leaf disease identification. IEEE Access, 8: 102188-102198.

Liu, J. and Wang, X. 2020. Early recognition of tomato gray leaf spot disease based on MobileNetv2-YOLOv3 model. Plant Methods, 16(1): 1-16.

Neelakantan, P. 2021. Analyzing the best machine learning algorithm for plant disease classification. Mater. Today Proceed., 2214-7853.

Nerkar, B. and Talbar, S. 2021. Cross-dataset learning for performance improvement of leaf disease detection using reinforced generative adversarial networks. Int. J. Inf. Technol., 13(6): 2305-2312.

Nihar, F., Khanom, N. N., Hassan, S. S. and Das, A. K. 2021. Plant disease detection through the implementation of diversified and modified neural network algorithms. J. Eng. Adv., 2(01): 48-57.

Pallathadka, H., Ravipati, P., Sajja, G.S., Phasinam, K., Kassanuk, T., Sanchez, D.T. and Prabhu, P. 2021. Application of machine learning techniques in rice leaf disease detection. Mater. Today Proceed., 6: 514.

Pang, S. and Yang, X. 2016. Deep convolutional extreme learning machine and its application in handwritten digit classification. Comp. Intell. Neurosci., 2016.

Patil, B.M. and Burkpalli, V. 2021. A perspective view of cotton leaf image classification using machine learning algorithms using WEKA. Adv. Hum. Comput. Interact., 2021.

Rahman, C.R., Arko, P.S., Ali, M.E., Khan, M.A.I., Apon, S.H., Nowrin, F. and Wasif, A. 2020. Identification and recognition of rice diseases and pests using convolutional neural networks. Biosyst. Eng., 194: 112-120.

Ramesh, S. and Vydeki, D. 2020. Recognition and classification of paddy leaf diseases using optimized deep neural network with Jaya algorithm. Inform. Process. Agric., 7(2): 249-260.

Rodrigues, I.R., da Silva Neto, S.R., Kelner, J., Sadok, D. and Endo, P.T. 2021. Convolutional extreme learning machines: A systematic review. Informatics, 8(1): 33

Sai Reddy, B. and Neeraja, S. 2022. Plant leaf disease classification and damage detection system using deep learning models. Multimedia Tool Appl., 6: 1-20.

Saleem, M.H., Khanchi, S., Potgieter, J. and Arif, K.M. 2020. Image-based plant disease identification by deep learning meta-architectures. Plants, 9(11): 1451.

Sethy, P.K., Barpanda, N.K., Rath, A.K. and Behera, S.K. 2020. Deep feature-based rice leaf disease identification using a support vector machine. Comput. Electron. Agric., 175: 105527.

Sharif, M., Khan, M.A., Iqbal, Z., Azam, M.F., Lali, M.I.U. and Javed, M.Y. 2018. Detection and classification of citrus diseases in agriculture based on optimized weighted segmentation and feature selection. Comput. Electron. Agric., 150: 220-234.

Shrivastava, V. K. and Pradhan, M. K. 2021. Rice plant disease classification using color features: A machine learning paradigm. J. Plant Pathol., 103(1): 17-26.

Singh, U.P., Chouhan, S.S., Jain, S. and Jain, S. 2019. Multilayer convolution neural network for the classification of mango leaves infected by anthracnose disease. IEEE Access, 7: 43721-43729.

Singh, V. 2019. Sunflower leaf disease detection using image segmentation based on particle swarm optimization. Artif. Intell. Agric., 3: 62-68.

Singh, R.K., Tiwari, A. and Gupta, R.K. 2022. Deep transfer modeling for classification of Maize Plant Leaf Disease. Multimedia Tool Appl., 15: 1-17.

Sladojevic, S., Arsenovic, M., Anderla, A., Culibrk, D. and Stefanovic, D. 2016. Deep neural networks-based recognition of plant diseases by leaf image classification. Comp. Intell. Neurosci., 2016.

Subramanian, M., Shanmugavadivel, K. and Nandhini, P.S. 2022. On fine-tuning deep learning models using transfer learning and hyper-pa-

rameters optimization for disease identification in maize leaves. Neural Comput. Appl., 10: 1-18.

Sun, J., Yang, Y., He, X. and Wu, X. 2020. Northern maize leaf blight detection under complex field environment based on deep learning. IEEE Access, 8: 33679-33688.

Syed-Ab-Rahman, S.F., Hesamian, M.H. and Prasad, M. 2022. Citrus disease detection and classification using end-to-end anchor-based deep learning model. Appl. Intell., 52(1): 927-938.

Thangaraj, R., Anandamurugan, S. and Kaliappan, V.K. 2021. Automated tomato leaf disease classification using transfer learning-based deep convolution neural network. J. Plant Dis. Prot., 128(1): 73-86.

Trivedi, N.K., Gautam, V., Anand, A., Aljahdali, H.M., Villar, S.G., Anand, D. and Kadry, S. 2021. Early Detection and Classification of Tomato Leaf Disease Using High-Performance Deep Neural Network. Sensors, 21(23): 7987.

Turkoglu, M., Yanikoğlu, B. and Hanbay, D. 2022. PlantDiseaseNet: Convolutional neural network ensemble for plant disease and pest detection. Signal, Image and Video Processing, 16(2): 301-309.

Vallabhajosyula, S., Sistla, V. and Kolli, V.K.K. 2021. Transfer learning-based deep ensemble neural network for plant leaf disease detection. J. Plant Dis. Prot., 1-14.

Vishnoi, V. K., Kumar, K. and Kumar, B. 2021 Plant disease detection using computational intelligence and image processing. J. Plant Dis. Prot., 128(1): 19-53.

Waheed, A., Goyal, M., Gupta, D., Khanna, A., Hassanien, A.E. and Pandey, H M. 2020. An optimized dense convolutional neural network model for disease recognition and classification in corn leaf. Comput. Electron. Agric., 175: 105456.

Wang, Y., Wang, H. and Peng, Z. 2021. Rice disease detection and classification using attention-based neural network and bayesian optimization. Expert Syst Appl., 178: 114770.

Wang, B. 2022. Identification of crop diseases and insect pests based on deep learning. Sci. Program., 1: 022.

Xiong, J., Yu, D., Liu, S., Shu, L., Wang, X. and Liu, Z. 2021. A review of plant phenotypic image recognition technology based on deep learning. Electronics, 10(1): 81.

Yan, Q., Yang, B., Wang, W., Wang, B., Chen, P. and Zhang, J. 2020. Apple leaf disease recognition is based on an improved convolutional neural network. Sensors, 20(12): 3535.

Yang, G., Chen, G., He, Y., Yan, Z., Guo, Y. and Ding, J. 2020. Self-supervised collaborative multi-network for fine-grained visual categorization of tomato diseases. IEEE Access, 8: 211912-211923.

Yebasse, M., Shimelis, B., Warku, H., Ko, J. and Cheoi, K.J. 2021. Coffee disease visualization and classification. Plants, 10(6): 1257.

Yuan, Y., Chen, L., Wu, H. and Li, L. 2021. Advanced agricultural disease image recognition technologies: A review. Inf. Process. Agric., 19: 534-546.

Yu, H., Song, J., Chen, C., Heidari, A. A., Liu, J., Chen, H. and Mafarja, M. 2022. Image segmentation of leaf spot diseases on maize using multi-stage Cauchy-enabled grey wolf algorithm. Eng. Appl. Artif. Intell., 109: 104653.

Zeng, Q., Ma, X., Cheng, B., Zhou, E. and Pang, W. 2020. Gans-based data augmentation for citrus disease severity detection using deep learning. IEEE Access, 8: 172882-172891.

Zekiwos, M. and Bruck, A. 2021. Deep learning-based image processing for cotton leaf disease and pest diagnosis. Journal of Electrical and Computer Engineering.

Zhang, L., He, Z. and Liu, Y. 2017. Deep object recognition across domains based on adaptive extreme learning machine. Neurocomputing, 239: 194-203.

Zhao, J., Fang, Y., Chu, G., Yan, H., Hu, L. and Huang, L. 2020. Identification of leaf-scale wheat powdery mildew (Blumeria graminis f. sp. Tritici) combining hyperspectral imaging and an SVM classifier. Plants, 9(8): 936.

Zou, X., Ren, Q., Cao, H., Qian, Y. and Zhang, S. 2020. Identification of tea diseases based on spectral reflectance and machine learning. J. Inf. Process. Syst., 16(2): 435-446.

Nature Environment and Pollution Technology
An International Quarterly Scientific Journal

p-ISSN: 0972-6268
(Print copies up to 2016)
e-ISSN: 2395-3454

Vol. 21 | No. 5 (Suppl) | pp. 2177-2187 | 2022

Original Research Paper

https://doi.org/10.46488/NEPT.2022.v21i05.012

Open Access Journal

Sensitivity of WRF Model for Simulation of 2014 Massive Flood Over Kashmir Region: A Case of Very Heavy Precipitation

Zahid Nabi and Dinesh Kumar†

Department of Environmental Science, Central University of Jammu, Bagla (Rahya-Suchani), District Samba-181143, J&K, India

†Corresponding author: Dinesh Kumar; dkumarcuj@gmail.com

Nat. Env. & Poll. Tech.
Website: www.neptjournal.com

Received: 10-06-2022
Revised: 15-08-2022
Accepted: 19-08-2022

Key Words:
RMSE
MBIAS
WRF model
Vertical velocity

ABSTRACT

The present study simulates the devastating floods in Kashmir that caused widespread damage in the valley from September 2-6 2014. The study used NCEP-NCAR FNL data for the initialization and simulation of the WRF ARW model. Statistical analysis of temperature over four places namely Anantnag, Srinagar, Pulwama, and Baramulla taking RMSE and MBIAS at 24, 48, 72, and 96 hours was also done against observed ECMWF-ERA5 temperature data. Further analysis of RMSE and MBIAS showed a minimum value at 48, 72, and 96 h indicating the improvement of prediction after 6 hours. Rainfall amount was under-predicted by the model with a time lag of 4 h while temperature time series over four districts were significantly closer to observation. Furthermore, the Model was able to capture the strong vertical velocities along with sufficient moisture content up to 600 hPa at the time of observed rainfall.

INTRODUCTION

Floods can well be described as natural disasters that occur across all countries and cause tremendous damage to life and property (Berz et al. 2001) and leave serious impacts on human societies. The impact of floods is seen more in developing countries due to poor infrastructure and the absence of any flood warning system. People living in mountainous regions are more prone to floods and landslides (Watson & Haeberli 2004). An increase in the frequency of disasters brought about by floods in the mountainous regions has seen an increase during the last few decades (Sepúlveda & Padilla 2008, Korup & Clague 2009). The Indian Himalayan region which witnesses erratic weather often has also witnessed some hydrological disasters in the recent past, which include the Kosi Floods (2008), the flash floods that occurred in Leh in 2010, and the unprecedented Ganga River floods (2010), Brahmaputra floods (2012), flash floods in Kedarnath in 2013 and Srinagar floods (2014). Floods have been described as the main threat to sustainable development in the Himalayas (2004). The Kashmir Valley receives rainfall from two distinctive meteorological systems, i.e. southwest monsoon and extratropical disturbances (western disturbances). Many researchers have simulated events related to flooding by heavy rainfall using the WRF model. Hong & Lee (2009) conducted a study using the Korean Peninsula for a case of very heavy rainfall (around 400 mm). The model was able to capture accumulated rainfall amount distribution, even though the rainfall amount at one station (Goyang) was less than the observed. Nooni et al. (2022), used Weather Research and Forecasting (WRF) model to simulate seven heavy precipitation events that occurred across East Africa in the summer of 2020. The results showed that the WRF model was able to produce heavy precipitation, with recorded rainfall ranging from 6 to >30 mm/day. Kumar et al. (2008), used the WRF model at 3. km resolution to simulate the heavy rainfall event of 26 July 2005 over Mumbai. The model reproduced the intensity, amount, and distribution of the rainfall and the results were at par with observations. Another study using the same event over Mumbai was carried out by Rama Rao et al. (2007) with a WRF model run with a grid resolution of 20 km. The model was able to simulate approximately 250 mm of rain with a location error of 50 km north of Mumbai. Srinivas et al. (2018) used the WRF model for the study of a case of heavy rainfall over Chennai. The researchers concluded that the Model produced the best prediction in terms of timing, intensity, and distribution of rainfall for the domain with 1 km. grid resolution. Chen et al. (2010) used the WRF model to study a high precipitation event over southwestern Taiwan associated with a sub-synoptic cyclone in 2003. They showed that a sub-synoptic cyclone formed at 850 hPa formed over the eastern Tibetan Plateau which in association with a 500 hPa trough intensified and resulted in heavy precipitation in

Taiwan. Several researchers have used the WRF model over the Himalayan region. Kumar et al. (2012) used the WRF model for the study of the cloudburst event of 2010 over Leh. Kumar et al. (2014) and Thayyen et al. (2013) used the WRF model to understand the atmospheric processes that led to the 2010 Leh event. Likewise, Chevuturi et al. (2015) simulated the heavy precipitation event of September 2012 in the central Himalayas using the WRF model. Hassan & Islam (2018) used the WRF model, with different parametrization schemes to forecast rainfall events during the year's monsoon season. The researchers found the Stony Brook University microphysics scheme (SU) along with the Tiedtke cumulus scheme (TD) to be the best-performing scheme over the southeastern hilly regions of Bangladesh. The second-best combination according to the researchers is using WRF single-moment 6-class microphysics scheme (WM) and Grell (GR) cumulus scheme. Ntwali et al. (2016) researched the impacts using the WRF model. The researchers concluded that the impacts of topography during the long rainy season and that of the short rainy season are not the same due to the position and the shift of ITCZ. The researchers further found out that all orographic influences are fundamentally caused by topographically driven ascending and descending atmospheric motions that result in condensation and evaporation. Baki et al. (2021), investigated the combination of various parametrization schemes available in the WRF model to find the best combination of microphysics (MP) and cumulus parameterization (CP) schemes for the simulation of Tropical Cyclones (TCs) over the Indian subcontinent region. Their results showed that the Kain–Fritsch scheme, in combination with all MP schemes, predicts the tracks best among all the available CP schemes, but the performance of microphysics schemes remains indistinguishable.

The present work has been undertaken to investigate the ability of the WRF model to predict the moisture and heat flux between the land surface and the lower atmosphere during a heavy rainfall event. Further, the study tries to analyze the reproducibility of the atmosphere above the observed station in terms of moisture and vertical wind along with near and surface meteorological parameters such as rainfall, and temperature. The current study will also evaluate model performance through statistical analysis such as root mean square error (RMSE) and mean bias (MBias). The paper is organized as a synoptic description of the event as seen in observed data followed by methodology and domain design. Finally, the results have been described.

SYNOPTIC WEATHER SYSTEM DURING 2014 FLOODS

Before the disaster of a massive flood hit Kashmir Valley, a noticeable low-pressure area was formed over the Bay of Bengal, which moved northwestwards through central parts of India and interacted with another low-pressure area that had developed over Saurashtra and Kutch and northeast Arabian Sea (September 2–4, 2014). These low-pressure areas resulted in the revival of monsoonal activity in central and northwest India. From September 4 these low-pressure areas moved northwards and interacted with a trough in the midlatitude westerlies lying in the lower troposphere. Due to this, torrential rainfall started in Jammu and Kashmir in the first week of September, which resulted in devastating floods (Nandargi & Dhar 2011). Fig. 1 shows synoptic conditions in terms of wind at 300, 500, and 950 hPa and surface pressure over the Indian subcontinent at the start of the model run (02:09:2014 00:00 hrs)

MATERIALS AND METHODS

For the present study, the WRF model has been used. A nested domain as shown in Fig. 2 was made over Jammu and Kashmir, with the inner domain centered at Srinagar. The parent domain covers an area at 9 km horizontal resolution and extends from 72° E to 77° E and from 32° N to 37° N, while the inner has a resolution of 3 km and covers the entire Kashmir valley where the major rainfall occurred. For the simulation and model initialization, six hourly 25° FNL data from NCAR archives were used. The experiment was conducted for a duration of 110 h. starting from 02:09:2014 to 06:09:2014. The configuration table used for the WRF model is shown in Table 1. The model simulation was chosen with the physical scheme combination already optimized using multiple case studies and their comparative statistical score against IMD-AWS observations has been presented in Table 3. Experiment naming was done by taking the first

Table 1: Configuration table used in the study.

Number of Domains	2	
East-west Dimension	48	91
South-north Dimension	51	76
Vertical Levels	51	
Grid Distance in X-direction in m	9000	3000
Grid Distance in Y-direction in m	9000	3000
Grid ratio	1	3
Microphysics Option	WSM-6 class Graupel Scheme	
Long wave radiation Option	RRTM Long wave Scheme	
Short wave radiation Option	Dudhia shortwave Scheme	
Land surface Option	Unified Noah Scheme (NOAH)	
Planetary Boundary option	Yonsei University Scheme	
Cumulus Parameterization option	Kain-Fritsch scheme (KF)	

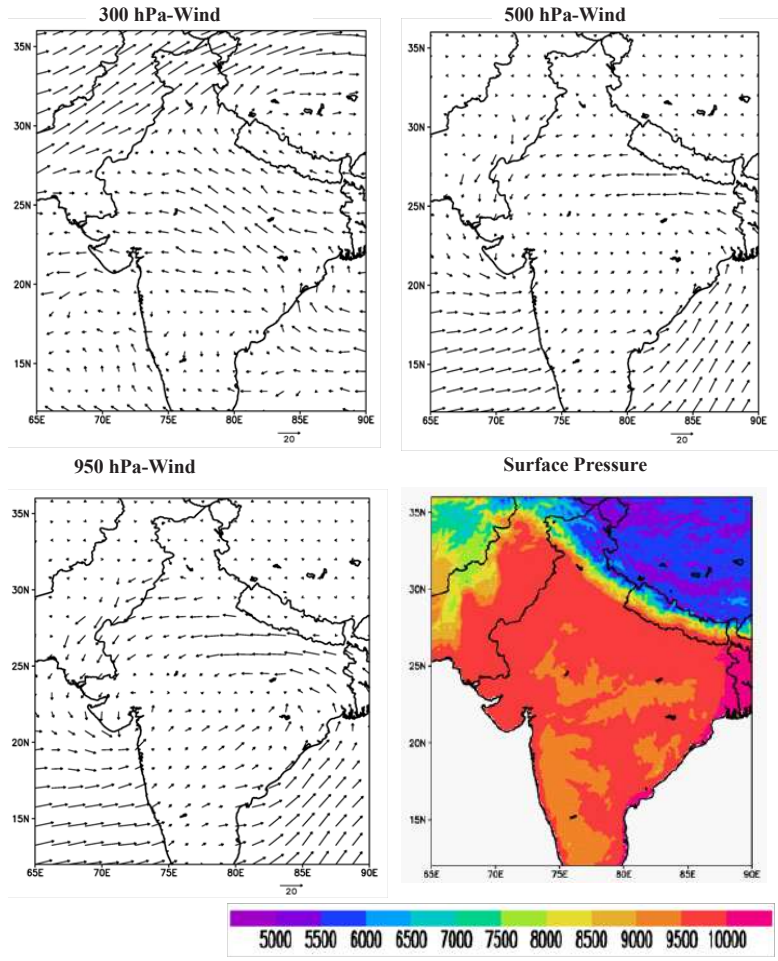

Fig. 1: Synoptic plots of (a) 300-hPa- wind, (b) 500-hPa-wind, (c) 950-hPa-wind and (d) surface pressure derived from ECMWF reanalysis data on 00UTC, 02 Sept., 2014.

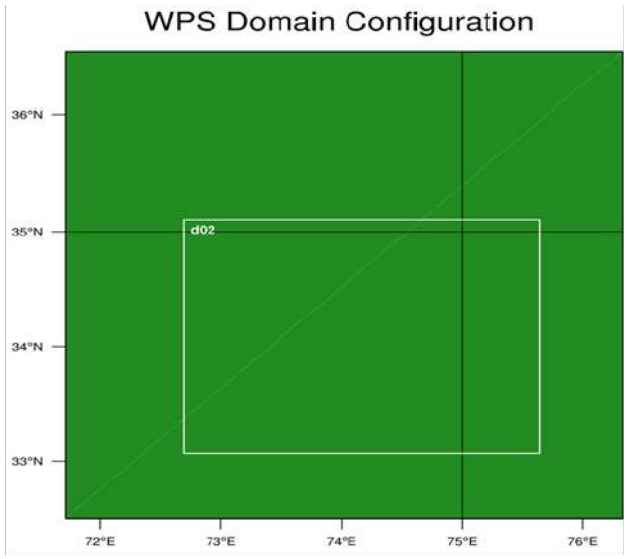

Fig. 2: Domain used in the study.

letter of microphysics, planetary boundary layer, and cumulus schemes mentioned in Table 3. The better-performing physical scheme based on the statistical score table was found to be the WYKF experiment. WYKF experiment had scored least RMSE i.e. 4.74 with least MBIAS of 3.03 among the parametrized schemes. Based on the above statistical score, the physical scheme combination named here as WYKF has been chosen for undertaken flashflood rainfall events that occurred over J&K.

RESULTS AND DISCUSSION

Results have been described in terms of spatial and time series analysis of meteorological parameters. Spatial plots of accumulated rainfall have been validated with CMORPH data. Time series of temperature and rainfall were respectively validated with ECMWF and CMORPH data. To develop an understanding of moisture and heat flux exchange between the lower atmosphere and land surface,

time series of land surface parameters like soil moisture, soil temperature, latent heat, and ground flux were also analyzed. Finally, to evaluate the performance of the model, the results were subjected to statistical analysis in terms of Mean Bias and Root Mean Square Error.

Air temperature drop at the time rain is often correlated. Therefore, to analyze rainfall time series progression, the ambient air temperature has been considered to correlate a dip in ambient temperature with rainfall. So, temperature and rainfall are analyzed together hereafter. Fig. 3 shows the hourly progression of temperature and rainfall in the four districts. As shown in the Figure, rainfall in the observation starts from 24 to the 25th hour at all four districts, whereas in the model output rainfall starts at 29 to the 30th hour thus showing a lag of 4-5 h. Observation at Anantnag has recorded a rainfall of 180 mm whereas the model shows rainfall up to 142 mm, which is closer to observed data with little under prediction. Further Srinagar has received 124 mm of rain and the model has simulated 64 mm of rain. Pulwama and Baramulla have recorded 114 mm and 126 mm of rain while

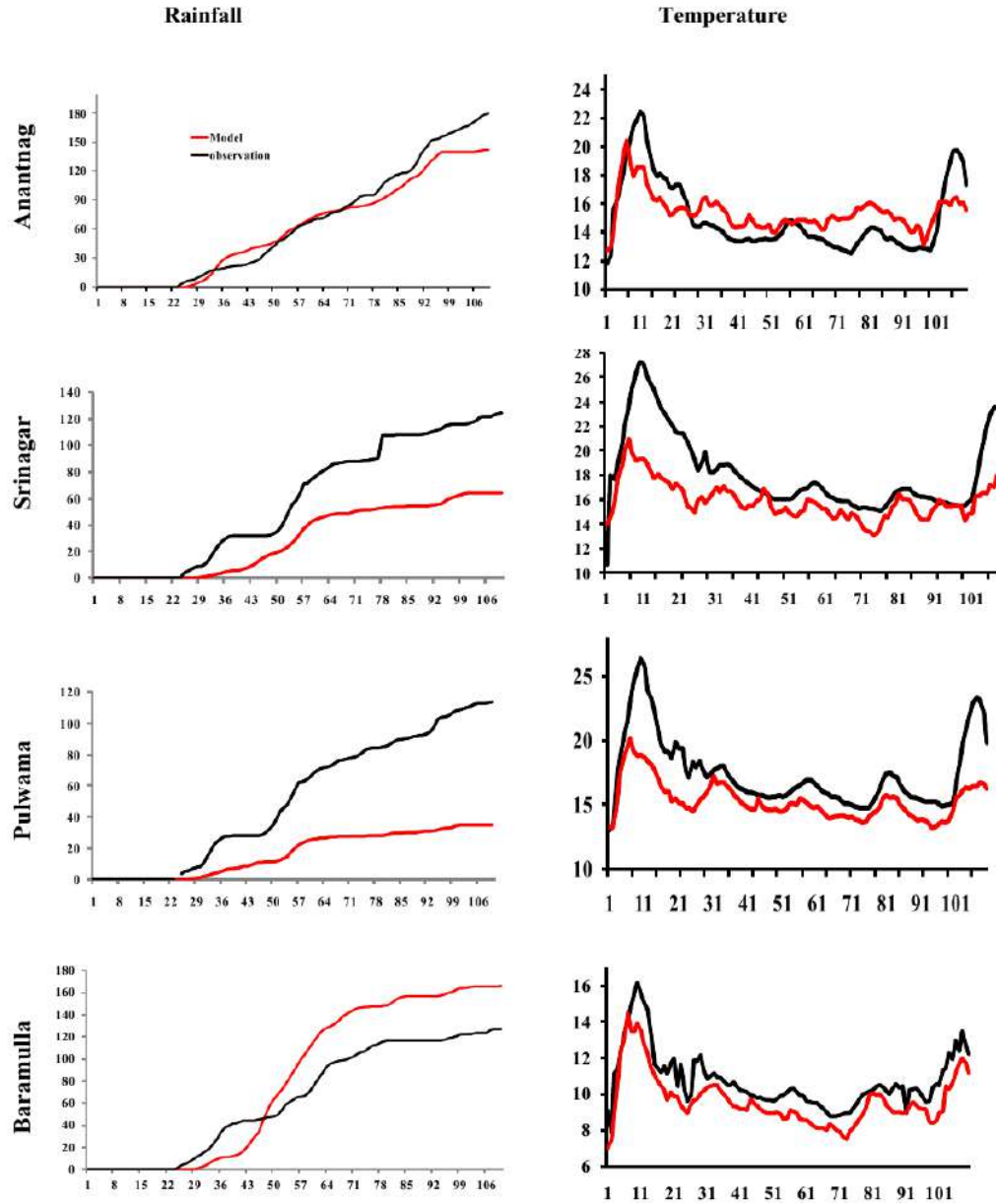

Fig. 3: Time series of rainfall (mm) and temperature (°C) over Anantnag, Srinagar, Pulwama and Baramulla.

the model has shown 34 mm and 165 mm of rain respectively. Similarly, temperature progression has been well captured by the model at all four districts with slight over-prediction. The declining trend in air temperature over Anantnag and Srinagar is 6°C at 24 h and 5°C at 24 h and the model has shown a similar trend. Further, a similar progression of temperature has been shown by the model at Pulwama and Baramulla also (Fig. 3).

Land surface parameters such as soil moisture, soil temperature, latent heat, and ground heat flux provide insight into moisture and flux between the lower atmosphere and land surface. The heat and moisture in the lower atmosphere are carried deeper into the atmosphere providing a convective atmosphere for convection to occur. Fig. 4 and Fig. 5 show time series of soil temperature, soil moisture, and latent heat, ground heat flux respectively at the four districts during

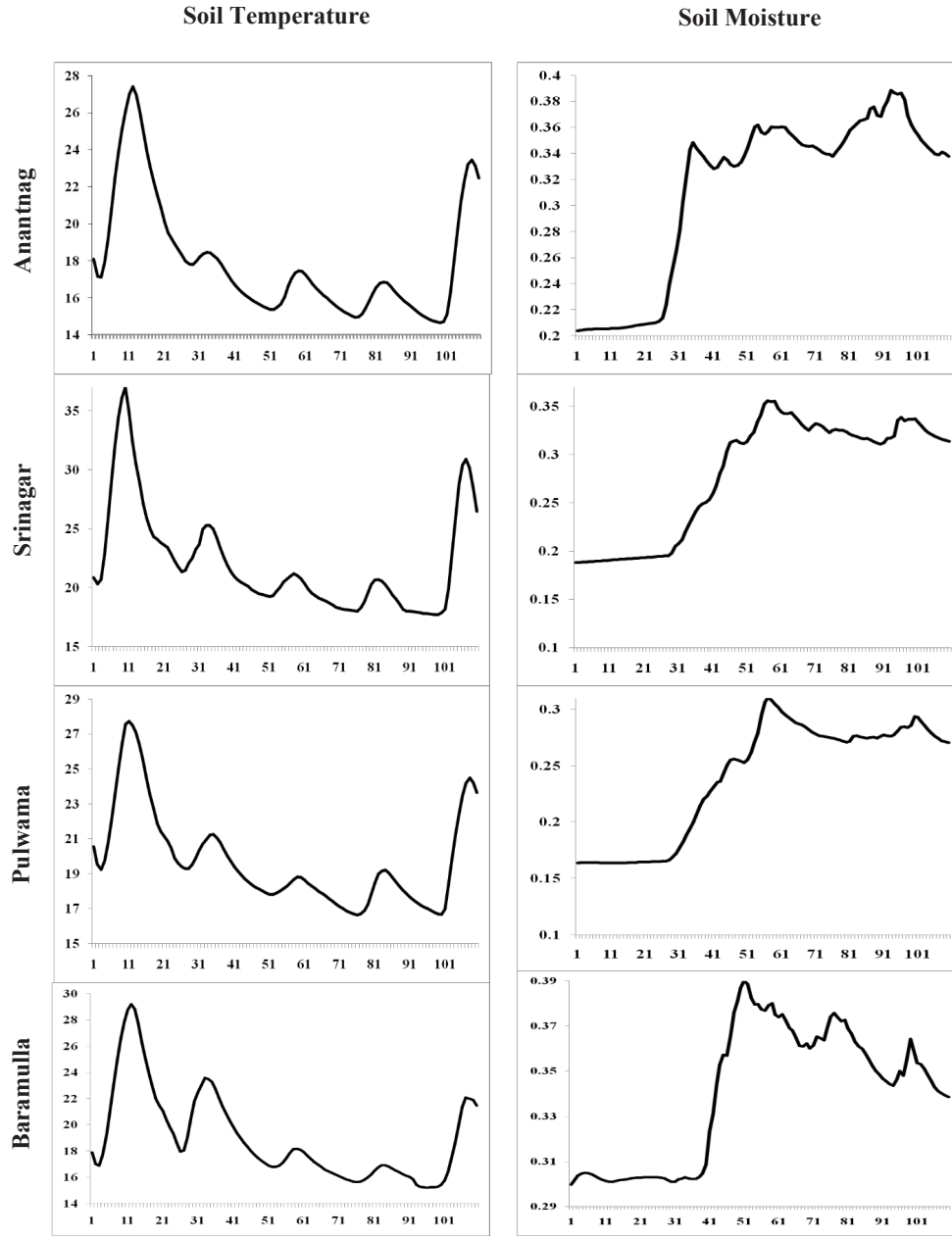

Fig. 4: Soil temperature (°C) and soil moisture (m/m^3) progression over Anantnag, Srinagar, Pulwama and Baramulla for simulation period.

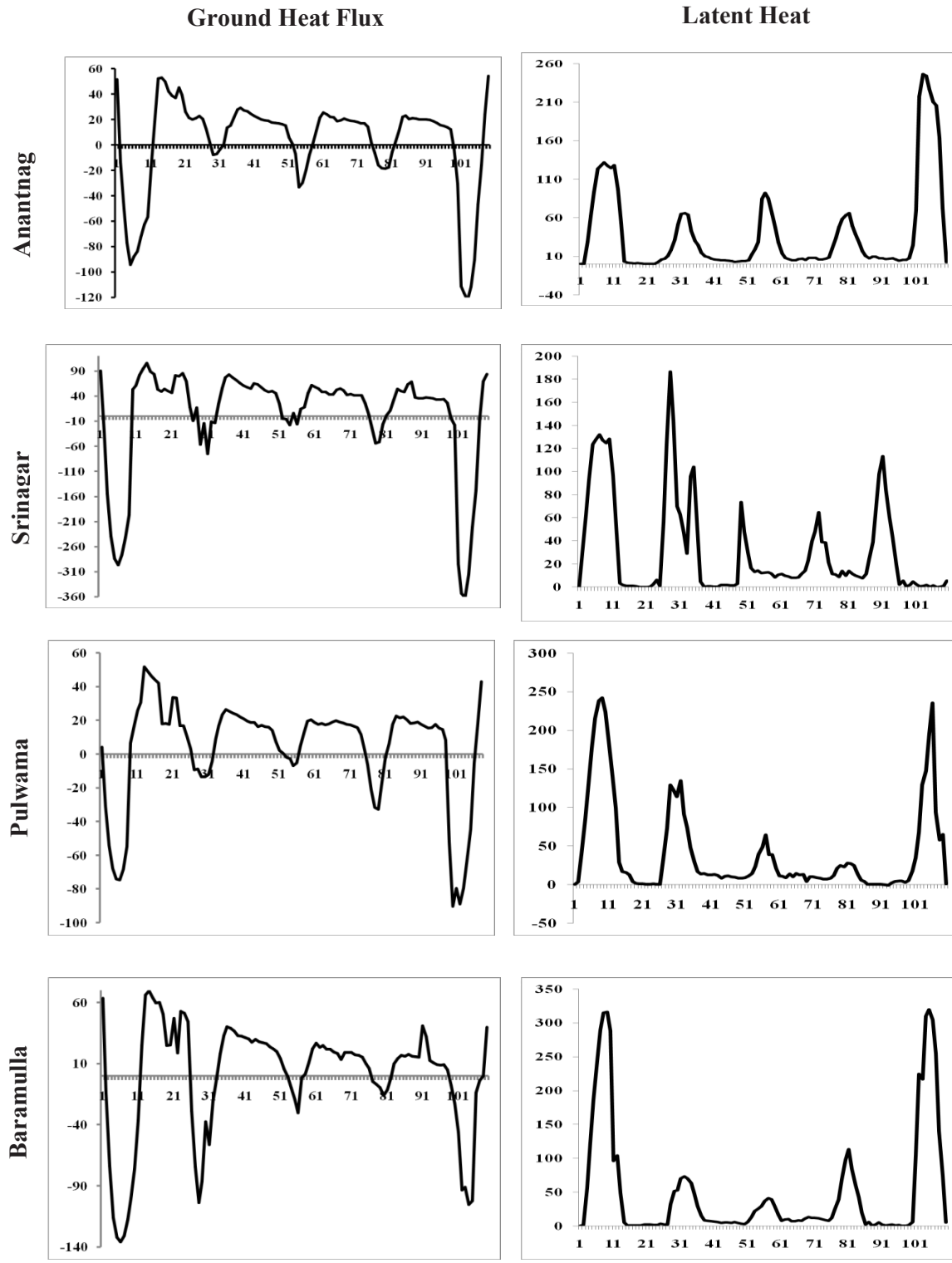

Fig. 5: Latent heat (watt/m^2) and ground heat flux (watt/m^2) progression over Anantnag, Srinagar, Pulwama and Baramulla for simulation period.

the event. As evident from the Figure, the soil temperature drops by over 10°C at around the 24th h of the model run as the rain starts. The reason could be a drop in temperature and rainfall may have brought down the temperature of the soil. Soil temperature further dips by 5°C around 45 h which could be attributed to colder air brought about by consistent rain. Soil temperature, later on, fluctuates till 100 h after which soil temperature shoots up by over 10°C at all four districts. Soil moisture starts increasing around 24th h when the rainfall begins and continues to increase till the 50th hr. after which there is a gradual decrease in the amount of moisture held by the soil. The reason could be the evaporation of moisture brought about by an increase in lower temperature also the soil may have reached saturation level. Ground heat flux helps to evaporate the soil moisture. The latent is used to evaporate the soil moisture which can be correlated with the diagram of the time series diagram of soil moisture. A decrease in ground heat flux contributes to an increase in the latent heat flux. The latent heat might have been consumed to evaporate soil moisture decreasing its value.

The vertical wind is responsible for carrying moisture into the atmosphere. The intensity of vertical wind would determine the vertical distribution of moisture providing a convective atmosphere for the condensation process. Therefore, the analysis of vertical wind velocity and moisture profile will help to understand the convective structure of the atmosphere and its available moisture which might contribute to a possible convective event. Fig. 6 shows the vertical profile of wind and moisture over four districts. Further, a strong updraft in the range of 15cm.s^{-1} at 48 h is seen over Anantnag up to 600 hPa with the presence of a downdraft of 3cm.s^{-1} which is coinciding with the time of observed rainfall. Over Srinagar, the model has simulated multiple strong updrafts at 36hr, 72, 84, and 96 h in the range of 15cm.s^{-1}. Availability of moisture is more over Anantnag than in Srinagar which could be a reason for the occurrence of more rainfall over Anantnag. The model has captured a strong

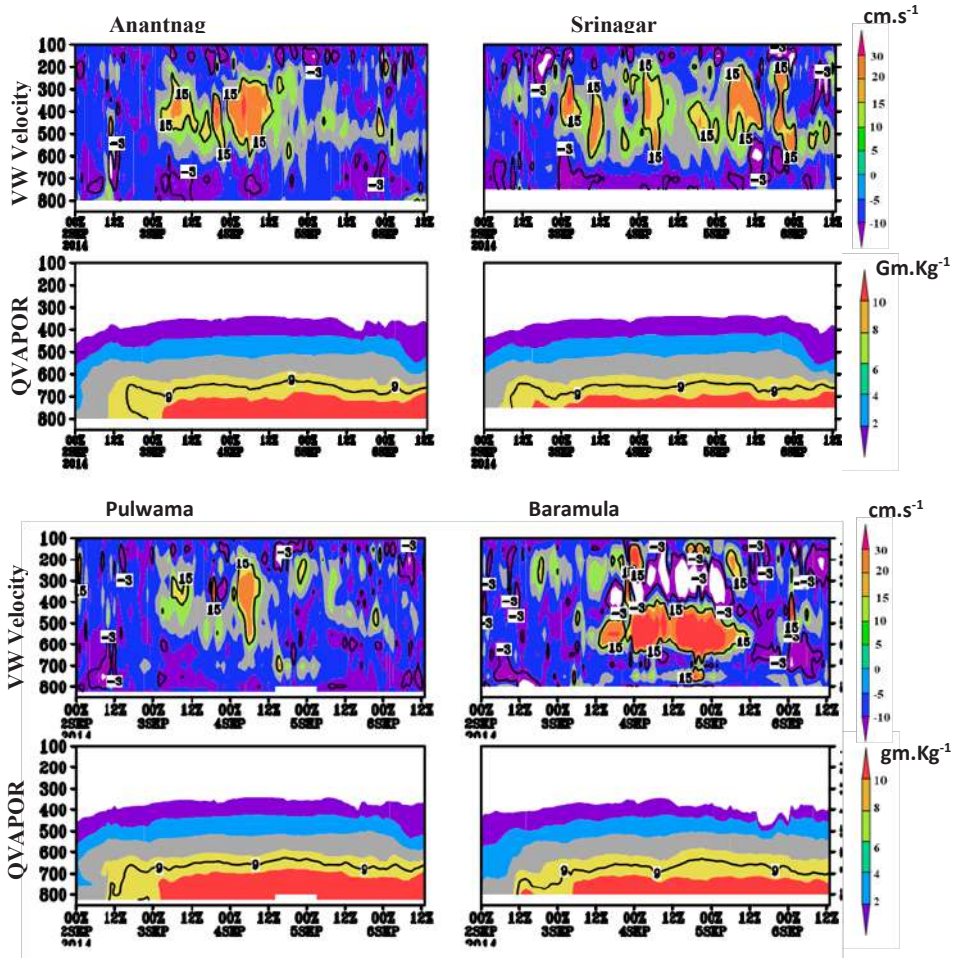

Fig. 6: Vertical Profile of QVAPOR (gm.kg^{-1}) and Verticle wind velocity (cm/s) over Anantnag, Srinagar, Pulwama and Baramulla.

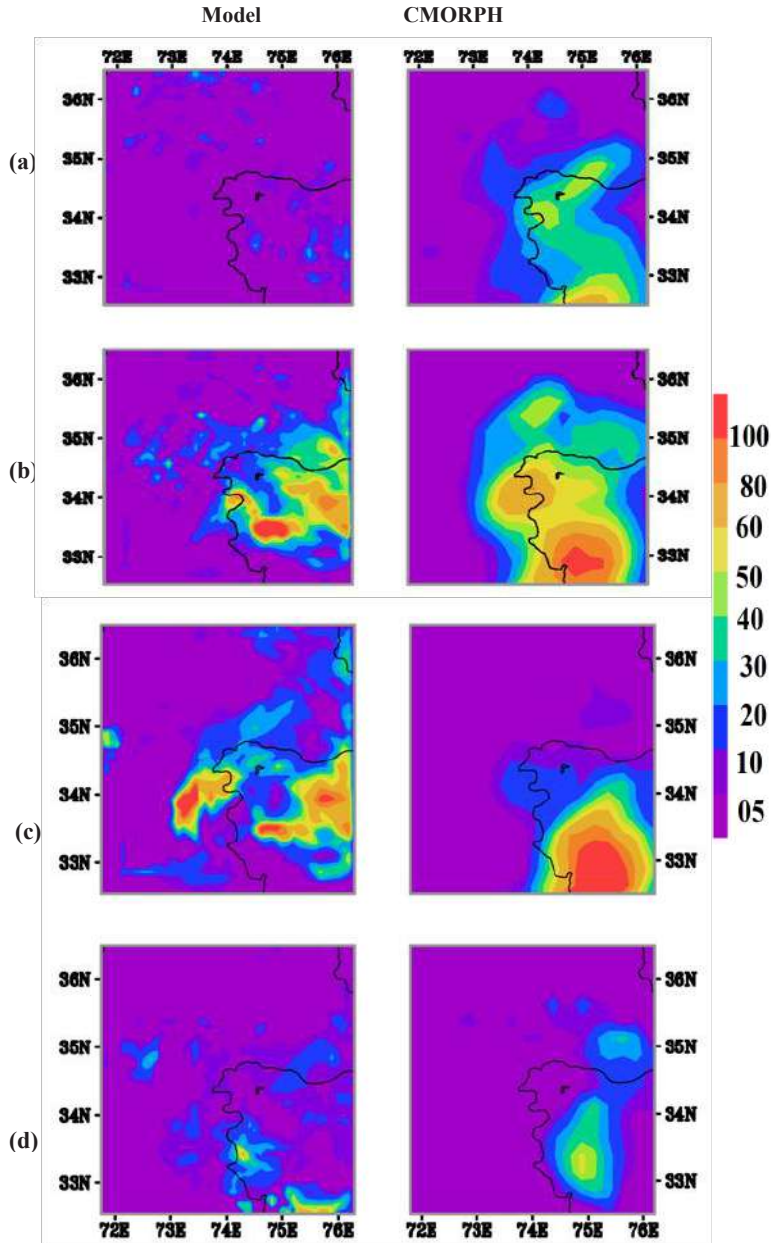

Fig. 7: Accumulated spatial rain plots at (a) 0-48, (b) 48-72, (c) 72-96 and (d) 96-110 hrs along with CMORPH observations.

updraft of 15 cm.s^{-1} at 48 hr along with moisture availability over Pulwama. Strong vertical wind in the range of 15 cm.s^{-1} is seen at 24-96 h over Baramullah. The persistence of updraft and downdraft for 48 h combined with moderate moisture availability may have resulted in more rain over Baramula. Strong updrafts/downdrafts accompanied by moderate to high moisture content (6-10 gm.kg^{-1}) have shaped the atmosphere more conducive over four chosen places i.e. Anantnag, Srinagar, Pulwama, and Baramulla. In addition to the above, the presence of strong updrafts and moisture are also coinciding with observed rainfall timing. Furthermore, the presence of strong vertical velocity in the range of -3 to 15 cm.s^{-1} (updraft and downdraft) coinciding with each other, provides a strong indication for convection to happen over all four districts and the model-generated vertical wind is coinciding with the observed rain time duration signifying the model results.

From Fig. 7 the following observations are drawn from CMORPH rain data. The southeastern part of the domain has received 40-60 mm of rain during 48-72 h of rain

(48 h accumulated rain). Further, the spatial pattern of rain has shown north-west expansion during the next 48 h (72 – 96 h) with >100 mm accumulated rain. On the other hand, the model has captured the accumulated rain from 48 h onwards. The results were also able to capture the northwestern expansion of spatial rain patterns with 60-100 mm of accumulated rain for 48-72 h and 72-96 h Spatial patterns of rain at 96-110 h were also represented quite well as seen in the model result. On a whole note, well representation of temperature, rainfall, soil moisture, and soil temperature along with a conducive atmosphere (vertical profile of moisture and vertical wind velocity) have shown a good agreement with an observed atmospheric feature found in ECMWF, CMORPH data.

Model performance can be accessed through (a) Error estimation and bias evaluation.Root Mean Square Error and Mean Bias have been analyzed by taking time series progression over four districts against the ECMWF (ERA5) temperature data. RMSE and Mean Bias were calculated at 24 h. difference. Mean Bias RMSE is two statistical operations for measuring the performance of a model. The mean bias deviation or mean bias tells difference between observed values and model output. Mean bias finds the average bias in the model. A positive bias or error in a variable (for example in soil temperature) represents that model has overestimated its value and vice versa. Root mean square error or root mean square deviation is one of the most commonly used measures for evaluating the quality of predictions. It shows how far

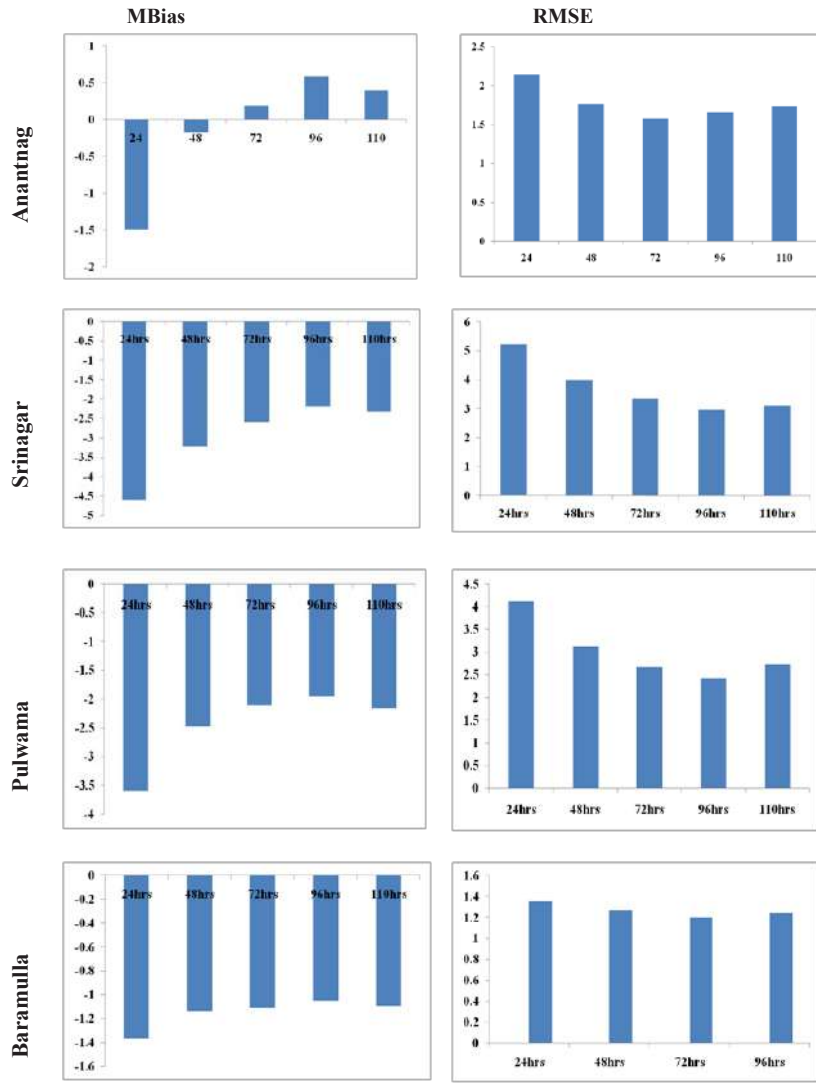

Fig. 8: 24-hourly calculated mean bias and RMSE of temperature time series against ECMWF ERA5 temperature data over Anantnag, Srinagar, Pulwama and Baramulla.

Table 2: Mean Bias and RMSE averaged for a simulation period of temperature time series data over Anantnag, Srinagar, Pulwama, and Baramulla.

Name of Districts	Mean Bias	Root Mean Square Error
Anantnag	0.3934	2.43
Srinagar	-2.3220	3.128
Pulwama	-2.1602	2.738
Baramulla	-1.09	1.246

predictions fall from measured true values using Euclidean distance. RMSE and MBIAS have been calculated at 24 h intervals against ECMWF-ERA5 temperature data over four districts. As shown in Fig. 8 and Table 2, MBIAS of -1.09 with 1.24 RMSE is calculated over Baramula while Srinagar has scored the highest MBIAS -2.32 with 3.12 RMSE value. Further, Anantnag has shown 0.39 MBIAS with a 2.43 RMSE value and -2.1 MBIAS with 2.7 RMSE is calculated for Pulwama. It is also observed that with the progression of time, MBIAS and RMSE have reduced significantly during 48hr to 96 hr over four districts. The statistical calculation was also done over Srinagar and Jammu coordinates only against IMD-AWS observed data. This is done to compare the statistical score of the model against ECMWF and IMD-AWS observed data. The unavailability of IMD-AWS data over Anantnag, Pulwama, and Baramula has limited the statistical analysis with reference o IMD-AWS data for Srinagar and Jammu only. The model has shown an RMSE of 2.6 and MBIAS of -1.38 (Table 4) over Srinagar against IMD observation which is a little more as compared to ECMWF. The statistical analysis has signified the satisfactory model performance as the model has scored MBIAS -1.29 with 2.38 RMSE for temperature averaged over four districts for 96 h.

CONCLUSIONS

The present research tested the performance of the WRF Model in simulating an extraordinary event of heavy rainfall that caused the flood in Kashmir valley in the first week of September 2014. FNL data from NCAR archives was used for Model initialization and simulation. To validate the model output CMORPH and ECMWF (ERA5) data was used. To test the statistical significance of the Model, MBIAS and RMSE errors were calculated from ERA5 temperature data. The results were described in terms of time series analysis of rainfall, temperature, soil temperature, soil moisture, latent heat, and ground heat flux. Spatial plots of rainfall were made for 0-48, 48-72, 72-96, and 96-110 h. The results showed the model has captured the amount of rainfall with slight underprediction and with a time lag of 4-5 h. In terms of temperature progression, the model is in good agreement with ECMWF ERA5 data. The temperature drop up to 6^{o}C at the start of rainfall was also well captured by the model. The model showed an increase in the amount of soil moisture from 24hrs. as the rainfall began till 50th hr. when soil may have reached saturation level. The model also captured a drop of up to 10^{o}C in soil temperature as the convective event

Table 3: Statistical score (Mean Bias and RMSE) of Parametrized schemes.

Experiment Name	Statistics	6	12	18	24	30	36	42	48	54	Average Score
WYKF	MBIAS	5.34	5.15	-0.59	0.30	2.93	5.11	1.84	3.82	3.39	3.03
	RMSE	6.62	5.71	4.32	3.43	4.15	6.17	3.17	3.86	5.20	4.74
WYGD	MBIAS	-0.67	1.65	-2.84	-3.68	-0.98	2.72	0.35	-3.70	-3.62	-1.20
	RMSE	6.65	5.84	3.66	4.02	4.24	5.89	3.15	8.73	8.42	5.62
WMGD	MBIAS	-2.10	3.36	-1.49	-4.53	-2.16	2.09	0.04	-1.20	-0.85	-0.76
	RMSE	5.16	7.18	3.17	4.77	5.54	6.73	4.20	4.65	4.69	5.12
WMKF	MBIAS	-2.23	3.11	-1.78	-5.01	-3.22	1.61	-0.38	-1.35	-0.30	-1.06
	RMSE	5.23	7.25	3.34	5.37	6.46	6.88	3.55	4.49	4.75	5.26

Each letter in the experiment name refers to the physical scheme mentioned in the WRF user guide and names are as follows:

W→WRF Double-Moment 6-class microphysics scheme; Y→Yonsei University PBL scheme; M→Mellor-Yamada-Janjic PBL scheme; KF→Kain-Fritsch Cumulus Scheme; GD→ Grell-Devenyi Cumulus Scheme

Table 4: Mean Bias and RMSE averaged at a 6-hourly interval over Srinagar and Jammu using IMD AWS temperature data.

	Time	06	12	18	24	30	36	42	48	54	Average Score
Srinagar	MBIAS	-4.52	-3.56	1.45	2.77	-0.13	-0.35	0.53	-0.95	-7.64	-1.38
	RMSE	4.52	3.57	1.78	2.95	0.59	0.37	0.6	1.27	7.78	2.6
Jammu	MBIAS	-2.16	-1.3	0.37	0.16	-1.18	0.26	0.66	0.99	-3.17	-0.6
	RMSE	2.17	1.45	0.57	0.45	1.33	0.63	0.93	1.34	3.34	1.36

starts. The model captured a decrease in surface heat flux and an increase in latent heat as the rainfall starts. Profile of the atmosphere in terms of vertical wind velocity and moisture availability shows the presence of strong updrafts and downdrafts around 600 hPa. The availability of moisture at the time was rainfall as shown by the model could well have resulted in heavy rainfall. The spatial pattern of rainfall showed northwestern expansion of rain from 48-72 and 72-96 h Model was able to capture the spatial distribution of rainfall. Statistical results reveal improvement in model performance with the progression of time. With a Mbias of -1.29 with an RMSE of 2.38, the performance of the model can be described as satisfactory.

ACKNOWLEDGEMENT

The author acknowledges the financial support provided by DST-SERB (Project Sanction No-EEQ_2017_000206). The author is also thankful to ECMWF, NCAR, and IMD for archiving data.

REFERENCES

Baki, H., Chinta, S., Balaji, C. and Srinivasan, B. 2021. A sensitivity study of WRF model microphysics and cumulus parameterization schemes for the simulation of tropical cyclones using GPM radar data. J. Earth Syst. Sci., 130(4): 1-30.

Berz, G., Kron, W., Loster, T., Rauch, E., Schimetschek, J., Schmieder, J. and Wirtz, A. 2001. World map of natural hazards: A global view of the distribution and intensity of significant exposures. Nat. Hazards, 23(2): 443-465.

Chen, C.S., Lin, Y.L., Peng, W.C. and Liu, C.L. 2010. Investigation of a heavy rainfall event over southwestern Taiwan associated with a subsynaptic cyclone during the 2003 Mei-Yu season. Atmos. Res., 95(2-3): 235-254.

Chevuturi, A. and Dimri, A.P. 2015. Inter-comparison of physical processes associated with winter and non-winter hailstorms using the Weather Research and Forecasting (WRF) model. Modeling Earth Systems and Environment, 1(3): 1-9.

Hassan, M.A. and Islam, A.K.M. 2018. Evaluation of microphysics and cumulus schemes of WRF for forecasting heavy monsoon rainfall over the southeastern hilly region of Bangladesh. Pure Appl. Geophys., 175(12): 4537-4566.

Hong, S.Y. and Lee, J.W. 2009. Assessment of the WRF model in reproducing a flash-flood heavy rainfall event over Korea. Atmos. Res., 93(4): 818-831.

Korup, O. and Clague, J.J. 2009. Natural hazards, extreme events, and mountain topography. Quat. Sci. Rev., 977-990 :(12-11)28.

Kumar, A., Dudhia, J., Rotunno, R., Niyogi, D. and Mohanty, U.C. 2008. Analysis of the 26 July 2005 heavy rain event over Mumbai, India using the Weather Research and Forecasting (WRF) model. Quart. J. Royal Meteorol. Soc., 134(636): 1897-1910.

Kumar, A., Houze Jr., R.A., Rasmussen, K.L. and Peters-Lidard, C. 2014. Simulation of a flash flooding storm at the steep edge of the Himalayas. J. Hydrometeorol., 15: 212-228.

Kumar, M.S., Shekhar, M., Krishna, S.R., Bhutiyani, M. and Ganju, A. 2012. Numerical simulation of cloud burst event on August 05, 2010, over Leh using WRF mesoscale model. Nat. Hazards, 62: 1261-1271.

Nandargi, S. and Dhar, O.N. 2011. Extreme rainfall events over the Himalayas between 1871 and 2007. Hydrol. Sci. J., 56(6): 930-945.

Nooni, I.K., Tan, G., Hongming, Y., SaidouChaibou, A.A., Habtemicheal, B.A., Gnitou, G.T. and Lim Kam Sian, K.T. 2022. Assessing the performance of the WRF model in simulating heavy precipitation events over East Africa using satellite-based precipitation products. Rem. Sens., 14(9): 1964.

Ntwali, D., Ogwang, B.A. and Ongoma, V. 2016. The impacts of topography on spatial and temporal rainfall distribution over Rwanda based on the WRF model. Atmos. Clim. Sci., 2)6): 145-157.

Rama Rao, Y.V., Hatwar, H.R., Salah, A.K. and Sudhakar, Y. 2007. An experiment using the high-resolution Eta and WRF models to forecast heavy precipitation over India. Pure Appl. Geophys., 164(8): 1593-1615.

Sepúlveda, S.A. and Padilla, C. 2008. Rain-induced debris and mudflow triggering factors assessment in the Santiago cordilleran foothills, Central Chile. Nat. Hazards, 47(2): 201-215.

Srinivas, C.V., Yesubabu, V., Prasad, D.H., Prasad, K.H., Greeshma, M.M., Baskaran, R. and Venkatraman, B. 2018. Simulation of an extreme heavy rainfall event over Chennai, India using WRF: Sensitivity to grid resolution and boundary layer physics. Atmos. Res., 210: 66-82.

Thayyen, R.J., Dimri, A., Kumar, P., and Agnihotri, G. 2013. Study of cloudburst and flash floods around Leh, India, during August 4-6, 2010. Nat. Hazards, 65: 2175-2204.

Watson, R.T. and Haeberli, W. 2004. Environmental threats, mitigation strategies, and high-mountain areas. AMBIO: J. Hum. Environ., 13)33): 2-10.

Nature Environment and Pollution Technology
An International Quarterly Scientific Journal

p-ISSN: 0972-6268
(Print copies up to 2016)
e-ISSN: 2395-3454

Vol. 21 | No. 5 (Suppl) | pp. 2189-2200 | 2022

Original Research Paper

https://doi.org/10.46488/NEPT.2022.v21i05.013

Open Access Journal

A Framework for Improving Urban Land Cover Using Object and Pixel-Based Techniques via Remotely Sensed Data

Ammar Shaker Mahmoud*†, Mustafa Ridha Mezaal, Mustafa Raad Hameed*** and Ahmed Samir Naje******

*Department of Civil Engineering, College of Engineering, University of Babylon, Babylon, Iraq
**Building & Construction Technology Engineering Department, Technical Engineering College, Northern Technical University, Mosul, Iraq
***School Buildings Department, the General Directorate of Education, Babylon, Iraq
****College of Engineering, Al-Qasim Green University, Babylon, Iraq
†Corresponding author: Ammar Shaker Mahmoud; ammar.shaker.eng@uobabylon.edu.iq

Nat. Env. & Poll. Tech.
Website: www.neptjournal.com

Received: 06-06-2022
Revised: 11-07-2022
Accepted: 13-07-2022

Key Words:
Pixel-based technique
Urban land cover
QuickBird satellite images
Object-based analysis
Remote sensing

ABSTRACT

Recently, the advancement of remote sensing technology played a key role in urban land/cover mapping, planning, tourism, and environmental management. Images with a high spatial resolution for urban classification are widely used. Despite the high spectral resolution of the image, spectral confusion happens among different land covers. Furthermore, the shadow problem also causes poor results in the classification based on traditional per-pixel spectral approaches. This study looks at ways of improving the classification of urban land cover using QuickBird images. Maximum likelihood (ML) pixel-based supervised as well as Rule-based object-based approaches were examined on high-resolution QuickBird satellite images in Karbala City, Iraq. This study indicates that the use of textural attributes during the rule-based classification procedure can significantly improve land-use classification performance. Furthermore, the results show that rule-based results are highly effective in improving classification accuracy than pixel-based. The results of this study provide further clarity and insight into the implementation of using the object-based approach with various classifiers for the extended study. In addition, the finding demonstrated the integration of high-resolution QuickBird data and a set of attributes derived from the visible bands and geometric rule set resulted in superior class separability, thus higher classification accuracies in mapping complex urban environments.

INTRODUCTION

The application of remote sensing technology is a major target for urban areas as centers of economic urban planning, and environmental and development of social (Banzhaf et al. 2009, Noori et al. 2019a). The spatial and spectral heterogeneity in an urban environment that usually involves structures built up (buildup area and roads), much vegetation (parks, gardens, crops, and agricultural areas), bare land area, and water causes problems common to remote sensing in detailed and accurate urban areas. Due to the urban spatial heterogeneity, high spatial resolution sensors (2.5 m) reflect urban cover artifacts in relatively few adjacent pixels (Sertel & Alganci 2016). Therefore the classification of the urban land cover from this kind of data could use an object-oriented image analysis instead of a pixel-based (Ma et al. 2017). Classification based on image segmentation will lead to a more homogeneous and reliable mapping product with a higher level of detail (Darwish et al. 2003).

The spectral resolution of satellite sensors such as QuickBird is relatively limited. Because of the complexities of the urban area, the separation of built-up and unbuilt material, roofs and roads, and various roof styles have unique limitations (Herold et al. 2003, Ruiz Hernandez & Shi 2018). Additional information about spatial shape and context should thus be included in the image classification (Mezaal et al. 2019). Object-based techniques have shown their potential to take spatial complexity into account when classifying images (Bruce 2008, Song et al. 2018, Mahmoud et al. 2021).

Supervised and unsupervised spectral-based methods have been applied in the fields of resource survey, forecast, environment evaluation, forest monitoring, and weather (Tehrany et al. 2014, Wang et al. 2004). Numerous studies on the use of multispectral data for land usage classification have been carried out since the launch of the Landsat satellite (Forkuor et al. 2018). Multi-spectral classification

approaches used in many of these studies assigned a pixel class mark dependent only on its spectral characteristics (Belgiu & Csillik 2018).

The implementation of high spatial dates and object-based strategies for big urban areas is a major challenge (Sameen et al. 2017, Hashim et al. 2022). The coverage of these large areas typically requires many separately acquired images and reflects a high spectral range within the class variation of different land cover types. To provide a highly homogenous image data set, geometric distortions and radiometric differences between images must be minimized.

Most methods are multi-spectral and dependent on pixels based (Noori et al. 2019b). Due to the presence of miscellaneous pixels, induced via low spatial sensor resolutions, many existing classificatory fail to produce high precision performance (Castillejo-González et al. 2009). Therefore, the object-based technique is needed.

The object-oriented analytical method (OOA) is an analysis method that explores the requirements from the class and object perspective of the problem domain vocabulary (Kohli et al. 2013, Mahmoud et al. 2021). In the OOA, many concepts and strategies for the management of complexity, such as abstraction, encapsulation, inheritance, the association have been compiled. The OOA methodology is used in the design and management field of object-based spatial data modeling to upkeep object-based analysis for land/ use and land cover classification in residential zones (Hussain et al. 2013).

The implementation of object-oriented approaches is a method to map specific land uses (Bhaskaran et al. 2010). This technique takes into account the pixel group and geometric qualities of objects in the image. The images are divided into uniform regions based on the spectral and spatial characteristics of neighboring pixels. In this project, therefore, an objective-oriented procedure was used to avoid the problem of mixed pixels.

The most important difference between pixel and object-based examines is linked to the improvement of results performance by using an object-based approach (Tehrany et al. 2014). Many studies have approved that object-based methods are accurate (Duro et al. 2012, Esetlili et al. 2018, Myint et al. 2011, Weih & Riggan 2010, Yan et al. 2006, Zhang & Jia 2014). In contrast, Adam et al. (2016) and Nugroho et al. (2017) mentioned that the pixel-based approach is slightly better than the object-based approach in the classification of land use land cover.

Therefore, the objective of this study is to examine pixel and object-based using QuickBird images of Karbala province in Iraq to classify a complex urban area. The pixel and object-based classification are implemented by ENVI software. Also, the performance of evaluations of two approaches was validated to know which one is most appropriate for urban land use. Finally, a comparison was conducted between these two approaches.

STUDY AREA AND DATA

Karbala city is placed between 3611461 to 3608525 X and 402565 to 406282 Y. The region covers an area of 1994.0 hectares and is situated in the northern part of the Iraqi city of Karbala (Mohammed et al. 2018). The province is situated

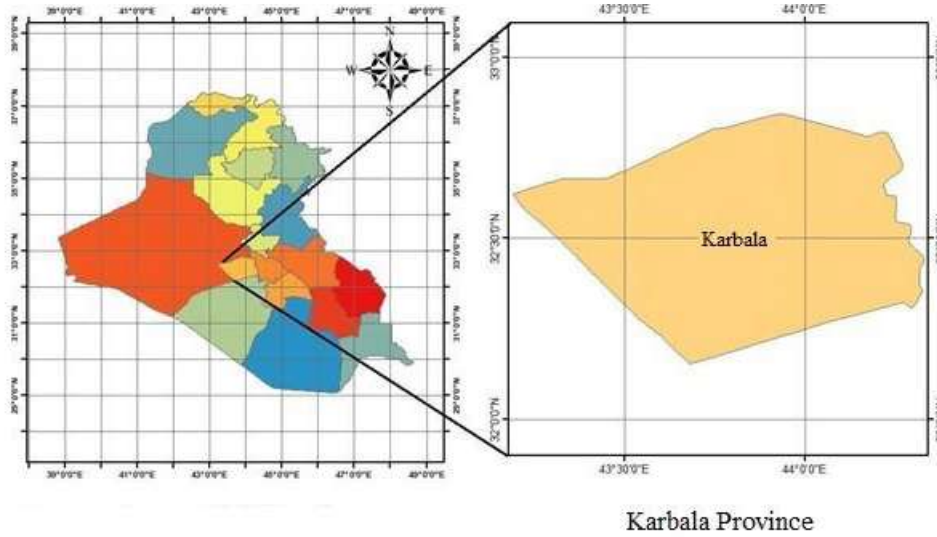

Fig. 1: Location map of the study area.

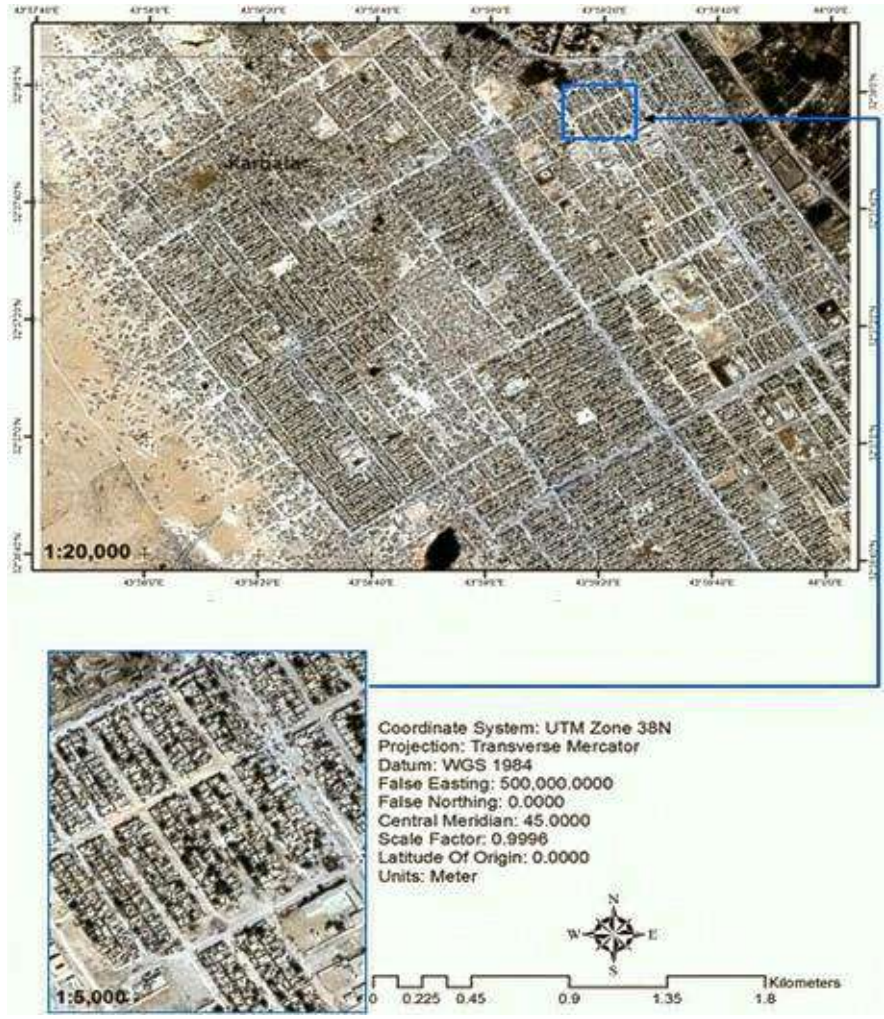

Fig. 2: The QuickBird satellite image.

in the Alluvial plain, in the sedimentary plane, and in the western plateau, where the warm desert climate prevails. It is located in the center of Iraq and near the capital of Iraq, Baghdad. Yearly precipitation ranges from 50 to 200 mm, and the bulk of the rainfall is from October to April. The temperature varies greatly between day and night, summer and winter, reaching an average of 45-50°C. The study area is shown in Fig. 1.

In this study, the data used are the high spatial resolution and multi-spectral (0.6 meters) spatial resolution QuickBird and the spectral three bands which covered the city of Karbala (Fig. 2).

MATERIALS AND METHODS

Digitally classified is a study of machine perception that defines pixels based on their numerical properties and because of their ability in the region calculation to count pixels. Preprocessing techniques have been applied to correct the atmospheric and radiometric of the image. Furthermore, two types of classification have been used to classify land-use types in the study area which are object-based and pixel-based. The results are quantified statistically and spatially to determine pattern continuity following classification methods applied to these data. Finally, an accuracy assessment has been applied to compare both classification types and approve which classification method is a performance for this specific data. Fig. 3. shows the overall methodology of this study.

Preprocessing

Atmospheric Correction

Remote sensing involves the passage of solar radiation through the atmosphere before the system is collected. This

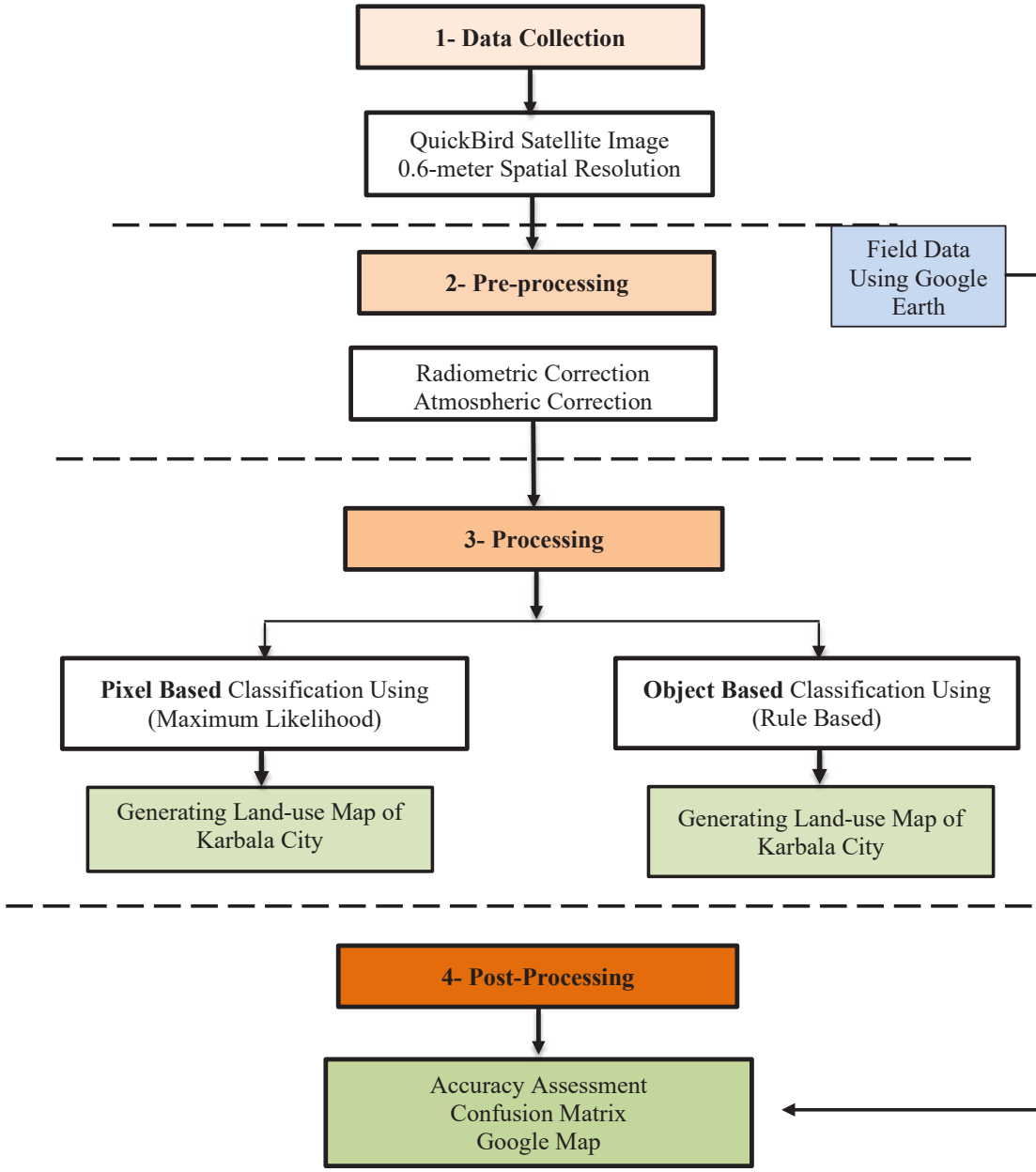

Fig. 3: The overall methodology flow chart.

means that remotely sensed images contain information on the atmosphere and the surface of the Earth. The elimination of the impact of the atmosphere is a crucial pre-processing step for those involved in the quantitative analysis of surface reflectance (Martins et al. 2017). Properties such as water vapor, aerosol delivery, and scene visibility should be understood to account for atmosphere effects. Since these atmospheric properties are seldom calculated directly, some techniques can be used to deduce them from their radiance results. A pixel per pixel can be added to atmospheric correction of this sort since each pixel found on the multi-spectral image includes an individual atmospheric vapor absorption strip measurement.

The procedure for the correction of atmospheric effects is used to correct the imagery. To recognize the presence of targets through the reference spectral library, atmospheric correction is necessary for image processing. In this analysis, the atmospheric correction method for Dark Object Subtraction has been used to eliminate a certain atmospheric attenuation.

Radiometric Correction

When the electromagnetic energy released or reflected is detected by a sensor, the energy measured will not correspond with the energy emitted or reflected by the same object observed for a short time. This is because of the sun azimuth and temperature, weather like aerosols, fog, sensor reactions, etc. This is due to the sun. Such radiometric errors must, therefore, be corrected to achieve true irradiance or mprovements are being used to promote vreflection (Vicente-Serrano et al. 2008). Iisual perception and imagery comprehension. Digital imagery has the advantage of allowing us to manipulate digital pixel values in an image.

Processing

Rule-Based Classification (Object-Based)

Because of its greater spatial resolution, conventional digital image processing algorithms are more difficult to obtain thematic facts from this new-fangled image. Given the spatial complexity of urban environments, high-spatial-resolution images (2.5m–0.6 m) in comparatively few adjacent pixels reflect urban cover items.

Using a trial-and-error method to optimize and develop a rule set is time-consuming and optimum rule sets are difficult to identify. The rule sets were automatically generated using a data mining algorithm that denotes to Decision Tree (DT) algorithm and was executed in MATLAB R2015b. The merit of utilizing MATLAB software is that it uses Gini's index as the separation criterion (Hamedianfar & Shafri 2016). Hence, this research applies a data mining algorithm called Decision Tree (DT) and important features to develop the rule sets. The 8 rule sets developed were utilized to distinguish between the classes. The governing Rule-based classification was introduced as a Level 1 hierarchical structure. 4 classes have been described for image classification in this analysis. Although the spatial resolution of QuickBird permits us to go further to level 2 (See Fig. 4).

This city has a homogeneous pattern of land use and the variety of classes was limited. Moreover, identification of the different types of residential areas was difficult because of the lack of ancillary data along with in situ ground control points. The description of classes is shown in Table 1.

In object-oriented analytics, a segmentation of the image is the first step. This process extracts meaningful image objects based on their spectral and textual properties (for example, streets, buildings, and vegetation parts). The segmentation is a half-automated process rule-based, which allows users to identify certain parameters that affect the image segments' size and shape. The artifacts that resulted refer not only to spectrum statistics but also to shape and context information in the surrounding objects and textures factors. The Fuzzy logic supervised approach (FbSP) optimizer was utilized to optimize the parameters of multiresolution segmentation such as scale, shape, and compactness. The optimized parameters contributed to

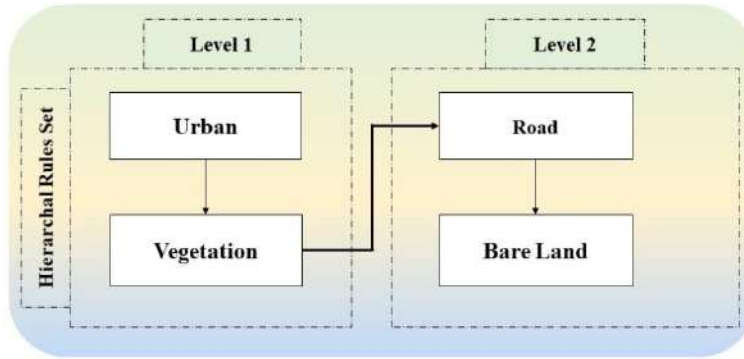

Fig. 4: The flow of hierarchal rule set between the Classes.

Table 1: Descriptions of Land Cover Classes.

S/N	Land Cover	Description (s)	Color
1	Urban or built-up areas	This class includes continuous and discontinuous urban fabric, industrial, commercial, and other related built-up areas.	Red
2	Open/bare land	Barren soil is a desert area without plants and unstructured lands.	Yellow
3	Vegetated areas	This comprises green urban areas, non-irrigated arable land, irrigated land, scrubs, and palm cover.	Green
4	Road	Asphalts, unpaved roads, and transportation	Gray

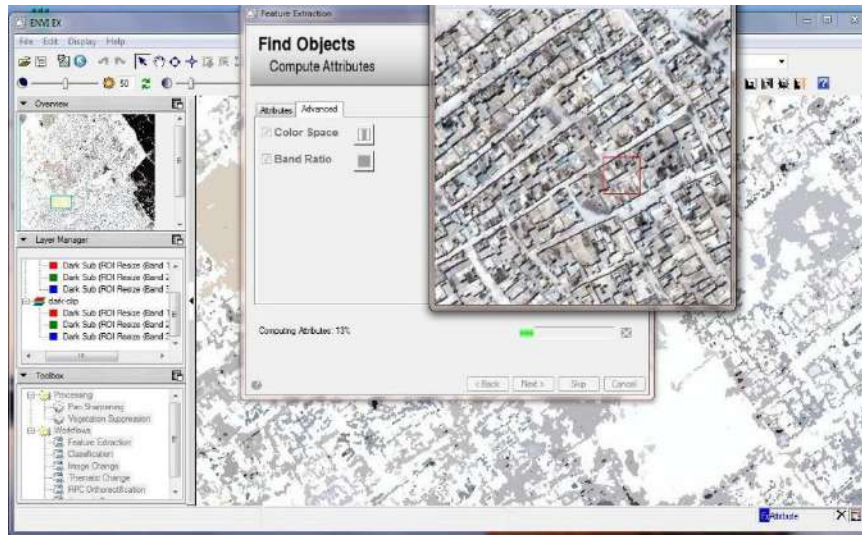

Fig. 5: Segmentation of the rule-based classification.

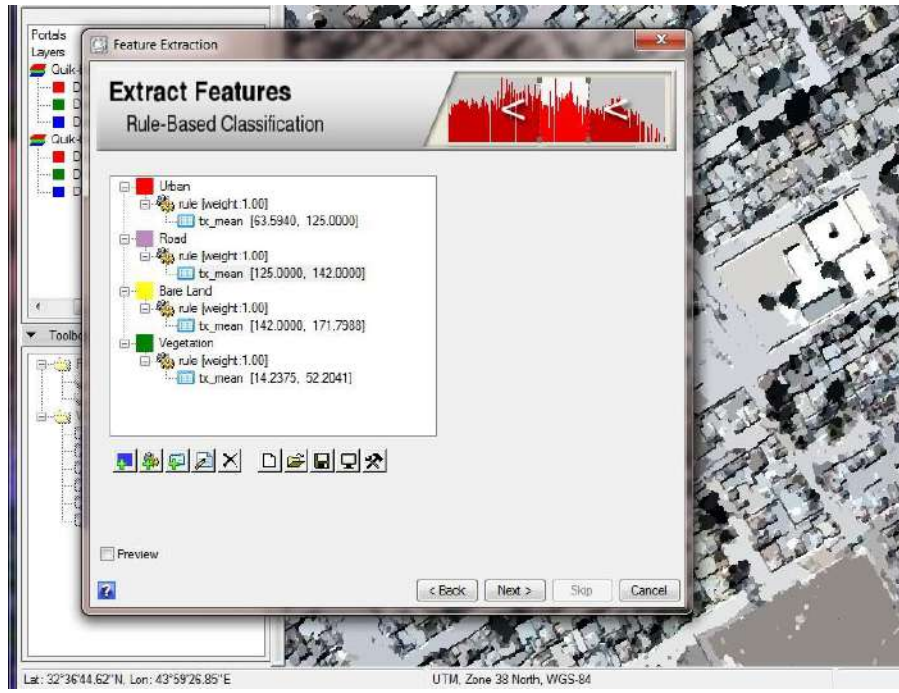

Fig. 6: Extract feature based on the reflectance of textural mean.

distinguishing between the classes. With a 0.6 m spatial resolution, several pixels reflect the typical individual land objects (built-up structures). The segmentation was rendered using the following criteria by measuring all 3 bands equally. Scale Level 50, Merge Level 30, Smoothness 0.4/ Compactness 0.5. Fig. 5. shows the segmentation of Rule-Based classification.

In this study, the rule-based algorithm classification has been applied based on wavelength measures and performs class assignments. The classification of the image as the key layer attribute (helpfulness, line, and max diff), a feature space based on the rule was chosen for this analysis. Various spectral measurements were used to determine textural and land-use classes of various reflections. Fig. 6. shows the

extraction feature based on the reflectance of the textural mean

Maximum Likelihood Image Classification (Pixel-Based)

One high-resolution and multispectral scene of QuickBird has been applied for this study. It was acquired in September 2007. First, the scene was sub-sat in a part of Karbala city. Having implemented the preprocessing on the image such as radiometric correction and Atmospheric correction, it was classified into 4 different classes according to the Anderson scheme using the pixel-based Maximum Likelihood method. Somehow the entire region of the analysis is cloudless, allowing for fast processing and exact classification. The same number class was extracted as a Rule-based approach (Urban, Road, Vegetation, and Bare Lands). There was a sufficient number of training sites for each Land/use class which was applied to the image by using ENVI 5.2 software. The class included trees, industrial areas, sports, and administrative buildings and large-scale structures, and bare land and roads (asphalted and primary networks and minor networks).

Accuracy Assessment

The accuracy of the LULC map was evaluated by comparing actual ground data to the classified area. Error matrix or confusion matrix is a common way to directly define and compare the percentage of the map area with reference data. In this analysis, the overall accuracy and kappa value provided by data coverage are compared and tested with the Google map topographical scale as a result of visual interpretation. Accuracy tests were carried out based on confusion matrices and kappa statistics for both classifications. A marginal homogeneity test was used to assess the statistical significance of the difference between the kappa coefficients for the pixel-based, main component, and object-based classification.

Table 2: Land use area using Rule-Based classification.

Land use	Area [m^2]	Area [ha]	Percentage
Bare Land	2507777.8	250.77	22.93
Road	2867484.6	286.75	26.22
Urban	4181496.5	418.15	38.22
Vegetation	998873.82	99.89	9.13
Unclassified	382196.14	38.22	3.49

RESULTS AND DISCUSSION

In this research, Karbala city, Iraq was utilized as a case study to generate and evaluate rules using high spatial resolution (0.6 meters) QuickBird. The segmentation parameters were optimized using the Fuzzy logic supervised approach (FbSP) optimizer approach. A technique developed by Bartels and Wei, 2010 was employed by using 10-fold cross-validation to have a high-accuracy prediction. Applying two methods for classifications have been illustrated different results for feature extractions.

The results of the rule-based classification showed that land use included a total of 1094 hectares. Such land uses have been categorized with high precision compared with other land use in the region of the case study, despite the spectral heterogeneity of urban and road. Table 2. shows land-use areas of Rule-based classification in the study area. Fig. 7. shows the chart of Land-use areas using the Rule-Based classification method.

According to the findings, urban areas of 418.15 hectares have the highest area relative to other uses, and plant ecosystems of almost 100 hectares (agricultural land and green lands) have a minimum area for the study site.

The result of the Maximum Likelihood showed different areas for each land-use class, however, the total area of the entire study is the same almost 1094 hectares. The area of land/uses classified by the Maximum Likelihood classifier

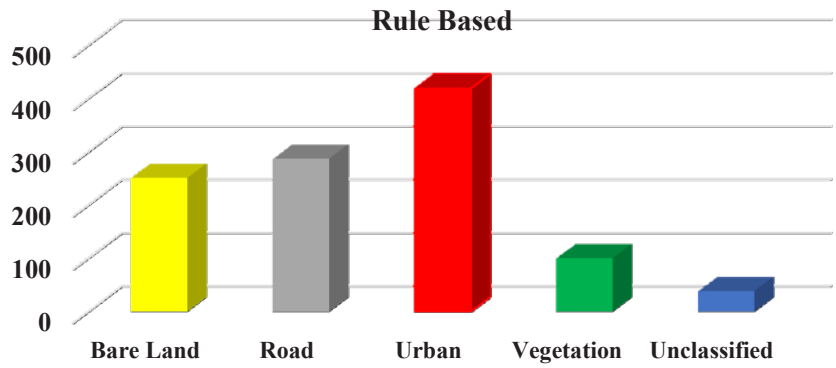

Fig. 7: Chart of Land-use area using rule-based classification method.

Table 3: Land use Area using Maximum Likelihood Classification.

Land use	Area [m^2]	Area [ha]	Percentage
Bare Land	1853207.68	185.32	16.94
Road	2398698.97	239.87	21.93
Urban	5601570.18	560.16	51.21
Vegetation	1084352.03	108.43	9.914

is shown in Table 3. However, Fig. 8. shows the chart of the land-use area using the Pixel-Based classification method.

These results in urban areas with 560.16 hectares (51.21%) which is the highest area compared to other land uses, while vegetation (farmland and green land) is almost 108.43 (9.914%) hectares which is low in comparison with other land uses. Road and Bare Land have almost (21.93%) and (16.94%) percentages respectively. Fig. 10. shows the map of Maximum Likelihood classification. These results sound reasonable considering the similarity of their spectral signatures.

In this research, Karbala City, Iraq was used as a case study to evaluate the performance of the object and pixel-based approaches in improving various urban land cover classes from High-Resolution QuickBird Imagery. The result illustrated that the rule-based classification enables differentiation between the classes accurately. Although, there was a decline in accuracy because of the differences between the characteristics of the classes and environmental conditions. Moreover, variations in the sensors utilize, illumination conditions, spatial resolutions of images, etc. are some other challenges that could impact the outcome as stated by (Ray et al. 2013).

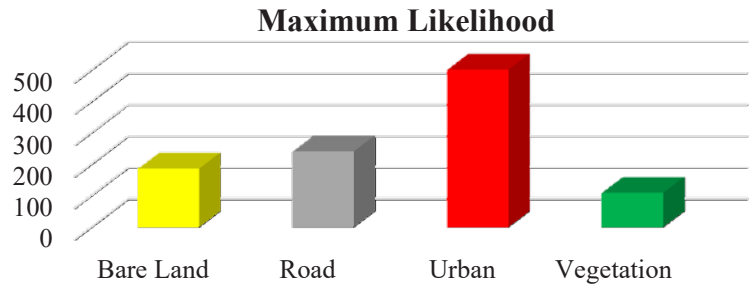

Fig. 8: Chart of Land use area using pixel-based classification method.

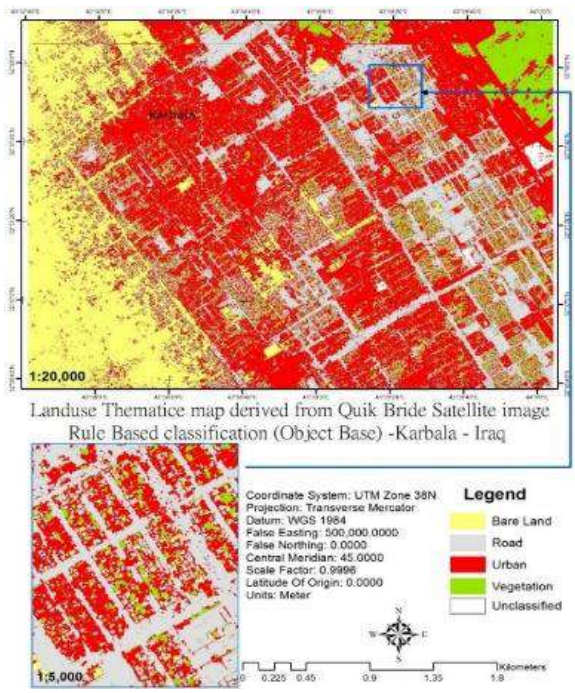

Fig. 9: Object-based classification.

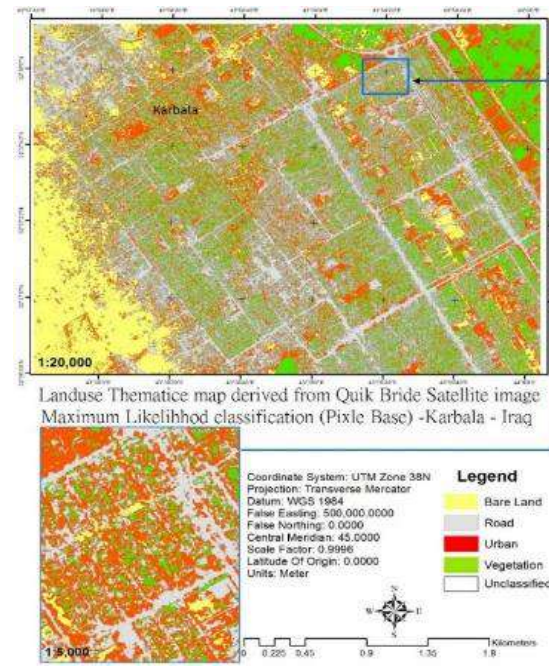

Fig. 10: Maximum likelihood classification.

Table 4: Maximum likelihood Accuracy assessment using a confusion matrix.

Land-use classes	Producer Accuracy %	User Accuracy %	Producer Accuracy pixels	User Accuracy Pixels
Bare Land	77.4	74.26	79117/102213	79117/106535
Road	60.55	84.09	56952/94051	56952/60528
Urban	92.38	26.9	12757/13809	12757/47418
Vegetation	95.68	90.92	99382/103872	99382/99464
Overall Accuracy			(248208/313945)	79.06%
Kappa Coefficient			0.78	

Table 5: Rule-Based Accuracy assessment using sampling of Google Earth.

Land-use classes	User Accuracy %	User Accuracy Pixels
Bare Land	89.85	44/50
Road	70.24	21/30
Urban	80.31	48/60
Vegetation	93.56	47/50
Overall Accuracy		86.02%
Kappa Coefficient		0.82

Table 6: Comparison of Land use classes derived from the object and pixel-based classification.

Land use	Maximum		Rule-Based	
	Area [ha]	Percentage	Area [ha]	Percentage
Bare Land	185.3	16.9	250.8	22.9
Road	239.9	21.9	286.7	26.2
Urban	560.2	51.2	418.1	38.2
Vegetation	108.4	9.9	99.9	9.1
Unclassified	0.0	0.0	38.20	3.5

Validation of Classifications

Classification accuracy is typically expressed by an error matrix. However, the matrix error is a quadratic sequence of rows and columns and also provides the related classified mage of the reference map. It is recommended and agreed as a common reporting norm that an error matrix is used to represent accuracy.

In this study, overall, the producer's and user's accuracy were considered for investigation of Maximum likelihood by using the confusion matrix while for assessment of Rule-based method 190 sample testing for all land use classes were performed from Google Map as shown in Table 4.

The Kappa coefficient was also measured as one of the most common measures to address the discrepancy between the agreement itself and the change agreement. The Maximum likelihood Accuracy assessment using a confusion matrix is shown in Table 4. and the Rule-Based Accuracy assessment using sampling of Google Earth is shown in Table 5.

The findings of the accuracy evaluation showed that rule-based classification is efficient and reliable for class differentiation. The accuracy of the user and the producer declined in both approaches for road class due to changes in road characteristics such as color changes and abstracted features.

Methods Comparison

Two classification techniques were applied to the same area

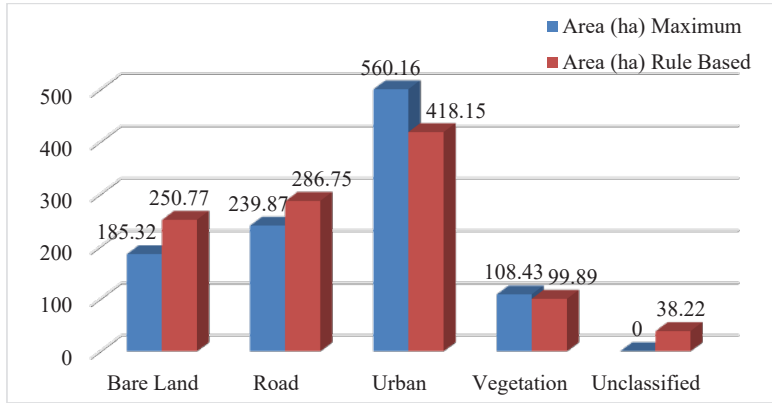

Fig. 11: Comparison ratio of land use classes derived from the object and pixel-based classification.

Table 7: Comparison between the pixel and object-based classifications according to user accuracy.

land-cover classes	User Accuracy %	
	Rule-based	Maximum-likelihood
Bare Land	89.85	74.26
Road	70.24	84.09
Urban	80.31	26.9
Vegetation	93.56	90.92

but different results were achieved for every single land/use class. Table 6. shows the comparison of Land-use classes derived from the object and pixel-based classification. Fig. 11. shows the comparison ratio of Land-use classes derived from the object and pixel-based classification.

Precision evaluation is a method used by comparing the classified result with a reference map to determine the accuracy of image classification. This is often known as an integral part of any classification technique of images. The spectral properties of an object in a very urbanized area may be inconsistent to be properly classed. Fig. 12 shows an area built up with a propensity for spectral signatures interfering with unpaved roads due to the reflectance of an old building roof. Table 7. shows the comparison between the pixel and Object-based classifications accuracy assessment. Fig. 12. shows the comparison between the pixel and Object-based classifications according to User Accuracy.

According to this graph user accuracy for extracting the urban area in the rule-based is much more precise than the maximum likelihood method 80% vs 27% almost. Vegetation classes show approximately the same amount of accuracy 91% vs 93% for Rule-based and Maximum respectively. Likewise in bare land class using object base, user accuracy is greater than maximum likelihood. However, Maximum likelihood is shown the better accuracy just in Road detection rather than Rule-based classification (70% versus 84% rule-based and Maximum respectively).

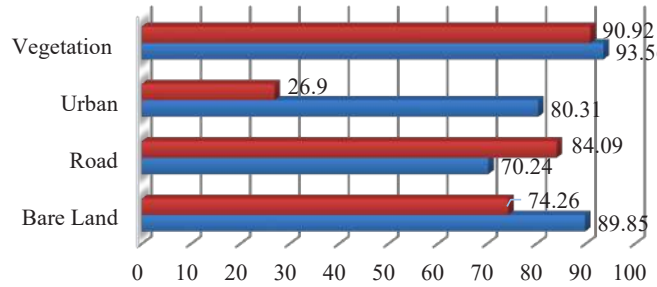

Fig. 12: Comparison between the pixel and object-based classifications according to user accuracy.

Fig. 13: Comprehensive comparisons between methods of classification.

As can be seen from Fig. 13, the urban extraction in the object-based classification method is more accurate and near to the original satellite image of QuickBird rather than pixel-based classification. While it is clear that Roads extracted by the pixel-based approach are near to the original image. Since it has shown a higher accuracy rather than a rule-based classification method.

CONCLUSION

Remote sensing is now an effective method for analyzing and mapping micro-, meso- and macro-level land use/cover. Repetitive coverage is important for remote sensing systems for change detection studies. The preparation of land and ground-cover maps is necessary to ensure planned growth and monitoring of land use patterns. This study shows the usefulness of satellite data to prepare accurate and up-to-date land-use and land cover maps. Classification results indicate consistently positive growth in urban planning and a balanced decrease in urban vegetation. In this study, two types of image classification were applied to a high-resolution satellite image (QuickBird) on a part of Karbala city in Iraq. Two sets of land use with four classes were generated, as a result, an object-based classification using the rule-based approach was not only more accurate in general but also, especially for urban and road classes, which are normally hard to make distinguish, had a great capability to extract features. It is also recommended that guidelines based on high-resolution satellite images such as QuickBird be used for the extraction of residential areas for future studies. It is proposed that the Iraqi Government will facilitate the use of modern GIS and remote sensing technologies to obtain rapid and precise digital information in support of the use of high-resolution satellite images and relegated techniques. As ground surveying methods are not easy and the production of aerial and photographic maps is very costly and time-consuming. A substantial finding from this research is that an improved detailed urban land cover classification based on high-resolution satellite data can be done via the combination of a set of features derived from the visible band and geometric ruleset. Further study is planned to examine the proposed methodology in various regions for land cover classification and informal settlements mapping.

REFERENCES

Adam, H. E., Csaplovics, E. and Elhaja, M. E. 2016. A comparison of pixel-based and object-based approaches for land use land cover classification in semi-arid areas, Sudan. In: IOP Conference Series: Earth and Environmental Science; 37(1): 012061.

Banzhaf, E., Grescho, V. and Kindler, A. 2009. Monitoring urban to peri-urban development with integrated remote sensing and GIS information: A Leipzig, Germany case study. Int. J. Remote Sens., 11: 297. https://doi.org/10.1080/01431160802642297

Belgiu, M. and Csillik, O. 2018. Sentinel-2 cropland mapping using pixel-based and object-based time-weighted dynamic time warping analysis. Remote Sens. Environ., 10: 05. https://doi.org/10.1016/j.rse.2017.10.005

Bhaskaran, S., Paramananda, S. and Ramnarayan, M. 2010. Per-pixel and object-oriented classification methods for mapping urban features using Ikonos satellite data. Appl. Geogr., 16: 112-132. https://doi.org/10.1016/j.apgeog.2010.01.009

Bruce, D. 2008. Object-oriented classification : case studies using different image types and different spatial resolutions. Int. Arch. Photohgramm. Remote Sens. Spat. Inform. Sci., 116: 1089.

Castillejo-González, I.L., López-Granados, F., García-Ferrer, A., Peña-Barragán, J.M., Jurado-Expósito, M., de la Orden, M.S. and González-Audicana, M. 2009. Object- and pixel-based analysis for mapping crops and their agro-environmental associated measures using QuickBird imagery. Comp. Electr. Agric., 25: 313-326. https://doi.org/10.1016/j.compag.2009.06.004

Darwish, A., Leukert, K. and Reinhardt, W. 2003. Image Segmentation for the Purpose of Object-Based Classification. International Geoscience and Remote Sensing Symposium (IGARSS), 21-25 July 2003, Toulouse, France, IEEE, Manhattan, NY, US, pp. 2039-2042. https://doi.org/10.1109/igarss.2003.1294332

Duro, D.C., Franklin, S.E. and Dubé, M.G. 2012. A comparison of pixel-based and object-based image analysis with selected machine learning algorithms for the classification of agricultural landscapes using SPOT-5 HRG imagery. Remote Sens. Environ., 16: 201-206. https://doi.org/10.1016/j.rse.2011.11.020

Esetlili, M.T., Bektas Balcik, F., Balik Sanli, F., Ustuner, M., Kalkan, K., Goksel, C., Gazioğlu, C. and Kurucu, Y. 2018. Comparison of the object and pixel-based classifications for mapping crops using rapid eye imagery: A case study of Menemen Plain, Turkey. Int. J. Environ. Geoinform., 2: 44-56. https://doi.org/10.30897/ijegeo.442002

Forkuor, G., Dimobe, K., Serme, I. and Tondoh, J.E. 2018. Landsat-8 vs. Sentinel-2: Examining the added value of sentinel-2's red-edge bands to land-use and land-cover mapping in Burkina Faso. GISci. Remote Sens., 5: 169 https://doi.org/10.1080/15481603.2017.1370169

Hamedianfar, A. and Shafri, H. Z. M. 2016. Integrated approach using data mining-based decision tree and object-based image analysis for high-resolution urban mapping of WorldView-2 satellite sensor data. Journal of applied remote sensing, 10(2): 025001.

Hashim, F., Dibs, H. and Jaber, H.S. 2022. Adopting Gram-Schmidt and Brovey methods for estimating land use and land cover using remote sensing and satellite images. Nat. Environ. Pollut. Technol., 21(2): 867-881.

Herold, M., Liu, X.H. and Clarke, K.C. 2003. Spatial metrics and image texture for mapping urban land use. Photogramm. Eng. Remote Sens., 11: 267-273. https://doi.org/10.14358/PERS.69.9.991

Hussain, M., Chen, D., Cheng, A., Wei, H. and Stanley, D. 2013. Change detection from remotely sensed images: From pixel-based to object-based approaches. ISPRS J. Photogramm. Remote Sens., 6: 114. https://doi.org/10.1016/j.isprsjprs.2013.03.006

Kohli, D., Warwadekar, P., Kerle, N., Sliuzas, R. and Stein, A. 2013. Transferability of object-oriented image analysis methods for slum identification. Remote Sens., 5: 420 https://doi.org/10.3390/rs5094209

Ma, L., Li, M., Ma, X., Cheng, L., Du, P. and Liu, Y. 2017. A review of supervised object-based land-cover image classification. ISPRS J. Photogramm. Remote Sens., 14: 315-326. https://doi.org/10.1016/j.isprsjprs.2017.06.001

Mahmoud, A.S., Kalantar, B., Al-Najjar, H.A., Moayedi, H., Halin, A.A. and Mansor, S. 2021. Object-Oriented Approach for Urbanization Growth By Using Remote Sensing and GIS Techniques: A Case Study in Hilla City, Babylon Governorate, Iraq. In Sharma, P. (ed), Geospatial Technology and Smart Cities, Springer, Cham, pp. 39-57.

Martins, V.S., Barbosa, C.C.F., de Carvalho, L.A.S., Jorge, D.S.F., Lobo, F.D.L. and de Moraes Novo, E.M.L. 2017. Assessment of atmospheric correction methods for sentinel-2 MSI images applied to Amazon floodplain lakes. Remote Sens., 9: 422. https://doi.org/10.3390/rs9040322

Mezaal, M.R., Pradhan, B., Shafri, H.Z.M., Mojaddadi, H. and Yusoff, Z.M. 2019. Optimized hierarchical rule-based classification for differentiating shallow and deep-seated landslides using high-resolution lidar data. Lect. Notes Civil Eng., 10: 16. https://doi.org/10.1007/978-981-10-8016-6_60

Mohammed, E.A., Hani, Z.Y. and Kadhim, G.Q. 2018 Assessing land cover/use changes in Karbala city (Iraq) using GIS techniques and remote sensing data. J. Phys. Conf. Ser., 12: 1047-1052. https://doi.org/10.1088/1742-6596/1032/1/012047

Myint, S.W., Gober, P., Brazel, A., Grossman-Clarke, S. and Weng, Q. 2011. Per-pixel vs. object-based classification of urban land cover extraction using high spatial resolution imagery. Remote Sens. Environ., 10: 172-193. https://doi.org/10.1016/j.rse.2010.12.017

Noori, A.M., Pradhan, B. and Ajaj, Q.M. 2019a. Dam site suitability assessment at the Greater Zab River in northern Iraq using remote sensing data and GIS. J. Hydrol., 24: 574. https://doi.org/10.1016/j.jhydrol.2019.05.001

Noori, A.M., Qader, W.M., Saed, F.G. and Hamdany, Z.A.L. 2019. Quantification of morphometric parameters to analyze the watershed characteristics: A case study of Rosti Watershed, Iraq. Int. J. Adv. Sci. Technol., 46: 541-556.

Nugroho, J. T., Sari, N. M. and Kushardono, D. 2017. A comparison of object-based and pixel-based approaches for land use/land cover classification using LAPAN-A2 microsatellite data. International Journal of Remote Sensing and Earth Sciences (IJReSES), 14(1): 27-36.

Ray, R., Mandal, S. and Dhara, A. 2013. Environmental monitoring of estuaries: Estimating and mapping various environmental indicators in Malta estuarine complex, using Landsat TM digital data. Int. J. Geomat. Geosci., 01: 4-17.

Ruiz Hernandez, I.E. and Shi, W. 2018. A random forests classification method for urban land-use mapping integrating spatial metrics and texture analysis. Int. J. Remote Sens., 17: 1011-1026. https://doi.org/10.1080/01431161.2017.1395968

Sameen, M.I., Pradhan, B., Shafri, H.Z.M., Mezaal, M.R. and Hamid, H.B. 2017. Integration of ant colony optimization and object-based analysis for LiDAR data classification. IEEE J. Sel. Topics Appl. Earth Observ. Remote Sens., 20: 956 https://doi.org/10.1109/JSTARS.2017.2650956

Sertel, E. and Alganci, U. 2016. Comparison of pixel and object-based classification for burned area mapping using SPOT-6 images. Geomat. Nat. Hazards Risk, 5: 608. https://doi.org/10.1080/19475705.2015.1050608

Song, J., Lin, T., Li, X. and Prishchepov, A.V. 2018. Mapping urban functional zones by integrating very high spatial resolution remote sensing imagery and points of interest: A case study of Xiamen, China. Remote Sens., 11: 737. https://doi.org/10.3390/rs10111737

Tehrany, M.S., Pradhan, B. and Jebuv, M.N. 2014. A comparative assessment between object and pixel-based classification approaches for land use/land cover mapping using SPOT 5 imagery. Geocarto Int., 13: 768. https://doi.org/10.1080/10106049.2013.768300

Vicente-Serrano, S.M., Pérez-Cabello, F. and Lasanta, T. 2008. Assessment of radiometric correction techniques in analyzing vegetation variability and change using time series of Landsat images. Remote Sens. Environ., 6: 113. https://doi.org/10.1016/j.rse.2008.06.011

Wang, Z., Wei, W., Zhao, S. and Chen, X. 2004. Object-oriented classification and application in land use classification using SPOT-5 PAN imagery. International Geoscience and Remote Sensing Symposium (IGARSS). https://doi.org/10.1109/igarss.2004.1370370

Weih, R.C. and Riggan, N. D. 2010. Object-based classification vs. pixel-based classification: Comparative importance of multi-resolution imagery. Int. Arch. Photogramm. Remote Sens. Spat. Inform. Sci., 53: 1125-1136.

Yan, G., Mas, J.F., Maathuis, B.HP., Xiangmin, Z. and Van Dijk, P.M. 2006. Comparison of pixel-based and object-oriented image classification approaches: A case study in a coal fire area, Wuda, Inner Mongolia, China. Int. J. Remote Sens., 14: 632. https://doi.org/10.1080/01431160600702632

Zhang, J. and Jia, L. 2014. A comparison of pixel-based and object-based land cover classification methods in an arid/semi-arid environment of Northwestern China. 3rd International Workshop on Earth Observation and Remote Sensing Applications, EORSA 2014 - Proceedings, 11-14 June 2014, Changsha, China, Manhattan, NY, pp. 291-302. https://doi.org/10.1109/EORSA.2014.6927922

Nature Environment and Pollution Technology
An International Quarterly Scientific Journal

p-ISSN: 0972-6268
(Print copies up to 2016)
e-ISSN: 2395-3454

Vol. 21 | No. 5 (Suppl) | pp. 2201-2209 | 2022

Original Research Paper

https://doi.org/10.46488/NEPT.2022.v21i05.014

Open Access Journal

Future Predictions of Precipitation and Discharge Using CMIP5 Models in the Western Ghats Region, India

Shilpa A. Veerabhadrannavar*† and B. Venkatesh**

*National Institute of Hydrology, Hard Rock Regional Centre, Visvesvaraya Nagar, Belagavi 590019, Karnataka, India
**National Institute of Hydrology, Hard Rock Regional Centre, Visvesvaraya Nagar, Belagavi 590019, Karnataka, India
†Corresponding author: Shilpa A. Veerabhadrannavar; shilpaveer56@gmail.com

Nat. Env. & Poll. Tech.
Website: www.neptjournal.com

Received: 15-04-2022
Revised: 31-05-2022
Accepted: 22-06-2022

Key Words:
Rainfall trend
Null hypothesis
Linear regression analysis
Ensemble
CORDEX-SA

ABSTRACT

Climate change is expected to exacerbate the hydrological cycle globally and have a significant impact on water resources. The Intergovernmental Panel on Climate Change (IPCC) Fourth Assessment Report states that observed and projected increases in both temperature and precipitation variability are the main reasons for projected climate change impacts on natural water resources. The examination of meteorological variables of the region, especially when agriculture is rainfall dependent, is very essential to formulate feasible adaptation strategies. As a result, using CORDEX-SA (Coordinated Regional Downscaling Experiment-South Asia) rainfall data (2021 to 2050), trend analysis was used to examine variations in rainfall data in the Kokkarne catchment of the Seetha river basin. Regression analysis was used to identify the season-wise rainfall trend. Annual, Summer, Monsoon, and Winter rainfall have depicted increasing trends with a rate of 2.46, 1.21, 2.77, and 0.009 mm per year respectively. The post-monsoon rainfall has projected a declining trend with a rate of -1.54 mm per year. Hence it is recommended that the designed strategies in the agricultural sector have to take the increasing, decreasing, and erratic nature of the trend of rainfall into consideration. Further considering the use of a Multi-Model Ensemble (MME) is reducing the SD and CV of rainfall data by 862 mm and 48.5% respectively. 87% of annual rainfall is contributed by monsoon season only with a Standard deviation of 424.4 mm and CV of 12%.

INTRODUCTION

Water is a very essential component of all the biological processes taking place on the earth, and there is no substitute for it. Water constitutes a vital resource for sustaining life on earth (Earman & Dettinger 2011, Hossain 2015). Water is regarded as a source of energy and is used for a variety of purposes in the home, agriculture, and business. But Water is a limited natural resource (Deka et al. 2021, Hossain 2015). Rainfall is the major source of supply of water in any region. The water requirements of Plants are met by natural sources and irrigation. Crop output, particularly in rain-fed locations, is highly dependent on rainfall occurrence, hence it is critical to study the variation of rainfall (Bhatla et al. 2020) to predict the likelihood of rainfall patterns from the available historical records of hydrological data. The probability distribution helps in relating the severity of extreme events like droughts, floods, and severe storms to their number of occurrences which enables the prediction of their likelihood pattern throughout time. By fitting a frequency distribution to a hydrological dataset, the likelihood of patterns of random parameters can be estimated. In the present study, the hydrological data is analyzed, and the variability in the data under consideration is studied concerning the statistical parameters, to fit the distribution. A slight change in any of the climatic variables has an impact on crop growth phases, lowering yield stability and quality (Mahilange & Das 2018). Crop growth and crop yield are negatively influenced by changes in climatic variables (Acquah & Kyei 2012, Panda & Sahu 2019). Crop yields are primarily dependent on rainfall received during the monsoon season, while crops sown in the winter season are also reliant on soil moisture maintained from the preceding monsoon. As a result of these influencing factors, the shifting rainfall pattern and its influence on agriculture and water supplies have become a significant climatic issue.

ORCID details of the authors:

S. A. Veerabhadrannavar: https://orcid.org/0000-0002-1566-1640
B. Venkatesh: https://orcid.org/0000-0002-9352-5230

The agricultural output reflects the economic well-being of the country (Cheng & Hu 2012, Goswami & Paul 2010, Hussain & Taqi 2014). To avoid water resource difficulties, it is vital to properly manage current resources. So having an idea about the pattern of rainfall and its trend is crucial from the standpoint of agriculture. To deliver the needed amount of water to the crops for their growth, it is critical to have comprehensive knowledge of rainfall trends. Climate scientists will benefit from the trend analysis in their hunt for climate change implications and repercussions. The primary goal of a trend test is to determine if the values of a data series are increasing or decreasing. Trend analysis is primarily used to assess the direction of a trend and to quantify its magnitude. The key objectives of this study, with the above considerations, are, to assess the multi-model ensemble data, to analyze the seasonal trend of rainfall, and to assess discharge patterns. This form of analysis will aid in the evaluation of actions aimed at ensuring enough irrigation and food security.

DATA USED AND METHODOLOGY

Study Area

The study area under consideration is the Kokkarne catchment, belonging to the Seetha river basin. Seetha river originates in the Western Ghats of India in Karnataka, which travels towards the west and drains into the Arabian sea. The Kokkarne catchment is located between 13.25° N and 13.75° N latitudes and between 74.75° E and 75.25° E longitudes. The delineated catchment area of Kokkarne catchment is 385 km^2 with a 30-year average rainfall of 3915.61 mm during the historical period (1991-2020). The drainage net is composed of small streams that originate in the Western Ghats, which are dominated by the younger Greenstone lithoclan. The Western Ghats, an important morpho element that works as a water barrier for the west-flowing and east-flowing rivers of the southwestern section of the Indian peninsula, is formed by these metasediments and metavolcanics. The location map of the study area is shown in Fig. 1.

Data

In this study, the rainfall dataset from the following five selected GCM (Global Climate Model) datasets (ACCESS1-0, GFDL-CM3, CNRM-CM5, MPI-ESM-LR, NorESM1-M) is obtained from http://cccr.tropmet.res.in. This CORDEX-SA data (Coordinated Regional Downscaling Experiment-South Asia) obtained for RCP 4.5 and the period of 2021-2050 is bias corrected before using as input to the Soil and Water Assessment Tool (SWAT) model. Table 1

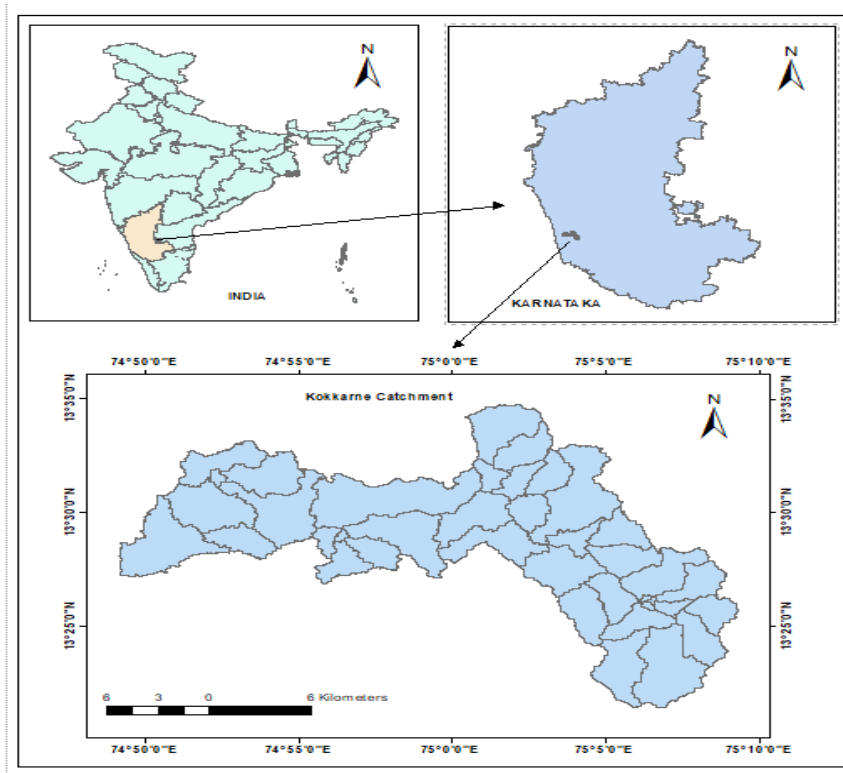

Fig. 1: Location map of the study area (Kokkarne catchment).

Table 1: Data source.

Component	Source
Rainfall (Daily)	India Meteorological Department (IMD)
Temperature (Daily)	India Meteorological Department (IMD)
Discharge (Daily)	Water Resources Development Organisation (WRDO)
Digital Elevation Model (DEM)	Shuttle Radar Topography Mission (SRTM)
Soil map	Food and Agricultural Organization (FAO)
Land-use/land-cover maps (LULC)	Water Base Worldwide Dataset

shows the data source for the study.

SWAT Model

The Soil and Water Assessment Tool (SWAT) model is used to simulate river outflows (Neitsch et al. 2011). It is a physically based rainfall-runoff model which normally operates on a daily time frame and basin scale and accounts for regional heterogeneities by dividing the watershed into several hydrological response units (HRUs). Each HRU has its unique combination of soil, land use, and elevation. The model estimates the hydrology of each HRU based on the precipitation, surface runoff, evapotranspiration, percolation, and return flows in the catchment. The output of the SWAT model helps to analyze each subbasin discharge of the catchment.

Representative Concentration Pathways

In the current study, RCP 4.5 scenario, which is a medium stabilization scenario is used. The IPCC Fifth Assessment Report (AR5) released in 2014 recommends RCP 4.5 as one of the representative concentration pathways (RCPs) in which radiative forcing is assumed not to overshoot beyond 4.5 W/m^2 by the end of 2100. Radiative forcing is the sum of the effects of greenhouse gases and other forcing components. RCP 4.5 takes into account long-term global greenhouse gas emissions in a global framework, as modeled by the Global Change Assessment Model, and adopts a cost-cutting method to attain the target radiative forcing (Thomson et al. 2011). RCPs can be used to highlight likely climate change impacts on watershed hydrology using GCM-predicted datasets (Hong et al. 2016; Mudbhatkal et al. 2017; Shrestha & Htut, 2016).

Methodology

The various steps followed in the present study were as follows:

1. The regression analysis in this study was based on IMD (India Meteorological Department) rainfall data from the Kokkarne catchment for the baseline period 1991 to 2020. The Linear regression analysis was employed to discover trends in the rainfall data. One of the most basic approaches for calculating the trend of data in a time series is linear regression analysis. A parametric test that assumes normally distributed data is regression analysis. The linear relationship between time and the variable of interest is utilized to test the trend. The variables must be normally distributed, as well as be temporally and spatially independent, to apply this strategy correctly. The regression analysis can be done on the time series of rainfall data directly by using regression analysis with time as the independent variable and rainfall as the dependent variable, the trend in rainfall can be determined. The linear regression equation is expressed as:

$$y = mk + c \quad (1)$$

The dependent variable is y, while the independent variable is x. The slope of the line is m, and the intercept (value of y when x = 0) is c. The rate of increase or decline of the variable is represented by the slope. k denotes the length of time in years. The rainfall trend has been described by the slope line. If the slope line is positive, it indicates that rainfall is increasing. However, if the slope line is negative, it indicates that rainfall is decreasing. The dependent variable y in this study is rainfall, whereas the independent variable x is the year. The assumption of a normal distribution is required for linear regression. The null hypothesis in this study is that the slope of the line in the graph is zero, or that the rainfall data shows no trend.

   The R^2 or square of the correlation value from the regression analysis was used to demonstrate the strength of the connection between the variables x and y. Which has a value ranging from 0.0 to 1.0. An R^2 score of 1.0 indicates that the connection is high and that all of the points are in a straight line. An R^2 value of 0.0, on the other hand, indicates that there is no connection and no linear relationship exists between x and y.
2. The multi-model ensemble data is analyzed with statistical parameters like standard deviation and Coefficient of variation.
3. The monthly distribution of rainfall in the catchment region is analyzed.
4. With the data inputs presented in Table 1, the SWAT model was used to simulate the Kokkarne catchment. The generated discharge output was used for the analysis.

RESULTS AND DISCUSSION

Trend Analysis

Fig. 2 and 3 show the trend of total annual and seasonal precipitation over the period under consideration. The rate of change in a linear regression model is determined by the slope of the regression line, which in the case of annual rainfall in the current study area is around 2.46 mm/year as shown in Fig. 3. The increasing trend of annual rainfall in the current study is matching with that of the increasing trend of precipitation as reported by Basappa et al. (2021) and Nandargi & Mulye (2014) in the study regions which belong to the Western Ghats. While the winter, spring, and summer seasons have shown an increasing trend in the study region, the post-monsoon season has shown a minor declining trend as presented in Fig. 2 and Table 2.

The rate of change is defined by the slope of the regression line, which in this case is roughly 1.21 mm/year, 2.77 mm.year^{-1}, -1.54 mm.year^{-1}, and 0.0093 mm.year^{-1} for summer, monsoon, post-monsoon, and winter rainfall

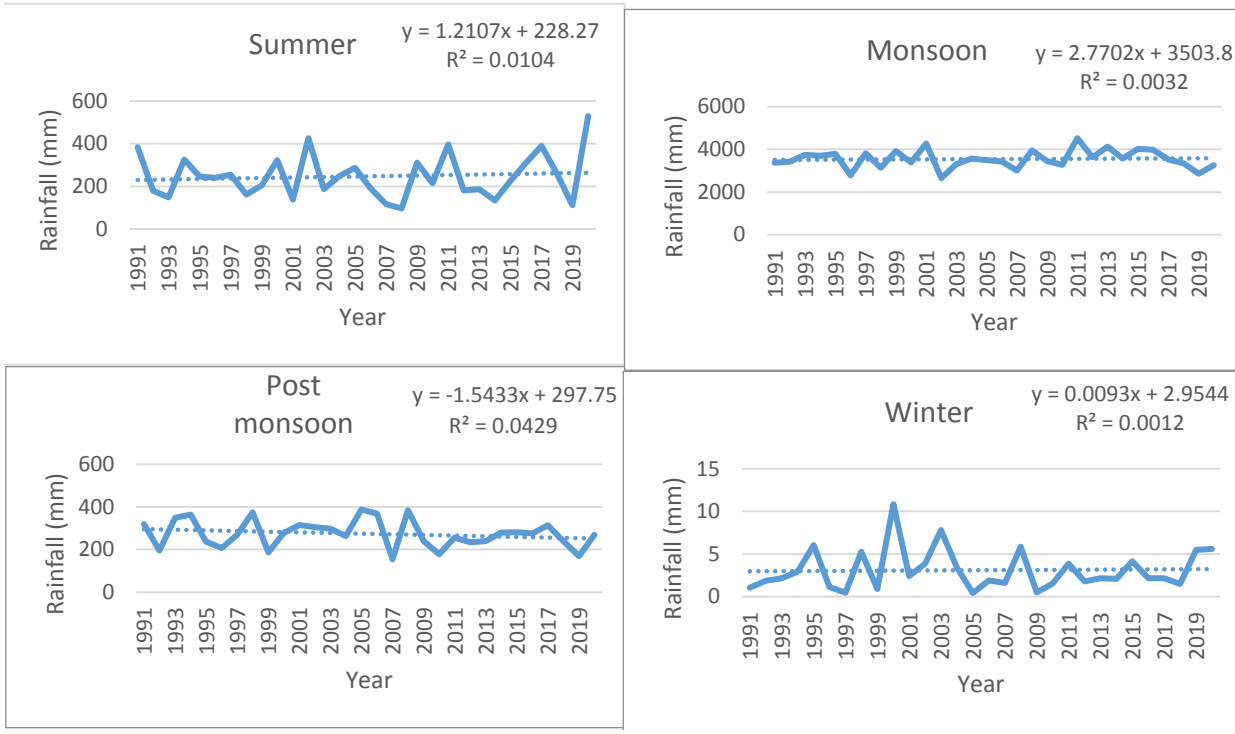

Fig. 2: Regression analysis of rainfall data (a) Summer, (b) Monsoon, (c) Post Monsoon (d) Winter

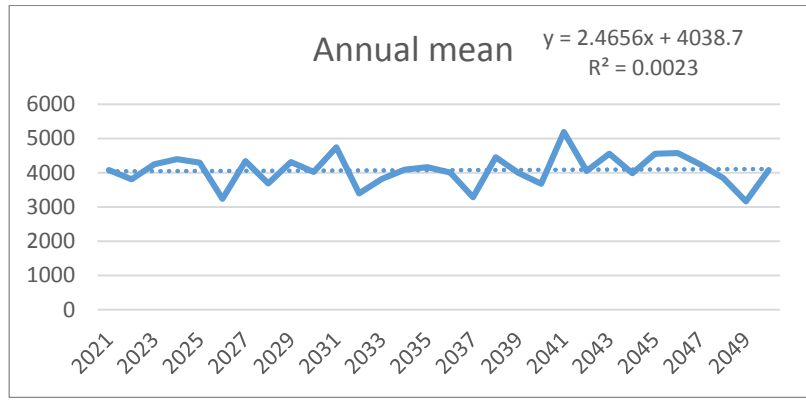

Fig. 3: Regression analysis of rainfall data (2021-2050) for Kokkarne catchment

Table 2: Regression analysis of rainfall data (a) Summer, (b) Monsoon, (c) Post Monsoon (d) Winter.

Season	Regression Equation	R^2
Summer	y = 1.21x + 228.27	0.0104
Monsoon	y = 2.77x + 3503.8	0.0032
Post monsoon	y = -1.54x + 297.75	0.0429
Winter	y = 0.0093x + 2.95	0.0012
Annual	y = 2.46x + 4038.7	0.0023

respectively, using a linear regression model (Fig. 2). The post-monsoon rainfall pattern was found to be fairly variable, while the winter trend was non-significant (Fig. 2). The post-monsoon rainfall season is showing a declining trend. This kind of seasonal variation in precipitation in different regions has also been reported by (Cheung et al. 2008, Gedefaw et al. 2018, Hussain & Lee 2013, Jain & Kumar 2012, Kumar et al. 2010, Łupikasza et al. 2011, Malik & Kumar 2020, Radhakrishnan et al. 2017). The weather system being different in different seasons of the year is the prime factor leading to seasonal variation in precipitation as reported by Arora et al. (2006).

GCM Uncertainty

Climate statistics for the near future are shown in Table 3 for the summer, monsoon, post-monsoon, and winter seasons and annual time scales. It is worth noting that the majority of the forecasts show a rise in mean annual rainfall when compared to the rainfall data of the baseline period (1777.7 mm). The ensemble means rainfall value for the catchment shows an increase of roughly 2299.2 mm. The annual rainfall projected by different GCM models ranges from 3555.7 mm (ACCESS1.0 GCM MODEL) to 4317.1 mm (MPI-ESM-LR GCM MODEL). During the monsoon season, all of the projections show similar variations.

As shown in Table 3, there are only minor variations in CV, which are 11 % and 12 % for the annual and monsoon seasons respectively, compared to 48.5 % and 58.9 % for the rainfall data of the baseline period, implying that variability will be reduced in the near future. Further, the CV of post-monsoon rainfall is 23.55 % which is higher than that of monsoon rainfall at 11.96%, implying that post-monsoon rainfall has more interannual variability than monsoon rainfall. Considering the above findings the use of Multi-Model

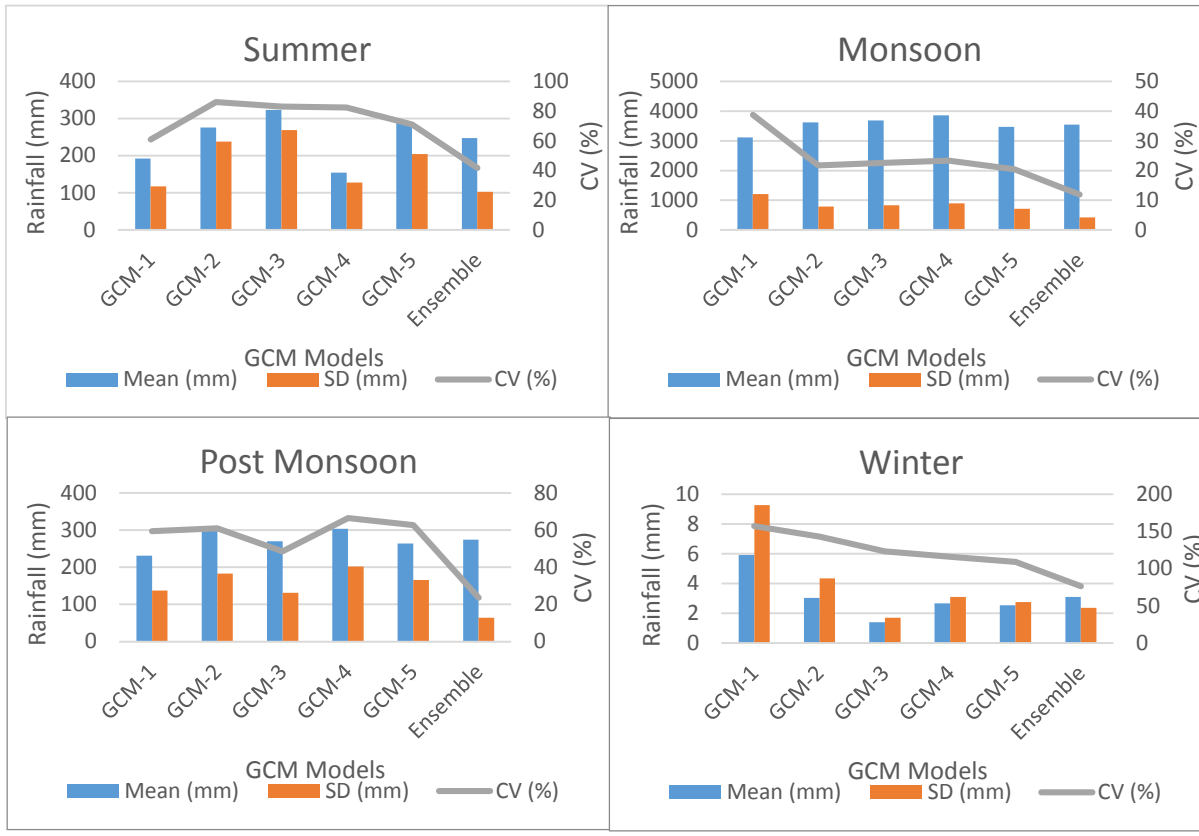

Fig. 4: Seasonal mean rainfall, standard deviation, and their corresponding CV.

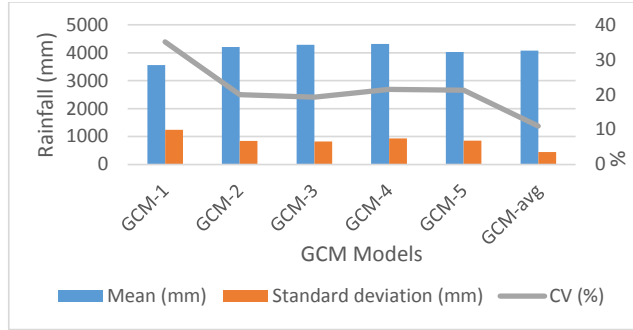

Fig. 5: Annual mean rainfall, standard deviation, and their corresponding CV.

Table 3: Climate statistics for near future bias-corrected GCM projections (2021-2050). The values in brackets represent the absolute change in the Bias corrected GCM data with reference period, i.e. IMD gridded data for the period (1991-2020).

		Mean (mm)	SD (mm)	CV (%)
IMD	Summer	119.34	57.50	48.18
	Monsoon	1451.36	854.60	58.88
	Post monsoon	193.11	104.73	54.23
	Winter	4.62	5.73	123.94
	Annual	1777.69	861.95	48.49
ACCESS1.0	Summer	192.3 (61.2)	117.3 (104.1)	61 (26.7)
	Monsoon	3114.6 (114.6)	1207.3 (41.3)	38.8 (-34.2)
	Post monsoon	231.2 (19.8)	137.2 (31.1)	59.4 (9.6)
	Winter	5.9 (27.6)	9.3 (62.3)	157.3 (27)
	Annual	3555.7 (100.1)	1245 (44.5)	35.1 (-27.7)
CNRM-CM5	Summer	276.1 (131.4)	237.8 (313.6)	86.2 (79)
	Monsoon	3617.1 (149.3)	785 (-8.2)	21.8 (-63)
	Post monsoon	300.5 (55.7)	183.4 (75.2)	61.1 (12.7)
	Winter	3.1 (-33)	4.4 (-23.3)	143 (15.4)
	Annual	4202.6 (136.5)	839.1 (-2.7)	20 (-58.8)
GFDL-CM3	Summer	323.6 (171.2)	268.6 (367.2)	83.1 (72.5)
	Monsoon	3687.9 (154.1)	832.2 (-2.7)	22.6 (-61.7)
	Post monsoon	270.2 (40)	131.4 (25.5)	48.7 (-10.2)
	Winter	1.4 (-69.8)	1.8 (-68.6)	123.3 (-0.6)
	Annual	4285.8 (141.1)	826.3 (-4.2)	19.3 (-60.2)
MPI-ESM-LR	Summer	154.8 (29.8)	127.5 (121.8)	82.4 (71.1)
	Monsoon	3851 (165.4)	897.8 (5.1)	23.4 (-60.3)
	Post monsoon	303.4 (57.2)	201.7 (92.6)	66.5 (22.7)
	Winter	2.7 (-41.7)	3.1 (-46)	115.9 (-6.5)
	Annual	4317.1 (142.9)	927.5 (7.7)	21.5 (-55.7)
NorESM1-M	Summer	288.7 (142)	204.7 (256.1)	70.9 (47.2)
	Monsoon	3463.5 (138.7)	709.4 (-17)	20.5 (-65.2)
	Post monsoon	264.1 (36.8)	165.6 (58.2)	62.8 (15.9)
	Winter	2.6 (-43.8)	2.8 (-51.2)	108.8 (-12.3)
	Annual	4023.8 (126.4)	856.4 (-0.7)	21.3 (-56.1)
Ensemble	Summer	247 (107)	102.9 (79)	41.7 (-13.4)
	Monsoon	3546.8 (144.4)	424.4 (-50.3)	12 (-79.6)
	Post monsoon	273.8 (41.8)	64.5 (-38.4)	23.6 (-56.5)
	Winter	3.1 (-33)	2.4 (-58.1)	76.4 (-38.4)
	Annual	4076.9 (129.3)	448 (-48)	11 (-77.3)

Ensemble (MME) data is encouraged as the process will reduce the uncertainties involved in individual GCM data (Ahmed et al. 2019, Colorado-Ruiz et al. 2018, Dai et al. 2001, Shiru et al. 2020, Wang et al. 2018).

The standard deviation of rainfall data projected by different GCM models under consideration varied from 826.3 mm (GFDL-CM3 GCM MODEL) to 1245 mm (ACCESS1.0 GCM MODEL), and the coefficient of variation varied from 19.3 mm (GFDL-CM3 GCM MODEL) to 35.1 mm (ACCESS1.0 GCM MODEL). Considering the ensemble of GCM values reduces the standard deviation of rainfall data for the period 2021-2050 to 448 mm, as shown in Fig. 5. Even the coefficient of variation is lowered to 11 %, along with the standard deviation. As a result, the rainfall variability of the projected data is reduced.

Monthly Distribution of Average Precipitation (2021-2050)

Kokkarne catchment receives annual precipitation ranging from 3201.82 mm to 5141.29 mm, with an average of 4069.38 mm. The highest monthly average precipitation is received during July (1230.73mm) (Krishnakumar et al. 2009), contributing 30.24 % to annual precipitation; August and September months with precipitation of 1018.39 mm and 387 mm ranked second and third, contributing 25.02 % and 9.51 % to annual precipitation, respectively. July is found to be the wettest month in the catchment as reported by other similar studies (Bhan et al. 2015, Singh & Mishra 2014, Zhang et al. 2019).

The monsoon season receives the highest precipitation of all the seasons, it is preferable to locate a feasible mechanism for storing extra precipitation in a reservoir, rather than letting it runoff or evaporate. A guideline for groundwater recharging might be constructed using this extra precipitation during the monsoon. With minimal extraction during the monsoon and by using groundwater recharging techniques, good groundwater can be conserved. It would be difficult to grow post-monsoon crops without additional irrigation since post-monsoon precipitation is more unpredictable and variable.

Decadal Analysis of Rainfall and Discharge

The box plot analysis of rainfall and discharge has been shown in Fig. 6. The rainfall is projected to decrease from 4164.64 mm in 2021-30 to 3999.02 mm in 2031-40 then projected to increase to 4157.16 mm in 2041-50. Similarly, the discharge output obtained from the simulation of the SWAT model was also analyzed and it was found that rainfall is projected to decrease from 218.40 $m^3.sec^{-1}$ in 2021-30 to 208.40 $m^3.sec^{-1}$ in 2031-40 and then projected to increase to 218.92 $m^3.sec^{-1}$ in 2041-50.

The increase in the discharge is correlated with an increase in the rainfall of the catchment as reported by studies like (Chiew et al. 1995, Fapeng et al. 2013; Miller & Russell 1992, Pfister et al. 2004, Van Steenbergen & Willems 2012).

CONCLUSIONS

The purpose of this study was to use regression analysis of the rainfall data for the catchment to detect the annual and seasonal rainfall patterns. The rate of change of the rainfall was obtained by fitting the linear regression line, and the slope of the simple least-square regression expressed the trend. The current study used linear regression analysis, a significant parametric model that can be utilized to construct functional correlations between variables, to examine the rainfall trend for the study area. Furthermore, from 2021 to

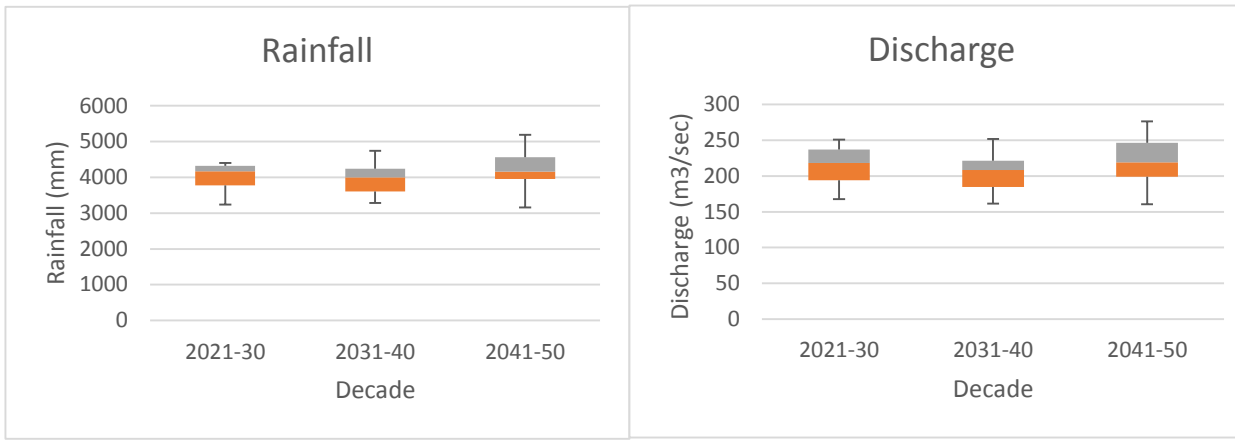

Fig. 6: Decadal analysis of 1) Rainfall 2) Discharge of Kokkarne catchment.

2050, the current study brings to light the impact of global climate change on rainfall and discharge patterns in the Kokkarne catchment.

Following are a few of the observations from the present research.

1. Except for the post-monsoon season, the trend m (the slope) in the equation y = mk + c of regression analysis revealed a positive trend for all three seasons.
2. Considering the Ensemble mean of rainfall data helps to reduce the uncertainty in the data.
3. The standard deviation of ensembled rainfall data has reduced to 448 mm.
4. CV of ensembled rainfall data has reduced to 11 mm.
5. July month is receiving the highest monthly average precipitation of 1230.73 mm.
6. The increase or decrease in the rainfall of the catchment is reflecting the increase or decrease in the discharge of the catchment.

Climate extreme events have an impact on farmers in the region and their agricultural activities with the increase in rainfall variability. The government may formulate climate-friendly water resource policies as a result of the findings of this study, which will promote self-sufficient and economical agricultural practices.

ACKNOWLEDGMENTS

The authors thank the Indian Institute of Tropical Meteorology (IITM), Pune for making CORDEX-SA data available. The authors also gratefully acknowledge the climate data provided by the India Meteorological Department, New Delhi, and discharge data provided by WRDO, Bangalore. The authors acknowledge gratefully the National Institute of Hydrology, Belagavi, Karnataka, India for helping to acquire all the data used in this study.

REFERENCES

Acquah, H. and Kyei, C. 2012. The effects of climatic variables and crop area on maize yield and variability in Ghana. Russ. J. Agric. Socio-Econ. Sci., 10(1): 10-13. https://doi.org/10.18551/rjoas.2012-10.02

Ahmed, K., Sachindra, D.A., Shahid, S., Demirel, M.C. and Chung, E. 2019. Selection of multi-model ensemble of general circulation models for the simulation of precipitation and maximum and minimum temperature based on spatial assessment metrics. Hydrol. Earth Syst. Sci., 23(11): 4803-4824.

Arora, M., Singh, P., Goel, N. and Singh, R. 2006. Spatial distribution and seasonal variability of rainfall in a mountainous basin in the Himalayan region. Water Resour. Manag., 20(4): 489-508.

Basappa, V., Nayak, P. C., Thomas, T., Jain, S. and Tyagi, J. 2021. Spatio-temporal analysis of rainfall pattern in the Western Ghats region of India. Meteorol. Atmos. Phys., 133(4): 1089-1109. https://doi.org/10.1007/s00703-021-00796-z

Bhan, S., Devrani, A. and Sinha, V. 2015. An analysis of monthly rainfall and the meteorological conditions associated with cloudburst over the dry region of Leh (Ladakh), India. Mausam, 66(1): 107-122. https://doi.org/10.54302/mausam.v66i1.371

Bhatla, R., Singh, S., Verma, S., Tyagi, P., Maurya, A. and Pant, M. 2020. The study of rainfall variability during pre and post-monsoon seasons over all of India and its different regions in changing climate. J. Indian Geophys. Union, 24(3): 57-71.

Cheng, H. and Hu, Y. 2012. Improving China's water resources management for better adaptation to climate change. Clim. Change, 112(2): 253-282.

Cheung, W.H., Senay, G.B. and Singh, A. 2008. Trends and spatial distribution of annual and seasonal rainfall in Ethiopia. Int. J. Clim. Royal Meteorol. Soc., 28(13): 1723-1734.

Chiew, F.H.S., Whetton, P.H., McMahon, T.A. and Pittock, A.B. 1995. Simulation of the impacts of climate change on runoff and soil moisture in Australian catchments. J. Hydrol., 167(1): 121-147. https://doi.org/10.1016/0022-1694(94)02649-V

Colorado-Ruiz, G., Cavazos, T., Salinas, J.A., De Grau, P. and Ayala, R. 2018. Climate change projections from Coupled Model Intercomparison Project phase 5 multi-model weighted ensembles for Mexico, the North American monsoon, and the mid-summer drought region. Int. J. Clim., 38(15): 5699-5716.

Dai, A., Meehl, G.A., Washington, W.M., Wigley, T.M. and Arblaster, J.M. 2001. Ensemble simulation of twenty-first-century climate changes Business-as-usual versus CO 2 stabilization. Bull. Am. Meteor. Soc., 82(11): 2377-2388.

Deka, J.R., Bordoloi, M. and Sarma, P. 2021. Historical ponds of Darrang district: Identification and mapping, their ecological relevance for management planning. Int. J. Geoherit. Parks, 9(4): 496-508. https://doi.org/10.1016/j.ijgeop.2021.11.008

Earman, S. and Dettinger, M. 2011. Potential impacts of climate change on groundwater resources: A global review. J. Water Clim. Change, 2(4): 213-229.

Fapeng, U., Zhang, Y., Xu, Z., Teng, J., Liu, C., Liu, W. and Mpelasoka, F. 2013. The impact of climate change on runoff in the southeastern Tibetan Plateau. J. Hydrol., 505(1): 188-201. https://doi.org/10.1016/j.jhydrol.2013.09.052

Gedefaw, M., Yan, D., Wang, H., Qin, T., Girma, A., Abiyu, A. and Batsuren, D. 2018. Innovative trend analysis of annual and seasonal rainfall variability in Amhara regional state, Ethiopia. Atmosphere, 9(9): 326-336.

Goswami, A. and Paul, A. 2010. Assessment of trends and variability of post-monsoon rainfall for some selected districts of sub-Himalayan West Bengal, India. Ind. Geogr. J., 85(1): 37-44.

Hong, N.N., Xu, C.Y., Beldring, S., Tallaksen, L.M. and Jain, S.K. 2016. Water resources under climate change in Himalayan basins. Water Resour. Manag., 30(2): 843-859.

Hossain, M. 2015. Water: The most precious resource of our life. Glob. J. Adv. Res., 2(9): 1-11.

Hussain, M. and Lee, S. 2013. The regional and seasonal variability of extreme precipitation trends in Pakistan. Asia-Pacif. J. Atmos. Sci., 9(4): 421-441. https://doi.org/10.1038/s41598-019-41334-7

Hussain, M. and Taqi, M. 2014. Impact of agricultural credit on agricultural productivity in Pakistan: An empirical analysis. Int. J. Adv. Res. Manag, Social Sci., 3(4): 125-139.

Jain, S.K. and Kumar, V. 2012. Trend analysis of rainfall and temperature data for India. Curr. Sci., 102(1): 37-49.

Krishnakumar, K.N., Rao, G.P. and Gopakumar, C.S. 2009. Rainfall trends in the twentieth century over Kerala, India. Atmos. Environ., 43(11): 1940-1944. https://doi.org/10.1016/j.atmosenv.2008.12.053

Kumar, V., Jain, S.K. and Singh, Y. 2010. Analysis of long-term rainfall trends in India. Hydrol. Sci. J., 55(4): 484-496.

Łupikasza, E.B., Hänsel, S. and Matschullat, J. 2011. Regional and seasonal variability of extreme precipitation trends in southern Poland

and central-eastern Germany 1951-2006. Int. J. Climatol., 31(15): 2249–2271.

Mahilange, M. and Das, G.K. 2018. Estimating rainfall variability over five districts of the northern hill zone of Chhattisgarh state. J. Pharmac. Phytochem., 7(5): 3370-3374.

Malik, A. and Kumar, A. 2020. Spatio-temporal trend analysis of rainfall using parametric and non-parametric tests: A case study in Uttarakhand, India. Theoret. Appl. Climatol., 140(1): 183-207.

Miller, J.R. and Russell, G.L. 1992. The impact of global warming on river runoff. J. Geophys. Res. Atmos., 97(D3): 2757-2764. https://doi.org/10.1029/91JD01700

Mudbhatkal, A., Raikar, R., Venkatesh, B. and Mahesha, A. 2017). Impacts of climate change on varied river-flow regimes of southern India. J. Hydrol. Eng., 22(9): 1-13. https://doi.org/10.1061/(ASCE)HE.1943-5584.0001556

Nandargi, S. and Mulye, S. 2014). Spatio-temporal rainfall variability over Goa, India. Int. J. Meteorol., 39(385): 99-121.

Neitsch, S.L., Arnold, J.G., Kiniry, J.R. and Williams, J.R. 2011. Soil and Water Assessment Tool Theoretical Documentation Version 2009. Texas Water Resources Institute. https://oaktrust.library.tamu.edu/bitstream/handle/1969.1/128050/TR-406_SoilandWaterAssessmentToolTheoreticalDocumentation.pdf?sequence=1

Panda, A. and Sahu, N. 2019. Trend analysis of seasonal rainfall and temperature pattern in Kalahandi, Bolangir and Koraput districts of Odisha, India. Atmos. Sci. Lett., 20(10),1-10. https://doi.org/10.1002/asl.932

Pfister, L., Drogue, G., El Idrissi, A., Iffly, J.F., Poirier, C. and Hoffmann, L. 2004. Spatial variability of trends in the rainfall-runoff relationship: A mesoscale study in the Mosel basin. Clim. Change, 66(1): 67-87. https://doi.org/10.1023/b:clim.0000043160.26398.4c

Radhakrishnan, K., Sivaraman, I., Jena, S. K., Sarkar, S. and Adhikari, S. 2017. A climate trend analysis of temperature and rainfall in India. Clim. Change Environ. Sustain., 5(2): 146-153.

Shiru, M.S., Chung, E.S., Shahid, S. and Alias, N. 2020. GCM selection and temperature projection of Nigeria under different RCPs of the CMIP5 GCMs. Theoret. Appl. Climatal., 141(3): 1611-1627. https://doi.org/10.1007/s00704-020-03274-5

Shrestha, S. and Htut, A.Y. 2016.. Modeling the potential impacts of climate change on the hydrology of the Bago River Basin, Myanmar. Int. J. River Basin Manag. 14(3): 287-297.

Singh, S. and Mishra, A. 2014. Spatiotemporal analysis of the effects of forest covers on stream water quality in the Western Ghats of peninsular India. J. Hyrdol., 519(1): 214-224.

Thomson, A.M., Calvin, K.V., Smith, S.J., Kyle, G.P., Volke, A., Patel, P., Delgado-Arias, S., Bond-Lamberty, B., Wise, M. A. and Clarke, L.E. 2011. RCP4. 5: A pathway for stabilization of radiative forcing by 2100. Climat. Change, 109(1): 77-94.

Van Steenbergen, N. and Willems, P. 2012. Method for testing the accuracy of rainfall-runoff models in predicting peak flow changes due to rainfall changes, in a climate-changing context. J. Hyrdrol., 414(1): 425-434. https://doi.org/10.1016/j.jhydrol.2011.11.017

Wang, B., Zheng, L., Ji, F., Clark, A. and Yu, Q. 2018. Using multi-model ensembles of CMIP5 global climate models to reproduce observed monthly rainfall and temperature with machine learning methods in Australia. Int. J. Climatol., 38(13): 4891-4902. https://doi.org/10.1002/joc.5705

Zhang, K., Wang, Q., Chao, L., Ye, J., Li, Z., Yu, Z., Yang, T. and Ju, Q. 2019. Ground observation-based analysis of soil moisture spatiotemporal variability across a humid to semi-humid transitional zone in China. J. Hydrol., 574(1): 903-914. https://doi.org/10.1016/j.jhydrol.2019.04.087

Nature Environment and Pollution Technology
An International Quarterly Scientific Journal

p-ISSN: 0972-6268
(Print copies up to 2016)
e-ISSN: 2395-3454

Vol. 21 | No. 5 (Suppl) | pp. 2211-2218 | 2022

Original Research Paper

https://doi.org/10.46488/NEPT.2022.v21i05.015

Open Access Journal

Prediction of Marine Water Quality Index Using a Stacked Classifier Under Machine Learning Architecture

K. Komathy*†

*Department of Information Technology, Academy of Maritime Education and Training, Chennai, India
†Corresponding author: K. Komathy; gomes1960@yahoo.com

Nat. Env. & Poll. Tech.
Website: www.neptjournal.com

Received: 28-04-2022
Revised: 25-06-2022
Accepted: 30-06-2022

Key Words:
Machine learning
Model training
Model optimizing
Ensemble learning
Marine water quality
Marine water quality index

ABSTRACT

The health of humankind is intrinsically associated with the health of the marine and ocean ecosystems. The pollution of the coastal region due to urbanization, for example, principally harms the growth of the ecosystem with poor-quality of water, which aggravates the survival of marine organisms and animals. The toxicity of the contaminated seafood would affect the human-ocean ecosystem thereby bringing down the economic rank of the region as well. Therefore, it is mandatory to assess the quality of the marine and ocean water to initiate any statutory measures to protect the regional marine water against pollution and dumping of toxic matter. This paper, therefore, presented an architecture of machine learning techniques to assist in classifying marine water quality. The proposed framework evaluated various classification models and selected the best fit out of the top-performing algorithms through training and optimizing. The finalized model was a *stacked classifier*, which was then deployed to predict the marine water quality index from the physicochemical and biological properties of the water.

INTRODUCTION

Physical, chemical, and biological processes undertake to transform a marine ecosystem into a complex one. Light, food, and nutrients are vital elements to a healthy marine ecosystem. Also, water temperature, depth, and salinity, as well as the local landscape have an impact on marine ecosystems. Variations of these conditions can result in new compositions of species as part of the marine community. Besides, a microbe present in the marine environment is an important biological indicator of water quality. Say, phytoplankton microbes constitute the basis of the food chain structure in marine environments, which serve as food for aquatic species such as zooplankton, shellfish, and finfish (Sridhar et al. 2006), and keep the biological balance of water quality. Marine microorganisms adapt quickly to changes in nutrients (Robertson & Blaber 1993). According to plant-animal relations showcased by Sverdrup et al. (1942), plants, as autotrophic organisms, transform inorganic material into organic particulate as food for marine animals. Therefore, it is vital phenomenon to monitor the quality of marine water so that the dependents including humankind in the food chain will be able to survive without infections and toxicity.

The water quality index (WQI) is an empirical expression, as per McClelland (1974), which integrates physical, chemical, and microbiological parameters of water quality to derive into a single number. Since 1965, several numerical water quality indices have originated on various approaches depending on the applications and water parameters. Horton started with a simple WQI model (Horton 1965) followed by Brown et al. (1970, 1972) to propose a general WQI. WQIs were derived from associating observed parameter values and the local norms. Different WQI approaches existing currently were derived from either the weighted sum method or amplitude technique. The weighted-sum method was used to generate a sub-index, which helped to normalize the water quality parameters differing in units of measurement (Banda & Kumarasamy 2015). On the other method, the overall WQI was calculated using the deviations of water quality metrics quantitatively from the targets (CCME 2001, Khan et al. 2005, Mostafaei 2014). Akhtar et al. (2021) have elaborated the multi-criteria decision-making (MCDM) approach, which included the processes namely MACBETH and AHP to distinguish the various water usages such as

ORCID details of the authors:

K. Komathy:
https://orcid.org/0000-0002-0721-1762

drinking, domestic, irrigation, and industrial requirements. The process involved the steps: collecting the users' demand for each of the criteria to be selected; selecting alternatives to the high-ranked criteria; getting the consumers' ranking of the criteria and alternatives; and a comparison of criteria and their counterparts.

This paper has reviewed the salient features of novel techniques used for arriving at WQI that were proposed by research scientists and brought out a suitable computational model developed over the machine learning platform for classifying the marine water quality and predicting further, the marine water quality index (MWQI) of seawater.

REVIEW OF METHODOLOGIES FOR WATER QUALITY INDEX ESTIMATION

Horton's Model for WQI

In 1965, Horton developed and extended the concept of WQI (Horton 1965). Horton followed the steps for creating an index as (i) selected the water quality indicators such as dissolved oxygen, pH, E.coli, specific conductivity, alkalinity, and chloride, commonly available in Europe, Africa, and Asia countries; (ii) selected rating scales for each indicator so that the sub-index ranges from 0 to 100, where the highest quality was rated 100; and (iii) fixed the weight of the parameters that ranged from 1 to 4.

The Horton WQI model employed physicochemical indicators of water quality such as DO, pH, coliforms, specific conductance, carbon, chloroforms extract, alkalinity, and chlorides. The parameters were chosen based on their importance, the relative effect of other parameters, and the reliability of the data. Horton applied a linear scaling function and assigned sub-index values based on concentration level or contamination level. The sub-index value ranged from 0 to 100, where 0 indicated worst quality and 100 to excellence. The parameter weights were determined using the Delphi method (Taylor et al. 2003). The panel of experts was asked to assign a weight of 1 to 4 to various water quality parameters. Final WQI was obtained by aggregating an additive function given by Equation (1) as,

$$WQI = \left[\frac{\sum_{i=1}^{n} W_i S_i}{\sum_{i=1}^{n} W_i}\right] m_1 m_2 \quad \ldots(1)$$

where S_i is the sub-index of the i^{th} variable; W_i is the relative weight of the i^{th} variable; m_1 is a temperature correction factor, which is equal to 0.5 for temperatures below 34°C; and otherwise, it is 1; m_2 is a pollution correction factor equal to 0.5 or 1. Selecting the right parameters for WQI was one of the challenges in the Horton model.

National Sanitation Foundation Water Quality Index (NSFWQI) Method

NSFWQI used the weighted arithmetic mean function to assess the significance of all water quality parameters obtained from 142 water quality assessment experts. To convert the score to weights, the most important parameter was assigned a temporary weight of 1, and the weights of all other parameters were derived by dividing the weight of the highest parameter by the average of the individual importance scores. The final weight for each parameter was obtained by dividing the individual temporary weights by the sum of the temporary weights so that the final sum of the weights, $\sum_{i=1}^{n} W_i = 1$. NSFWQI was estimated using Equation (2) as,

$$Additive\ quality\ index, WQI = \sum_{i=1}^{n} W_i Q_i \quad \ldots(2)$$

where W_i is the unit weight of the i^{th} parameter; Q_i is the sub-index of the quality parameter derived from the parameter-to-value conversion curve in the interval of 0 to 100, and n is the number of parameters. Based on the WQI values obtained in the range of 0 to 100, quality classes would then be assigned as *excellent, good, fair, and bid* accordingly. McClelland (1974) found that though the additive model is a good choice when all the parameters are within a reasonable range it lacks the sensitivity of a low-impacted parameter on the overall water quality. Hence, a multiplicative model was originated (McClelland 1974), which is given by Equation (3),

$$Multiplicative\ quality\ index, WQI = \prod_{i=1}^{n} {Q_i}^{w_i} \quad \ldots(3)$$

where Q_i is the quality of the i^{th} parameter, a value between 0 to 100; W_i is the unit weight of the i^{th} parameter, and n is the number of parameters.

Oregon Water Quality Index (OWQI) Method

Originally developed in 1970 by Brown et al. (Brown 1970, Brown 1972, Cude 2001), OWQI had been improved in subsequent years after understanding more about the water quality behavior. The OWQI, a statistical tool is used to analyze a defined set of water quality parameters and generate a rating that describes the overall water quality of a particular monitoring site. The OWQI score takes a value from 10 to 100. The OWQI is also helpful for assessing water quality for recreational purposes like fishing and swimming. The OWQI approach utilized the arithmetic mean and is given by Equation (4),

$$OWQI = \sqrt{\frac{n}{\sum_{i=1}^{n} \frac{1}{{SI_i}^2}}} \quad \ldots(4)$$

where n is the number of parameters, and SI_i is the sub-index

of the i[th] parameter (Darvishi et al. 2016). The weighted harmonic helped the impaired parameter to influence the OWQI by its presence and also observed that OWQI was dependent on the environmental changes hence their impacts on water quality were considered. However, all the toxic elements for health such as bacteria, metals, and toxins (Tyagi et al. 2013) were not part of it.

Weighted Arithmetic Water Quality Index (WAWQI) Method

WAWQI's strategy classified water quality from the most influential water quality indicators. It is a simple and easy technique to utilize. It is observed that most scientists have utilized the WAWQI to decide the water quality of surface waters and groundwater. The algorithm of WAWQI is given below:

- Identify the water quality indicators for WQI calculation
- Calculate the *proportionality constant, k* value from, $k = \frac{1}{\sum_{i=1}^{n} \frac{1}{S_i}}$ where S_i is the standard value for the i[th] parameter and n is the number of parameters considered.
- Q_i, the quality rating for the i[th] parameter is estimated by, $Q_i = 100 * \{\frac{V_{oi} - V_i}{V_{Si} - V_i}\}$ where V_{oi} is the observed value from the sample for the i[th] parameter; Vi is the ideal value of the it[h] parameter in distilled water; V_{si} is the standard or permissible value for the i[th] parameter
- W_i, the unit weight of the individual parameter is derived from, $W_i = k/S_i$
- Finally, the water quality index (WQI) is arrived at by Equation (5) as,

$$WQI = ((\sum_{i=1}^{n} W_i Q_i) / \sum_{i=1}^{n} W_i) \quad \ldots(5)$$

The authors of (Chandra et al. 2017) have studied the groundwater quality of Vijayawada, India using the WAWQI model for analyzing the physicochemical properties such as pH, total dissolved solids (TDS), Cl, SO4, Na, K, Ca, Mg, and total hardness (TH) at nineteen different stations of the study area. Oni et al. (2016) studied the impact of municipal solid waste on the quality of the groundwater and surface water bodies at Ado Ekiti, Nigeria by using the algorithm of WAWQI. However, this index did not include all the parameters, which could describe the quality of a water source and this index only quantified the direct impact of physiochemical indicators (Tyagi et al. 2013)

Canadian Council of Ministers of the Environment Water Quality Index (CCME WQI) Method

CCME WQI (CWQI 2022, CCME 2001) is implemented generally to test a multi-boundary water quality against the permissible limit kept by the user. The WQI considers three variables such as scope, frequency, and amplitude to produce the water quality at that particular location with the benchmarks chosen. The output is a number ranging from 0 to 100, where a score of 100 indicates that all variables meet the selected benchmarks. F1 represents the scope variable in terms of failed parameters, which does not satisfy the benchmark at least once, and Equation (6) is arrived as,

$$F_1 = \frac{No.\ of\ failed\ parameters}{Total\ no.\ of\ parameters} * 100 \quad \ldots(6)$$

F_2 indicates the frequency variable, in terms of failed tests, which do not meet the target as given in Equation (7),

$$F_2 = \frac{No\ of\ failed\ tests}{Total\ no.\ of\ tests} * 100 \quad \ldots(7)$$

F_3 refers to the amplitude of the test values, by which they did not meet the benchmark. The non-compliance with the test values is calculated as:

(i) The test value should not exceed the target:

$$excursion_i = \left\{\frac{Failed\ Test\ Value}{Target}\right\} - 1.0$$

(ii) The test value should not fall below the target:

$$excursion_i = \left\{\frac{Target}{Failed\ Test\ value}\right\} - 1.0$$

Then, the sum of excursions under the non-compliance category is calculated as, *Normalized sum of excursions*

$$(nse) = \frac{\sum_{i=1}^{n} excursion_i}{No.of\ tests}$$

F_3 is then calculated as given in Equation (8),

$$F_3 = \left\{\frac{nse}{0.01nse + 0.01}\right\} \quad \ldots(8)$$

CCME WQI method suits to calculate the quality index for different water bodies and it does not get influenced by the presence of missing data. The limitation of the method stated by the authors (Călmuc et al. 2018) is that physiochemical indicators included in the estimation of WQI are selected in such a way that they do have the same level of influence. The water quality estimated is also partial since the other physiochemical indicators and biological indicators are not considered in the algorithm. Lastly, the F_1 variable is not consistent when the quality indicator list has only very few parameters

Bhargava Method

The Bhargava approach considered the parameters corresponding to each of the applications separately and applied the sensitivity function that selects a value between 0 and 1 and the results are accumulated using the geometric mean

(Bhargava 1983a, 1983b, Noori et al. 2017). The geometric mean-based WQI suggested by Bhargava is expressed in Equation (9) as,

$$WQI = (\prod_{i=1}^{n} f_i())^{1/n} * 100 \quad \ldots(9)$$

where function $f_i()$ indicates the sensitivity function for the i^{th} parameter, which is related to the weighting of the i^{th} parameter and varies from 0 to 1; and n is the number of water quality parameters considered. Water quality index (WQI), used six water quality parameters namely dissolved oxygen (DO), biochemical oxygen Demand (BOD), most probable number (MPN), turbidity, total dissolved solids (TDS), and pH measured at eight different stations along the river basin. Rating curves were drawn based on the quality of river water and gave importance with weight to every parameter. Lastly, a rating scale in the order of 0 to 4 was used to classify water quality in each of the study areas such as, *excellent* to *poor* range by the Bhargava WQI method.

Recreational Water Quality Index (RWQI) Method

Recreational water bodies are characterized and classified to determine their suitability for recreational use, based on susceptibility to fecal contamination, development of HABs, and proliferation of specific free-living microbial pathogens (WHO 2003). The water quality criterion is to set a recreational water quality index for fresh bathing waters. The World Health Organization (WHO) aggressively promoted the safety of human health while using recreational waters. In (WHO 2003, WHO 2005, WHO 2021) reports, WHO laid out the guidelines that provide an assessment of the health risks associated with the recreational use of water. Risks arising from contacting the contaminated water include infection from microbes and toxicity of physical and chemical properties of the water.

The RWQI was developed by Almeida et al. (2012) using physical, chemical, and microbiological parameters. The opinions of 17 experts were used from the rating curves and all rating curves were fitted with a coefficient regression bigger than 0.98 for each one. WHO has fixed a maximum value (Almeida et al. 2012) for recreational waters as 2 $mg.L^{-1}$ for Q_i, which is equivalent to 100; with 75 for values up to 0.1 $mg.L^{-1}$; and the Q_i reaches10 for values above 2 $mg.L^{-1}$. The RWQI included the water quality indicators namely pH, turbidity, detergents, nitrate, COD, PO_4^{3-}, total coliforms, coliforms, and enterococci. Equation (10) shows the calculation of RWQI as,

$$RWQI = \prod_{i=1}^{n} Q_i^{W_i} \quad \ldots(10)$$

where Q_i is the rating value of the i^{th} parameter expressed as concentration or other analytical measurements and W_i is the weightage given to the i^{th} parameter in such a way, $\Sigma W_i = 1$. W_i is calculated as, $W_i = \frac{\frac{1}{a_i}}{\Sigma\frac{1}{a_i}}$, where a_i is the coefficient that varies from 1 to 4 as per the significance of the parameter i. RWQI is a result ranging from 0 to 100.

THE FRAMEWORK OF MACHINE LEARNING TECHNIQUES FOR THE CLASSIFICATION AND PREDICTION OF MARINE WQI

This Section discusses the design of a framework of machine learning techniques for classifying and further predicting marine water quality index (MWQI) using eight water quality parameters like salinity, dissolved oxygen (DO), dissolved inorganic carbon (DIC), alkalinity, phosphate, nitrate+nitrite, dissolved organic carbon (DOC), and heterotrophic bacteria from the dataset collected by the Center for Microbial Oceanography Research & Education Data System (C-MORE DS 2021). The framework has embedded the machine learning platform to predict marine water quality. In this framework, different supervised machine-learning models were examined to predict water quality more accurately. Fig.1 illustrates the process flow for arriving at the MWQI. The observations of physiochemical and biological parameters collected from 11 cruises were

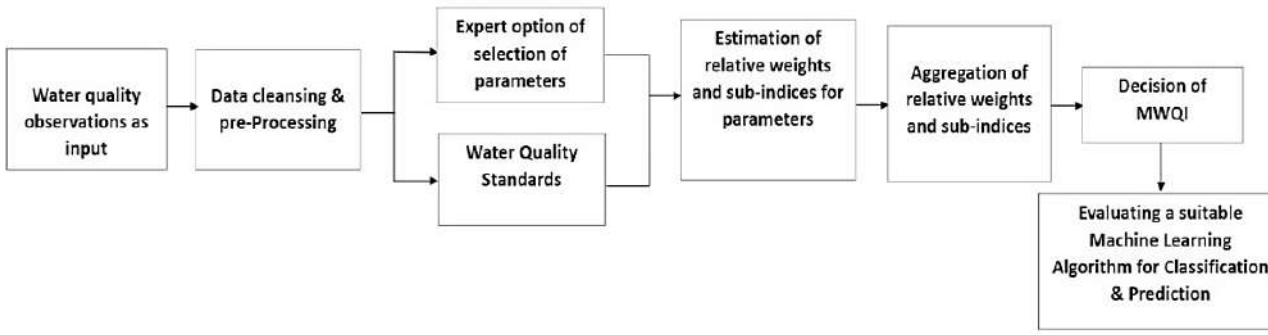

Fig. 1: Process flow of arriving MWQI from the input observations.

used in this study. The data pre-processing phase involved data cleansing using outlier detection, missing data, and normalization. After pre-processing, the dataset taken for the study contained 1361 observations. The weighted arithmetic water quality index (WAWQI) algorithm discussed in Section 2 (iv) was embedded in this framework. The parameters used for estimating MWQI have been thoroughly explored with their significance to marine water quality.

Correlation analysis is to determine the association among water quality parameters involved in the study. Correlation analysis as given in Fig. 2 helps to conclude the positive, negative, or no-correlation effects of those chosen parameters. Table 1 gives the statistic of input parameter values and the outcome of the correlation. The standard deviation shows the average distance of each observation from the mean. A larger value indicates that the data are more spread out. Salinity, for example, showed a low variation, which made 25%, 50%, and 75% of the observations stick around the mean value. Looking at the minimum and maximum range of the DO, DIC, Alkalinity, DOC, and h-bacteria, the standard deviations also proved that the data are widely spread out. The parameters such as DIC, alkalinity, phosphate, nitrate +nitrite, and DOC showed the minimum value and 25%, 50%, and 75% observations as zero, which was reflected in their correlation too. The coefficient of variation (CV) and the index of dispersion (ID) displayed the relative dispersion of the observations around the mean.

The correlation matrix given in Table 2 shows the degree of linear correlation by means of coefficient R between any two parameters. R-value helps to identify the water quality parameters, which may influence the seawater quality. Some of them exhibit negative correlations too. Salinity, DO, DIC, nitrate+nitrite, phosphate, alkalinity, DOC, and h-bacteria from the given dataset were found to be more significant in the water quality. Marine water quality standards of those chosen parameters were also considered for estimating the relative weights and sub-indices and aggregating these two computed outcomes. The estimated value of water quality of each observation was found to be lying in the range of 0 to 100. The water quality results were then classified as *excellent, good, and poor* represented numerically as classes 2, 1, and 0 respectively. The classes that arrived are therefore called *marine water quality index (MWQI)*.

The framework has further employed the machine learning model to classify and predict MWQI, which is shown in Fig. 2. Lastly, the correlation of each parameter with MWQI was studied to understand the linear association between each parameter with MWQI and is represented in Table 3. Determination of the best-fit classification model for the marine water quality adapted training, evaluation, and optimization as discussed in the following sections.

Training and Optimizing the Classification Models

Process flow to determine the best-fit machine learning algorithm for predicting the MWQI has followed: (i) create models, (ii) tune models, (iii) compare models, and (iv) ensemble model. An integrated software development tool, namely, the Anaconda platform unified with python programming (Python 2020) and PyCaret (PyCaret 2022) was used in the model evaluation and optimization. The dataset (C-MORE DS 2021) after pre-processing was split

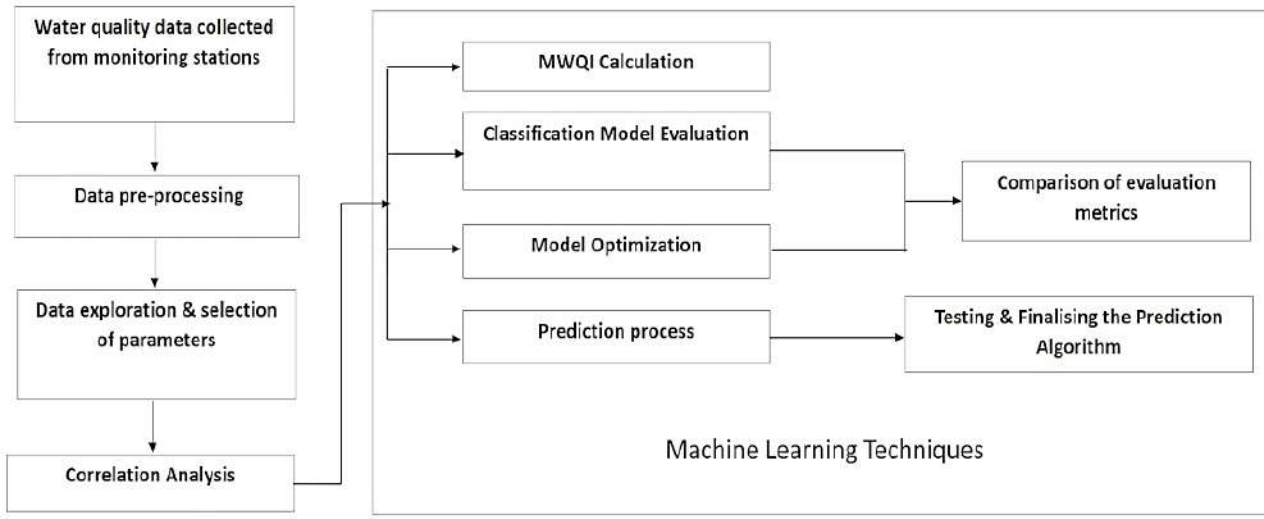

Fig. 2: Framework of machine learning techniques for classifying and predicting MWQI.

Table 1: Descriptive statistics to analyse the input parameters for prediction.

Descriptive Statistics	Salinity µmol.kg^{-1}	DO µmol.kg^{-1}	DIC µmol.kg^{-1}	Alkalinity µmol.kg^{-1}	Phos µmol.kg^{-1}	Nitrate +Nitrite µmol.kg^{-1}	DOC µmol.kg^{-1}	H-Bact CFU.100mL^{-1}	Water quality %
Observations	1361	1361	1361	1361	1361	1361	1361	1361	1361
Mean	35.12	200.86	437.43	498.65	0.086	0.353	3.563	455.80	59.25
Std dev	0.253	40.11	837.76	954.50	0.274	1.946	15.46	188.68	6.25
Min	34.039	0.0	0.0	0.0	0.0	0.0	0.0	123.70	50.47
25%	34.95	204.10	0.0	0.0	0.0	0.0	0.0	337.40	55.62
50%	35.203	208.20	0.0	0.0	0.0	0.0	0.0	441.10	57.68
75%	35.293	213.60	0.0	0.00	0.10	0.07	0.0	528.90	60.65
Max	35.988	265.90	2328.1	2409.0	2.71	29.64	83.50	2469.7	100.0
CV	0.007	0.199	1.915	1.914	3.175	5.519	4.339	0.4139	0.105
ID	0.002	8.011	1604.4	1827.07	0.870	10.74	67.11	78.11	0.659

Table 2: Correlation matrix of marine water quality indicators.

	Salinity	DO	DIC	Alkalinity	Phos	Nit+Nit	DOC	H-bact
Salinity	1.0000							
DO	0.3689	1.0000						
DIC	0.0280	0.0204	1.0000					
Alkalinity	0.0320	0.0308	0.9994	1.0000				
Phos	-0.2338	-0.3443	0.3305	0.3050	1.0000			
Nit+Nit	-0.2276	-0.3943	0.2107	0.1855	0.9410	1.0000		
DOC	-0.1097	0.0554	-0.1230	-0.1231	-0.0688	-0.0383	1.0000	
H-Bact	-0.3420	-0.0166	0.1131	0.1109	0.2651	0.1355	-0.0496	1.0000

into training, validation, and test data with eight water quality parameters. Training and validation data were used to evaluate the classification models under the machine learning framework. Training the classification models is to select an optimum one in classifying marine water quality. PyCaret is a python-based machine learning library, that assists the framework for fitting the best model. To optimize the selection further, tuning the hyperparameters of the individual model was also added. The performance metrics namely, accuracy, AUC, recall, precision, F1, kappa, MCC, and TT helped to appraise the top-performing models as demonstrated in Table 4. From the comparison, it is found that the decision tree algorithm was the best-fit one. Additionally, ensemble and stacking processes would also help to identify a more suitable algorithm.

Table 3: Correlation of MWQI with each Water Quality Indicator.

MWQI	1.000
Hbact	0.646
Phos	0.562
Nit	0.525
Doc	0.264
Dic	0.135
alk	0.122
Csal	-0.478
Coxy	-0.661

Ensemble Learning Techniques in Prediction

Machine learning models sometimes favor biasing and therefore, ensemble learning is preferred to recover from biasing. An ensemble is a machine-learning approach, in which several machine-learning algorithms are bundled together and trained. The top four classification methods from Table 4 namely, decision tree, ada boost, gradient boosting, and random forest were tuned first and then ensembled using bagging or boosting algorithms. Stacking was finally applied to combine the four ensembled algorithms. Evaluation of the stacked classifier by their performance was appraised as portrayed in Table 5. The finalized prediction algorithm was saved as *MWQI Classifier* in the server where the algorithm could be deployed and worked stand-alone thereon.

Table 4: Comparison of the performance of classification models.

Classifier Model	Accuracy	AUC	Recall	Precision	F1	Kappa	MCC	TT (Sec)
Decision tree	1.0000	1.0000	1.0000	1.0000	1.0000	1.0000	1.0000	0.0110
Ada boost	1.0000	1.0000	1.0000	1.0000	1.0000	1.0000	1.0000	0.0120
Gradient boosting	1.0000	1.0000	1.0000	1.0000	1.0000	1.0000	1.0000	0.0830
Random forest	0.9987	1.0000	0.9986	1.0000	0.9993	0.9850	0.9860	0.2040
Extra trees	0.9974	0.9995	0.9973	1.0000	0.9986	0.9701	0.9720	0.1700
Logistic regression	0.9961	1.0000	0.9986	0.9973	0.9979	0.9494	0.9531	0.0490
Light gradient boosting machine	0.9948	1.0000	0.9973	0.9973	0.9973	0.9345	0.9391	0.0310
SVM - linear kernel	0.9935	0.0000	0.9959	0.9973	0.9966	0.9252	0.9301	0.0140
Ridge classifier	0.9935	0.0000	0.9986	0.9946	0.9966	0.9041	0.9150	0.0150
Linear discriminant analysis	0.9935	1.0000	0.9973	0.9959	0.9966	0.9195	0.9251	0.0110
K Neighbors	0.9895	0.9691	0.9973	0.9919	0.9945	0.8453	0.8611	0.0280
Naive Bayes	0.9777	0.9986	0.9767	1.0000	0.9881	0.8031	0.8246	0.0100
Dummy classifier	0.9580	0.5000	1.0000	0.9580	0.9786	0.0000	0.0000	0.0100
Quadratic discriminant analysis	0.8777	0.8787	0.8849	0.9881	0.9181	0.4815	0.5397	0.0120

Table 5: Performance of the Stacked Classifier Model Finalized for Marine Water Quality Prediction.

Model	Accuracy	AUC	Recall	Prec.	F1	Kappa	MCC
Stacking Classifier	1.0000	1.0000	1.0000	1.0000	1.0000	1.0000	1.0000

Testing the Prediction Algorithm

MWQI classifier was loaded in the integrated machine learning platform of Anaconda, Python, and PyCaret and tested the sample data accessed from the given water quality dataset. Table 6 displays a sample output from the prediction. The outcome of the prediction was 100% accurate.

CONCLUSION

This paper proposed a machine learning framework for evaluating the classification models, optimizing the models, and finally selecting the best-fit model with higher performance for the given dataset and application. The chosen model was then applied for prediction. The classification method called *stacked classifier* was proposed as a top-performing machine learning model under the supervised learning category to classify the marine water quality. The application dataset from C-MORE DS with eight selected physio, chemical, and biological properties are involved to train, evaluate and test the model for arriving at the marine water quality index (MWQI). The estimated and predicted values of MWQI matched with 100% accuracy.

ACKNOWLEDGMENT

This study was granted by the Department of Science and Technology (DST), India under optimal water usage for the industrial sector (OWUIS).

Table 6: A sample of predicted output.

Salinity $\mu mol.kg^{-1}$	DO $\mu mol.kg^{-1}$	DIC $\mu mol.kg^{-1}$	Alkalinity $\mu mol.kg^{-1}$	Phos $\mu mol.kg^{-1}$	Nitrate +Nitrite $\mu mol.kg^{-1}$	DOC $\mu mol.kg^{-1}$	H-Bacteria $CFU.100mL^{-1}$	MWQI calculated	MWQI predicted	Score
34.578	211.2	0	1.33	6.75	0	1543.9	85.307	0	0	1
34.94	214.1	0	0	0	0	538.9	58.658	1	1	1
35.289	211.2	0	0	0	0	665.5	62.060	1	1	1
34.854	265.8	0	0.77	0	0	1540.1	75.588	0	0	1
35.175	210.7	0	0.12	0.01	0	575.1	60.025	1	1	1
35.195	212.2	0	0	0	0	140.8	50.468	0	1	1

REFERENCES

Akhtar, N., Ishak, M. I. S., Ahmad, M. I., Umar, K., Md Yusuff, M. S., Anees, M. T., Qadir, A. and Ali Almanasir, Y.K. 2021. Modification of the water quality index (WQI) process for simple calculation using the multi-criteria decision-making (MCDM) method: A review. Water, 13(7): 905. https://doi.org/ 10.3390/w13070905

Almeida, C., González, S.O., Mallea, M. and González, P. 2012. A recreational water quality index using chemical, physical and microbiological parameters. Environ, Sci. Pollut. Res., 19(8): 3400-3411. https://doi.org/10.1007/s11356-012-0865-5

Banda, T.D. and Kumarasamy, M.A. 2020. Development of water quality indices (WQIs): A review. Pol. J. Environ. Stud., 29(3): 2011-2021. https://doi.org/10.15244/pjoes/110526

Bhargava, D.S. 1983a. Most rapid BOD assimilation in Ganga and Yamuna rivers. J. Environ. Eng., 109(1): 174-188. https://doi.org/10.1061/(ASCE)0733-9372(1983)109:1(174).

Bhargava, D.S. 1983b. Use of water quality index for river classification and zoning of Ganga River. Environ. Pollut. Ser. B. Chem. Phys., 6(1): 51-67. https://doi.org/10.1016/0143-148X(83)90029-0

Brown, R.M., McClelland, N.I., Deininger, R.A. and O'Connor, M.F. 1972. A water quality index—crashing the psychological barrier. Environ. Qual., 15: 173-182. https://doi.org/10.1007/978-1-4684-2856-8_15

Brown, R.M., McClelland, N.I., Deininger, R.A. and Tozer, R.G. 1970. A water quality index-do we dare. Water Sew. Works, 117(10): 339-343.

Călmuc, V.A., Călmuc, M., Topa, M.C., Timofti, M., Iticescu, C. and Georgescu, L.P. 2018. Various methods for calculating the water quality index. Ann. Dunarea De Jos Univ. Galati. Fascicle II Math. Phys. Theor. Mech, 41(1): 171-178. https://doi.org/10.35219/ann-ugal-math-phys-mec.2018.2.09.

Canadian Water Quality Index (CWQI) 2022. Accessed on 11th February 2022. https://www.gov.nl.ca/ecc/waterres/quality/background/cwqi/

CCME 2001. Canadian water quality guidelines for the protection of aquatic life: CCME Water Quality Index1.0 Technical Report. Canadian Council of Ministers of the Environment (CCME). Accessed on 10th Feb 2022. https://prrd.bc.ca/wp-content/uploads/post/prrd-water-quality-database-and-analysis/WQI-Technical-Report-en.pdf

Center for Microbial Oceanography: Research & Education Data System (C-MORE DS) 2021. Data Accessed on 7thSeptember 2021. https://hahana.soest.hawaii.edu/cmoreserver/datasearch/data.php

Chandra, D.S., Asadi, S.S. and Raju, M.V.S. 2017. Estimation of water quality index by weighted arithmetic water quality index method: a model study. Int. J. Civil Eng. Tech., 8(4): 1215-1222.

Cude, C.G. 2001. Oregon water quality index is a tool for evaluating water quality management effectiveness 1. JAWRA J. Am. Water Resour. Assoc., 37(1): 125-137. https://doi.org/10.1111/j.1752-1688.2001.tb05480.x

Darvishi, G., Kootenaei, F. G., Ramezani, M., Lotfi, E. and Asgharnia, H. 2016. Comparative investigation of river water quality by OWQI, NSFWQI, and Wilcox indexes: Case study: The Talar River–Iran). Arch. Environ. Protect., 42(1): 41-48. https://doi.org/10.1515/aep-2016-0005

Horton, R.K. 1965. An index number system for rating water quality. J. Water Pollut. Contr. Fed., 37(3): 300-306.

Khan, A. A., Tobin, A., Paterson, R., Khan, H. and Warren, R. 2005. Application of CCME procedures for deriving site-specific water quality guidelines for the CCME Water Quality Index. Water Quality Research Journal, 40(4): 448-456.

McClelland, N.I. 1974. Water quality index application in the Kansas River basin. U.S. Environmental Protection Agency Region 7, Kansas City, Missouri. Accessed on 4th February 2022. National Service Center for Environmental Publications (NSCEP). https://www.epa.gov/nscep

Mostafaei, A. 2014. Application of multivariate statistical methods and water-quality index to the evaluation of water quality in the Kashkan River. Environ. Manag., 53(4): 865-881. https://doi.org/10.1007/s00267-014-0238-6

Noori, M.M., Abdulrazzaq, K.A. and Mohammed, A.H. 2017. Evaluation of water quality using Bhargava water quality index method and GIS, case study: Euphrates river in Al-Najaf City. Int. J. Sci. Res., 6(7): 1286-1295. https://doi.org/10.21275/art20175545

PyCaret Official. 2022. Accessed on 2nd January 2022. https://pycaret.gitbook.io/docs/get-started/functions.

Python for Windows. 2020. Accessed on 12th June 2020. https://www.python.org/downloads/windows/

Robertson, A.I., and Blaber, S.J.M. 1992. Plankton, epibenthos, and fish communities. Coast. Estuar. Stud., 29: 173-224. https://doi.org/10.1029/CE041p0173

Sridhar, R., Thangaradjou, T., Kumar, S.S. and Kannan, L. 2006. Water quality and phytoplankton characteristics in the Palk Bay, southeast coast of India. J. Environ. Biol., 27(3): 561-566.

Sverdrup, H.U., Johnson, M.W. and Fleming, R.H. 1942. The Oceans: Their Physics, Chemistry, and General Biology. Prentice-Hall Inc., New York.

Taylor, J.G. and Ryder, S.D. 2003. Use of the Delphi method in resolving complex water resources issues. JAWRA J. Am. Water Resour. Assoc., 39(1): 183-189. https://doi.org/10.1111/j.1752-1688.2003.tb01570.x

Tyagi, S., Sharma, B., Singh, P. and Dobhal, R. 2013. Water quality assessment in terms of water quality index. Am. J. Water Resour., 1(3): 34-38. https://doi.org/10.12691/ajwr-1-3-3

World Health Organization (WHO). 2003. Guidelines for Safe Recreational Water Environments. Volume 1, Coastal and Fresh Waters. https://apps.who.int/iris/handle/10665/42591

World Health Organization (WHO). 2005. Guidelines for Safe Recreational Water Environments. Volume 2: Swimming Pools and Similar environments. https://www.who.int/publications/i/item/9241546808

World Health Organization (WHO). 2021. Guidelines on Recreational Water Quality. Volume 1: Coastal and Freshwaters. https://www.who.int/publications/i/item/9789240031302

Nature Environment and Pollution Technology
An International Quarterly Scientific Journal

p-ISSN: 0972-6268
(Print copies up to 2016)
e-ISSN: 2395-3454

Vol. 21 | No. 5 (Suppl) | pp. 2219-2229 | 2022

Original Research Paper

https://doi.org/10.46488/NEPT.2022.v21i05.016

Open Access Journal

Study of the Effectiveness of Making a Retention Pond for Urban Flood Management: A Case Study of the Barabai River, South Kalimantan

Nely Ana Mufarida* and Nanang Saiful Rizal†**
*Departement of Mechanical Engineering, University of Muhammadiyah Jember, Jember, Indonesia
**Departement of Civil Engineering, University of Muhammadiyah Jember, Jember, Indonesia
†Corresponding author: Nanang Saiful Rizal; nanangsaifulrizal@unmuhjember.ac.id

Nat. Env. & Poll. Tech.
Website: www.neptjournal.com

Received: 04-06-2022
Revised: 24-07-2022
Accepted: 03-08-2022

Key Words:
River hydraulics
Retention ponds
Flood Management
Barabai city

ABSTRACT

The upstream of the Barabai River is experiencing land conversion from forest to agricultural and mining areas. In 2021, floods and river overflows will inundate nearly 75% of Barabasi City. The solution given is to build a Retention Pool so that the flow of the Barabai River before entering Barabai City is diverted to the Retention Pool. By conducting hydrological and hydraulic flow analysis with the application of HEC RAS with unsteady flow conditions, the water level profile along the Barabai River can be displayed including the flow behavior in the retention pond during flooding. As a result, the retention pond is only effective at accommodating 25% of the discharge during a flood. By optimizing using the HEC RAS program, alternatives to inundation or flooding in Barabai City are obtained, namely: widening the Barabai river 2x, expanding the regulation pool to 95 ha, building a second retention pond of 40 ha, and normalizing the Barabai River that enters Barabai City.

INTRODUCTION

The Barabai River is a tributary of the state and is part of the Barito River Basin with a catchment area of 550 km^2 and a length of the main river of 113.35 km. In the lower reaches of the Barabai River through Barabai City, South Kalimantan Province, there has been a narrowing. When there is heavy rain upstream, there will be floods and overflows of river water downstream which inundate almost 75% of Barabai City (Prabowo 2018). Floods and overflows in Barabai City occur regularly every year starting in 2018, 2019, and 2020 so there is moderate vulnerability to buildings in Barabai City (Muslim et al. 2017). For flood control, drainage has been built, but its effectiveness is only 62.75% (Anam et al. 2015). Normalization or widening of the Barabai River is no longer possible in urban areas. The only way is to make a temporary reservoir in the event of a flood. The planned flood discharge that occurs needs to be studied hydrologically because 4 rivers enter the lower reaches of the Barabai River, namely the Kahakan River, Udung River, Kuli River, and Kitir River with varying river lengths (Ls) and river slopes (So), which certainly have an impact on time concentration (Tc), and the amount of flood discharge that occurs are presented as fluctuating in the form of a calibrated flood hydrograph (Chay 2002, Harto 1993). To regulate the incoming discharge, it is necessary to build a threshold in the Barabai river and side spills in the regulation pond so that the function of the reservoir pond is effective (Anis et al. 2017). The discharge that enters the Barabai River is regulated with a certain threshold elevation so that there is no overflow in the Barabai River. Similarly, the elevation and width of the side spillway (B) that will enter the regulation pool are set at a certain elevation so that the regulation pool can accommodate a certain volume of flood discharge. The elevation of the side spillway must be higher than the elevation of the threshold light that enters the lower reaches of the Barabai River (AH). Setting the threshold height and volume of regulation pool regulation is an important part that needs to be analyzed and optimized so that there will be no more flooding in Barabai City (Cahyono 2010, Czahchor et al. 2010). The threshold elevation was made higher than the elevation of the side spillway entering the Regulation Pond and then analyzed by HEC RAS. Analysis with HEC RAS for the Barabai river has been carried out with flood discharges at the 100th return period (Faizal & Nizam 2005, Hauer et al. 2021).

RESEARCH SIGNIFICANCE

Inflow modeling using HEC RAS, the flow behavior is made unsteady, and then the flow behavior in 2 places is evaluated, namely in the lower reaches of the Barabai

River and in the Regulatory Pond (Istiarto 2012) by analyzing and simulating threshold elevation, the elevation of side beam crest, and the width of side spillway. So, the purpose of this study is to obtain the most effective regulatory pool construction (optimum area and height) including complementary building models (shape and elevation of the threshold lighthouse and side spillway including the width) to reduce flooding that occurred in Barabai City.

The components for perpetual flow were developed for subcritical flow calculations. Hydraulic calculations for cross-sections, bridges, culverts, and other hydraulic structures developed for permanent flow components are combined with non-permanent flow calculations. Components for perpetual flow are used for reservoir models and hydraulic linkages with reservoirs. HEC – RAS is now able to perform one-dimensional water table profile calculations for continuous flow changes in natural and artificial channels. Subcritical, supercritical, and combined system flow profiles of the water table can be analyzed (Istiarto 2012). The water level profile calculated from one cross-section to the next is solved by an energy equation called the Standard – Step method. The energy equation used can be seen as follows (Rizal 2014):

$$Y_2 + Z_2 + \frac{\alpha_2 V_2^2}{2g} = Y_1 + Z_1 + \frac{\alpha_1 V_1^2}{2g} + h_e \quad \ldots(1)$$

The energy loss height (h_e) between the 2 cross-sections is due to friction loss and loss due to narrowing or widening. The high energy loss equation is as follows (Rizal 2014):

$$h_e = L.S_f + c.\left[\frac{\alpha_2 v_2^2}{2g} - \frac{\alpha_1 v_1^2}{2g}\right] \quad \ldots(2)$$

(a). The overflowing barabai river (b). Flow on the channel

(c). Flow on intake (d). Overflowing stream to the city of barabai

Fig. 1: The condition of the area during the flood on November 15, 2021, in the Barabai River.

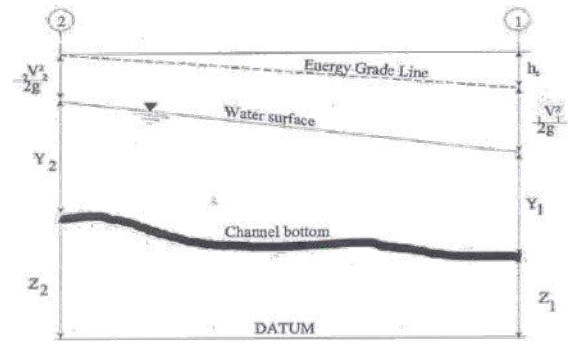

Fig. 2: Components in the energy equation. (Source: Chow et al. 1989).

Determination of the total ow rate and velocity coefficient for a cross-section requires dividing the flow into units because the flow velocity is not uniformly distributed. In HEC – RAS the approach used is to divide the area in the embankment area using the boundaries of the n values that exist in the cross-section (the location where the value of n changes) as the basis for division (Fig. 3). The discharge calculated in each of the sub-areas in the embankment area is used by the Manning formula. Since HEC-RAS is a one-dimensional program for determining the water level profile, only one water level and average energy is calculated for each cross-section. For a given water level, the average energy is obtained by calculating the flow energy portion of the 3 subsections of a cross-section (left of the embankment, middle, and right of the embankment). Fig. 3 shows how the average energy will be obtained for a cross-section with the composition of the main flow and the right area of the embankment (no left area of the embankment).

MATERIALS AND METHODS

Data Collection

The data inputted in this study from the Central Kalimantan River Basin (BBWS) III agency include 1) Rainfall data 1 daily and water level data (AWLR) for data input in the HEC-RAS application Rainfall data 1 daily from the nearest Rain Station for at least the last 10 years. 2) Observation data or minimum field discharge measurements when flooding occurs in 5 rivers. 3) Elevation digital model (DEM) owned by the Information & Geospatial Agency, land use map based on aerial photography in 2015 from data from the Department of Public Works & Spatial Planning (PUPR) of South Kalimantan Province as well as land maps belonging to the 2016 Agricultural Land Resources Research and Development Agency, which are used to hydrological analysis and modeling. 4) Data from the measurement of the cross-section and long section of the Barabai River from upstream to downstream. 5) Regulation pool planning data which includes inundation area and a peak elevation of the regulation pool. 6) Data on types of supporting buildings in the entry of flow to the retention pond.

Data Processing Stage

The activity stages include: 1) Analysis of the design flood hydrograph of 5 (five) rivers using HEC-HMS, 2) Inputting the long and cross-section data of the Barabai River into the HEC RAS program, 3) Entering the input data for the regulatory pool to be made, 4) Entering input spillover data for the entry of Barabai River water into the retention pond, 5) Entering boundary conditions at the upstream and downstream of the Barabai River (upstream is the flood hydrograph of each river, downstream is the bottom slope of the Barabai River).

Analysis Stage

In the next analysis, the following things were carried out: 1) Performing a flow hydraulics analysis with HEC RAS with unsteady flow conditions, 2) displaying input results on all cross rivers and regulatory ponds and side spillways, 3) optimizing the output results of the HEC RAS program, 4) determine alternative inundation or flood management, 5) proposed recommendations for flood management in Barabai City.

RESULTS AND DISCUSSION

Modeling of flow behavior in retention ponds is strongly influenced by the input of discharge data entering the river which is expressed in the form of a flow hydrograph for 24 hours (Martin & Fransiskus 2015, Noor 2013). The input does not always flow downstream but can be seeped into the soil and this depends on the physical properties of the soil. The flow that enters the largest regulation pool from the Barabai River is then added to the flow from the Kahakan River, Udung River, Kuli River, and Kitir River whose results are presented in a schematic form in Fig. 4.

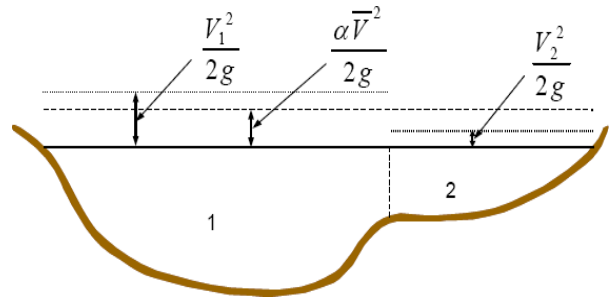

Fig. 3: Average energy distribution in HEC RAS. (Source: Chow et al. 1989).

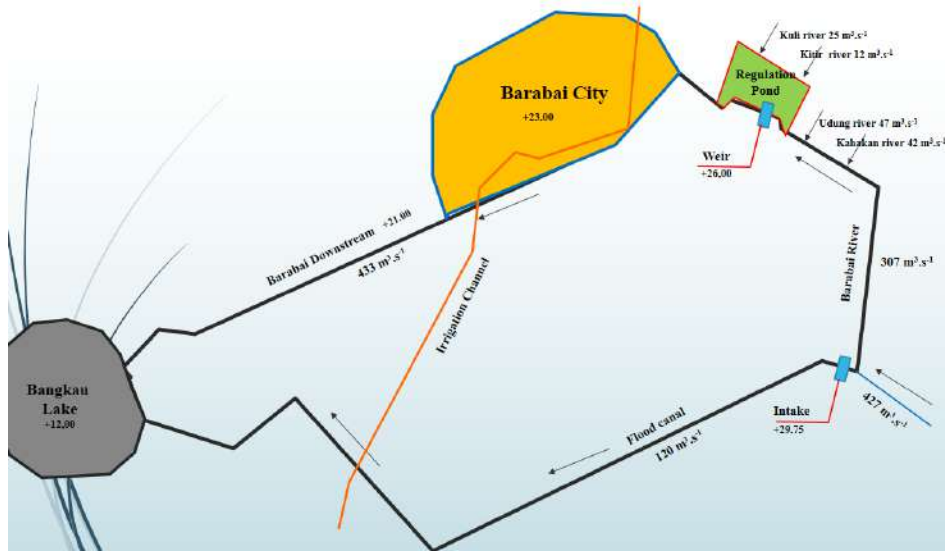

Fig. 4: Flow scheme in the Barabai Sungai River. (Source: Consultant Study Results, 2021).

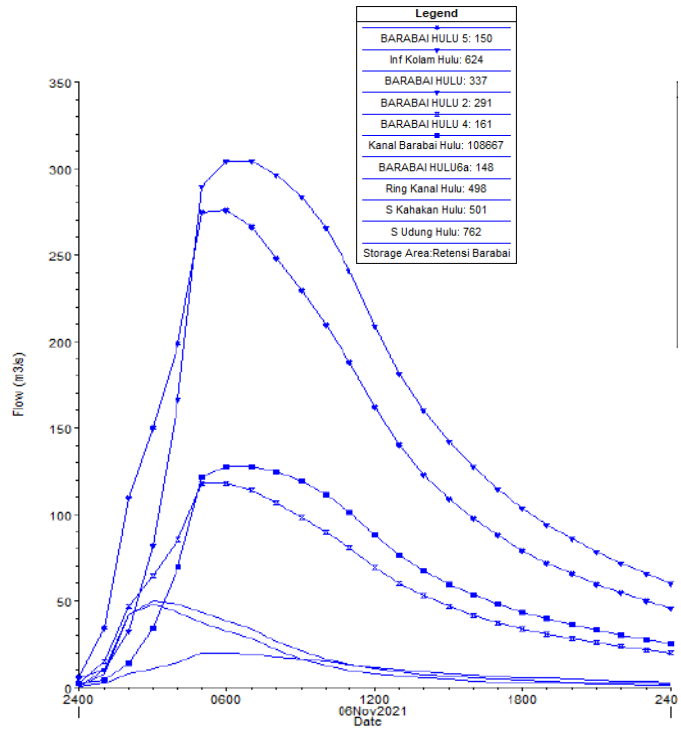

Fig. 5: Calibrated flood hydrograph. (Source: Calculation Result, 2021)

The results of the flood hydrograph calculation have been calibrated by observing flood events on the 15th. November 2021, the results of which are presented in Fig. 2. Validation of the discharge value has been carried out on all STA as the results of the measurement of the discharge at the time of the incident from STA 188 to STA 272 which were compared with the results of the HEC RAS modeling. The total flood discharge that enters the lower reaches of the Barabai River

is 579.24 $m^3.s^{-1}$ which is the accumulation of 4 rivers. All accumulated discharges from the Barbai River, Kahakan River, Udung River, Ulin River, and Kitir River are planned to enter the holding pond for several hours. The storage pond is planned with an inundation area of 58 ha, then the highest elevation of the regulation pond is planned to be +18 m. The flow that enters the reservoir first passes through the side spillway with a width of 8 m and a height of 3 m. In determining the discharge that enters the downstream of the Barabai River, a hydrological analysis is carried out to obtain flood hydrographs for the 5 rivers mentioned above. Frequency analysis can be calculated using the Gumbel or Pearson log method. The results of the hydrograph analysis must pay attention to the suitability of the relationship between parameters (Yan et al. 2013). The results of the calculation of the peak flood discharge were calibrated based on the results of flood observations in the five rivers mentioned above so that the hydrograph parameters of each river were obtained. Furthermore, these parameters can be used to calculate the flood hydrograph (Zhang & Singh 2006) in the 5 rivers, so that the result is that the peak flood time (Tr) occurs at the 6th h with varying peak discharge quantities which are presented in Fig. 5.

Furthermore, the results of the calculation of the flood discharge plan are entered as the upstream boundary condition in the HEC RAS program, while the downstream boundary conditions use the data of the downstream river bed slope. In accordance with the storage pond development plan, it must be ensured that the size and dimensions of the planned storage pond include the dimensions of the side girder. Furthermore, from the dimensions of the reservoir Komal, the inundation area will be obtained which will be included as input in the HEC RAS program. Similarly, the width of the next side girder is used as input in the HEC RAS program.

The results of the measurement of the situation map and river cross-section are first entered into the HEC RAS program. In this study, the total length of the river studied was 20 km and there were 150 cross rivers included in the HEC RAS. The results are presented in Fig. 6. Running is carried out using unsteady flow conditions with the aim of getting an overview of the flow behavior pattern in the river, side spillway, and the holding pond within 24 hours. The results of the analysis in the HEC RAS program will show the water level profile along the Barabai River including the water level profile in the side spillway and storage pond. In the reservoir pond, a graph or table will be obtained showing the relationship between time and the highest elevation of the reservoir pond and a graph showing the relationship between time and the flow rate entering the regulation pond. Based on initial calculations, it was determined that the regulation pool needed to be at least +44 meters above sea level or 26 meters high to accommodate the maximum flood discharge of 579.24 $m^3.s^{-1}$.

After running based on the data that has been entered in the HEC RAS program, the results show that the peak discharge occurs at 16.00 WIB, and to accommodate flood

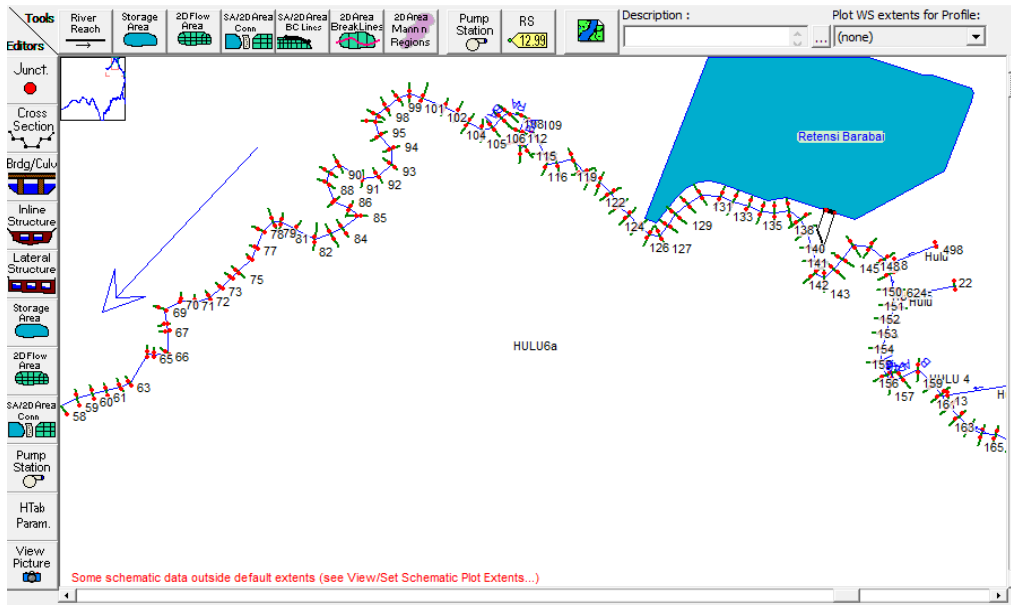

Fig. 6: Barabai River modeling with Hec Ras Program. (Source: Calculation Result, 2021)

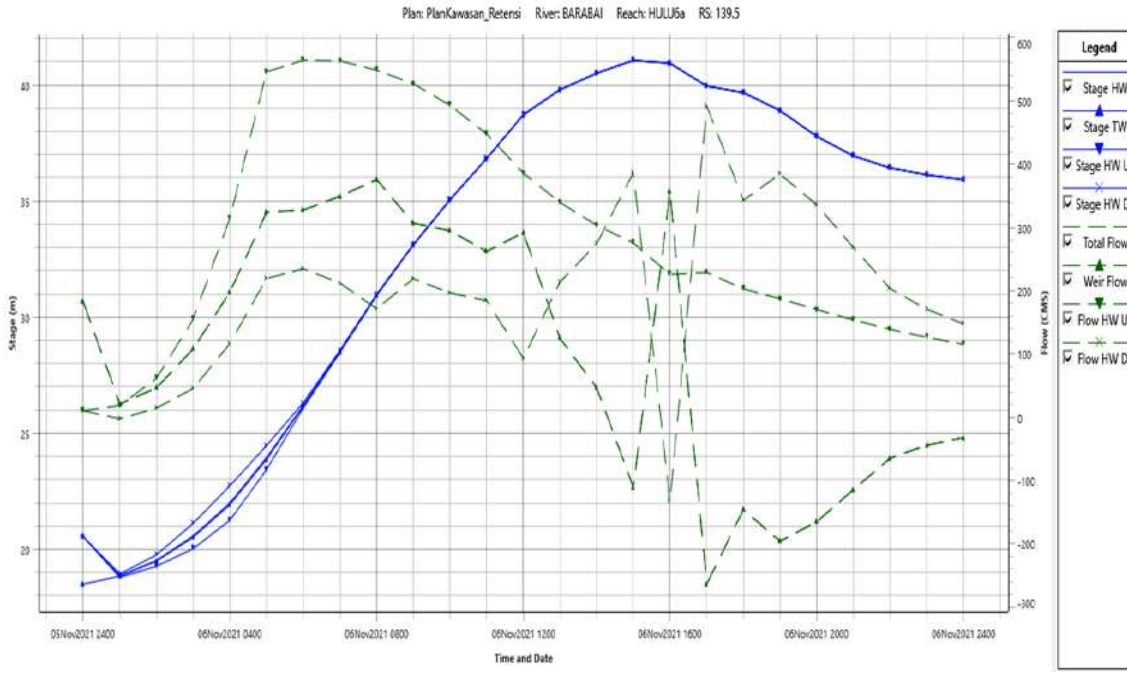

Fig. 7: Simulation of flow in regulation pool with 40% discharge. (Source : Calculation Result, 2021)

discharges from 5 rivers for 24 hours the required reservoir pool elevation is +48 m. Based on the plan, only a maximum elevation of +25 m is provided or the height of the storage pool is only 7 m. As illustrated in Fig. 7, the HEC RAS application's results also revealed a connection between the water level profile on the side spillway and the storage pond. The water level elevation during flooding above the side spillway crest is between +18 and +25, as can be observed on the side spill. This shows that due to the installation of the side spillway, there will be an overflow of water up to +25 m, meaning that the guard height of the side spillway must be even higher. So based on the modeling of the flow through the side perforation and the storage pond, it can be seen that the storage pond is no longer able to accommodate all the flood discharges that occur. The side spillway and regulation ponds that are planned are only able to accommodate about 40% of the flood discharge that occurs within 24 hours after the downstream river recedes and then flows into the downstream river. So the remaining 60% of the discharge must still be channeled downstream of the Barabai River which enters Barabai City. Efforts are being made to re-calculate the capacity of the regulation pool to accommodate flood discharge with reference to the planned elevation of +25 m, so that new hydraulic flow behavior will also be obtained, both in the regulation pool and on the side ledge. Then the water level profile in the lower reaches of the Barabai River will be based on the discharge capacity that can be stored by the regulatory pool. After re-modeling, it was found that the regulation pool was only effective at accommodating 40% of flood discharge. The remaining 60% of the discharge flows downstream of the Barabai River. The results of the modeling of flow behavior and rating curve in the regulation pool as well as the flow behavior sideways are presented in Fig. 7. From the picture, it can be seen that the water level has met the top elevation of +25. It is also necessary to examine the intake, it needs to be screened because it affects the incoming discharge (Rizal et al. 2020) and (Rizal et al. 2021) and the need for water balance for irrigation (Salim & Rizal 2020).

After 40% can be absorbed by the regulation pond, then 60% of the flood discharge flows to the lower reaches of the Barabai River and through Barabai City with a flow profile presented in Fig. 7. In the Fig., it appears that there is still quite a high runoff when the Barabai River water enters Barabai City. At 0-5 km the average water level elevation is around +35 but at 5-8 km the average water level elevation drops to +22, so, there is a significant difference. The very high elevation of the water table indicates that the distribution of the puddle is quite wide, but in this HEC RAS only one-dimensional modeling is presented, so visualization of the inundation area or inundation zoning needs to be reworked in the 2-dimensional HEC RAS modeling. In detail, at STA 139 to STA 62, there are quite extreme inundations

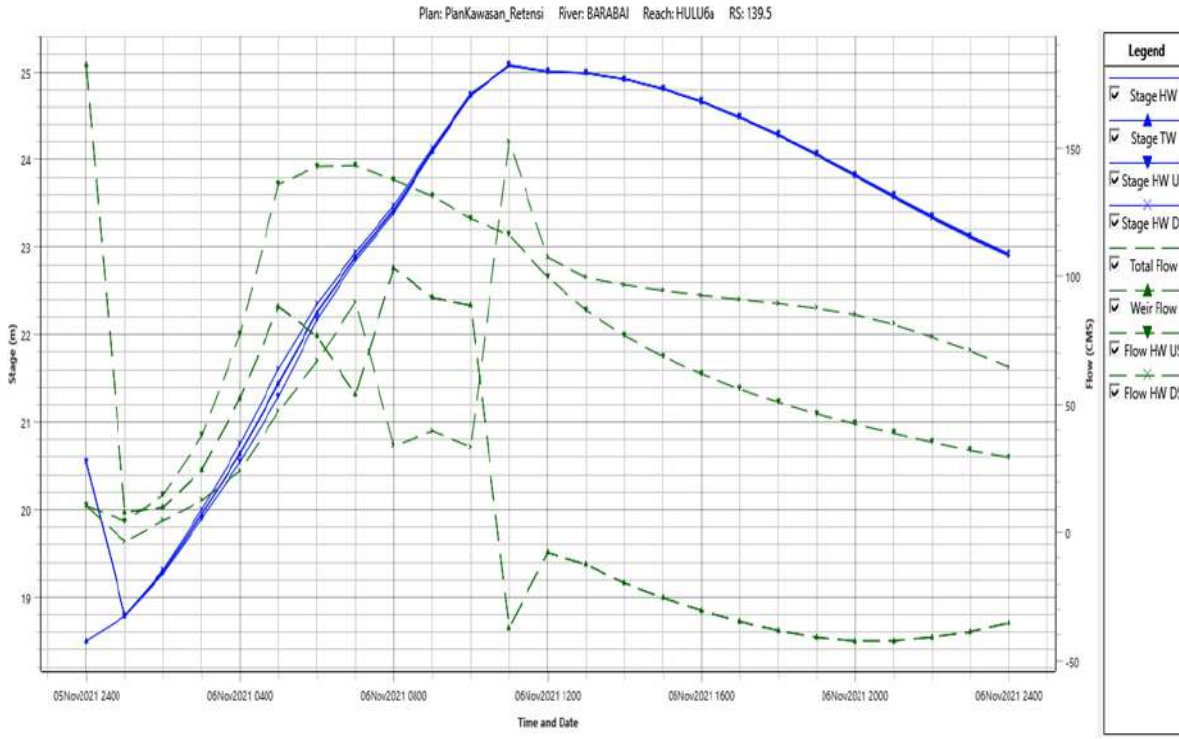

Fig. 8: Simulation of flow profile on side spillway with 40% discharge. (Source: Calculation Result, 2021)

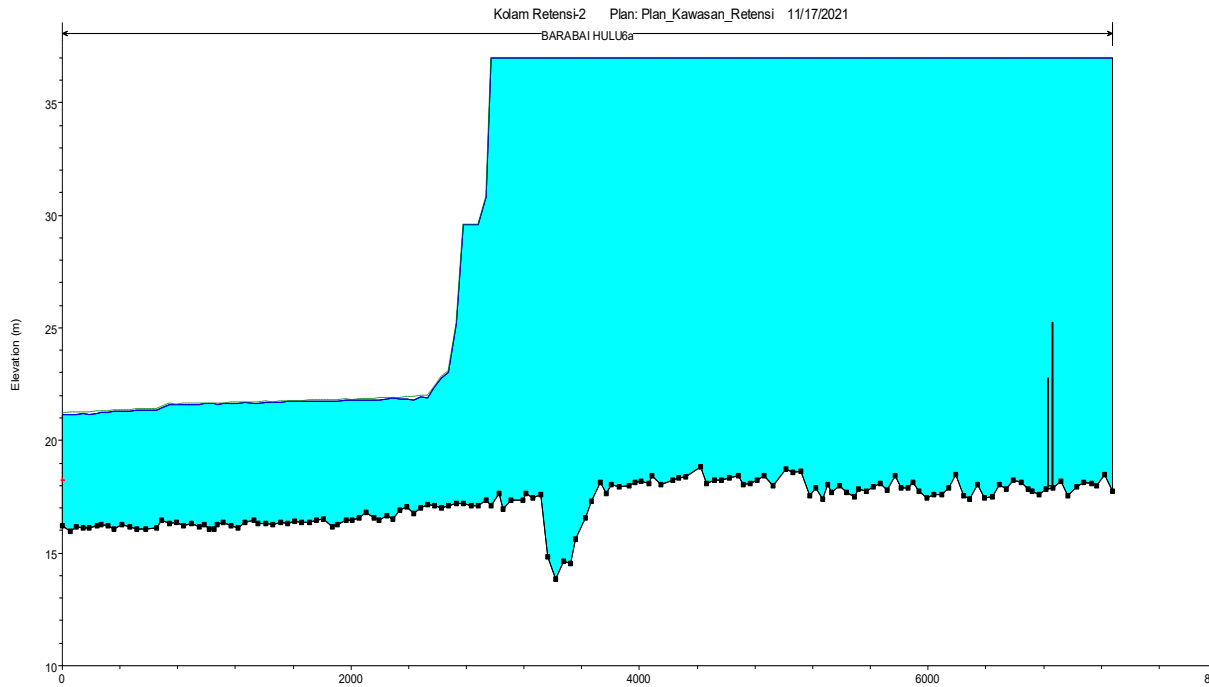

Fig. 9: Profile of the water level passing through the city of Barabai with a discharge of 60% of the Planned Discharge. (Source: Calculation Result, 2021)

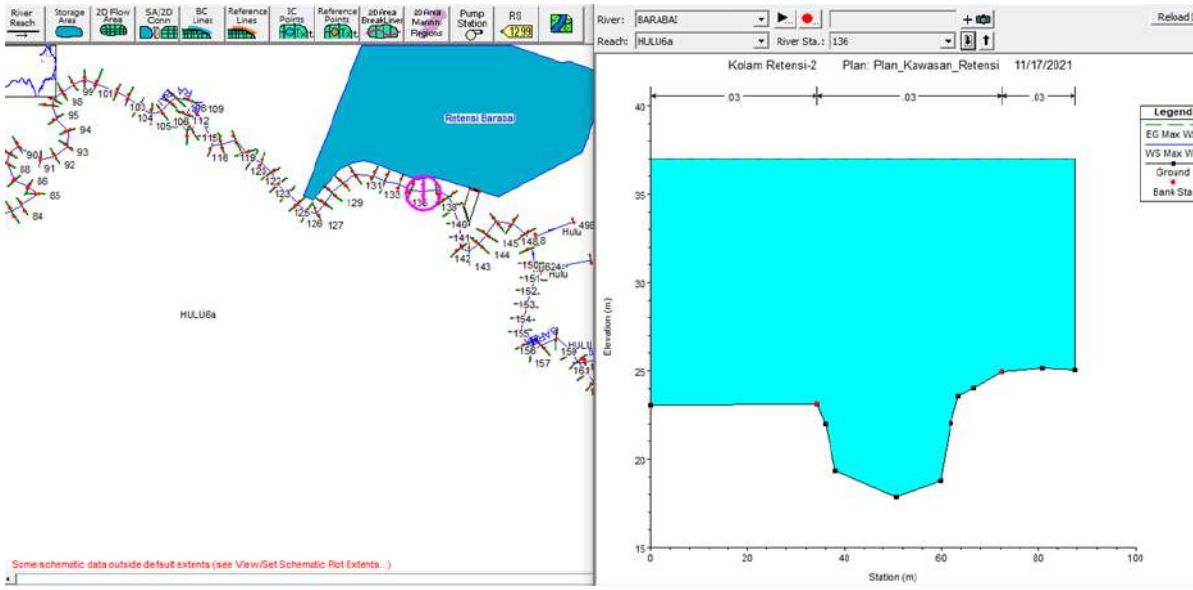

Fig. 10: Water level profile at STA 138 with 60% discharge. (Source: Calculation Result, 2021).

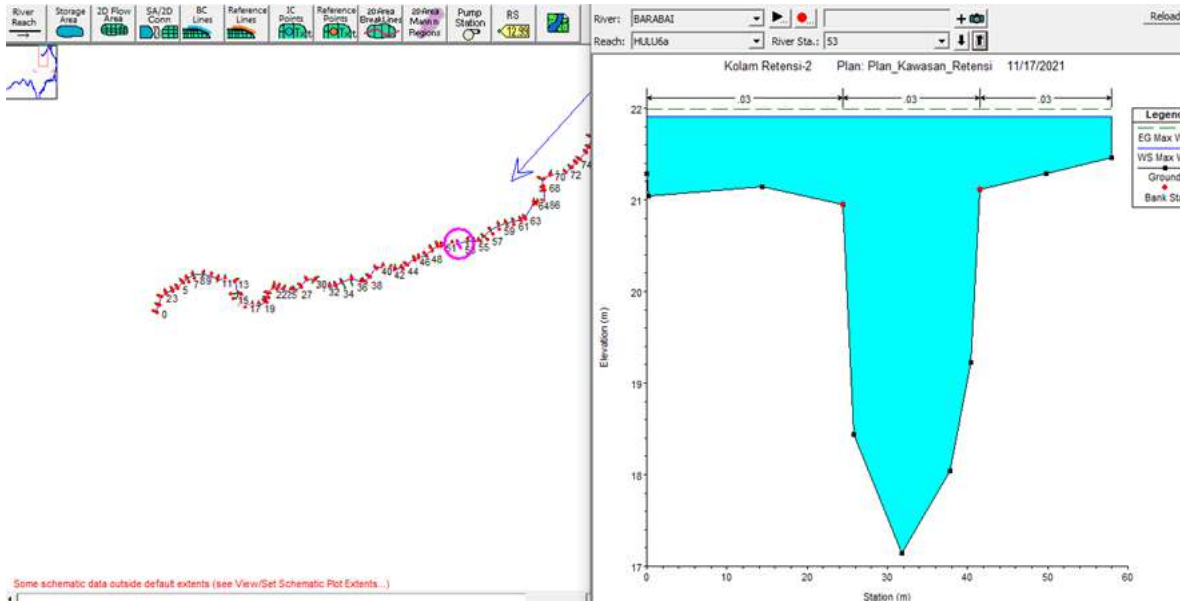

Fig. 11: Water level profile at STA 53 with 60% discharge. (Source: Calculation result, 2021).

up to an altitude above +35. Then at STA 53, it started to decline at an elevation of +23 to STA 0 at an elevation of +21, as shown in Fig. 8 and Fig. 9. The cross-section of the river which is quite small is an indicator of the occurrence of water overflow in the Barabai River that passes through Kota Barabai. Care must be taken in reviewing the Barabai River's maximum storage capacity in the form of an estimate of the percentage of flood discharge that can flow without flooding. Furthermore, the rest needs to be given a solution by making a reservoir upstream of the Barabai River. Based on field verification, it is possible to carry out river normalization because there is a violation of river boundaries. There are 10 cross-sections. In field visualization, it is clear that there are river border violations.

As a visualization, the water level profile is presented at STA 138, it appears that the water level profile is

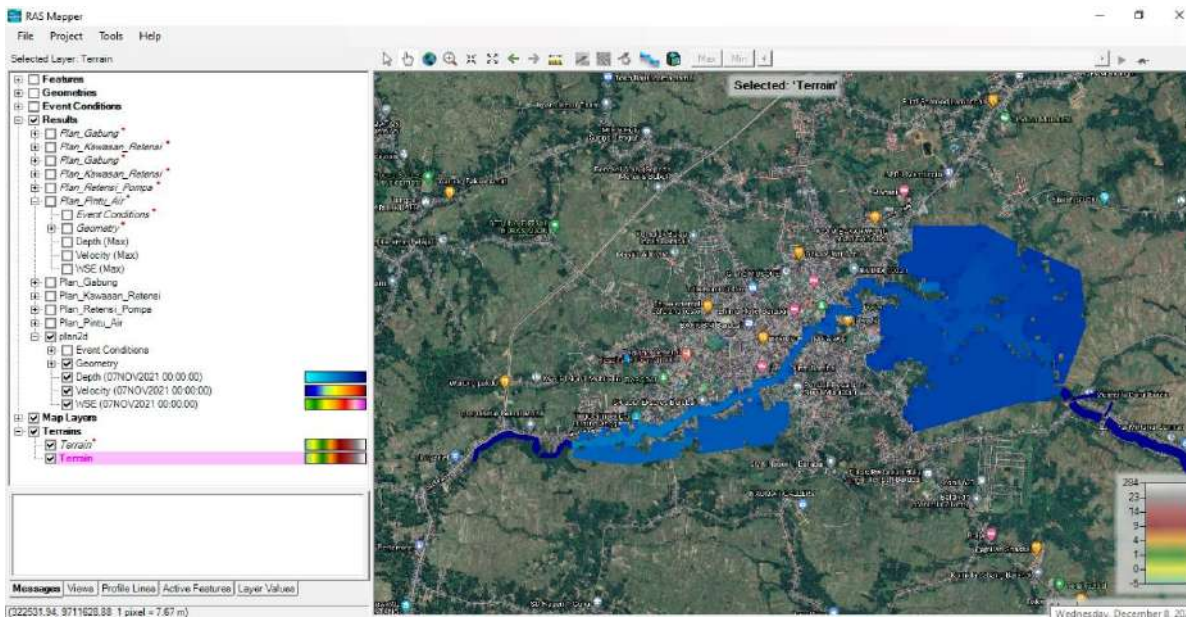

Fig. 12: Areas experiencing inundation in Kota Barabai. (Source: Calculation result, 2021)

quite high, namely 5 meters above the river embankment elevation as shown in Fig. 10. Visualization of water level conditions is also presented in Fig. 11. At STA 53 the water level profile is also high but lower than STA 138 only 2 m above the embankment. This is possible because the cross-sectional area of the river at STA 53 is larger than that of STA 138.

After conducting a study using HEC RAS 1D, almost all cross sections of rivers passing through Barabai City overflowed. The solution given is to do another analysis to

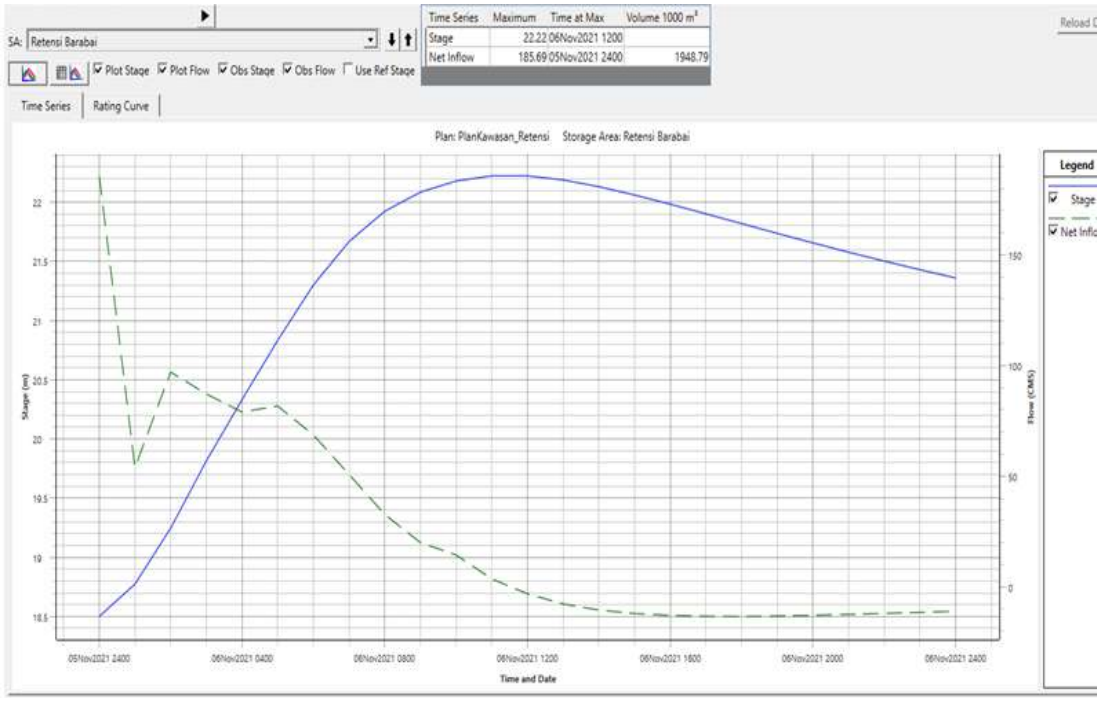

Fig. 13: Result of f1ow simulation in retention pond with expansion and addition of retention pond.

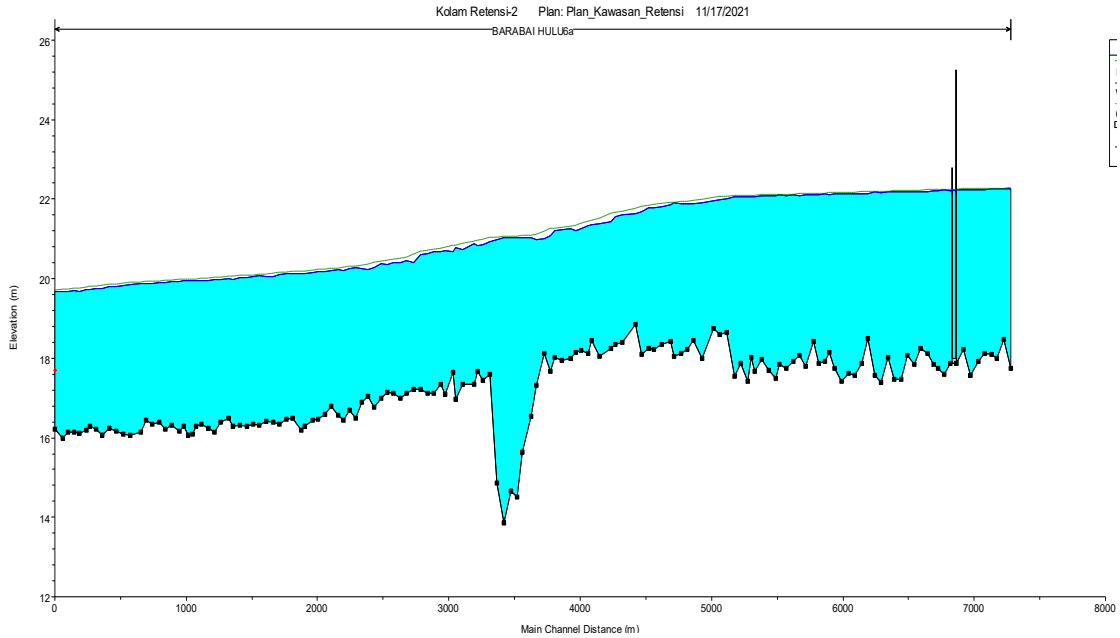

Fig. 14: Long section and cross conditions section after repair. (Source: Calculation result, 2021)

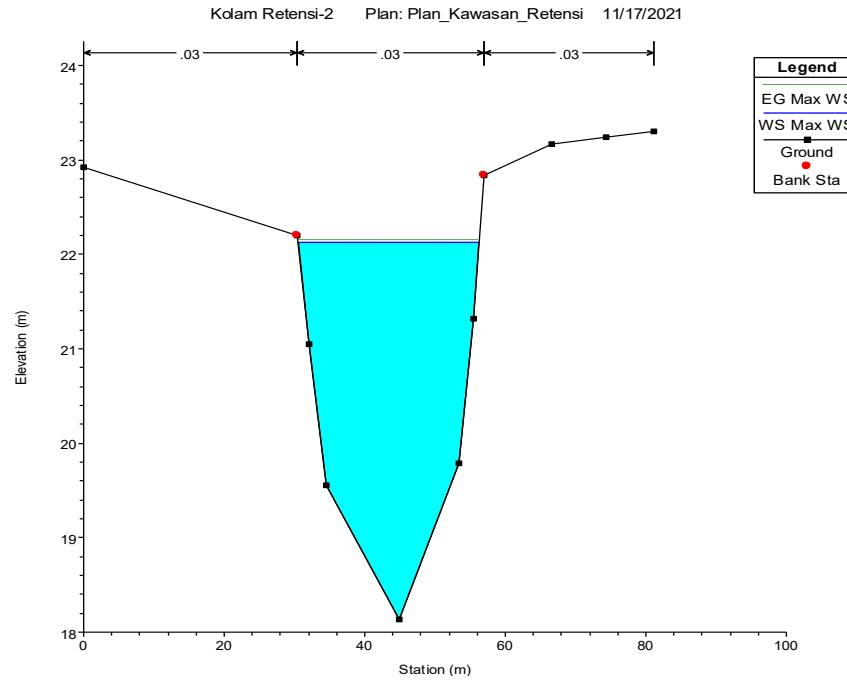

Fig. 15: Long section and cross conditions section after repair. (Source: Calculation Result 2021)

find out the level of overflow or inundation by doing 2D modeling as described previously. In modeling, boundaries of the area to be analyzed must be made. So in this analysis, the study boundary zone uses all areas of Barabai City, South Kalimantan Province. Based on the study, the results are presented in Fig. 12. In the picture, it can be seen that 70% of the Barabai City area experiences inundation during floods. The largest distribution occurs in the eastern river area,

especially at the point where the Retention Pool will be built.

Given the explanation in the preceding section, it is clear that despite the construction of a retention pond, the flooding issue in Barabai City has persisted despite multiple modeling iterations (Ljubenkov 2015). So some of the solutions are as follows:

1. The Barabai Canal is maximized so that it can drain a maximum flood discharge of 200 $m^3.s^{-1}$ by widening the Barabai canal 2x from the initial plan, then the planned regulation pool expansion is carried out from an inundation area of 58 ha to 95 ha.
2. The Barabai Canal is maximized so that it can drain a maximum flood discharge of 200 $m^3.s^{-1}$ by widening the Barabai canal 2x from the initial plan, then a 2nd regulation pool is made upstream of the Barabai River with an area of 40 ha and a height of 7 m. Visualization of alternative selection is presented in Fig. 13.
3. The Barabai Canal, which is in the upper reaches of the Barabai River, is widened by 2 meters from the original plan, and the river entering Barabai City is widened by at least 4 meters on each side so that it can drain a maximum flood flow of 200 $m^3.s^{-1}$. After normalizing 4 m to the right cliff and 4 m to the left cliff, it seems that there are no more puddles in Barabai City. After running using the HEC RAS Program, the water level profile is quite good and there are no more puddles, as shown in Fig. 14 and Fig. 15.

CONCLUSION

This study is quite important as a solution to flooding management in Barabai City based on a priority scale. By enlarging the retention pond from 58 ha to 95 ha or by constructing another retention pond in the Barabai River's upstream section, flooding in Barabai City can be prevented. If this is not possible, the Barabai River, which flows through Barabai City, is normalized on both sides.

ACKNOWLEDGMENTS

This research did not receive any specific grant from funding agencies in the public, commercial, or not-for-profit sectors. The authors would like to thank the editor and anonymous reviewers for their comments that help improve the quality of this work.

REFERENCES

Anam, S., Dermawan. V. and Sisinggih D. 2015. Evaluation of the functions of the Barabai river flood control building, Hulu Sungai Tengah Regency, South Kalimantan Province. J. Irrig. Eng., 6(2): 271-286.

Anis, M.B., Suhardjono, M. and Andawayanti, U. 2017. The reservoir pond is a flood control building in Sampang District. J. Irrig, Eng., 8 (1): 39-47.

Cahyono, A.T. 2010. Perencanaan Pengendalian Banjir Kali Kemuning Sampang. Thesis, ITS Jawa Timur, East Java, p.72.

Chay, A. 2002. Hydrology and Watershed Management. Gadjah Mada University Press, Yogyakarta, p. 38.

Chow, V.T., Rosalina, N. 1989. Hidrolika Saluran Terbuka. Erlangga, Jakarta, p. 609.

Czahchor, H., Doerr, S.H.. and Lichner, L. 2010. Water retention of repellent and subcritical repellent soils: New insights from model and experimental investigations. J. Hydrol., 380(2): 104-111.

Faizal, F. and Nizam, M. 2005. Analysis of the Barabai River Water Level in Planning for Flood Control at Kemuning River, Sampang. Thesis., ITS Jawa Timur, Wast Java, p.72.

Muslim, F., Kumalawati, R. and Aristi, N.F. 2017. The Vulnerability of Residential Buildings to Floods in Barabai District, Hulu Sungai Tengah Regency. J. Geogr. Educ., 4(1): 1-7.

Harto, S. 1993. Hydrological Analysis. PT Gramedia Pustaka Utama, Jakarta, Indonesia, pp. 38.

Hauer, C., Flodl, P., Habersack, H. and Pulg, U. 2021. Critical flows in semi-alluvial channels during extraordinarily high discharges: Implications for flood risk management. J. Flood Risk Manag., 14(4): 12741.

Istiarto. 2021. 1-Dimensional Flow Simulation with the Help of the HEC-RAS Hydrodynamics Program. Department of Civil Engineering FT UGM, Jakarta, Indonesia, p.38.

Ljubenkov, I. 2015. Hydrodynamic modeling of a stratified estuary: A case study of the Jadro River (Croatia). J. Hydrol. Hydromech., 63(1) : 29-37.

Martin, M. and Fransiskus, H. 2013. Normalization of the Rantauan River as an alternative to flood management in Jelimpo District, Landak Regency. J. Tanj. Univ. Civil Eng. Stud., 1: 39.

Prabowo, E. 2018. The flood control study in Barabai city is related to the plan to build the Pancur Hanau Dam on the Barabai River, Hulu Sungai Tengah Regency. J. Sustain Technol., 7(1): 43-51.

Noor, M.A. 2013. Riam Kiwa River Capacity Study Using HEC – RAS 4.1.0. Lambung Mangkurat University, South Kalimantan., p. 34.

Rizal, N., Bisri, M., Juwono, P. and Dermawan, V. 2020. Effect of the coefficient of discharge at the bottom intake Weir with a screen of a circular perforated plate. J. Water Land Dev., 45(6): 13- 22.

Rizal, N.S. 2014. Irrigation Planning Application and Waterworks. LPPM Muhammadiyah University Jember, East Java, p. 56.

Rizal, N.S., Munfarida, N. and Kosjoko. 2021. Effect of diagonal formation of plate perforations on the Tyrol Weir discharge coefficient value. Int. J. Geomate, 21(87): 28- 35.

Salim, N. and Rizal, N.S. 2020. Study of Water Balance for Irrigation in Coastal Areas Jember District. Int. J. Eng. Res. Technol., 1(12): 4992-4999.

Yan, B., Guo, S. and Yu, W. 2013. Coincidence risk of flood hydrographs between Yangtze River and Qing River Shuili Fadian Xuebao. J. Hydroelectr. Eng., 32(1): 50-53.

Zhang, L. and Sing, V.P. 2006. Bivariate flood frequency analysis using the copula method. J. Hydrol. Eng. ASCE, 11(2): 150-164.

Nature Environment and Pollution Technology
An International Quarterly Scientific Journal

p-ISSN: 0972-6268
(Print copies up to 2016)
e-ISSN: 2395-3454

Vol. 21 | No. 5 (Suppl) | pp. 2231-2240 | 2022

Original Research Paper

https://doi.org/10.46488/NEPT.2022.v21i05.017

Open Access Journal

Selective Detection of Zn^{2+} Ions by Ratiometric Receptor (E)-N′-(1-(2, 5-Dihydroxy phenyl) Ethylidene) Isonicotinohydrazide: A DFT Study

N. S. Patil*(**), R. B. Dhake*, R. Phalak*, U. A. Fegade†, C. Ramalingan*** and V. Saravanan*****

*Department of Chemistry, D. D. N. Bhole College, Bhusawal, Jalgaon 425201, Maharashtra, India

**Department of Chemistry, Bhusawal Arts, Science and P. O. Nahata Commerce College, Bhusawal, Jalgaon 425201, Maharashtra, India

***Department of Chemistry, Kalasalingam Academy of Research and Education (Deemed to be University), Krishnankoil 626 126, Tamilnadu, India

†Corresponding author: U. A. Fegade; umeshfegade@gmail.com

Nat. Env. & Poll. Tech.
Website: www.neptjournal.com

Received: 21-05-2022
Revised: 26-06-2022
Accepted: 30-06-2022

Key Words:
Detection of zinc
Ratiometric receptor
Isonicotinohydrazide
DFT study

ABSTRACT

The metal ion sensing characteristics of a novel Schiff-based ratiometric UV-visible chemosensor (E)-N'-(1-(2,5-dihydroxy phenyl)ethylidene) isonicotinohydrazide) (R1) has been explored. In EtOH:H_2O (7:3, v/v), it has high sensitivity and selectivity for Zn^{2+} among a series of metal ions. With the addition of Zn^{2+} ions solution, R1 displayed discriminating spectral activity. The other metal ions did not affect R1 in any way. Furthermore, the addition of Zn^{2+} ions to R1 and LMCT action caused the shifting of the peak to a longer wavelength of 406 nm. The interaction of Zn^{2+} ions with R1 was further investigated using Density Functional Theory (DFT) investigations. Zn^{2+}-R1 combination has a lower energy (2.2667 kcal.mol^{-1} to 0.9339 kcal.mol^{-1}) than R1, indicating a strong connection with excellent stability. The Zn^{2+}-R1 complex's association constant (Ka) was discovered to be 6795M^{-1} and 6836M^{-1} using Benesi-Hildebrand and Scatchard plots respectively. The detection limit was determined to be 276 nM.

INTRODUCTION

Many industrial processes rely heavily on transition metals including iron, zinc, and nickel. For the production of ammonia and fertilizers, iron is employed as a catalyst. Nickel is a key component of various steel-based alloys due to its high strength and resilience to corrosion and heat in the steel industry. Galvanization of iron is generally done with zinc. In the paint and dye-based industries, iron and zinc oxides are extensively employed as pigments (Lehn 1995, Atood et al. 1996).

Zinc is often seen securely bound in proteins in the human body. It plays a range of vital roles in biological processes. Infantile diarrhea, Parkinson's disease, and Alzheimer's disease, immunological dysfunction might all be caused by a disturbance of Zn(II) homeostasis (Lehn 1995, Atood et al. 1996, De Silva et al. 1997, Kumar et. al. 2018, An et al. 2016). As a result, creating probes that can properly detect and understand in vivo Zn(II) biological processes requires the ability to observe Zn(II) concentration in biological systems.

Because of their importance in a range of biological and industrial processes, effective real-time atomic detection of all of these metals is critical. For detecting them, several analytical approaches are available (Zhang et al. 2019a, 2020, Khanna et al. 2019, Ghorai et al. 2019, Yan et al. 2018, Dong et al. 2017). Metal sensing based on optical phenomena is a growing subject of study (Fegade et al. 2014a). Because of its simplicity, ease of use, real-time detection, cheap cost, excellent selectivity, and sensitivity, in the environmental, analytical, and biological realms, this technique has a wide range of applications (Fegade et al. 2014b, 2015a, 2015b, Patil et al. 2014, Kuwar et al. 2013, Tayade et al. 2014, Pawar et al. 2015, Patil et al. 2015, 2014, 2020, Bhosale et al. 2015, Kaur et al. 2017, Kolate et al. 2020, Fegade et al. 2021a, 2021b).

In comparison to fluorescence-based chemosensors, other detection techniques such as AAS, XRF, radioisotopes, ICP-MS (Berrones-Reyes et al. 2019), modified nanotube carbon

ORCID details of the authors:

Umesh Fegade:
https://orcid.org/0000-0002-2599-668X

electrodes (Khanra et al. 2019), voltammetry (Zhang et al. 2019b), and ion-selective membrane electrodes (Diana et al. 2019, Jung et al. 2019) have a substantial benefit. Fluorescent chemosensors are appealing approaches because of their low cost, high selectivity, sensitivity, and ability to detect in real-time (Ghorai et al. 2019, Yan et al. 2018, Dong et al. 2017, Fegade et al. 2014c, Fegade et al. 2015a, 2015b, Patil et al. 2014,). Chemosensors have played a significant role in gaining a better knowledge of biological processes and their applications in the environment. In recent years, chromogenic zinc sensing molecules have been extensively produced for the goal of monitoring and/or detecting the transient and dynamic distribution of zinc ions inside the cell (Fegade et al. 2014d, 2015a, 2015b, 2020, 2021a, 2021b, Patil et al. 2014, 2015, 2021, Jethave et al. 2018, 2019, 2021, Xu et al. 2018, Yan et al. 2018).

Many transition metals are required for the chemistry of biological systems, with Fe, Co, Cu, and Mo being the most prevalent examples. However, because of the severe toxic consequences, simple, sensitive, selective, and Reliable sensing systems or sensors are required for detecting and eliminating metals from diverse environmental matrices (Lehn 1995, Atood et al. 1996, De Silva et al. 1997, Khan et. al 2013). However, these procedures have significant disadvantages, including a time-consuming sample preparation process, expensive costs, and the need for specialized instrumentation. Furthermore, due to the color change effect visible to the naked eye, identifying trace elements with a colorimetric probe is simple. The response time between the analyte and the probe is relatively short, and apparent color changes allow detection to move from the lab to on-site applications (An et al. 2016, Maniyazagan et al. 2017, Dong et al. 2017, Ghosh et al. 2017, Yang et al. 2019, Naha et al. 2020). In Schiff UV-visible/fluorescent probes, with metal ions, the C=N bond results in the formation of a stable complex., demonstrating the discriminating spectral activity. As a result, Schiff base probes have attracted the attention of several scientists in the fields of environmental and chemical sciences (Pendin et al. 2019).

For a few years, our team has been working on detecting and removing organic and inorganic contaminants from the environment (Fegade et al. 2014e, 2015a, 2015b, 2020, 2021a, 2021b, Patil et al. 2014, 2015, 2021, Jethave et al. 2018, 2019, 2021). In this study, (E)-N'-(1-(2,5-dihydroxyphenyl) ethylidene) isonicotinohydrazide) (R1) a Schiff base, was produced and tested in fluorescence and UV-visible spectrophotometers for the detection of Zn^{2+} ions. Color shift was observed by the human eye and wavelength enhancement and the shift was examined for the validation of Zn^{2+} interaction with the R1.

MATERIALS AND METHODS

Fisher Scientific Chemicals Ltd. in India provided all reagents, which were utilized without being purified further. The "1H NMR" spectra were acquired on a "Bruker Avance II 400 NMR" operating at 400 MHz in DMSO. The MASS and IR spectra were generated using water "QTOF-Q micro mass" and "Bruker FTIR spectrometers", respectively. A Shimadzu UV-1800 model with 1 cm quartz cells was used to perform the UV-visible spectrophotometric examination.

Synthesis of R1

A solution of isoniazide (0.411 g, 3 mmol) and 2,5-dihydroxy benzaldehyde (0.414 g, 3 mmol) are mixed in 50 mL of CH_3OH and provided 2 h of stirring at room temperature results in the yellow precipitate, which was purified, dehydrated, and recrystallized from ethanol (85%) to yield pure R1 (Fig. 1).

Photographic and Physical Examination

UV-visible spectrophotometer was used for the analysis of working solution R1 to assess metal ion selectivity, then various metal ions were added. R1 demonstrated a discriminating spectrum shift when Zn^{2+} ions were added, but other metal ions did not, resulting in photometric titrations.

DFT Research

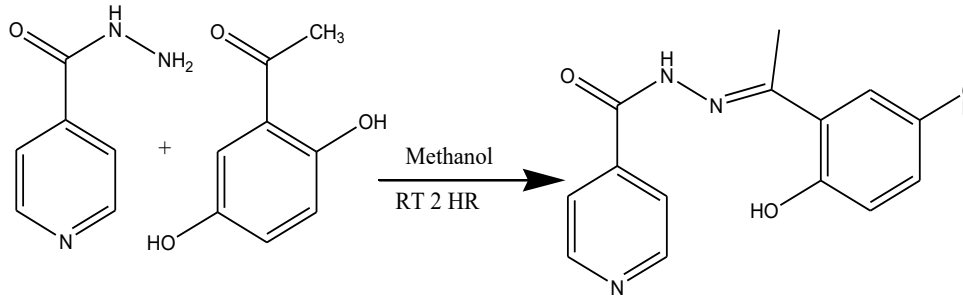

Fig. 1: Synthesis of R1.

GAUSSIAN 09 software was applied for all computational calculations. The optimal research was conducted at the B3LYP level, utilizing the Gaussian 09 program's 6-311G** basis set (for Zn atom). To establish the nature of the reaction, LUMO and HOMO values were used to monitor the interaction of Zn^{2+} ions with R1.

Calculation of the LOD

The detection limit was calculated using the equation below.

LOD (limit of detection) = 3/S

S = Slope.

RESULTS AND DISCUSSION

Chemosensor R1 was made by condensation reaction between isoniazide and 2,5-dihydroxy benzaldehyde in methanol (Fig. 1) and analyzed using Spectro-analytical methods. The purity of the R1 has been established based on IR, ^{1}H-NMR, and mass spectroscopic techniques. ^{1}H-NMR (CDCl3, 400 MHz, ppm, δ): 2.43 (s, 3H, CH_3), 6.72-6.79 (m, 2H, Ar-H), 6.980 (s, 1H, Ar-H), 7.82-7.83 (m, 2H, Ar-H), 8.76-8.77 (m, 2H, Ar-H), 8.84 (s, 1H, -OH), 11.49 (s, 1H, -NH), 12.436 (s, 1H, -NH), IR (KBr, cm^{-1}) υ = 668.34, 752.60, 781.20, 831.42, 1149.44, 1208.93, 1292.38, 1504.27, 1533.90, 1665.88, 3452.81, MS (EI): m/z = 271.0957 ($C_{14}H_{13}N_3O_3$) cald m/z = 272.55163 for $C_{14}H_{13}N_3O_3$ [39-43].

The behavior of R1 (C = 1 × 10^{-5} M) absorption in the presence of different metal ions (C = 1 × 10^{-4} M) was investigated using UV-visible spectrophotometric measurements. R1's UV-Visible spectra revealed two peaks at 396 nm, with n→Π* transitions ascribed to the peak. In addition, the addition of Zn^{2+} ion solution to R1 produced a ratiometric spectrum pattern, but the insertion of different ionic species had no effect. Because of the LMCT action, the addition of Zn^{2+} ion solution to R1 resulted in a red shift of the 396 nm peak to 406 nm, as seen in Fig.2a. The complex bond form between Zn^{2+}, OH of R1, and C=N was identified. The redshift is generated by the -OH group being deprotonated,

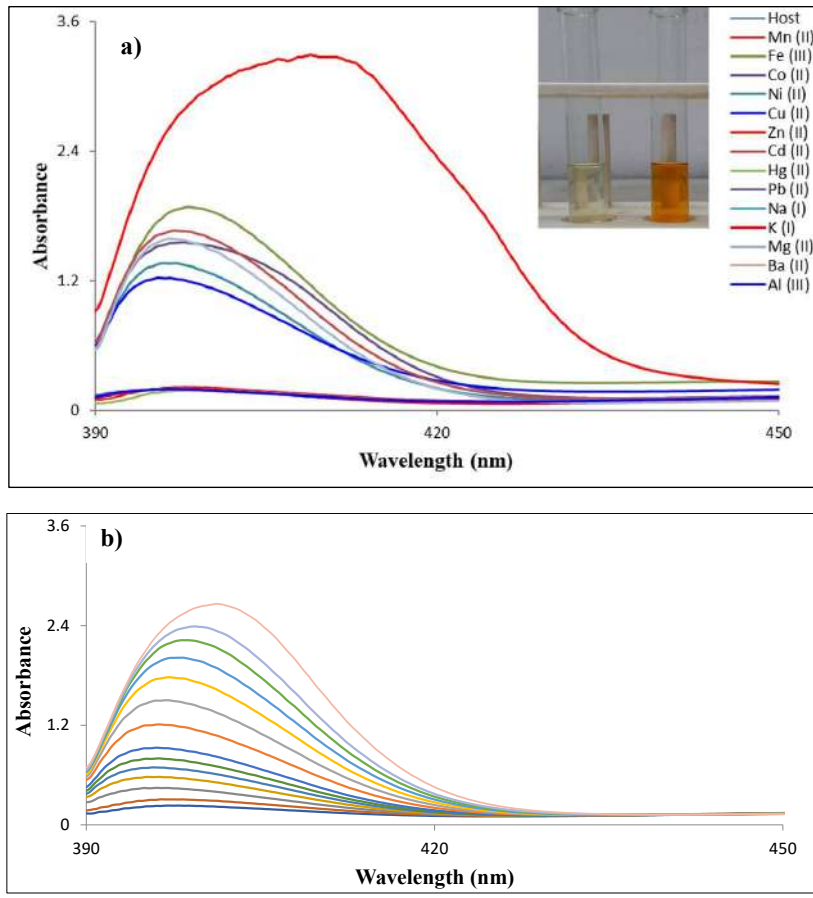

Fig. 2: a) Metal ion selectivity utilizing R1, Inset Fig. 2a Colour change of R1 (Pale yellow) with the addition Zn^{2+} (Orange) and b) R1 absorption profile with gradual addition of Zn^{2+} ion.

which leads to the formation of an O-Zn covalent bond. The addition of Zn^{2+} to R1 results in not only spectral shifts but there are also chromatic changes from yellow to orange, as measured by colorimetry. The color shift is visible with the naked eye (Fig. 2a Inset), increasing R1 efficiency in today's industrially polluted world (Benesi & Hildebrand 1949, Scatchard 1949, Xu et al. 2018).

Titrations were performed to have a better grasp of occurrence. The spectra of R1 were initially recorded, as shown in Fig, 1b, and then a Zn^{2+} ion solution varying in concentration from 0 to 200 µL was introduced to R1 (2 mL). The absorbance at 396 nm increases as the amount of Zn^{2+} ions increase, allowing Zn^{2+} ions to be detected in both synthetic and actual samples. The absorption ratiometric response of R1 with Zn^{2+} in the presence of different metal ions was investigated to evaluate selectivity, as shown in Fig. 3a. The interference study is crucial in the detection of target analytes because interfering ions have a major impact on the method's detection capabilities as well as the detection limit (Fig. 3b).

In the FTIR spectra of pure ligand, broadbands were seen at 3423 cm^{-1} and 3095 cm^{-1}, which correspond to the –OH and –NH stretching frequencies, respectively. Carbonyl and imine stretching frequency characteristic bands formed sharply at 1668 cm^{-1} and 1525 cm^{-1}, respectively. In the FTIR spectra of the equivalent R1-Zn^{2+} complex, the unique bands associated with -OH and -NH are diminished/ decreased, and the band for carbonyl and imine stretching is moved to a lower wavelength in the complex at 1664cm^{-1} and 1517cm^{-1}, respectively (Yan et al. 2018, Meng et al.

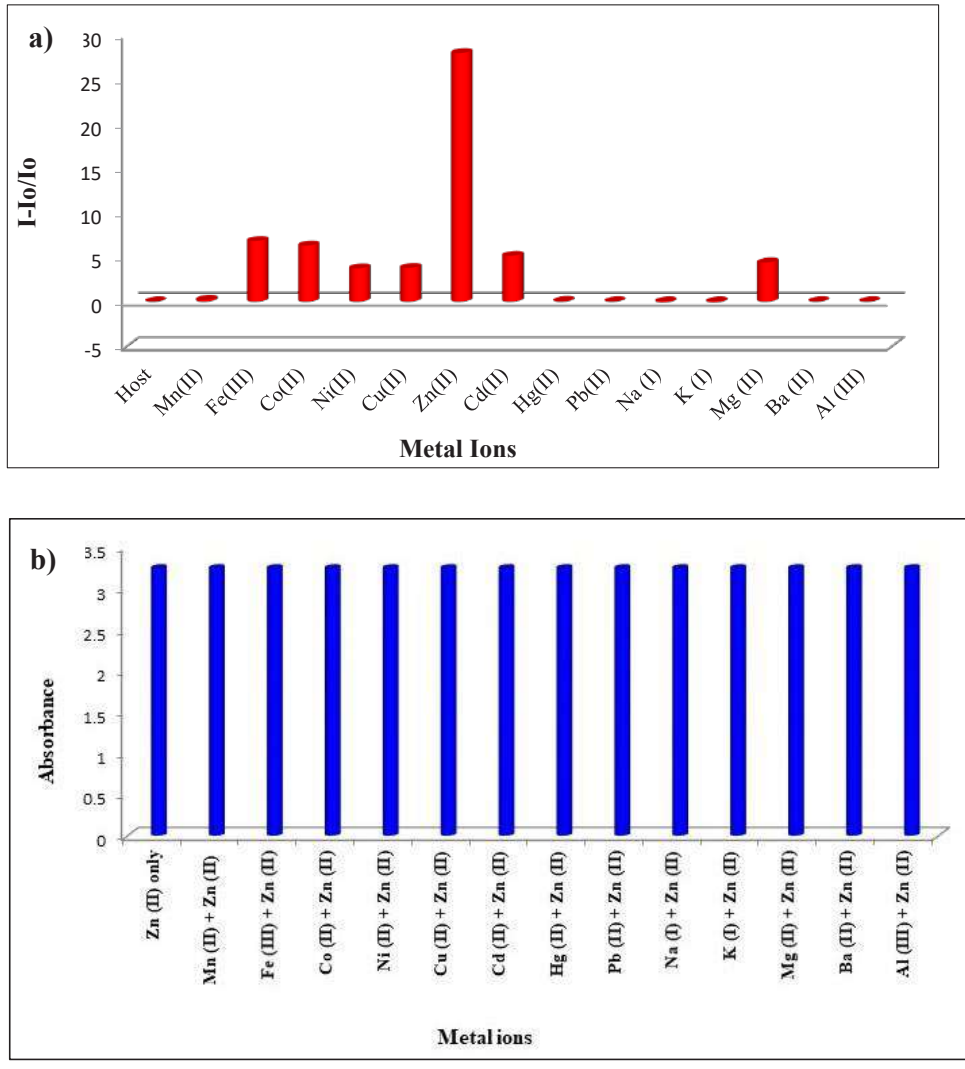

Fig. 3: a) Ratiomeric graph of R1 with other metals and b) R1 interference investigations with Zn^{2+} in the existence of some of the other metal cations.

2018). For the imidol structure to become the dominant one during complexation, the ligand's amide functionality must have undergone amido-imidol tautomerism, according to the preceding facts. The band for the carbonyl and imine functional groups also shifts to a lesser wavelength due to the participation of N in the C=N with the Zn. $m.z^{-1}$ = 335.6534 ($C_{14}H_{12}N_3O_3Zn$) cald $m.z^{-1}$ = 336.0901 for ($C_{21}H_{18}ClCuN_4O_2$).

The highest occupied MO and lowest unoccupied MO energy levels of the title sensor ligand R1 and the corresponding sensor ligand R1+Zn^{2+} are calculated computationally at the B3LYP level using the basis function system 6-311++ G(d,p) to realize the impact of Zn^{2+} binding with the sensor ligand R1 and its electronic properties. 3D plots of the highest occupied MO and lowest unoccupied MO are furnished in Fig. 4 and the energy values are depicted in Table 1. The calculated highest occupied MO and lowest unoccupied MO energies of the sensor ligand R1 are -6.3356 eV and -4.0689 eV, respectively and the resulting bandgap energy (ΔE) of the sensor ligand R1 is 2.2667 eV. Alike, in the sensor ligand R1+Zn^{2+}, the HOMO has an energy of -4.3732 eV, whereas the LUMO has an energy of -3.4393 eV, and the bandgap energy is 0.9339 eV. As can be seen from the figure, the electron density in the highest occupied MOs of sensor ligand R1 is mainly confined to the dihydroxyphenyl structural motif while electron density in the lowest unoccupied MOs of the same is chiefly occupied on the pyridinyl scaffold. Besides, the density of electrons in the highest occupied MOs of sensor ligand R1+Zn^{2+} is primarily located on the dihydroxyphenyl unit akin to the pure sensor ligand R1, however, the density of electrons in the lowest unoccupied MOs of the same is positioned predominantly on the metal and its surroundings such as imine, carbonyl and one of the hydroxyl moieties coordinated with the metal. Precisely, when the highest occupied MOs and lowest unoccupied MOs are concerned, the predominant electron distribution region transfers from one province to another in both cases (Gangatharan et al. 2018, Khanra et al. 2019). On comparing the highest occupied MOs and the lowest unoccupied MOs energy difference between the sensor ligand R1+Zn^{2+} and the sensor ligand R1, the former has a lower value when compared to the latter reflecting the higher stability of the

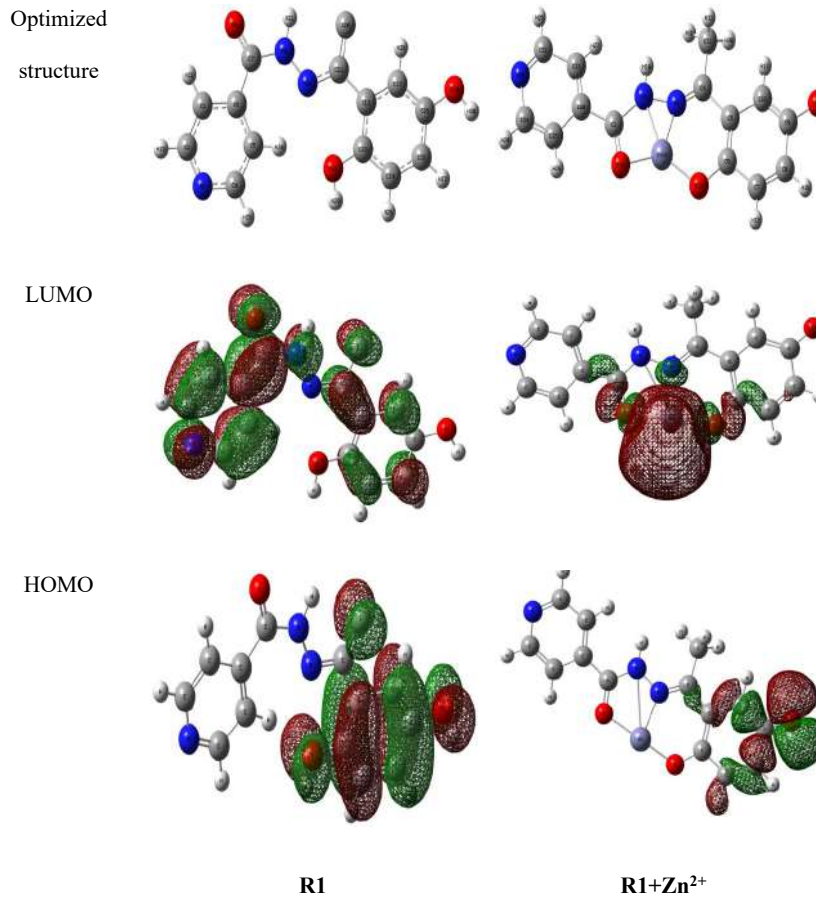

Fig. 4: DFT calculation (a) R1 and R1. Zn^{2+}, (b) LUMO, (c) HOMO diagrams.

Table 1: Energies value of S1and Sensor 3+Zn^{2+}

Parameter	Energies (eV)	
	R1	R1+Zn^{2+}
HOMO	-6.3356	-4.3732
LUMO	-4.0689	-3.4393
ΔE	2.2667	0.9339

sensor ligand R1+Zn^{2+}. Consequently, the results obtained from computational calculations are in good harmony with the experimental analysis of the Zn^{2+} binding (Ghorai et al. 2019, Zhang et al. 2019a, 2019b, Awad et al. 2019).

The complex's binding constant may also be calculated by titrating R1 with a Zn^{2+} ion solution. Using Benesi-Hildebrand and Scatchard plots, the association constant (Ka) of the Zn^{2+}-R1 complex was determined to be 6795M^{-1} and 6836M^{-1}, respectively (Fig. 5a and 5b). As seen in Fig. 6, the binding stoichiometry is a constantly fluctuating process. The absorbance of the host H/([H]+[G]) was also shown in Fig. 6 for a range of total concentrations (Berrones-Reyes

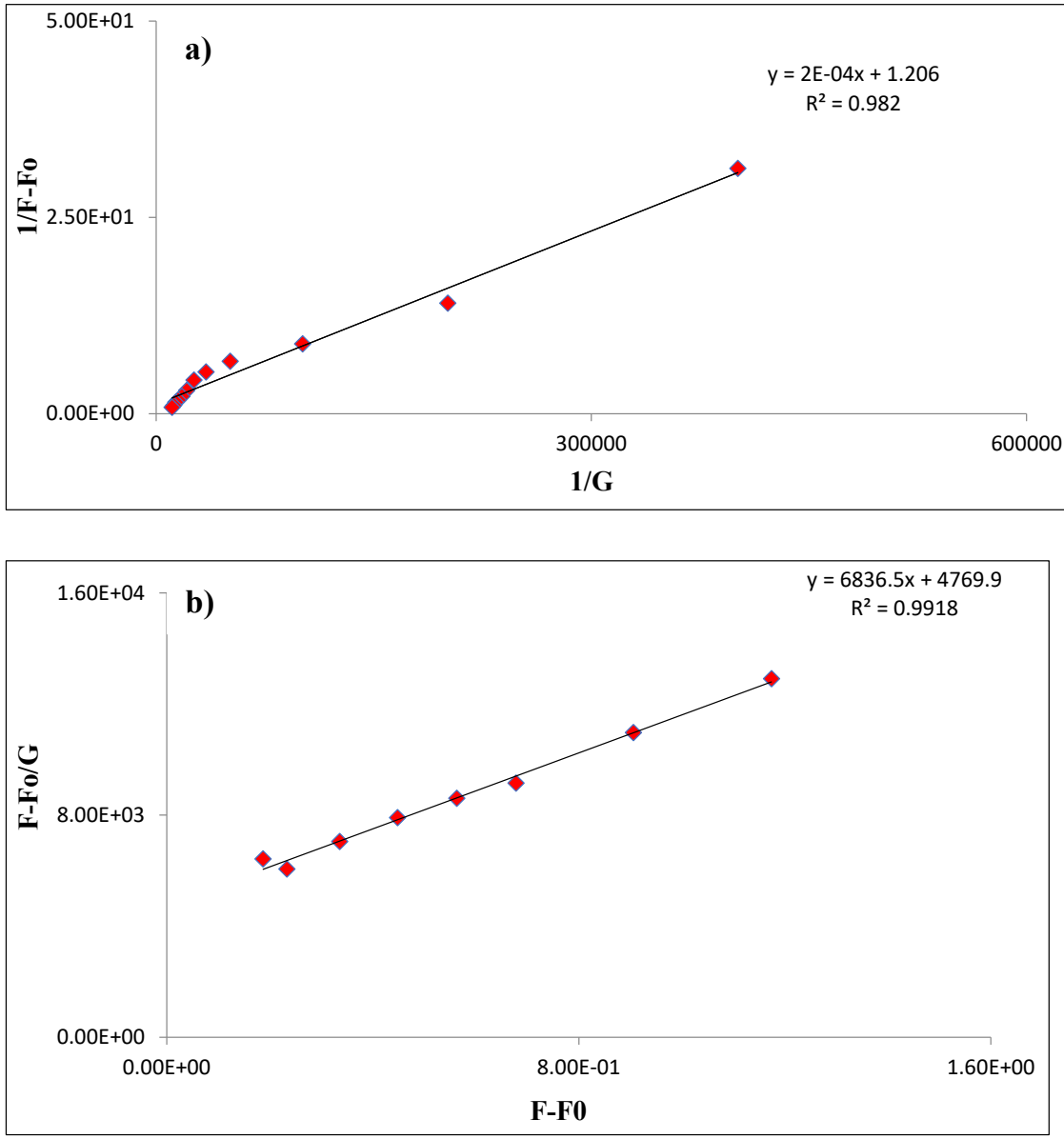

Fig. 5: a) Benesi-Hildebrand for R1 where the K_a value at 6795M^{-1} and R^2 = 0.982, and b) Scatchard graph for R1 where the K_a value at 6836 M^{-1} and R^2 = 0.9981.

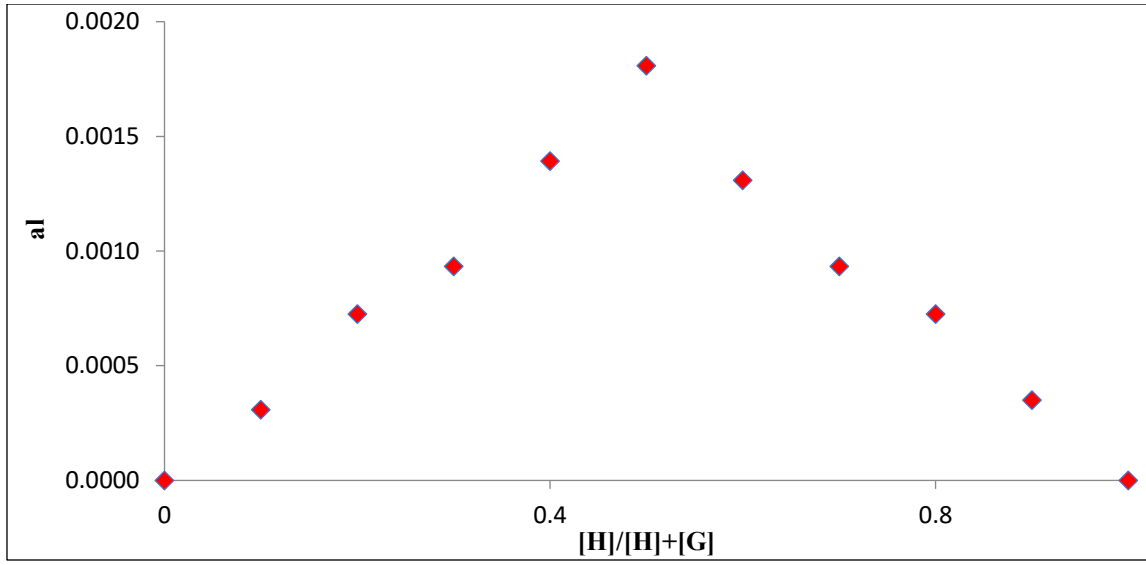

Fig. 6: Job plot between R1 and Zn^{2+} showing 1:1 complexation.

et al. 2019). The concentration of Zn^{2+} and R1 complex was found to be at a maximum of 0.5 units in Fig. 6. 276 nM detection limit (LOD) was found for the 1:1 stoichiometry of Zn^{2+} and R1 (Panunzi et al. 2019).

Reversibility and Colorimetrically Naked Eye Detection

Using absorption spectra, many ions were employed to investigate the reversible binding of Zn^{2+} ions. The brown hue of the Zn^{2+}-R1 was only removed with the addition of $EDTA^{2-}$. It's easy to see how the addition of $EDTA^{2-}$ may shatter the Zn^{2+}-R1 combination. The reversible reagent $EDTA^{2-}$ is used to demetallize the compound and restore R1 to its natural color. Fig. 7 shows that R1 has greater reversibility of 6 cycles. The resulting complex was extracted with the $EDTA^{2-}$ after the Zn^{2+} ion sensing technique. In comparison to the published sensors (Li et al. 2019, Gu et al. 2019, Xu et al. 2019, Zhang et al. 2019a, 2019b), the regenerated R1 may be used numerous times to better detect Zn^{2+} ions, signifying sensitivity and cost-effectiveness. With the recommended colorimetric R1, the color shift from pale yellow to orange (Fig. 8) may be seen with the naked eye, as a consequence of this a reliable and selective sensor system for in-situ applications was designed (Mao et al. 2013, Guan et al. 2019, Park et al. 2014).

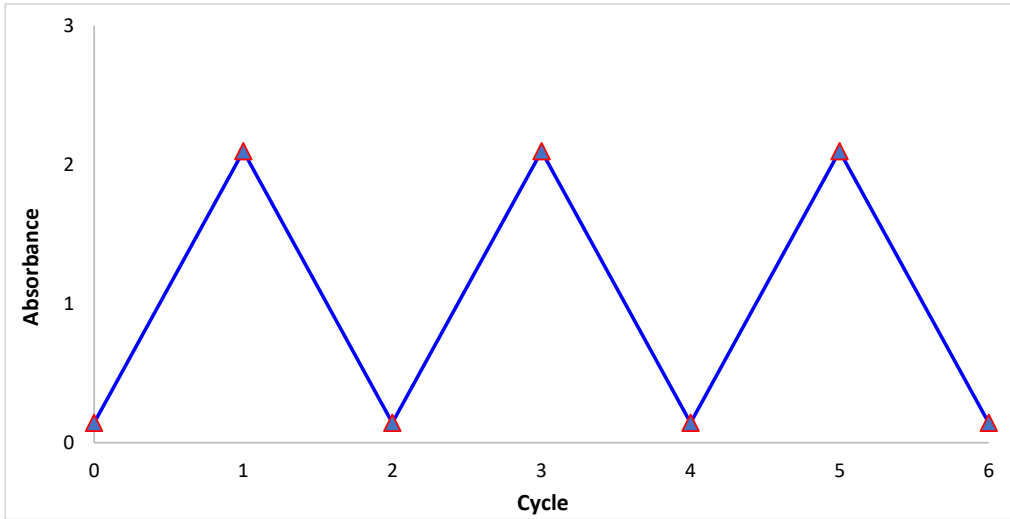

Fig. 7: A Receptor 1 reversible cycle with Zn^{2+} and $EDTA^{2-}$

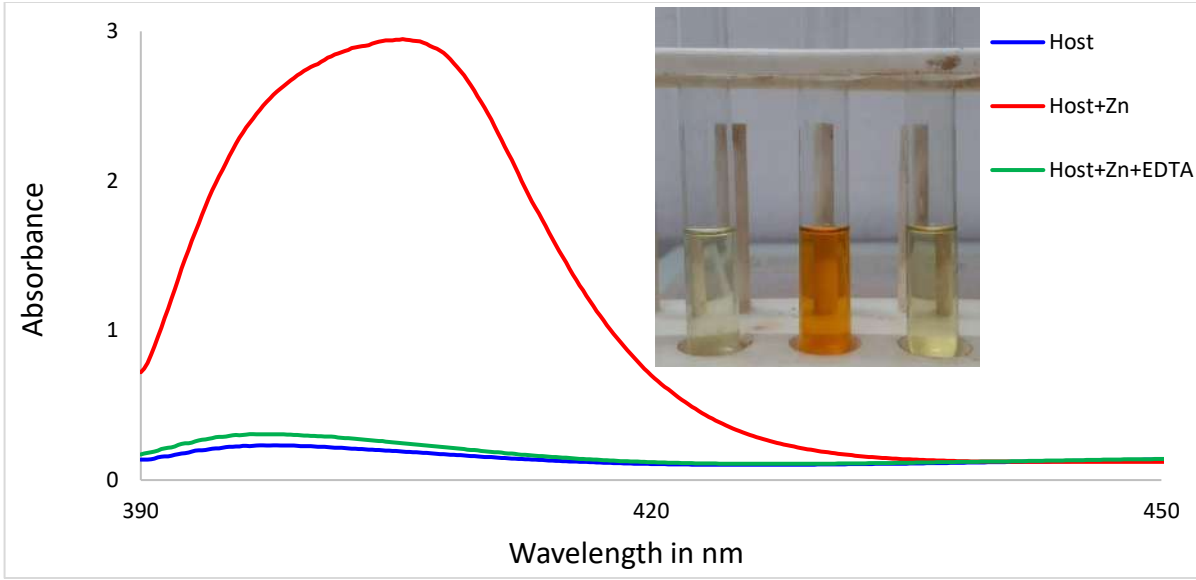

Fig. 8: a) Reversible cycle of R1 with Zn^{2+} and $EDTA^{2-}$, and b) graph of the reversible study, Inset figure capture of reversibility (R1, R1+Zn and R1+Zn+ EDTA).

ANALYTICAL APPLICATIONS

Recovery tests with real samples were done to assess the proposed colorimetric probe's selectivity, sensitivity, and reliability. Tap water and Mineral samples were taken from the industrial region of Bhusawal, Maharashtra, for the recovery tests. Zn^{2+} ions solutions with concentrations ranging from 10 to 25 $g.L^{-1}$ were introduced into the water samples. Table 2 showed that utilizing R1 resulted in better Zn^{2+} recoveries (> 97%) and lower percentage relative standard deviation (percent RSD) values (Cox et al. 2019, Bagheri et al. 2020, Zhou et al. 2014, Yang et al. 2019, Pendin et al. 2019, Yang 2019, Huang et al. 2019, Swami et al. 2018, Sargenti et al. 2014, Zhao et al. 2015, Kang et al. 2013).

CONCLUSIONS

Chemosensor R1 was made by condensation reaction between isoniazide and 2,5-dihydroxy benzaldehyde in methanol and analyzed using Spectro-analytical methods. The UV-Visible spectra of R1 revealed two peaks 396nm and n→Π* 396 nm transitions are assigned to the peak. In addition, the addition of Zn^{2+} ion solution to R1 produced a ratiometric spectrum pattern, other metal ions, however, had no effect. Because of the LMCT action, the addition of Zn^{2+} ion solution to R1 resulted in a red shift of the 396nm peak to 406 nm. The Zn^{2+}-R1 complex's association constant (Ka) was discovered to be $6795M^{-1}$ and $6836M^{-1}$ using Benesi-Hildebrand and Scatchard plots respectively. The 1:1 stoichiometry of Zn^{2+} and R1 having a detection limit (LOD) of 276 nM.

REFERENCES

An, R., Zhang, D., Chen, Y. and Cui, Y.Z. 2016. A "turn-on" fluorescent and a colorimetric sensor for selective detection of Cu^{2+} in aqueous media and living cells. Sensors Actuat. B Chem., 222: 48-54.

Atood, J., Davies, J., MacNicol, D. and Vogetle, F. 1996. Comprehensive Supramolecular Chemistry. Elsevier Exeter, The Netherlands.

Table 2: Results of a Real sample of Zn^{2+} sensing

Sample	Zn^{2+} added ($\mu g.L^{-1}$)	Zn^{2+} found ($\mu g.L^{-1}$) using R1	Recovery (%) by R1 (n=3)
Mineral water	10	9.86 ± 0.045	99.01
	15	13.99 ± 0.084	99.24
	25	24.72 ± 0.053	99.32
Tap water	10	9.89 ± 0.049	98.42
	15	14.71 ± 0.047	98.61
	25	24.71 ± 0.037	98.88

N = Number of samples.

Awad, I., Said, Nikolai I. Georgiev, Vladimir B. and Bojinov, A. 2019. Smart chemosensor: Discriminative multi-detection and various logic operations in aqueous solution at biological pH. Spectrochim. Acta A Mol. Biomol. Spectrosc., 223: 117304.

Bagheri, M. and Masoomi, M.Y. 2020. Sensitive ratiometric fluorescent metal-organic framework sensor for calcium signaling in human blood ionic concentration media. ACS Appl. Mater. Interfaces, 12(4): 4625-4631.

Benesi, H.A. and Hildebrand, J.H.J. 1949. A spectrophotometric investigation of the interaction of iodine with aromatic hydrocarbons. J. Am. Chem. Soc., 71(8): 2703-2707.

Berrones-Reyes, J.C., Muñoz-Flores, B.M., Cantón-Diáz, A.M., Treto-Suárez, M.A., Páez-Hernández, D., Schott, E., Zarate, X. and Jiménez-Pérez, V.M. 2019. Quantum chemical elucidation of the turn-on luminescence mechanism in two new Schiff bases as selective chemosensors of Zn^{2+}: Synthesis, theory and bioimaging applications. RSC Adv., 9(53): 30778-30789.

Bhosale, J., Fegade, U., Bondhopadhyay, B., Kaur, S., Singh, N., Basu, A., Dabur, R., Bendre, R. and Kuwar, A. 2015. Pyrrole-coupled salicylimine-based fluorescence "turn on" probe for highly selective recognition of Zn^{2+} ions in mixed aqueous media: Application in living cell imaging. J. Mol. Recog., 28(6): 369-375.

Cox, R.P., Sandanayake, S., Scarborough, D.L.A., Izgorodina, E.I., Langford, S.J. and Bell, T.D.M. 2019. Investigation of cation binding and sensing by new crown ether core substituted naphthalene diimide systems. New J. Chem., 43(4): 2011-2018.

De Silva, A.P., Gunaratne, H.N., Gunnlaugsson, T., Huxley, A.J., McCoy, C.P., Rademacher, J.T. and Rice, T.E. 1997. Signaling recognition events with fluorescent sensors and switches. Chem. Rev., 97(5): 1515-1566.

Diana, R., Panunzi, B., Tuzi, A., Piotto, S., Concilio, S., Caruso, U. 2019. An amphiphilic pyridinoyl-hydrazone probe for colorimetric and fluorescence pH sensing. Molecules 24(21): 3833-3855.

Dong, W.K., Akogun, S.F., Zhang, Y., Sun, Y.X. and Dong, X.Y, 2017. A reversible "turn-on" fluorescent sensor for selective detection of Zn^{2+}. Sensors Actuat. B Chem., 238: 723-734.

Fegade, U., Bhosale, J., Sharma, H., Singh, N., Bendre, R. and Kuwar, A. 2015a. Fluorescence chemosensor for HSO_4^- ion based on pyrrole-substituted salicylimine Zn^{2+} complex: Nanomolar detection. J. Fluoresc., 25(4): 819-824.

Fegade, U., Jethave, G., Attarde, S., Kolate, S., Inamuddin, Altalhi, T. and Kanchi, S. 2021a. statistical physics model of EBT adsorption on Pb (II) doped zinc oxide nanoparticles: Kinetics, isotherm and reuse study. Int. J. Environ. Anal. Chem., 16: 1-15.

Fegade, U., Jethave, G., Hong, W.G., Khan, I., Marwani, H.M., Wu, R.J. and Dhake, R. 2020. Multifunctional $Zn_{0.3}Al_{0.4}O_{4.5}$ crystals: An efficient photocatalyst for formaldehyde degradation and EBT adsorption. Arab. J. Chem., 13(11): 8262-8270.

Fegade, U., Kolate, S., Gokulakrishnan, K., Ramalingan, C., Altalhi, T. and Kanchi, S. 2021b. A selective ratiometric receptor 2-((E)-(3-(prop-1-en-2-yl) phenylamino) methyl)-4-nitrophenol for the detection of Cu^{2+} ions supported by DFT studies. J. Fluoresc., 31(3): 625-634.

Fegade, U., Patil, S., Kaur, R., Sahoo, S.K., Singh, N., Bendre, R. and Kuwar, A. 2015b. A novel chromogenic and fluorogenic chemosensor for the detection of trace water in methanol. Sensors Actuat. B. Chem., 210: 324-327.

Fegade, U., Sahoo, S.K., Singh, A., Mahulikar, P., Attarde, S., Singh, N. and Kuwar, A. 2014a. A selective and discriminating noncyclic receptor for HSO_4^- ion recognition. RSC Adv., 4(29): 15288-15292

Fegade, U., Saini, A., Sahoo, S.K., Singh, N., Bendre, R. and Kuwar, A. 2014b. 2, 2□-(Hydrazine-1, 2-diylidenedimethylylidene) bis (6-isopropyl-3-methylphenol) based selective dual-channel chemosensor for Cu^{2+} in semi-aqueous media. RSC Adv., 4(75): 39639-39644.

Fegade, U., Sharma, H., Singh, N., Ingle, S., Attarde, S. and Kuwar, A. 2014c. An amide-based dipodal Zn^{2+} complex for multinationals recognition: Nanomolar detection. J. Luminesc., 149: 190-195.

Fegade, U., Singh, A., Chaitanya, G.K., Singh, N., Attarde, S. and Kuwar, A. 2014d. Highly selective and sensitive receptor for Fe^{3+} probing. Spectrochim. Acta Part A Mol. Biomol. Spectrosc., 121: 569-574.

Fegade, U., Tayade, S., Chaitanya, G.K., Attarde, S. and Kuwar, A. 2014e. Fluorescent and chromogenic receptor bearing amine and hydroxyl functionality for iron (III) detection in aqueous solution. J. Fluoresc., 24(3): 675-681.

Gangatharan, Vinoth Kumar Gujuluva, Kesavan Mookkandi Palsamy, Sivaraman Gandhi, Annaraj Jamespandi, Anitha Kandasamy, Tamilselvi Arunachalam, Athimoolam Shenmuganarayanan, Sridhar Balasubramaniyam, and Rajesh Jegathalaprathaban. 2018. Reversible NIR fluorescent probes for Cu^{2+} ions detection and its living cell imaging. Sensors and Actuators B: Chemical, 255: 3235-3247.

Ghorai, P., Banerjee, S., Nag, D., Mukhopadhyay, S.K. and Saha, A. 2019. Design and synthesis of a novel fluorescent-colorimetric chemosensor for selective detection of Zn (II) and Cu (II) ions with applications in live cell imaging and molecular logic gate. J. Luminesc., 205: 197-209.

Ghosh, U., Bag, S.S. and Mukherjee, C. 2017. Bis-pyridobenzene as a fluorescence light-up sensor for Hg2+ Ion in water. Sensors Actuat. B. Chem., 238: 903-907.

Gu, Y.Q., Shen, W.Y., Mi, Y., Jing, Y.F., Yuan, J.M., Yu, P., Zhu, X.M. and Hu, F.L. 2019. Dual-response detection of Ni^{2+} and Cu^{2+} ions by a pyrazolopyrimidine-based fluorescent sensor and the application of this sensor in bioimaging. RSC Adv., 9(61): 35671-35676.

Guan, J., Tu, Q., Chen, L., Yuan, M.S. and Wang, J. 2019. A benzothiazole-rhodol based luminophor: ESIPT-induced AIE and an application for detecting Fe^{2+} ion. Spectrochim. Acta Part A Mol. Biomol. Spectrosc., 220: 117114.

Huang, M.X., Lv, C.H., Huang, Q.D., Lai, J.P. and Sun, H. 2019. A novel and fast responsive turn-on fluorescent probe for the highly selective detection of Cd^{2+} based on photo-induced electron transfer. RSC Adv., 9(62): 36011-36019.

Jung, J.M., Yun, D., Lee, H., Kim, K. and Kim, C. 2019. Selective chemosensor capable of sensing both CN– and Zn^{2+}: Its application to zebrafish. Sensors Actuat. B Chem., 297: 126814

Jethave, G. and Fegade, U. 2018. Design and synthesis of $Zn_{0.3}Fe_{0.45}O_3$ nanoparticle for efficient removal of congo red dye and its kinetic and isotherm investigation. Int. J. Ind. Chem., 9(1): 85-97.

Jethave, G., Attarde, S., Fegade, U., Altalhi, T., Kanchi, S., Ingle, S. and Dhake, R. 2021. Statistical modeling and interpretation of sono-assisted adsorption mechanism of crystal violet dye on FeTiPbO nanocomposite. J. Mol. Liq., 340: 116878.

Jethave, G., Fegade, U., Attarde, S. and Ingle, S. 2019. Decontamination study of eriochrome Black-T from wastewater by using AlTiPbO nanoparticles (ATPO-NPs) for a sustainable clean environment. J. Water Environ. Nanotechnol., 4: 263-274.

Kang, J., Kang, H.K., Kim, H., Lee, J., Song, E.J., Jeong, K.D., Kim, C. and Kim, J. 2013. Fluorescent chemosensor based on bispicolylamine for selective detection of magnesium ions. Supramol. Chem., 25(2): 65-68.

Kaur, N., Kaur, G., Fegade, U.A., Singh, A., Sahoo, S.K., Kuwar, A.S. and Singh, N. 2017. Anion sensing with chemosensors having multiple NH recognition units. TrAC Trends Anal. Chem., 95: 86-109.

Khan, M.S., Al-Senaidy, A.M., Priyadarshini, M., Shah, A. and Bano, B. 2013. Different conformation of thiol protease inhibitor during amyloid formation: Inhibition by curcumin and quercetin. J. Fluoresc., 23(3): 451-457.

Khanna, Kanika, Vijay Lakshmi Jamwal, Anket Sharma, Sumit G. Gandhi, Puja Ohri, Renu Bhardwaj, Asma A. Al-Huqail, Manzer H. Siddiqui, Najat Marraiki, and Parvaiz Ahmad. 2019. Evaluation of the role of rhizobacteria in controlling root-knot nematode infection

in Lycopersicon esculentum plants by modulation in the secondary metabolite profiles. AoB Plants, 11(6): 69.

Khanra, S., Ta, S., Ghosh, M., Chatterjee, S. and Das, D. 2019. Subtle structural variation in azine/imine derivatives controls Zn^{2+} sensitivity: ESIPT-CHEF combination for nano-molar detection of Zn 2+ with DFT support. RSC Adv., 9(37): 21302-21310.

Kolate, S., Patil, N., Phalak, R., Waghulde, G.P., Patil, C.J., Dhake, R.B. and Fegade, U. 2020. Colorimetric" off-on" probe for Cu^{2+} nanomolar detection in aqueous solution. J. Adv. Sci. Res., 11: 112-136.

Kumar, G.G.V., Kesavan, M.P., Tamilselvi, A., Rajagopal, G., Raja, J. D., Sakthipandi, K., Rajesh, J. and Sivaraman, G. 2018. A reversible fluorescent chemosensor for the rapid detection of Hg^{2+} in an aqueous solution: It is logic gates behavior. Sensors Actuat. B Chem., 273: 305-315.

Kuwar, A., Fegade, U., Tayade, K., Patil, U., Puschmann, H., Gite, V., Dalal, D. and Bendre, R. 2013. Bis(2-Hydroxy-3-Isopropyl-6-Methyl-Benzaldehyde) ethylenediamine: A novel cation sensor. J Fluoresc., 23: 859-864.

Lehn, J.M. 1995. Supramolecular Chemistry. Wiley and Sons, NJ.

Li, S., Cao, D., Hu, Z., Li, Z., Meng, X., Han, X. and Ma, W. 2019. A chemosensor with a paddle structure based on a BODIPY chromophore for sequential recognition of Cu^{2+} and HSO_3^-. RSC Adv., 9(59): 34652-34657.

Maniyazagan, M., Mariadasse, R., Jeyakanthan, J., Lokanath, N.K., Naveen, S., Premkumar, K., Muthuraja, P., Manisankar, P. and Stalin, T. 2017. Rhodamine-based "turn–on" molecular switch FRET–sensor for cadmium and sulfide ions and live cell imaging study. Sensors Actuat. B Chem., 238: 565-577.

Mao, X., Su, H., Tian, D., Li, H. and Yang, R. 2013. Bipyrene-functionalized graphene as a "Turn-On" fluorescence sensor for manganese (II) ions in living cells. ACS Appl. Mater. Interfaces, 5(3): 592-597.

Meng, X., Cao, D., Hu, Z., Han, X., Li, Z. and Ma, W. 2018. A highly sensitive and selective chemosensor for Pb^{2+} based on quinoline–coumarin. RSC Adv., 8(59), pp.33947-33951.

Naha, S., Wu, S.P. and Velmathi, S. 2020. Naphthalimide-based smart sensor for CN^-/Fe^{3+} and H_2S. Synthesis and application in RAW264. 7 cells and zebrafish imaging. RSC Adv., 10(15): 8751-8759.

Panunzi, B., Diana, R., Concilio, S., Sessa, L., Tuzi, A., Piotto, S. and Caruso, U. 2019. Fluorescence pH-dependent sensing of Zn (II) by a tripodal ligand. A comparative X-ray and DFT study. J. Luminesc., 212: 200-206.

Park, G.J., Na, Y.J., Jo, H.Y., Lee, S.A. and Kim, C. 2014. A colorimetric organic chemo-sensor for Co^{2+} in a fully aqueous environment. Dalton Trans., 43(18): 6618-6622.

Patil, N., Dhake, R.B., Fegade, U., Gokulakrishnan, K., Ramalingan, C., Inamuddin, Altalhi, T. and Kanchi, S. 2021. N'-(4-(diethylamino)-2-hydroxybenzylidene) isonicotinohydrazide based chemosensor for nanomolar detection of Ni (II) ion. Int. J. Environ. Anal. Chem., 10: 1-17.

Patil, N.S., Dhake, R.B., Ahamed, M.I. and Fegade, U. 2020. A mini-review on organic chemosensors for cation recognition (2013-19). J. Fluoresc., 30(6): 1295-1330.

Patil, R., Fegade, U., Kaur, R., Sahoo, S.K., Singh, N. and Kuwar, A. 2015. Highly sensitive and selective determination of Hg^{2+} by using 3-((2-(1H-benzo [d] imidazol-2-yl) phenylimino) methyl) benzene-1, 2-diol as fluorescent chemosensor and its application in the real water sample. Supramol. Chem., 27(7-8): 527-532.

Patil, S., Fegade, U., Sahoo, S.K., Singh, A., Marek, J., Singh, N., Bendre, R. and Kuwar, A. 2014. Highly sensitive ratiometric chemosensor for selective naked-eye nanomolar detection of Co^{2+} in semi-aqueous media. Chem. Phys. Chem., 15(11): 2230-2235.

Patil, S., Patil, R., Fegade, U., Bondhopadhyay, B., Pete, U., Sahoo, S.K., Singh, N., Basu, A., Bendre, R. and Kuwar, A. 2015. A novel phthalazine based highly selective chromogenic and fluorogenic chemosensor for Co^{2+} in semi-aqueous medium: application in cancer cell imaging. Photochem. Photobiol. Sci., 14(2): 439-443.

Pawar, S., Fegade, U., Bhardwaj, V.K., Singh, N., Bendre, R. and Kuwar, A. 2015. 2-((E)-(2-aminophenylimino) methyl)-6-isopropyl-3-methylphenol based fluorescent receptor for dual Ni^{2+} and Cu^{2+} recognition: Nanomol. Detect. Polyhed., 87: 79-85.

Pendin, D., Norante, R., De Nadai, A., Gherardi, G., Vajente, N., Basso, E., Kaludercic, N., Mammucari, C., Paradisi, C., Pozzan, T. and Mattarei, A. 2019. A synthetic fluorescent mitochondria-targeted sensor for ratiometric imaging of calcium in live cells. Angewan. Chem., 131(29): 10022-10027.

Sargenti, A., Farruggia, G., Malucelli, E., Cappadone, C., Merolle, L., Marraccini, C., Andreani, G., Prodi, L., Zaccheroni, N., Sgarzi, M. and Trombini, C. 2014. A novel fluorescent chemosensor allows the assessment of intracellular total magnesium in small samples. Analyst, 139(5): 1201-1207.

Scatchard, G.D. 1949. The attractions of proteins for small molecules and ions. Ann. NY Acad. Sci., 51: 660-672.

Swami, S., Agarwala, A., Behera, D. and Shrivastava, R. 2018. Diaminomaleonitrile-based chromo-fluorescent receptor molecule for selective sensing of Mn (II) and Zn (II) ions. Sensors Actuat. B Chem., 260: 1012-1017.

Tayade, K., Bondhopadhyay, B., Sharma, H., Basu, A., Gite, V., Attarde, S., Singh, N. and Kuwar, A., 2014. "Turn-on" fluorescent chemosensor for zinc (ii) dipodal ratiometric receptor: application in live cell imaging. Photochemical & Photobiological Sciences, 13(7): 1052-1057.

Xu, J., Yang, Y., Baigude, H. and Zhao, H. 2019. New ferrocene–triazole derivatives for multisignaling detection of Cu^{2+} in aqueous medium and their antibacterial activity. Spectrochim. Acta Part A Mol. Biomol. Spectrosc., 229: 117880.

Xu, K., Li, Y., Si, Y., He, Y., Ma, J., He, J., Hou, H. and Li, K. 2018. A "turn-on" fluorescent chemosensor for the detection of Hg (II) in buffer-free aqueous solution with excellent selectivity. J. Luminesc., 204: 182-188.

Yan, R., Wang, Z., Du, Z., Wang, H., Cheng, X. and Xiong, J. 2018. A biomimetic fluorescent chemosensor for highly sensitive zinc (II) detection and its application for cell imaging. RSC Adv., 8(58): 33361-33367.

Yang, M., Chae, J.B., Kim, C. and Harrison, R.G. 2019. A visible chemosensor based on carbohydrazide for Fe (II), Co (II), and Cu (II) in an aqueous solution. Photochem. Photobiol. Sci., 18(5): 1249-1258.

Yang, X., Wang, Y., Liu, R., Zhang, Y., Tang, J., Yang, E.B., Zhang, D., Zhao, Y. and Ye, Y. 2019. A novel ICT-based two-photon and NIR fluorescent probe for labile Fe^{2+} detection and cell imaging in living cells. Sensors Actuat. B Chem., 288: 217-224.

Zhang, Q., Ma, R., Li, Z. and Liu, Z. 2020. A multi-responsive crown ether-based colorimetric/fluorescent chemosensor for highly selective detection of Al^{3+}, $Cu^{2+,}$ and Mg^{2+}. Spectrochim. Acta Part A Mol. Biomol. Spectrosc., 228: 117857.

Zhang, Y., Li, H., Gao, W. and Pu, S. 2019a. Dual recognition of Al^{3+} and Zn^{2+} ions by a novel probe based on diarylethene and its application. RSC Adv., 9(47): 27476-27483.

Zhang, Y., Zhang, C., Wu, Y., Zhao, B., Wang, L. and Song, B. 2019b. A novel water-soluble naked-eye probe with a large Stokes shift for selective optical sensing of Hg^{2+} and its application in water samples and living cells. RSC Adv., 9(40): 23382-23389.

Zhao, B., Xu, Y., Fang, Y., Wang, L. and Deng, Q. 2015. Synthesis and fluorescence properties of phenanthrene [9, 10-d] imidazole derivative for Ag^+ in aqueous media. Tetrahed. Lett., 56(19): 2460-2465.

Zhou, J.R., Liu, D.P., He, Y., Kong, X.J., Zhang, Z.M., Ren, Y.P., Long, L.S., Huang, R.B. and Zheng, L.S. 2014. A highly selective colorimetric chemosensor for cobalt (II) ions based on a tripodal amide ligand. Dalton Trans., 43(30): 11579-11586.

Nature Environment and Pollution Technology
An International Quarterly Scientific Journal

p-ISSN: 0972-6268
(Print copies up to 2016)
e-ISSN: 2395-3454

Vol. 21 | No. 5 (Suppl) | pp. 2241-2248 | 2022

Original Research Paper

https://doi.org/10.46488/NEPT.2022.v21i05.018

Open Access Journal

Estimation of Soil Contamination with Heavy Metals in the Streets of Al-Diwaniyah City in Al-Qadisiyah Governorate, Iraq

Kawthar Hassan Obayes
Department of Physics, College of Education, University of Al-Qadisiyah, Qadisiyah Governorate, Iraq
†Corresponding author: Kawthar Hassan Obayes; kawthar.aljelehawy@qu.edu.iq

Nat. Env. & Poll. Tech.
Website: www.neptjournal.com

Received: 25-06-2022
Revised: 21-07-2022
Accepted: 30-07-2022

Key Words:
Heavy metals
Al-Diwaniyah city
Soil contamination
Human health

ABSTRACT

This study aims to calculate the contamination levels of the elements (Pb, Cr, Ni and Cd) in soil samples taken from the Iraqi city of Al-Diwaniyah in the Al-Qadisiyah Governorate. Twenty samples of dust collected between the street and the sidewalk were collected for some areas of Al-Diwaniyah city, and then analyses were conducted to determine the concentrations of toxic and carcinogenic elements with the global determinants. The study's findings revealed that there were very high concentrations of heavy metals compared to the internationally permissible limits, where the highest concentration of lead and chromium was in Main Street - Al-Asry District (112.6 ppm) and (115.1 ppm), respectively, and the lowest concentration of them was in Health Center Street - Al-Furat District (15.8 ppm) and (48.8 ppm), respectively, where the lowest lead value exceeded the internationally permitted limits and the lowest chromium value fell below the permissible limit. As for nickel and cadmium, the highest values of nickel and cadmium appeared in Main Street - Eastern Republican District which amounted to (135.2 ppm) and (2ppm), respectively, which is significantly greater than the internationally permissible limit, while the lowest values appeared in University Street - University District, which is (3.6 ppm) (0.05 ppm) respectively, which is less than the internationally permissible limit. It is noted from the results obtained that high rates of heavy metals concentrations in the soil samples of Al-Diwaniyah City indicate that the main factor in this rise is pollution caused by human activities, and the reason for this is due to the effect of vehicle launchers and some launchers of workshops and factories, as well as its presence in sand-laden dust of various sources. This rise might have an effect on the environment and human health at all of the selected sites.

INTRODUCTION

Heavy metals are natural elements from the Earth's crust that cannot be decomposed or broken down to a small degree. They enter the human body through air, food, and drinking water (Ibe et al. 2018). Some heavy metals are necessary for the human body, however, an increase in their concentration leads to poisoning (Al-Jaberi 2014). Exposed soils in many regions of the world pollute toxic heavy metals as a result of human activity in many fields, especially in industry, agriculture, and addition phosphate fertilizers, manufacturing, mining, and waste disposal. These activities are a significant source of the heavy metal-laden particles that pollute the air (Al-Dabbas et al. 2018). These particles are deposited directly on the surface of the soil or other surfaces, as rain washes them and transfers them to dissolved or suspended water, and ultimately to the soil (Banjanac et al. 2006). The sources of other pollution with heavy metals and important human activity in the sewage disposal plants water, reflected this pollution problem when using soil contaminated for food production by crop plants as easy to enter these elements in the food chain, which increases the risk to human health (Salman et al. 2021). Metal and semi-metal ions are environmental pollutants resulting from industrial human activity such as mining, metal smelting, internal combustion machine exhaust, petroleum production, dyes, and their waste, agricultural applications (fertilizers and pesticides), sewage, waste disposal, and others (Muhammad et al. 2021). The problem lies in the ions of these heavy elements (metals and metalloids). When available in high concentrations, they are toxic to humans and other organisms, even though some of this is necessary for living things in small concentrations (Jaradat & Momani 1999). When the concentration of these elements is high in the soil solution, they may seep into the surface and groundwater or be absorbed by plants, and then enter the food web and directly or indirectly be absorbed by humans or animals. Numerous elements are present in these metals, some of which are known for their physiological role in plants, such as copper (Cu), cobalt (Co), iron (Fe), nickel (Ni)

and zinc (Zn). Among them are those whose physiological function is not known, such as cadmium (Cd), lead (Pb), selenium (Se), aluminum (Al), mercury (Hg), chromium (Cr), arsenic (As), and others (Al-Khashman 2007). It can be said that pollution with these heavy elements is one of the biggest problems at present for soils and water sources (Aydin et al. 2012). The study seeks to compare the results with the internationally permitted limits by measuring the concentrations of (Pb, Cr, Ni, and Cd) in soil samples taken from Al-Diwaniyah city in Al-Qadisiyah Governorate, Iraq.

THE HEAVY METALS

Lead (Pb)

Lead is one of the elements that must be monitored continuously due to its high danger to humans and the environment. Continuous and regular exposure to lead leads to mental retardation. This element may accumulate in the bones and does not remain there all the time. It is transmissible through the bloodstream and may pass, for example, to the fetus through the placenta in pregnant women. It may also come out dissolved in the mother's milk for her newborn (Arifin et al. 2015). Long exposure to lead or one of its compounds leads to lower levels of intelligence, and an increase in lead level can lead to miscarriage, infertility, hormonal changes, menstrual disorders, and delayed puberty (Borošová & Klöslová 2006).

Chrome (Cr)

Inhalation of chromium-containing dust produced by laboratories leads to severe damage to the nasal tissue, which leads to perforation of the nasal septum. Chromium fumes are harmful as they cause asthma, shortness of breath, and coughing and lead to pneumonia. Inhalation of large quantities of chromium dust leads to the occurrence of lung tumors (Ferreira-Baptista & De Miguel 2005). Eating foods containing high concentrations of chromium leads to stomach cancer (Ferreira-Baptista & De Miguel 2005). Also, skin contact with chromium for a long time leads to itching (allergy in the skin), which leads to skin redness, and the appearance of a rash on it similar to eczema (Gowd et al. 2010).

Nickel (NI)

Found on a large scale in the environment, the natural sources of nickel are volcanic dust emissions, erosion of rocks and dust, burning of fuel, emissions during mining and refining processes, and consumption of large quantities of nickel-containing products inevitably lead to environmental pollution (Tapsoba et al. 2009). The most significant sources of this element's pollution are landfills, which contaminate groundwater, and acid rain, which raises the concentration of this element in the soil and then the groundwater, which increases the consumption of this element by microbes, plants, and animals. Exposure to nickel occurs through inhalation and ingestion are the most common cases among workers in the metallurgical industry. Epidemiological studies show an increase in mortality rates among refinery workers from cancer in the lung and sinuses, and chronic exposure to dust and nickel fumes is associated with smelting, welding, and the oil refining industry (Tapsoba et al. 2009).

Cadmium (Cd)

Cadmium is one of the most dangerous elements, toxic to humans and animals. Cadmium is found in all natural soils, which is very low, not exceeding a maximum of one part per million. Industrial development has led to the pollution of soil, water, air, and plants with this element, and it results from various industries that throw their waste into the surrounding environment without treatment. Studies reveal a significant concentration of cadmium in soils close to industrial facilities that discharge this element into the environment, whether by chimney nozzles discharging gases or dust that can poison people and animals. The risk of this element to the human body comes from the fact that it can accumulate in key organs and tissues and that the excretion process for it can be nearly nonexistent (Morais et al. 2012).

MATERIALS AND METHODS

Twenty soil samples were collected from some areas of Al-Diwaniyah city in Al-Qadisiyah Governorate, Iraq (Fig. 1), distributed over industrial, commercial, residential, and traffic areas. The samples were taken from the dust collected between the street and the sidewalk and kept inside nylon bags equipped with a special modeling form for each area, including the sample number, the name of the area, information about the nature of the area, the movement of transportation and the coordinates of the site shown in (Table 1). Then the samples were prepared for the final analysis according to the Jackson method, where the sample was crushed and placed in a beaker washed with distilled water and dried, and placed in the oven at a temperature of (100°C) for 2h utilizing a delicate balance and a beaker with a capacity of, for drying the dried sample (250 mm). The sample was then digested by adding (15 mL) of acid HCl and (5 mL) of concentrated nitric acid HNO3 to the sample. The sample was then placed in a sand bath at a temperature of (200-225) for (45-60) min, after which the beaker was cooled to laboratory temperature and added (5 mL) of acid HCL and heated in a sand bath until dryness, where this stage took about (10-15)

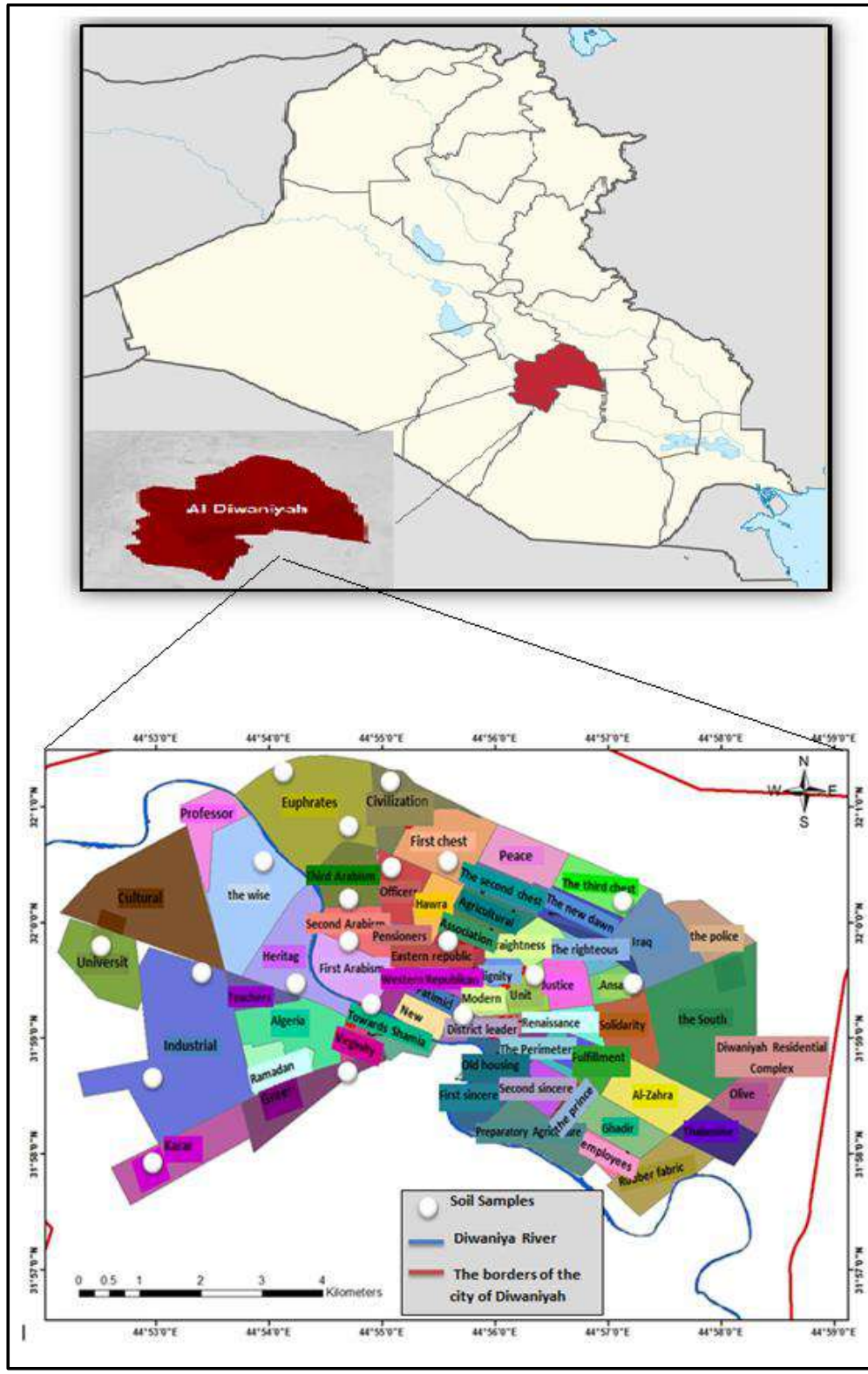

Fig. 1: Iraqi map with sampling locations from Al-Diwaniyah city.

Table 1: The regions for collecting samples in the streets of Al-Diwaniyah city.

Sample No.	Area name	Nature of the area	Transportation movement	Coordinates X	Coordinates Y
S1	University Street / University District	Residential + Commercial	High	44°52’25”	31°59’39”
S2	Al-Jawahiri Street / Al-Hakim District	Residential + Commercial	High	44°53’42”	32°0’17”
S3	Al-Gomhoria School Street / Al-Askari District	Residential + Commercial	High	44°55’22”	32°0’47”
S4	College of Medicine Street / Al-Furat District	Traffic	High	44°54’37”	32°0’59”
S5	Main Street / Eastern Republican District	Old residential + commercial + industrial (blacksmith shops)	High	44°55’42”	31°59’33”
S6	Main Street / Al Wahda District	Residential + Industrial (Black-smith shops)	High	44°56’16”	31°59’35”
S7	General Teaching Hospital Street / Al-Orouba Third District	Traffic	High	44°55’14”	32°0’52”
S8	Maternity Hospital Street / Al-Orouba District	Traffic	High	44°54’44”	31°59’29”
S9	Main Street / Industrial District	Industrial (auto repair shops)	High	44°53’9”	31°58’58”
S10	Main Street/ Al-Hadara District	Residential + Industrial (fuel filling station + ice lab)	High	44°55’5”	32°0’58”
S11	Al-Qadisiyah Filling Station Street / Al-Sadiq District	Traffic	High	44°56’4”	31°58’37”
S12	Health Center Street / Al-Furat District	residential	medium	44°54’37”	32°0’59”
S13	Main Street - Al-Asry District	Residential + Industrial (gas filling station + ice lab + black-smith shops)	High	44°55’54”	31°59’21”
S14	Al Thawra Street - Sob Al Shamiya District	Residential + commercial + industrial (car repair shops + gas station + blacksmith shops)	High	44°55’10”	31°59’7”
S15	Old Camp Street - Al-Karar District	Residential + Industrial (car repair shops + blacksmith shops)	High	44°52’47”	31°57’57”
S16	Car Showroom Street - Industrial District	Industrial (car repair shops + gas filling station)	High	44°53’18”	31°59’7”
S17	Main Street/ Officers District	Traffic	High	44°55’9”	32°0’10”
S18	Al-Saah Square Street / Al-Adaria District	Traffic	High	44°54’44”	31°59’9”
S19	Algeria Street - Algeria District	Residential + Commercial	High	44°54’9”	31°58’57”
S20	City Street - New District	Old residential + commercial + industrial (car repair shops + blacksmith shops)	High	44°55’22”	31°59’23”

minutes. Then the beaker was cooled and (5 ml) of HCL acid and (50 ml) of hot distilled water were added to wash the sides of the beaker from the traces of the sample. Then heat the mixture to boiling point for 2-3 minutes. Then the filtration was done with filter paper, where the filtrate was placed in a volumetric vial with a capacity of (100 mL). The insoluble precipitate was washed with distilled water, the washing water was added to the filtrate, and the volume was completed to 100 mL (Al-Dabbas et al. 2018), and then sent for analysis by atomic absorption spectrometer in the service laboratory of the Department of Biology, College of Science/University of Baghdad.

RESULTS AND DISCUSSION

The concentrations of (Pb, Cr, Ni, Cd) were calculated in soil samples for the streets of Al-Diwaniyah city in Al-Qadisiyah Governorate, Iraq using atomic absorption spectroscopic device after conducting geochemical analyzes on all samples, where the calculations and statistical equations

were performed within the values and concentrations that were obtained for the elements. The concentration rates of lead, chromium, nickel, and cadmium in the soil of some streets of Al-Diwaniyah city reached (59.04 ppm) (83.075 ppm) (58.515 ppm), and (0.579 ppm), respectively, as shown in (Table 2).

Lead (Pb)

The results of the research showed that the concentration of this element in the soil in some selected sites from Al-Diwaniyah city in Al-Qadisiyah Governorate, Iraq were higher than the internationally permissible limit. The general

Table 2: Concentrations of heavy metals in units (ppm) in soil samples for the streets of Al-Diwaniyah city.

Sample No.	Pb	Cr	Ni	Cd
S1	20.3	66.7	3.6	0.05
S2	29.5	78.3	15.7	0.12
S3	18.9	61.2	8.9	0.09
S4	38.0	78.2	16.7	0.20
S5	88.7	95.3	135.2	2.00
S6	98.2	103.0	49.0	0.33
S7	18.6	60.6	54.4	0.70
S8	27.5	75.3	56.0	0.72
S9	63.5	88.7	82.2	0.60
S10	110.2	109.5	65.2	0.65
S11	32.8	70.3	45.9	0.60
S12	15.8	48.8	64.9	0.55
S13	112.6	115.1	67.6	0.70
S14	97.7	102.3	88.2	0.40
S15	93.8	99.5	59.0	0.82
S16	88.3	95.1	98.5	1.60
S17	60.2	85.9	62.5	0.30
S18	50.4	70.3	43.8	0.25
S19	37.3	73.5	54.3	0.40
S20	78.5	83.9	98.7	0.50
Average	59.04	83.075	58.515	0.579
World average (Lindsay 1979)	10	100	40	0.5

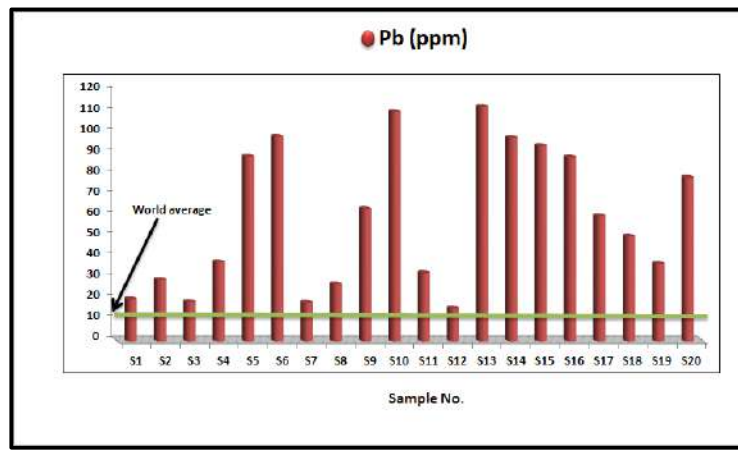

Fig. 2: Pb concentration in soil samples selected from Al-Diwaniyah city.

average of lead concentration in the soil of Al-Diwaniyah city areas according to the results of the current study was (59.04 ppm) when compared with the global average concentration of lead in unpolluted soils (10 ppm) (Lindsay 1979). The concentration of lead exceeded the normal rate by nearly (5 times), as shown in (Fig. 2). This rise is evident in the industrial areas if the results are compared to the natural rate of lead concentrations in uncontaminated soil, as these areas contain many factories such as the ice factory and the Al-Kashi factory, as well as containing electric power plants, blacksmithing workshops, and vehicle repair workshops of various kinds. In addition, it can be considered that heavy traffic in these areas is the second main cause of lead pollution in these areas. The more factories there are in the region, the more vehicles, cars, and various means of transportation move, and this, in turn, releases large amounts of burnt fuel exhaust containing lead compounds added to tetraethyl lead (Steinbock 1979).

Chromium (Cr)

The results showed that the average concentration of chromium in soil samples selected from Al-Diwaniyah city was (83.075 ppm) less than the internationally permissible rate (Lindsay 1979). However, its concentrations exceeded the permissible limit globally in some areas, including (S6, S10, S13, and S14) which are shown in (Fig. 3). These areas are considered industrial because they contain car repair workshops, paint shops, car garages, gas filling plant, and the widespread use of electric power generators.

Industrial wastes and emitted gases and vapors release chromium into the air and then deposit it on the surface of the soil. As for residential areas and commercial areas, the concentration of chromium is less than the permissible limit, because these areas are considered free from the reasons and factors mentioned previously that helped the high concentration of the chromium in the environment (Muhammad et al. 2020).

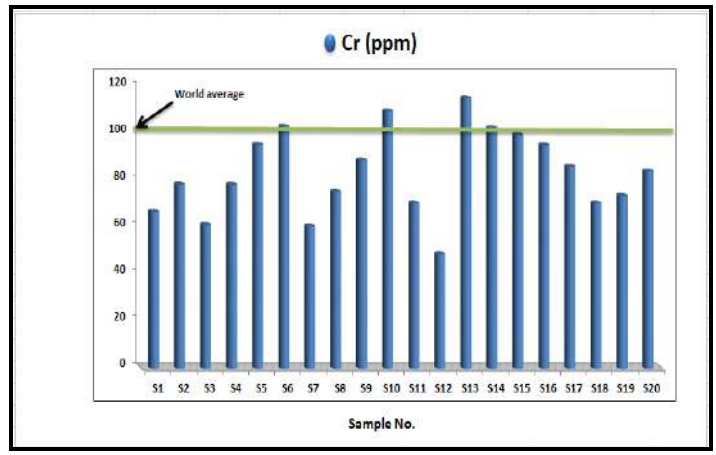

Fig .3: Cr concentration in soil samples selected from Al-Diwaniyah city.

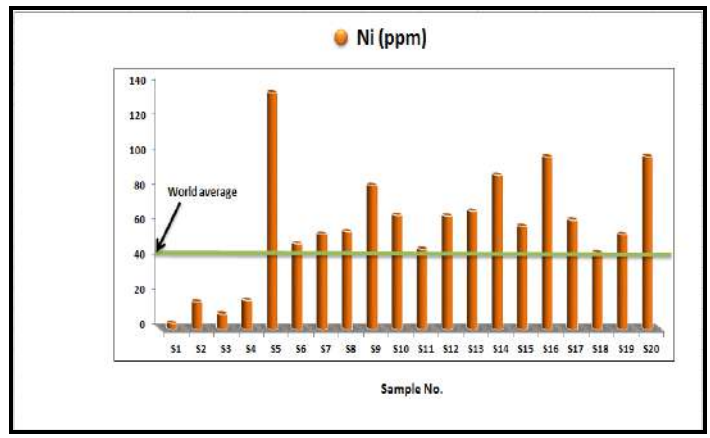

Fig .4: Ni concentration in soil samples selected from Al-Diwaniyah city.

Nickel (Ni)

It was noted through the results of this research that the average concentration of this element in soil samples selected from Al-Diwaniyah city exceeded the permissible limits globally (Lindsay 1979), which amounted to (58.515 ppm) as shown in Fig. 4. This is because the areas contain a gas and fuel filling plant and the frequent use of electric power generators. As used fuel burns, a high concentration of elements, including nickel, is released into the atmosphere and deposits itself on the soil's surface as smoke. The direct dumping of sewage and household waste into the soil increases the concentrations of heavy metals in the soil because sewage water contains high amount of nickel. This is another major factor that led to the high concentrations of nickel in the study area. Hence, the main cause of pollution with this element is the presence of factories, electric power plants, sewage water, and household wastes (Muhammad et al. 2020).

Cadmium (Cd)

Through the results of the research, it was found that the concentration of this element in soil samples selected from Al-Diwaniyah city in many areas has exceeded the permissible limit globally (Lindsay 1979), as shown in Fig. 5. One of the reasons for the increase in the concentration of cadmium in the soil is the burning of plastic materials, as these combustion products increase the concentration cadmium in the atmosphere and then its deposition in the soil. Fuel combustion (during vehicle movements and transportation) increases the concentration of cadmium in the atmosphere and then it is also deposited on the surface of the soil. The direct dumping of sewage and household waste into the soil, as well as the byproducts of fuel combustion in electric power generators, both contribute to an increase in the concentration of cadmium (Arifin et al. 2015).

CONCLUSIONS

Through the results of the research, very high concentrations of heavy metals were found in soil samples selected from the city of Al-Diwaniyah in Al-Qadisiyah Governorate, Iraq. Whereas the results indicated that lead concentration values (Pb) exceeded the internationally recognized limit, most concentrations of chromium, nickel, and cadmium (Cr, Ni, Cd) exceeded the permitted levels. The reason is due to the presence of a gas filling plant, an ice plant, a Kashi factory, blacksmith shops, and car repair workshops that dump their industrial waste directly into the soil, as well as crowding the streets with vehicles, which are the main pollutant with lead because the gasoline supplied to vehicles contains additives such as (tetraethyl lead and tetramethyl lead). Also, the practice of dumping domestic waste directly into the ground, which when it decomposes raises the concentrations of elements in the soil and sewage that contains high concentrations of elements, are contributing factors. To reduce pollution with heavy metals, quick solutions must be developed for traffic jams, which have become a major

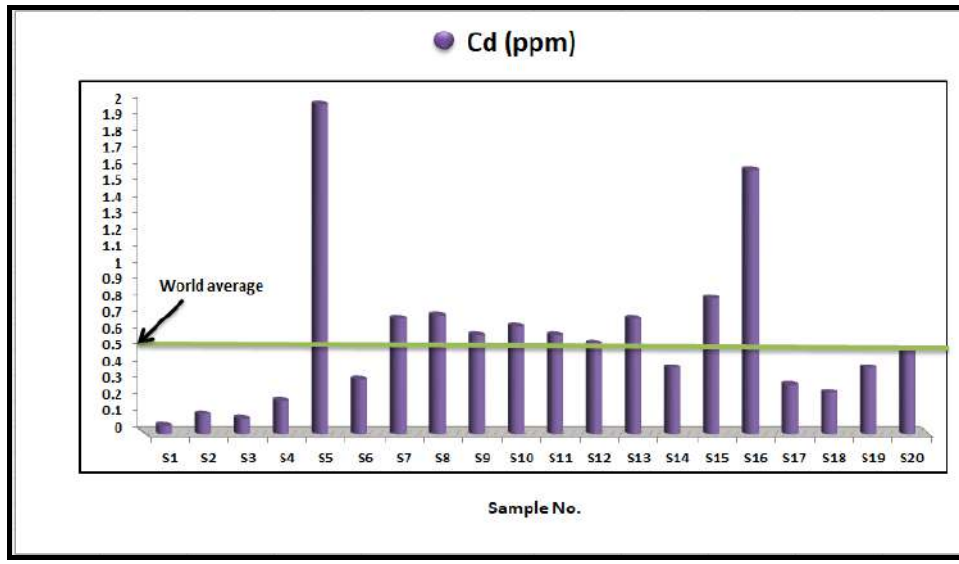

Fig. 5: Cd concentration in soil samples selected from Al-Diwaniyah city.

problem as a result of the increase in the number of vehicles and means of transport in recent years. Additionally, it is important to measure the percentage of emissions emitted from the exhaust of these vehicles, and conduct a study of the use of unleaded gasoline, and replace the lead added to gasoline with less toxic substances and damage to the public the environment.

ACKNOWLEDGEMENTS

The author would like to thank workers in the service laboratory of the Department of Biology, College of the Science/University of Baghdad. for his help in accomplishing this study.

REFERENCES

Al-Dabbas, M.A., Mahdi, K.H., Al-Khafaji, R. and Obayes, K.H. 2018. Heavy metals characteristics of settled particles of streets dust from Diwaniyah City-Qadisiyah Governorate-Southern Iraq. J. Phys. Conf. Ser., 1003(1): 12023.

Al-Jaberi, M.H.A. 2014. Heavy metals characteristics of settled particles during dust storms in Basrah city-Iraq. J. Phys. Conf. Ser., 3(10): 14-18.

Al-Khashman, O.A. 2007. The investigation of metal concentrations in street dust samples in Aqaba city, Jordan. Environ. Geochem. Health, 29(3): 197-207.

Arifin, Y.I., Sakakibara, M. and Sera, K. 2015. Impacts of artisanal and small-scale gold mining (ASGM) on the environment and human health of Gorontalo Utara Regency, Gorontalo Province, Indonesia. Geosciences, 5(2): 160-176.

Aydin, F., Aydin, I., Erdogan, S., Akba, O., Isik, B. and Hamamci, C. 2012. Chemical characteristics of settled particles during a dust storm. Pol. J. Environ. Stud., 21(3): 65.

Banjanac, R., Dragić, A., Grabež, B., Joković, D., Markushev, D., Panić, B. and Aničin, I. 2006. Indoor radon measurements by nuclear track detectors: Applications in secondary schools. Facta Univ. Ser. Phys. Chem. Technol., 4(1): 93-100.

Borošová, D. and Klöslová, Z. 2006. Estimating uncertainty and lead quality determination in blood in the occupation exposure. Trans. Univ. Košice, 11: 2-3.

Ferreira-Baptista, L. and De Miguel, E. 2005. Geochemistry and risk assessment of street dust in Luanda, Angola: A tropical urban environment. Atmos. Environ., 39(25): 4501-4512.

Gowd, S.S., Reddy, M.R. and Govil, P.K. 2010. Assessment of heavy metal contamination in soils at Jajmau (Kanpur) and Unnao industrial areas of the Ganga Plain, Uttar Pradesh, India. J. Hazard. Mater., 174(1-3): 113-121.

Ibe, F.C., Opara, A.I., Ibe, B.O., Adindu, B.C. and Ichu, B.C. 2018. Environmental and health implications of trace metal concentrations in street dust around some electronic repair workshops in Owerri, Southeastern Nigeria. Environ. Monit. Assess., 190(12): 1-12.

Jaradat, Q.M. and Momani, K.A. 1999. Contamination of roadside soil, plants, and air with heavy metals in Jordan: A comparative study. Turk. J. Chemi., 23(2): 209-220.

Lindsay, W.L. 1979. Chemical Equilibria in Soils. John Wiley and Sons Ltd, NJ.

Morais, S., Costa, F.G. and Pereira, M.L. 2012. Heavy metals and human health. Environ. Health–Emerg. Issues Pract., 10(1): 227-245.

Muhammad, J. S., Jasim, K. A. and Shaban, A. H. 2020. Evaluation of (Ni, Cr, Cu) concentration in the soil of Diyala utilizing GIS techniques. IOP Conference Series: Materials Science and Engineering, 928(7): 72111. IOP Publishing.

Muhammad, J.S., Jasim, K.A. and Shaban, A.H. 2021. Determining heavy metals and other elements concentrations in the soil at Baquba-Iraq. Key Eng. Mater., 886: 273–280.

Salman, N.A., Al-Saad, H.T. and Al-Imarah, F.J. 2021. The status of pollution in the southern marshes of Iraq: A short review. South. Iraq's Marshes, 11: 505-516.

Steinbock, R.T. 1979. Lead ingestion in history. New Eng. J. Med., 301(5): 277.

Tapsoba, I., Bourhis, S., Feng, T. and Pontié, M. 2009. Sensitive and selective electrochemical analysis of methyl-parathion (MPT) and 4-nitrophenol (PNP) by a new type p-NiTSPc/p-PPD coated carbon fiber microelectrode (CFME). Electroanal. Int. J. Devoted Fund. Pract. Aspects Electroanal., 21(10): 1167-1176.

Nature Environment and Pollution Technology
An International Quarterly Scientific Journal

p-ISSN: 0972-6268
(Print copies up to 2016)
e-ISSN: 2395-3454

Vol. 21 | No. 5 (Suppl) | pp. 2249-2258 | 2022

Original Research Paper

https://doi.org/10.46488/NEPT.2022.v21i05.019

Open Access Journal

Comparison of GIS-Based Intrinsic Groundwater Vulnerability Assessment Methods: DRASTIC and SINTACS

Indrajeet Sahu†, A. D. Prasad and Ishtiyaq Ahmad
Department of Civil Engineering, National Institute of Technology, Raipur 492010, India
†Corresponding author: Indrajeet Sahu; iamindraa14@gmail.com

Nat. Env. & Poll. Tech.
Website: www.neptjournal.com

Received: 07-07-2022
Revised: 22-08-2022
Accepted: 07-09-2022

Key Words:
Groundwater vulnerability
DRASTIC index model
SINTACS method
GIS

ABSTRACT

The possibility of contaminants percolating and diffusing into the groundwater system is referred to as groundwater vulnerability. When groundwater once gets polluted it is very difficult to process/clean it so, measures must be taken to assess the vulnerability of the groundwater for effective groundwater conservation and management planning. This study aims to evaluate and map the vulnerability of Raipur city using the SINTACS and DRASTIC models and to compare their effectiveness between them. To assess the hydrogeological setting and evaluate aquifer vulnerability, each model includes seven environmental parameters (aquifer hydrogeologic features, effective infiltration, topographic slope, soil media, water table depth, unsaturated conditions, and hydraulic conductivity). The parameter data sets are evaluated in a Geographical Information system (GIS) environment to get the vulnerability index (VI), the index is categorized into five classes that show low to high vulnerability. The area under the low class for DRASTIC and SINTACS is 26.14% and 20.34% respectively whereas for the highly vulnerable class it is 15.54% and 22.54% respectively of the total area. By comparing the 15-groundwater sample value of nitrate concentration on the two vulnerability maps it was found that the SINTACS method result was shown to be significantly associated with the nitrate concentration with an accuracy of 86.7 percent.

INTRODUCTION

A good way to safeguard groundwater is vulnerability assessment since it identifies the locations that are most exposed to pollution. The actions of humans, such as farming, urbanization, and industry, have irreversibly damaged the quality of groundwater. Vulnerability is typically supposed as an "intrinsic" property of a groundwater system, determined by its sensitivity to environmental and/or human influences (Vrba & Zaporozec 1994). An aquifer's intrinsic vulnerability is the ease with which a pollutant deposited to the ground surface can reach and spread in groundwater. In the study area, the groundwater present in permeable aquifers provides the majority of water needed to meet demand. The coexistence of permeable aquifers, farming land, and industries, together with the excessive use of fertilizers in farming, effluent, and leakage from sewage has exacerbated nitrate contamination of groundwater. The amount of nitrate concentration in groundwater is regarded as a sign that the quality of the water is deteriorating.

Various methods mainly overlay/index statistical techniques, and process-based methods approaches were developed and then utilized for groundwater vulnerability assessment (GVA) (Tesoriero et al. 1998). As the information/data required for GVA is readily available over large areas, overlay/index approaches are frequently preferred (Shirazi et al. 2013). In overly and index approaches, elements (such as geology, soil, the impact of the vadose zone, etc.) that control the transport of pollutants from the ground surface into the saturated zone are mapped using existing and/or developed data. Each model depends mainly on the hydro-geological environment and aquifer characteristics. Then, each element is given a subjective numerical value (rating) based on how crucial it is for regulating the circulation of contaminants. The final vulnerability map of a region is created by linearly combining the rate maps. These techniques provide a qualitative and situational assessment of groundwater vulnerability.

DRASTIC and SINTACS are two of the most well-known and commonly utilized overlay/index approaches for evaluating GVA (Iqbal et al. 2012). The DRASTIC index model combines several thematic layers to generate vulnerability scores for various areas (Aller et al. 1987). The parameters characterization of vulnerability that was identified in the SINTACS approach is the same as those of the DRASTIC method (Civita & De Maio 1997). The key advantage of such methods is that they may be used for regional-scale evaluation since they allow for the assessment

of some of the elements influencing the migration of pollutants over large areas. Geographic information systems (GIS) and Remote sensing (RS) methods were applied to collect and prepare the inputs parameter layer for the overlay/index models.

The objective of this study is to evaluate the Raipur city groundwater vulnerability using both DRASTIC and SINTACS overlay/index methods and compare the effectiveness of the method to the region. Also, it shows that combining the overlay/index method with a geographic information system (GIS) is a useful technique for determining groundwater pollution risk and managing water resources.

STUDY AREA

Raipur is the capital of Chhattisgarh state located in the central part of the state. The city is enclosed between 21°10' to 21°20' (N) latitudes and 81°35' to 81°40' (E) longitude (Fig. 1). It is around 290 m above sea level having an area of about approximately 226 km^2. According to Indian Metrological Department (IMD) Raipur, the region's average rainfall is about 1460 mm. The city has a moist climate and is tropically dry, with warm temperatures all year. In the winter months of November to January, temperatures drop to 10°C, and in the summer months of March to May-June, temperatures can reach 48°C. The state experiences the rainy season from July to November, area depends on rain for irrigation and groundwater recharge as the main crop of the state is paddy (Rice), which is also known as the rice bowl of India. The water table depth of the city is found to be 3-40 meters below ground level (mbgl) (CGWB-Central Ground Water Board). The research region has mature soil types consisting of Inceptisols, Alfisols, and Vertisols and comes under the Seonath-Mahanadi alluvial plain. The Chandi and Gunderdehi formations can be found across the study region. The city is having many steel/iron and cement industries as the state is rich in iron ore and limestone which are raw materials for these industries.

MATERIALS AND METHODS

A vulnerability assessment has been done for Raipur city using overlay/index-based methods that are DRASTIC and SINTACS. Each method uses seven parameters for the analysis, and this parameter layer is developed in a GIS system using some hydrogeological, precipitation, and satellite image data. With the use of the prepared layer, the vulnerability index was evaluated by applying both methods as illustrated in Fig. 2.

DRASTIC Method

The DRASTIC approach evolved through the offerings of the US Environmental Protection Agency's (USEPA) services and is based on a parameter weighting and indexing system (Aller et al. 1987). The DRASTIC is the abbreviation of seven criteria that determine the vulnerability index: Depth to water (D); Recharge (R): effective recharge of the aquifer;

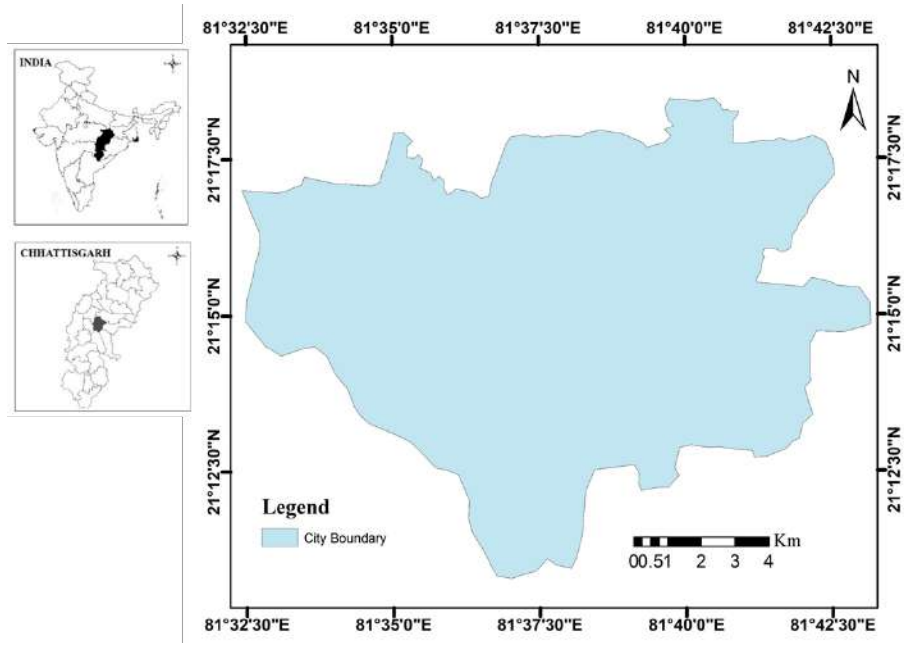

Fig. 1: The study area.

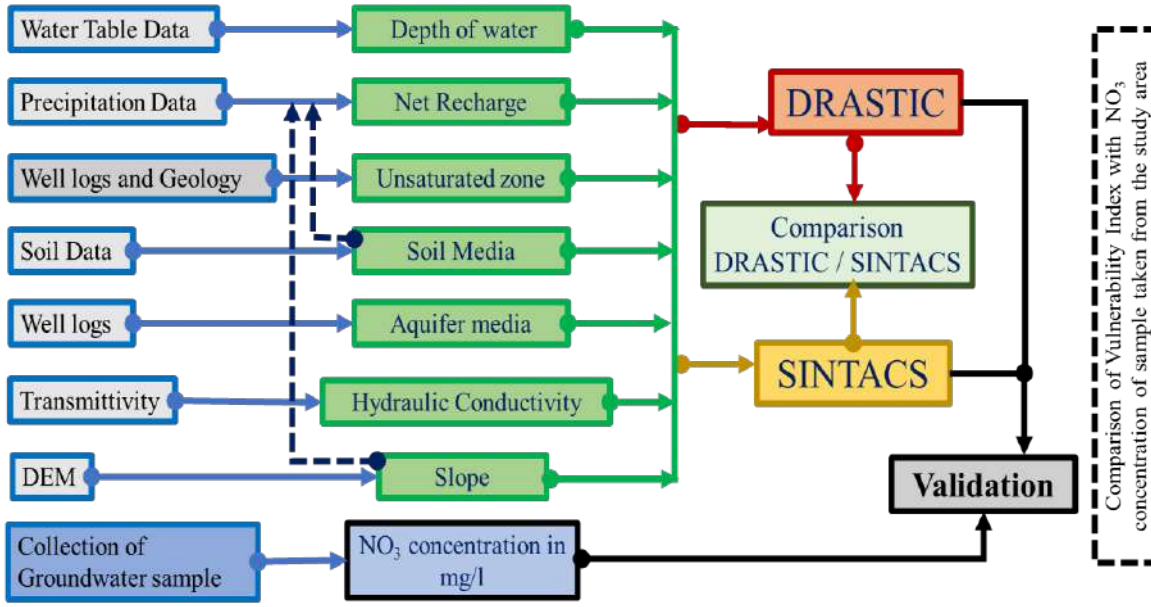

Fig. 2: Methodology flow chart.

Aquifer media (A); Soil media (S): refers to the type of soil; Topography (T): refers to the land's topographic slope; Impact of vadose zone (I): unsaturated zone; Hydraulic Conductivity of the aquifer (C).

The model generates a numerical index based on the weights and ratings applied to the seven parameters. The rate, evaluated on a 10 to 1 scale depending upon the relative effect on the vulnerability of groundwater, is represented by the significant media types or classes of individual parameters. After that, weights ranging from 1 to 5 are applied to the seven parameters to indicate their respective importance (Rahman 2008, Samey & Gang 2008, Prasad et al. 2011, Yin et al. 2013, Kazakis & Voudouris 2015, Baghapour et al. 2016). Each parameter rating for each interval was multiplied by a multiplier designated as weight, and the results were then added up to determine the final DRASTIC Vulnerability Index (DVI). The DVI is computed according to the subsequent equation (1) using ArcGIS software:

$$\text{DRASTIC VI} = (De*Dd) + (Re*Rd) + (Ae*Ad) + (Se*Sd) + (Te*Td) + (Ie*Id) + (Ce*Cd) \quad \ldots(1)$$

Table 1: Class distribution for DRASTIC method (Aller et. al 1987).

Degree of Vulnerability	Vulnerability Index
Very high	> 200
High	161 – 200
Average	121 – 160
Low	80 – 120
Very low	< 80

Where, 'd' is the weight of the parameter and 'e' is the rating, and D, R, A, S, T, I, and C are DRASTIC parameters.

SINTACS Method

SINTACS is a GVA method that employs the same parameters as DRASTIC (Rahman 2008). Using the same criteria as DRASTIC, the SINTACS approach was developed for typical Mediterranean climatic and hydrogeological environments. However, SINTACS has a more flexible rating and weighting process (Kapelj et al. 2013). The SINTACS is a tool for data and analysis optimization with a remarkable amount of versatility. It can function in a GIS setting, hence being utilized frequently in vulnerability analysis (Mali & Janža, 2005, Al Kuisi et al. 2006).

The five various weighing systems are influenced by the hydrogeological setting. The weighting systems show how important the parameters are concerning one another in various contexts, including normal, drainage, relevant, fissured, and karst. The characteristics used to evaluate vulnerability in this methodology are the same as those used in the DRASTIC method. SINTACS stands for (S)-depth of water, (I)- infiltration, (N)-unsaturated zone, (T)- soil, (A)-aquifer hydrogeological properties; (C)- hydraulic conductivity; (S)-the topographic surface's average slope (Civita & De Maio, 1997). The hydrological setting of a place is defined by the seven parameters listed above. According to the classification scale, these seven factors are further separated into ranges of 1 to 10, each of which represents a specific hydrological state (Kuisi et al. 2006, Sener & Davrez

Table 2: Weights attributed to parameters in the different scenarios of the SINTACS method (Civita 1990, Civita & De Maio 1997).

Parameter	Normal Impact	Important Drainage	Severe Impact	Cracked land	Karsts
S	5	4	5	3	2
I	4	4	5	3	5
N	5	4	4	3	1
T	4	2	5	4	3
A	3	5	3	4	5
C	3	5	2	5	5
S	2	2	2	4	5

2013). The rating given to each of these zones or ranges identifies their relative significance within each parameter in terms of increasing aquifer susceptibility. When assessing vulnerabilities, the seven characteristics are not thought to be equally significant. Weights from 1 to 5 are allocated to each of these criteria to indicate their relative importance (Table 4). The equation (2) is used to compute the SINTACS Vulnerability Index (SVI) (Al Kuisi et al. 2006, Guastaldi et al. 2014, Rutharvel Murthy et al. 2015, Al-Shatnawi et al. 2016, Jahromi et al. 2021)

SINTACS VI = (Se*Ss) + (Ie*Is) + (Ne*Ns)+ (Te*Ts) + (Ae*As) + (Ce*Cs) + (Se*Ss) ...(2)

Where S, I, N, T, A, C, and S are SINTACS parameters, 's' and 'e' are the weights and rates allocated to each parameter.

Parameter Layer Preparation

Parameter layers for GVA are developed in GIS systems using precipitation, hydrogeological, and satellite data. The parameters are described below:

Depth to the Water Table

The depth of the water table is a measure of the distance between the ground's surface and the top of the groundwater table. To acquire depth to the groundwater table layer parameter, the good data at different locations in the study region was interpolated using the Inverse Distance Weighted (IDW) method in the GIS environment (Fig. 3). The interpolation results obtained show that water depth in the area ranges from 3 to 41 meters below ground level (mbgl) Table 4. The lesser the depth of the water table from the ground more the threat of contamination from the pollutant present on the surface, in a view of its importance in GVA the weight given to the depth of water is 5.

Infiltration

The water that percolates from the surface, through the sub-surface into the water table (aquifer) is known as infiltration.

Table 3: Criteria for the vulnerability assessment in the SINTACS method (Civita & De Maio 1997).

Degree of Vulnerability	Vulnerability Index
Low	< 105
Average	105 – 186
High	186 – 210
Very high	> 210

Infiltration is crucial in evaluating the sensitivity of aquifers because it can introduce contaminants into groundwater through a variety of mechanisms, such as percolation and dilution from the saturated zone to the unsaturated zone. (Fig. 4). Formula established (Eq. 3) by Piscopo (2001) has been used for the evaluation of infiltration. A net recharge layer parameter was created using data on average rainfall (mm), soil permeability(m.day^{-1}), and slope (%) percentage in a GIS framework (Table 4).

Recharge value = Rainfall + Slope% + Soil permeability ...(3)

Unsaturated Zone

The unsaturated zone is the area that is above the water table and below the typical soil horizon. Based on the interpretation of the lithological drilling data, the impact parameter of the unsaturated zone is evaluated. One of the most important factors in assessing susceptibility is the unsaturated zone parameter and hence the weight given to it is 5 according to its relative importance in evaluating the GVA (Fig. 5).

Soil

The topmost part of the unsaturated zone is referred to as the soil, which is also the primary layer of the physio-chemical

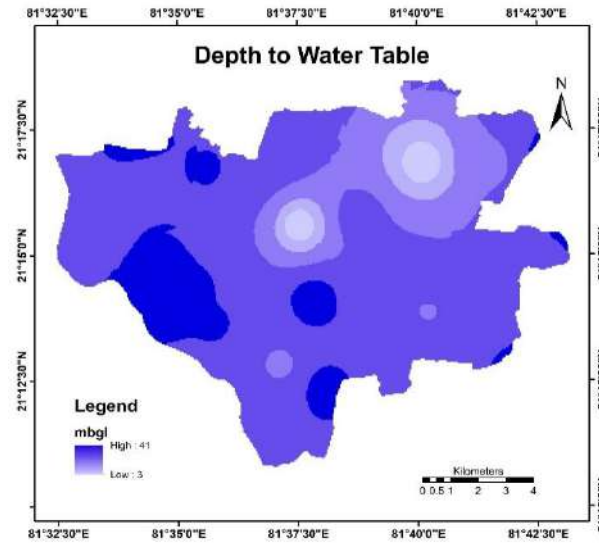

Fig. 3: Depth of the water table.

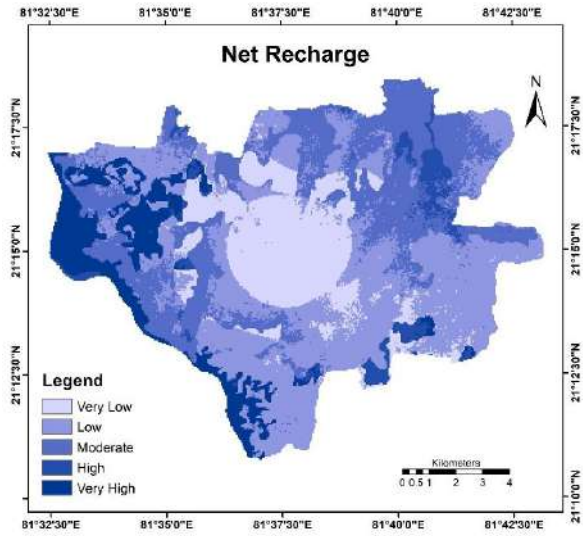

Fig. 4: Net recharge.

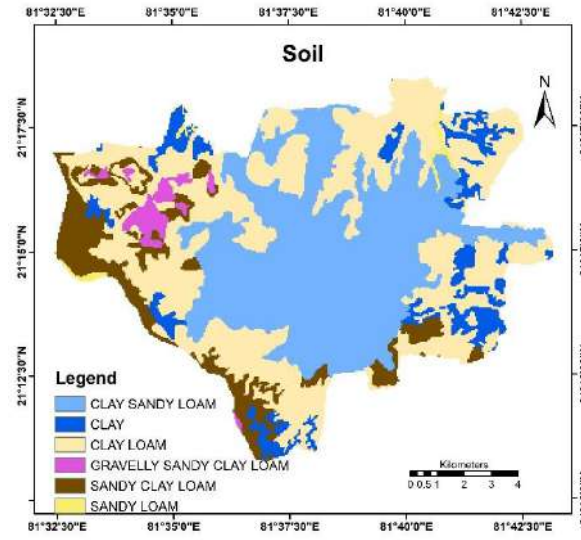

Fig. 6: Soil.

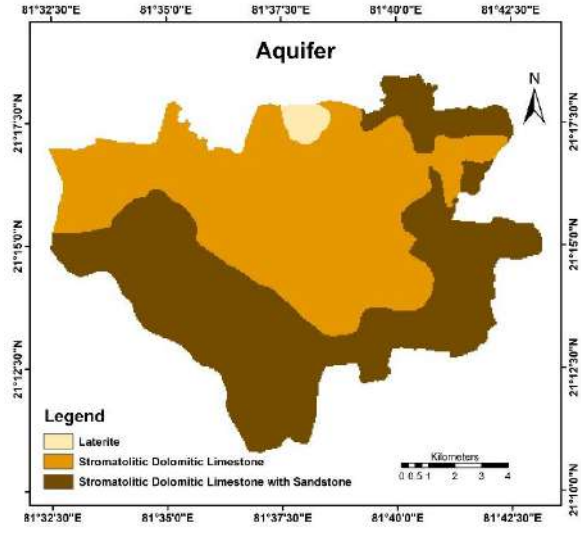

Fig. 5: Aquifer.

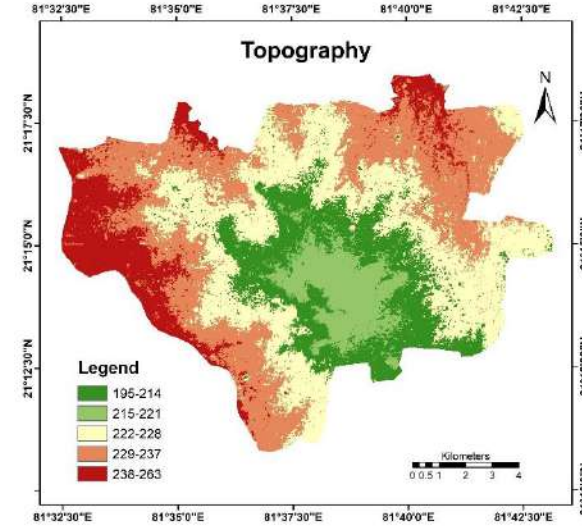

Fig. 7: Topography.

interface between potential pollutants and the subsoil (vadose zone). The soil significantly affects how much recharge can penetrate the groundwater and, as a result, how easily contaminants can travel into the unsaturated zone (Srinivasamoorthy et al. 2011). Additionally, where the zone of soil is sufficiently broad, the processes of volatilization, filtration, and sorption are highly important and are to be considered during analysis. The study area's soil is divided into six subgroups, as indicated in Fig. 6, including clay sandy loam, and clay loam and its rating and weights are depicted for both cases (DRASTIC and SINTACS) in Table 4.

Aquifer

An aquifer has enough saturated permeable material to produce a sizable amount of water for springs or wells. The drilling well records and geological map data of the basin were applied to develop the aquifer layer. The aquifer media in the study basin was divided into three regions (Mali & Janža 2005, Kumar et al. 2013, Busico et al. 2017). The study area contains mainly three aquifer types that are Stromatolitic Limestone with Sandstone, Stromatolitic Dolomitic Limestone, and Laterite as shown in Fig. 7, whereas its rating and weights are represented in Table 4.

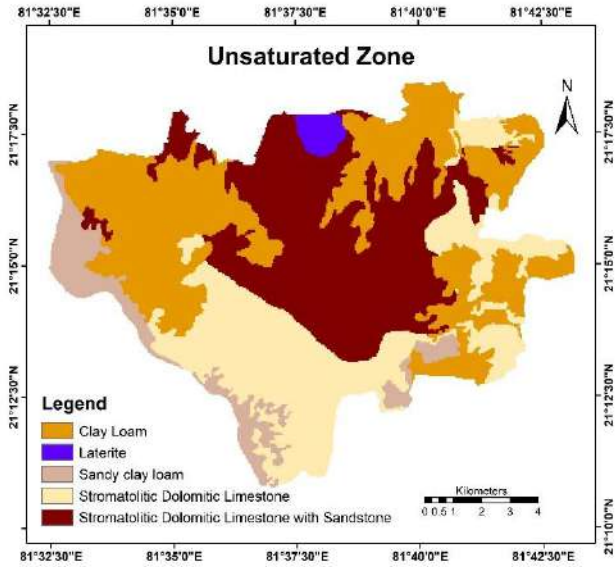

Fig. 8: Unsaturated zone.

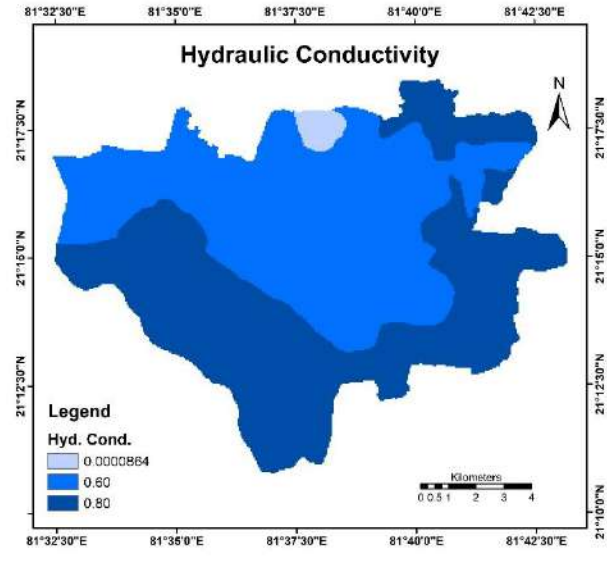

Fig. 9: Hydraulic Conductivity.

Topography

In terms of vulnerability assessment, the slope of the bed or topography influences whether water and contaminants will preferentially drain off or stay on the surface for enough time to penetrate (Kapelj et al. 2013). If the slope is low the runoff rate will be low and the deposition of water will be there which will ultimately lead to an aquifer through the subsurface layer. Using the CartoSAT Digital Elevation Model (DEM), which has a resolution of 30m, it is possible to determine the topographical slope in the GIS environment. Fig. 8 demonstrates the area's gradient, weight, and rate for both methods are shown in Table 4.

Hydraulic Conductivity

The hydraulic conductivity of the aquifer is a gauge of its water-carrying capacity. This property controls how quickly groundwater will flow when subjected to a particular hydraulic gradient; higher conductivity levels often equate to high sensitivity to pollutants (Fig. 9). The parameter layer was prepared using the data obtained from CGWB through GIS analysis.

RESULTS AND DISCUSSION

The seven parameter layers were put together using Equations (1) and (2) to calculate the DRASTIC and SINTACS vulnerability index of Raipur city. The Vulnerability index of DRASTIC for the region of study is 70 to 207 as the vulnerability index of the SINTACS method ranges from 84 to 215 (Fig. 10 and 11).

The acquired vulnerability map illustrates the different levels of aquifers' sensitivity to contamination. The result is standardized and divided into five classes. Both DRASTIC and SINTACS-based categories are termed as low, very low, high, very high, and moderate vulnerability (Fig. 10 and 11). The result obtains from the DRASTIC method shows that 26.14% i.e 59.08 km^2 of the complete region demonstrate low susceptibility, 42.75% 96.62 km^2 indicates moderate vulnerability and 10.25% that is 23.17 km^2 of the study region is having vulnerability in the very-high range (Table 5). The outcome of SINTACS VI shows that out of 226 km^2 area 20.34% which is 45.97 km^2 contributes to low vulnerability, 36.4% which is 82.26 km^2 of the entire area indicates moderate vulnerability and 12.26% which is 27.71km^2 of the section is demonstrating vulnerability in a very high zone (Table 5).

To identify areas that belonged to the same or different categories of vulnerability classes, the findings from the DRASTIC and SINTACS models were compared.VI obtained from each model are compared pixel by pixel for the five-vulnerability class done in ArcGIS. Fig.-12 represents the difference in vulnerability classes in both methods. The comparison result is categorized into 3 groups, the pixel with no difference in VI is placed under the No difference class, with ±10 change in pixel value kept under slight difference whereas if the change is between 10 to 24 it is kept under moderate. According to the analysis, there is only a slight difference between low (DVI) and low (SVI) classes, and moderate (DVI) to moderate (SVI) classes, although there is an average difference between higher classes.

Table 4: The DRASTIC and SINTACS models' rating and weighting of each parameter (Aller et al. 1987, Civita & De Maio, 1997).

Parameters	Sub-Parameter	DRASTIC				SINTACS		
		Rating	Weight	Index rating		Rating	Weight	Index rating
Groundwater depth [m] [Sd]	0-10	10	5	50		10		50
	10-20	8		40		7	5	35
	20-30	6		30		5		25
	30-40	3		15		3		15
	>40	1		5		1		5
Net recharge (I)	Very-high	10		40		10		40
	High	9		36		9	4	36
	Medium	7	4	28		8		32
	Low	5		20		6		24
	Very-low	2		8		2		8
Impact of Vadose (N)	Stromatolitic lime and dolomite with flaggy limestone	9	5	45		9	5	45
	Stromatolitic limestone and dolomite	7		35		8		40
	Sandy clay loam	3		15		3		15
	Laterite	2		10		2		10
	Clay loam	1		5		1		5
Soil Media (T)	Sandy loam	5		10		4		16
	Gravelly sandy Clay loam	3	2	6		3	4	12
	Sandy clay loam	3		6		3		12
	Clay sandy loam	2		4		2		8
	Clay loam	2		4		2		8
	Clay	1		2		1		4
Aquifer Media (A)	Stromatolitic limestone with Sandstone	10	3	30		10	3	30
	Stromatolitic dolomitic limestone	9		27		9		27
	Laterite	1		3		1		3
Hydraulic Conductivity (C)	0.80 $m.day^{-1}$	9		27		9		27
	0.60 $m.day^{-1}$	8	3	24		8	3	24
	0.000864 $m.day^{-1}$	1		3		1		3
Slope (S)	Very low	10		10		10		20
	Low	9	1	9		9	2	18
	Moderate	7		7		8		16
	High	6		6		7		14
	Very High	5		5		6		12

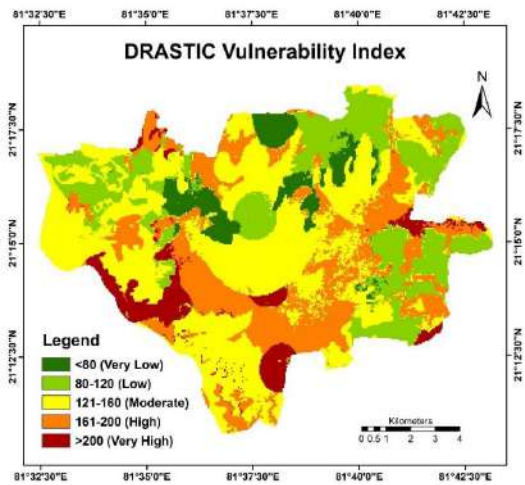

Fig. 10: DRASTIC Vulnerability Index.

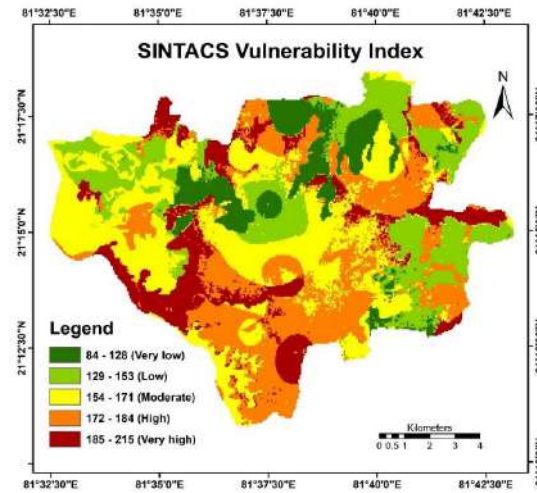

Fig. 11: SINTACS Vulnerability Index.

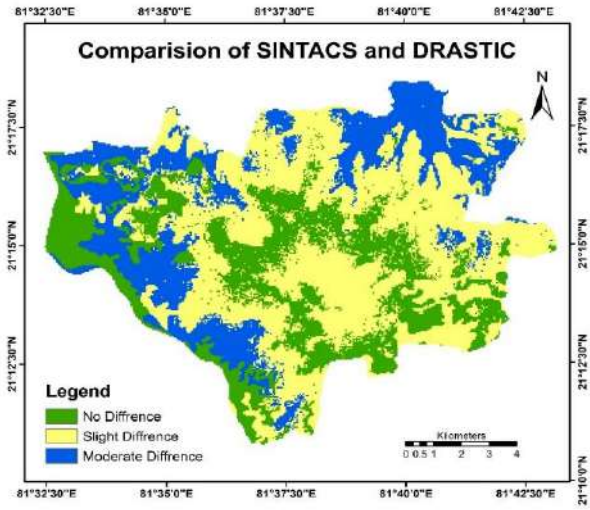

Fig. 12: Comparison of SINTACS, DRASTIC vulnerability index.

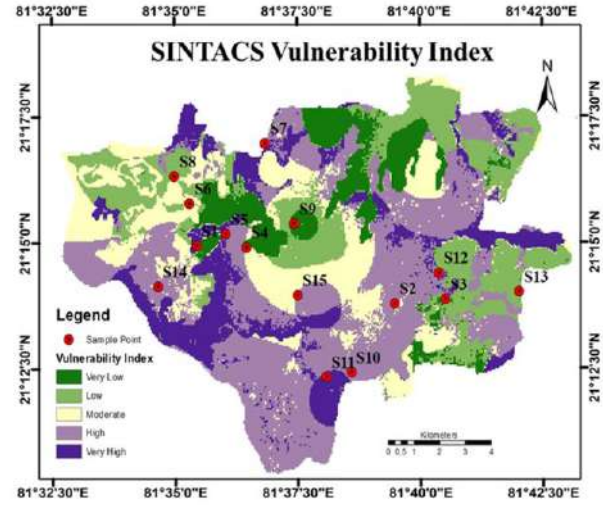

Fig. 13: Nitrate sample point location.

Table 5: Vulnerability index range categorization.

	DRASTIC		SINTACS	
Classes	Area [%]	Area [km^2]	Area [%]	Area [km^2]
Very Low	5.32	12.02	8.46	19.12
Low	26.14	59.08	20.34	45.97
Moderate	42.75	96.62	36.4	82.26
High	15.54	35.12	22.54	50.94
Very High	10.25	23.17	12.26	27.71

VALIDATION

For a more accurate evaluation, the vulnerability index maps generated by the overlay and index method (DVI and SVI) can be compared and validated with the field measurements of the physical and chemical properties of groundwater. Nitrate concentrations in groundwater are viewed as a warning that the water's quality is declining. The level of nitrate discovered in the region, which is one of the main groundwater pollutants, validated the

Table 6: Nitrogen concentrations at various sample sites and their associated vulnerability index.

Location		Sample number	Nitrate concentration [mg.L^{-1}]	class	DRASTIC Vulnerability Index	SINTAC Vulnerability Index
(Latitude) E	(Longitude)N					
81.5884	21.2527	S-1	48.12	h	H(Similar)	H(Similar)
81.6058	21.2522	S-2	64.34	h	H(Similar)	H(Similar)
81.5986	21.2565	S-3	14.20	l	M(Dissimilar)	M(Dissimilar)
81.5805	21.2752	S-4	10.86	l	L(Similar)	L(Similar)
81.6224	21.2600	S-5	32.45	m	H(Dissimilar)	M(Similar)
81.6422	21.2124	S-6	21.64	m	M(Similar)	M(Similar)
81.6336	21.2108	S-7	52.36	h	H(Similar)	H(Similar)
81.6731	21.2442	S-8	29.3	m	L(Dissimilar)	M(Similar)
81.5746	21.2396	S-9	9.2	l	L(Similar)	L(Similar)
81.6237	21.2371	S-10	24.46	m	H(Dissimilar)	M(Similar)
81.6338	21.2107	S-11	68.26	h	H(Similar)	H(Similar)
81.6730	21.2443	S-12	84.34	h	H(Similar)	H(Similar)
81.7010	21.2384	S-13	12.52	l	L(Similar)	L(Similar)
81.5748	21.2398	S-14	40.62	m	M(Similar)	H(Dissimilar)
81.6237	21.2371	S-15	10.34	l	M(Dissimilar)	L(Similar)

Note: 1. DVI and SVI- (L = low, M = moderate, H = high); 2. Nitrate Conc.- (l = low, m = moderate, h = high)

Table 7: Accuracy of the applied methods using Nitrate concentration of sample point location.

	DRASTIC	SINTACS
Nitrate sample (Which does not have similarities)	S5, S8, S10, and S15	S3 and S14
Accuracy % (similarities/total sample)	73.4	86.7

delineated groundwater-sensitive zones (Ramesh & Elango 2012, Kumar et al. 2013, Neshat & Pradhan 2017, Noori et al. 2018). Although nitrate is not naturally present in groundwater, excessive fertilizer uses in agricultural practices, leakage from the septic tank and sewage, and effluent from industries cause it to contaminate the aquifer system. To determine the model's efficacy in determining groundwater vulnerability to pollution, the association between the GVA model (DRASTIC, SINTACS), and groundwater nitrate levels was examined (Table 6). In the study area's identified groundwater risk zones, 15 groundwater samples were therefore collected from the various wells (Table 6). The Ultraviolet Spectrophotometric Screening Method (4500-NO3-B) was used to evaluate the nitrate concentration (Fig. 13). The results of the chemical analysis show that NO3 concentrations for all groundwater samples range from 9 $mg.L^{-1}$ to 125 $mg.L^{-1}$. Given that according to (IS:10500) Drinking Water Standards, the highest permissible and most acceptable nitrate limit that is suitable for human consumption is 45 $mg.L^{-1}$. Groundwater with nitrate concentrations over that level is dangerous for human consumption. In comparing the concentration of nitrate found at the location and the VI obtain from the analysis, the SINTACS method shows better accuracy (Table 7).

CONCLUSION

The overlay/index method combined with GIS is a highly precise way of determining how sensitive groundwater is to contamination. The study region's following DRASTIC and SINTACS maps show that the majority of the area; 42.75 percent and 36.4%, respectively are in the intermediate vulnerability zone. The yearly net recharge, which is 250+mm, is the main cause of the extremely high vulnerability with a high rate near industrial areas (chemical pollutants and wastewater) and the agricultural land (use of pesticides for farming) are the major reason for the high VI of those particular regions. In addition, the Unsaturated/ Vodas zone is also a factor contributing to vulnerability most of the area contains limestone with Sandstone making it simpler for water to infiltrate into the ground. The results obtained from the DRASTIC and SINTACS models were compared to pinpoint regions that fell into the same or different categories of vulnerability classes. From the analysis, it is found that there is a slight difference in the low (DVI) to low (SVI) class and moderate (DVI) to moderate (SVI) class, whereas it is an average difference in a higher class.

On comparing the 15-groundwater sample value of Nitrate concentration on the two maps we find that the SINTACS model gives the best result and more than 60% of the area comes under the low and moderate vulnerability class. The SINTACS results were shown to be significantly associated with the nitrate concentration of groundwater sample collected from the study area, with an accuracy of 86.7 percent, and is more suitable for evaluating Raipur's groundwater-sensitive zones.

REFERENCES

Al Kuisi, M., El-Naqa, A. and Hammouri, N. 2006. Vulnerability mapping of shallow groundwater aquifer using SINTACS model in the Jordan Valley area, Jordan. Environ. Geol., 50(5): 651-667.

Aller, L., Lehr, J., Petty, R. and Bennett, T. 1987. A standardized system to evaluate groundwater pollution using a hydrogeologic setting. J. Geol. Soc. India, 29(1): 23-37.

Al-Shatnawi, A.M., El-Bashir, M.S., Khalaf, R.M.B. and Gazzaz, N.M. 2016. Vulnerability mapping of groundwater aquifer using SINTACS in Wadi Al-Waleh Catchment, Jordan. Arab. J. Geosci., 9(1): 1-13.

Baghapour, M.A., Fadaei Nobandegani, A., Talebbeydokhti, N., Bagherzadeh, S., Nadiri, A.A., Gharekhani, M. and Chitsazan, N. 2016. Optimization of the DRASTIC method by the artificial neural network, nitrate vulnerability index, and composite DRASTIC models to assess groundwater vulnerability for the unconfined aquifer of Shiraz Plain, Iran. J. Environ. Health Sci. Eng., 14(1): 1-16.

Busico, G., Kazakis, N., Colombani, N., Mastrocicco, M., Voudouris, K. and Tedesco, D. 2017. A modified SINTACS method for groundwater vulnerability and pollution risk assessment in highly anthropized regions based on NO3- and SO42- concentrations. Sci. Tot. Environ., 609: 1512-1523.

Central Ground Water Board (CGWB), Raipur. http://cgwb.gov.in/index.html

Civita M. 1990. Legenda unificata per le carte della vulnerabilita dei corpi idrici soutterranei. In: *Studi sulla vulnerabilita degli Acquiferi*. Pitagora: Bologna.

Civita, M. and De Maio, M. 1997. Un sistema parametrico per la valutazione e la cartografia della vulnerabilita' degli acquiferi all'inquinamento. Metodol. Automat., 60: 515-525

Guastaldi, E., Graziano, L., Liali, G., Brogna, F.N.A. and Barbagli, A. 2014. Intrinsic vulnerability assessment of Saturnia thermal aquifer by means of three parametric methods: SINTACS, GODS, and COP. Environ. Earth Sci., 72(8): 2861-2878.

Iqbal, J., Gorai, A.K., Tirkey, P. and Pathak, G. 2012. Approaches to groundwater vulnerability to pollution: A literature review. Asian J. Water Environ. Pollut., 9(1): 105-115.

Jahromi, M.N., Gomeh, Z., Busico, G., Barzegar, R., Samany, N.N., Aalami, M.T., Tedesco, D., Mastrocicco, M. and Kazakis, N. 2021. Developing a SINTACS-based method to map groundwater multi-pollutant vulnerability using evolutionary algorithms. Environ. Sci. Pollut. Res., 28(7): 7854-7869.

Kapelj, S., Loborec, J. and Kapelj, J. 2013. Assessment of aquifer intrinsic vulnerability by the SINTACS method. Geol. Croat., 66(2): 119-128.

Kazakis, N. and Voudouris, K.S. 2015. Groundwater vulnerability and pollution risk assessment of porous aquifers to nitrate: Modifying the DRASTIC method using quantitative parameters. J. Hydrol., 525: 13-25.

Kumar, S., Thirumalaivasan, D., Radhakrishnan, N. and Mathew, S. 2013. Groundwater vulnerability assessment using the SINTACS model. Geomat. Nat. Hazards Risk, 4(4): 339-354.

Mali, N. and Janža, M. 2005. A GIS-based SINTACS model for assessing aquifer vulnerability. Geologija, 48(1): 127-140.

Murali, K. and Elangovan, R. 2013 Assessment of groundwater vulnerability in Coimbatore South Taluk Tamilnadu India using DRASTIC approach International Journal of Scientific and Research Publications. 3(6):1.

Neshat, A. and Pradhan, B. 2017. Evaluation of groundwater vulnerability to pollution using DRASTIC framework and GIS. Arab. J. Geosci., 10(22): 1-8.

Noori, R., Ghahremanzadeh, H., Kløve, B., Adamowski, J.F. and Baghvand, A. 2019. Modified-DRASTIC, modified-SINTACS, and SI methods for groundwater vulnerability assessment in the southern Tehran aquifer. J. Environ. Sci. Health Part A, 54(1): 89-100.

Piscopo, G. 2001. Groundwater Vulnerability Map, Explanatory Notes: Castlereagh Catchment. Australia NSW Department of Land and Water Conservation, Parramatta NSW.

Prasad, R.K., Singh, V.S., Krishnamacharyulu, S.K.G. and Banerjee, P. 2011. Application of drastic model and GIS: For assessing vulnerability in hard rock granitic aquifer. Environ. Monitor. Assess., 176(1): 143-155.

Rahman, A. 2008. A GIS-based DRASTIC model for assessing groundwater vulnerability in shallow aquifer in Aligarh, India. Appl. Geogr., 28(1): 32-53.

Ramesh, K. and Elango, L. 2012. Groundwater quality and its suitability for domestic and agricultural use in the Tondiar river basin, Tamil Nadu, India. Environmental monitoring and assessment, 184(6): 3887-3899.

Rutharvel Murthy, K., Dhanakumar, S., Sundararaj, P., Mohanraj, R. and Kumaraswamy, K. 2015. GIS-based modified SINTACS model for assessing groundwater vulnerability to pollution in Vellore District (Part of Palar River Basin), Tamil Nadu, India. Springer, Cham.

Samey, A.A. and Gang, C. 2008. A GIS-based DRASTIC Model for the assessment of groundwater vulnerability to pollution in West Mitidja: Blida City, Algeria. J. Appl. Sci., 3(7): 500-507.

Sener, E. and Davraz, A. 2013. Assessment of groundwater vulnerability based on a modified DRASTIC model, GIS and an analytic hierarchy process (AHP) method: the case of Egirdir Lake basin (Isparta, Turkey). Hydrogeol. Jour., 21(701–714). DOI: 10.1007/s10040-012-0947-y.

Shirazi, S.M., Imran, H.M., Akib, S., Yusop, Z. and Harun, Z.B. 2013. Groundwater vulnerability assessment in the Melaka State of Malaysia using DRASTIC and GIS techniques. Environ. Earth Sci., 70(5): 2293-2304.

Tesoriero, A.J., Inkpen, E.L. and Voss, F.D., 1998, April. Assessing ground-water vulnerability using logistic regression. In: Proceedings for the source water assessment and protection 98 conference, Dallas, TX (157165).

Srinivasamoorthy, K., Nanthakumar, C., Vasanthavigar, M., Vijayaraghavan, K., Rajivgandhi, R., Chidambaram, S., Anandhan, P., Manivannan, R. and Vasudevan, S. 2011. Groundwater quality assessment from a hard rock terrain, Salem district of Tamilnadu, India. Arabian Journal of Geosciences, 4(1): 91-102.

Vrba, J. and Zaporozec, A. 1994. Guidebook on Mapping Groundwater Vulnerability. Vol. 16. International Contributions to Hydrogeology, IAH, HeiseVerlag, Hannover.

Yin, L., Zhang, E., Wang, X., Wenninger, J., Dong, J., Guo, L. and Huang, J. 2013. A GIS-based DRASTIC model for assessing groundwater vulnerability in the Ordos Plateau, China. Environ. Earth Sci., 69(1): 171-185.

Nature Environment and Pollution Technology
An International Quarterly Scientific Journal

p-ISSN: 0972-6268
(Print copies up to 2016)
e-ISSN: 2395-3454

Vol. 21 | No. 5 (Suppl) | pp. 2259-2267 | 2022

Original Research Paper

https://doi.org/10.46488/NEPT.2022.v21i05.020

Open Access Journal

Anthropogenic Influence on Protected Areas: A Case Study of Achanakmar Tiger Reserve (ATR), Chhattisgarh, India

Anupama Mahato† and S. S. Singh
Department of Forestry, Wildlife and Environmental Sciences, Guru Ghasidas Vishwavidyalaya, Bilaspur, CG, India
†Corresponding author: Anupama Mahato; anupamamahato4@gmail.com

Nat. Env. & Poll. Tech.
Website: www.neptjournal.com

Received: 17-02-2022
Revised: 09-05-2022
Accepted: 15-05-2022

Key Words:
Achanakmar tiger reserve
Anthropogenic influence
Conservation
Habitat suitability

ABSTRACT

India's broad network of protected areas, which encompasses 4.93% of the country's geographical area, is exposed to immense anthropogenic pressures that can create an imbalance and also hinder the prime objective of wildlife conservation and protection. The present study assesses some of these problems in relation to the Achanakmar Tiger Reserve (ATR). The main anthropogenic influence in ATR is the presence of eighteen core villages, five buffer villages, and 49 fringe villages in the periphery of the reserve area. The population density of the core zone was higher (16.0 people/km^2) as compared to the buffer zone (7.41 people/km^2). Another important disturbance in the protected area is state highway 8 which bisects the entire core zone into two halves. This highway also connects the neighboring state of Madhya Pradesh and there is the continuous movement of traffic, which hampers the smooth movement of wild animals. ATR also has a wide network of tourist roads of 192 km passing through the core zone. The average population density of livestock in ATR is relatively high compared to the average population of wild ungulates. It creates competition between wild ungulates for food, and they are also under constant threat of infectious diseases. The livestock depredation by apex predators is one of the major reasons for man-wildlife conflict in ATR. The cattle kill incidences by both the apex predator (tiger and leopard) was 378 during the period of three years (2015 to 2018) and these incidences were recorded more in the core zone as compared to the buffer zone. In the present study, anthropogenic effects on ATR have been studied and evaluated. It concludes that for effective management and conservation of tigers in ATR, these aspects need to be considered. To restore the tiger population in ATR, there must be a proper balance between human (anthropogenic) approaches and conservation benefits for the effective sustainability of the protected areas.

INTRODUCTION

The world has lost 95% of the tiger population (Thompson 2010) four subspecies and 93% of their historical range (Thatte et al. 2018) in the last century. Wild tigers continue to be threatened by poaching, habitat destruction and loss (Jhala et al. 2015), depletion of prey, diseases, and trade in body parts (Dinerstein et al. 2007, Sunquist 1999). Tiger is one of the critically endangered mammals of the Felidae family and is known for maintaining ecological sustainability.

The largest population of global wild tigers (*Panthera tigris tigris*) is found in India, having a population of 2,967. The charismatic megafauna Royal Bengal Tiger bears the position of India's national animal and is spread across 20 states (Jhala et al. 2020). About 40% total tiger population in India is restricted to the Central Indian landscape (Jhala et al. 2011).

The Achanakmar Tiger Reserve (ATR) is a part of the Central Indian Landscape and acts as a conduit for movement for tigers from many different tiger reserves and protected areas of the region, thereby promoting genetic exchange and dispersion of the wild tiger population. The corridors connect ATR with many important tiger reserves of Central India such as Kanha Tiger Reserve, Pench Tiger Reserve, and Bandhavgarh Tiger Reserve. The ATR is also well linked with Guru Ghasidas Tiger Reserve on the northern side. On South Western side, ATR connects with Phen Wildlife Sanctuary and Bhoramdev Wildlife Sanctuary.

ATR is also an integral part of the Achanakmar Amarkantak Biosphere Reserve (AABR) situated in the lap of the Maikal ranges and is enriched with a rich pool of germplasm. It is the 32nd tiger reserve in India and the third tiger reserve in Chhattisgarh State. ATR owes its name to the village called Achanakmar, which lies within the green limits of the Maikal ranges. The word 'Achanakmar' means

'sudden attack'. This protected area has a long history of conservation. Considering, the uniqueness and richness of biodiversity, Achanakmar declared a Wildlife Sanctuary in 1975 under the Wildlife (Protection) Act, of 1972. Due to the presence of magnificent carnivores and endangered tiger species, Achanakmar was declared a tiger reserve in the year 2009.

The ATR is constantly exposed to anthropogenic influences. At the time of its formation, 24 villages existed within the core zone. In addition, five buffer villages and many fringe villages are situated outside the reserve area which directly or indirectly affects the sole objective of conservation. To create an inviolable space for the movement of wildlife, six forest villages (Jalda, Kuba, Bahud, Bakal, Bokra Kachhar, and Sambhar Dhasan) were relocated from the tiger reserve in December 2009 as the first phase of relocation.

Kumari et al. (2020) and Angulo et al. (2016) reported that the Tiger reserve areas are subjected to various types of anthropogenic disturbances which are threatening its biodiversity. Seidensticker et al. (1999) illustrated that tiger abundance is determined by the quality and quantity of available habitat. The cumulative effect of population density, land-use patterns, roads, and railways results in a highly resistant landscape for tiger movement (Dutta et al. 2016, 2018). The major threat is habitat loss due to the rapid conversion of natural habitats outside protected areas resulting in isolation (DeFries et al. 2005) and poaching.

Previous studies also suggest that the ATR area bears high anthropogenic disturbance (Mathur et al. 2011) and high levels of poaching (Jhala et al. 2011). The settlements and the roads are the greatest disruptions to wildlife (Kumar et al. 2014). The present paper is an overview of the anthropogenic influence of ATR on effective management and protection for the wild tiger population.

STUDY AREA

The geographical extent of the Achanakmar Tiger Reserve area lies between 22°17' and 22°38' North latitudes and 81°31' and 81°57' East longitude. It extends over an area of 914.017 km^2, out of which 626.195 km^2 falls under the core zone (critical tiger habitat) and 287.822 km^2 comes under the buffer zone (Fig. 1 & Fig. 2). It is located in the Lormi tehsil of the Mungeli district. 113 beats of the ATR area is covered under ten territorial ranges which includes Achanakmar, Belghana, Chhaparwa, Gaurela, Khuriya, Kota, Lamni, Lamni (Tiger Reserve), Lormi, and Surhi range.

Champion & Seth (1968) categorized forest vegetation under Northern Tropical Moist Deciduous and Southern Dry Mixed Deciduous Forest. Sal (*Shorea robusta*) is the dominant tree species in the area, followed by Sal mixed

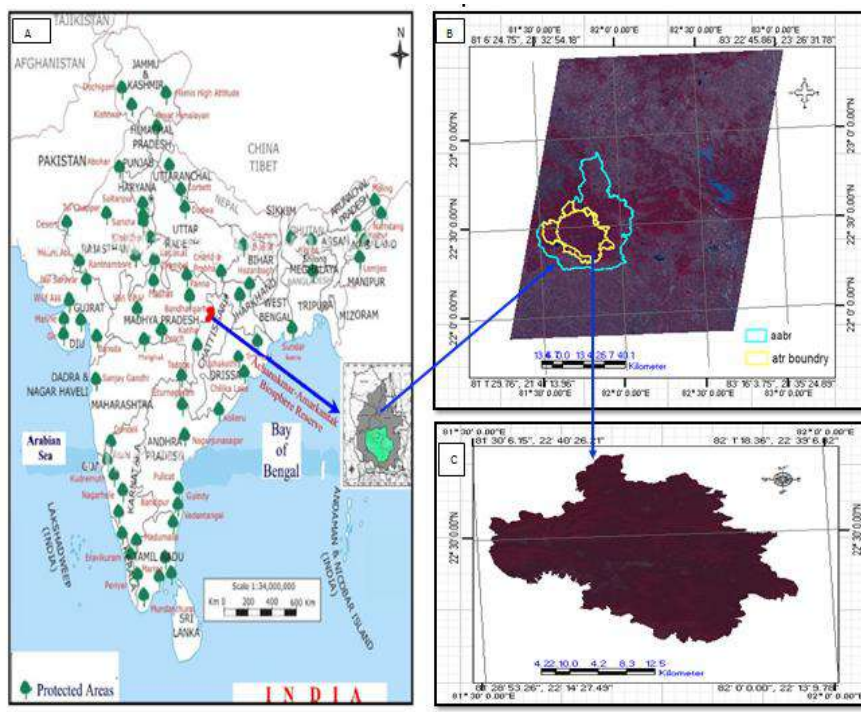

Fig. 1: The location map of ATR A-Protected Areas of India, B- Location of AABR and ATR in IRS LISS III image, C-Location of ATR Area.

forest, which includes tree species such as Saja (*Terminalia tomentosa),* Tendu (*Diospyros melanoxylum),* Haldu (*Adina cordifolia),* Bija (*Pterocarpus marsupium),* Mahua (*Madhuca indica),* Dhaora (*Anogeissus latifolia),* Teak (*Tectona grandis* (plantation)). Bamboo (*Dendrocalamus strictus*) is also found in higher and lower slopes with miscellaneous tree species (Mandal et al. 2017).

MATERIALS AND METHODS

- The Achanakmar Tiger Reserve boundary was obtained from Forest Department, Govt. of Chhattisgarh.
- A preliminary interpretation of the study area is done on topographical sheets. For digitalization, the Survey of India (SOI) topographic maps of 64F10, 64F11, 64 F14, and 64F15 on 1:50,000 scales published by SOI, Dehradun have been used.
- Detailed information on the villages within the core and buffer zones is collected from ground truthing and also from the forest department.
- Demographic details such as census data were downloaded from the Government of India's official website for the years 2001 and 2011. Population Density for core and buffer villages was calculated with the help of the following formula:

$$\text{Population Density} = \frac{\text{Number of people}}{\text{Land area in sq. km}}$$

- The data on cattle predation and conflicts within ATR were obtained from the C.G Forest department. The limitation of such secondary data is that they only include the cases that have been recorded or registered by the forest department.
- IGIS Version 1.0 was used for image processing such as layer stacks, a subset of the study area, preparation of the base map, road network map, identification of core, buffer, and fringe villages, etc.
- The road networks within the ATR area have been prepared with the help of IGIS software and Survey of India (SOI) toposheets as primary roads (state highway), and secondary roads (all other roads such as unmetalled roads, cart track roads/footpaths, etc) which crisscross this landscape (Fig. 5).
- Field data, including the field photographs and the ground control points, have been collected during the field survey.
- For identifying the actual location GPS (Global Positioning System) - Garmin (eTrex 10) and the "Trimble Geo Explorer" series with an accuracy of 2-6 m have been used.

RESULTS AND DISCUSSION

Protected areas of India are under constant threat and pressure from anthropogenic influence. Kerley et al. (2002) used human population density and transportation networks (roads and railways) as anthropogenic variables in their study because tigers are known to avoid human settlements and roads. In most forested areas, anthropogenic disturbances and a lack of prey bases do not allow the existence of wild tigers (Karanth & DeFries 2010). High human population density causes increased anthropogenic pressure on large mammals, which can lead to a decrease in their numbers (Harihar & Pandav 2012).

The ATR is also under the influence of many anthropogenic pressures such as villages, roads, and livestock populations causing overgrazing of vegetation, human-wildlife conflict, etc.

Settlements Inside the ATR Area

Eighteen villages (Fig. 3) are still in the core zone and five buffer villages are situated inside the ATR area. The main inhabitants of these villages are Baiga followed by Gond, Kol, Oraon, and Yadav communities. The population density of the core zone ranges from 12.64 inhabitants/km^2 during the year 2001. Despite of relocation of six villages in the first phase of relocation (2009), the population density increased in the year 2011 to 16.05 inhabitants/km^2. On the other hand, the human population density of the buffer zone increased from 6.12 people/km^2 to 7.41 people/km^2 between 2001 to 2011.

The activities and dependence of core villagers on forests affect the management of the tiger reserve. The villagers

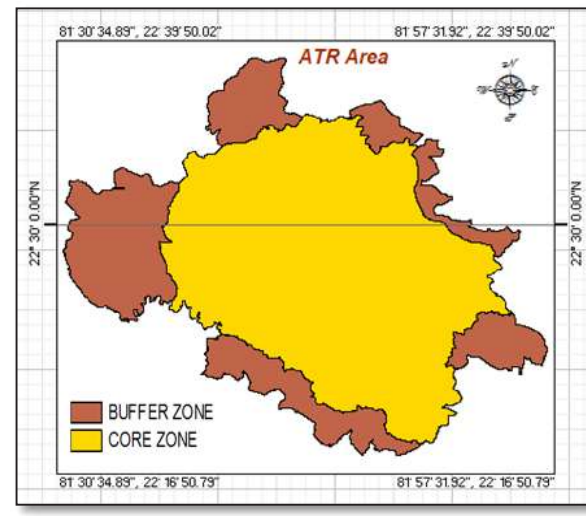

Fig. 2: Zonation map of ATR showing core and buffer zone.

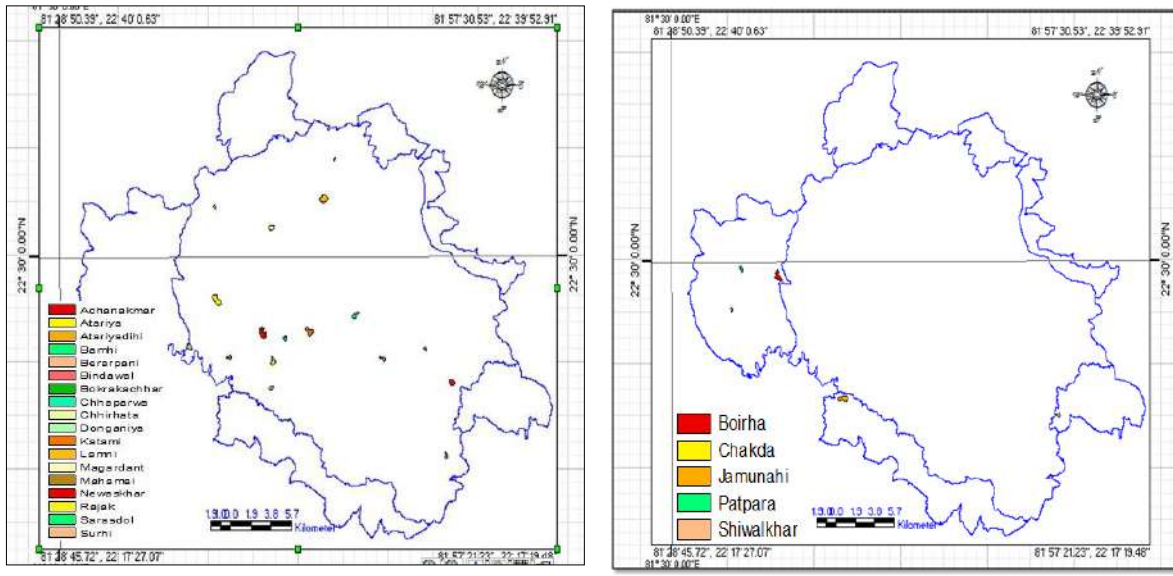

Fig. 3: Location of core and buffer villages of ATR a) Core villages of ATR b) Buffer villages of ATR.

are mainly dependent on forests for their livelihood. They are employed in forestry activities such as road repairing, engineering works, fire safety, wildlife protection, etc. The tribes residing inside the ATR area, cultivate rain-fed annual cereal crops, especially rice. The rise in the human settlement near the forests leads to a decline in wildlife population and

Agricultural land of Achanakmar village

Forest village sarasdol

Core village Bindawal

Housing pattern of Chhaparwa village

Fig. 4: (A to D) Core villages of ATR.

degradation of its natural environment. People residing in the reserve area directly or indirectly depend on the forest for wood, firewood, and non-timber forest products (NTFPs) as there is little to no alternative for them.

The tribes residing inside the ATR area grow annual cereal crops, especially rice. But, the presence of wild animals such as langur, deer, sambhar, etc often leads to crop damage in the core, buffer, and fringe villages.

ATR has a very low human population density as compared to other tiger reserves such as Kaziranga (437 people/km^2) and Namdapha (27 people/km^2). In India, human population density around the tiger reserves did not correlate with the success or failure of the reserves (Post & Pandav 2013).

The main reason behind the success of tiger reserves like Corbett, Kaziranga, Kanha, and Nagarhole is that their core area remains inviolate despite human interference at the periphery of the reserve area (Post & Pandav 2013). Harihar & Pandav (2012) observed that to create an inviolate breeding space for tigers, villages must be relocated from the reserve area. Resettlement has been used in India for over 30 years to remove human settlements from the habitat of tigers and Lions which has resulted in significant recovery of the carnivore population and conflict at many locations (Karnath et al. 1999). Lasgorceix & Kothari (2009) examined the relocation and displacement of core villagers from protected areas and tiger reserves in India and reported a maximum displacement of 24 villages each from Kanha National Park and the tiger reserve (around 650 families) in 1973-74 and Kuno Wildlife Sanctuary, M.P (1400 families) between 1996-2002.

In contrast, human use has favored biodiversity as found in Kanha Tiger Reserve (KTR), M.P (Maan & Chaudhry 2019). Here, the existence of villagers in forests has led to the formation of open grasslands. The forage availability increased for herbivores and these grasslands were managed regularly by using fire and pruning techniques even after village relocation. However, controlled extraction of resources from the reserve area has proven to be sustainable.

Transportation Network

The highways have a serious impact on wildlife and their habitats. Roads are the main cause of habitat fragmentation and there have been increased anthropogenic activities in these areas. A network of main roads and villages was used to understand the spatial pattern of human pressures in the landscape. Proximity to road networks and human habitations is known to have negative effects on habitat quality (Dutta et al. 2016, Joshi et al. 2013).

A large number of roads exist within ATR (Fig 5). State highway 8, approximately 55 km from south to north is the largest and busiest road within the Tiger Reserve. It divides the entire tiger reserve area into two halves. This highway, which runs from south to north, divides the ATR into a larger western area and a smaller eastern area. A stretch of this highway passes through ATR which starts at Shivtarai, the first forest check post, and ends at the last checkpoint of the reserve at Keonchi. In between, there are four other checkpoints. These checkpoints are in the order Shivtarai Barighat Achanakmar Chhaparwa Lamni Keonchi. The authorities are trying to keep unwanted elements out by

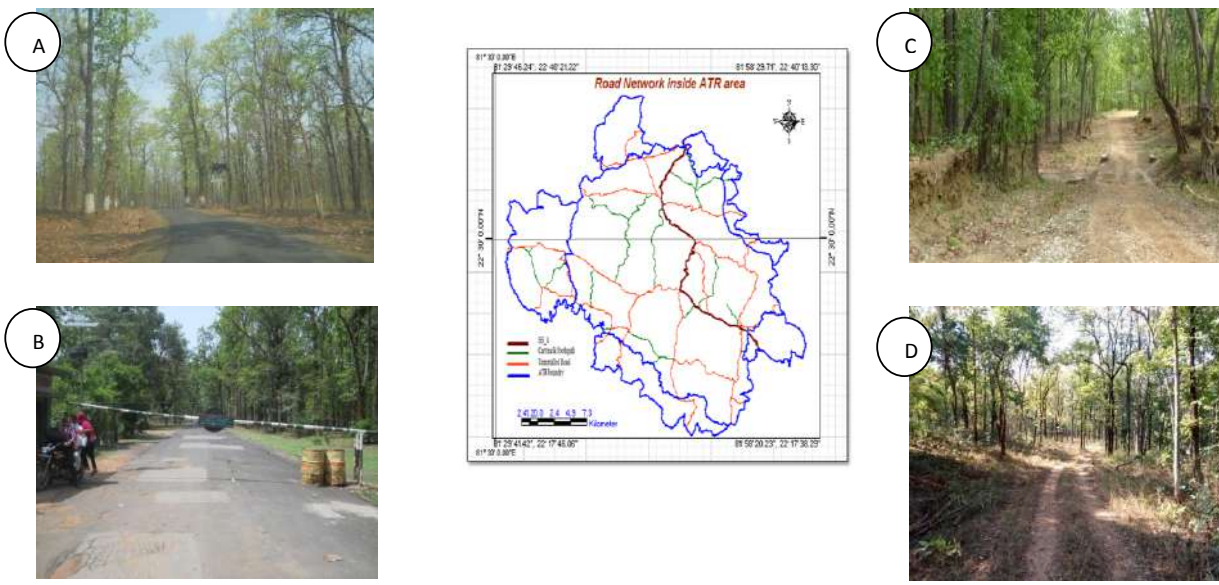

Fig. 5: Road network inside ATR (A & B) State Highway 8 passing through Chhaparwa, (C & D) unmetalled road and tourist road inside ATR.

making the crossing to Keonchi compulsory when entering Shivtarai. Despite the alternative route Ratanpur- Majwani-Kenda-Kevchi (RMKK) route and Bilaspur - Pendra Road - Amarkantak road people often use state highway to reach Amarkantak (an important tourist and religious place).

ATR also has a wide network of tourist roads that facilitate the transportation of safari vehicles. The entire tourist road in ATR is divided into two areas. One is 90 km long in the Achanakmar range. The other road 102 km long is situated in the Chhaparwa range. NCTA guidelines limit tourism to 20% of the core area (Tyagi et al. 2019). But in ATR all the tourist roads are situated in the core zone which hampers the smooth movement of wild animals.

Tyagi et al. (2019) examined the anthropogenic disturbance especially tourism in two tiger reserves of the Central Indian Landscape (Bandhavgarh Tiger Reserve & Kanha Tiger Reserve) and the physiological stress responses of tigers. Their study concluded that the concentration of fecal glucocorticoid metabolite (FGM) was significantly higher in tigers during the tourism period as compared to the non-tourism period. Thus, research has proven that anthropogenic influence not only influences the natural behavior of tigers (dispersal, hunting, and breeding) but also causes physiological changes.

Livestock Population

The villagers residing in and around the protected areas are largely dependent on livestock (Mann & Chaudhry 2019). The tiger reserve area has a large livestock population of around 9000 (Mandal et al. 2017). A high livestock density ($25.44 \pm 11.10/km^2$) in ATR areas has deleterious harmful effects on wild ungulates and their habitat (Mandal et al. 2017). Cattle grazing affects the forage available in the area and the presence of a high density of livestock can lead to competition between wild ungulates for food, resources, etc. Since, ATR area is having low wild ungulate prey density ($32.5/km^2$) (Mandal et al. 2017) as compared to other protected areas such as Sariska Tiger Reserve ($103.4/km^2$) and Rajaji National Park ($90.8/km^2$) (Harihar et al. 2009) which sustain similar predators such as tiger, leopard and striped hyena (Mandal et al. 2017).

The main livestock in the area is buffalo (*Bubalus bubalis*), Cow (*Bos indicus*), and goat (*Capra hircus*) (Fig 6). Few livestock camps have also been reported in the core zone of ATR by local newspapers as well as by Management Effective Evaluation Report, 2010-2011. Yadav families generally prefer to raise cattle for milk production and trade.

These cattle usually graze in the forest area and often lead to livestock deaths from predators like tigers and leopards. The uncontrolled grazing by cattle can lead to the removal of biomass and younger seedlings from the forest. The regeneration of forest tree species is adversely affected due to soil loss through the trampling of the forest floor. Mann & Chaudhry (2019) reported that the 500 families of buffalo herding Maldharis tribe were relocated from the core zone of Gir National Park, Gujarat as a result, the number of cows predated by lions decreased.

Fringe Villages and Their Influence on the ATR Area

There are many forms of anthropogenic pressure on protected areas of India. The main biotic pressures include the felling of firewood, harvesting of timber, grazing and browsing of domestic livestock, lopping of fodder species, and collection of broom grass by fringe villagers thereby causing negative pressure on wildlife and their habitat. There are more than 49 fringe villages within 5 km of the ATR border. The peripheral areas of Tiger Reserve area are under the pressure of heavy grazing.

Conflicts in ATR

Indian protected areas support a huge array of wildlife that is prone to conflict with humans. The expansion of human

Fig. 6: View of livestock population (a &c) cattle grazing in the core zone and (b) construction of the bamboo house for livestock.

activities in and around protected areas has led to major cases of conflict (Karnath et al. 2012, Packer et al. 2005). Several studies have been carried out on the human-animal conflict (Treves & Karnath 2003, Struebig et al. 2018). Livestock depredation is the main reason for human-wildlife conflicts worldwide (Singh et al. 2015, Graham et al. 2005).

High livestock depredation is reported in the ATR area by both tigers and leopards. Major livestock losses are associated with grazing animals both within and near the proximity of the protected areas. Due to the high livestock population, there is an increased possibility of human-wildlife conflict (Mandal et al. 2017) and this is a common phenomenon in both core and buffer areas. No human casualty has been reported by tigers in the reserve area in the past seven decades. The cattle kill incidences by both the apex predator (tiger and leopard) was 378 during the period of three years (2015 to 2018) (Fig 7). Several conflict cases have been published in local newspapers by a sloth bear, leopard, etc.

Man-wildlife conflicts still arise as the crop-raiding herbivores such as chitals (*Axis axis*), nilgais (*Boselaphus tragocamelus*), wild boars (*Sus scrofa*), etc often graze the agricultural field of the villagers. The incidences of crop raiding are more in the fringe areas as compared to the core and buffer because of limited agricultural operations in the area.

The Kaziranga Tiger Reserve recorded 518 cattle kills by tigers over three years (2008-2011) (Borah et al. 2018). Chouksey et al. (2018) examined the human-wildlife conflicts near Bandhavgarh Tiger Reserve and the study reported that maximum conflicts were reported by jackals (37.57%), followed by sloth bears (27.64%), wild boars (20.99%), tigers (8.84%), leopards (3.31%) and 1.65% by other carnivores during the year 2001 to 2011. Singh et al. (2015) studied the human-tiger conflicts in pastoral villages adjacent to Ranthambhore Tiger Reserve between 2006-2011 and reported that maximum conflicts (88.5%) between humans and tigers are due to attacks on domestic animals. Leopard is the main carnivore involved in cattle killings in the Kanha-Achanakmar corridor (Ahmed et al. 2012).

To address the human-animal conflict between the villagers who have lost their livestock, WWF-India has taken steps to provide the villagers with immediate interim financial aid. The compensation from the forest department helps to reduce the initial anger and hostility of the people. Compensation is not the only solution, but it is an important conservation strategy to reduce the retaliatory killing of tigers (Bose et al. 2011). Another permanent and cost-effective solution needs to be implemented for the sustained survival of tigers.

CONCLUSION

The status of anthropogenic influence of core, buffer, and fringe villages of the ATR area was examined to study the degradation in the ecosystem and habitats around the tigers. An uncontrolled human intrusion and traffic movement within the entire reserve area is threatening the conservation goals of ATR. Since tigers avoid locations closer to human settlements, the presence of 18 core villages and 5 buffer villages restrict the movement of tigers in the core zone. Another problem with this tiger reserve is habitat fragmentation, as The State Highway 8 of 55 km

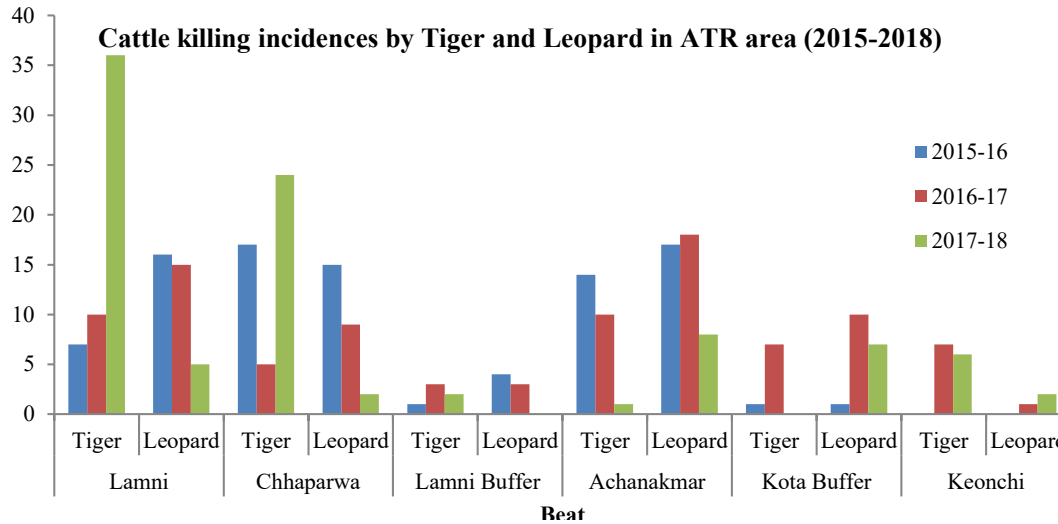

(Source: C.G Forest Department)

Fig. 7: Livestock depredation incidences in different beats of ATR (2015-2018).

divides the entire ATR into two halves. Regular movement of vehicles hinders the smooth movement of wild animals. Thus, vehicular movement should be regulated and restricted. The presence of a large livestock population increases the competition between wild ungulates for fodder and cattle depredation by apex predators can accelerate the conflict between humans and animals.

ATR area can support a good population of tigers by minimizing anthropogenic activity in the core, buffer, and fringe areas. This is possible by village relocation to provide inviolate space for tigers and movement of vehicles in the SH 8 should be restricted as an alternative route is available. The area should be managed properly with proper allocation of resources, land use planning, and sustainable management of natural resources. There is a need to reduce the livelihood dependency on the resources of the reserve area and subsequent anthropogenic pressure to protect the habitat of apex predator *Panthera tigris tigris* and several other rare and endangered flora and fauna.

RECOMMENDATIONS

1. Relocation of core villages from the reserve area.
2. In the dry summer months, special attention should be paid to the availability of water for wild animals.
3. The economic valuation of cattle must be increased by improving their breed to improve the economy of cattle owners and the removal of old and unproductive cattle can reduce the impact of grazing on the nearby forest area.
4. To reduce the impact of heavy grazing by domestic livestock and wild animals, artificial water sources must be created in less-used habitats.

ACKNOWLEDGMENTS

Anupama Mahato is thankful to the University Grand Commission (UGC), Government of India for providing the fellowship (JRF) for the research work. She is also grateful to the Forest Department, Government of Chhattisgarh for providing necessary information and constant support for the study.

REFERENCES

Ahmed, R.A., Prusty, K., Jena, J., Dave, C., Das, S. K., Sahu, H.K. and Rout, S.D. 2012. Prevailing human-carnivore conflict in Kanha-Achanakmar corridor, Central India. World Journal of Zoology, 7(2): 158-164.

Angulo, E., Boulay, R., Ruano, F., Tinau, A. and Cerda, X. 2016. Anthropogenic impacts in protected areas: assessing the efficiency of conservation efforts using Mediterranean ant communities. Peer J., 4: e2773. https://doi.org/10.7717/peerj.2773

Borah, J., Bora, P.J., Sharma, A., Dey, S., Sarmah, A., Vasy, N.K. and Sidhu, N. 2018. Livestock depredation by Bengal tigers in fringe areas of Kaziranga Tiger Reserve, Assam, India: Implications for large carnivore conservation. Human-Wildlife Interact., 12(2): 186-197.

Bose, J., Kandpal K. D., Anwar M., Guleria H., Vattakaven J., Ahmed A. and Ghose D. 2011. Interim Relief Scheme for Cattle depredation by Tigers around Corbett Tiger Reserve, WWF-India, New Delhi.

Champion, H.G. and Seth, S.K. 1968. A revised survey of the forest types of India, Government of India Publication, New Delhi.

Chouksey, S., Singh, S., Pandey, R., and Tomer, V.S. 2018. Monitoring the status of Human-wildlife conflict and its impact on community-based conservation in Bandhavgarh tiger reserve, Madhya Pradesh, India. J. Appl. Nat. Sci., 10(2): 710-715

DeFries, R., Hansen, A., Newton, A. C. and Hansen, M.C. 2005. The increasing isolation of protected areas in tropical forests over the past twenty years. Ecol. Appl., 15(1):19-26.

Dinerstein, E., Louks, C., Wikramanayake, E., Ginsberg, J.J., Sanderson, E., Seidensticker, J., Forrest, J., Bryja, G., Heydlauff, A., Klenzendorf, S., Leimgruber, P., Mills, J., O'Brien, T.G., Shrestha, M., Simons, R. and Songer, M. 2007. The fate of wild tigers. Bio Sci., 57: 508-514.

Dutta, T., Sharma, S. and DeFries, R. 2018. Targeting restoration sites to improve connectivity in a tiger conservation landscape in India. Peer J., 6: e5587.

Dutta, T., Sharma, S., McRae, B.H. and Roy, P.S. 2016. Connecting the dots: Mapping habitat connectivity for tigers in Central India. Reg. Environ. Change, 16(I): 853-867.

Graham, K., Beckerman, A.P. and Thirgood, S. 2005. Human-predator-prey conflicts: ecological correlates, prey losses, and patterns of management. Biol. Conserv., 122 (2): 159-171.

Harihar, A. and Pandav, B. 2012. Influence of connectivity, wild prey, and disturbance on occupancy of tigers in the human-dominated western terai arc landscape. PLoS One, 7: e40105.

Harihar, A., Pandav, B. and Goyal, S.P. 2009. Responses of tiger (Panthera tigris) and their prey to the removal of anthropogenic influences in Rajaji National Park, India. Europ. J. Wild. Res., 55: 97-105.

Jhala, Y., Qureshi, Q. and Gopal, R. 2011. Can the abundance of tigers be assessed from their signs? J. Appl. Ecol., 48: 14-24.

Jhala, Y.V., Qureshi, Q. and Nayak, A.K. (eds). 2020. Status of tigers, co-predators, and prey in India, 2018. National Tiger Conservation Authority, Government of India, New Delhi, and Wildlife Institute of India, Dehradun.

Jhala, Y.V., Qureshi, Q. and Gopal, R. 2015. Status of Tigers in India. 2014. National Tiger Conservation Authority and Wildlife Institute of India, New Delhi and Dehradun.

Joshi, A., Vaidyanathan, S., Mondol, S., Edgaonkar, A. and Ramakrishnan, U. 2013. Connectivity of tiger (*Panthera tigris*) populations in the human-influenced forest mosaic of central India. PloS One, 8(11): e77980.

Karanth, K.K. and DeFries R. 2010. Conservation and management in human-dominated landscapes: Case studies from India. Biol. Conserv., 143: 2865-2869. https://doi.org/10.1016/j.biocon.2010.05.002

Karnath, K.U, Sunquist, M.E. and Chinnappa, K.M. 1999. Long-Term Monitoring of Tigers: Lessons from Nagarhole. Cambridge University Press, Cambridge, United Kingdom, pp. 114-122

Karnath, K.U., Gopalaswamy, A.M., DeFries, R. and Ballal, N. 2012. Assessing patterns of human-wildlife conflicts and compensation around a central Indian protected area. PLOS One,7(2): 1-13.

Kerley L.L., Goodrich J.M., Miquelle D.G., Smirnov E.N., Quigley H.B. and Hornocker M.G. 2002. Effects of roads and human disturbance on Amur tigers. Conserv. Biol., 16: 97-108. https://doi.org/10.1046/j.1523-1739.2002.99290.x

Kumar, N., Mohan, D., Jhala, Y.V., Qureshi Q. and Sergio, F. 2014. Density, laying date, breeding success, and diet of black kites *Milvus migrans*

Govinda in the city of Delhi (India). Bird Study, 61(1):1-8. https://doi.org/10.1080/00063657.2013.876972

Kumari, B., Pandey, A.C and Kumar, A. 2020. Remote sensing approach to evaluate anthropogenic influences on forest cover of Palamau Tiger reserve, Eastern India. Ecol. Process., 9: 17. https://doi.org//10.1186/s/13717-020-0219-z

Lasgorceix, A. and Kothari, A. 2009. Displacement and relocation of protected areas: a synthesis and analysis of case studies. Econ. Polt. Week., 16: 37-47.

Maan, J.S. and Chaudhry, P. 2019. People and protected areas: Some issues from India. Anim. Biodiv. Conserv., 42(1): 79-90.

Mandal, D., Basak, K., Mishra, R.P., Kaul, R. and Mondal, K. 2017. Status of leopard Panthera pardus and striped hyena Hyaena hyaena and their prey in Achanakmar Tiger Reserve, Central India. J. Zool. Stud., 4: 34-41

Mathur, V.B., Gopal, R., Yadav, S.P. and Sinha, P.R. 2011. Management Effectiveness Evaluation (MEE) of Tiger Reserves in India: Process and Outcomes. National Tiger Conservation Authority, Government of India, Delhi, p. 97.

Packer, C., Ikanda, D., Kissui, B. and Kushnir, H. 2005. Lion attacks on humans in Tanzania. Nature, 436(7053): 927-928.

Post, G., and Pandav, B. 2013. Comparative evaluation of tiger reserves in India. Biodiv. Conserv., 22(12): 2785-2794.

Seidensticker, J., Jackson, P. and Christie, S. 1999. Riding the tiger: Tiger conservation in human-dominated landscapes. Cambridge University Press, Cambridge.

Singh, R., Nigam, P., Quershi, Q., Sankar, K., Krausman, P.R., Goyal, S.P. and Nicholoson, K.L. 2015. Characterizing human-tiger conflict in and around Ranthambhore Tiger Reserve, Western India. Eur. J. Wildl. Res., 61: 255-261.

Struebig, M.J., Linkie, M., Deere, N.J., Martyr, D.J., Millyanawati, B., Faulkner, S.C., Comber, S.C.L., Mangunjaya, F.M., Williams, N.L., McKay, J.E. and Freya A.V. 2018. Addressing human-tiger conflict using socio-ecological information on tolerance and risk. Nature Commun., 9: 1-9

Sunquist, M. 1999. Ecology, Behavior, and Resilience of the Tiger and Its Conservation Needs. Cambridge University Press, Cambridge, pp. 5-18.

Thatte, P., Joshi, A., Vaidyanathan, S. Landguth, E. and Ramakrishnan, U. 2018. Maintaining tiger connectivity and minimizing extinction into the next century: Insights from landscape genetics and spatially-explicit simulations. Biol. Conserv., 218: 181-191. https://doi.org/10.1016/j.biocon.2017.12.022.

Thompson, C. 2010. Tigers on the Brink: Facing Upto the Challenge in the Greater Mekong: Cambodia, Laos, Myanmar, Thailand, and Vietnam. WWF Greater Mekong, Vientiane, pp. 1-26.

Treves, A. and Karanth, K.U. 2003. Human-carnivore conflict and perspectives on carnivore management worldwide. Conserv., Biol., 17(6): 1491-1499.

Tyagi, A., Kumar, V., Kittu, S., Reddy, M., Naidenko, S., Ganswindt, A. and Umapathy, G. 2019. Physiological stress responses of tigers due to anthropogenic disturbance especially tourism in two central Indian tiger reserves. Conserv. Physiol., 7(1): 45. https://doi.org/10.1093//cnphy/coz045.

Nature Environment and Pollution Technology
An International Quarterly Scientific Journal

p-ISSN: 0972-6268
(Print copies up to 2016)
e-ISSN: 2395-3454

Vol. 21 | No. 5 (Suppl) | pp. 2269-2274 | 2022

Original Research Paper

https://doi.org/10.46488/NEPT.2022.v21i05.021

Open Access Journal

Evaluation of Heavy Metals in Vegetables from Two Origins Marketed in Northern Peru

J. Grández*, M. Oliva, E. Morales**(***)(****)†, M. Goñas**, S. Chavez** A. Guivin***, L. Quiñones**** and M. Milla*******

*Facultad de Ingeniería Civil y Ambiental (FICIAM), Universidad Nacional Toribio Rodríguez de Mendoza (UNTRM), Chachapoyas 01001, Perú

**Instituto de Investigación para el Desarrollo Sustentable de Ceja de Selva (INDES-CES), Universidad Nacional Toribio Rodríguez de Mendoza (UNTRM), Chachapoyas 01001, Perú

***Universidad Nacional Intercultural Fabiola Salazar Leguía de Bagua (UNIFSLB), Bagua 01721, Perú

****Instituto de Ciencias de Datos (INSCID), Universidad Nacional de Jaén, Jaén 06801, Perú

*****Facultad de Ingeniería, Universidad Nacional de Jaén, Jaén 06801, Perú

†Corresponding author: E. Morales; eli.morales@untrm.edu.pe, emorales@unibagua.edu.pe

Nat. Env. & Poll. Tech.
Website: www.neptjournal.com

Received: 31-05-2022
Revised: 01-07-2022
Accepted: 08-07-2022

Key Words:
Heavy metals
Contamination
Food
Vegetables
Consumers

ABSTRACT

The objective of the study was to evaluate the concentration of arsenic, chromium, cadmium, and lead in onion (*Allium fistulosum* and *Allium cepa*), tomato (*Solanum lycopersicum*), and celery (*Apium graveolens*) from two origins (local - Chachapoyas province and from the coast-province of Chiclayo) that are sold in the model market of the city of Chachapoyas. Six samples were taken on three different dates in November 2020, which were collected by non-probabilistic sampling (by convenience), which allowed choosing the most appropriate sample (according to its origin). For the determination of heavy metals, the Agilent 4100 MP-AES spectrometer was used. The concentration of As, Cr, and Cd in the vegetables remained below the Maximum Allowable Limits of the international standards with which they were compared; however, the concentration of Pb exceeded the Maximum Allowable Limits in all the samples analyzed, obtaining the lowest value in the celery samples from the local origin (0.15 $mg.kg^{-1}$) and the highest value in the tomato samples from the coast (0.21 $mg.kg^{-1}$). Therefore, it is concluded that only Pb is higher than the Maximum Allowable Limits with which it was compared.

INTRODUCTION

Vegetables are the most important sector in agriculture, however, technological advances and innovations are still dependent on the climatological, environmental, and soil conditions for their development (Burbano-Orjuela 2016).

Vegetables occupy an important place in the daily diet because of their vitamin and mineral content. However, exposure to heavy metals through the consumption of contaminated vegetables and their toxicity is a concern (Manzoor et al. 2018).

The presence of heavy metals in foods of vegetable origin, such as vegetables, is generally due to the excessive use of agrochemicals and occasionally the use of wastewater for irrigation (Durán et al. 2017). It was determined that the absorption of agrochemicals in vegetables depends on the type of plant, especially in leafy vegetables, which are not eliminated through food preparation (Guzmán et al. 2016). Also, the presence of heavy metals in vegetables is related to mining, causing socio-environmental conflicts due to the generation of toxic substances. Heavy metals are concentrated in the soil, then they are impregnated in the plants (Madueño & García 2019).

Improper use of pesticides disturbs the components of the environment and can cause pesticide residues in vegetables (Guerrero 2003). In this sense, contamination by mercury (Hg), arsenic (As), cadmium (Cd), and lead (Pb) is closely related to the cultivation scenarios; due to this, the consumption of vegetables with heavy metals affects different parts of the organism (Buendia 2018, González et al. 2020). Vegetables containing cadmium can have harmful consequences on human health, including cancer if consumed for an extended period of time (Estupiñan 2016, Giuffré et al. 2005, Mirabent 2015).

Fiallos (2017)found that the heavy metal content and microbiological quality in fruits and vegetables sold in

markets in the city of Ambato, Colombia, exceeded the permissible limits in food quality for Zn, Mn, Hg, Pb, Cd, and Cu. Also, Juan de Dios (2018) found concentrations of Cadmium and Arsenic in onion (*Allium cepa*) in Metropolitan Lima, which exceed the maximum limit specified by WHO/FAO. Similarly, Marín (2019) compared the concentration of two heavy metals in oregano (Oreganum vulgare) and olives (Olea europaea) in Tacna; based on this background, it can be inferred that there is a presence of heavy metals in vegetables.

However, in northern Peru, there is no study of this type, which leads to a vacuum of information that the authorities require for decision-making. This will benefit public health and the economic prosperity of Peru (Galagarza et al. 2021).

Based on the above, the objective of the study was to evaluate the concentration of heavy metals in vegetables from two sources sold at the Modelo market in Chachapoyas.

MATERIALS AND METHODS

Study Area

The city of Chachapoyas is located in northern Peru, in the region of Amazonas, at an altitude of 2483 meters above sea level, and has a population of 32,026 inhabitants (INEI 2017). Chachapoyas has six markets that sell both groceries and agricultural products: Modelo market (central), La Unión market, Yance market, Requejo market, Pedro Castro market and the wholesale market. The study was carried out with samples obtained from the Modelo market since this market is where vegetables of different origins are concentrated.

Sample Collection

Triplicate samples were taken in November 2020. The non-probabilistic sampling method (by convenience) was used, which allowed for choosing the appropriate sample (according to its origin) (Wang et al. 2019a).

Samples were collected during the morning (6:00 am) because local vegetables are brought to the market at that time to be sold and found fresh. The samples were composed of three vegetables (onion, tomato, and celery) both local and from the coast. To identify the origin of the samples, the traders were consulted about the place of origin. Hermetically sealed polyethylene bags were used and these were transported for analysis to the Water and Soil Laboratory of the Research Institute for Sustainable Development of Ceja de Selva (INDES-CES) of the National University Toribio Rodriguez de Mendoza (UNTRM).

Sample Preparation

Samples of tomato, onion, and celery were washed (Sharma et al. 2008). The edible part of each vegetable was cut into small pieces, the samples were left to dry in aluminum foil, the samples were placed in the oven at 105°C for approximately 24 h, the samples were crushed using the mortar, then 2 g of the samples were weighed in beakers. Finally, the samples were placed in the muffle at 450°C for 6 h.

Methodology for the Detection of Heavy Metals

The determination of heavy metals such as cadmium, lead, arsenic, and chromium in samples of tomato (*Solanum lycopersicum*), onion (*Allium fistulosum*, *Allium cepa*), and celery (*Apium graveolens*) was performed by the Atomic Emission Spectrometry method, using the principle of atomic emission spectrometry method 132 (Azcarate 2017). In the emission process in the spectrometer, the sample is transported by means of a pump to the nebulizer system where it is converted into an aerosol; the aerosol passes into the center of the hot plasma, dries, decomposes, and is then atomized. The plasma is generated by subjecting a flow of nitrogen gas to a zone where microwave radiation is applied. The atoms of the sample emit radiation at a wavelength that is characteristic of each element. The detector then measures the intensity of this radiation; this information is processed by a computer system (Fig. 1).

Statistical Analysis

Data was analyzed using Minitab statistical software version 19.1 (Fachelli 2018). Descriptive statistics was used to calculate the means and standard deviations of heavy metal concentrations by vegetable species and place of origin. An Excel spreadsheet was used to compare the maximum levels allowed by Codex and the EU.

RESULTS

Table 1 shows the results of the heavy metal concentration levels analyzed in the 18 samples of tomato, onion, and celery from two origins.

Fig. 2 shows graphically the concentration of heavy metals according to the origin of the vegetables, where the concentration of arsenic in local and coastal celery was 0.31 and 0.30 $mg.kg^{-1}$, respectively. Likewise, the concentration of chromium for celery from the coast had the highest value reaching 0.33. While the chromium concentration levels for tomatoes were not reported. With respect to the high values of lead, it belongs to the tomato from the coast, and the lowest value can be seen in celery. Lead concentration levels for locally sourced celery showed the lowest concentration (0.15 $mg.kg^{-1}$), while tomatoes from the coast showed the highest values (0.21 $mg.kg^{-1}$).

Table 2 shows that lead exceeds the maximum permissible limits of the Codex Alimentarius (FAO/WHO) and Europe-

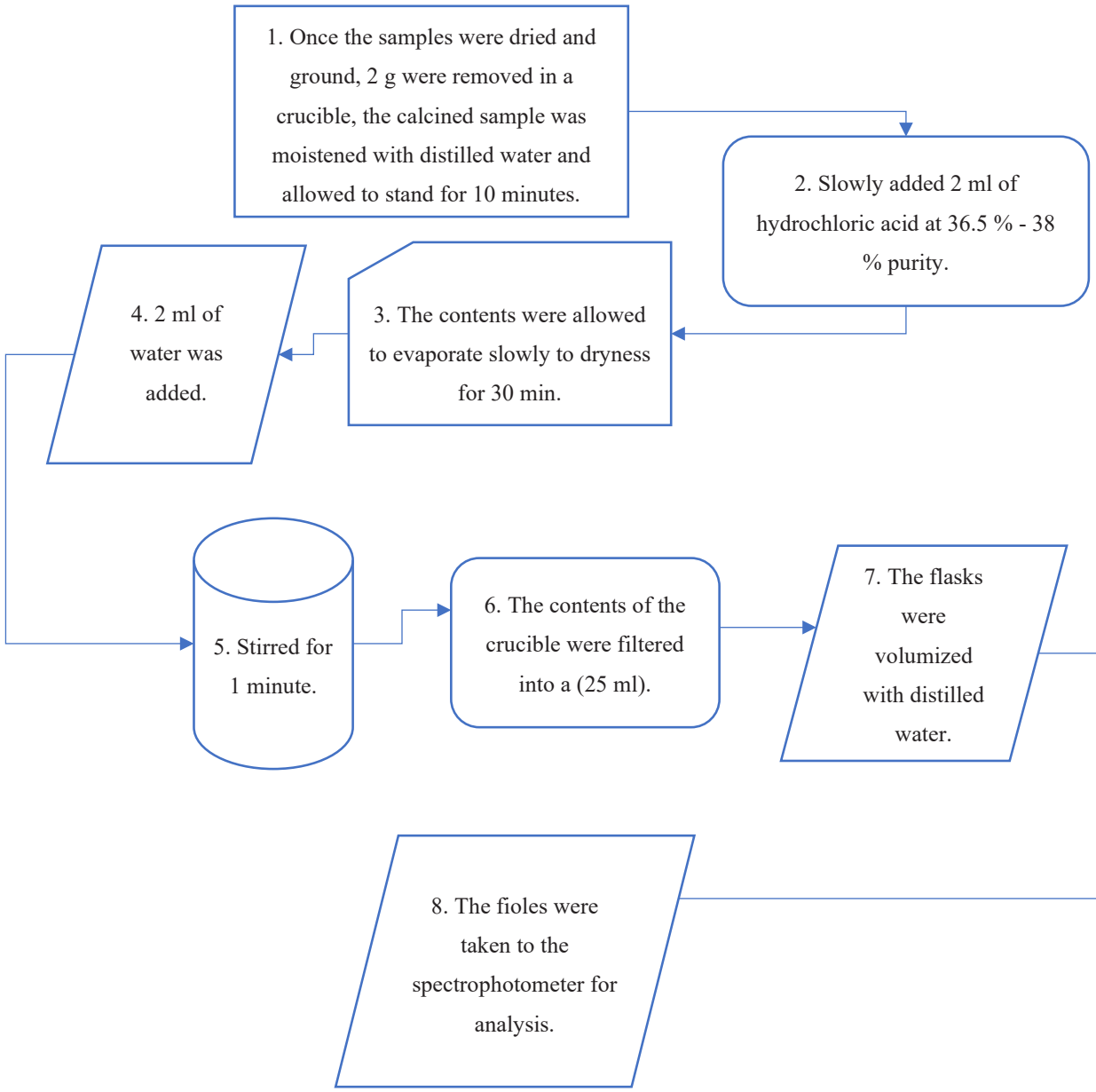

Fig.1: Flow chart of the heavy metal determination methodology.

Table 1: Heavy metal concentrations in vegetable species from two source locations (mean ± standard deviation in $mg.kg^{-1}$).

Cultivation	As	Cr	Cd	Pb
Local tomato	0.23 ± 0.08	0.00 ± 0.00	0.00 ± 0.00	0.18 ± 0.02
Tomato coast	0.25 ± 0.03	0.00 ± 0.00	0.00 ± 0.00	0.21 ± 0.04
Local onion	0.23 ± 0.08	0.01 ± 0.01	0.00 ± 0.00	0.20 ± 0.01
Onion Coast	0.22 ± 0.06	0.00 ± 0.00	0.00 ± 0.00	0.17 ± 0.01
Local celery	0.31 ± 0.05	0.03 ± 0.01	0.00 ± 0.00	0.15 ± 0.02
Celery coast	0.30 ± 0.02	0.03 ± 0.03	0.00 ± 0.00	0.17 ± 0.01

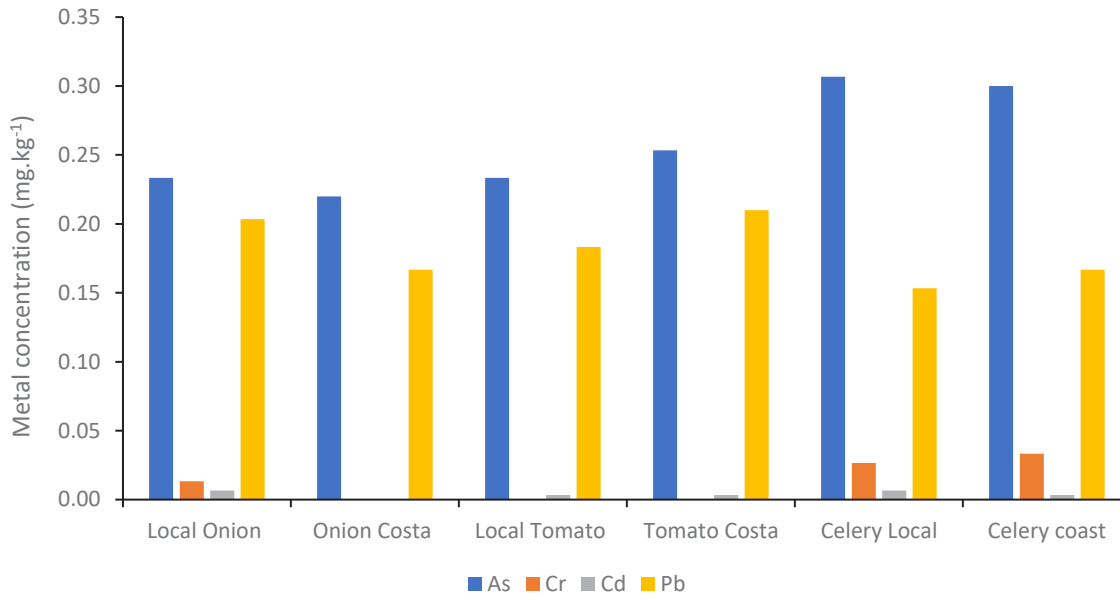

Fig. 2: Concentration of heavy metals for vegetables according to their origin.

Table 2. Concentration of heavy metals in vegetable species compared with the maximum permissible limits of international standards.

Parameters	Vegetables evaluated						Maximum allowable limit		
	Local Onion	Onion Costa	Local Tomato	Tomato Costa	Celery Local	Celery Coast	CODEX [mg.kg^{-1}]	UE [mg.kg^{-1}]	ECA SOILS [mg.kg^{-1}]
As	0.233	0.220	0.233	0.253	0.307	0.300	0.5	NC	50
Cr	0.013	0.000	0.000	0.000	0.027	0.033	NC	0.1	0.4
Cd	0.007	0.000	0.003	0.003	0.007	0.003	0.05	NC	1.4
Pb	0.203*	0.167*	0.183*	0.210*	0.153*	0.167*	0.1	0.1	70

ECA = Environmental Quality Standards for Soil; NC = Not covered by the standard; * = Values exceeding maximum permissible limits.

an Union (EU) food safety standards. The comparison with the Environmental Quality Standards (EQS) for soils is also shown.

DISCUSSION

High concentration of heavy metals is a risk to human health due to exposure during vegetable consumption (Birghila 2022). Arsenic in food can be acquired by the effects of volcanic ash, water, soil, and pesticides; it can also be due to the use of arsenic or phosphorus-based insecticides because they induce the accumulation of arsenic in plant tissues (Fiallos 2017). Another problem is the presence of arsenic, which may be due to the soils in which it is grown, the sediments, and the water used for irrigation (Chuan-Ping et al. 2012). However, due to crop permeation, the highest concentrations are directly related to mining regions and are becoming a global concern (Alonso et al. 2014, Tripathi et al. 2007).

The highest chromium concentration was 0.03 mg.kg^{-1} for local and coastal celery since celery can accumulate chromium in its edible and inedible parts (Wang et al. 2019b). Generally, the concentration of chromium is due to the natural components of the soil (Mihaileanu et al. 2019). Chromium in lower concentrations may help stabilize blood glucose levels; however, if these values were excessive, it would cause irregular heartbeat, and stomach upset (Järup 2003). Even worse if these vegetables are consumed without adequate washing (Nabulo et al. 2012).

Lead was the metal found in high concentrations in celery, onion, and tomato. Contamination is generally higher in plant foods, especially leafy vegetables, due to plant uptake and the existence of soil contaminated with this metal (Malavolti et al. 2020, Reyes et al. 2016). It may also be due to the use of agrochemicals such as pesticides and fertilizers, sewage sludge, and compost (Olivares 2013). It

can also be attributed to other anthropogenic activities such as the dumping of paint and garbage dumps containing electronic parts (Ds et al. 2017). They may also be influenced by roadside crops (Nabulo et al. 2006).

Lead exposure occurs mostly through the food chain, and as long-term Pb intake through food can have negative health effects (even at relatively low levels), it is being researched for risk assessment of human health (Ćwieląg-Drabek et al. 2020). The irrigation of vegetables with wastewater should be monitored and controlled through some management plans, in order to avoid health risks for consumer groups (Atamaleki et al. 2019). To reduce contaminants such as heavy metals in crops, the transportation system and handling of agricultural products must be improved to reduce the introduction of heavy metals into crops (Onwuka et al. 2019).

With respect to lead concentrations, the highest level found was 0.21 ppm in tomatoes from the coast; this value is higher than the one obtained by Heshmati et al. (2020) (0.007 $mg.kg^{-1}$ for tomatoes). Likewise, Sharma et al. (2016), found elevated lead values (1.20 $mg.kg^{-1}$) in sites that were close to sewage drainage but irrigated with groundwater. In that regard, it is crucial to define corrective variables for future research, such as the principles of sound agricultural practices for consumer protection purposes (CODEX 1999).

It should be noted that the concentrations of heavy metals such as cadmium, chromium, and arsenic, compared to the limits established for vegetables (onion, tomato, and celery) both from the coast and from local sources, did not exceed the Maximum permissible limits established by the Codex Alimentarius (FAO/WHO) and European Union food safety standards. Donkor et al. (2017) also found that 18.99% of leafy vegetable samples had metal detections below the FAO/WHO reference values. However, studies show that the metal content varies greatly between samples (different origins), indicating that there is no standard composition (Çelik et al. 2018). The RCTs were significant for the comparison of the evaluated parameters because they served as a reference for the amount of heavy metals and other contaminants present in soils as a receiving body. They were also significant for the population's health because the levels of heavy metals in vegetables shouldn't pose a risk to human health or the environment (MINAM 2017).

CONCLUSIONS

The concentration of cadmium, chromium, and arsenic for tomato, onion, and celery vegetables sold in the Central Market of Chachapoyas from local and coastal sources did not exceed the maximum permissible limits established by the Codex Alimentarius (FAO/WHO) and European Union food safety standards. Lead concentrations in tomatoes, onions, and celery from local and coastal sources exceeded the maximum permissible limits established by Codex Alimentarius (FAO/WHO) and European Union food safety standards. Finally, future studies on vegetables are needed, with a larger number of samples, over longer periods of time, for the implementation of food safety measures.

ACKNOWLEDGMENTS

The authors acknowledge and thank the funding of the CEINCAFE Public Investment Project (SNIP N° 352439), executed by the Research Institute for the Sustainable Development of Ceja de Selva (INDES-CES) of the National University Toribio Rodriguez de Mendoza of Amazonas (UNTRM).

REFERENCES

Alonso, D.L., Latorre, S., Castillo, E. and Brandão, P.F.B. 2014. Environmental occurrence of arsenic in Colombia : A review. Environ. Pollut., 186: 272-281. https://doi.org/10.1016/j.envpol.2013.12.009

Atamaleki, A., Yazdanbakhsh, A., Fakhri, Y., Mahdipour, F., Khodakarim, S. and Mousavi, A. 2019. The concentration of potentially toxic elements (PTEs) in the onion and tomato irrigated by wastewater : A systematic review; meta-analysis and health risk assessment. Food Res. Int., 125: 108518. https://doi.org/10.1016/j.foodres.2019.108518

Azcarate, R. 2017. Optimization of Variables for the Determination of Arsenic by Hydride Generation by Microwave Plasma Atomic Emission Spectrometry (MPAES). Bachelor Thesis, National University of La Pampa, Argentina.

Buendia, B.F. 2018. Evaluation of the Concentration of Heavy Metals in Passiflora ligularis Fruits Due to the Intensive Use of Agrochemicals Oxapampa, Pasco. Doctoral Thesis, Postgraduate Unit of the Faculty of Forestry and Environmental Sciences, National University of Central Peru, Lima.

Burbano-Orjuela, H. 2016. Soil and its relationship with ecosystem services and food security. J. Agric. Sci., 33(2): 117. https://doi.org/10.22267/rcia.163302.58.

Birghila, S., Matei, N., Dobrinas, S., Popescu, V., Soceanu, A., & Niculescu, A. 2022. Assessment of heavy metal content in soil and Lycopersicon esculentum (tomato) and their health implications. Biol. Trace Element Res., 11: 1-10.

Çelik, A., Yaman, H., Turan, S., Kara, A., Kara, F., Zhu, B., Qu, X., Tao, Y., Zhu, Z., Dhokia, V., Nassehi, A., Newman, S.T., Zheng, L., Neville, A., Gledhill, A., Johnston, D., Zhang, H., Xu, J.J., Wang, G. and Dutta, D. 2018. No covariance structure analysis of health-related indices for the elderly at home, focusing on subjective feelings of health title. J. Mater. Process. Technol., 1(1): 1-8.

Chuan-Ping, L., Chun-ling, L., Xiang-Hua, X., Chuang-An, W., Fang-Bai, L. and Gan, Z. 2012. Chemosphere effects of calcium peroxide on arsenic uptake by celery (Apium graveolens L.) grown in arsenic-contaminated soil. Chemosphere, 86(11): 1106-1111. https://doi.org/10.1016/j.chemosphere.2011.12.033

CODEX. 1999. General Standard of Codex Stan 193-1995, for Contaminants and Toxins, Present in Food and Feed. https://www.fao.org/fao-who-codexalimentarius/sh-proxy/en/.pdf

Ćwieląg-Drabek, M., Piekut, A., Gut, K. and Grabowski, M. 2020. Risk of cadmium, lead, and zinc exposure from consumption of vegetables produced in areas with mining and smelting past. Sci. Rep., 10(1): 3363. https://doi.org/10.1038/s41598-020-60386-8

Donkor, A., Fordjour, L.A., Tawiah, R., Asomaning, W., Dubey, B., Osei-Fosu, P., Ziwu, C. and Mohammed, M. 2017. Evaluation of trace metals in vegetables sampled from farm and market sites of Accra Metropolis, Ghana. Int. J. Environ. Stud., 74(2): 315-324. https://doi.org/10.1080/00207233.2016.1261599

Ds, J., Eo, E., Ma, S., Bs, D. and Ab, M. 2017. Assessment and effects of lead (Pb) and chromium (Cr) from vegetables grown by wastewater irrigation at doctor's s quarters in Bauchi metropolis, Nigeria. J. Pharmacog. Phytochem., 6(6): 2083-2085.

Durán, A., González, M. I., Vargas, G. and Mora, D. 2017. Potential risk situations related to the application of agrochemicals in horticultural systems. Costa Rican Agron., 41(2):, 67-77. https://doi.org/10.15517/rac.v41i2.31300

Onwuka, K., Christopher, A. and Victor, A. 2019. A study on heavy metals comparison in processed tomato paste and fresh tomatoes sold in a market in Umuahia Metropolis of Abia State Nigeria. J. Anal. Tech. Res., 01(01): 26-32. https://doi.org/10.26502/jatri.004

Estupiñan, J. M. 2016. Evaluation of the Risk in Human Health Due to the Consumption of Vegetables Irrigated with Waters That Contain Heavy Metals in A Sector of the Tunjuelo River Basin. Research Paper, National University of Colombia Bogota Campus Faculty of Engineering Department of Civil and Agricultural Engineering, pp. 1-160.

Fachelli, S. 2018. Methodology of quantitative social research. Educ. Law Mag., 17: 13-27. https://doi.org/10.1344/reyd2018.17.13

Fiallos, M. 2017. Quantification of heavy metals and microbiological quality of fruits and vegetables that are sold in the Wholesale Market of the city of Ambato. Technical University of Ambato Faculty of Food Science and Engineering Biochemical, Ecuador, p. 61.

Galagarza, O.A., Ramirez-Hernandez, A., Oliver, H.F., Álvarez Rodríguez, M.V., Valdez Ortiz, M., Pachari Vera, E., Cereceda, Y., Diaz-Valencia, Y. K. and Deering, A.J. 2021. Occurrence of chemical contaminants in Peruvian produce: A food-safety perspective. Foods, 10(7): 1461. https://doi.org/10.3390/foods10071461.

Giuffré, L., Ratto, S., Marbán, L., Schonwald, J. and Romaniuk, R. 2005. The risk from heavy metals in urban agriculture. Soil Sci., 23(1): 101-106.

González, C., Orué, R., Morel, M., Adorno, C. and Bañuelos, F. 2020. Risk factors for chronic non-communicable diseases in dental students. Rev. Sci. Odontol., 2(1): 5-11.

Guerrero, J. 2003. Study of pesticide residues in fruits and vegetables in specific areas of Colombia. Redalyc, 21: 198-209.

Guzmán, P., Guevara, R., Olguín, J. and Mancilla, O. 2016. Peasant perspective, pesticide poisoning and use of agrochemicals. Idea, 34(3): 69-80.

Heshmati, A., Mehri, F., Karami-Momtaz, J. and Khaneghah, A.M. 2020. Concentration and risk assessment of potentially toxic elements, lead, and cadmium, in vegetables and cereals consumed in western Iran. J. Food Prot., 83(1): 101-107. https://doi.org/10.4315/0362-028X.JFP-19-312

INEI. 2017. Peru: Growth and distribution of the total population, 2017. Censused population plus omitted population. J. Chem. Inform. Modeling, 53(9): 76.

Järup, L. 2003. Hazards of heavy metal contamination. Brit. Med. Bull., 68: 167-182. https://doi.org/10.1093/bmb/ldg032

Juan de Dios, M. 2018. N Arsenic and cadmium levels in samples of onion (Allium cepa) sold in the city of Lima. National University of San Marcos Faculty of Pharmacy and Biochemistry Professional School of Toxicology Levels, Lima, pp.1-103.

Madueño, F. and García, M. 2019. Determination of heavy metals (Lead and Cadmium) in lettuce (*Lactuca sativa*) from markets in Metropolitan Lima. Sci. Res., 21: 19-23.

Malavolti, M., Fairweather-Tait, S.J., Malagoli, C., Vescovi, L., Vinceti, M. and Filippini, T. (2020). Lead exposure in an Italian population: Food content, dietary intake, and risk assessment. Food Res. Int., 137: 109370. https://doi.org/10.1016/j.foodres.2020.109370

Manzoor, J., Sharma, M. and Wani, K. A. 2018. Heavy metals in vegetables and their impact on the nutrient quality of vegetables: A review. J. Plant Nutr., 41(13): 1744-1763. https://doi.org/10.1080/01904167.2018.1462382

Marín, L.A. 2019. Comparison of the concentration of Two Heavy Metals (Cadmium and Lead) in Oregano (*Oreganum vulgare*) and Olives (*Oleo europaea*) Harvested in Pampa Sitana and La Yarada in the Tacna Region, 2019. Doctoral Thesis, Jorge Basadre Grohmann National University, Tacna, pp. 1-86.

Mihaileanu, R.G., Neamtiu, I.A., Fleming, M., Pop, C., Bloom, M.S., Roba, C., Surcel, M., Stamatian, F. and Gurzau, E. 2019. Assessment of heavy metals (total chromium, lead, and manganese) contamination of residential soil and homegrown vegetables near a former chemical manufacturing facility in Tarnaveni, Romania. Environ. Monit. Assess., 19(1): 142. https://doi.org/10.1007/s10661-018-7142-0

MINAM. 2017. They approve environmental quality standards (ECA) for soil D.S. N° 011-2017-mINAm. The Peruvian, 6: 12-15. http://www.minam.gob.pe/wp-content/uploads/2017/12/DS_011-2017-MINAM.pdf

Mirabent, C. 2015. Determination of metals in vegetables and physical-chemical parameters of irrigation water from two organogenic in Camagüey Student: Marta Abreu de Las Villas Central University. Faculty, 11: 1-66.

Nabulo, G., Black, C. R., Craigon, J. and Young, S. D. 2012. Does the consumption of leafy vegetables grown in peri-urban agriculture pose a risk to human health? Environ. Pollut., 162: 389-398. https://doi.org/10.1016/j.envpol.2011.11.040

Nabulo, G., Oryem-Origa, H. and Diamond, M. 2006. Assessment of lead, cadmium, and zinc contamination of roadside soils, surface films, and vegetables in Kampala City, Uganda. Environ. Res., 101(1): 42-52. https://doi.org/10.1016/j.envres.2005.12.016

Olivares, S. 2013. Cadmium, lead, copper, and zinc levels in vegetables grown in a highly urbanized area of the city of Havana, Cuba. Int. J. Environ. Pollut., 29(4): 285-293.

Reyes, Y., Vergara, I., Torres, O., Díaz, M. and González, E. 2016. Heavy metal pollution: Implications on health, environment and food safety. Indian J. Pediat., 16(1): 66-77. https://doi.org/10.1007/BF02796157

Sharma, A., Katnoria, J.K. and Nagpal, A.K. 2016. Heavy metals in vegetables: Screening health risks involved in cultivation along wastewater drain and irrigating with wastewater. SpringerPlus, 5(1): 1-16. https://doi.org/10.1186/s40064-016-2129-1

Sharma, R.K., Agrawal, M. and Marshall, F.M. 2008. Heavy metal (Cu, Zn, Cd, and Pb) contamination of vegetables in urban India: A case study in Varanasi. Environ. Pollut., 154(2): 254-263. https://doi.org/10.1016/j.envpol.2007.10.010

Tripathi, R.D., Srivastava, S., Mishra, S., Singh, N., Tuli, R., Gupta, D.K. and Maathuis, F. J.M. 2007). Arsenic hazards : Strategies for tolerance and remediation by plants. Trends Biotechnol., 25(4): 158-165. https://doi.org/10.1016/j.tibtech.2007.02.003

Wang, L., Yang, D., Li, Z., Fu, Y., Liu, X., Brookes, P. C. and Xu, J. 2019a. A comprehensive mitigation strategy for heavy metal contamination of farmland around mining areas – Screening of low accumulated cultivars, soil remediation, and risk assessment. Environ. Pollut., 245: 820-828. https://doi.org/10.1016/j.envpol.2018.11.062

Wang, P., Yin, N., Cai, X., Du, H., Li, Z., Sun, G. and Cui, Y. 2019b. Variability of chromium bioaccessibility and speciation in vegetables: The influence of in vitro methods, gut microbiota and vegetable species. Food Chem., 277: 347-352. https://doi.org/10.1016/j.foodchem.2018.10.120

Nature Environment and Pollution Technology
An International Quarterly Scientific Journal

p-ISSN: 0972-6268
(Print copies up to 2016)
e-ISSN: 2395-3454

Vol. 21 | No. 5 (Suppl) | pp. 2275-2281 | 2022

Review Research Paper

https://doi.org/10.46488/NEPT.2022.v21i05.022

Open Access Journal

Association Between $PM_{2.5}$ Induced Diseases and COVID-19: A Systematic Review

Gulshan Sharma*, Era Upadhyay*† and Pawan Tiwari**
*Amity Institute of Biotechnology, Amity University, Jaipur, Rajasthan, India
**School of Excellence in Pulmonary Medicine, Netaji Subhash Chandra Bose Medical College, Jabalpur, India
†Corresponding author: Era Upadhyay; era.upadhyay@gmail.com

Nat. Env. & Poll. Tech.
Website: www.neptjournal.com

Received: 18-03-2022
Revised: 06-05-2022
Accepted: 08-05-2022

Key Words:
Air pollution
Particulate matter
COVID-19
Health impact
$PM_{2.5}$

ABSTRACT

A novel severe acute respiratory syndrome coronavirus 2 (SARS-CoV-2) caused a global pandemic that started in China (Wuhan, Hubei region) in December 2019, called Coronavirus disease. This systematic review intends to evaluate the correlation of pre-existing particulate matter ($PM_{2.5}$) induced comorbidities along with COVID-19 spread and mortality. A search was operated to report the association between $PM_{2.5}$ and COVID-19 outbreak and evaluating the $PM_{2.5}$ related disease affected by COVID-19 infection. The research was conducted in consent with the criteria of PRISMA (Preferred Reporting Items for Systematic Reviews, and Meta-Analyses). We filtered the review and research articles published only in the English language and selected these keywords: air pollution, particulate matter, COVID-19, health impact. We obtained a total of 27 appropriate published articles in their final version. Additional articles were rectified by searching through Scopus, PubMed and Google Scholar. We concluded that the values of coagulation biomarkers in all SARS-CoV-2 patients were considerably higher as compared with healthy people. It was noted that Hypertension, Diabetes, COPD, CVD, Asthma and Cancer possess an evident relation with COVID-19 severity. Globally, air pollutants affect the body's immunity, leading to people being more susceptible to pathogens. In addition, transmission from person-to-person dynamic of the new respiratory virus was considered the environmental factors' role in accelerating coronavirus spread and its lethality. COVID-19 patients with pre-existing comorbidities induced by particulate matter show a high risk of mortality as compared to COVID-19 patients without these comorbidities.

INTRODUCTION

A novel (COVID-19) pandemic caused by Severe Acute Respiratory Syndrome Coronavirus 2 (SARS-COV- 2) emerged from Wuhan, China in December 2019 and spread all over the world (Han et al. 2020). The diameter of Coronavirus is approx.70–90 nm, single-stranded RNA viruses (He et al. 2020). The life cycle of SARS CoV-2 in human lung cells is completed in several stages including infiltration, inhalation, in the upper respiratory tract (Mallapaty 2020). Therefore, it is necessary to examine the various correlated issues related to particulate matter that are being introduced in this section.

$PM_{2.5}$ and COVID-19

Air pollution exposure has become a main public health issue due to increasing sources of pollutants (Kim et al. 2015). The particulate matter ($PM_{0.1}$, $PM_{2.5}$, and PM_{10}) can stick to viruses. If the virus carrying particulate matter inhaled, may transport the virus in the alveolar and tracheobronchial region and may weaken the immunity (Qu et al. 2020, Chauhan & Singh 2020). The Italian Society of Environmental Medicine launched a discussion paper on 16 March, for the first time presumed a possible correlation between the higher particulate matter concentration ($PM_{2.5}$ and PM_{10}) and the impact of COVID-19 pandemic in Northern Italy, in association with its weather conditions. These observations revealed that ambient particulate matter could not serve as a "boosting factor" but at least imitate as an indicator for COVID-19 severity in terms of health outcomes seen in Northern Italy (Setti et al. 2020, Badawi & Ryoo 2016).

Impact of Climate on COVID-19 Spread

The local environment such as weather, particle source, microenvironments influence PM exposure (Kim et al. 2015). It seems that air pollution plays a role in the airborne spread of SARS-CoV-2 and in the severity of coronavirus (Dehghani et al. 2017, Deepak et al. 2020). In this context, it may be assumed that a high level of air pollutants in an atmosphere together with some climatic parameters might

encourage longer stability of the virus in the air. It would support an indirect dispersal of SARS-CoV-2 with the direct physical spreading of the virus in person to person (Copat et al. 2020). Ho et al. reported that long-term $PM_{2.5}$ exposure affects the cardiovascular and respiratory system, and some COVID-19 symptoms may increase the chance of mortality in COVID-19 patients (Ho et al. 2020, Comunian et al. 2020).

Particulate matter is regulated in the environment, but PM less than 2.5μm is of main concern because of its greater penetration into the alveoli of the lungs and high reactive surface area. It causes cardiovascular disease including thrombosis and endothelial dysfunction (Raji et al. 2020, Hampel et al. 2015). Emerging evidence established correlation between environmental factors (climate, air pollution, chemical exposures, built environment) and transmission of SARS-CoV-2 susceptibility and severity (Weaver et al. 2022, Wang et al. 2022, Diffenbaugh 2022).

Effect of Particle Size and Particle Components

After inhalation, the deposition of particles in the respiratory tract depends on the pattern of breathing and particle size. A particle diameter of more than 10 μm (PM_{10}) can pass through the nose but too broad to reach the respiratory tract. But fine particles ($PM_{2.5}$) and ultrafine particles ($PM_{0.1}$), can deeply penetrate the human lungs and then deposited in alveolar regions at the time of mouth breathing (Dehghani et al. 2017). That's why the researchers and the government of countries should estimate exposure of $PM_{2.5}$ in areas exposed to the high levels of particulate pollution, at the time of framing policies to overcome the rate of COVID-19 (Dehghani et al. 2017, Kamf et al. 2020, Leikauf et al. 2020).

MATERIALS AND METHODS

We followed a systematic review method to report the association between $PM_{2.5}$ and COVID-19 outbreak and evaluating the $PM_{2.5}$ related disease affected by COVID-19 infection. The research was conducted in consent with the criteria of PRISMA (Preferred Reporting Items for Systematic Reviews and Meta-Analyses), and the Flow Diagram is shown in Fig. 1. The research was guided in the Scopus database using Advanced Search Builder, and the keywords were searched in (Abstract OR Title). We have filtered the review and research articles published only in the English language and selected the keywords: air pollution, particulate matter, COVID-19, health impact. We have excluded articles, short surveys, letter, opinion, commentary, or non-relevant articles. We obtained a total of 27 appropriate published articles in their final version. For some of the papers, we select only principal findings that precisely fit the aim of this review.

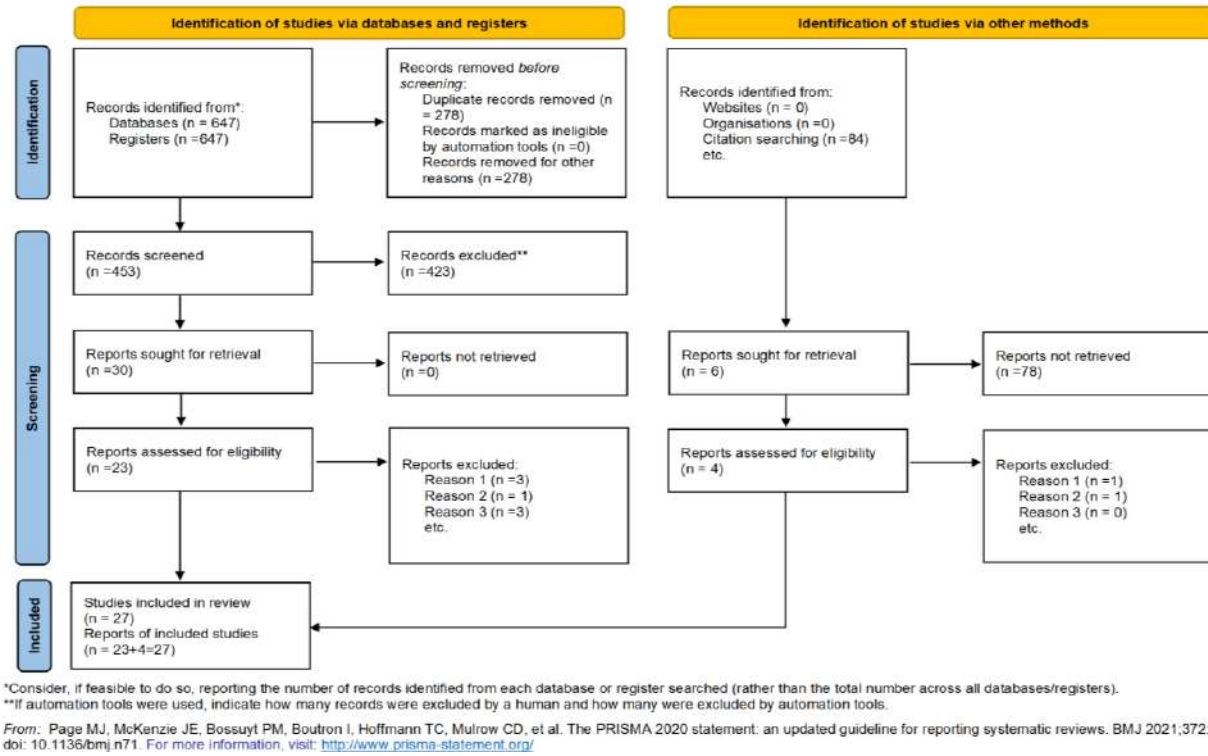

Fig. 1. PRISMA flow diagram of identification, screening, and inclusion of studies.

Morbidity/Mortality Evidence on the Correlation between $PM_{2.5}$ and COVID-19

It can be assumed that SARS-CoV-19 using a species of "highways", made up of atmospheric particulates helps in increasing its indirect viral transmission. The air pollutants exposure can cause oxidative stress, lead to free radicals' production, which in turn might damage the respiratory system, and results in decreasing the resistance towards viral infections. The COVID-19 pandemic is spreading via particulate matters, air, and aerosols which act as a major factor in mediating severity in COVID-19 confirmed cases because the SARS-CoV-2 virus can prolong survival in aerosols for up to 3 hours (Marques & Domingo 2020). Air pollution is positively associated with Angiotensin-Converting Enzyme 2 (ACE-2) receptor (that behaves as a binding receptor for SARS-CoV-2) in respiratory cells of humans and that may speed up the severity in susceptible people from Coronavirus Disease leading to death (Agarwal et al. 2020, Morawska et al. 2020, Zeng et al. 2022).

Significantly, the seriousness of COVID-19 is dependent on the interconnections between viral infection and chronic diseases such as respiratory and cardiovascular diseases which are themselves impacted by environmental stressors (Barouki et al. 2021). Outdoor airborne transmission probability depends on a few parameters, still quite uncertain: viability and lifetime, virus-loaded aerosol concentrations, and the minimum dose required to spread the disease (Marques & Domingo 2020). Therefore, particulate matter pollution should be lessened in regions where positive cases of COVID-19 are unpredictably high (Paital et al. 2020, Newby et al. 2015). The morbidity and mortality may be understood by a systematic framework shown in Fig. 2.

Viral Transmission and Symptoms

COVID-19 transmission appears to spread human–to–human when a person is in the stage of showing symptoms or incubation stage. Transmission occurs via touching non-living objects, and infected surfaces (skin-to-skin) (He et al. 2020). COVID-19 viruses may survive on sterile sponges, aluminum, and surgical gloves for a long period and later can transmit via touch (Qu et al. 2020). SARS- CoV- 2 has also been noticed in tears, which is similar to SARS- CoV (He et al. 2020). Human coronaviruses can be contagious on non-living surfaces for 9 days at room temperature. Larger aerosol droplets may fall on objects such as desks and can be active for 3- 5 days. Fecal transmission may also be possible because COVID -19 has been detected in stool samples (Qu et al. 2020). The mean incubation time is about 5 days, from 1 to 14 days (He et al. 2020). Coronavirus can stay last on copper for 1 hour period, on cardboard for 3 hours, and can stay for up to 5.6 hours on stainless steel surfaces, and 6.8 hours on plastic, resulting in fomite transmission (Marques & Domingo 2020). People standing near an infected patient within less than 2 meters of the area can also get that infection by sneezing or being coughed by an infected person. An elevated temperature greater than 100.4°F along with other symptoms like runny nose, body aches, sore throat, etc. may occur during the infection (Fang et al. 2020). Generally, the air pollution-to-person transmission mechanism plays a major role instead of human-to-human transmission (Coccia 2021, Schiffrin et al. 2020).

Biomarkers

Red blood cells, Haemoglobin, Coagulation factors, Platelet count, Fibrinogen, C-reactive protein, Protein oxidation and Interleukin-6 measured in blood plasma and found that PM exposure was interconnected with increased C-reactive protein (CRP), plasma viscosity, and blood coagulation. Blood parameters change with plaque misbalance, which leads to coronary disease in patients (Ruckerl et al. 2006).

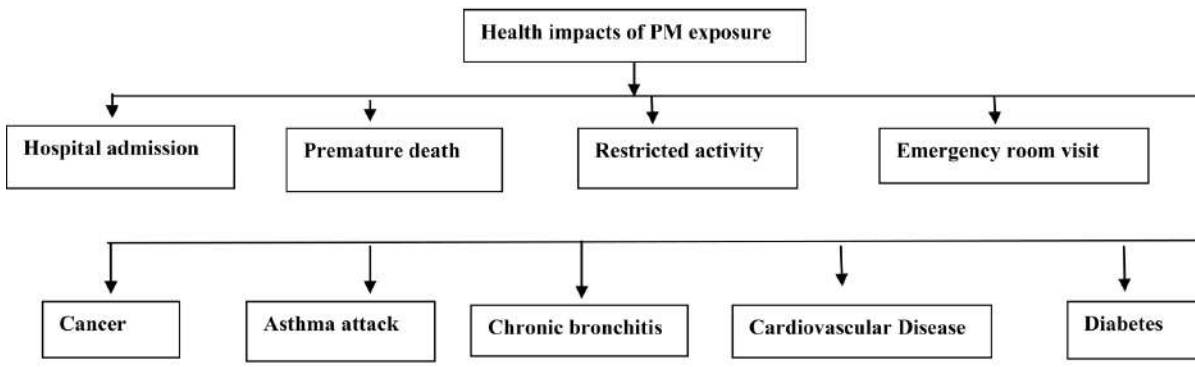

Fig. 2. Systematic framework for morbidity and mortality due to PM exposure.

Fibrinogen, a glycoprotein complex is produced in the liver. It is converted enzymatically by thrombin to fibrin and then to a fibrin-based blood clot. The amount of fibrinogen is responsible for clot formation (Bonzini et al. 2010). The Particulate effect increases with less diameter because of easier vascular penetration, high pulmonary deposition efficiency. These effects could develop within 2 hours after PM exposure and become powerful within the first 12 or 24 hours (Chen et al. 2015). High exposure to PM may increase the amount of C- reactive protein (CRP), coagulation of blood, plasma viscosity, fibrinogen, and platelet count. However, biomarkers such as inflammation marker (interleukin 6), haemostasis (platelet counts and coagulation factors) are used in clarifying the mechanism of action. Production of IL-6 stimulates by exposure to particulate matter causes the formation of thrombosis (Ruckerl et al. 2006, Zhu et al. 2020).

The Disarray of Fibrinolytic and Coagulation System in Covid-19 Patients

One of the important discoveries replicated over most preliminary COVID-19 studies includes disarray of the fibrinolytic and coagulation system. Hospitalized patients affected from severe and moderate COVID-19 infection are prominently showing elevated D-dimer, prolonged prothrombin time (PT), and activated partial thromboplastin time (APTT) (Han et al. 2020). It is found through pulmonary inflammation stimulating macrophages activation and release of Interleukin 6 (IL-6). Inhalation of PM enters the human lung and deposited on alveoli, leads to an inflammatory reaction (Fig. 3) that causes an elevation in circulating inflammatory biomarkers like C-reactive protein and fibrinogen but favours formation of thrombus which in turn triggers acute events. Fibrinogen in high amounts acts as a marker for acute inflammation, while they show activation of

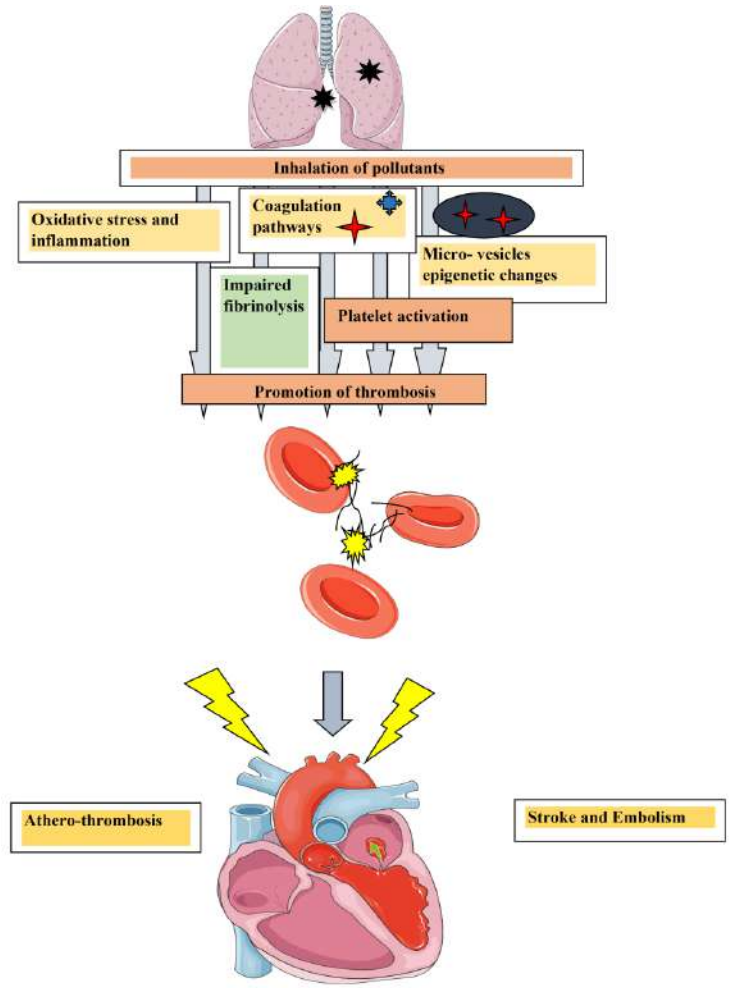

Fig. 3. Inhalation mechanisms and thrombosis formation.

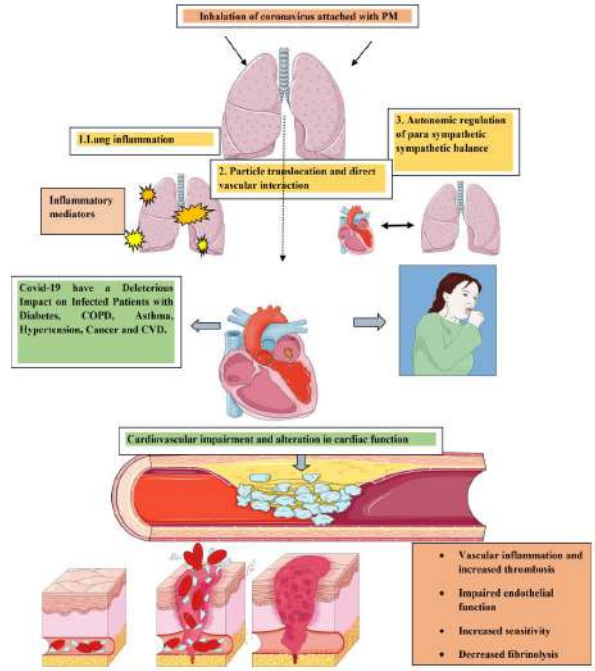

Fig. 4. Mechanism for cardiovascular impairment due to PM attached coronavirus inhalation.

clotting cascade in moderate amounts (Bonzini et al. 2010).

It is evidenced that air pollution exposure promotes coagulation and damages fibrinolysis, leads to an imbalance in haemostatic factors, and then can cause risk of thrombotic in individuals (Fig. 4).

COVID-19: Deleterious Impact on Infected Patients

Prominent changes in blood coagulation of patients with COVID-19 infection: The haemostasis function differences between SARS-CoV-2 patients and healthy controls composed the evaluation of nine parameters, as prior indicated. In comparison with healthy controls, values of antithrombin (AT) were accounted lower in COVID-19 cases. Thrombin time was found to be lower than that in healthy controls. The Prothrombin time (PT) was accounted low in COVID-19 patients as compared with healthy controls although the FDP and D-dimer values were found to be higher in COVID-19 patients than healthy controls. Remarkably, in SARS-CoV-2 cases, FIB values were also found to be higher as compared with the healthy control group (Han et al. 2020). The coagulation function of SARS-CoV-2 infected patients is undoubtedly unbalanced as compared with healthy individuals but controlling FDP and D-dimer values might be useful for the early recognition of serious cases (Han et al. 2020).

Diabetes and COVID-19: Diabetic patients are prone to get infections because of the potential of impaired phagocytic cells, however, some other factors elevate the COVID-19 risk in diabetic susceptible individuals (Ejaz et al. 2020). The spike (S) protein of SARS-CoV-2 connects to the ACE-2 receptors and is turned on by huge furin levels. Consequently, an unbalanced immune response with furin expression and increased ACE-2 receptors may result in lower insulin levels and an increase in lung inflammation rate (Ejaz et al. 2020). Diabetes-induced hyperglycemia resulting in several issues, such as chronic inflammation and weaken immune system through oxidative stress and decreased functioning of macrophages, antibodies, and chemokines. It also causes diabetes related problems like endothelial dysfunction and coagulation (Bradley et al. 2022).

COPD and COVID-19: The COVID-19 disease resulted in hypoxemia development in 15–20% of the cases, which needed the support of a ventilator in critical situations (Qu et al. 2020). However, primary studies did not report COPD with increased COVID-19 cases, the ACE-2 receptors expression is elevated in this disease, which leads to the development of serious symptoms in COVID-19 cases, such as weak immunity, structural damage to lungs, and mucous production (Newman et al. 2020).

Asthma and COVID-19: Air quality has an impact on

symptoms of asthma and on activating asthma attacks as explained in figure 2. Still, COVID-19 can be a serious disease for already damaged lungs from chronic asthma, especially in asthma–chronic obstructive pulmonary disease (COPD) overlaps syndrome (ACOS) patients (Yin et al. 2018). Although asthma is not directly correlated with COVID-19 disease, people with respiratory diseases and other complications are more prone to being infected during asthma (Ejaz et al. 2020). $PM_{2.5}$ can lead to asthma attacks and risk of chronic obstructive pulmonary disease (Nishida & Yatera 2022).

Hypertension and COVID-19: COVID-19 infection is correlated with uncontrolled blood pressure along with an increased case fatality rate (CFR) (Fang et al. 2020, Schiffrin et al. 2020). Pneumonia with increased blood pressure was noted in hypertensive patients with the covid-19 disease while blood pressure controlling should be important among COVID-19 cases to reduce the burden of disease (Ejaz et al. 2020).

CVD and COVID-19: CVD had a strong correlation with MERS (30%) and SARS (8%) (Nishiga et al. 2020). However, the increased prevalence of COVID-19 cases was mostly observed among patients with serious signs and symptoms of CVD (Zhou et al. 2020). Among pre-existing CVD cases having a high risk of COVID-19 disease can be due to the presence of ACE-2 receptors on cardiac muscle cells, implying the cardiovascular system in the SARS-CoV-2 infection (Ejaz et al.2020).

Cancer and COVID-19: According to a Chinese cohort, cancer patients are more prone to COVID-19 infection. Cancer patients are especially vulnerable towards their immunocompromised state (Han et al. 2022). Cancer patients found to be the highly susceptible group in this COVID-19 outbreak as studied cancer shows poor outcomes and worsen conditions such as dry cough (81%), fever (82.1%), and dyspnoea (50.0%), along with increased C-reactive protein (82.1%), lymphopaenia (82.1%), hypoproteinaemia (89.3%) and anaemia (75.0%) (Yu et al. 2020).

Impact of COVID-19 on children: Additionally, studies found that children younger than 10 years old seem to get contaminated from COVID as adults, but they don't show any serious symptoms. A logical theory for why most of the children show milder symptoms is that they have fewer ACE2 receptor proteins that act as an entry receptor for the SARS-CoV-2 virus in cells (Mallapaty 2020). Another study concluded that the association of higher mortality due to COVID-19 to PM2.5 in the region of northern Italy imparts a sharp piece of evidence that individual living in a region over high $PM_{2.5}$ level are more prone to promoting respiratory diseases, mostly in children (Senthilumaran et al. 2020).

Mortality due to air pollution and COVID-19: Ambient PM exposure and household air may be dangerously polluted, resulting in seven million avoidable deaths every year. Moreover, there is more evidence for $PM_{2.5}$ which shows negative effects on the cardiovascular system of heart failure, diabetes, hypertension, and cardiac arrhythmias through mechanisms of thrombosis (Fig. 4), and inflammation (Isaifan 2020).

CONCLUSION

Despite the strong hypothesis and evidence, people seem to be locked in the old perspectives that only direct links can cause the spread of viral infection. It will be too late when this pandemic is over, and backward data will reveal the importance of airborne-based transmission. Furthermore, the lessons we learned now will make us prepare better for the next viral pandemic, then we will strongly consider the transmission of this virus through air. Therefore, reduction of air pollution mainly $PM_{2.5}$ emission is essential to minimize the COVID-19 infection.

REFERENCES

Agarwal, K.M., Mohapatra, S., Sharma, P., Sharma, S., Bhatia, D. and Mishra, A. 2020. Study and overview of the novel coronavirus disease (COVID-19). Sens. Int., 1: 100037.

Badawi, A. and Ryoo, S.G. 2016. Prevalence of comorbidities in the Middle East respiratory syndrome coronavirus (MERS-CoV): A systematic review and meta-analysis. Int. J. Infect. Dis., 49: 129-133.

Barouki, R., Kogevinas, M., Audouze, K., Belesova, K., Bergman, A. and Birnbaum, L. 2021. The COVID-19 pandemic and global environmental change: Emerging research needs. Environ. Int., 146: 106272.

Bonzini, M., Tripodi, A., Artoni, A., Tarantini, L., Marinelli, B., Bertazzi, P.A. and Baccarelli, A. 2010. Effects of inhalable particulate matter on blood coagulation. J. Thromb. Haemost., 8(4): 662-668.

Bradley, S.A., Banach, M., Alvarado, N., Smokovski, I. and Bhaskar, S.M. 2022. Prevalence and impact of diabetes in hospitalized COVID-19 patients: A systematic review and meta- analysis. J. Diab., 14(2): 144-157.

Chauhan, A. and Singh, R.P. 2020. The decline in $PM_{2.5}$ concentrations in major cities around the world is associated with COVID-19. Environ. Res., 187: 109634.

Chen, R., Zhao, Z., Sun, Q., Lin, Z., Zhao, A., Wang, C. and Kan, H. 2015. Size-fractionated particulate air pollution and circulating biomarkers of inflammation, coagulation, and vasoconstriction in a panel of young adults. Epidemiology, 26(3): 328-336.

Coccia, M. 2021. The effects of atmospheric stability with low wind speed and of air pollution on the accelerated transmission dynamics of COVID-19. Int. J. Environ. Stud., 78(1): 1-27.

Comunian, S., Dongo, D., Milani, C. and Palestini, P. 2020. Air pollution and COVID-19: the role of particulate matter in the spread and increase of COVID-19's morbidity and mortality. Int. J. Environ. Res. Pub. Health, 17(12): 4487.

Copat, C., Cristaldi, A., Fiore, M., Grasso, A., Zuccarello, P., Santo Signorelli, S. and Ferrante, M. 2020. The role of air pollution (PM and NO_2) in COVID-19 spread and lethality: A systematic review. Environ. Res., 191: 110129.

Dehghani, M., Keshtgar, L., Javaheri, M.R.. Derakhshan, Z., Oliveri Conti, G., Zuccarello, P. and Ferrante, M. 2017. The effects of air pollutants on

the mortality rate of lung cancer and leukemia. Mol. Med. Rep., 15(5): 3390-3397.

Diffenbaugh, N.S. 2022. COVID-19 and the environment: Short-run and potential long-run impacts. Annual Rev. Environ. Resour., 47: 1-28.

Ejaz, H., Alsrhani, A., Zafar, A., Javed, H., Junaid, K., Abdalla, A.E. and Younas, S. 2020. COVID-19 and comorbidities: Deleterious impact on infected patients. J. Infect. Pub. Health, 13(12): 1833-1839.

Fang, L., Karakiulakis, G. and Roth, M. 2020. Are patients with hypertension and diabetes mellitus at increased risk for COVID-19 infection? Lancet Resp. Med., 8(4): e21.

Hampel, R., Peters, A., Beelen, R., Brunekreef, B., Cyrys, J., de Faire, U. and Lanki, T. 2015. Long-term effects of the elemental composition of particulate matter on inflammatory blood markers in European cohorts. Environ. Int., 82: 76-84.

Han, H., Yang, L., Liu, R., Liu, F., Wu, K., Li, J. and Zhu, C.L. 2020. Prominent changes in blood coagulation of patients with SARS-CoV-2 infection. Clinic. Chem. Lab. Med., 58(7): 1116-1120.

Han, S., Zhuang, Q., Chiang, J., Tan, S.H., Chua, G.W.Y., Xie, C. and Yang, V.S. 2022. Impact of cancer diagnoses on the outcomes of patients with COVID-19: A systematic review and meta-analysis. BMJ Open, 12(2): e044661.

He, F., Deng, Y. and Li, W. 2020. Coronavirus disease 2019: What we know? J. Med. Virol., 92(7): 719-725.

Ho, H.C., Wong, M.S. and Chan, T.C. 2020. Spatially differentiating the effects of long-term air pollution on specific causes of death from cardiovascular and respiratory mortality in Hong Kong: a territory-wide register-based study. Air Qual. Atmos. Health, 13(6): 721-730.

Isaifan, R.J. 2020. The dramatic impact of coronavirus outbreak on air quality: Has it saved as much as it has killed so far?. Glob. J. Environ. Sci. Manag., 6(3): 275-288.

Kampf, G., Todt, D., Pfaender, S. and Steinmann, E. 2020. Persistence of coronaviruses on inanimate surfaces and their inactivation with biocidal agents. J. Hosp. Infect., 104(3): 246-251.

Kim, K.H., Kabir, E. and Kabir, S. 2015. A review on the human health impact of airborne particulate matter. Environ. Int., 74: 136-143.

Leikauf, G.D., Kim, S.H. and Jang, A.S. 2020. Mechanisms of ultrafine particle-induced respiratory health effects. Exper. Mol. Med., 52(3): 329-337.

Mallapaty, S. 2020. How do children spread the coronavirus? The science still isn't clear. Nature, 581(7807): 127-129.

Marquès, M. and Domingo, J. L.2021. Contamination of inert surfaces by SARS-CoV-2: Persistence, stability and infectivity. A review. Environ. Res., 193: 110559.

Morawska, L. and Cao, J. 2020. Airborne transmission of SARS-CoV-2: The world should face the reality. Environ. Int., 139: 105730.

Newby, D.E., Mannucci, P. M., Tell, G.S., Baccarelli, A.A., Brook, R.D., Donaldson, K. and Storey, R.F. 2015. Expert position paper on air pollution and cardiovascular disease. Europ. Heart J., 36(2): 83-93.

Newman, J.D., Bhatt, D.L., Rajagopalan, S., Balmes, J.R., Brauer, M., Breysse, P.N. and Brook, R.D. 2020. Cardiopulmonary impact of particulate air pollution in high-risk populations: JACC state-of-the-art review. J. Am. Coll. Cadriol., 76(24): 2878-2894.

Nishida, C. and Yatera, K. 2022. The impact of ambient environmental and occupational pollution on respiratory diseases. Int. J. Environ. Res. Pub. Health, 19(5): 2788.

Nishiga, M., Wang, D.W., Han, Y. Lewis, D.B. and Wu, J.C. 2020. COVID-19 and cardiovascular disease: from basic mechanisms to clinical perspectives. Nat. Rev. Cardiol., 17(9): 543-558.

Paital, B. and Agrawal, P.K. 2021. Air pollution by NO_2 and $PM_{2.5}$ explains COVID-19 infection severity by overexpression of angiotensin-converting enzyme 2 in respiratory cells: A review. Environ. Chem. Lett., 19(1): 25-42.

Qu, G., Li, X., Hu, L. and Jiang, G. 2020. An imperative need for research on the role of environmental factors in the transmission of novel coronavirus (COVID-19). Complete the reference? Environ. Sci. Technol., 23: 01102

Raji, H., Riahi, A., Borsi, S.H., Masoumi, K., Khanjani, N., AhmadiAngali, K. and Dastoorpoor, M. 2020. Acute effects of air pollution on hospital admissions for asthma, COPD, and bronchiectasis in Ahvaz, Iran. Int. J. Chron. Obstruct. Pulmon. Dis., 15: 501.

Ruckerl, R., Ibald-Mulli, A., Koenig, W., Schneider, A., Woelke, G., Cyrys, J. and Peters, A. 2006. Air pollution and markers of inflammation and coagulation in patients with coronary heart disease. Am. J. Resp. Crit. Care Med., 173(4): 432-441.

Schiffrin, E.L., Flack, J.M., Ito, S., Muntner, P. and Webb, R.C. 2020. Hypertension and COVID-19. Am. J. Hyper., 33(5): 373-374.

Senthilkumaran, S., Meenakshisundaram, R., Shah, S. and Thirumalaikolundu, S.P. 2020. Coronavirus disease (COVID-19) in children: Indian perspectives. Ind. Pediat., 57(6): 585.

Setti, L., Passarini, F., De Gennaro, G., Barbieri, P., Pallavicini, A., Ruscio, M. and Miani, A. 2020. Searching for SARS-COV-2 on the particulate matter: A possible early indicator of COVID-19 epidemic recurrence. Int. J. Environ. Res. Pub. Health, 17(9): 2986.

Wang, D., Wu, X., Li, C., Han, J. and Yin, J. 2022. The impact of geo-environmental factors on global COVID-19 transmission: A review of evidence and methodology. Sci. Tot. Environ., 15: 1-12.

Weaver, A.K, Head, J.R, Gould, C.F., Carlton, E.J. and Remais, J.V. 2022. Environmental Factors Influencing COVID-19 Incidence and Severity. Annual Rev. Pub. Health, 43: 271-291.

Yin, Y. and Wunderink, R. G. 2018. MERS, SARS and other coronaviruses as causes of pneumonia. Respirology, 23(2): 130-137.

Yu, J., Ouyang, W., Chua, M.L. and Xie, C. 2020. SARS-CoV-2 transmission in patients with cancer at a tertiary care hospital in Wuhan, China. JAMA Oncol., 6(7): 1108-1110.

Zeng, X., Liu, D., Wu, W. and Huo, X. 2022. $PM_{2.5}$ exposure inducing ATP alteration links with NLRP3 inflammasome activation. Environ. Sci. Pollut. Res., 29: 1-12.

Zhou, P., Yang, X.L., Wang, X.G., Hu, B., Zhang, L., Zhang, W. and Shi, Z.L. 2020. A pneumonia outbreak associated with a new coronavirus of probable bat origin. Nature, 9(8): 270-273.

Zhu, Y., Xie, J., Huang, F. and Cao, L. 2020. Association between short-term exposure to air pollution and COVID-19 infection: Evidence from China. Sci. Total Environ., 727: 138704.

Nature Environment and Pollution Technology
An International Quarterly Scientific Journal

p-ISSN: 0972-6268
(Print copies up to 2016)
e-ISSN: 2395-3454

Vol. 21 | No. 5 (Suppl) | pp. 2283-2290 | 2022

Original Research Paper

https://doi.org/10.46488/NEPT.2022.v21i05.023

Open Access Journal

A Critical Review of the Impact of COVID-19 on Plastic and Food Waste

Prashant Shukla*† and Sachi Choudhary**
*School of Engineering, University of Petroleum & Energy Studies, Dehradun, Uttarakhand, India
**School of Computer Science, University of Petroleum & Energy Studies, Dehradun, Uttarakhand, India
†Corresponding author: Prashant Shukla; prashantshukla1617@gmail.com

Nat. Env. & Poll. Tech.
Website: www.neptjournal.com

Received: 21-03-2022
Revised: 09-05-2022
Accepted: 16-05-2022

Key Words:
COVID-19
Solid waste management
Medical waste
Recyclable waste
Domestic waste
Commercial waste

ABSTRACT

This research aims to show the positive and negative indirect effects of COVID-19 on municipal solid waste management systems, especially for plastic waste and food waste. The COVID-19 pandemic has affected the entire waste management sector. As the pandemic spread and lockdowns were enforced in many countries, government and municipal waste operators had to quickly adapt their waste management programs and procedures to the situation. In the pandemic condition, waste generation has switched from industry and commercial to domestic areas. Reduced recycling activities have made municipal waste collection and disposal more difficult. This paper focuses on all the challenges and it's possible resolutions for managing food and plastic waste during the pandemic of COVID-19.

INTRODUCTION

The outbreak of the pandemic, which forced the closure of businesses and educational institutions, raised concerns among the general public about how the COVID-19 pandemic might influence the composition and pattern of waste generation. This may also be taken to mean that, depending on the place, the pandemic may cause the waste level to rise or fall. When places like educational institutions, businesses, and industrial facilities that produced enormous volumes of waste were shut down, waste production also decreased. The generation of domestic, medical, and agricultural waste has increased in some places, however, not all groups are completely closed (Naughton 2020). While the world has observed the favorable environmental consequences of COVID-19 national locks like the clear sky and clean rivers, municipal solid waste management systems are facing various challenges at different levels (Gardiner 2020). The spread of COVID-19 changed the dynamics of waste generation, causing despondency among sanitation workers and policymakers (Calma 2020). Various kinds of hazardous & medical waste are generated during an outbreak, including used gloves, masks, and other protective equipment, along with a huge amount of similar non-infected items (Calma 2020). Though medical waste is not part of municipal solid waste but pandemic has made masks and gloves essential for daily routine. Therefore such infectious waste started coming with municipal solid waste. Hence inappropriate collection may cause contamination of municipal solid waste and may cause transmission of disease risk because the virus will live hours to days in cardboard, plastic, and metals (Aylin & Gal 2020, Chasan & Kaufman 2020, Van Doremalen et al. 2020a). Fig. 1 shows the duration of survival of the virus on different surfaces, according to the data, the virus survives on a mask for a period longer than any other surface. Indiscriminately tossing or disposing of such waste will cause risk to the lives of waste management staff. In developing, nations where waste management employees are not provided with adequate personal protective equipment (PPE), this may cause the condition much more serious (Jerie 2016). Across these areas, rag pickers and informal waste collectors are at the high-risk region of contamination from virus-infected waste. Pre-pandemic waste-treatment devices planned for moderate variability may now function abnormally due to drastic volume and waste content shifts. The pandemic resulted in major challenges in the management of Solid municipal waste (SMW) and medical hazardous waste. Hence proper management of this type of waste is a key function of effective emergency response (Kulkarni & Anantharama 2020, Sharma et al. 2020).

Fig. 1: Survival time of the SARS-Cov-2 virus on different surfaces (Gal 2020).

Few early news articles reported the rise in recyclable, domestic, and agricultural waste. Such a rise forced the recycling industries in Ohio, New York, South Carolina, and Arizona to recycle 45 percent more waste than the previous year (Staub 2020). Initially hit hard by the pandemic, New York City had an increment of 3.3% in municipal solid waste and a 13.3% increase in organic waste over the previous year (Staub 2020). Many recycling plants had to bring down their capacity to protect their workers from infection, which diverted their goods to dump sites (Staub 2020). Even if most of the crops were disposed of on-site, large amounts were overturned with disturbance to food-supply chains (Naughton 2020). COVID-19 Social distancing measures led to the closure of businesses and schools which minimized the generation of waste but the contribution had shifted to households. In addition, COVID-19 led to many Americans purchasing online articles and foodstuffs that contain more packaging waste. Americans also harvested food and items that could lead to some spoilage waste.

The paper focuses on the rising problems and global challenges of managing municipal solid waste in the current scenario of the COVID-19 crisis. This paper also highlights the new trend of biomedical, plastic, and food waste production as a result of the pandemic, aside from its exposition of existing worldwide biomedical waste management practices. Furthermore, it seeks to investigate ingenious approaches in the management of the current crisis, and suggests viable changes to existing practices to minimize and address the identical situation in probable future pandemics. This paper also highlights various paths which are useful in the development of effective MSW management systems for policymakers and regulators in the pandemic and post-pandemic world.

Effect of the Pandemic on Plastic Waste Generation

One of the pandemic's immediate environmental consequences is the rapid increase in the production and usage of disposable goods to protect the general population,

doctors, community staff, and services from infection. Since the human-to-human coronavirus transmission news, there was a hike in the requirement for masks, gloves, hand sanitizers, and other important safeties. WHO forecasted that there will be an annual need for 89 million surgical masks and 76 million test gloves, although worldwide demand for goggles was 1.6 million a month (WHO 2020). Widespread usage of safety equipment globally because the pandemic causes major upstream production chain instability and downstream waste management issues, therefore infectious contamination is not limited to clinics and facilities. Market patterns are expected to coincide with the worldwide pandemic trend of many plastic products, including PPE, gloves and masks, disposable plastic products for life-support systems, respirators, and general syringes (Klemeš et al. 2020). The plastic products used are often contaminated and should be treated as hazardous waste. Before the beginning of the COVID-19 pandemic, plastic waste management was seen as a major environmental problem because of growing pollution concerns in land and marine ecosystems (Rajmohan et al. 2019). In developing, nations current waste management system is inefficient in managing plastic waste whereas the imminent rise in COVID-19 waste quantity created more challenges for current waste and healthcare systems. Although virus retains on plastic for a longer period disposability is seen by customers as a significant hygiene advantage (Kampf et al. 2020, Sharma et al. 2020, Van Doremalen et al. 2020b). This has led to increased use and disposal, even for non-medical applications, of plastic products. In contrast, plastic demand in the probable global economic recession, other sectors (e.g. automotive and aviation applications) are declining. The demand for packaging used to supply food and foodstuffs to houses has also increased due to Lockdown. Such an inevitable scenario may intensify the environmental issues with the waste plastics that were already there before the pandemic. In particular, metrics should be created and fully used for the design and comparison of alternatives and their footprints on the environment. With total locks and the closure of food stores (cafés) as well as in restaurants worldwide to promote physical distancing, the demand for food supply and food services has increased, which has resulted in increased production of common plastic packaging waste-polypropylene (PP), Polyethylene Low Density (LDPE), Polyethylene High Density (HDPE), Terephthalate polyethylene (PET), Polystyrene (PS), etc. (Tenenbaum 2020, Sharma et al. 2020). Due to the outbreak of the coronavirus and reduced recycling (Emily & Kaufman 2020) the management of plastic waste has become a new challenge for the waste management sector. In addition, the demand for critical medical logistics worldwide is expected to rise in the volume of waste plastic from medical sectors (Chasan & Kaufman 2020). In line with existing public health concerns, individuals can opt to use single-use plastic which contradicts the limitations on their use imposed by many countries. (Tenenbaum 2020).

According to the press releases of the State Council's Joint Mechanism for Prevention and Control in China, on 11 March (Chinese Government Network 2020), the generation of MSW was cut down by 30 percent during the lockdown period. However, medical waste generation in Hubei Province increased sharply (approx. 370 percent) with a high percentage of plastic. The total stockpiled medical waste in China was observed as 207 kt from 20 January to 31 March. Such waste rose from 40 $t.d^{-1}$ to a peak of 240 $t.d^{-1}$ in Wuhan, which is more than the defined capacity of incineration i.e. 49 $t.d^{-1}$ (Weike 2020). Compared to USD 14.1 per ton of MSW (Weike 2020), Therefore the cost of incineration of hazardous medical waste has increased from USD 14.1 per ton to USD 281.7–422.6/t in China. Fig. 2 (Klemeš et al. 2020) shows worldwide waste flow trends in comparison with treatment capacity, which indicates that

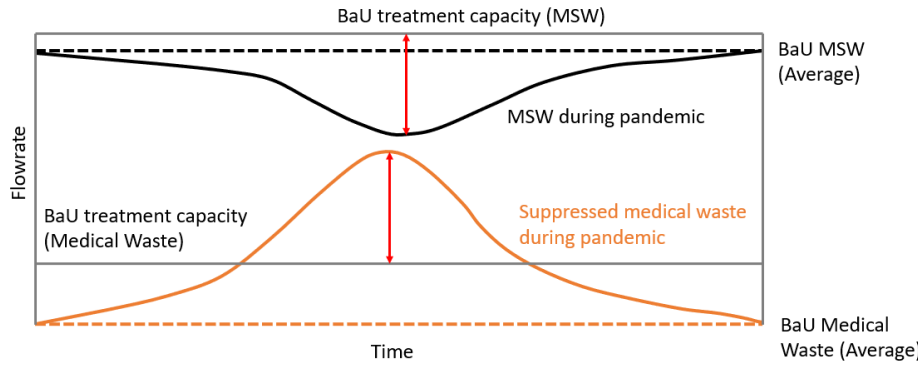

Fig. 2: Flow trend- MSW Vs Medical waste (Klemeš et al. 2020).

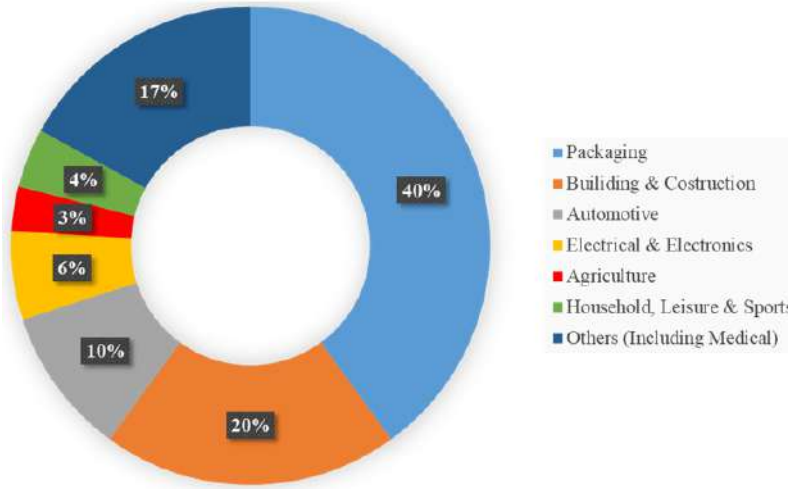

Fig. 3: Sources of plastic waste.

waste treatment systems have tackled drastic changes that led the system to irregular operations.

Technical analysis is important if these systems are to be able to handle the pandemic's dynamic and evolving nature. The fact that much is unknown about the virus itself is another challenge as the products and procedures available to handle the pandemic are not yet clear. The COVID-19 crisis highlighted the major role of plastics in daily life. Virus management requires single-use plastic even if, in most other applications, disposability is seen to be largely an environmental liability (Greenpeace USA 2020). An efficient evaluation tool can summarize the major impact of plastic products on the environment. Fig. 3 (PlasticsEurope 2019) shows the different sources of plastic waste in the environment. Medical product and packaging demand rise rapidly during the period of the pandemic. Therefore countries are working together for changing the quantity and quality of plastic waste.

Whereas a strong strategy to manage plastic waste can be helpful to bring down the unexpected effects on living species. Efficient handling of medical waste needs a suitable approach for identification, collection, segregation, storage, transportation, treatment, disposal, and other essential precautions like disinfection, personnel protection, and training. Fig. 4 (AISBL ACR+ 2020, Centers for Disease Control and Prevention 2015, Klemeš et al. 2020, Marshall 2020, UK Health Security Agency, 2021) explains the process to treat the waste during the pandemic, where the source of contaminated waste is not limited to hospitals.

Even hospitals with modern equipment have failed in coping with the fast-growing numbers of COVID-19 patients. The one with mild symptoms goes for self-isolation at home itself and causes virus-laden waste. This needs a sustainable change in the waste management infrastructure. In European Union, the entire Corona body safety kit is required to be packed in double bags. In Germany recyclable food containers are now will be considered hazardous waste as they may be contaminated with viruses (AISBL ACR+ 2020). It was also precautionary advised that if a house is found with a positive or suspected corona patient, so follow the specified municipal waste management guidelines (AISBL ACR+ 2020). However such practice promotes the usage of plastic and a neutral response toward source segregation.

Treatment of hazardous medical waste through incineration and steam sterilization (90 min, 120°C) is the most widely used approach (Centers for Disease Control and Prevention 2015). In Germany, it is advised strictly to maintain 1000°C just to achieve a safe treatment of medical waste (AISBL ACR+ 2020). WHO has also recommended maintaining 900 to 1200°C for the thermal treatment process (WHO 1999). Due to COVID-19, the hike in waste generation is demanding high-capacity treatment facilities also. In Spain, the incineration of contaminated waste by cement plants has been adopted for future reference (AISBL ACR+ 2020).

The Repercussion of COVID-19 on Food Waste and the Food Supply Chain

COVID-19 has given a severe impact on industry on several fronts (Kahlert & Bening 2020). Few cases like the U.S. food producers struggled due to the non-operational restaurants, schools, and other institutions that generally demand large amounts of food. A significant amount of food waste was produced during the beginning of the lockdown (Waste 360

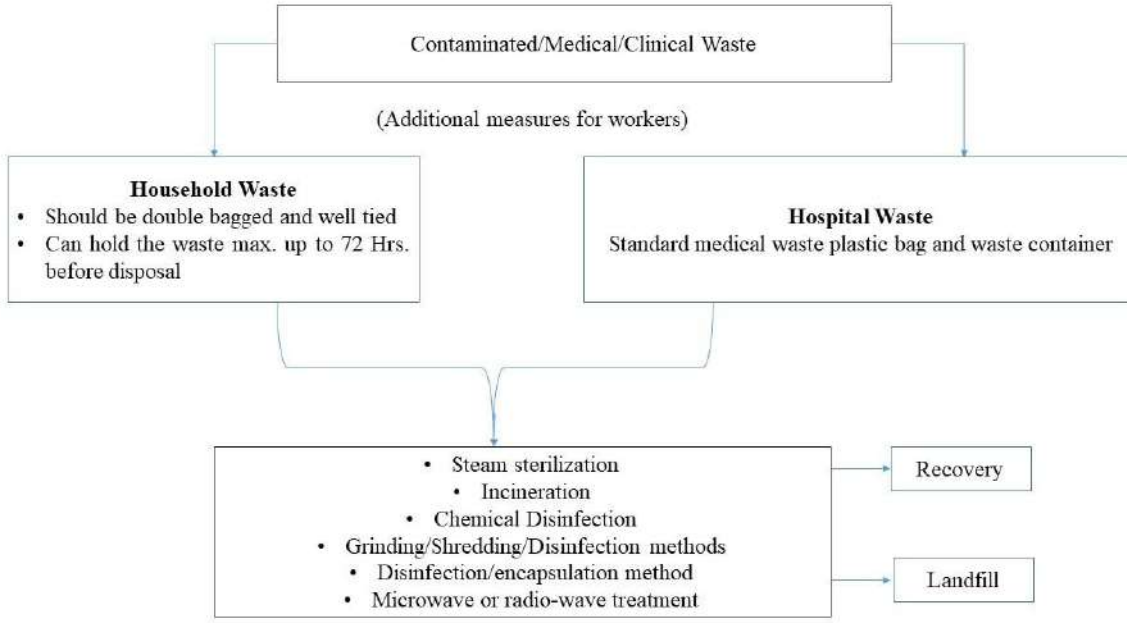

Fig. 4: Process of managing the waste during COVID 19.

2020). The United States Environmental Protection Agency (US EPA) reacted to the emergency of COVID-19 by issuing recommendations for recycling and sustainable management of food waste. These guidelines target household, institutional and business-level food waste management (US EPA n.d.). In India, the lockdown started parallel with seasonal crop harvesting. The plants of wheat, paddy, and barley were ready for harvest, and vegetables and fruits were also ready for the consumer. However, most goods were wasted due to the sudden shutdown in the country (Pothan 2020). The Indian government has also made attempts to tackle the diversion of perishable goods to implement an economic stimulus package. Food inspectors have worked to ensure that food products are distributed to restaurants, stores, and impacted individuals. Importantly, initiatives like food distribution allowed the government to reach localized and remote communities, to ensure successful food management and food waste reduction (Pothan 2020). Storage of food products leads to disrupted dynamics of food waste generation (Sharma et al. 2020), whereas the fractured supply chain leads to the dumping of food, milk, and fruits at local dumpsites/landfill or on the roadside (Sharma et al. 2020). Therefore a flexible supply chain system needs to be developed

Household Food Waste Generation

COVID-19-induced panic buying, where lockdowns forced the population to store refrigerated edible items and ignore their expiry dates. Mandating statistics on shelf-life and public recognition of its importance can be an efficient way to minimize food waste. Authors (Jribi et al. 2020) stated that the pandemic situation has drawn people's attention toward food waste due to anticipated supply shortages. The report, however, indicated that this pro-behavioral shift was motivated by socioeconomic background, not just because of environmental concerns. Moreover, in the current scenario, consumers tend to stock rather than dump, resulting in less waste generation (Durante & Laran 2016, Jribi et al. 2020). It is also noted that consumer-conscious food purchases as confirmed by other research undertaken during the extreme recessions in Greece and Italy (Fanelli & Florio 2016, Jribi et al. 2020, Martinengo 2015). Nonetheless, the study also indicated that the storage limits, weak cooking habits, or overcooking and overstocking brought the downfall in the generation of household food waste during the complete lockdown.

Supply Chain

COVID-19 reached urban areas deeper than rural areas. Consequently, COVID-19's effect on food production was attributed, given the availability of farm labor, to the lack of resource materials for agricultural activities. Moreover, fear of getting infected, limits on the commute, and lockdowns in cities and towns have stopped food supply employees from continuing to provide their services. Therefore, people are

scared of resourcing food and its transportation from storage facilities to markets. Furthermore, the closing of borders has made interstate food transportation, complicated and time taking. Furthermore, the food supply chain was disrupted in the containment zone. Owing to the lack of sufficient manpower and the use of available manpower under the strict surveillance of social distance, the food processing, and packaging industry was hit hard. This scenario not only affected the food supply but also caused the devastation of food products in stores and fields. The following media articles are showing the cases of burial and dumping of food items due to the damaged supply chain.

- The New York Times: The New York Times, the Insider, and the Milwaukee newspaper sentinel reported that due to closed restaurants, hostels, and schools, farms are forced to dump the fresh vegetables, milk, and eggs, that can not be sold anymore (Barrett 2021).
- Times of India: According to the Times of India, farmers in Punjab are worried about their business and its ongoing losses, and they demanded a rest in the shutdown to sell their goods and their crops in fields (Kamal 2020).
- Business Line: In another case from India, it was reported that the transport network got disconnected with the lockdown and the entire supply chain got crumpled. This leads to the dumping of vegetables and fruit supplies in Mumbai and Pune (Jadhav 2020).
- CNA: In Singapore, farmers are unable to work on the farms, and transporters are struggling to supply food to markets due to the lockdown. CNA Singapore reported huge amounts of fruits were left abandoned or thrown on dumpsites (Jadhav 2020).
- Anadolu Agency: Due to the unavailability of manpower and transport facilities during the lockdown period, millions of farmers in India & Pakistan are going through another tragedy, seeing their goods rot in their fields. Professionals believe the scenario will have a negative impact on food security (Jadhav 2020).

Way-Forward to Managing Food Waste During the Pandemic

Although the current crisis brought some problems, it also created the right set of circumstances to unveil new solutions for viable, efficient supply chains. These solutions could help for preparing nations for such pandemics. The food supply chain starts with sourcing seeds, processing, inventory, and transport, and finally ends with consumers. COVID-19's spread has affected this chain's efficiency at different levels. Therefore, at each level, innovative solutions are needed to tackle food shortages and reduce food waste. Second, the supply of raw materials should be hassle-free and the group delivery channel should route this. The local governing and other voluntary bodies such as NGOs will distribute seeds, equipment, resources, etc. directly to a community that belongs to the grower. This approach can help to make the system mechanized for easy storage and minimizing food waste. Food items may be stocked in local warehouses in partnership with government or private entities for the intermediate duration. Food stocked in warehouse units requires adequate transport and distribution releases. Special licenses must be held for trucks transporting food, such as interstate charges and tolls. Proper provision for truck drivers, warehouse workers, and other support teams of safety equipment, food, water, and washroom facility should be guaranteed. Such measures will contribute directly to a decrease in food waste while at the same moment providing food quality that is less likely to spoil because of lack of storage, transportation, or packaging material contamination (Parfitt et al. 2010, Saini & Kozicka 2014, Va et al. 2007).

As online delivery gains prominence from COVID-19, Online service providers can pool capital to obtain and distribute food supplies. The participation of local administrative bodies like Residence Welfare Associations (RWAs) in municipal areas, panchayats in village areas, and Non-Governmental Organizations (NGOs) are important for providing food supplies. Such public bodies will run on mobile applications (apps) for collecting essential orders. An app will be used to collect the list of household essentials, on which local administration will arrange weekly markets. The Apps will also have information on appropriate ways of storage, helps to avoid overbuying the food, clarify the difference between non-essential and essential goods, and pass on the details of suppliers, food service providers, etc. It is necessary to promote and support organizations like religious organizations, and NGOs working tirelessly to provide food to the poor and facilitate food supply. Another alternative may be to use the nearby restaurant and dining joints. Since they buy bulk raw food, these raw food material stocks can be sourced and sold to customers. A temporary food market would emerge as a result of this approach, generating income for the restaurant. Customers would also benefit from a food supply. This activity will also lessen food waste (Sharma et al. 2020). In the fight against pandemics, "hotspots" of poor food security Due to hoarding, inadequate storage, and improper food supply channels, chains can contribute to food waste.. Therefore, drone distribution can be coordinated in these cities, through which food supply can be managed with a contactless approach. Therefore, wholesale markets can supply perishables to the food market at lower bulk prices, selling them directly to customers through their retail networks.

Due to lockdowns and social distances, the labor force is left unemployed. This labor can be absorbed by the supply chain, for the operation of trucks, the loading and unloading of inventories, and the maintenance of warehouses. Throughout the pandemic, small-scale enterprises and cooperatives will remain involved. Development models such as AMUL (Umarji 2020) and Shri Mahila Griha Udyog Lijjat Papad (Naik 2005) can serve as prototypes in India. Such industries do not require large manpower. Households must be self-reliant to any degree as regards food production and the elimination of food waste. Sustainable cultivation and permaculture activities should be promoted to ensure food security during the potential pandemic. It may not have many effects because it combines the production of food waste by limiting purchases to goods that are not made or cultivated at home. As a result, the food supply chain will be significantly impacted by this technique.

CONCLUSION

This paper discussed the current scenario of municipal solid waste management in the world that appeared in the ongoing COVID-19 crisis. The entire focus is on the issue specifically food and plastic waste, because food waste and plastic waste are the two components of MSW that stand out the most and harm the environment. On one side where minimized commercial affairs bring out clean air and water as stated in many cases, the new trend in the generation of plastic and food waste has brought big trouble in the area of waste management and handling on another side. Discarded corona protective body kits like gloves and masks are causing severe health hazards to sanitary workers. The increasing demand for corona safety body kits will also increase the amount of plastic waste in the environment. The adverse effects may be minimized by plotting the efficient facilities for handling the manufacturing and recycling facilities. Similarly, a few socioeconomic factors such as rationing, and conscious shopping caused a low generation of domestic food waste during lockdowns. Large amounts of food were wasted as a result of a disruption in the food supply chain, which calls for the use of cutting-edge technology solutions. To combat comparable potential future pandemics, creating sustainable supply chains against food crises and wastage will be more beneficial. To prevent similar cries in the future, an adaptable socioeconomic-environmental approach must also be devised.

REFERENCES

AISBL ACR+. 2020. Municipal Waste Management and Covid-19. Retrieved September 2, 2020, from https://www.acrplus.org/en/municipal-waste-management-covid-19.

Aylin, W. and Shayanne, G. 2020. One Graphic Shows How Long the Coronavirus Lives on Surfaces Like Cardboard, Plastic, and Steel. Retrieved August 11, 2020, from https://www.businessinsider.in/science/news/one-graphic-shows-how-long-the-coronavirus-lives-on-surfaces-like-cardboard-plastic-and-steel/articleshow/74720814.cms

Barrett, R. 2021. Wisconsin Farmers Forced to Dump Milk as Coronavirus Slams a Fragile Dairy Economy. Retrieved August 7, 2020, from https://www.jsonline.com/story/money/2020/04/01/coronavirus-forces-dairy-farmers-dump-milk-wisconsin-covid-19/5108609002/

Calma, J. 2020. The COVID-19 Pandemic Is Generating Tons of Medical Waste. Retrieved April 13, 2022, from https://www.theverge.com/2020/3/26/21194647/the-covid-19-pandemic-is-generating-tons-of-medical-waste

Centers for Disease Control and Prevention. 2015. Medical Waste. Retrieved September 2, 2020, from https://www.cdc.gov/infectioncontrol/guidelines/environmental/background/medical-waste.html

Chasan, E. and Kaufman, L. 2020. Cities Wonder Whether Recycling Counts as Essential During the Virus. Retrieved August 6, 2020, from https://www.bloomberg.com/news/articles/2020-03-27/cities-wonder-whether-recycling-counts-as-essential-during-the-virus

Chinese Government Network. 2020. Authoritative Release of the State Council's Joint Defense and Joint Control Mechanism. Retrieved August 1, 2020, from http://www.gov.cn/xinwen/gwylflkjz53/index.htm

Durante, K.M. and Laran, J. 2016. The effect of stress on consumer saving and spending. J. Market. Res., 53(5): 814–828. https://doi.org/10.1509/jmr.15.0319

Fanelli, R.M. and Florio, A.D. 2016. Domestic food waste, the gap in times of crisis. Rivista Di Econ. Agr., 71(2): 111–125. https://doi.org/10.13128/REA-20075

Gal, A.W. 2020. One Graphic Shows How Long the Coronavirus Lives On Surfaces Like Cardboard, Plastic, and Steel. Retrieved April 15, 2022, from https://www.businessinsider.in/science/news/one-graphic-shows-how-long-the-coronavirus-lives-on-surfaces-like-cardboard-plastic-and-steel/articleshow/74720814.cms

Gardiner, B. 2020. Pollution Made the Pandemic Worse, But Lockdowns Clean the Sky. Retrieved August 4, 2020, from https://www.nationalgeographic.com/science/2020/04/pollution-made-the-pandemic-worse-but-lockdowns-clean-the-sky/

Greenpeace USA. 2020. How the Plastic Industry Is Exploiting Anxiety about COVID-19 -. Retrieved August 2, 2020, from https://www.greenpeace.org/usa/how-the-plastic-industry-is-exploiting-anxiety-about-covid-19/

Jadhav, R. 2020. Lockdown Impact: Maharashtra Farmers Dump Vegetables and Fruits in Trash Containers. Retrieved August 7, 2020, from https://www.thehindubusinessline.com/economy/agri-business/lockdown-impact-maharashtra-farmers-dump-vegetables-and-fruits-in-trash-in-garbage-containers/article31328165.ece#

Jerie, S. 2016. Occupational risks associated with solid waste management in the informal sector of Gweru, Zimbabwe. J. Environ. Pub. Health, 20: 160. https://doi.org/10.1155/2016/9024160

Jribi, S., Ben Ismail, H., Doggui, D. and Debbabi, H. 2020. COVID-19 virus outbreak lockdown: What impacts on household food wastage? Environ. Develop. Sustain., 22(5): 3939–3955. https://doi.org/10.1007/s10668-020-00740-y

Kahlert, S. and Bening, C.R. 2020. Plastics recycling after the global pandemic: Resurgence or regression? Resour. Conserv. Recycl., 160: 104948. https://doi.org/10.1016/j.resconrec.2020.104948

Kamal, N. 2020. Punjab Farmers Start Dumping Vegetables Due to Curfew. Retrieved August 5, 2020, from https://timesofindia.indiatimes.com/city/chandigarh/punjab-farmers-start-dumping-vegetables-due-to-curfew/articleshow/74801554.cms

Kampf, G., Todt, D., Pfaender, S. and Steinmann, E. 2020. Persistence of coronaviruses on inanimate surfaces and their inactivation with biocidal agents. J. Hospital Infect., 104: 246–251. https://doi.org/10.1016/j.jhin.2020.01.022

Klemeš, J.J., Fan, Y., Van, T.R.R. and Jiang, P. 2020. Minimizing the present and future plastic waste, energy, and environmental footprints related to COVID-19. Renewable and Sustain. Energy Rev., 127: 109883. https://doi.org/https://doi.org/10.1016/j.rser.2020.109883

Kulkarni, B.N. and Anantharama, V. 2020. Pandemic on municipal solid waste management: Challenges and opportunities. Sci. Tot. Environ., 14: 693. https://doi.org/10.1016/j.scitotenv.2020.140693

Marshall, J. 2020. Pandemic: Could the U.S., like China, face a medical waste crisis? Retrieved September 2, 2020, from https://www.eenews.net/stories/1062690625

Martinengo, M.C. 2015. Household food waste and consumer culture: Reflections on Italian behavior. J. Nutri. Ecol. Food Res., 2(1): 73–77. https://doi.org/10.1166/jnef.2014.1062

Naik, J. 2005. The Incredible story of Lijjat Papad! - Rediff.com Business. Retrieved August 8, 2020, from The Smart Manager website: https://www.rediff.com/money/2005/apr/15spec.htm

Naughton, C.C. 2020. Will the COVID-19 pandemic change waste generation and composition?: The need for more real-time waste management data and systems thinking. Resour. Conserv. Recylc., 62: 10142.

Parfitt, J., Barthel, M. and Macnaughton, S. 2010. Food waste within food supply chains: quantification and potential for change to 2050. Phil. Trans. Royal Soc. B: Biol. Sci., 365(1554): 3065–3081. https://doi.org/10.1098/rstb.2010.0126

PlasticsEurope 2019. Plastics-the Facts 2019 An analysis of European plastics production, demand and waste data. https://plasticseurope.org/knowledge-hub/plastics-the-facts-2019/

Pothan, P.E. 2020. Local Food Systems and COVID-19: A Glimpse on India's Responses for Food for the Cities Program. Retrieved August 2, 2020, from http://www.fao.org/in-action/food-for-cities-programme/news/detail/en/c/1272232/

Rajmohan, K.V.S., Ramya, C., Raja Viswanathan, M. and Varjani, S. 2019. Plastic pollutants: Effective waste management for pollution control and abatement. Curr. Opinion Environ. Sci. Health, 12: 72–84. https://doi.org/10.1016/j.coesh.2019.08.006

Saini, S. and Kozicka, M. 2014. Evolution and Critique of Buffer Stocking Policy of India. Retrieved August 7, 2020 from: https://www.econstor.eu/handle/10419/176301

Sharma, H.B., Raja Vanapalli, K., Cheela, S., Ranjan, V.P., Kumar Jaglan, A., Dubey, B. and Bhattacharya, J. 2020. Challenges, opportunities, and innovations for effective solid waste management during and post-COVID-19 pandemic. Resour. Conserv. Recycl., 162: 105052. https://doi.org/10.1016/j.resconrec.2020.105052

Staub, C. 2020. City data shows COVID-19 impacts on recycling tonnages - Resource Recycling News. Retrieved August 1, 2020, from https://resource-recycling.com/recycling/2020/04/28/city-data-shows-covid-19-impacts-on-recycling-tonnages/

Tenenbaum, L. 2020. The Amount of Plastic Waste Is Surging Because of the Coronavirus Pandemic. Retrieved August 5, 2020, from https://www.forbes.com/sites/lauratenenbaum/2020/04/25/plastic-waste-during-the-time-of-covid-19/#1780e5fd7e48

UK Health Security Agency. 2021. COVID-19: Cleaning in Non-Healthcare Settings Outside the Home. Retrieved September 2, 2020, from https://www.gov.uk/government/publications/covid-19-decontamination-in-non-healthcare-settings/covid-19-decontamination-in-non-healthcare-settings

Umarji, V. 2020. Amul Brings Nostalgia Back in Ads to Stay Relevant Amid Covid-19 Lockdown. Retrieved August 8, 2020, from https://www.business-standard.com/article/companies/amul-brings-nostalgia-back-in-ads-to-stay-relevant-amid-covid-19-lockdown-120041401652_1.html

US EPA n.d. Recycling and Sustainable Management of Food During the Coronavirus (COVID-19) Public Health Emergency. Retrieved from https://www.epa.gov/coronavirus/recycling-and-sustainable-management-food-during-coronavirus-covid-19-public-health

Va, R., Prof, M. and Ramanayya, T.V. 2007. Procurement Policy for Food Corporation of India Modifications and Implications. IIM Bangalore Research Paper No 250, IIMB, Bangalore, pp. 1-29. https://ssrn.com/abstract=2147608

Van Doremalen, N., Bushmaker, T., Morris, D.H., Holbrook, M.G., Gamble, A., Williamson, B.N. and Munster, V.J. 2020a. Aerosol and surface stability of SARS-CoV-2 as compared with SARS-CoV-1. New Eng. J. Med., 382: 1564-1567. https://doi.org/10.1056/NEJMc2004973

Van Doremalen, N., Bushmaker, T., Morris, D.H., Holbrook, M.G., Gamble, A., Williamson, B.N. and Munster, V.J. 2020b. Aerosol and surface stability of SARS-CoV-2 as compared with SARS-CoV-1. New Eng. J. Med., 382: 1564-1567. https://doi.org/10.1056/NEJMc2004973

Waste 360. 2020. New Challenges (and Solutions) for Food Waste During COVID-19 Pandemic. Retrieved August 2, 2020, from https://www.waste360.com/food-waste/new-challenges-and-solutions-food-waste-during-covid-19-pandemic

Weike, T. 2020. The Medical Waste Related to COVID-2019 Is Cleaned Up Every Day: The Medical Waste Treatment Market Needs to Be Standardised. Retrieved August 1, 2020, from http://www.21jingji.com/2020/3-12/xNMDEzODFfMTU0MjIxNQ.html

World Health Organization (WHO) (1999). Safe management of wastes from health-care activities. WHO, Geneva

World Health Organization (WHO) (2020). Shortage of Personal Protective Equipment Endangering Health Workers Worldwide. Retrieved August 6, 2020, from https://www.who.int/news-room/detail/03-03-2020-shortage-of-personal-protective-equipment-endangering-health-workers-worldwide

Nature Environment and Pollution Technology
An International Quarterly Scientific Journal

p-ISSN: 0972-6268
(Print copies up to 2016)
e-ISSN: 2395-3454

Vol. 21 | No. 5 (Suppl) | pp. 2291-2297 | 2022

Original Research Paper

https://doi.org/10.46488/NEPT.2022.v21i05.024

Open Access Journal

Analysis and Characterization of Municipal Solid Wastes Generated in a Community in the Northern Philippines

J. M. Ngohayon†* and J. Tulagan*
*Ifugao State University, Potia Campus, Potia, Alfonso Lista, Ifugao, Philippines
†Corresponding author: J. M. Ngohayon; engrjoelngohayon@gmail.com

Nat. Env. & Poll. Tech.
Website: www.neptjournal.com

Received: 26-05-2022
Revised: 30-06-2022
Accepted: 01-07-2022

Key Words:
Municipal solid waste
Waste generation
Waste composition
Waste volume

ABSTRACT

The residential community of Potia in the Northern Philippines experiences various problems arising from mismanaged municipal solid waste. Hence, a waste analysis and characterization study on the generated municipal solid wastes was conducted to determine the municipal solid waste generation data which can be used for planning and formulation of potential solutions. For three consecutive days, the generated municipal solid wastes were gathered from the sample which included residential sources, commercial sources (food establishments, service centers, general stores, and markets), industrial sources, and institutional sources (institutions and health units). The total generated municipal solid waste in Potia is about 508.30 kg.day^{-1} of which most were contributed by the residential sources (70.59%), followed by commercial (25.09%), industrial (2.64%), and institutional (1.70%). The overall composition of the generated MSW is also dominated by biodegradable waste (76.90%), followed by residual waste (14.66%), recyclable waste (7.35%), and special waste (1.08%). The total volume of daily generated MSW is about 3.37 m^3.day^{-1}.

INTRODUCTION

The management of municipal solid waste (MSW) is one of the major problems in developing countries (Ferronato & Torretta 2019) including the Philippines. Even with the existence of the Republic Act 9003 (Ecological Solid Waste Management Act 2000) which enforces proper MSW management, it remains a relentless problem that, unfortunately, is widely ignored in the country. The study by Guisansana et al. (2020) has cited several reasons for the persistence of this problem: (1) Lack of willingness and/or very low priority of the local government unit in implementing the law. (2) Rising population growth. The increase in population will result in an increase in the rate of consumption and also the waste generation rate (Liu et al. 2019, Supangkat & Herdiansyah 2020). In relation to this is the increasing family size which also increases the rate of consumption and rate of waste generation (Suthar & Singh 2015, Xiao et al. 2015, Noufal et al. 2020). (3) Lack of initiatives and discipline of the Filipino people especially on waste generation and segregation. A lot of people are still throwing their waste anywhere. Even if there are trash bins available, only a few are following the waste segregation at source (Paz et al. 2020).

Mismanaged MSW can be a precursor to various community problems and ecological disturbances: (1) it can affect the overall aesthetics of the community (Abdel-Shafy & Mansour 2018), (2) it can clog the drainage and pipe systems (Daniels 2014), (3) it attracts and promotes proliferation of disease-causing vectors (Krystosik et al. 2020), (4) it can pollute the surface water and groundwater through the leachate it produces, and (5) it can pollute the air through the greenhouse gases and other toxic gases it emits upon burning (Ejaz et al. 2010, Liao & Chiu 2011, Alam & Ahmade 2016).

Potia is one of the developing communities in the Northern Philippines. It has a population of approximately 2,188 residents and has had a positive growth rate of 2.30% since 2015 (Philippine Statistics Authority 2021). Currently, the community experiences the following problems regarding MSW management: (1) The absence of an engineered and centralized MSW storage facility. The community has a designated Materials Recovery Facility (MRF), but it only functions as a temporary storage location as it doesn't contain any MRF elements such as weighing equipment, sorting equipment, and designated sorting area among others (Asian Development Bank 2013). The capacity of the designated temporary storage location is also not enough, hence trash containers are lying around the storage structure. (2) The absence of a proper disposal facility for biodegradable wastes. The waste collectors are only collecting nonbiodegradable wastes, thus the

responsibility for the disposal of the biodegradable wastes is tasked to the community and its constituents. While some have backyard compost pits and other ways to utilize the biodegradables (e.g. feeding vegetable and fruit peels to livestock), most are still thrown out and left to rot in nearby ravines. (3) Mixed wastes. Some of the wastes brought to the temporary storage facility contain biodegradables, hence these end up not being collected by the waste collectors. (4) The lack of recycling facilities. While there are efforts to recycle, generally there is no recycling facility to receive the recyclables. Thus, these recyclables are also sent to the storage facility for collection and disposal. Hence, there is a need for the community to plan an MSW management that can effectively minimize or eliminate these aforementioned problems. However, before planning the MSW management strategy, it is important to conduct an initial assessment to know the profile and location of the waste generators and the characteristics of the generated MSW such as the quantity, the composition, the bulk density, and the volume as this information can help in planning the appropriate handling, storage, collection, treatment, and disposal of the generated MSW.

Until now, there are no studies in the community of Potia regarding the characteristics of the generated MSW, hence the primary aim of this paper is to initially assess the baseline MSW generation data. This assessment study is limited to providing the MSW generation data such as waste generation rate, MSW generated daily, waste composition, bulk density, and volume of MSW generated daily. The results obtained from the study can be used by the community as a basis for future planning on MSW management including the formulation of strategies, programs, campaigns, projects, and activities that would address the issues and concerns aforementioned. Furthermore, the results can be used to design long-term waste processing and diversion facilities such as MRFs and composting facilities among others. Moreover, the results can be used by succeeding waste characterization studies to assess the changes and determine trends in the MSW generation data for the community.

MATERIALS AND METHODS

The waste analysis and characterization study (WACS) approach used in this study was adapted from the set of guidelines published in the "Waste Analysis and Characterization Study – A Manual" by the Philippine Environmental Governance Project (EcoGov Project 2011). The guidelines are in accordance with R.A. 9003 and were designed for use by the communities within the country.

The study was conducted at Potia, a residential community that is located in the Northern Philippines. The inventory of the waste generators (residential and non-residential including commercial, institutional, and industrial) was obtained from the office of the community. For a relatively small community like Potia, a sample size of at least 30 households for the residential waste generators was included in the sample size. The following considerations were taken into account in narrowing down the target households: (1) it must have 4 - 6 members to reduce the variability of waste generated, (2) it must not be operating a home-based business, (3) the residents must be willing to cooperate with the researcher, and (4) there are no celebrations during the data gathering. Random sampling was done to obtain a total of 33 households which consist of 153 people. For the non-residential waste generators, at least 10% of the inventory of the non-residential waste generators was included in the sample size. The summary of the inventory and the actual number of samples used for the data gathering is given in Table 1.

Table 1: The inventory of waste generators in the community and the actual sample size.

Waste Generator	Included	Unit	No. of Geneators	Sample Size
Residential	Households	capita	2,188	152
Commercial				
Food Establishments	restaurants, eateries, snack houses, bakeries, and food stalls	store	18	5
Service Centers	computer shops, tailor shops, transport terminals, barber shops, repair shops, and gasoline stations	shop	19	3
General Stores	small-scale groceries, neighborhood sundry stores (sari-sari stores), dry goods stores, and hardware shops	store	95	10
Markets	wet market	stall	9	4
Industrial	furniture-making and rice mills	industry	4	2
Institutional				
Institutions	offices, churches, and schools	capita	176	85
Health Units	health centers and pharmacies	capita	21	16

Before the conduct of the data gathering, permission was obtained from the head of the community and the heads and owners of the households and non-households included in the sample. They were briefly oriented about the study and its objectives, how they will store their generated waste in the provided containers, and how the collection will be done. They were also assured of their anonymity and the confidentiality of the obtained data.

The data gathering was done for three consecutive days from November 12 to 14, 2020. Two waste containers were provided to the identified sampling points: a container for biodegradables and nonbiodegradables (including recyclables, residuals, and special wastes). The collection for each sampling day was on the following day e.g. waste generated on Thursday starting from 8:00 AM will be collected on Friday at 8:00 AM. The collected MSW were then brought to the laboratory in Ifugao State University Potia Campus for analysis.

The total mass of the MSW from each waste generator was measured using a calibrated weighing scale. The generation rate for each type of waste generator was calculated using the formula (Kawai & Tasaki 2016):

$$Generation\ Rate = \frac{Total\ Mass\ of\ MSW}{Number\ of\ Units\ per\ Sample} \quad \ldots(1)$$

The total volume of the MSW from each type of waste generator was measured using a calibrated container. The bulk density was then calculated using the formula (Palanivel & Sulaiman 2014):

$$Bulk\ Density = \frac{Total\ Mass\ of\ MSW}{Bulk\ Volume\ of\ MSW} \quad \ldots(2)$$

The containers for biodegradable and nonbiodegradable were checked for any mixed waste contents. After that, the nonbiodegradables were segregated into residuals, recyclables, and special wastes. Furthermore, the recyclables were segregated into papers, tins, bottles, and textiles. The description of each waste category is presented in Table 2. After segregation, the masses of each type of waste per waste generator were measured using a weighing scale. The gravimetric composition of each type of waste was calculated using the formula (Miguel et al. 2016):

$$\%\ type\ of\ waste = \frac{Mass\ of\ Type\ of\ Waste}{Total\ Mass\ of\ MSW} \times 100 \quad \ldots(3)$$

After the analysis, the collected MSW were disposed of - the biodegradable wastes were buried in a compost pit, while the nonbiodegradable wastes were packaged and brought to the nearest waste collection point for pickup by the waste collectors of the community.

The average of the obtained MSW generation data from the three-day sampling was calculated and was used for the succeeding analysis and discussion.

RESULTS AND DISCUSSION

MSW Generation Rate and MSW Generated Daily

The summary of the calculated MSW generation rate and the daily generated MSW per type of waste generator in Table 3 shows that the largest portion of the generated MSW came from residential sources (70.59%). This is because the community is largely utilized as a residential area. In addition, because of the prevalence of the COVID-19 pandemic and the quarantine restrictions, most of the commercial establishments, industries, and institutions were either closed or not operating at full capacity, thus there were relatively fewer MSW generated in these sources as compared to the residential sources. Moreover, since most people were forced to stay and work within the confinements of their homes, waste production must have shifted from

Table 2: Description of the categories used in the gravimetric characterization of the generated MSW.

Category*	Description*	Sample Waste Recovered from the Study
Biodegradable	Waste can be easily decomposed and can be turned into compost once it is exposed to various agents of decomposition.	food wastes, fruit and vegetable peelings, meat and fish scraps, garden and yard wastes, wet/soiled paper wastes, used tissue paper, wood shavings, and rice husk
Recyclables	Wastes that are in relatively good condition enough to be recovered and converted into new products.	dry/unsoiled paper wastes, cartons, cardboard, metal scraps, glass bottles, plastic bottles, tin cans, textile trimmings, and rubber
Residual	Wastes cannot be recycled anymore due to several factors such as market demand, technological limitations, costs, and quality of recycled products, among others. These are immediately transported to sanitary landfills for disposal.	ashes, soot, dirt, tattered packaging materials, plastic straw, laminates, and composite materials, sando bags, food wrappers, and packaging, used napkins and diapers
Special	Household hazardous waste.	chemical containers, broken light bulbs, expired drugs, used dry cell batteries and used face masks

*Source: National Solid Waste Management Commission 2018

Table 3: The MSW generation rate and MSW generated daily in Potia.

Waste Generator	MSW Generation Rate	No. of Generator	MSW Generated Daily*	
			kg.day^{-1}	%
Residential	0.164 kg.day^{-1}.capita^{-1}	2,188 capita	358.83	70.59
Commercial			127.46	25.09
Food Establishments	1.425 kg.day^{-1}.store^{-1}	18 store	25.65	5.05
Service Centers	0.812 kg.day^{-1}.shop^{-1}	19 shop	15.43	3.04
General Stores	0.728 kg.day^{-1}.store^{-1}	95 store	69.16	13.61
Markets	1.913 kg.day^{-1}.stall^{-1}	9 stall	17.22	3.39
Industrial	3.350 kg.day^{-1}industry^{-1}	4 industry	13.40	2.64
Institutional			8.62	1.70
Institutions	0.040 kg.day^{-1}.capita^{-1}	176 capita	7.04	1.39
Health Units	0.075 kg.day^{-1}.capita^{-1}	21 capita	1.58	0.31
Total			508.30	100.00

*MSW Generated Daily = MSW Generation Rate × No. of Generators

institutional, industrial, and commercial to residential (Roy et al. 2021, Sinha et al. 2020).

While most commercial establishments in the community were not operating at full capacity, a considerable amount of MSW is still being generated in these sources (25.09%). In particular, the general stores, which include mostly small-scale groceries and neighborhood sundry stores, have the highest contribution (13.61%) to the generated MSW from commercial sources. Since the residents don't have the luxury anymore to travel to the nearby city to buy their household necessities, they are relegated to consuming the goods available within the community. Food is still a daily necessity for the population, pandemic or not, therefore food establishments and markets also contribute a sizable amount of MSW from commercial sources. Since people could not use shared services like transit terminals, computer stores, and barbershops among others due to quarantine laws at the time, the service centers make up the least of the MSW generated.

Daily, the total generated MSW from all the waste generators is approximately 508.30 kg.day^{-1}. On a yearly basis, this is about 185,529.50 kg.yr^{-1} or 185.52 MT.yr^{-1}

MSW Composition

The summary of the waste composition from the various waste generators is shown in Table 4. Most of the waste generators, except for the service centers, generated MSW that was dominated by biodegradable wastes, followed by residual waste, recyclable waste, and special wastes. The relatively high biodegradable fraction for the generated MSW in the community is similar to the results of several studies (Adeleke et al. 2021, Montero et al. 2019, Enteria & Orig 2019) which have also observed this trend among communities dominated by residential areas.

Table 4: The composition of the generated MSW in Potia.

Waste Generator	Bio [%]	Recyclable [%]				Residual [%]	Special [%]
		Paper	Tin	Bottle	Textile		
Residential	79.03	0.66	1.22	1.68	1.59	15.14	0.68
Commercial							
Food Establishments	72.71	0.00	0.53	1.48	0.00	25.23	0.04
Service Centers	0.36	27.81	0.00	1.62	65.18	4.53	0.50
General Stores	78.54	0.00	0.00	3.01	0.00	14.27	4.18
Markets	94.86	0.00	0.00	0.12	0.00	5.02	0.00
Industrial	100.00	0.00	0.00	0.00	0.00	0.00	0.00
Institutional							
Institutions	51.59	18.52	0.34	2.01	0.00	26.23	0.92
Health Units	59.26	9.24	1.16	1.16	0.00	26.99	2.20
Overall	76.90	1.59	0.90	1.76	3.10	14.66	1.08

The service centers are the only group of waste generators that generated MSW that was not dominated by biodegradable wastes. This is because the stores and shops belonging to this group don't primarily engage in activities that consume goods that produce biodegradable wastes such as food waste. The few biodegradable wastes recovered were mostly yard wastes from their cleaning activities. Instead, the generated MSW is dominated by recyclable wastes, such as paper waste and textile trimmings due to the nature of activities in the various service centers such as computer shops, tailor shops, and repair shops.

The industries produced the highest biodegradable fraction as the rice mills and the furniture shops in the community are only producing rice hull and wood shavings, respectively, from their activities.

The generated MSW from the institutional source also has a relatively high fraction of paper waste among the recyclable waste generated. This result is very similar to the observations from several studies (Goa & Sota 2017, Montero et al. 2019, Pathak et al. 2020) on the generated MSW from institutional sources. This is because the activities in the institutional sources heavily involve the usage of paper products for printing, note-taking, and crafting among others.

The overall composition shows that the bulk of the generated MSW is biodegradable (76.90%). Daily, this amounts to approximately 390.88 kg of biodegradable waste generated. With this many biodegradables, these must be properly handled and disposed of because mismanaged biodegradable wastes can easily attract disease-causing vectors and can be unsightly and smelly in just a few hours. As mentioned, this type of waste is not being collected for disposal in the sanitary landfill, and the responsibility for handling and disposal of the generated biodegradable wastes is left to the individual waste generators. Some residents are utilizing their food wastes as animal feed for their pets and livestock. However, not all biodegradable wastes, such as garden waste and soiled paper waste, can be used as animal feed. In addition, not all residents have pets or livestock. While there are some efforts to compost, these are only limited to those who are knowledgeable about composting and those who have spare backyard space. Hence, the community can develop a centralized facility that will receive the generated biodegradable wastes from residents who don't own pets or livestock and/or who don't have spare backyard space for backyard composting. The centralized facility can then employ various treatment methods for biodegradable wastes like composting and waste-to-energy processes among others.

Recyclable waste is just a small percentage (combined with 7.35%) of the overall generated MSW. Since the community has no dedicated treatment or recovery facilities, such as junk shops and recycling facilities, these potentially-recyclable materials end up as residuals and are sent to the sanitary landfill for disposal. Similarly, this is also the case for special waste (1.08%) which has no dedicated receiving and treatment facility within the community. Hence, this brings to a total of 23.1% residuals of the overall generated MSW daily.

Bulk Density and Volume of MSW Generated Daily

The summary of the calculated bulk densities and the volumes of generated MSW daily per type of waste generator is shown in Table 5. The generated MSW from the markets has the highest bulk density (245.58 $kg.m^{-3}$) among the waste generators. This can be attributed to

Table 5: The bulk density and the volume of MSW generated daily in Potia.

Waste Generator	Bulk Density [$kg.m^{-3}$]	MSW Generated Daily [$kg.day^{-1}$]	The volume of MSW Generated Daily* [$m^3.day^{-1}$]
Residential	162.00	358.83	2.21
Commercial			
Food Establishments	166.55	25.65	0.15
Service Centers	128.76	15.43	0.12
General Stores	117.01	69.16	0.59
Markets	245.58	17.22	0.07
Industrial	162.28	13.40	0.08
Institutional			
Institutions	62.88	7.04	0.11
Health Units	61.77	1.58	0.03
Total		508.30	3.37

* Volume of MSW Generated Daily = Bulk Density × MSW Generated Daily

the high biodegradable content (94.86%) of the generated MSW which is mostly food waste that has relatively high bulk densities (Foday et al. 2017). This is similar to the observation of Hailu et al. (2018) where the highest bulk density was recorded on the waste generator having the highest amounts of biodegradable in the generated waste. While the generated MSW from the industries is 100% biodegradable, the type of biodegradable wastes generated (rice hull and wood shavings) have relatively higher volume owing to their porous and loose nature as compared to the market's biodegradables (food waste) which are less porous and are more compact.

The generated MSW from the institutions and the health units have the lowest bulk densities because of the relatively high fraction of paper waste and residuals (mostly plastics). Since paper and plastics have low densities (Foday et al. 2017), then the overall generated MSW which is dominated by these components is also expected to have low bulk densities (Bowan & Tierobar 2014). The generated MSW in the service centers, despite having a higher fraction of paper waste than either of the former two, have a higher bulk density. This can be attributed to the following: (1) the generated MSW in the service centers has lower residual (plastics) content as compared to generated MSW in the institutions and the health units, and (2) the generated MSW in the service centers have a high fraction of textile trimmings (65.18%) which have high densities (United States Environmental Protection Agency 2016).

The residential and the food establishments have almost similar bulk densities because of the similarities in their waste composition - both are dominated by biodegradable wastes. While the general stores have close amounts of biodegradables with the residential and food establishments, it has a lower bulk density than the former two. This can be attributed to the higher fraction of recyclable bottles and chemical containers (special waste) which adds to the bulkiness and volume of the generated MSW.

Similarly, since the community is largely utilized as a residential area, the bulk of the volume of generated MSW daily came from residential sources. The total volume of the generated MSW is approximately 3.37 $m^3.day^{-1}$. If packed in a cube, the generated MSW daily will be approximately 1.5 m on each side. On a yearly basis, the volume of generated MSW is approximately 1,230.05 $m^3.yr^{-1}$.

CONCLUSIONS

The total generated MSW in Potia is about 508.30 $kg.day^{-1}$ of which most were contributed by the residential sources (70.59%), followed by commercial (25.09%), industrial (2.64%), and institutional (1.70%). The overall composition of the generated MSW is also dominated by biodegradable waste (76.90%), followed by residual waste (14.66%), recyclable waste (7.35%), and special waste (1.08%). Without a receiving treatment facility for recyclable waste and special waste, these types of waste can also end up in the sanitary landfill, hence bringing a total of 23.1% residual waste. The large amount of biodegradable waste generated and the lack of proper treatment and disposal for this type of waste can also be a good starting point for the community to explore potential treatment methods for this type of MSW. The highest bulk density was recorded on the generated MSW which is dominated by biodegradable wastes. The total volume of daily generated MSW is about 3.37 $m^3.day^{-1}$ of which most were also contributed by the residential sources. The MSW generation data obtained from Potia is similar to most communities which are also largely utilized as a residential areas.

ACKNOWLEDGEMENT

The authors would like to acknowledge the residents of Potia for their willingness to participate in the data gathering and for the manpower provided during the actual experiment. The authors would also like to acknowledge the assistance provided by the Ifugao State University, especially during the sample collection.

REFERENCES

Abdel-Shafy, H.I. and Mansour, M.S. 2018. Solid waste issue: Sources, composition, disposal, recycling, and valorization. Egypt. J. Petrol., 27(4): 1275-1290.

Adeleke, O.A., Akinlabi, S.A., Jen, T.C. and Dunmade, I. 2021. An overview of factors affecting the rate of generation and Physical Composition of Municipal Solid Waste. IOP Conf. Ser. Mater. Sci. Eng., 1107(1): 012096.

Alam, P. and Ahmade, K. 2016. Impact on health and the environment. Live Cell Assays, 13: 197-217.

Asian Development Bank. 2013. Materials Recovery Facility Tool Kit. Asian Development Bank, Tokyo.

Bowan, P.A. and Tierobaar, M.T. 2014. Characteristics and management of solid waste in Ghanaian markets: A study of WA municipality characteristics and management of solid waste in Ghanaian Markets. Civil Environ. Res., 6: 114-119.

Daniels, N.C. 2014. Drainage system cleaner is a solution to environmental hazards. Int. Ref. J. Eng. Sci., 3(3): 54-60.

EcoGov Project. 2011. Waste Analysis and Characterization Study: A Manual. Second Edition. Philippine Environmental Governance Project, Diliman, Quezon City, The Philippines.

Ecological Solid Waste Management Act. 2000. R.A. 9003, 2000. https://www.officialgazette.gov.ph/2001/01/26/republic-act-no-9003-s-2001/

Ejaz, N., Akhtar, N., Nisar, R. and Ali Naeem, U. 2010. Environmental impacts of improper solid waste management in developing countries: A case study of Rawalpindi City. WIT Trans. Ecol. Environ., 142: 379-387.

Enteria, O. and Orig, A. 2019. Comparative waste analysis and characterization study (WACS) among the selected rural areas in the northern part of Mindanao, Philippines. Int. J. Sci. Res., 8(2): 1549-1553.

Ferronato, N. and Torretta, V. 2019. Waste mismanagement in developing countries: A Review of Global issues. Int. J, Environ, Res. Pub. Health, 16(6): 1060.

Foday, E.H., Ramli, N.A., Nabilah Ismail, H., Malik, N.A., Basri, H.F., Aziz, F.S.A., Nor, N. S.M. and Jumhat, F. 2017. Municipal solid waste characteristics in Taman Universiti, Skudai, Johore, Malaysia. J. Adv. Res. Design, 38(1): 13-20.

Goa, E. and Sota, S.S. 2017. Generation rate and physical composition of solid waste in Wolaita Sodo Town, southern Ethiopia. Ethiop. J, Environ. Stud. Manag., 10(3): 415.

Guisansana, L.G.G., Mag, J.D.R.U., Nabing, C.B.P. and Festijo, F. 2020. Solid waste management: The enactment of the ecological solid waste management act of 2000 (R.A 9003) in addressing the waste crisis. Europ. J. Mol. Clinic. Med., 7(2): 4186-4196.

Hailu, H., Rao, R.S.V., Dawit, M. and Feyisa, A. 2018. Assessment of reuse, recycle, and recoverable potential of solid waste. MATEC Web oConf., 276: 06007.

Kawai, K. and Tasaki, T. 2016. Revisiting estimates of municipal solid waste generation per capita and their reliability. J. Mater. Cyc. Waste Manag., 18(1): 1-13.

Krystosik, A., Njoroge, G., Odhiambo, L., Forsyth, J.E., Mutuku, F. and LaBeaud, A.D. 2020. Solid wastes provide breeding sites, burrows, and food for biological disease vectors, and urban zoonotic reservoirs: A call to action for solutions-based research. Front. Pub. Health, 7: 56

Liao, C.H. and Chiu, A.S.F. 2011. Evaluate municipal solid waste management problems using a hierarchical framework. Proced. Social Behav. Sci., 25: 353-362.

Liu, J., Li, Q., Gu, W. and Wang, C. 2019. The impact of consumption patterns on the generation of municipal solid waste in China: Evidence from provincial data. Int. J< Environ. Res. Pub. Health, 16(10): 1-19.

Miguel, M.G., Paixao Filho, J.L.D., Benatti, J.C.B., Leme, M.A.D.G., Mortatti, B.C., Gabrielli, G., Elaiuy, M.L C., Pereira, S.Y. and Teixeira, E.N. 2016. Gravimetric composition of municipal solid waste disposed of in a large-scale experimental cell in Southeastern Brazil. Int. J. Environ. Waste Manag., 17(2): 128.

Montero, S., Hapinat, H. and Penaflorida, M. 2019. Waste Analysis and Characterization Study (WACS): Measures Towards Effective Municipal Waste Management in Batad, Iloilo, Philippines. Food and Fertilizer Technology Center for the Asian and Pacific e-Journal. Retrieved from https://ap.fftc.org.tw/article/1650

Noufal, M., Yuanyuan, L., Maalla, Z. and Adipah, S. 2020. Determinants of household solid waste generation and composition in Homs city, Syria. J. Environ. Pub. Health, 2: 20.

Palanivel, T.M. and Sulaiman, H. 2014. Generation and composition of municipal solid waste (MSW) in Muscat, Sultanate of Oman. APCBEE Proced., 10: 96-102.

Pathak, D.R., Mainali, B., Abuel-Naga, H., Angove, M. and Kong, I. 2020. Quantification and characterization of municipal solid waste for sustainable waste management in newly formed municipalities of Nepal. Waste Manag. Res. J. Sustain. Circular Econ., 38(9): 1007-1018.

Paz, V.D., Domingo, R. and Roxas, F.M. 2020. Strategy to improve the solid waste management of Barangay Matictic, Norzagaray, Bulacan. IOP Conf. Ser. Earth Environ. Sci., 511(1): 012004.

Philippine Statistics Authority 2021. 2020 Census of Population and Housing [Data Set]. Philippine Statistics Authority. Retrieved from https://psa.gov.ph/sites/default/files/attachments/ird/pressrelease/CAR.xlsx

Roy, P., Mohanty, A.K., Wagner, A., Sharif, S., Khalil, H. and Misra, M. 2021. Impacts of COVID-19 outbreak on the municipal solid waste management: Now and beyond the pandemic. ACS Environ., (1): 32-45.

Sinha, R., Michelsen, J.D., Akcura, E. and Njie, L. 2020. COVID-19's Impact on the Waste Sector. International Finance Corporation.

Supangkat, S. and Herdiansyah, H. 2020. Analysis correlation of municipal solid waste generation and population: Environmental perspective. IOP Conf. Ser. Earth Environ. Sci., 519(1): 012056.

Suthar, S. and Singh, P. 2015. Household solid waste generation and composition in different family size and socioeconomic groups: A case study. Sustain. Cities Soc., 14(1): 56-63.

United States Environmental Protection Agency 2016. Volume-to-Weight Conversion Factors for Solid Waste. US EPA. Retrieved from https://www.epa.gov/smm/volume-weight-conversion-factors-solid-waste

Xiao, L., Lin, T., Chen, S., Zhang, G., Ye, Z. and Yu, Z. 2015. Characterizing urban household waste generation and metabolism considering community stratification in a rapidly urbanizing area of China. PLoS ONE, 10(12): 1-16.

Nature Environment and Pollution Technology
An International Quarterly Scientific Journal

p-ISSN: 0972-6268
(Print copies up to 2016)
e-ISSN: 2395-3454

Vol. 21 | No. 5 (Suppl) | pp. 2299-2305 | 2022

Original Research Paper

https://doi.org/10.46488/NEPT.2022.v21i05.025

Open Access Journal

Chromate Reduction by *Allochromatium* sp. Isolated from the Coastal Area of Visakhapatnam

Kadari Rajyalaxmi*†, S. Girisham*, S. M. Reddy* and E. Sujatha*
*Department of Microbiology, Kakatiya University, Warangal, Telangana-506009, India
†Corresponding author: Kadari Rajyalaxmi; laxmi.kadari10@gmail.com

Nat. Env. & Poll. Tech.
Website: www.neptjournal.com

Received: 01-04-2022
Revised: 13-05-2022
Accepted: 16-05-2022

Key Words:
Allochromatium sp.
Chromate reduction
Free cells
Immobilized cells
Incubation period

ABSTRACT

A phototrophic purple bacterium *Allochromatium* sp. strain GSKRLMBKU–01 was used in this study for the reduction of hexavalent chromium. This phototrophic bacterium was isolated from samples collected from the coastal area of Visakhapatnam, India. Both the cells (free (FC) and alginate entrapped immobilized (IC)) are used for the reduction of chromate. Among them, chromate reduction was increased using immobilized cells. Immobilized cells entrapped in sodium alginate reduced the chromate up to 33 ± 3.0 µM on the 8th day of incubation by *Allochromatium* sp., incubated in presence of light (2000 lx) under the strictly anaerobic conditions, while a chromate reduction up to 26 ± 0.20 µM was recorded by FC of *Allochromatium* sp. Chromate reduction can be recorded even up to the 20th day by both FC and IC. An incubation period of 8 days was found to be optimum for its growth and chromate reduction. The maximum growth in terms of dry cell weight (DCW) of FC is recorded up to 1.7 ± 0.20 g.L^{-1} and IC is 2.0 ± 0.30 g.L^{-1}. The growth was recorded even on complete chromate reduction. The final pH of the FC was recorded at pH 8.5 ± 0.10, while the final pH of 8.6 ± 0.20 was recorded for the IC of *Allochromatium* sp. in the growth medium. The obtained results were mentioned in terms of mean and standard deviation which are statistically significant at P ≤ 0.001 level. The detoxification of chromium in the large-scale systems by employing a purple phototrophic bacteria *Allochromatium* sp., is proposed.

INTRODUCTION

Microorganisms have to cope and adapt to the various stressors of natural or anthropogenic origin in their environment (Mariann Kis et al. 2015). Scientists are assigned with developing useful applications for environmental protection, including protecting the biodiversity of aquatic habitats (Koblizek et al. 2005, Falkowski et al. 2007, Hojerova et al. 2011, Medova et al. 2011, Ferrera et al. 2011, Douglas et al. 2016) and monitoring and remediating pollutants (Borsetti et al. 2009, Kushalatha et al. 2010, Idi et al. 2015) in the environment. One of the most important factors affecting toxicity can be the metal ions produced by contamination. Low concentrations of important metal ions play an essential part in the natural development of microorganisms: They act as catalysts for several biochemical reactions, transition metals such as iron, copper, and nickel participate in redox processes, stabilize magnesium and zinc, various enzymes and DNA by electrostatic forces, and iron, magnesium, nickel, and cobalt are part of complex molecules with diverse functions (Mariann Kis et al. 2015, Nies 1992). Among heavy metals, the second most common metal is chromium which is considered a serious environmental inorganic pollutant widely spread in nature. This is very important in the treatment of different industrial wastes contaminated with metal (Williams & Silver1984). A huge number of industrial applications such as metallurgical and refractory are associated with chromium. The oxyanions of Cr(VI) are widely distributed in leather treating processes, metal plate removal, rust prevention, water cooling tower treatment, color manufacture, masking, and wood preservation (Shanker et al. 2005). The metal toxicity will depend upon its state of oxidation, whereas the compounds of Cr(VI) are dissolved in water and move in nature. Although, the insoluble chromium hydroxides of Cr(III) are slightly acidic and alkaline (Cieslak-Golonka 1995). The hexavalent chromium species are carcinogenic, teratogenic, and mutagenic in nature and are highly toxic to all life forms. The CrO_4^{2-} tends to cross the cell membrane through external anion transport systems (channels of SO_4^{2-} and HPO_4^{2-}) and reacts with nucleic acids as well as alternative cell constituents that affect oxidation and damage the cells (Bagchi et al. 2002, Rajyalaxmi et al. 2019). Previously the removal of chromium-polluted wastes are executed by conventional methods which were more expensive and required higher energy and a larger number of chemicals. To overcome these current problems, the employment of biological systems and their uses in the

biodegradation of pollutants has gained much consideration in the past few years (Gadd 2000). In the reduction of toxicity, various microorganisms are exposed to Cr(VI) by altering the elements of the genes into a dangerous and subtle trivalent type (Daulton et al. 2002).

Because of their unique nature, these phototrophic bacteria are a great fit for their application in biotechnological industries as they get energy from solar radiation and are highly resistant to several heavy metals. These bacteria have strong capabilities in decomposing as well as transforming several organic compounds, which are highly resistant to toxicants such as phenols, cyanides, chlorine, and salts involved in synthesizing cell materials (Zhou et al. 2015). He et al. (2017) reported the combination of nanoparticles and microbes for the treatment of wastewater using phototrophic bacteria. *Rsp. rubrum* and *Rhodobacter sphaeroides* were used for the bioaccumulation and biosorption of cadmium (Watanabe et al. 2003, Smiejan et al. 2003). The high concentrations of chromium, cobalt, molybdenum, as well as nickel, were also removed by using *Rhodobacter sphaeroides* (Buccolieri et al. 2006). The *Rba. capsulatus* was found to be cadmium (Cd) tolerant (Gad El-Rab et al. 2006). The bioaccumulation of cobalt and nickel as well as oxyanions reduction as selenite and tellurite was also reported (Borsetti et al. 2003, Italiano et al. 2009). The reduction and oxidation of metals using hydrogenases produced from *Thiocapsa roseopersiciana* were studied by Zadvorny et al. (2006). The chromate reductases produced by bacteria and some phototrophic bacteria were used for the detoxification of toxic chromate to less toxic Cr(III) form (Philip et al. 1998; Ramchander et al. 2011, Rajyalaxmi et al. 2019). Panwichian et al. (2012) have undertaken detailed studies on the remediation of heavy metals and treatment of water collected from contaminated shrimp ponds using purple non-sulfur bacteria (PNSB). A purple phototrophic bacteria such as *Allochromatium* sp., isolated from a marine source was used for phosphate solubilization (Rajyalaxmi et al. 2015). Takaiekhozani and Rezania (2017) have excellently reviewed heavy metals removal from polluted water by employing photosynthetic bacteria. These phototrophic purple bacteria are not only used in bioremediation processes but are also used in the production of other high-value-added products (Sasikala et al. 1995a, Ramchander et al. 2010a,b, Rajyalaxmi et al. 2018, Rajyalaxmi et al. 2021). Ramchander et al. (2011) and Rajyalaxmi et al. (2019) investigated the reduction of chromate by employing *Rhodobacter capsulatus* KU002 and *Rhodobacter* sp. strain GSKRLMBKU-02. Very few reports are published on anoxygenic phototrophic bacteria. The results of this investigation carried out on phototrophic purple bacteria such as *Allochromatium* sp. intended to show its possibilities in the field of remediation of chromium in the presence of light under anaerobic conditions. This is the first report on chromate reduction by this bacterium.

MATERIALS AND METHODS

Chemicals

0.25% Diphenyl-carbazide (DPC) solution, 0.05 µM potassium dichromate ($K_2Cr_2O_7$), 3% sodium nitride (NaN_3) solution, 1N H_2SO_4, 0.01 M $KMnO_4$ solution, Distilled water, $MgSO_4{\cdot}7H_2O$, $KH_2PO_4{\cdot}7H_2O$, NaCl, NH_4Cl, 0.4; $CaCl_2.2H_2O$, Sodium acetate, Ferric citrate, Yeast extract, ZnCl, $MnCl_2.4H_2O$, H_3BO_3, $CoCl_2.6H_2O$, $NiCl_2.6H_2O$, $CuCl_2.2H_2O$, $NaMO_4.2H_2O$, Hydrochloric acid (25%v/v) and Cyanocobalamin (Vitamin B_{12}). All the above-mentioned chemicals used for this study are purchased from Hi-Media and Sigma Aldrich (Mumbai, India).

Basal Medium (Modified Biebl and Pfennig's Media)

The media employed for this study is taken from the previous literature reported by Rajyalaxmi *et al*. (2018). The media contains (in g.1000mL^{-1}) KH_2PO_4, 1.0; NH_4Cl, 1.0; $MgCl_2.5H_2O$, 0.5; Yeast extract, 0.1; Organic carbon (sodium acetate), 1.0; H_2S, 0.25; Sodium bicarbonate, 3.0; Yeast extract, 0.1; double distilled H_2O, 1000 mL; Trace element solution (modified SL4 (Pfennig & Lippert 1966)): ($MnCl_2$, 100; $CoCl_2$, 190; H_3BO_3, 300; $NiCl_2.6H_2O$, 24; $CuCl_2.2H_2O$, 0.2; $NaMO_4.2H_2O$, 10; $ZnCl_2$, 70; Ethylenediaminetetraacetate-Na(Na_2-EDTA), 3.0) (mg.L^{-1}), 1.0 mL and the mixture of vitamin solution contains (Biotin, 10; Calcium pantothenate, 10; Pyridoxal HCl, 10; PABA, 20; Thiamine dichloride, 30; vitamin B12, 5 and Niacinamide, 35) (mg.L^{-1}), 1.0 mL. The initial pH of the basal medium was maintained at pH 8.0.

Isolation and Identification of *Allochromatium* sp.

Allochromatium sp. strain GSKRLMBKU-01 used in this present investigation was isolated by enrichment techniques (Pfennig & Truper 1992, Rajyalaxmi et al. 2015). Bacteria thus isolated were identified morphologically (Staley et al., 1994) and further confirmed molecularly by 16S rRNA sequencing analysis (Rajyalaxmi et al. 2019).

Immobilization

The method used for the immobilization was adopted from the method suggested by Johnsen and Flink (1986) and Rajyalaxmi et al. (2019). Freshly cultured cells of *Allochromatium* sp. were separated by centrifugation at 5000 rpm for 10 minutes at 4°C. The obtained cells were washed and resuspended in sterile 0.3 % saline and fixed with an alginate cell trap by immobilization. A 3.0 % solution of sodium

alginate was prepared by dissolving 3.0 g of sodium alginate in 100 mL of boiling distilled water and kept for autoclaving for 15 minutes at 121°C. On cooling, the cell and alginate suspension were mixed and stirred thoroughly for 10 minutes to form a homogenous mixture. Drop this mixture into an ice-cold solution of 0.2 M $CaCl_2$ with a sterile syringe from the height of 5 cm and be subject to curing at 4°C for about 4 h. These cured beads were washed with sterile distilled H_2O about 4 times and are stored in the refrigerator by preserving in the 0.9% solution of sodium chloride (Rajyalaxmi et al. 2019).

Estimation of Chromium

The Uv-Vis spectrophotometric method was suggested for chromium determination using diphenyl–carbazide (DPC) (Greenberg et al. 1992, Rajyalaxmi et al. 2019). The reddish-violet complex is observed when chromium (VI) reacts with diphenyl-carbazide. This reaction is very sensitive and selective for chromium. To a 15 mL sample solution, add 1.0 mL of 1 N sulphuric acid (H_2SO_4) and a solution prepared with 0.5 mL of 0.01 M potassium permanganate ($KMnO_4$) and heat the solution for 40 minutes in boiling water. A 4% sodium azide (NaN_3) solution was added and kept for warming for 3 minutes at 60°C to reduce the excess amount of $KMnO_4$. After cooling in ice water, add 2.0 mL of the solution prepared with 0.25% diphenyl-carbazide and make up the volume to 25 mL using distilled H_2O. Allow the reaction mixture for about 20 minutes and measure the absorbance at 540 nm against a blank prepared using only the reagent. Different concentrations of potassium dichromate ($K_2Cr_2O_7$) are used for the preparation of the standard graph (Rajyalaxmi et al. 2019).

Estimation of Biomass

The UV-Vis spectrophotometer (turbidimetric analysis) is used to determine the growth of the *Allochromatium* sp. by reading the optical density at 660 nm. The biomass of the cells was also determined in terms of the dry weight, for this, aluminum cups were prepared and weighed before and after the experimental procedure (Rajyalaxmi et al. 2019). The culture suspension was transferred into the cups and dried at 80°C. After cooling at room temperature, the aluminum cups were weighed in a single pan balance, whereas the uninoculated media was used as blank.

Statistical Analysis

The obtained results were subjected to statistical analysis to record the mean and SD by using GraphPad Prism.InStat Version 6 (GraphPad Software Inc., USA) and subjected to analysis of variance (ANOVA) to test the significance level of the treatment at P □ 0.05 (Rajyalaxmi et al. 2019).

RESULTS AND DISCUSSION

Isolation and Identification

Allochromatium sp. strain GSKRLMBKU-01 was isolated from the water sampled from the coastal area of Visakhapatnam, India using modified Biebl and Pfennig's media (Rajyalaxmi et al. 2018). The cells were motile, Gram – ve, appear as ovoid to rod-shaped, 2.0 to 5.0 µm in size, multiplied by binary fission and they form single or paired cells. This bacterium appears in brown because of the presence of bacteriochlorophyll *a* and carotenoids of the spirilloxanthin series i.e., spirilloxanthin as the main carotenoid. Further, growing on the agar plates they form smooth round as well as slimy colonies. After 3-5 days of its incubation at a temperature of 30±2°C in the presence of light (2000 lx) under strict anaerobic conditions, the light brown colored cells were transformed to dark brown in liquid media. This phototrophic bacteria grows photoorganoheterotrophically in the presence of light (2000lx) by utilizing acetate (0.1% w/v) under anaerobic conditions.

Thus the morphologically identified *Allochromatium* sp. was further confirmed molecularly by 16S rRNA sequencing analysis (Rajyalaxmi et al. 2015). The obtained sequence was analyzed at the NCBI (Bethesda, MD) (http://www.nbi.nlm.nih.gov/BLAST) (Rajyalaxmi et al. 2019) to find out the closed homology by means of a BLAST algorithm and also deposited in the National Centre for Biotechnology Information based on obtained evolutionary analysis. Fig. 1 illustrates that isolated and identified strain GSKRLMBKU-01 of *Allochromatium* species differed hereditarily from other species because of the source from where it is isolated. The obtained sequence data showed that a new isolate was observed and branched separately, however, it is grouped with other members of *Allochromatium* which were varied with the genera of other anoxygenic phototrophic bacteria (Tamura et al. 2011). The gene sequence obtained from 16S rRNA gene sequence analysis of an *Allochromatium* sp. strain GSRLMBKU-01 was deposited at the NCBI database with GenBank Accession Number HF677171.1 (Rajyalaxmi et al. 2015).

Estimation of Chromium

The Uv-Vis spectrophotometric method with diphenyl-carbazide (DPC) is used for the determination of chromate reduction at different incubation time intervals. In the present study both the FC and IC of *Allochromatium* sp. were used for the chromate reduction. The concentration of 0.05 mM potassium dichromate is added to the 15 mL screw-capped glass tubes containing growth medium which are incubated at a temperature of 30 ± 2°C for 4 to 20 days in the presence

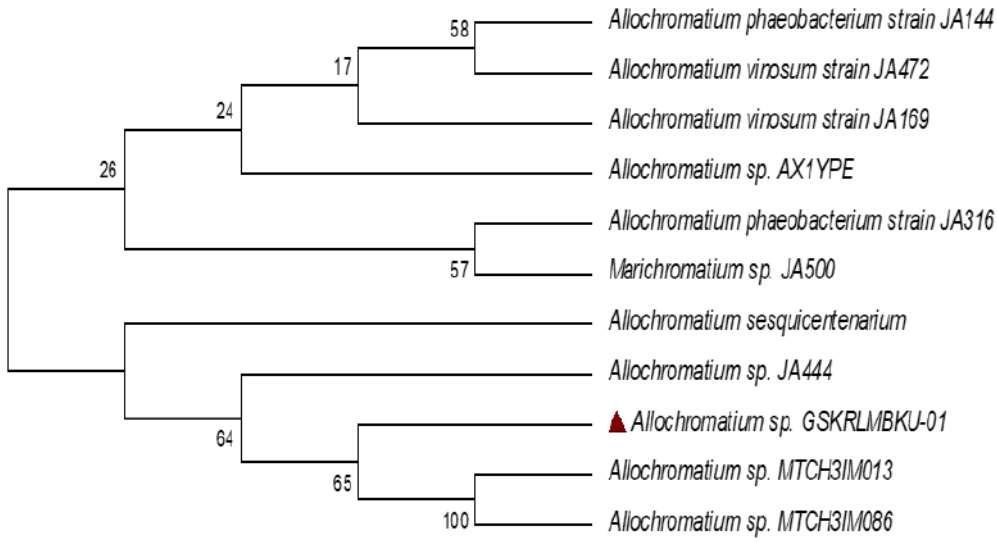

Fig. 1: Phylogenetic tree showing the genetic diversity of *Allochromatium* sp., based on partial 16s rRNA gene sequences of isolate and NCBI reference strains, obtained by the neighbor-joining method using the MEGA 5.0 software (Tamura et al. 2011).

of light (2000lx) and strict anaerobic conditions are maintained throughout the investigations. The immobilization of bacterial cells increased the percentage of reduction of chromate (Fig. 2). From Table 1 and Table 2, it is evident that the reduction of chromate was initiated from the 4th day by FC (10.0 ± 2.0 µM) and IC (14.0 ± 1.0 µM) of *Allochromatium* sp., and it was even recorded on the 20th day. These investigations carried out are similar to the study reported by Rajyalaxmi et al. (2011) and Rajyalaxmi et al. (2019) where they recorded the reduction of chromate even on the 20th day. The benefit of this investigation might be that the reduction of chromate was observed for a persistent period (up to 20 days).

The chromate up to 33.0 ± 3.0 µM is reduced by alginate entrapped cells of *Allochromatium* sp. (Table 2), whereas chromate up to 26.0 ± 2.0 µM is reduced by FC of *Allochromatium* sp. (Table 1). Eight days of incubation proved to be optimum for the reduction of chromate by both the immobilized and free cells. The chromate reduction was increased up to the 8th day and it gradually decreased on a further increase of the incubation period (Fig. 2). Similarly, Rajyalaxmi et al. (2019) reported the maximum chromate reduction of up to 40 µM on the eighth day of the incubation by alginate entrapped cells of *Rhodobacter* sp. Nepple et al. (2000) examined the growth conditions of *Rba. sphaeroides* and found that it can grow anaerobically even in the presence of chromate up to 46 µM and also converted Cr (VI) to trivalent Cr (III). He also recorded the chromate reduction up to 20 µM anaerobically in the presence of light by using some phototropic bacteria (*Rhodobacter capsulatus, Rhodospirillum rubrum, Rcy. tenuis,* and

Table 1: The Growth, pH changes, and chromate reduction recorded at different incubation days by free cells of *Allochromatium* sp.

Days of incubation	Growth in optical density	Dry cell weight [g.L^{-1}]	Final pH	Chromate reduction by Free cells (µM)
4	0.3 ± 0.10	0.5 ± 0.06	8.2 ± 0.06	10 ± 2.0
6	1.0 ± 0.20	1.2 ± 0.20	8.4 ± 0.15	20 ± 1.5
8	1.4 ± 0.25	1.7 ± 0.20	8.5 ± 0.10	26 ± 2.0
10	1.2 ± 0.15	1.5 ± 0.30	8.6 ± 0.20	24 ± 1.0
12	1.0 ± 0.10	1.3 ± 0.10	8.8 ± 0.20	21 ± 3.0
16	0.7 ±0.10	1.0 ± 0.15	9.2 ± 0.25	15 ± 2.0
20	0.4 ± 0.10	0.6 ± 0.10	9.5 ± 0.10	8 ± 1.0

This experiment was carried out in triplicates and the obtained results were noted in terms of mean and SD which are analyzed for ANOVA and the obtained results are statistically significant at the level of $P < 0.001$.

Rhodobacter blasticus). Ramchander et al. (2011) reported the immobilized cells of *Rba. capsulatus* showed enhanced growth and reduction of chromate up to 28 µM within 12 to 16 days of its incubation period.

The UV-Vis spectrophotometer is used to determine the growth of *Allochromatium* sp. by reading optical density at 660 nm and the growth of the bacterium was estimated in terms of the DCW (Italiano et al. 2012). The maximum growth in optical density of free cells was recorded as 1.4 ± 0.25, whereas DCW (dry cell weight) was recorded up to 1.7 ± 0.20 $g.L^{-1}$ (Fig. 2). The 8^{th} day is considered as the optimum incubation period for maximum growth and chromate reduction. On the other hand, the immobilized cells of the bacterium showed maximum growth in O.D as 1.8 ± 0.20, while the DCW was recorded as 2.2 ± 0.30 $g.L^{-1}$. Similarly, Rajyalaxmi et al. (2019), reported the maximum growth of both FC and IC of *Rhodobacter* sp. in terms of optical density (1.5 to 1.8) and dry cell weight (1.8 to 2.2) was observed on the 8^{th} day respectively. Italiano et al. (2012) reported the total reduction of 0.2 mM concentration of chromate within 3 to 4 days in a growth medium containing *Rhodobacter sphaeroides*. A very long lag phase is observed in their investigations for the reduction of a very small concentration of CrO_4^{2-} which takes place very.

Table 2: Growth, pH changes, and chromate reduction recorded at different incubation days by sodium alginate immobilized cells of *Allochromatium* sp.

Das of incubation	Growth in optical density	Dry cell weight ($g.L^{-1}$)	Final pH	Chromate reduction by Immobilized cells (µM)
4	0.6 ± 0.10	0.8 ± 0.10	8.3 ± 0.10	14 ± 1.0
6	1.3 ± 0.30	1.7 ± 0.20	8.5 ± 0.30	25 ± 2.0
8	1.8 ± 0.20	2.2 ± 0.30	8.6 ± 0.20	33 ± 3.0
10	1.5 ± 0.10	2.0 ± 0.20	8.8 ± 0.20	30 ± 2.0
12	1.4 ± 0.20	1.8 ± 0.20	9.0 ± 0.30	26 ± 3.0
16	0.9 ± 0.20	1.2 ± 0.10	9.5 ± 0.10	18 ± 2.0
20	0.6 ± 0.15	0.8 ± 0.20	9.8 ± 0.20	12 ± 2.0

This experiment was carried out in triplicates and the obtained results were noted in terms of mean and standard deviations which are analyzed for ANOVA and the obtained results are statistically significant at the level of $P < 0.001$.

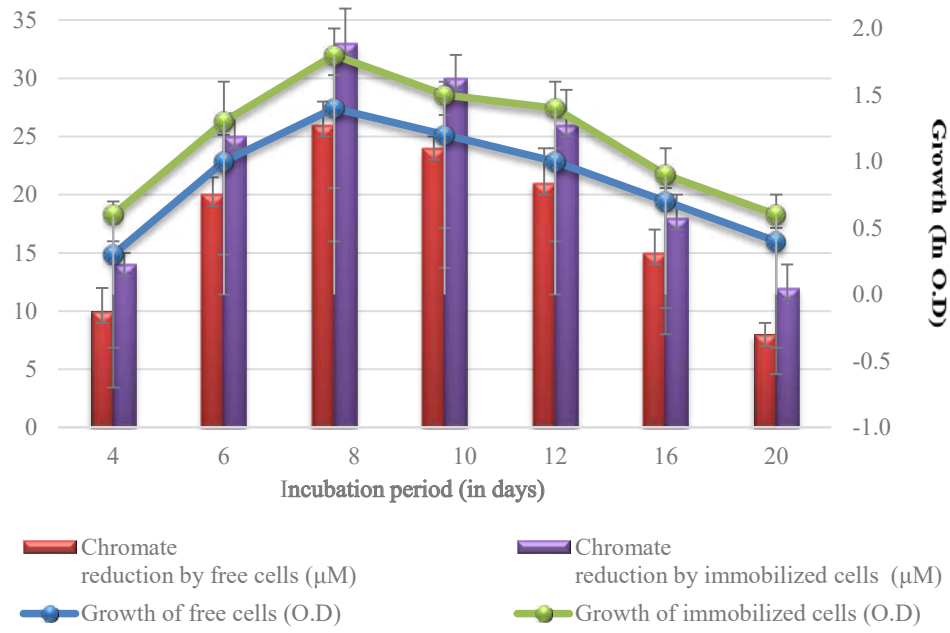

Fig. 2: Graph shows the growth in optical density and chromate reduction by free and immobilized cells of *Allochromatium* sp., in the presence of light under strictly anaerobic conditions. The obtained results are analyzed for ANOVA which are showing statistically significant at $P < 0.001$ level. The error bars in the graph indicate the mean and ± standard error noted from the triplicate samples tested in the laboratory.

The initial pH of the growth medium is changed to the alkaline side on the 8th day, which was recorded in the range of 8.5 ± 0.10 to 8.6 ± 0.20 by free cells and alginate entrapped immobilized cells of *Allochromatium* sp. on 8th day. On the other hand, the final pH was changed to alkaline in the range of 9.5 ± 0.10 to 9.8 ± 0.20 at the end of the incubation period. These investigations are identical to the investigation carried out by Ramchander *et al.* (2011), wherever he recorded the final pH at pH 8.2 (alkaline) in the growth medium containing *Rhodobacter capsulatus* KU002). Rajyalaxmi et al. (2019) studied the maximum reduction of chromate at pH 7.6 ± 0.15 by *Rhodobacter* sp., whereas Nepple et al. (2000) studied the maximum reduction of chromate at neutral pH 7.0 and temperature 30°C. During this investigation, the optimal growth conditions are directly proportional to the optimal chromate reduction by these bacteria. The statistical analysis was performed on the results obtained and the ANOVA of the obtained results revealed that the significance of the experiment is at P □ 0.001 level. A positive relationship has been recorded between the growth of the *Allochromatium* sp. as well as chromate reduction at different incubation periods.

CONCLUSION

The present investigations on chromate reduction by *Allochromatium* sp. provide the information that this bacterium is found to be very efficient in reducing chromate and to date, there is no information is available on chromate reduction by *Allochromatium* sp., hence this investigation is considered the first report on *Allochromatium* sp. However, more studies are required to expose the determination mechanism involved in chromate reduction by *Allochromatium* sp. in comparison with other anoxygenic phototrophic bacteria involved in chromate reduction. Bioremediation using *Allochromatium* sp. is cost-effective as well as environmentally best for treating the different water sources contaminated with different heavy metals.

ACKNOWLEDGEMENT

Our sincere thanks to the University Grants Commission (UGC), New Delhi, India for financial assistance and the Head, Department of Microbiology, Kakatiya University, Warangal for providing the necessary facilities.

REFERENCES

Bagchi, D., Stohs, S.J., Downs, B.W., Bagchi M. and Preuss, H.G. 2002. Cytotoxicity and oxidative mechanisms of different forms of chromium. Toxicology, 180: 5-22.

Staley J.T, Byrant, M.P, Pfennig, N. and Holt, J.C. (eds.). 1994. Bergey's Manual of Systematic Bacteriology: Enrichment and isolation of purple photosynthetic bacteria. Springer, NY.

Borsetti, F., Toninello, A. and Zannoni, D. 2003. Tellurite uptake by cells of the facultative phototroph *Rhodobacter capsulatus* is a delta pH-dependent process. FEBS Lett., 554: 315-318.

Borsetti, F., Martelli, P.L., Casadio, R. and Zannoni, D. 2009. Metals and metalloids in photosynthetic bacteria: Interactions, resistance and putative homeostasis revealed by genome analysis. Springer, Dordrecht, The Netherlands. pp. 655-689.

Buccolieri, A, Italino, F., Dell'Atti, A., Buccolieri, G., Giotta, L., Agostiano, A., Milano, F. and Trotta, M. 2006. Testing the photosynthetic bacterium *Rhodobacter sphaeroides* as a heavy metal removal tool. Ann. Chim., 96: 195-203.

Cieslak-Golonka, M. 1995. Toxic and mutagenic effects of Chromium (VI). A review, Polyhedron., 15: 3667-3689.

Daulton, T.L., Little, B.J., Lowe, K. and Meehan, J.J. 2002. Electron energy loss spectroscopy techniques for the study of microbial Chromium (VI) reduction. J. Microbiol. Methods, 50: 39-54.

Douglas, G.B., Lurling, M. and Spears, B.M. 2016. Assessment of changes in potential nutrient limitation in an impounded river after application of lanthanum-modified bentonite. Water Res., 97: 47-54.

Falkowski, P.G. and Raven, J.A. 2007. Aquatic Photosynthesis. Second Edition, Princeton University Press, Princeton.

Ferrera, I., Gasol, J.M., Sebastian, M., Hojerova, E. and Koblízek, M. 2011. Comparison of growth rates of aerobic anoxygenic phototrophic bacteria and other bacterioplankton groups in coastal Mediterranean waters. Appl. Environ Microbiol., 77(21): 7451-7458.

Gad El–Rab, S.M.F., Shoreit, A.A.F. and Fukumori, Y. 2006. Effects of cadmium stress on growth, morphology, and protein expression in *Rhodobacter capsulatus* B10. Biosci. Biotechnol. Biochem., 70: 2394-2402.

Gadd, G.M. 2000. Bioremedial potential of microbial mechanisms of metal mobilization and immobilization, Curr. Opin. Biotechnol., 11: 271-279.

Greenberg, A., Clescerl, L. and Eaton, A. 1992. Standard Methods for the Examination of Water and Wastewater. Eighteenth Edition. American Public Health Association, Washington DC.

He, S., Zhong, L,, Duan, J., Feng, Y., Yang, B. and Yang, L. 2017. Bioremediation of wastewater by iron oxide-biochar nanocomposites loaded with photosynthetic bacteria. Frontiers in Microbiol., 8: 823. doi:10.3389/fmicb.2017.00823.

Hojerova, E., Masin, M., Brunet, C., Ferrera, I., Gasol, J.M. and Koblízek, M. 2011. Distribution and growth of aerobic anoxygenic phototrophs in the Mediterranean Sea. Environ. Microbiol., 13(10): 2717-2725.

Idi, A., Muhamadd Nor, M.H. and Abdul Wahab, M.F. 2015. Photosynthetic bacteria: an eco-friendly and cheap tool for bioremediation. Rev. Environ. Sci. Biotechnol., 14(2): 271- 285.

Italiano, F., Rinalducci, S., Agostiano, A., Zolla, L., De Leo, F., Ceci, L.R. and Trotta, M. 2012. Changes in morphology, cell wall composition, and soluble proteome in *Rhodobacter sphaeroides* cells exposed to chromate. Biometals, 25: 939–949.

Italiano, F., Buccolieri, A., Giotta, L., Agostiano, A., Valli, L., Milano, F. and Trotta, M. 2009. Response of the carotenoids mutant *Rhodobacter sphaeroides* growing cells to cobalt and nickel exposure. Int. Biodeter. Biodegrad., 63(7): 948-957.

Johnsen, A. and Flink, J.M. 1986. Influence of alginate properties and gel reinforcement on fermentation characteristics of immobilized yeast cells. Enz. Microb. Technol., 8: 737-748.

Koblizek, M., Shih, J.D., Breitbart, S.I., Ratcliffe, C., Kolber, Z.S., Hunter, C.N. and Niederman, N.A. 2005. Sequential assembly of photosynthetic units in *Rhodobacter sphaeroides* as revealed by fast repetition rate analysis of variable bacteriochlorophyll fluorescence. Biochim. Biophys Acta., 1706: 220-231.

Kushalatha, M., Vidya, G. and Chandrakant, K. 2010. Photobiodegradation of halogenated aromatic pollutants. Adv. Biosci. Biotechnol., 1: 238-240.

Mariann Kis., Gabor Sipka., Emese Asztalos., Zsolt Razga. and Peter Maroti. 2015. Purple non-sulfur photosynthetic bacteria monitor environ. J. Photochem. Photobiol. B: Biol., 151: 110-117.

Medova, H., Boldareva, E.N., Hrouzek, P., Borzenko, S.V., Namsaraev, Z.B., Gorlenko, V.M., Namsaraev, B.B. and Koblízek, M. 2011. High abundances of aerobic anoxygenic phototrophs in saline steppe lakes. FEMS Microbiol. Ecol., 76(2): 393-400.

Nepple, B., Kessi, J. and Bachofen, R. 2000. Chromate reduction by *Rhodobacter sphaeroides*. J Ind. Microb. Biotechnol., 25: 198-203.

Nies, D.H. 1992. Resistance to cadmium, cobalt, zinc, and nickel in microbes. Plasmid, 27: 17-28.

Panwichian, S., Kantachote, D., Wittayaweerasak, B. and Mallavarapu, M. 2012. The use of selected purple non-sulfur bacteria to remove heavy metals and salts from sediment and water collected from contaminated areas to decrease their phytotoxicity. Afr. J. Biotechnol., 11(29): 7434-7444.

Pfennig, N. and Lippert, K.D. 1966. On the vitamin B12 requirement of phototrophic sulfur bacteria. Arch Microbiol., 155:245-256.

Pfennig, N. and Truper, H.G. 1981. Isolation of Members of the Families *Chromatiaceae* and *Chlorobiaceae*. In: Starr, M.P., Stolp, H., Truper, H.G., Balows, A. and Schlegel, H.G (eds.) The Prokaryotes: A Handbook on Habitats, Isolation, and Identification of Bacteria. Universite Bordeaux, Berlin Springer, pp. 279-289.

Pfennig, N. and Truper, H.G. 1992. The Family *Chromatiaceae*. In: Balows, A., Truper, H.G., Dworkin, M., Harder, W. and Schleifer, K.H. (eds) The Prokaryotes. Springer, New York, NY. https://doi.org/10.1007/978-1-4757-2191-1_8

Philip, L., Iyengar, L. and Venkobachar, C. 1998. Cr(VI) reduction by *Bacillus coagulans* isolated from contaminated soils. J. Environ. Eng., 124: 1165-1170.

Rajyalaxmi, K., Girisham, S. and Reddy, S.M. 2021. Biology and Biotechnological applications of Anoxygenic Phototrophic Bacteria. Scientific Publishers, Jodhpur, India.

Rajyalaxmi, K., Ramchander, M., Girisham, S. and Reddy, S.M. 2015. Phosphate solubilization by *Allochromatium* sp. GSKRLMBKU–01 isolated from the marine water of Visakhapatnam. Int. J. Appl. Bio. Pharm. Techno., l6: 1-6.

Rajyalaxmi, K., Ramchander, M., Girisham, S. and Reddy, S.M. 2018. Impact of cultural conditions on photoproduction of hydrogen by *Allochromatium* sp. GSKRLMBKU-01 isolated from marine water of Visakhapatnam. Inter. J. Hydr. Ener., 43(12): 6060-6065.

Rajyalaxmi, K., Ramchander, M., Girisham, S. and Reddy, S.M. 2019. Chromate reduction by purple non-sulfur phototrophic bacterium *Rhodobacter* sp. GSKRLMBKU-03 isolated from pond water. Proc. Natl. Acad. Sci. India. Sect. B. Biol. Sci., 89: 259-265.

Ramchander, M., Girisham, S. and Reddy, S.M. 2010a. Bioproduction of hydrogen by *Rhodobacter capsulatus* KU002 isolated from leather industry effluents. Inter. J. Hydr. Ener., 35: 9591-9697.

Ramchander, M., Girisham, S. and Reddy, S.M. 2010b. Production of PHB (Polyhydroxy butyrate) by *Rhodopseudomonas palustris* KU003 under nitrogen limitation. Int. J. Appl. Bio. Pharm. Tech., 2: 686-688.

Ramchander, M., Pratap Rudra, M.P., Thirupathaiah, A., Girisham, S. and Reddy, S.M. 2011. Chromate reduction by a purple non-sulfur phototrophic bacterium *Rhodobacter capsulatus* KU002 isolated from tannery Effluents. J. Pure Appl. Microbiol., 5(2): 66-69.

Sasikala, C. and Ramana, C.V. 1995a. Biotechnological potentials of anoxygenic phototrophic bacteria: Production of single-cell protein, vitamins, ubiquinones, hormones, and enzymes and use in waste treatment. Adv. Appl. Microbiol., 41: 173-226.

Shanker, A.K., Cervantes, C., Loza–Tavera, H. and Avuainayagam, S. 2005. Chromium toxicity in plants. Review article. Environ. Int., 31: 739-753.

Smiejan, A., Wilkinson, K.J. and Rossier, C. 2003. Cadmium bioaccumulation by a freshwater bacterium, *Rhodospirillum rubrum*. Environ. Sci. Tech., 37: 701-706.

Talaiekhozani, A. and Rezania, S. 2017. Application of photosynthetic bacteria for removal of heavy metals, macro-pollutants, and dye from wastewater: A review. J. Water Process Eng., 19: 312-321.

Tamura, K., Peterson, D., Peterson, N., Stecher, G., Nei, M. and Kumar, S. 2011. MEGA5: Molecular evolutionary genetics analysis using maximum likelihood, evolutionary distance, and maximum parsimony methods. Mol. Biol. Evol., 28: 2731-2739.

Watanabe, M., Kawahara, K., Sasaki, K. and Noparatnaraporn, N. 2003. Biosorption of cadmium ion using a photosynthetic bacterium, *Rhodobacter sphaeroides* S, and a marine photosynthetic bacterium, *Rhodovulum* sp., and their biosorption kinetics. J. Biosci. Bioengin., 95: 374-378.

Williams, J.W. and Silver, S. 1984. Bacterial resistance and detoxification of heavy metals. Enzyme Microb. Technol., 6: 530-537.

Zadvorny, O.A., Zorin, N.A. and Gogotov, I.N. 2006. Transformation of metals and metal ions by hydrogenases from phototrophic bacteria. Arch. Microbiol., 184: 279-285.

Zhou, Q., Zhang, P. and Zhang, G. 2015. Biomass and pigments production in photosynthetic bacteria wastewater treatment: Effects of light sources. Bioresour. Technol., 179: 505-509.

Nature Environment and Pollution Technology
An International Quarterly Scientific Journal

p-ISSN: 0972-6268
(Print copies up to 2016)
e-ISSN: 2395-3454

Vol. 21 | No. 5 (Suppl) | pp. 2307-2313 | 2022

Original Research Paper

https://doi.org/10.46488/NEPT.2022.v21i05.026

Open Access Journal

Local Community-Based Management Model in Karimunjawa National Park

Rizal Akbar Aldyan*†, MTh. Sri Budiastuti*, Warto and Wiwik Setyaningsih*****

*Department of Environmental Science, Post Graduate, Sebelas Maret University, Surakarta-57126, Jawa Tengah, Indonesia

**Department of Culture Studies, Sebelas Maret University, Surakarta-57126, Jawa Tengah, Indonesia

***Department of Engineering, Sebelas Maret University, Surakarta-57126, Jawa Tengah, Indonesia

†Corresponding author: Rizal Akbar Aldyan; rizalakbar@student.uns.ac.id

Nat. Env. & Poll. Tech.
Website: www.neptjournal.com

Received: 22-06-2022
Revised: 02-08-2022
Accepted: 03-08-2022

Key Words:
Local community
Management model
Karimunjawa National Park
Tree planting

ABSTRACT

This research aims to study the management model of Karimunjawa National Park Based on Local Communities. Activities are carried out in all sections of Karimunjawa National Park Management. Data sources are informants involved in Karimunjawa National Park Management and secondary data was collected using rapid monitoring methods, namely in-depth interviews, field observations, FGDs, and various other data collection techniques (technique triangulation). Methods of Data Analysis were observation using interactive data analysis. Empowerment of local communities in the Karimunjawa National Park in the Karimunjawa National Park area is carried out in three ways: coral reef rehabilitation activities, mangrove forest planting, and lowland tropical forest tree-planting efforts to develop a conservation village model.

INTRODUCTION

National Park, both land and water, is a protected natural area with the uniqueness and uniqueness of natural resources regulated by Law no. 5 of 1990 concerning the conservation of living natural resources and their ecosystems (Suherman et al. 2015). The Karimunjawa National Park area is located in Jepara Regency, which is designated as a National Park based on the Decree of the Minister of Forestry and Plantations No. 78/Kpts II/1999 dated 22 February 1999 regarding the change in the function of the Karimunjawa nature reserve area and the surrounding waters in a national park called (Taman Nasional Karimunjawa) TNKJ.

Management of National Parks cannot be separated from the community's interests around the National Park area, where there has been a strong bond in sociocultural and economic relations between the community and the existence of the National Park (Nyirarwasa et al. 2020). Therefore, in managing buffer zones outside the area and other utilization zones, the community's interests around the area should be considered. In other words, to preserve the environment of the Karimunjawa National Park, community participation is needed. According to Harjasoemantri (1988), development cannot be carried out without the participation of the community, for everyone has the right and obligation to participate in environmental management to realize development.

The Karimunjawa National Park area's potential invites various parties to utilize the existing potential (Wungo et al. 2020). The interests of various parties in utilizing the potential of natural resources in the Karimunjawa National Park area are pretty diverse, including coral reef ecosystems, seagrass and seaweed fields, mangrove forests, coastal forests, lowland tropical rain forests, and fisheries (BTNKJ 2011). In utilizing natural resources in the Karimunjawa National Park, some are in line, and some are contrary to the conservation objectives.

The Karimunjawa National Park area is directly adjacent to the community, so there are residential residents within the Karimunjawa National Park area. This implies the need for community involvement in natural resource management activities. Besides that, the community does not fully understand the rules in the management of Natural Resources and Conservation, so it is necessary to continue to carry out socialization and counseling efforts to improve understanding and institutionalization of existing rules. Based on the above background, researchers are interested in conducting research that focuses on making local community-based management models increase their participation in the conservation of Karimunjawa National Park.

MATERIALS AND METHODS

Determination of the research area is done through purposive sampling with villages in the Karimunjawa National Park area. This activity is carried out in all Karimunjawa National Park Management Sections, namely in the Kemujan Region I Section and the Karimunjawa Region II Section.

Researchers studied local community development and empowerment with a qualitative approach. The rationale for participation is that community development programs, projects, or activities that come from "above" or "outside" the community often fail and do not meet the needs of local communities. The reorientation of community development strategies emerged by prioritizing community participation and empowerment as a strategy in community development (Adimihardja & Hikmat 2003).

Sources of data in this study are the words and actions of critical informants/stakeholders involved in the management of Natural Resources and ecosystems in the Karimunjawa National Park area (primary data), which comes from institutions directly involved: Indonesian Tour Guide Association (HPI Karimunjawa), Association Karimunjawa Tourism Bureau (PBWK), Mosquito Village Management Group (KPDN), Rural Forestry Extension Center (SPKP), and Village Government Institutions.

The rapid monitoring method used in the research is an in-depth interview, field observation, and FGD (Focus Discussion Group) so that various data collection techniques (technique triangulation) are used. FGDs are built on the assumptions: a) Individual limitations are always hidden in the ignorance of these personal weaknesses; b) Each group member gives knowledge to each other in group association; c) Other individuals control each individual so that he tries to be the best; d) Subjective weakness lies in individual weakness which is difficult to control by the individual concerned; e) Intersubjective always approaches the best truth.

The data collected in the FGDs are:

1. Study of community development and empowerment models in the Karimunjawa National Park area
2. The data from the FGDs is used to develop a local community-based management model so that the empowerment program is carried out more effectively and its sustainability can be expected.

The FGD participants are key informants/stakeholders who directly or indirectly manage natural resources in the Karimunjawa National Park area. The FGD participants were: the Indonesian Tour Guide Association (HPI Karimunjawa), Karimunjawa Tourism Bureau Association (PBWK), Mosquito Village Management Group (KPDN), Rural Forestry Extension Center (SPKP), Higher Education Institutions and Village Government Institutions.

Analysis of data collected by in-depth interview and observation using interactive data analysis from Miles and Huberman. According to Sugiyono (2009), in qualitative research, data is obtained from various sources, using various data collection techniques (triangulation), and is carried out continuously until the data is saturated. With continuous observations, the variation in the data is very high. The data obtained is generally qualitative (although they accept quanatitative data), so the data analysis technique does not have a clear pattern. Miles & Huberman (1992) suggested conducting data analysis using an interactive model to overcome the difficulties in conducting the analysis. It was also added that qualitative data analysis was carried out simultaneously with the data collection process. The analysis technique carried out includes three simultaneous activities: (1) data reduction, (2) data presentation, and (3) concluding (verification).

RESULTS

Analysis of the Karimunjawa National Park Community Resources Network

According to Suharto (2009), to see the strengths of the Karimunjawa National Park community in solving problems and meeting needs, it is necessary to do a Resource Network Analysis (RNA). Source Network Analysis is one of the techniques used to map and measure the relationships and interactions of various sources within a single social entity (institution or society) involving community groups or institutions, both formal and informal, which are depicted in circles. The lines connecting the circles show the interrelationships of the institutions concerned. The entire fabric of interaction and the dynamics and functioning between institutions is called a network-approach to describe and identify network quality. The results of the Source Network Analysis based on the FGD technique and in-depth interviews of several key informants are depicted in Fig. 1. It will be transformed into Source Network Analysis Matrix (AJS).

Source Network Analysis is designed to map the dynamics of interaction between internal and external sources related to the target community, namely the Karimunjawa National Park community so that an intervention plan can be made for the social functioning of the Karimunjawa National Park community.

Key elements involved in the Social Network Analysis (AJS) matrix are as follows:

1. Type and quality of sources: namely, the benefits obtained from these groups or institutions in improving

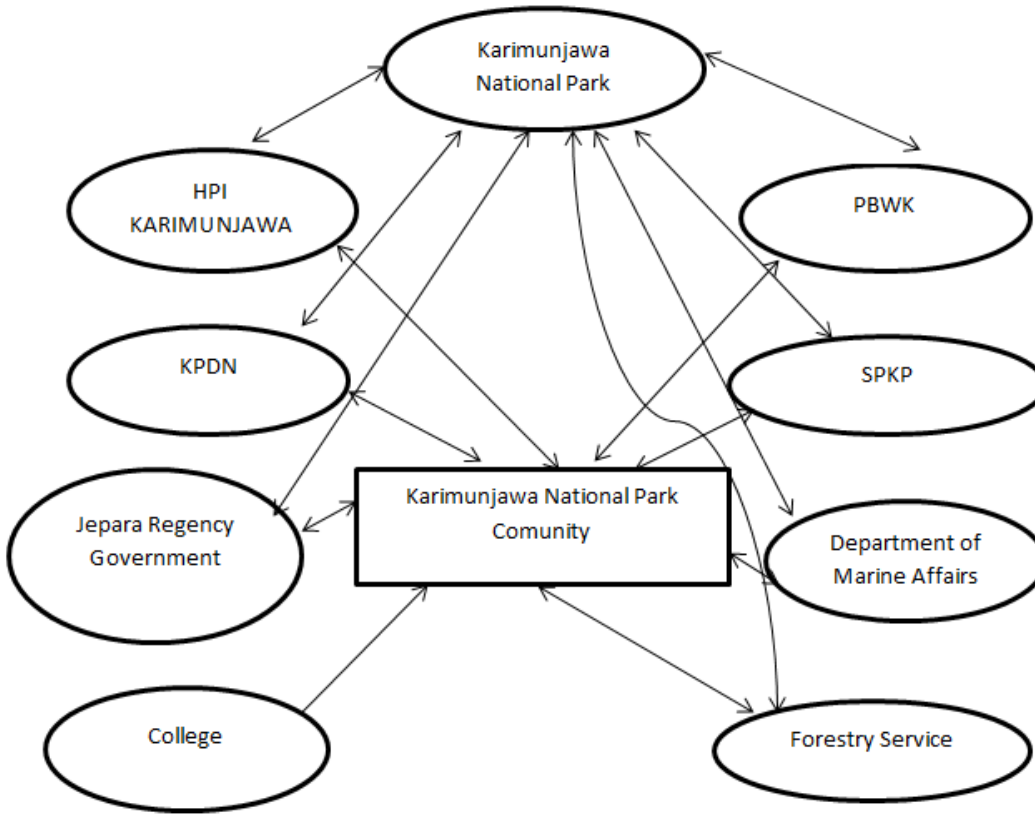

Fig. 1: Map of Community Resource Network Analysis of Karimunjawa National Park with stakeholders (institutions related to environmental conservation and management).

the quality of life of the people of Karimunjawa National Park

2. Accessibility is the group most frequently accessed by the Karimunjawa National Park community, the contribution and involvement of the group, and the obstacles experienced by the Karimunjawa National Park community.
3. Interaction between sources, namely the relationship between existing groups/institutions (robust, weak, or moderate) and the form of interaction (cooperation or competition) that occurs

The Source Network Analysis Matrix only maps the object/target community and its related external environment (group/institution). Meanwhile, the relationship between groups/institutions has not been mapped. Matrix Analysis of the Resource Network (AJS) of the Karimunjawa National Park community is given in Table 1.

DISCUSSION

Local Community-Based Management Model in Karimunjawa National Park

The scheme of community development and involvement programs is an alternative development model. The idea of alternative development appears in the development discourse as a reaction to the failure of the pro-economic growth development model in overcoming the problem of poverty, paying attention to environmental sustainability, and solving various social problems that crush the community (Zubaedi 2013).

The essence of empowerment activities is the participation of the community as actors or subjects of development (People-centered development). The fact shows that many still view community participation as merely the delivery of information (public information), counseling, and even public relations so that the project can run without obstacles. Community participation is not only used as a means to achieve goals but also as a goal (participation is an end itself).

Based on the results of the Source Network Analysis (AJS) in the Karimunjawa National Park community in Table 1., it can be concluded that local communities have sociocultural potentials, local knowledge, and processes that can be developed to achieve development goals in general

Table 1: Community Source Network Analysis (AJS) Matrix, Karimunjawa National Park.

No.	Institution name	Source Type and Quality	Source Accessibility	Source Interaction
1	Karimunjawa National Park	Empowerment of communities around national parks, formation of local organizations, training, equipment assistance, mentoring	Easy access but limited human resources	Medium (reciprocal)
2	HPI Karimunjawa	It is a local institution formed by the community to encourage sustainable tourism in the Karimunjawa National Park.	HPI Karimunjawa is an institution that improves the quality and competitiveness of Karimunjawa tourism and preserves natural resources and the environment in Karimunjawa.	Strong (reciprocal)
3	PBWK	It is a local institution formed by the community to coordinate tourism bureau actors so that they have formal legality as tour operators.	PBWK is an institution that assists the government in preserving and developing regional tourism, carrying out and carrying out various activities to improve the quality of human resources, and embracing all tourism actors to be involved in an independent system without destroying nature.	Medium (reciprocal)
4	KPDN	It is a local institution located in the Karimunjawa Mosquito Village that is engaged in conservation	KPDN is an institution that controls the activities of the community around the Mosquito Village	Medium (reciprocal)
5	SPKP	It is a local institution formed in the Karimunjawa National Park community to develop self-help extension workers, develop independent, productive community groups, increase community participation in conserving forests, improving the welfare of the Karimunjawa National Park communities.	Almost all Karimunjawa villages have this institution; it is just that the dynamics in each institution are different from one another.	In some villages, it is vital such as in Kemujan Village and Karimunjawa Village, while in Parang Village, it is weak (reciprocal).
6	Jepara Regency Government	Government institutions that assist with cleaning facilities in Karimunjawa villages	The government assists in the form of carts and trash cans in the four villages in Karimunjawa.	Medium (reciprocal)
7	Department of Marine Affairs and Fisheries	Government institutions that assist in the form of 2.5 tons of seaweed seeds	The seaweed seeds are distributed to villages in Karimunjawa	Medium (reciprocal)
8	Forestry Service	A government agency that assists the people of the Karimunjawa National Park	Facilitating the needs of SPKP groups in Karimunjawa National Park	Medium (reciprocal)
9	College	Is an institution that develops technology by conducting research and community service	The community still has difficulty accessing higher education institutions due to the lack of facilitators. There have been several studies and services carried out by several lecturers, both in groups and independently, but they are still partial.	Weak (unidirectional)

Source: Primary Data processed 2022

and the preservation of Karimunjawa National Park and welfare in particular. Interactions between local institutions already have a weak to a strong reciprocal relationship with the Karimunjawa National Park Authority as the authority for managing conservation areas. Non-governmental organizations such as HPI Karimunjawa have a solid and reciprocal relationship with the Karimunjawa National Park. Universities, especially Sebelas Maret University, do not yet have strong interactions because cooperation in research and service activities is limited to individual activities.

Capacity building is a development approach based on natural (local) strengths from the ground up. These strengths are the power of natural resources, economic resources, and human resources to become local capacities, namely the capacity of local governments, the capacity of private institutions, universities, and the capacity of local communities to develop the natural and economic potential of local communities (Fachrudin 2010). Local institutions such as the Rural Forestry Extension Center (SPKP), the Mosquito Village Management Group (KPDN), PBWK (Karimunjawa

Tourism Bureau Association), HPI Karimunjawa (Indonesian Karimunjawa Guides Association) have the freedom to determine community needs in the context of preserving and improving welfare. The participation of government institutions, the private sector, universities, and NGOs needs to be increased in enabling, empowering, and protecting the developing and empowering local community-based communities. This process is not only the responsibility of the Karimunjawa National Park Office as the authority for managing natural resources in the Karimunjawa National Park. The community-based Karimunjawa National Park management model is presented in Fig. 2.

The Karimunjawa National Park management model in Fig. 2. emphasizes the importance of community-based management with a bottom-up and locality paradigm. This management model is based on efforts to develop and encourage the Karimunjawa National Park community structure to become more independent through justice-based regulations. The approach used in this model is management at the local level, including the participation of local communities, so that local communities can simultaneously become management actors in their communities while maintaining cultural values that already exist and are rooted in the Karimunjawa National Park community, the social structure of local communities, and the culture and traditions of the local community of Karimunjawa National Park.

The concept of community-based Karimunjawa National Park management requires knowledge of the local community, working with the community, and identifying local resources owned by the Karimunjawa National Park community. Identification of local resources, including social capital owned by local communities. Helping communities understand their problems and respond to community needs to improve welfare. The facilitation and mentoring process is not always carried out because, in time, the community is considered to have sufficient confidence so facilitation is gradually eliminated. To become new subjects in implementing local community development, they must be able

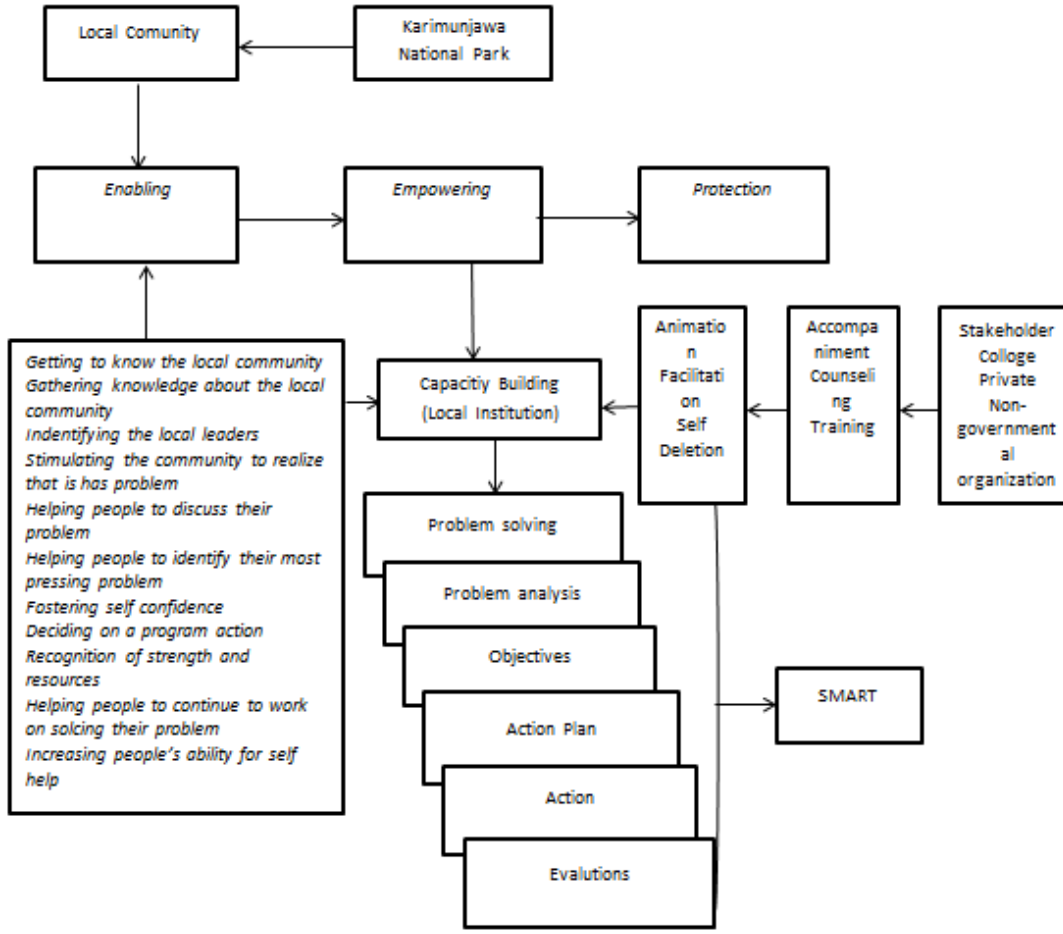

Fig. 2: The community-based Karimunjawa National Park management model.

to help themselves identify the problems they face and find the best solutions to achieve community goals (Nyirawarsa et al. 2020).

Empowerment of a community has the following meanings: 1) Authority, namely specifically empowerment means giving greater rights to specific communities; and 2) Capacity, which means energy, meaning that empowerment means "giving energy" from a solid community to a vulnerable community (Prijono & Pranaka. 1996). Community development programs often emphasize the application of CBM (Community Based Management) as a program management approach based on local community knowledge and awareness. CBM is a strategy to realize human-centered management activities. The center of decision-making regarding the sustainable use of natural resources in the Karimunjawa National Park Area is in the Karimunjawa National Park community. CBM is intended to increase the opportunities and responsibilities of the community in managing the natural resources contained in the Karimunjawa National Park. The people of the Karimunjawa National Park are the people who identify and define their needs, goals, and aspirations and make decisions for their well-being but always within a conservation and sustainable framework.

The preparation of management activities is carried out in several steps, namely:

1. The stage of problem exposure is carried out to determine the problems faced by the people of the Karimunjawa National Park
2. The problem analysis stage is to collect information faced by the Karimunjawa National Park community, and interested parties can access that information.
3. The stage of determining goals and objectives refers to long-term goals in which the entire community of Karimunjawa National Park plays an active role in maintaining the conservation and sustainability of natural resources and improving their welfare.
4. The Karimunjawa National Park community carries out the action planning stage to achieve the conservation and sustainability goals of natural resources, taking into account the potential of natural resources or the strength of local potential.
5. The implementation stage is implementing an action plan that has been identified/designed by the people of the Karimunjawa National Park and must pay attention to the possible impacts.
6. The evaluation stage is a continuous step in developing the Karimunjawa National Park community, formally and informally, every month, and annually.

The community-based Karimunjawa National Park management program strives to meet the SMART criteria, namely simple (easy to understand), measurable (measured), achievable (achievable), realistic (can be done according to local resources), and time-related (can be done according to the available time). Capacity building is understood as a process of improving or adjusting the behavior of individuals, organizations, and community systems of the Karimunjawa National Park community to achieve the goals that have been set in a timely, efficient and effective manner; especially the strategy of strengthening institutional support capacity to anticipate problems and needs. The strategy for developing the institutional capacity of the Karimunjawa National Park community can be studied through cultural, structural, and interactive aspects. Cultural aspects include existing systems, values, ethics, and norms; structural aspects related to the existence of institutions as a means of empowerment (increasing individual and collective capacity); the interaction aspect involves organizations that can develop social networks (networks) for the welfare of individuals and local communities in the Karimunjawa National Park.

CONCLUSION

The community development model carried out in the Karimunjawa National Park community is the development of local communities. The parameters used are goal orientation, assumptions about community structure, assumptions about community interests, conceptions of public interest, orientation to power structures, client systems or change systems, conceptions of clients or service recipients, community roles, social workers' roles, change media, change strategy, change technique. According to the Source Network Analysis Map (AJS) results, local groups/institutions in the Karimunjawa National Park, preserving the Karimunjawa National Park, and improving the community's welfare have a reciprocal relationship. The interaction between non-government organizations and universities is still fragile. Empowerment of local communities in the Karimunjawa National Park in the Karimunjawa National Park area is carried out in three ways: coral reef rehabilitation activities, mangrove forest planting, and lowland tropical forest tree-planting efforts to develop a conservation village model. The strategy uses a mezzo approach by forming local community groups such as HPI Karimunjawa, PBWK, KPDN, and SPKP. The empowerment strategy aimed at the group is the mezzo strategy with the target group, Peer Group, or Self-help group. The techniques used are education, training, and group dynamics. Empowerment aims to increase awareness, knowledge, and skills and change attitudes to overcome problems independently and in groups.

REFERENCES

Adimihardja, K. and Hikmat, H. 2003. Participatory Research Appraisal in the Implementation of Community Service. Humanities, Bandung.

Harjasoemantri, S. 1988. Environmental Management Law. Third Edition. Gadjah Mada University Press. Yogyakarta.

Miles, M.B. and Huberman, M. 1992. Qualitative Data Analysis: A Resource Book on New Methods. University of Indonesia, Jakarta.

Ministry of Forestry Directorate General of Forest Protection and Nature Conservation Karimunjawa National Park Office (BTNKJ). 2021. Karimunjawa National Park Agency Statistics for 2021. BTNKJ, Semarang.

Nyirawarsa, A., Fang. H., Xumei, P., Richard, M., Albert. P.M., Aboubakar, G., Madeleine U., Zacharia, F.M. and Edovia, D.U. 2020. Evaluating the relationship between national park management and local communities perceptions based on the survey: A case of Nyungwe National Park, Rwanda. J. Geosci Environ. Protect., 8(12): 108-126.

Prijono, O.S. and Pranarka, A.M.W. 1996. Empowerment: Concept, Policy, and Implementation. CSIS, Jakarta.

Sugiyono. 2009. Understanding Qualitative Research. Alphabet, Bandung.

Suharto, E. 2009. Building A Community Empowering the People. Aditama Refika, Bandung.

Suherman, M.H.K., Yuyun, Y. and Trisna, I.N. 2015. Conservation of living natural resources and their ecosystems. Int. J. Sci. Technol. Res., 4(9): 357-366.

Wungo, G.L., Mussadun, M. and Samsul, M. 2020. Education on the application of the ecotourism concept in the Karimunjawa Islands. J. Pasopati, 2(3): 142-148.

Zubaedi, L.M. 2013. Community Development Discourse and Practice. Kencana Prenada Media Group, Jakarta.

Nature Environment and Pollution Technology
An International Quarterly Scientific Journal

p-ISSN: 0972-6268
(Print copies up to 2016)
e-ISSN: 2395-3454

Vol. 21 | No. 5 (Suppl) | pp. 2315-2321 | 2022

Original Research Paper

https://doi.org/10.46488/NEPT.2022.v21i05.027

Open Access Journal

Satellite-Based Statistical Analysis of Hilla River Water Quality Parameters, Iraq

Fatimah D. Al-Jassani*, Hussein A. M. Al-Zubaidi† and Nisren J. Al-Mansori*****
Department of Environmental Engineering, College of Engineering, University of Babylon, Babylon, Iraq
†Corresponding author: Hussein A. M. Al-Zubaidi; alzubaidih10@gmail.com

Nat. Env. & Poll. Tech.
Website: www.neptjournal.com

Received: 17-06-2022
Revised: 21-07-2022
Accepted: 30-07-2022

Key Words:
Linear regression
Statistical analysis
Water quality modeling
Hilla river

ABSTRACT

Since industrial and human activities have been developed, water quality intensely degrades in Hilla River, Iraq. Using remote sensing technology provides data for assessing and monitoring water quality in surface water bodies. Thus, in this study, Landsat 8 satellite images (2016 to 2021) were statistically tested for developing linear models capable of estimating water quality parameters in the river based on field data, including turbidity (turb), electric conductivity (EC), hydrogen ions (pH), total suspended solids (TSS), chloride ions (Cl), sulfate ions (SO_4), Alkalinity (ALK), total hardness (TH), calcium (Ca), potassium (K), sodium (Na), magnesium (Mg), and total dissolved solids (TDS). The results showed that seven parameters have a significant relationship with the spectral bands ratio (p-value less than 0.05). Some of them (TDS, SO_4, and ALK) are positively correlated with bands ratio (Band10/Band3, Band10/Band3 and Band10/Band4, and Band3/Band7), respectively. Others (Mg, Ca, TH and pH) are inversely correlated with (Band4/Band7, Band1/Band4, Band1/Band4, and Band1/Band2), respectively. However, K, Na, TDS, Cl, EC and turb have an insignificant correlation with any band ratio.

INTRODUCTION

Surface water bodies are used for many purposes involving drinking water sources, recreation, transportation, and aesthetics. With several uses, these water forms are subjected to natural and human activities that can impact water quality. As a result, mechanisms to help protection of surface water, maintain present water quality, or prevent surface water deterioration seem to be critical. Water quality can be assessed according to its chemical, physical, and biological characteristics (Al-Zubaidi 2012, Issa et al. 2013). Water quality indicators, involving biological, chemical, and physical characteristics, have been usually measured by taking samples in the field and then studying them in the laboratory. Though in-situ measurement offers excellent accuracy, it is a labor-intensive and time-consuming operation, making a simultaneous water quality database on a regional scale geographically and temporally impractical (Goetz et al. 2008, Kibena et al. 2014). Remote sensing (RS) methods have become helpful instruments to attain this objective due to the improvements in space science, greater usage of computer applications, and improved computational power in recent periods. Remote sensing methods provide more effective and effectual observing and identification of large-scale areas and water bodies that suffer from qualitative issues (Al-Masaodi & Al-Zubaidi 2021, Alparslan et al. 2007, El-Amier et al. 2017, Hadjimitsis et al. 2010, Markogianni et al. 2018).

To explore the relationships between water quality indicators and spectral data from satellite images, decision-makers in water resources may utilize remote sensing data to better monitor water bodies (Chabuk 2022). Gholizadeh et al. (2016) summarized the characteristics of the main sensor (temporal, spatial, and spectral) utilized for water quality monitoring. This study also examines the methodologies and sensors utilized to assess and quantify the water quality parameters such as COD, BOD, dissolved oxygen, sea surface salinity, total phosphorus, water temperature, turbidity, TSS, Secchi disk depth, colored dissolved organic matter, and chlorophyll-a (chl-a). Japitana & Burce (2019) gave a global perspective of the earth's surface that may be utilized to monitor and analyze water quality using Landsat 8 and regression analysis to predict pH, dissolved oxygen, TDS, TSS, and BOD. The input images were radiometrically calibrated utilizing FLAASH and then atmospherically adjusted to create surface reflectance (SR) bands for comparison. Input data included SR bands produced by FLAASH and DOS algorithm, water indices, band ratios, and PCA images. The input bands' feature vectors were then regressed utilizing the water quality data.

All water quality metrics exhibited relatively high R-squared magnitudes except TSS and conductivity which had 60.1 and 67.7%, respectively. In addition, pH, BOD, TSS, and conductivity regression models are extremely significant to SR bands calculated utilizing DOS. The findings also revealed the possibility of employing RS-based water quality models for periodic water quality monitoring and evaluation. Al-Bayati et al. (2018) investigated field Spector-radiometers by developing relationships between water quality parameters and spectral data. The study included 20 stations for sampling on Hilla River, Babylon Province, Iraq to measure the physical and chemical parameters (pH, TSS, EC, TDS, CL). Landsat 8 satellite images were employed to be linked with field data statistically for only one day of investigation. It has been found that apposite spectral ranges and bands for water quality parameters, EC, and CL associated with a spectra range of (0.851-0.87) µm and (2.107-2.294) µm, respectively. Also, (TSS and Turb), and TDS at a spectral range of (0.533-0.590) µm and (1.566-1.561) µm, respectively. Abbas et al. (2021) utilized Landsat 8 satellite images to estimate total TDS, EC, NO_3, and pH. These models offer the capability of evaluating the water quality parameters dispersal lengthways of the Shatt Al-Arab River in the south of Iraq. Results built on R-squared, RMSE, SE, and p-value highlighted the feasibility of these models for the study area. The four bands (band 2, band 3, band 4, and band 5) of Landsat 8 were used to develop the water quality models. EC models are estimated for the winter, summer, and autumn seasons based on band 5 for winter and band 4 for the summer and autumn seasons. For NO_3 models, it was linked with band 4, band 3, and band 2 for winter, spring, and summer, respectively. pH models were developed depending on a single band for all seasons (band 4, band 5, band 4, and band 5 for winter, spring, summer, and autumn, respectively). For the remaining parameter (TDS), it was a too complex model in this study. One of them was estimated by combining band 3, band 4, and band 5 in terms of band ratios.

Thus, to cover the region of interest in this paper, statistical linear models and correlation analyses were performed between Landsat 8 images and water quality measurements for Hilla River at Hilla City, Iraq spatially along the river and temporally from 2016 to 2021 based on available data from the Ministry of Water Resources, Iraq.

MATERIALS AND METHODS

Study Area and Datasets

Hilla City is located in the center of Iraq on the Hilla River. The river is a branch of the Euphrates River, 100 km south of Baghdad City. Hilla City is the capital of Babylon Province where the ancient city of Babylon is located. It is located in a mainly agricultural region that is widely irrigated from the river, producing a wide range of crops, fruit, and textiles. Fig. 1 shows the present study area. It is situated between, Longitude (44º26'55" & 44º31'10") E and Latitude (32º26'30" & 32º31'33") N.

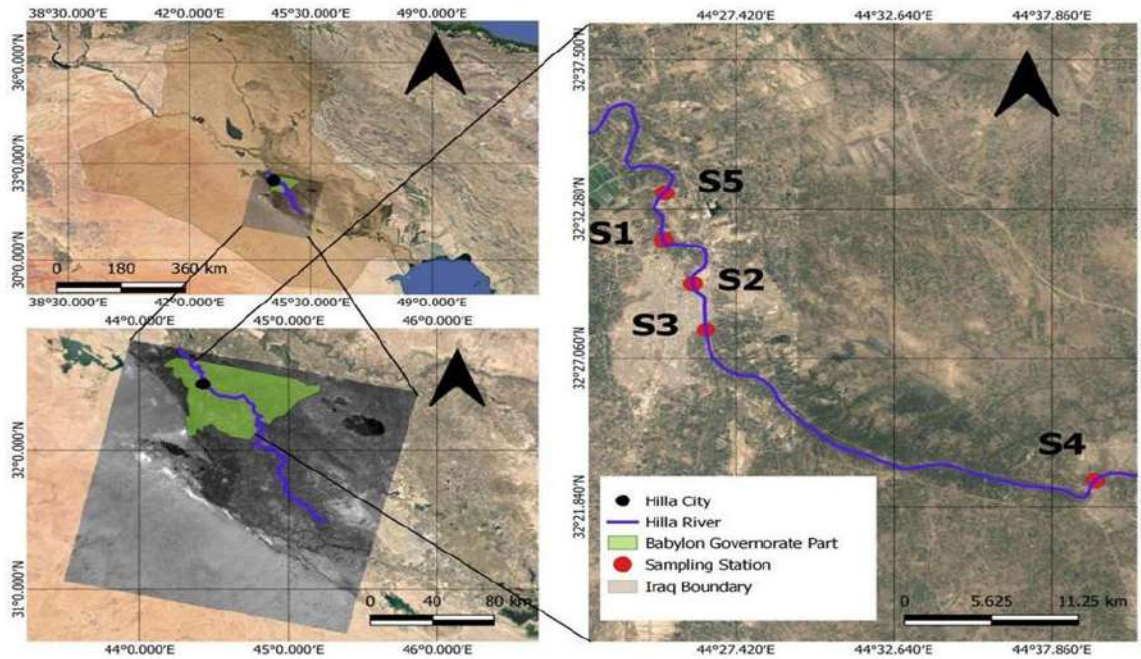

Fig. 1: Map of the study area.

Five stations were selected along the Hilla River. Station 1 (S1): The New Hilla Water Treatment Plant is located in the center of Hilla City in the Zuweir district. It was built in 1991 and produces about 6000 $m^3.h^{-1}$ for Hilla City consumption; Station 2 (S2): The Old Al-Tayarah Water Treatment Plant is located in the Hilla City center of the Al-Tayarah district. It was built in 1972 and produces about 1200 $m^3.h^{-1}$ for the Hilla City consumption too; Station 3 (S3): Al-Hashmiya Water Project with a capacity of 6000 m^3 to serve the districts of Al-Hashmiya, Al-Shuwaili, Al-Qasim and Al-Tali`ah in the Province of Babylon; Station 4 (S4): Al-Atayej Project is located in the city center (in the tourist area), and it produces 900 $m^3.h^{-1}$, and Station 5 (S5): The Annanah Water Project is situated on the right bank of the Hilla River near the village of Annanah. Samples were collected sparsely by Babylon Water Resources Directorate, Iraq at each sampling station from January 2016 to June 2021. The collection process included taking one or two samples monthly during this period. Table 1 displays the yearly averaged water quality parameters magnitudes.

Hilla City is situated between path 168 and row 38 of the Landsat 8 satellite. To discover the relations between water quality indicators and spectral data from the satellite, Landsat 8 senses were downloaded from the United States Geological Survey (USGS) website at the same sampling time and for the entire study period, covering the sampling process spatially and temporally (Fig. 1).

Methodology

The general structure of this study is displayed in Fig. 2 which is the conceptual model of the study. In-site water quality data from the five sampling stations and the related images from the Landsat 8 satellites were linked by linear models statistically. In-situ data was split into two datasets: train and test. The Landsat 8 images were collected 2 level 2 (surface reflectance) that contains 8 spectral bands (1 to 7 and 10) (Hereher et al. 2010, Kontopoulou et al. 2017). The GIS analysis was carried out utilizing QGIS software in order to display the spatial distribution of the spectral bands to be correlated with field data. The boundary of the river was digitized to make the polygon shape of the river extract the river water (El-Zeiny & El-Kafrawy 2017). After extracting the surface reflectance of each band from Landsat senses, RStudio software was utilized to develop linear models

Table 1: *In-situ* water quality parameters employed in this study.

Sampling Station	Year	Water Quality Parameter												
		k	Na	TSS	TDS	SO_4	Cl	Mg	Ca	TH	ALK	EC	pH	Turb
S1	2016	4.0	84.2	62.7	704.0	297.3	111.8	40.2	87.2	381.7	120.0	1086.5	7.8	15.4
	2017	3.0	81.3	25.0	662.0	230.3	107.3	29.8	74.0	314.0	134.0	1015.5	7.8	6.4
	2018	3.2	82.6	32.0	685.2	273.8	123.2	34.8	89.8	362.4	138.4	1135.8	7.2	7.0
	2019	2.9	48.7	44.7	596.0	250.3	75.3	25.0	105.7	366.3	147.3	949.0	7.4	24.2
	2020	3.7	72.0	38.0	630.0	248.0	85.0	33.5	96.5	378.5	108.0	960.0	7.3	10.1
	2021	3.3	72.5	36.0	645.0	280.0	87.0	34.0	93.0	371.5	101.0	1019.0	7.9	6.4
S2	2016	3.2	85.5	44.5	707.0	324.8	106.3	36.8	94.0	385.5	113.5	1105.0	7.9	15.1
	2017	3.0	67.1	29.6	653.2	247.0	109.6	33.2	76.0	330.6	134.8	1052.6	7.8	11.6
	2018	3.4	86.7	44.7	685.3	285.3	120.7	32.0	86.7	347.7	128.7	1139.7	6.9	7.4
	2019	2.8	47.3	32.0	605.3	249.7	74.3	24.0	106.0	362.7	146.0	954.0	7.5	15.5
	2020	3.2	67.5	37.5	606.0	252.8	82.3	34.0	98.3	385.3	123.5	952.8	7.5	12.5
	2021	3.3	71.0	68.7	600.7	254.3	90.0	36.7	80.7	352.0	110.0	996.0	7.6	12.8
S3	2016	6.8	91.0	42.0	758.0	365.0	122.0	41.0	106.0	432.0	112.0	1175.0	8.1	19.0
	2019	3.1	66.0	46.0	630.0	244.0	95.0	32.0	101.0	384.0	140.0	1048.0	7.2	2.9
	2021	3.4	72.0	42.0	554.0	206.0	91.0	35.0	69.0	314.0	110.0	947.0	7.1	7.1
S4	2016	3.3	85.5	70.0	731.0	317.5	110.0	38.5	89.0	380.0	109.0	1132.5	8.0	12.4
	2017	3.0	83.7	61.3	660.7	266.7	109.3	36.3	75.3	341.0	126.7	1036.3	7.7	13.9
	2018	2.9	86.0	14.0	630.0	258.0	116.0	35.0	84.0	352.0	120.0	1072.0	6.7	5.2
	2021	3.7	69.0	30.0	552.0	217.5	89.5	37.0	68.0	321.0	110.0	937.0	7.7	5.6
S5	2016	3.1	84.0	37.0	690.0	314.0	114.5	37.0	91.0	379.5	118.0	1079.0	7.9	8.4
	2017	3.0	79.7	29.3	660.7	242.7	113.7	32.0	79.0	334.7	127.3	1054.7	8.0	3.1
	2018	3.2	87.5	30.0	723.0	259.5	142.0	38.0	87.0	372.0	143.0	1174.0	7.4	7.4
	2020	4.7	76.0	22.0	544.0	212.0	85.0	39.0	78.0	353.0	116.0	912.0	7.5	27.4

between the train water quality parameters and the spectral bands. Finally, the test dataset was utilized to validate the developed model's robustness.

RESULTS AND DISCUSSION

Data Exploration

Many water quality parameters were measured from 2016 to 2021 including turbidity magnitude (Turb), (EC), (pH), (TSS), (Cl), (SO_4), (ALK), (TH), (Ca), (TDS), (Mg), (Na), and (K). A graphical summary (boxplots) of the water quality parameters is shown in Figs. 3 and 4. Raw data statistically reveals outliers' existence, however, these outliers will be kept because they could be related to errors or mistakes during sample gatherings such as errors due to parameter measurements, calculations, or any other source that could change the measured magnitudes (Al-Zubaidi et al. 2021). Fig. 5 highlights the correlation between water quality parameters. The best relation between parameters has a correlation coefficient close to 1 and a p-value less than 0.05 such as TDS with EC, TDS with SO4, SO4 with TH, and CL with EC. Many parameters have a normal distribution in the river. This can be visually noticed in the correlation plot, see the histogram plots of the parameters in Fig. 5. The Shapiro–Wilk test was utilized to confirm the normality quantitatively, see Table 2. The test showed that the w-value was close to 1 and the p-value greater than 0.05 for many parameters, except for TSS, K, Na, SO_4, and Turb.

Linear Models Development and Statistical Analysis

The linear regression model for the water quality parameters and the band ratio values of the satellite data are shown in Table 3. Statistical results for the 13 water quality parameters showed that 7 parameters have a significant relation with band ratio (p-value less than 0.05). These parameters were lineally regressed with the related band ratio by a linear model. The resulting models of the 7 parameters with bands ratio have a p-value less than 0.05. TDS is positively correlated with B10/B3 (P = 0.034), SO4 is positively correlated with B10/B3 and B10/B4 (P = 0.001), Mg is inversely correlated with B4/B7 (P = 0.003), Ca is inversely correlated with B1/B4 (P = 0.038), TH is inversely correlated with B1/B4 (P = 0.024), ALK is positively correlated with B3/B7 (P = 0.016), and pH is inversely correlated with B1/B2 (P = 0.003). The remaining parameters (K, Na, TDS, Cl, EC, and Turb) have an insignificant correlation with the bands ratio (p-value greater than 0.05). The MAE and RMAE show the difference between the measured data and the

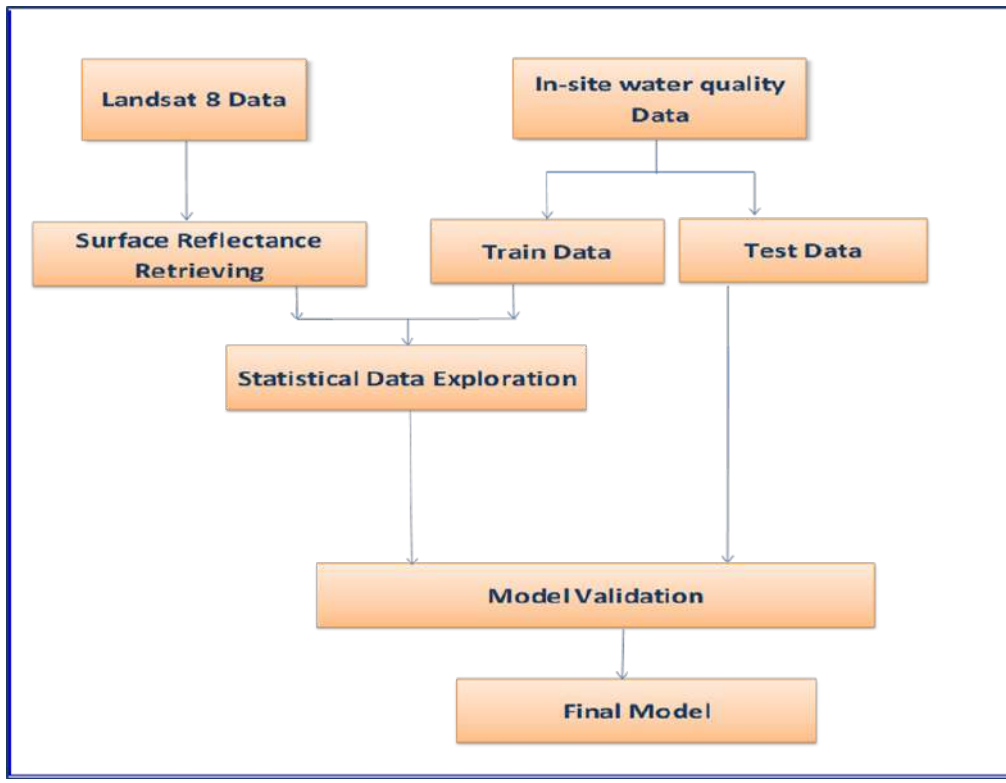

Fig. 2: Data processing flowchart.

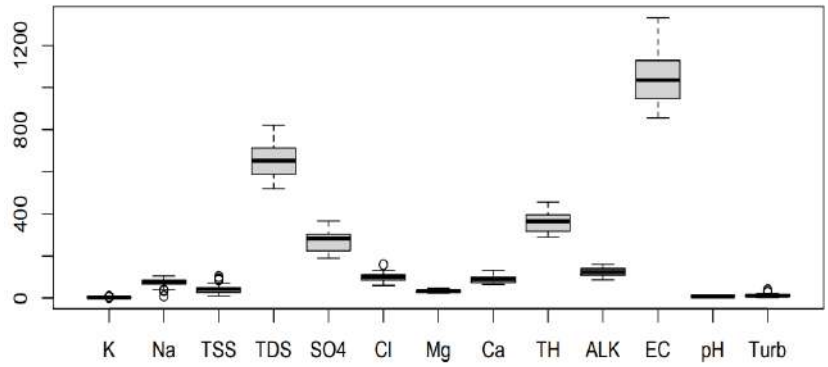

Fig. 3: Boxplots of all water quality parameters used in the study.

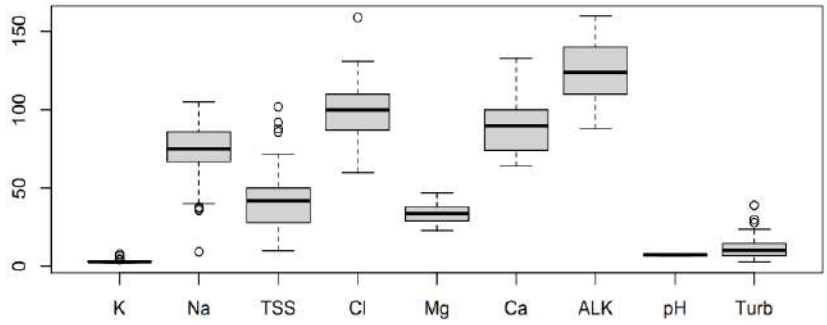

Fig. 4: Boxplots of the water quality parameters used in the study after excluding EC, TH, SO_4, and TDS.

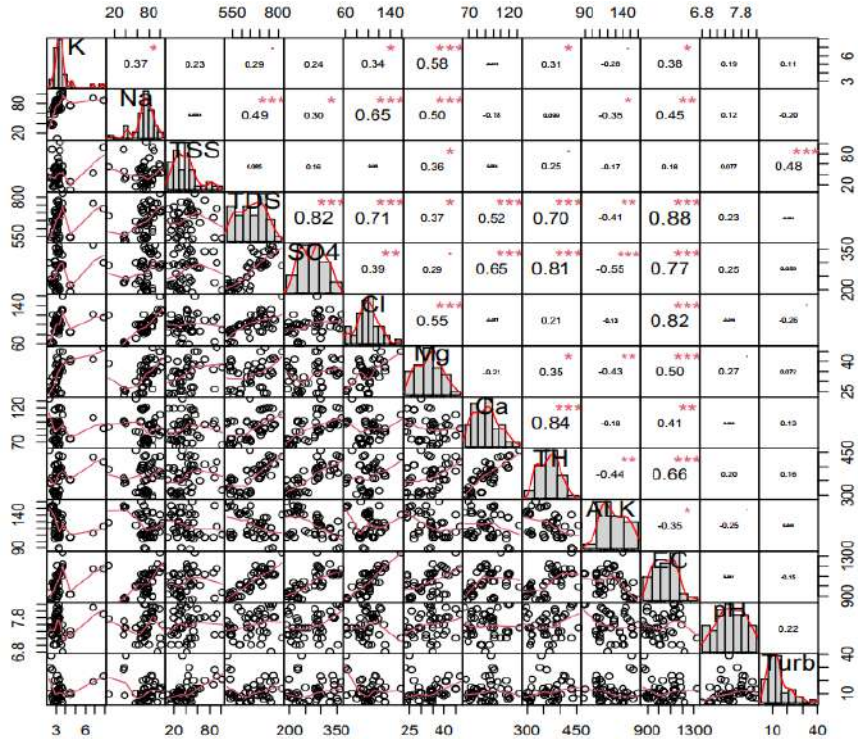

Fig. 5: Correlation plot of water quality parameters.

Table 2: Shapiro-Wilk test for water quality parameter.

Water quality parameter	w-value	p-value	Normality case
pH	0.9736	0.3879	Normal
TDS	0.9562	0.0873	Normal
TSS	0.9221	0.005	Not normal
K	0.62398	1.68E-09	Not normal
Na	0.9126	0.0024	Not normal
SO_4	0.9337	0.0127	Not normal
Cl	0.9742	0.4078	Normal
Mg	0.96445	0.1803	Normal
Ca	0.9555	0.0825	Normal
TH	0.95907	0.1125	Normal
ALK	0.95459	0.07588	Normal
EC	0.9624	0.1513	Normal
Turb	0.88487	0.000331	Not normal

model predictions. The best result was for pH with very low errors.

CONCLUSION

Remote sensing and GIS techniques in combination with in-situ measurements are the most effective, cheaper, and more dependable tools for observing water quality parameters in several surface water bodies (rivers, lakes, and reservoirs). The main findings of this study showed a significant correlation between in-situ measurements and remote sensed-based datasets in Hilla River, Iraq. The developed linear models can be utilized in estimating water quality parameter parameters (TDS, SO_4, Mg, Ca, TH, ALK, and pH) and predicting their seasonal changes. To apply the developed models for future predictions, it is not essential to obtain high-resolution and commercial satellite images since a free satellite image such as the Landsat series can be a dependable input image if the accurate pre-processing method is employed. In addition, MAE and RMAE are effective scales to validate the regressed model since they depict the difference between the model predictions and real data in the same unit of measurement.

ACKNOWLEDGMENT

The authors thank the Department of Environmental Engineering, at the University of Babylon for their support in doing this research.

REFERENCES

Abbas, M.R., Ahmad, B.B. and Abbas, T.R. 2021. Statistical remote sensing for prediction of inland water quality parameters for Shatt Al-Arab River in Iraq. IOP Conf. Ser. Earth Environ. Sci., 16: 111

Al-Bayati, Z.M.K., Nayle, I.H. and Jasim, B.S. 2018. Study of the relationship between spectral reflectivity and water quality index in Hilla River. Int. J. Eng. Technol., 7(3): 196-200.

Al-Zubaidi, H.A.M., Naje, A.S., Abed Al-Ridah, Z., Chabuck, A. and Ali, I M. 2021. A statistical technique for modeling dissolved oxygen in salt lakes. Cogent Eng., 8(1): 1875533.

Al-Zubaidi, H.A.M. 2012. Effect of heavy metals in wastewater effluents of Textile Factory-Hilla on the characteristics of Hilla River. J. Kerbala Univ. Sci., 10(3): 5-16.

Al-Masaodi, H.G.O. and Al-Zubaidi, H.A.M 2021. Spatial-temporal changes of land surface temperature and land cover Babylon Governorate, Iraq. Mater. Today Proceed., 5: 179. https://doi.org/10.1016/j.matpr.2021.05.179.

Alparslan, E., Aydöner, C., Tufekci, V. and Tüfekci, H. 2007. Water quality

Table 3: Remote sensing-based regression models for the selected water quality parameter parameters.

Water quality parameter	cor.	p-value	Bands ratio	Model	MAE	RMAE
pH	-0.43	0.00352	B1/B2	pH = 13.886 - 6.841*B1/B2	0.35	0.46
TDS	0.32	0.034	B10/B3	TDS = 276 + 86.16*B10/B3	76.1	89.7
TSS	-0.03	0.37276	B1/B2	-	-	-
K	0.24	0.10946	B6/B1	-	-	-
Na	-0.28	0.06742	B4/B7	-	-	-
SO_4	0.39	0.001604	B10/B3 +B10/B4	SO_4= 156.99 + 134.19*B10/B3 - 99.2*B10/B4	44.9	47.0
Cl	0.21	0.08636	B1/B2	-	-	-
Mg	-0.42	0.00385	B4/B7	Mg = 65.215 - 28.599*B4/B7	4.6	6.1
Ca	-0.31	0.0382	B1/B4	Ca = 158.18 - 77* B1/B4	11.4	13.5
TH	-0.33	0.02451	B1/B4	TH = 547.91 - 210.5* B1/B4	36.0	40.7
ALK	0.4	0.01675	B3/B7	ALK = 55.95 + 57.95* B3/B7	12.4	14.5
EC	0.08	0.58264	B1/B2	-	-	-
Turb	-0.25	0.09302	B7/B10	-	-	-

cor.: Pearson Correlation, MAE: Mean Absolute Error, RMAE: Root Mean Squared Error.

assessment at Ömerli Dam using remote sensing techniques. Environ. Monit. Assess., 135(1): 391-398.

Chabuk, A., Al-Zubaidi H.A.M., Abdalkadhum A.J., Al-Ansari N., Ali Abed S., Al-Maliki A. and Ewaid, S. 2022. Application ArcGIS on the Modified-WQI Method to Evaluate the Water Quality of the Euphrates River, Iraq, Using Physicochemical Parameters. Proceedings of Sixth International Congress on Information and Communication Technology, 25-26 Feb 2022, Brunei University, London, Springer, Singapore, pp. 657-675.

El-Amier, Y.A., Elnaggar, A.A. and El-Alfy, M.A. 2017. Evaluation and mapping spatial distribution of bottom sediment heavy metal contamination in Burullus Lake, Egypt. Egypt. J. Basic Appl. Sci., 4(1): 55-66.

El-Zeiny, A. and El-Kafrawy, S. 2017. Assessment of water pollution induced by human activities in Burullus Lake using Landsat 8 operational land imager and GIS. Egypt. J. Remote Sens. Space Sci., 20: S49-S56.

Gholizadeh, M.H., Melesse, A.M. and Reddi, L. 2016. A comprehensive review on water quality parameters estimation using remote sensing techniques. Sensors, 16(8): 1298.

Goetz, S., Gardiner, N. and Viers, J. 2008. Monitoring freshwater, estuarine and near-shore benthic ecosystems with multi-sensor remote sensing: An introduction to the special issue. Remote Sens. Environ., 112(11): 3993-3995.

Hadjimitsis, D.G., Hadjimitsis, M.G., Toulios, L. and Clayton, C. 2010. Use of space technology for assisting water quality assessment and monitoring of inland water bodies. Phys. Chem. Earth Parts A/B/C, 35(1-2): 115-120.

Hereher, M., Salem, M. and Darwish, D. 2010. Mapping water quality of Burullus Lagoon using remote sensing and geographic information system. J. Am. Sci., 7(1): 138-143.

Issa, I., Al-Ansari, N., Sherwany, G. and Knutsson, S. 2013. Trends and future challenges of water resources in the Tigris–Euphrates Rivers basin in Iraq. Hydrol. Earth Syst. Sci. Discussions, 10(12): 14617-14644.

Japitana, M.V. and Burce, M.E.C. 2019. A satellite-based remote sensing technique for surface water quality estimation. Eng. Technol. Appl. Sci, Res., 9(2): 3965-3970.

Kibena, J., Nhapi, I. and Gumindoga, W. 2014. Assessing the relationship between water quality parameters and changes in land use patterns in the Upper Manyame River, Zimbabwe. Phys. Chem. Earth, Parts A/B/C, 67: 153-163.

Kontopoulou, E., Kolokoussis, P. and Karantzalos, K. 2017. Water quality estimation in Greek lakes from Landsat 8 multispectral satellite data. Europ. Water, 58: 191-196.

Markogianni, V., Kalivas, D., Petropoulos, G.P. and Dimitriou, E. 2018. An appraisal of the potential of Landsat 8 in estimating chlorophyll-a, ammonium concentrations, and other water quality indicators. Remote Sens., 10(7): 1018.

Nature Environment and Pollution Technology
An International Quarterly Scientific Journal

p-ISSN: 0972-6268
(Print copies up to 2016)
e-ISSN: 2395-3454

Vol. 21 | No. 5 (Suppl) | pp. 2323-2327 | 2022

Original Research Paper

https://doi.org/10.46488/NEPT.2022.v21i05.028

Open Access Journal

Preparation of Carboxymethyl Cellulose from *Musa paradisiaca* Pseudo Stem Using an Alkaline Treatment

Vijayaraghavan Gopal*, Dharani Dharan Dharmarajan* and Sivamani Sivalingam*†
*Department of Chemical Engineering, Rajalakshmi Engineering College, Thandalam-602105, Chennai, India
†Corresponding author: Sivamani Sivalingam; sivamchem@gmail.com, sivamani.s@rajalakshmi.edu.in

Nat. Env. & Poll. Tech.
Website: www.neptjournal.com

Received: 08-07-2022
Revised: 22-08-2022
Accepted: 06-09-2022

Key Words:
Musa paradisiaca
Carboxymethyl cellulose
Pseudo stem
Alkaline treatment

ABSTRACT

Carboxymethyl cellulose (CMC) extraction from *Musa paradisiaca* (MP) pseudo stem by alkaline treatment and their properties were examined in the current research work. One of the most well-known types of lignin biomass waste that is readily available globally is MP. In many nations, including Taiwan, Sri Lanka, the Philippines, India, and the Philippines, these plants have been used for traditional reasons. Whole plant parts have been used as food, including the pseudo-stem, flower buds, trunk, fruits, and leaves. Sequestration of cellulose was attained by alkaline treatment and bleaching from raw fibers. Cellulose fiber is a biodegradable, naturally occurring, and renewable polymer that is used in a variety of industries, including the food, paper, cosmetic, and pharmaceutical sectors. The cellulose obtained from forest and agricultural residue has numerous advantages such as being environmentally safe, recyclable, and economically feasible respectively. The main process of cellulose extraction from MP pseudo stem are digesting process using a digester, bleaching, and neutralization which shows a zero-waste process. The alkali treatment takes less time to get a final product whereas enzyme treatment, and steam explosion treatment takes high energy and more cost. Hence, cellulose extract from alkaline treatment is economically feasible and environmentally friendly.

INTRODUCTION

In recent years, there is an increasing trend in the application of plant fibers and products. The main advantages of using these products from natural resources are bio-degradability and ease of handling. Deforestation of trees for the production of cellulose can be reduced when cellulose is extracted from agricultural waste. Lignocellulosic resources such as agricultural residues (straw, bark, leaves, and stems), and forest residues (hardwood and softwood) can be reused (Pires et al. 2019). The word 'lignocellulose waste' refers to the part of the crop that can not be harvested (Garcia et al. 2016). Lignocellulosic is the most available and regenerative biomass resource in nature and is underused, approximately 200 billion tonnes of lignocellulosic biomass supply from timber, forestry, industrial, and farm waste worldwide (Kocar et al. 2013). A significant amount of residual biomass (solid, liquid, and gaseous) is generated annually from the worldwide agricultural market, which should be the most available, physical, and renewable natural resource on earth (Santana-Meridas et al. 2014). Many of these residues are considered ecological liabilities unless recycled in an environmentally friendly manner (Hendriks & Zeeman 2009).

The lignocellulose waste, which primarily consists mainly of cellulose, and hemicellulose lined together and provides an enormous amount of energy resources and is an effective and regenerative supply of alternative fuels and useful chemical compounds (WeLi et al. 2015). In the biomass system, cell walls consist mainly of cellulose, hemicellulose, and lignin at a ratio of 4:3:3. This is distinct from sources like hardwood, softwood, and herbs (2014). Natural fibers have many advantages, they have low density, are recyclable, and are biodegradable. Additionally, they are sustainable raw materials and have comparatively immense strength and stiffness (Hendriks & Zeeman 2009). The natural fiber is a heterogeneous polymer network composed of cellulose, hemicellulose, and lignin (WeLi et al. 2015). In tropical and subtropical countries fibrous plants are available abundantly like bananas as an agricultural crop. Banana plants are a member of the *Musaceae* family. The edible banana species belong to the Australimusa and Eumusa groups, a member of *Musa accuminata* and *M. sapientum,* is usually a human convenient eatable banana (Mohapatra et al. 2010). The fiber of bananas is a perfect bast fiber. The chemical composition of banana fiber is cellulose, hemicellulose, and lignin, banana fiber is biodegradable and has no harmful environmental effects and can therefore be graded as eco-friendly fiber.

MP pseudo-stem is a waste product during MP cultivation. Hence it can be collected directly from the MP plants for value-added product-making like CMC (Huber et al. 2012).

Carboxyl methyl cellulose (CMC) is a water-soluble, anionic biopolymer and is one of the cellulose derivatives. Physical and chemical characteristics of CMC include hydrophilicity, pH-sensitivity, non-toxicity, and the ability to gel-forming (Siamak & Ahmad 2019). Because of the CMC's unique features, it has been used in various applications such as lithium-sulfur batteries, elimination of water contaminants, food packaging, etc. (Wang et al. 2018). Various techniques such as enzyme treatment, steam explosion treatment, and alkali treatments have been used to excerpt cellulose fibers from biomass resources (Manilal et al. 2011). The steam explosion behavior requires high pressure, and high temperature and is quite costly similarly enzyme treatment needs a long time and the activity of a low enzyme is hard for industrial production purposes. However, in alkali treatment the cellulose molecule reacts quickly with a strong base, with less energy like reactivity order is LiOH >NaOH >RbOH >CaOH.

Natural fibers are cured using chemicals to expel lignin covering resources like natural oils, waxy stuff, pectin, and so on. NaOH is a quite frequently used chemical for the ablution of the surface of plant fibers. This process is known as mercerization (WeLi et al. 2015). The standard explanation for mercerization recommended by ASTM D1695 is (ASTM 1983) "the process of subjecting a vegetable fiber to the action of a fairly concentrated aqueous solution of a strong base to produce great swelling with resultant changes in the fine structure, dimension, morphology, and mechanical properties". Zeronian proposes another definition of Mercerisation, as Mercerized cellulose is "a sample of cellulose which has been treated with a solution of an alkali metal hydroxide of sufficient strength for complete conversion" (Long Pang et al. 2019).

Cellulose is a homopolymeric, linear syndiotactic (molecular formula $C_6H_{10}O_{5n}$) that is formed by D-anhydrous glucopyranose units (AGU) joined together via □- 1,4-glycosidic bonds commonly called glucose units (Demirbas 2008). Cellulose has a high surface area since it contains well-structured bear hydroxyl groups which lead to great activity and the ability to react with different particular groups (Juntao Tang et al. 2017). Cellulose has the highest degree of polymerization (DP) among biopolymers, consisting of lignocellulosic fibers that can differ the maximum values of 20,000 units and more that depends on the source of cellulose. One of the key properties of cellulose is that it is insoluble in H_2O but absorbs about 14% of water at 60 % relative humidity at a temperature of 20°C.

After harvesting a bunch of *Musa paradisiaca* from trees over a field, vast amounts of pseudo-stem residues are left over because each *Musa paradisiaca* plant cannot be used for the next crop. These pseudo-stems are frequently discarded in soil planting to become organic waste and cause degradation of the ecosystem. Extracting fibers from these pseudo-systems can assist with natural degradation, thereby contributing to ecological equilibrium. Hence, the use of the pseudo-system *Musa paradisiaca*, which was historically called waste, would be greatly beneficial to the ecosystem and would bring additional profits. The reuse of by-products and processes with low environmental impact may be safe and an alternative novel material (Archana Das et al. 2016). Therefore, In the present study, an attempt was made to extract the cellulose from the *Musa paradisiaca* pseudo-stem which is available locally using the alkaline treatment, and to analyze the characteristics.

MATERIALS AND METHODS

Raw Materials

MP pseudo-stem was obtained after harvesting banana trees, the fruits and leaves are used for various purposes, Beater, Digester, Sodium hydroxide solution (NaOH) of 5% concentration, distilled water, and Hydrogen peroxide (H_2O_2) solution, Monochord acetic acid (MCAA) of 10% concentration and Ethanol for neutralization. The cellulose content present in different plants is listed in Table 1. From Table 1 it was inferred that the raw material chosen has approximately 50% cellulose content which is next to cellulose content in wood and cotton waste.

Methodology

The MP pseudo-stem is harvested, firstly the raw material has washed to remove impurities, and then water is sprinkled on the pseudo-stem at a higher velocity so that the impurities get washed away. Later it was chopped into small pieces with help of sharp knives as it increases the surface area

Table 1: Cellulose content present in different plants.

S. No	Raw material	Cellulose Content %
1	Cotton waste	80.95
2	Wood	80.90
3	*Musa paradisiaca* Pseudo-stem	43.0
4	Bagasse	40.0
5	Corn Stalk	35.0
6	Tomato stems	27.0
7	Coconut Shell	19.8
8	Tomato Leaves	10.9

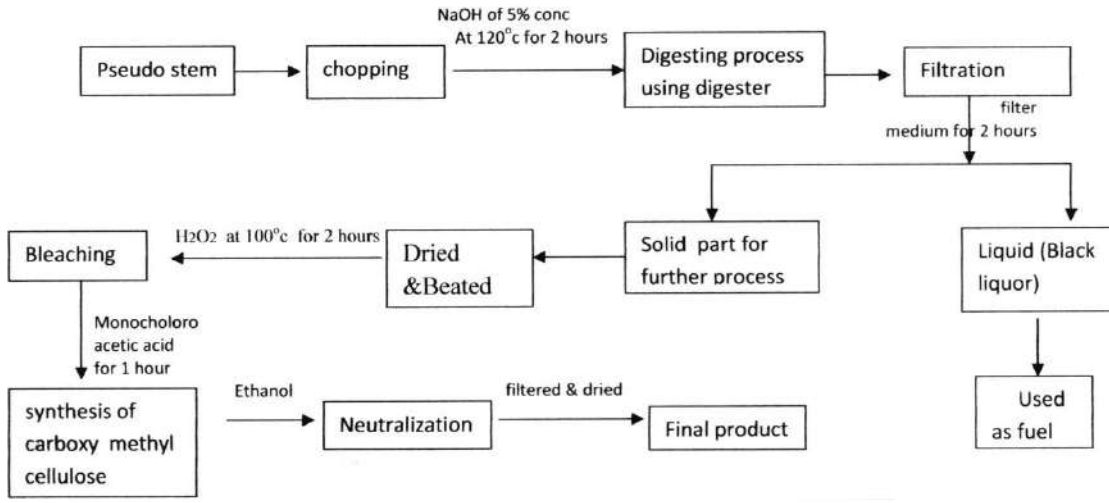

Fig. 1: Extraction of cellulose from *Musa paradisiaca* pseudo-stem.

and easier for further processing of the pseudo-stem. The chopped pieces must be of equal size it is better to use a cutting machine so that the size will be uniform. The detailed process of extracting the cellulose from the MP pseudo-stem was shown in Fig. 1. At that time chopped pieces are given as feed into a digester and 5% NaOH solution was added to eliminate the alkali-based soluble constituents like hemicellulose and other contaminations existing in the outer surface cell walls (Rani et al. 2019) i.e. for 30 g of feed 300 mL of NaOH is required feed to liquor ratio is (1:10), the temperature of the digester is maintained at 120°C and the pressure is maintained at 1.4 bar, and the process takes place for 2 hours (Tadeusz et al. 2020). Once the process is completed the outlet from the digester is taken with a mixture of digested stem and liquid obtained in black color, then the solid and liquid parts were separated by filtration process using a filter medium.

The filtrate, also known as the black liquor, was collected and used as fuel for the digester, and the solid portion kept in the filter medium was taken for additional processing. Then the obtained solid part is washed with water 2 to 3 times with water until they have become alkali-free. The washed fibers are allowed to deplete in free-flowing water. The dried part is added to potassium hydroxide and organic solvent acetone to remove lignin, hemicellulose, and other components without any loss of cellulose (Salam et al. 2007). After that, the product was dried and the solution was filtered. 90% of the lignin and hemicellulose were removed, which is a more effective removal method. The residue biomass underwent a 5-h bleach treatment at room temperature using a 2-percent H_2O_2 solution while being stirred because the residual was black. The chemical changes and fractional delignification of lignocellulosic were attained by oxidizing agents H_2O_2 to improve their properties for make use in various application purposes (Obi Reddy et al. 2017). The substance changed to white color then it was dried for 1 hour, the dried material looks similar to the cellulose obtained from normal wood processing. The bleached material was filtered using a filter medium and then dried for 30 min, later it was processed with Monochloro acetic acid (MCAA). This was the main process for cellulose fiber synthesis, which takes place for nearly one hour so that it forms a small thread-like structure as fiber and it was dried for 30 min. At last, the addition of ethanol for neutralization gives the final product after the filtration and drying process at 90°C.

RESULTS AND DISCUSSION

Chemical Analysis

The chemical composition of *Musa paradisiaca* pseudo-stem was calculated using the standards of Technical Association of the Pulp and Paper Industry (TAPPI) methods for various components, namely: T203 classical method (cm) -99 for cellulose and T 222 official method (om)-06 for lignin (Mwaikambo & Ansell 2001). The cellulose content was found to be 43% and lignin content is 18% and hemicellulose is 28% in the *Musa paradisiaca* pseudo-stem. Following the procedure, cellulose and lignin were chemically analyzed using TAPPI techniques, and for hemicellulose, three liters of ethanol were made for the filtrate produced from the processed biomass following alkaline neutralization. The precipitate produced using a vacuum pump was filtered through a glass funnel. The precipitated substance (i.e. hemicelluloses) was washed with 70 percent ethanol after

Table 2: Comparison of chemical composition in raw material and product.

Content	Cellulose %	Lignin %	Hemi cellulose%
Raw material	43	18	28
Processed	41	2	4

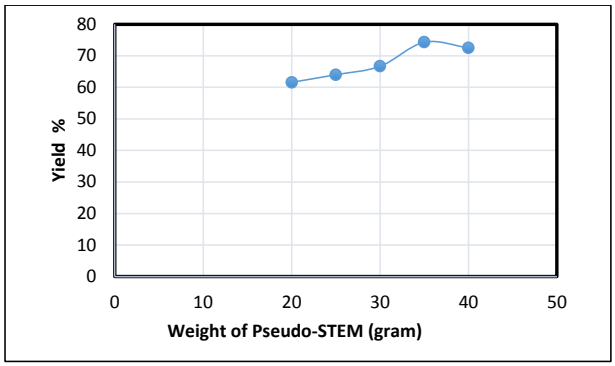

Fig. 2: Percentage yield of cellulose.

filtration and allowed to air dry (Obi Reddy et al. 2017). Table 2 shows the comparison of the chemical composition of raw material and the product.

Cellulose Yield

The cellulose fiber was extracted from the *Musa paradisiaca* pseudo-stem and the yield of cellulose content in the fiber was analyzed. The fresh banana pseudo stems moisture content was estimated to be 96%. Many trials have been carried out with different amounts of feed content, Fig. 2 shows the percentage of yield for different trials, from the graph it was found that the average yield of 60-70%.

Cellulose Confirmation Test

To confirm the presence of cellulose in the extracted fiber two confirmation tests were made - Schulze's reagent test: Schulze's reagent (Chloro-Zinc-Iodide) was added to the final product obtained after the extraction, and it turned purple color which confirms the presence of cellulose. Schulze reagent is an oxidizing mixture composed of a saturated aqueous potassium chlorate solution ($KClO_3$) and varying amounts of concentrated nitric acid (HNO_3) in the ratio of 1:1. Schulze and Tollens believed that Schulze's reagent is insoluble with hemicellulose (Rani et al. 2019). The reagents preparation technique is done by adding $ZnCl_2$ to 8.5 mL water, then dissolving followed by cooling. Lastly, we added $ZnCl_2$ solution dropwise in 20 mL of KI solution until Iodine precipitated, then proceeded to shake.

Determination of Viscosity

First, the cuprammonium reagent is prepared by dissolving solid cupric hydroxide in an ice bath with ammonium hydroxide. This approach makes storage superfluous. Cellulose is then dissolved in the reagent, and cuprous chloride and copper wire are added to prevent oxidation of air (Mwaikambo & Ansell 1999). Mechanical agitation makes the operation easier. In a redwood viscometer, the time of flow of the resulting solution was measured. Dynamic viscosity (also known as absolute viscosity) is the calculation of internal cellulose resistance to movement, whereas kinematic viscosity refers to the dynamic viscosity ratio to cellulose density. From Table 3, it was inferred that the cellulose viscosity is increased with an increase in the solution temperature indicating that the cellulose fiber extracted can withstand high temperatures.

Table 3: Effect of temperature on viscosity of cellulose.

Temperature °C	Density [kg.m^{-3}]	Time taken for 50 mL collection [sec]	Kinematic viscosity [v] m^2.s^{-1}	Dynamic viscosity[μ] Ns.m^{-2}
20	45.24	65	16.055	4.02
30	67.7	78	19.266	6.02
50	72.8	92	22.724	6.47
60	89.7	120	29.64	7.98
70	120.54	180	44.46	10.72

Production Cost

The cost for one piece of Pseudo-stem is Rs 10 of length 20 cm. A banana tree can be made into 10 pieces; hence, the cost of the main raw material is Rs 100. The cost of 1 kg of sodium hydroxide pellet is Rs 80 and the cost of 1 kg of Monocholoro acetic acid (MCAA) is Rs 90. The cost of 500 mL of Liquid ethanol is Rs 135. The overall cost of producing 1 kg of CMC is Rs 300, which is considerably less expensive than the standard method for extracting cellulose. Additionally, there are more raw materials available for CMC manufacturing than there are for wood pulp.

CONCLUSION

In the present work, CMC has been isolated and characterized from *Musa paradisiaca* pseudo-stem fiber waste. Cellulose separation from raw fibers was accomplished with alkaline treatment and bleaching, and there was no wastage in the production of CMC. Highly accessible cellulose was prepared and the deforestation of trees for the cellulose extraction from wood pulp was reduced. Results showed that the yield of cellulose from MP pseudo-stem was 60-70 %. The chemical composition of raw material and the product was analyzed by the standard Technical Association of the Pulp and Paper Associations (TAPPI) methods and the cost

for the process was also compared with the general process of cellulose extraction. Alkali treatment can therefore be utilised to extract CMC from biomass resources like MP, which offer viable solutions and are inexpensive.

ACKNOWLEDGMENT

The authors would like to acknowledge their sincere thanks to Rajalakshmi Engineering College (Autonomous), Thandalam, Chennai for the support.

REFERENCES

Archana Das, M., Manash, H.P., Monmi, G., Archana, Y. and Pradip, K. 2016. Extraction of cellulose from agricultural waste using Montmorillonite K-10/LiOH and its conversion to renewable energy: Biofuel by using *Myrothecium gramineum*. Carbohydr. Polym., 141: 20-27.

ASTM D 123-83a, 1983. Annual Book of ASTM Standards, Textiles Yarns, Fabrics, General Tests Methods, 7: 07

Demirbas, A. 2008. Heavy metal adsorption onto agro-based waste materials: A review. J. Hazard. Mater., 157: 220-229.

Garcia, A., Gandini, A., Labidi, J., Belgacem, N. and Bras, J. 2016. Industrial and crop wastes: A new source for Nanocellulose biorefinery. Ind. Crops Prod., 93: 26-38.

Hendriks, A.T.W.M and Zeeman. G. 2009. Pretreatments to enhance the digestibility of lignocellulosic biomass. Bioresource. Technol., 100: 10-18.

Huber,T., Mussig, J., Curnow, O., Pang, S.S., Bickerton, S. and Staiger. M.P. 2012. Acritical review of all-cellulose composites. J. Mater. Sci., 47: 1171-1186.

Juntao, T., Jared, S., Nathan, G. and Kam Chiu, T. 2017. Functionalization of cellulose nanocrystals for advanced applications. J. Colloid Interface Sci., 494: 397-409.

Kocar, G. and Civas, N. 2013. An overview of biofuels from energy crops: current status and future prospects. Renew. Sustain. Energy Rev., 28: 900-916.

Long, P., Zideng, G., Haojie, F. and Shunyi, W. 2019. Cellulose-based materials for controlled release formulations of agrochemicals: A review of modifications and applications. J. Contr. Rel., 316: 105-115.

Manilal, B.V., Jayaprabha, J.S. and Brahmakumar, M. 2011. Banana pseudostem characterization and its fiber property evaluation on physical and bio extraction. J. Nat. Fibers., 8(3): 149-160.

Mohapatra, D., Mishra, S. and Sutar, N. 2010. Banana and its by-product utilization an overview. J. Sci. Ind. Res., 69: 323-329.

Mwaikambo, L.Y. and Ansell, M. P. 1999. The effect of chemical treatment on the properties of hemp, sisal, jute, and kapok for composite reinforcement. Die Angewandte Makromol. Chemie., 272: 108-116.

Mwaikambo, L.Y. and Ansell, M.P. 2001. The determination of porosity and cellulose content of plant fibers by density methods. J. Mater. Sci. Lett., 20: 2095-2096.

Obi Reddy, K., Uma Maheswari, C., Dhlamini, M.S., Mothudi, B.M., Kommula, V.P., Jinming, Z., Jun, Z.A, and Varada, R. 2017. Extraction and characterization of cellulose single fibers from native African napier grass. Carbohydr. Polym., 188: 85-91.

Pires, J.R.A., Gomes, V., De Souza, L. and Fernando, A.L. 2019. Production of nanocellulose from lignocellulosic biomass wastes: Prospects and limitations. Innov. Eng. Entrep., 505: 719-725.

Rani, K., Gomathi, T., Vijayalakshmi, K., Saranya, M. and Sudha, P.N. 2019. Banana fiber cellulose nanocrystals grafted with butyl acrylate for heavy metal lead (II) removal. Int. J. Biol. Macromol., 131: 461-472.

Salam, A., Reddy, N. and Yang, Y. 2007. Bleaching of kenaf and Cornhusk fibers. Ind. Eng. Chem. Res., 46: 1452-1458.

Santana-Meridas, O., Polissiou, M., Izquierdo, M., Astraka, K., Tarantilis, P.A., Herraiz Penalver, D. and Sanchez, V.R. 2014. Polyphenol composition, antioxidant and bio plaguici deactivities of the solid residue from hydro distillation of Rosmarinusocinalis, L. Ind. J. Crop. Prod. Process., 59: 125-134.

Siamak, J. and Ahmad, S. 2019. Carboxymethyl cellulose-based oral delivery systems. Int. J. Biol. Macromol., 133: 21-29.

Tadeusz, J.S., Lukasz, K. and Teofil, J. 2020. Recent developments in modification of lignin using ionic liquids for the fabrication of advanced materials-A review. J. Mol. Liq., 301: 112417.

Wang, W., Yue, X., Meng, J., Wang, X., Zhou, Y., Wang, Q. and Fu, Z. 2018. Comparative study of water-based LA133 and CMC/SBR binders for the sulfur cathode in advanced lithium-sulfur batteries. J. Phys. Chem. C., 123: 250-257.

WeLi, Y., Zhang, J.L., Yijun, Z., Ruisong, L. and Wei, Z. 2015. Characterization of cellulose from banana pseudo-stem by heterogeneous liquefaction. Carbohydr. Polym., 132: 513-519.

... Continued from inner front cover

- The text of the manuscript should run into **Abstract, Introduction, Materials & Methods, Results, Discussion, Acknowledgement** (if any) and **References** or other suitable headings in case of reviews and theoretically oriented papers. However, short communication can be submitted in running with **Abstract and References.** The references should be in full with the title of the paper.
- The figures should preferably be made on a computer with high resolution and should be capable of withstanding a reasonable reduction with the legends provided separately outside the figures. Photographs may be black and white or colour.
- Tables should be typed separately bearing a short title, preferably in vertical form. They should be of a size, which could easily be accommodated in the page of the Journal.
- References in the text should be cited by the authors' surname and year. In case of more than one reference of the same author in the same year, add suffix a,b,c,.... to the year. For example: (Thomas 1969, Mass 1973a, 1973b, Madony et al. 1990, Abasi & Soni 1991).

List of References

The references cited in the text should be arranged alphabetically by authors' surname in the following manner: (Note: The titles of the papers should be in running 'sentence case', while the titles of the books, reports, theses, journals, etc. should be in 'title case' with all words starting with CAPITAL letter.)

Dutta, A. and Chaudhury, M. 1991. Removal of arsenic from groundwater by lime softening with powdered coal additive. J. Water Supply Res. Techno. Aqua., 40(1) : 25-29.

Hammer, D.A. (ed.) 1989. Constructed Wetlands for Wastewater Treatment-Municipal, Industrial and Agricultural. Lewis Publishers Inc., pp. 831.

Haynes, R. J. 1986. Surface mining and wetland reclamation. In: Harper, J. and Plass, B. (eds.) New Horizons for Mined Land Reclamation. Proceedings of a National Meeting of the American Society for Surface Reclamation, Princeton, W.V.

Submission of Papers

- The paper can be submitted by e-mail as an attachment in a single WORD file at **contact@neptjournal.com**
- The paper can also be submitted online in a single WORD file through the **online submission portal** of journal's website: **www.neptjournal.com**

Attention

1. Any change in the authors' affiliation may please be notified at the earliest.
2. Please make all the correspondence by e-mail, and authors should always quote the manuscript number.

Note: In order to speed up the publication, authors are requested to correct the galley proof immediately after receipt. The galley proof must be checked with utmost care, as publishers owe no responsibility for mistakes. The papers will be put on priority for publication only after receiving the processing and publication charges.

Nature Environment and Pollution Technology

(Abbreviation: Nat. Env. Poll. Tech.)

(An International Quarterly Scientific Journal)

Published by

Technoscience Publications

A-504, Bliss Avenue, Opp. SKP Campus
Balewadi, Pune-411 045, Maharashtra, India

In association with

Technoscience Knowledge Communications

Mira Road, Mumbai, India

For further details of the Journal, please visit the website. All the papers published on a particular subject/topic or by any particular author in the journal can be searched and accessed by typing a keyword or name of the author in the 'Search' option on the Home page of the website. All the papers containing that keyword or author will be shown on the home page from where they can be directly downloaded.

www.neptjournal.com

Published for Proprietor, Printer and Publisher: Mrs. T. P. Goel, A-504, Bliss Avenue, Balewadi, Pune, Maharashtra, India; Editors: Dr. P. K. Goel (Chief Editor) and Prof. K. P. Sharma